THE UNIVERSITY OF HULL

**SYNTHESIS OF TETRAAZAMACROCYCLIC COMPLEXES:
BIOMEDICAL APPLICATIONS**

being a Thesis submitted for the Degree of Doctor of Philosophy
in the University of Hull

by

Ryan Edward Mewis, MChem (Hons)

January 2009

Abstract

Tetraazamacrocyclic frameworks of 1,4,7,10-tetraazacylcododecane (cyclen) and 1,4,8,11-tetraazacyclotetradecane (cyclam) with functional pendent arms and porphyrins with solubilising polyethylene glycol (PEG) chains have been synthesised. The pendent arms possess different properties which tailor the metal complex towards a particular role.

Both transition metal and lanthanide complexes of cyclam and cyclen metal complexes have been prepared with phenolate and thiophenolate pendent arms. The phenolate and thiophenolate pendent arms have *tert*-butyl groups in the *ortho* and *para* positions to stabilise radical formation. Cyclic voltammograms show that the phenoxyl and thiyl radical species can be generated by one electron oxidation processes at values around +0.5 to 0.7 V and +0.6 to 1.0 V respectively. Formation of the phenoxyl radical is reversible whereas formation of the thiyl radical is irreversible. The cyclic voltammogram of the europium(III) complex of cyclen bearing a thiophenolate and three acetate pendent arms ([Eu**56**]⁻) is temperature dependent as the thiyl radical is 0.31 V easier to oxidise at −40°C than at room temperature (RT). The formation of the phenoxyl radical was also observed using UV-visible spectroscopy after the one electron oxidation by ferricyanide. Fluorescence spectra of the europium(III) and terbium(III) complexes of cyclen bearing a phenolate and three acetate pendent arms ([Eu**52**]⁻ and [Tb**52**]⁻) possess two and four emission peaks respectively. Europium(III) and terbium(III) complexes of the corresponding thiophenolate ligand ([Eu**56**]⁻ and [Tb**56**]⁻) also possess two and four emission peaks respectively. T1 weighted images of [Gd**52**]⁻ and [Gd**56**]⁻ show enhanced image brightness relative to water.

A cyclen ligand with a single aspartic acid derived pendent arm (**27**) and three acetate arms has been synthesised. This was used to attach a further cyclam macrocyclic component towards dual-imaging probe synthetics.

Transition metal and p-block metal complexes of porphyrins have been produced with chains on the periphery which can enhance water solubility (either hydroxyl or PEG chains). Cyclic voltammetry of the tetra(3,5-dihydroxyphenyl)porphyrin (**62**) leads to the formation of a poly-porphyrin species. This was deposited on to the

surface of carbon paper electrochemically and was visualised using scanning electron microscopy (SEM). PEGylated tetra(pentafluorophenyl)porphyrins have also been synthesised. The PEG chains aid water solubility and also have an effect on the light induced cytotoxicity of the compound. Zinc(II), nickel(II) and gallium(III) complexes have also been produced. Zinc(II) and nickel(II) complexes are not light induced toxic whereas the gallium(III) complexes are. Furthermore, the anion in the gallium(III) complexes can also dictate the light induced cytotoxicity of the complex.

Acknowledgements

I would firstly like to thank my supervisor, Dr Steve Archibald, for all of his help and advice during my PhD studies and also whilst writing up. I would also like to thank him for all his encouragement and support in pursing my future career aspirations. Thanks also to Dr Ross Boyle, my second supervisor, for his help with the porphyrin chemistry.

I would also like to express my thanks to all those people who I have worked with, especially (in no particular order) Gaz, Amanda, Abid, Jon, Graeme, Aaron, Christina, Mike and Chris. Special thanks go to Jon for teaching me how to collect and solve crystallographic data and for fuelling my interest in this area, Graeme for being my research companion for the last three years and Gaz for showing me how to obtain cyclic voltammograms. I would also like to thank all the members of the inorganic group, past and present, for their support and help.

I would like to thank all of the technical staff in the chemistry department for their help and assistance for helping me to obtain analytical data. People I would like to especially thank include Dr Steve Clark for being on hand to help with crystallographic problems, Carol Kennedy for running CHNs, Tony Sinclair for spending a couple of afternoons with me to obtain SEM images and Hugette Savoie for performing all the cellular studies.

I am also very grateful to my Mum, Dad and my sister, Laura, for taking an interest in my studies and the work that I've been doing. I would like to thank them for the weekly 8 pm phone call! In addition, I would like to thank my Dad especially as well as Matthew Wellock for their help in various DIY jobs. I would also like to thank Jenny Wellock for kindly volunteering to read through my entire thesis, and also for taking me to B&Q more or less every Wednesday for yet more DIY goods!

Lastly, a big thank-you goes to my wife Ruth. Ruth has been tremendously supportive whilst I've been writing up and her encouraging words of "so you've almost finished then" has spurred me on many a time. Now you can finally find out what I've been doing these last three years!

Abbreviations

^{62}Cu-PTSM	^{62}Cu-pyruvaldehyde-bis(N^4-methylthiosemicarbazone)
AIDS	acquired immunodeficiency syndrome
AOT	sodium bis(2-ethylhexyl)sulfo-succinate
BFC	bi-functional chelator
B_{max}	binding maximum
BN	bombesin
BOC	*tert*-butyl carbamate
BopCl	bis(2-oxo-3-oxazolidinyl)phosphonic chloride
Caco	human Caucasian colon adenocarcinoma
CEST	chemical exchange saturation transfer
Chk-1	checkpoint kinase 1
CT	catalytic therapy
CV	cyclic voltammogram
Cyclam	1,4,8,11-tetraazacyclotetradecane
Cyclen	1,4,7,10-tetraazacylcododecane
DCC	dicyclohexylcarbodiimide
DCM	dichloromethane
DEFRET	diffusion enhanced fluorescence resonance energy transfer
DFO	desferoxamine
DHE	dihydroethidium
DIBAL	diisobutyl aluminium hydride
DMA	dimethylacetamide
DMAP	dimethylamino-pyridine
DMEM	Dulbecco's modified Eagle's medium
DMF	dimethylformamide
DMSO	dimethyl sulfoxide
DNA	deoxyribonucleic acid
DO3A	1,4,7,10-tetraazacyclodecane-1,4,7-triacetic acid
DO3A-TB	1,4,7,10-tetraazacyclodecane-1,4,7-*tert*-butyl-methyl ester
DOTA	1,4,7,10-tetraazacyclodecane-1,4,7,10-tetraacetic acid
Dtma	1,4,7,10-tetrakis(carbamoylmethyl)-1,4,7,10-tetraazacyclododecane
DTPA	diethylenetriamine pentaacetate
EDC	1-ethyl-3-(3-dimethylaminopropyl) carbodiimide hydrochloride
EtOH	ethanol
GRPR	gastrin-releasing peptide receptor
HEPES	4-(2-hydroxyethyl)-1-piperazinoethanesulfonic acid
HIV	human immunodeficiency virus
HIV-1 Tat	human immunodeficiency virus I

	transcriptional activator
HOBT	hydroxybenzotriazole
HpPNP	2-hydroxypropyl-4-nitrophenyl phosphate
HSA	human serum albumin
ID	injection dose
IR	infra-red
LRET	luminescence resonant energy-transfer
MeCN	acetonitrile
MeOH	methanol
MICs	minimum inhibitory concentrations
MNPP	*p*-nitrophenyl phosphate
MOMCl	methoxymethyl chloride
MRI	magnetic resonance imaging
MRS	magnetic resonance spectrosopy
NBS	N-bromo succinimide
NBT	nitro blue tetrazolium
NEAA	non-essential amino acid solution
NIR	near-infrared
NLS	nuclear localisation signals
NMB-R	neuromedin B receptors
NMR	nuclear magnetic resonance
NOTA	1,4,7-triazacyclononane-*N,N',N''*-triacetic acid
NTI	naltrindole
OEP	2,3,7,8,12,13,17,18-octaethylpoprhyrin
OMP	2,3,7,8,12,13,17,18-octamethylpoprhyrin
PARACEST	paramagnetic chemical exchange saturation transfer
Pc	phthalocyanine
PcCo	Co phthalocycanine
PDA	2,6-pyridinedimethaneamine
PDT	photodynamic therapy
PEA	2,5,8,17,20,23-hexaaza[9.9]paracyclophane
PEG	polyethylene glycol
PEG4	15-amino-4,7,10,13-tetraoxopentadecanoic acid
PET	positron emission tomography
PFL	pyruvate formate-lyase
PPTS	pyridinium *p*-toluenesulfonate
PVC	poly(vinyl chloride)
q	hydration number
RF	radio-frequency
RNA	ribonucleic acid
RNR	ribonucleotide reductases
ROS	reactive oxygen species
RT	room temperature
Salen	salicylidene(amine)diaminoethane
SEM	scanning electron microscopy

SOD	super-oxide dismutase
SPECT	single photon emission computed tomography
TACN	triazacyclononane
TAG	tumour-associated glycoprotein
TBTA	*tert*-butyl-2,2,2-trichloroacetimidate
TETA	1,4,8,11-tetraazacyclotetradecane-1,4,8,11-tetraacetic acid
TF$_5$PP	5,10,15,30-tetrakis(pentafluorophenyl)porphine
TFA	trifluoroacetic acid
THP	3,4-di-hydro-2H-pyrane
TLC	thin layer chromatography
TPP	tetraphenylporphyrin
TRLLM	time-resolved long-lived luminescence microscopy
UV	ultra-violet
WSC	water-soluble carbodiimide

Table of contents

4.   Synthesis of cyclen derived macrocyclic systems with phenolate, thiophenolate and amino-acid pendent arms 128

xi

List of figures

List of graphs

List of schemes

List of tables

1. Introduction

1.1. Macrocyclic ligands

Macrocyclic ligands are polydentate ligands which contain donor atoms either incorporated in or attached to a cyclic backbone. Usually macrocyclic ligands possess at least three donor atoms and the macrocyclic ring consists of no less than nine atoms.[1] The number of atoms in the polydentate chain is the main factor that determines the cavity size, but this is also affected by the rigidity in the backbone and by the hybridisation and nature of the donor atom. Bonds between atoms in the cyclic chain can be saturated or unsaturated, although extensive unsaturation results in loss of flexibility, therefore decreasing the propensity for metal chelation. These factors can be used advantageously to develop macrocyclic derivatives that can be tailored towards binding certain types of metal ions e.g. transition or lanthanide metal ions.

The donor atoms of the macrocyclic ligand are arranged so that it can form five, six and seven-membered chelate rings with a metal centre. Thus ring sizes for a macrocycle containing three donor atoms possess usually between nine to thirteen atoms in the macrocyclic ring. For four donors, between twelve and seventeen atoms are required. Therefore macrocyclic ring sizes tend to possess between $3x$ and $4x+1$ (where $x=$ the number of donor atoms) atoms in its chain.

Enhanced kinetic and thermodynamic stabilities of the respective metal complexes offer distinct advantages over acyclic systems. This is because the propensity for decomplexation to occur is significantly lower and therefore, this does not affect the desired function of the metal complex. Such a property is highly desirable in biological systems.

1.1.1. The chelate and macrocyclic effect

The chelate effect is the gain of free energy when a bidentate or polydentate ligand is bonded to a metal ion instead of the corresponding number of unidentate ligands. The chelate effect is driven by a favourable entropic factor.[2]

The macrocyclic effect is an extension of the chelate effect. This term was first coined by Cabbiness and Margerum in the late 1960's after studying the copper(II)

complexes of the reduced Curtis macrocycle and an open chain tetramine analogue, '2.3.2-tet'.[3,4]
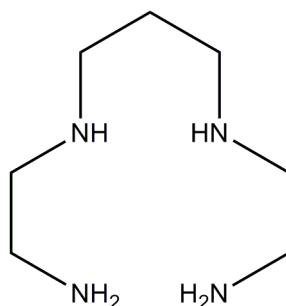
Figure 1: Chemical Structure of 2.3.3-tet.

A macrocycle has the donor atoms arranged so that it is *preorganised* to accept an incoming metal centre.[5] This means that there is less of an entropic effect in the binding energy of the resultant metal complex when compared with bidentate or polydentate ligands of the same donor type and number. The enthalpy of the reaction is governed by the following equation

$$M^{2+}(aq) + L(aq) \rightleftharpoons ML^{2+}(aq)$$
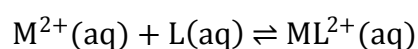
which can be determined calorimetrically for both the macrocyclic and open-chain systems. The difference between the respective enthalpy values gives the macrocyclic enthalpy for the following equation

$$ML^{oc}(aq) + L^{mac}(aq) \rightleftharpoons ML^{mac}(aq) + L^{oc}(aq)$$
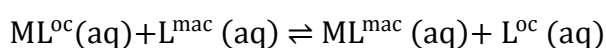
where L^{mac} is the macrocycle and L^{oc} is the open chain analogue. The entropy for such a reaction is always favourable; whereas the enthalpy term can be either favourable or unfavourable. Table 1^6 shows the thermodynamic parameters for a series of macrocyclic ligands relative to their open chain analogues for high spin nickel(II) complexes. Clearly, the enthalpy and entropy terms contribute differently to each complex in the series.
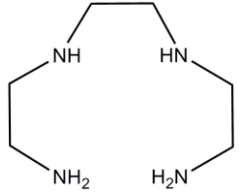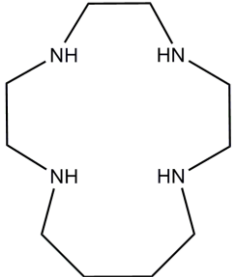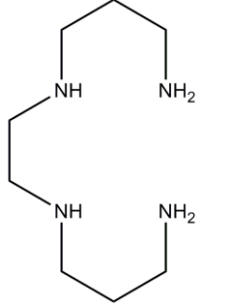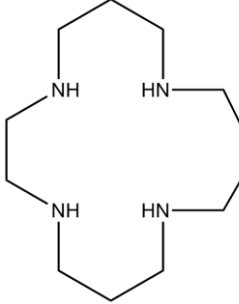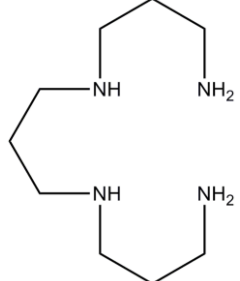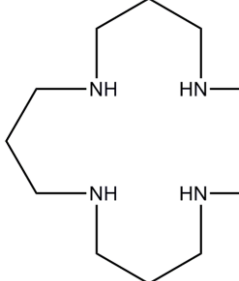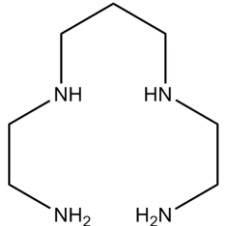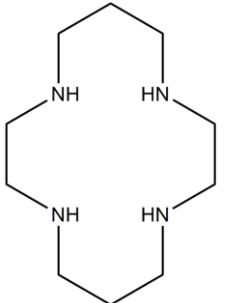
L^{oc}	L^{mac}	$-\Delta G$ (kJ mol^{-1})	ΔH (kJ mol^{-1})	$T\Delta S$ (kJ mol^{-1})
		2.43	5.1	7.4
		21.05	5.3	26.4
		15.69	3.5	19.2
		33.67	-20.5	13.2

Table 1: Thermodynamic parameters for a series of open chain nickel(II) complexes relative to their macrocyclic counterparts.

1.1.2. Macrocyclic systems incorporating pendent arms

Macrocyclic ligands are involved in a number of fundamental biological processes e.g. photosynthetic pathways and mammalian oxygen transport. Synthetic macrocyclic complexes have been prepared to mimic these systems. In addition, macrocyclic complexes have also been synthesised towards therapeutic and diagnostic applications. These compounds can be used as positron emission tomography (PET) imaging radiopharmaceuticals, magnetic resonance imaging (MRI) contrast agents, anti-cancer therapeutics and chemokine receptor antagonists. Pendent arms are frequently attached to the macrocyclic backbone for a number of reasons. Firstly, they can provide additional donor atoms to coordinate to the metal centre. Secondly, the pendent arms can be used as a linker group, providing additional functionality which can be used to attach further moieties to the complex. This is especially important in the synthesis of bioconjugate assemblies. Thirdly, the pendent arm can be responsive to a certain set of conditions which alters or attenuates the coordination sphere around the metal centre. This effect can then be monitored by analytical techniques. Pendent arms are therefore an important aspect in macrocycle design. A review on the topic of macrocyclic complexes bearing pendent arms as models for biological molecules was published in 2000.[7]

The aim of this introduction is to highlight selected examples in four key areas in which macrocyclic complexes are exploited. These are enzyme mimicry, therapeutic and diagnostic applications and optical probes. These four areas include several key topics of current interest, including anti-human immunodeficiency virus (HIV) drugs and magnetic resonance contrast agents. The examples discussed within this introduction offer a cross-section of the literature available but are not comprehensive due to the large volume of research in this area. The selected examples discussed focus on aza-macrocyles and mixed donor systems and their complexes. A recent review on the medical applications of macrocyclic polyamines has been published by Liang *et al*., which provides further information.[8] The introduction is divided in to sections based on the number of nitrogen atoms incorporated in the macrocyclic framework.

1.2. Tri-aza macrocyclic ligands and their analogues

Tri-aza macrocyclic ligands are currently being investigated for a number of diagnostic applications, which includes PET and MRI. They are also used in enzyme mimicry, such as in the production of photosystem II models. A further application for tri-aza macrocycles is for hydrolytic ribonucleic acid (RNA) and deoxyribonucleic acid (DNA) cleavage catalysts. The rest of this section will focus upon these areas and selected examples are discussed.

1.2.1. Enzyme mimics

1.2.1.1. Hydrolytic cleavage catalysts

A number of triazacyclononane (TACN) complexes have been produced in order to investigate their properties as hydrolytic cleavage catalysts. For example, zinc(II) complexes have been produced in order to study the mechanism of P-O bond cleavage occurring in the phosphate moiety of RNA model systems.[9] A dinuclear zinc(II) complex of **L**[1] (see Figure 3) with a bridging methoxide ion has been used to investigate the progressive change in mechanism from rate-limiting P-O bond cleavage to substrate binding.[10] The two zinc(II) centres were shown to be coordinated via a bridging methoxide. At pH 9.8, the catalyst is maximally active, catalysing the cyclisation of a range of phosphate esters with an acceleration of 1 - 4 x 10^{12} relative to the background reaction at the same pH.

A copper(II) methoxide bridged complex of **L**[1] has also been reported as a hydrolytic cleavage catalyst.[11] In this case, each TACN compartment holds a copper(II) ion, and it also exhibits efficient catalytic cleavage of phosphate esters. The catalyst exhibits Michaelis-Menten kinetics with a k_{cat}/K_M value of 30 $M^{-1}s^{-1}$ which is 3.8 x 10^7 fold greater than the methoxide promotion of the phosphate ester methyl *p*-nitrophenyl phosphate (MNPP). The transition state is stabilised by −24 kcal mol^{-1} relative to that of methoxide promoted reactions.

Further hydrolytic catalysts have been produced to cleave the more stable phosphate bonds in DNA. Zinc(II) and copper(II) bis-TACN complexes have been synthesised with bridging *p*-methyl phenol groups towards this aim.[12] The two metal centres are held in an almost perfect square based pyramidal geometry (τ values of 0.02 and

0.07 for dinuclear copper(II) (crystal structure shown in Figure 2) and zinc(II) complexes respectively). τ is a geometric parameter applicable to five coordinate structures to determine whether a metal ion adopts either a square-based pyramidal or trigonal bipyramidal geometry.[13,14] τ is defined as (β-α)/60, where β and α are the bond angles involving the *trans* donor atoms in the basal plane. Both complexes effectively cleave DNA in the presence of either mercaptoethanol (k_{cat} = 1.61 hr^{-1}, K_m =1.35 x 10^{-5} M, where M = copper(II)) or hydrogen peroxide (k_{cat} = 2.48 hr^{-1}, K_m = 5.5 x 10^{-5} M, where M = zinc(II)).
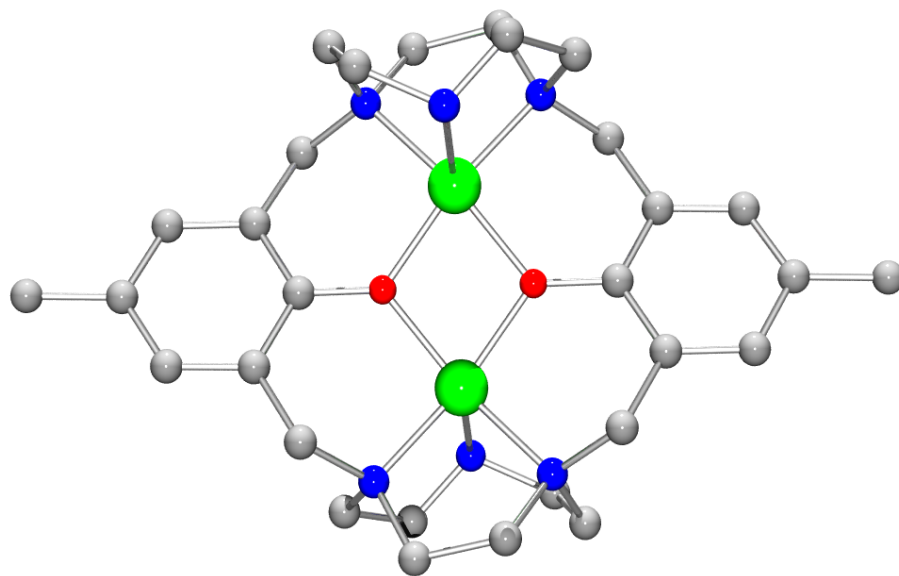
Figure 2: Ball and stick representation of the X-ray crystal structure of a bis-TACN bridged dinuclear copper(II) complex. H-atoms and perchlorate anions omitted for clarity (Qian *et al.*).[12]
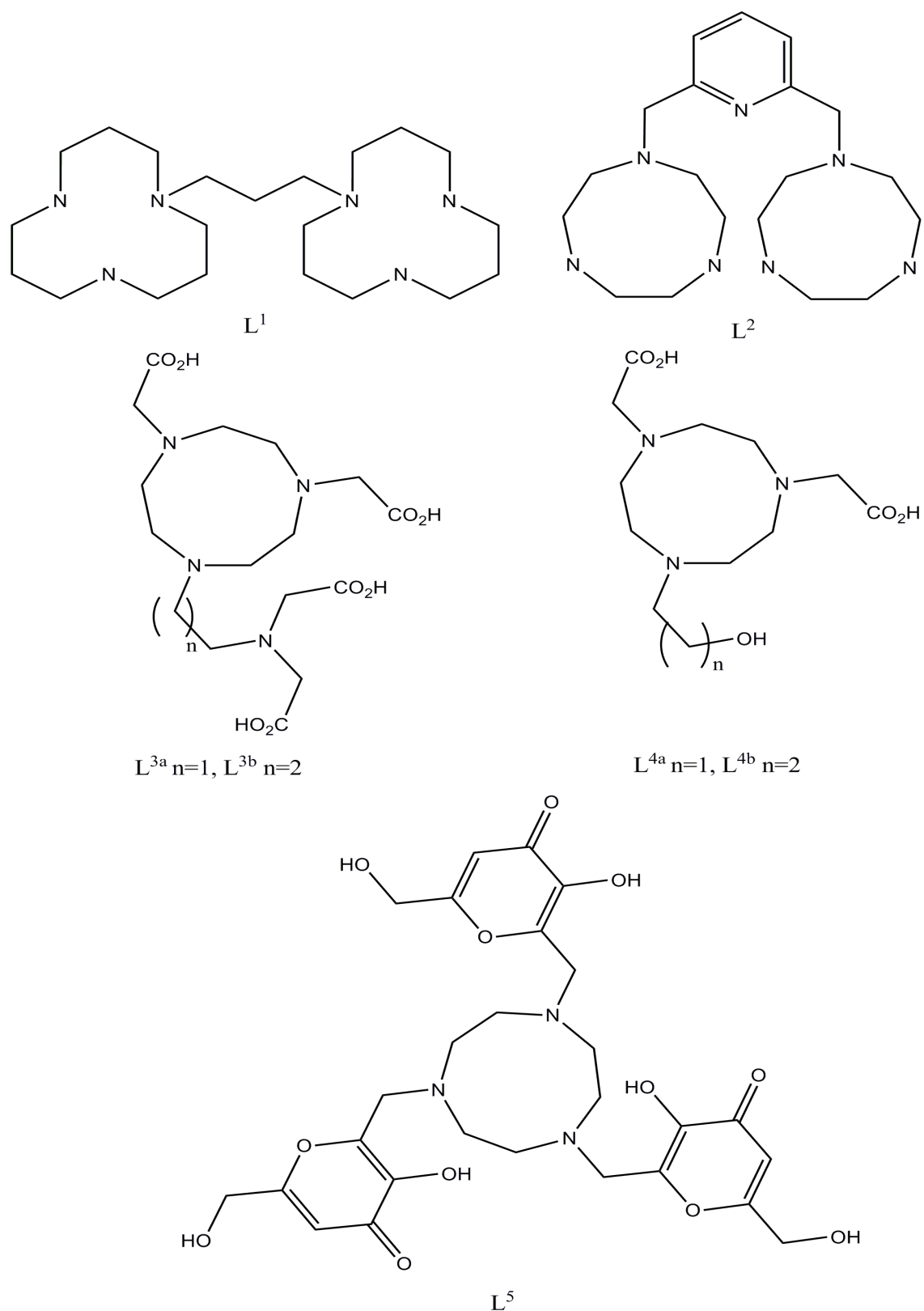
Figure 3: Chemical structures of L[1]-L[5].

Further examples of dinuclear zinc(II) hydrolytic DNA cleavage catalysts have been synthesised.[15] The zinc(II) ions are held in each TACN cleft of **L[2]**. Binding affinity

for this dinuclear complex for calf thymus DNA was found to be higher than the mononuclear TACN complex (3.57×10^6 M^{-1} and 1.43×10^5 M^{-1} respectively). Kinetic data for the dinuclear complex showed a 10^7-fold acceleration of DNA cleavage ($k_{obs} = 0.136$ h^{-1}) over uncatalysed supercoiled DNA. A hydrolytic process was suggested as the mechanism for cleavage.

1.2.1.2. Photosystem II and superoxide dismutase mimics

Tri-aza complexes have been used in enzyme mimicry. Two illustrative enzymes investigated using this type of complex are photosystem II and superoxide dismutase (SOD). Tetra- to nonanuclear transition metal complexes incorporating manganese ions, oxidisable phenolates and tris(2,2'-bipyridyl)ruthenium(II)-type units have been synthesised as a model for photosystem II.[16] The manganese centres were shown to exist in several oxidation states (II, III and IV) which are capable of undergoing one-electron transfer steps. Electrochemically, very slow heterogeneous electron-transfer was observed in several cases. This transfer was found to be dependent on the length of spacer between the manganese ion and the tris(2,2'-bipyridyl)ruthenium(II) unit. A long spacer unit enabled the observation of particularly slow electron-exchange kinetics by thin-layer electrochemical methods.

Other systems have been developed as SOD mimics. Oliveria and co-workers used several low molecular weight mixed oxygen and nitrogen donor macrocycles to complex copper(II) in order to investigate possible applications as superoxide scavenging agents.[17] All the complexes except 1,4-diaza-6-oxo-nonane showed reasonably high stability constants. Two different endpoints were used to evaluate the ability of the complexes to scavenge the superoxide anions generated by the xanthine-xanthine oxidase system; the nitro blue tetrazolium (NBT) reduction assay and the dihydroethidium (DHE) oxidation assay. Low micromolar IC_{50} (the molar concentration of antagonist which produces 50% of the maximum inhibitory response for that antagonist) values were found for most of the compounds tested (circa 13-31 μM).

1.2.2. Diagnostic agents

Triaza-macrocyclic complexes have been prepared for use as radiopharmaceuticals and as magnetic resonance imaging contrast agents. The following two sections discuss relevant examples for each area.

1.2.2.1.   Radiopharmaceuticals

Diagnostic agents for use in PET have been prepared using TACN derived macrocycles with either transition or p-block metal ions. For example, Brechbiel and co-workers synthesised 1,4,7-triazacyclononane-*N,N',N''*-triacetic acid (NOTA) based octadentate ligands as potential yttrium chelators.[18] A pendent bis(carboxymethyl)-amino donor group is linked to the macrocyclic ring by either an ethyl or propyl chain (**L**[3a] and **L**[3b]). The length of this alkyl chain was important with regard to the serum stability. The ethyl linker had 100% stability over 14 days whereas the propyl linker only 75%. *In vivo* distribution was shown to mirror that of the [86]Y complex of 1,4,7,10-tetraazacyclodecane-1,4,7,10-tetraacetic acid (DOTA).

Copper isotopes are also of interest as complexes of PET imaging agents. [62]Cu, ^{64}Cu and [67]Cu have been or are in current use as labels of compounds such as [62]Cu-pyruvaldehyde-bis(*N*[4]-methylthiosemicarbazone) ([62]Cu-PTSM) and monoclonal antibodies.[19] Brechbiel and co-workers have produced ^{64}Cu radiopharmaceuticals by modification of **L**[3a] and **L**[3b]. Replacing the pendent bis(carboxymethyl)-amino donor in **L**[3a] and **L**[3b] with a hydroxypropyl or hydroxyethyl (**L**[4a] and **L**[4b]) has been shown to lead to *in vivo* instability, with 59% and 29% of copper radioisotope dissociating from each macrocycle respectively.[20] The hydroxypropyl can form a six-membered chelate ring with the copper which gives rise to increased stability over the hydroxyethyl derivative. Aminocarboxylate groups were found to efficiently hold the ^{64}Cu in place, with no measurable loss of radioactivity over a 48 hr period.

Further examples of TACN based radiopharmaceuticals have been produced by Brechbiel's group. The ligands produced have both macrocyclic and acyclic clefts.[21] Two chelators were synthesised; both comprising of a modified *p*-isothiocyanate phenylalanine pendent arm which possessed either a secondary (*C*-NE3TA-NCS) or tertiary amino group (*C*-NETA-NCS). Both chelators were radiolabelled with ^{177}Lu, ^{90}Y, [203]Pb, [205/6]Bi and [153]Gd; and the *in vitro* stability of the complexes assessed in

human serum. All complexes were stable for up to 11 days in serum apart from the lead(II) complexes of both chelators which displayed significant dissociation of the metal from the complex. Relaxivity data indicated that Gd-*C*-NETA (4.77 mM^{-1}s^{-1}) and Gd-*C*-NE3TA (5.89 mM^{-1}s^{-1}) possess enhanced relaxivity compared to Gd(*C*-DOTA) (3.96 mM^{-1}s^{-1}). The varying number of coordination donors of NETA (8 donors) and NE3TA (7 donors) provided to the metal centre was believed to be responsible for the difference in relaxivities between the two complexes. ^{177}Lu and ^{90}Y labelled *C*-NETA and *C*-NE3TA exhibited rapid blood clearance from arythmic mice and also displayed relatively low radioactivity levels in normal organs as well as a favourable distribution profile. NE3TA and NETA have also been assessed for use in iron depletion tumour therapy.[22] Enhanced cytotoxicities were displayed in both HeLa and HT29 cells by NE3TA compared with desferoxamine (DFO).

Radio-labelled peptide-conjugates have been produced. NODAGATOC, a chelator-coupled somatostatin analogue with $^{67/68}$Ga and ^{111}In has been designed for application in single photon emission computed tomography (SPECT), PET and targeted therapeutic applications of somatostatin receptors (hsst2).[23] ^{67}Ga and ^{111}In are both γ emitters, whilst ^{68}Ga is β$^+$ emitter with a half-life of 68 min.[24] The two former radioisotopes are therefore suited for SPECT imaging and the latter for PET. The chelator produced uses a di-protected glutamic derived amino acid linker synthesised previously.[25] The ^{111}In radiolabelled complexes displayed notably higher binding affinity to both sstr2 and sstr5 (factor of 2 and 4 times higher respectively when compared with ^{67}Ga-NODAGATOC). The receptor binding affinities for the radiolabelled conjugates are shown in Table 2.

Peptide/ conjugate	hsst 1	hsst 2	hsst 3	hsst 4	hsst 5
Somatostatin-28	4.1 ± 0.3 (15)	2.6 ± 0.2 (16)	5.4 ± 0.6 (13)	4.1 ± 0.3 (16)	3.9 ± 0.4 (17)
DOTA-Tyr^3-octreotide (DOTATOC)	>10000 (7)	13.9 ± 2.8 (6)	13.9 ± 2.8 (6)	>1000 (5)	393 ± 85 (6)
Y-DOTA-Tyr^3-octreotide	>10000 (6)	11.4 ± 1.7 (6)	11.4 ± 1.7 (6)	>100000 (6)	204 ± 92 (6)
Ga-DOTA-Tyr^3-octreotide	>10000 (6)	2.5 ± 0.5 (7)	2.5 ± 0.5 (7)	>1000 (2)	106 ± 37 (7)
NODAGA-Tyr^3-octreotide (NODAGATOC)	>10000 (2)	3.2 ± 1.0 (2)	3.2 ± 1.0 (2)	>1000 (2)	305 ± 85 (2)
Ga-NODA-Tyr^3-octreotide	>1000 (2)	3.5 ± 1.6 (2)	3.5 ± 1.6 (2)	>1000 (2)	185 ± 35 (20
In-NODA-Tyr^3-octreotide	>1000 (3)	1.7 ± 0.2 (3)	1.7 ± 0.2 (3)	320 ± 17 (3)	44 ± 8 (3)

Table 2: Affinity profiles (IC$_{50}$ (nM ± SE)) for Human sst1-sst5 receptors for a series of somatostatin anologues. Number of independent studies is given in brackets.

A related peptide-conjugate has been synthesised for targeted uptake. The synthesis of a TACN derivative with two pyridyl methyl pendent arms and one single carboxylic arm provided a point of attachment for a bombesin (BN) stabilised derivative (βAla-βAla-[Cha^{13}, Nle^{14}]BN(7-14)).[26] The resulting ^{64}Cu complex was highly stable both in the presence of cyclam as a competing ligand and copper-seeking superoxide dismutase (SOD). Biodistribution studies showed a high uptake for the kidneys, which was believed to be due to the high affinity that BN displays for the gastrin-releasing peptide receptor (GRPR) which is present in high levels within the organ. As GRPR is over expressed in a large number of breast and prostrate carcinomas, this would point to a possible application as a cancer diagnostic agent.

Development of synthetic chemistry to produce macrocyclic ligands for use in radiopharmaceuticals has been reported. An example of such a ligand was produced by a Mannich aminomethylation of kojic acid at the *ortho* position in the presence of formaldehyde and TACN (**L^5**).[27] Complexation to copper(II), gallium(III) and iron(III) produced solid structures where the metal either adopted a distorted square-pyramidal coordination (copper) or distorted octahedral (gallium and iron). Cyclic voltammetry highlighted that the ligand stabilised both the iron(III) and copper(II)

oxidation states, therefore suggesting the complexes would be stable enough for radiolabelling and use as a target-specific radiotracer.

1.2.2.2. Magnetic resonance imaging contrast agents

An example of a gadolinium contrast agent has already been discussed in section 1.2.2.1. TACN iron complexes also have potential application in MRI, because the iron centre can possesses un-paired electrons, resulting in the complex being paramagnetic. TACN iron complexes have been investigated by Hasserodt and co-workers.[28] Using two previously literature prepared compounds, $[Fe^{II}(tptacn)](ClO_4)_2$[29,30] and $[Fe^{II}(dptacn)(Cl)](PF_6)$[31], the magnetic properties of both complexes were probed. This data showed that the former was diamagnetic (low spin iron(II)) whereas the latter was paramagnetic (high spin iron(II)) in both the solid and liquid phase. Relaxivity measurements of $[Fe^{II}(dptacn)(Cl)](PF_6)$ gave an observed value of $r1$ of 1.29 mM^{-1}s^{-1} which compares to gadolinium(III) DOTA (2.44 mM^{-1}s^{-1}).

1.3. Tetraazamacrocycles and their analogues

This section on tetraazamacrocycles will mainly focus on ligands derived from cyclam and cyclen and their complexes. The suitability of complexes of cyclen and cyclam for medical applications with regard to their thermodynamic stability constants and structural data has been reported.[32] Because of the volume of literature published on these two ligand systems, a section is dedicated to each. In each section selected examples are discussed to highlight current applications.

1.3.1. Cyclam derivatives

Cyclam complexes are pursued for a variety of reasons. The role of cyclam complexes and their applications in medicine has been highlighted in a review by Sadler and Liang.[33] In addition topologically constrained ligands are of interest because the ligand can then dictate coordination chemistry of a chelated metal centre and offer enhanced complex stability.[34] Cyclam type complexes can be used as PET imaging agents and as CXCR4 antagonists. Pendent arms attached to the macrocyclic framework can increase the stability of these complexes. Selected examples of ligand systems and their complexes of this type are discussed below.

1.3.1.1. Diagnostic agents

1.3.1.1.1. Copper-64 radiopharmaceuticals

1,4,8,11-tetraazacyclotetradecane-1,4,8,11-tetraacetic acid (TETA) (Figure 4) has been extensively used as a bi-functional chelator (BFC) for copper radionuclides in clinical imaging and therapy studies involving both antibodies and peptides.[35] ^{64}Cu is often used as the radionuclide because it can be used in both PET imaging and targeted radiotherapy due to its half life ($t_{1/2}$=12.7 hr), decay characteristics (β^+ (19%); β^- (39%)) and the ability for large-scale production with high specific activity on a biomedical cyclotron.[36]

Cyclam ligands complexed to ^{64}Cu have been investigated by numerous groups as radiopharmaceuticals. Weisman, Wong and co-workers have developed a cyclam based macrocycle to act as a copper-64 radionuclide carrier.[37] Three amide derivatives of CB-TE2A (see Figure 4 for structure) were produced, all of which had carboxylic and amide pendent arms. CB-TE2A is a configurationally restricted

macrocycle. Compared with TETA, these compounds had better *in vivo* clearance, with liver and bone marrow uptake at 24 hr being less than 10% of the uptake at 30 min. In comparison, ^{64}Cu-TETA displayed greater than 60% of 30 min uptake in the same tissues at 24 hr. Kinetic stability data for these compounds could not be obtained due to hydrolysis of the amide bond in 5M HCl.
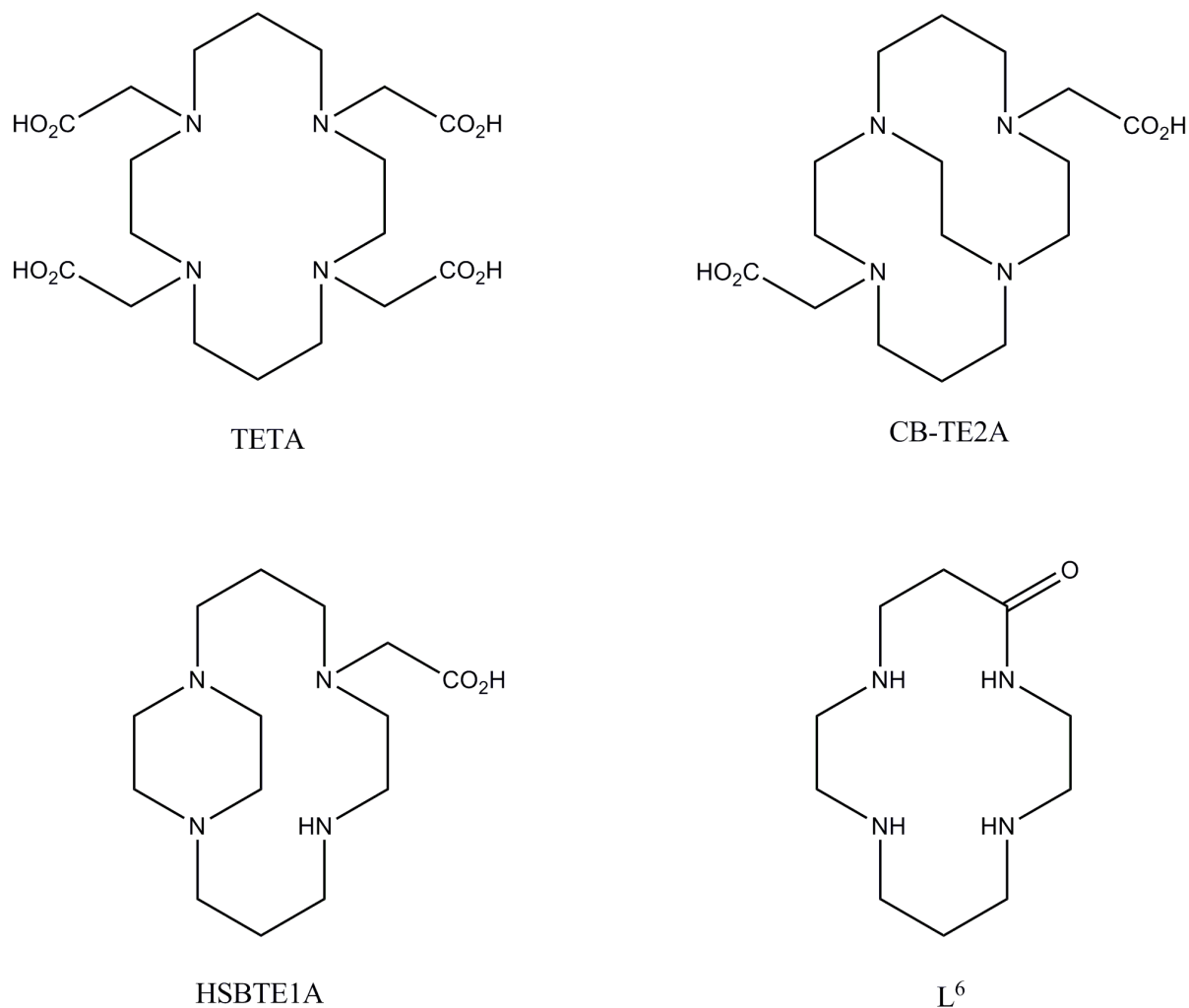
Figure 4: Chemical structures of TETA, CB-TE2A, HSBTE1A and L^6.

The influence of pendent arms on the *in vitro* and *in vivo* behaviour of copper cross-bridged copper complexes has been investigated.[38] *N*-carboxymethyl pendant arms gave the resulting copper cyclam cross bridged complex considerably better kinetic inertness and resistance to reduction than its *N*-carboxyethyl (crystal structure shown in Figure 5) analogue and cyclen cross bridged derivatives. The crystal structure of the *N*-carboxyethyl copper(II) complex shows that both of the carbonyl arms are coordinated to the copper(II) ion. The five coordinate copper(II) species was also

isolated in which one of the carbonyl arms is not coordinated to the copper centre. The copper ion adopts a square pyramidal geometry, with one of the nitrogens from the ring system providing the axial coordination site. The *N*-carboxymethyl cross-bridged cyclam and cyclen copper complexes had better clearance than both *N*-carboxyethyl complexes. As the *N*-carboxyethyl cross bridged cyclam complex was less resistant to reduction by 400 mV than the *N*-carboxymethyl analogue, it was presumed that this was important for optimal *in vivo* clearance.
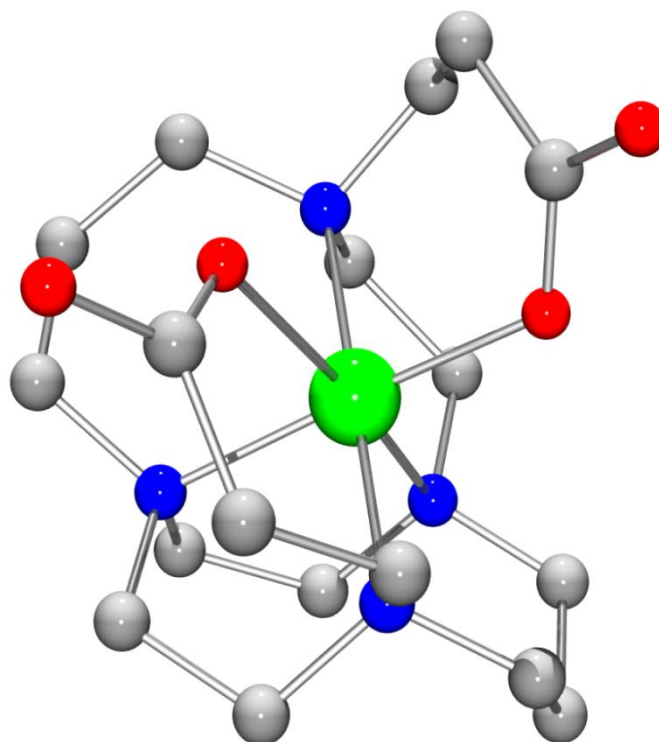
Figure 5: Ball and stick representation of the X-ray crystal structure of a copper(II) cross-bridged cyclam complex with two ethyl acetate arms. Sodium and perchlorate ions omitted for clarity (Sprague *et al.*).[38]

Other examples in the literature of side- and cross-bridged configurationally restricted complexes have been synthesised. For example, a cross-bridged cyclam derivative bearing carboxylic acid and amide pendant arms has been synthesised.[39] The cross-bridged cyclam compound with two carboxylic arms cleared quickly from all tissues whereas cross-bridged cyclams with amide arms cleared far slower, being taken up by the liver and kidney over a period of 24 hr. The rapid clearance of the copper-64 complex of the cross-bridged cyclam with two pendant arms suggests that it is highly stable *in vivo*. The *in vivo* stability of cross-bridged complexes has been

studied further. Data shows that the cross-bridged compounds have enhanced *in vivo* stability by reduction of metal loss to protein in both cyclam and cyclen cross-bridged ^{64}Cu complexes.[35] Lower levels of protein associated ^{64}Cu were observed for ^{64}Cu-CB-TE2A than ^{64}Cu-TETA ($13 \pm 6\%$ vs $75 \pm 9\%$ at 4 hr). Anderson and co-workers have also observed dissociation in bioconjugates such as ^{64}Cu-TETA-OC.[40]

Archibald and co-workers[41] have focused on the design and characterisation of copper(II) complexes of H_4TETA and HSBTE1A, which are both side-bridged cyclam compounds. Two different crystal structures were obtained for $Cu(H_2TETA)$ displaying Jahn-Teller distortion through either the macrocyclic plane or through the axially coordinated carboxylate pendent arms. A side bridged cyclam copper(II) complex with one carboxylic pendent arm was also isolated with the copper ion adopting a square based pyramidal structure.

^{64}Cu radiopharmaceuticals of monooxo tetraazamacrocycles have also been synthesised.[42] Copper(II) complexes were synthesised which had comparable *in vivo* properties. The copper(II) complex of the 14-membered ring with the oxo at the 5 position (**L^6**) had the best biodistribution, although this was still not as good as traditional BFCs based on DOTA and TETA.

1.3.1.1.2. Bioconjugate radiopharmaceuticals

Radio-labelled complexes with targeting vectors are crucial for selective imaging of particular tumour/tissue types. Vectors include peptides and antibodies. A comprehensive review on labelling macrocyclic radiometal complexes with monoclonal antibodies has been published.[43] Radio-labelled complexes enable the diagnostic imaging of a particular tissue or organ type. Octreotate, for example, has received considerable interest from research groups as it can be used to selectively target somatostatin receptor subtype 2 (SSTr2)-positive tissues.[44-47] A cross-bridged cyclam bearing an attached octreotate vector has been synthesised (**L^7**).[44] Compared with copper-64 TETA and TETA-conjugates, the copper-64 complex of **L^7** displayed improved *in vivo* stability as well as a reduction of *in vivo* transchelation. In addition, the additional stability was thought to be responsible for the broader specificity in that SSTr1, SSTr3 and SSTr5 as well SSTr2 were targeted as evidenced from the

significant difference in the B_{max} (binding maximum) values (^{64}Cu-TETA-octreotate 192 fmol/g; ^{64}Cu-cross bridged TETA-octreotate 1551 fmol/g).

Further peptides have been incorporated into structurally reinforced peptide conjugates. Recently, Brechbiel and co-workers have developed a cross-bridged cyclam cyclic RGD peptide conjugate radiolabelled with ^{64}Cu,[48] which utilised a bromide-functionalised glutamic acid derivative.[25] Structurally, the conjugate is a derivative of CB-TE2A. *In vitro* studies conducted demonstrated that the complex remained intact over a 48 hr period as no transchelation was observed.

$$L^7$$
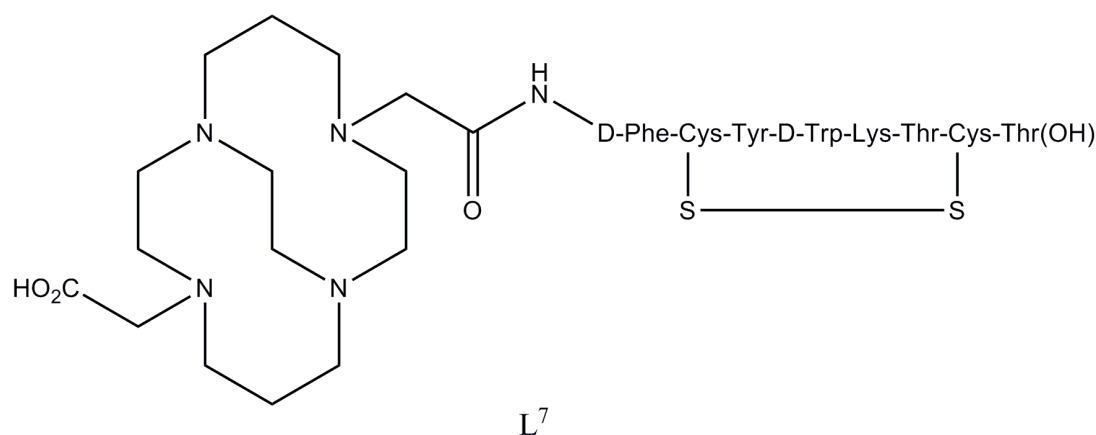
Figure 6: Chemical structure of L^7.

1.3.1.2.   Therapeutic agents

1.3.1.2.1. CXCR4 antagonists

One of the main areas in which cyclam complexes have been investigated as therapeutics is in the treatment of acquired immunodeficiency syndrome (AIDS). In particular, cyclam complexes are widely investigated as potential CXCR4 antagonists. AMD3100 (Figure 7), a configurationally unrestricted bi-cyclam was, until recently, in clinical trials against HIV. Sadler and co-workers investigated the bi-metallic complexes of AMD3100 which had been evaluated for their anti-HIV activity. Zinc(II) perchlorate complexes were produced towards this aim.[49] NMR studies showed that the complexes have two major conformers; trans-I (nitrogen chirality R, S, R, S) and trans-III (S, S, R, R). The six conformations of cyclam are shown in Figure 8. Addition of acetate to the perchlorate salts induced major structural change to the cis-V (R, R, R, R) configuration which was evidenced from

X-ray crystallography data. In solution phase, the trans-I conformer is also present. The mixed conformations present in the acetate complexes enable binding to CXCR4 (via a cis-V site) whilst the second cyclam adopts a trans-I conformation to bind to Asp[171].

AMD3100

L[8]
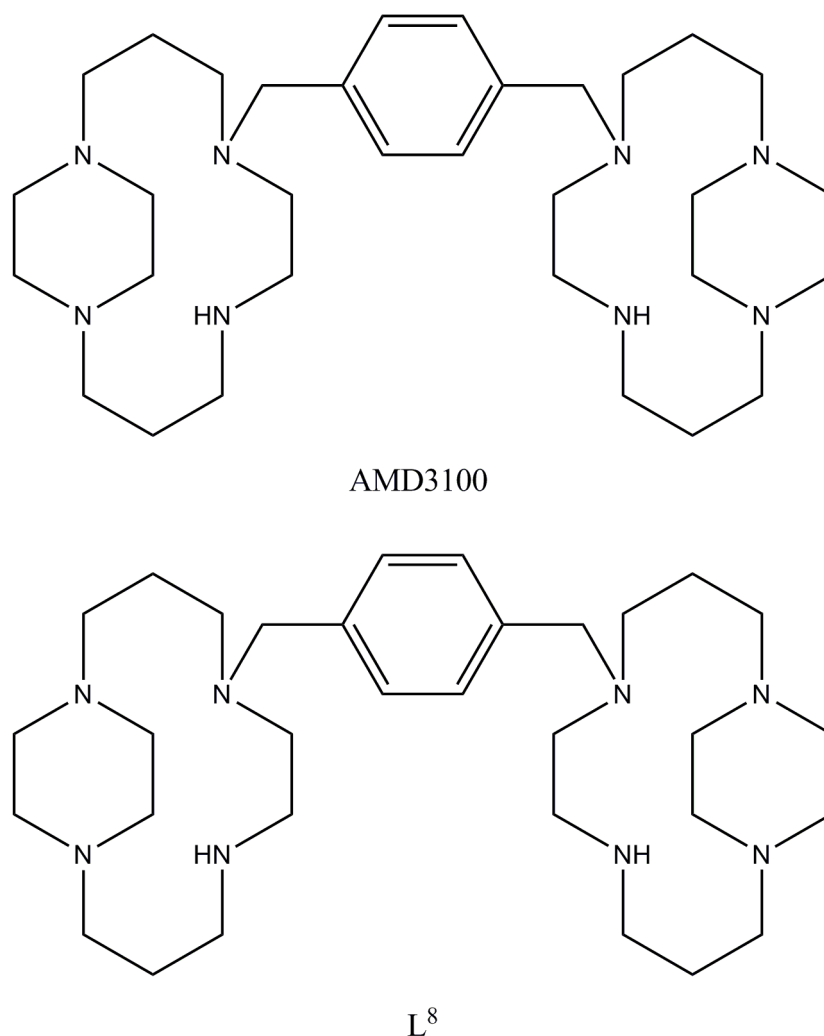
Figure 7: Chemical structures of AMD3100 and L[8].

The configurational activity of cyclam and its effect on the docking of the antagonist with the receptor has been further modelled. The configurational equilibria of nickel(II)-cyclam derivatives have been investigated.[50] [Ni(cyclam)(OAc)$_2$].H$_2$O and [Ni(benzylcyclam)(NO$_3$)$_2$] were found to adopt a *trans*-III configuration with either axial acetate or nitrate ligands, whereas [Ni(benzylcyclam)(OAc)](OAc). 2H$_2$O adopted a *cis*-V configuration. X-ray diffraction studies showed that crystals of lysozyme soaked in either nickel(II) cyclam or nickel(II)$_2$-xylbicyclam contain two major binding sites. One involves the coordination of nickel(II) to Asp[101] and

hydrophobic interactions between the cyclam ring and Trp[62] and Trp[63], and the second is hydrophobic interactions with Trp[123]. For nickel(II) cyclam bound to the Asp[101] residue, the *cis*-V configuration was found to dominate.

trans-**I**   *trans*-**II**   *trans*-**III**

trans-**IV**   *trans*-**V**   *cis*-**V**
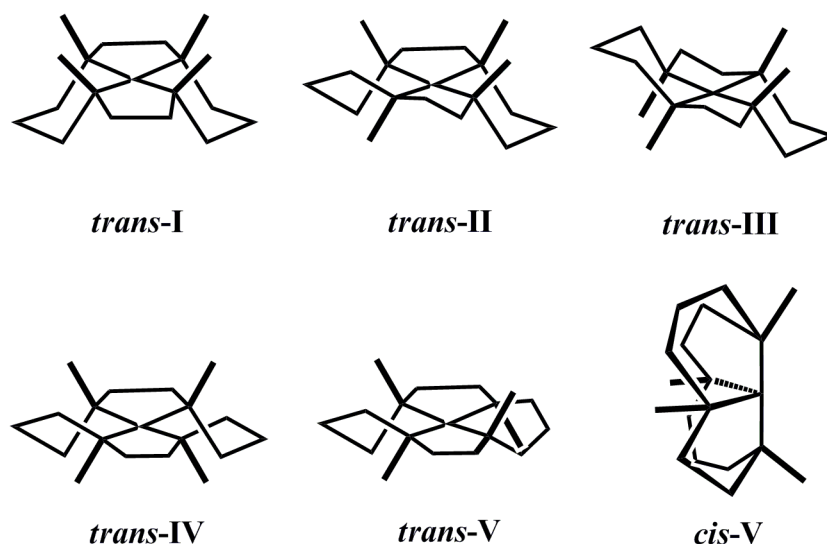
Figure 8: The six configurations of cyclam.[51]

Development of configurationally restricted AMD3100 derivatives to produce more potent compounds has been carried out. For example, mono- and bis-macrocyclic copper(II) complexes have been synthesised and their anti-HIV efficacy measured.[52] The restricted di-copper(II) complex of **L^8** is more active (average EC_{50} (the molar concentration of an agonist, which produces 50% of the maximum possible response for that agonist) $=0.026$ μM against HIV-1) than the corresponding di-copper(II) AMD3100 complex (average $EC_{50}=0.047$ μM against HIV-1). Interestingly the di-zinc(II) restricted macrocyclic complex has an EC_{50} in the nanomolar range (average $EC_{50}=8$ nM against HIV-1).[53]

Furthermore, fluorescent CXCR4 chemokine receptor antagonists have been evaluated with regard to metal activated binding.[54] Antibody competition studies show binding of the fluorescent conjugate to CXCR4 in Jurkat cells. However, both a CXCR4 negative control and Jurkat gave positive fluorescent response by flow cytometry. To investigate the uptake of the conjugates, cell surface blocking studies were carried out, highlighting that an active transport mechanism is used. A ball and stick representation of the crystal structure of the copper(II) benzyl side-bridged cyclam complex is shown in Figure 9. In the crystal structure, the ring system has

adopted a trans-II configuration with the copper(II) ion having distorted square-based pyramidal geometry.
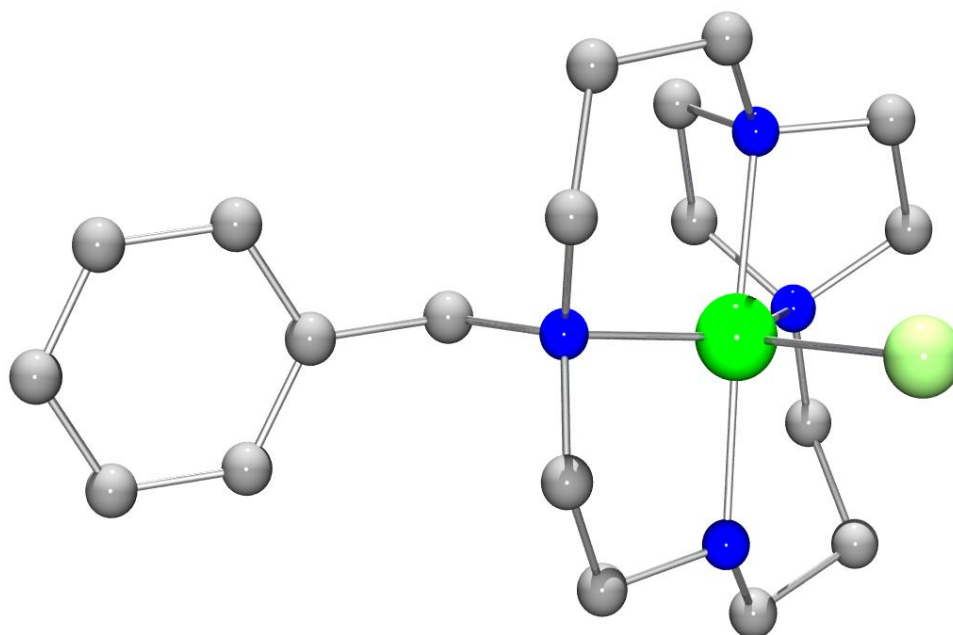
1.3.1.2.2. Anti-cancer therapeutics

Cyclam complexes are also used as anti-cancer drugs. Lipophilic derivatives of cyclam which show inhibition of tumour cell growth have been synthesised.[55] The use of isopropyl and isobutyl appendages was found to increase lipophilicity without diminishing overall water solubility. Against the cell line L1210, effective inhibition was achieved with IC_{50} values of 6.2 and 8.7 μM for the isopropyl and isobutyl derivatives respectively. Cyclam was found to be an ineffective inhibitor even at the highest concentration studied (25 μM).

1.3.2. Cyclen derivatives

Cyclen ligands and their analogues have found applications in a variety of different areas of biomedical chemistry. Complexation occurs to lanthanide ions as well as transition metal ions. Pendent arm selection is important to generate the high coordination numbers required by the lanthanide ion which sits above the ring cavity.

1.3.2.1.   Enzyme mimics

1.3.2.1.1. Hydrolytic catalysts

Cyclen derivatives have been developed as enzyme mimics. A lot of research effort has been focused on the production of hydrolytic catalysts. For example, RNA hydrolytic catalysts have been produced with either transition metal or lanthanide ions at the catalytic centre. Europium(III) cyclen complexes with pendent arms have been synthesised by Morrow *et al*. These were designed to promote cleavage of, and bind to, models for the 5'-cap of mRNA.[56] By modifying the coordination sphere around the europium(III) centre, different rates of cleavage of GpppG were achieved. With all four pendent arms present as hydroxyethyls a pseudo first order rate constant of 5.3×10^{-5} s^{-1} was reported.[57] Replacing one hydroxyethyl for an amide reduces the rate constant to 2.6×10^{-5} s^{-1}. Both europium(III) complexes cleave the 5' cap of mRNA by attack of an ethyl alcohol pendent group on the phosphoric anhydride linkage. Replacing all four pendent arms for 2-hydroxypropyl groups causes the complex to bind to the 5' cap of mRNA but does not promote cleavage. This was attributed to the difference in nucleophilicity of 2-hydroxypropyl compared with hydroxyl ethyl which results in a diminished promotion of transesterification.

A transition metal complex has also been prepared as a hydrolytic RNA cleavage catalyst. Two 1-oxa-4,7-10-triazacyclodecane macrocycles, a cyclen analogue where one nitrogen has been replaced by an oxygen, with either a single methyl or acridine pendent arm (**L^9**) have been synthesised.[58] The zinc(II) complexes of both ligands were tested for catalytic activity in the presence of 2-hydroxypropyl-4-nitrophenyl phosphate (HpPNP), a simple RNA analogue. Transesterification of the HpPNP by zinc(II) complexes was followed by monitoring the increasing absorbance of 4-nitrophenolate at 400 nm. Cleavage of HpPNP produces a single phosphate

containing product as identified from ^{31}P nuclear magnetic resonance (NMR). Pseudo first rate constants of 6.3×10^{-6} s^{-1} and 2.2×10^{-6} s^{-1} were obtained for **L^9**(R=Me) and **L^9**(R=Acr) respectively (see below). pH profiling of both zinc complexes identified that basic conditions gave better rates of cleavage of HpPNP. This was attributed to the catalyst-substrate complex being converted to its active form by loss of a proton.
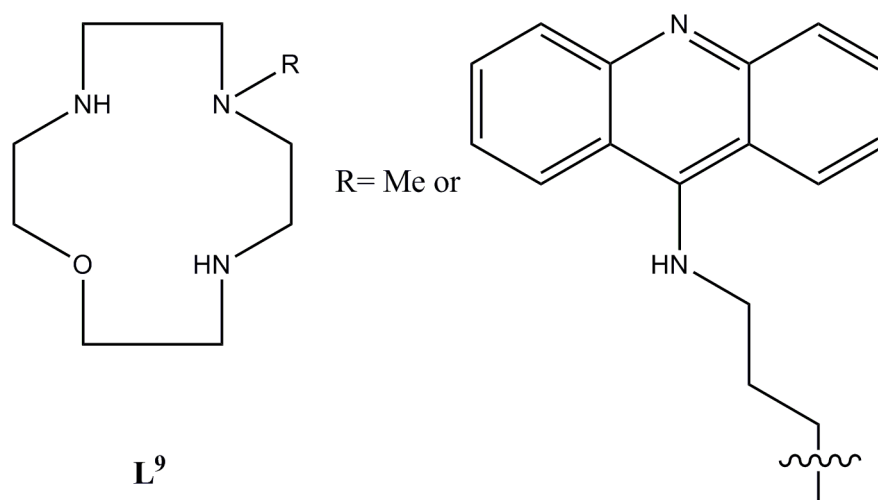
Figure 10: Chemical structures of the derivatives of L^9.

Carboxy-ester hydrolysis is also of interest. Tren-(tris(2-aminoethyl)amine)-based tris-macrocycles have been synthesised and characterised with the aim of investigating both their catalytic carboxy- and phosphate-ester hydrolysis.[59] The tris-zinc(II) complex was synthesised (see Figure 11 for crystal structure). In the crystal structure the zinc(II) ions are five coordinate and adopt a distorted square pyramidal geometry. The tris-zinc(II) complexes displayed elevated hydrolysis rates compared with the mononuclear zinc(II) [12]aneN$_4$ complex. Bis(*p*-nitrophenyl) phosphate cleavage occurs through a bridging interaction with at least two metals with simultaneous nucelophilic attack at phosphorous by a Zn-OH function. In *p*-nitrophenyl acetate hydrolysis, the three zinc(II) ions are not involved in substrate activation.
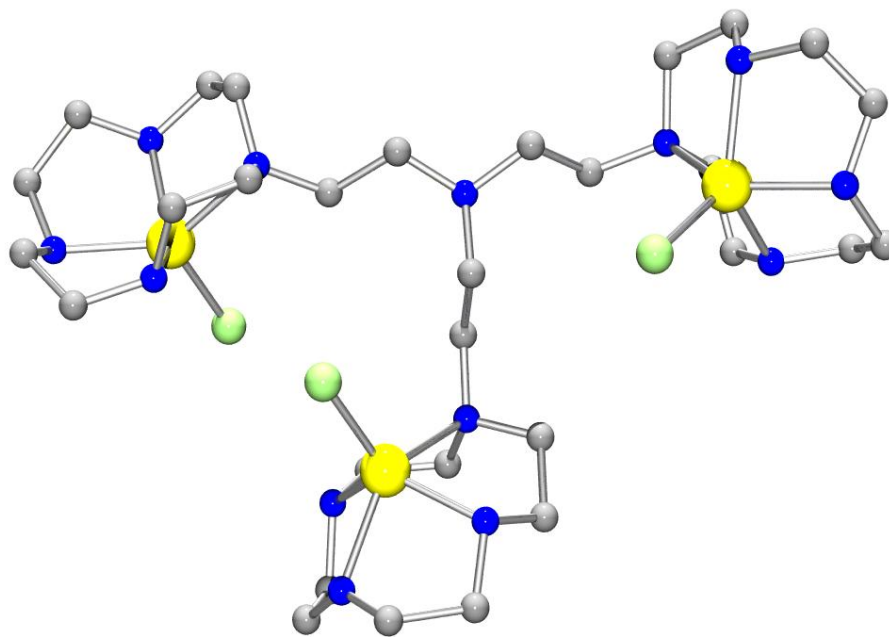
Figure 11: Ball and stick representation of the X-ray crystal structure of tri-zinc(II) chloride complex of a tren-based tris-[12]aneN₄ ligand. H-atoms are omitted for clarity (Bazzicalupi *et al.*).[59]

1.3.2.2. Diagnostic agents

1.3.2.2.1. Radiopharmaceuticals

Another main area in which cyclen macrocycles are used is in the production of radiopharmaceuticals. Radiopharmaceuticals have been synthesised for either whole organism or site specific imaging. Selected examples for both areas are now discussed.

1.3.2.2.1.1. ^{64}Cu Radiopharmaceuticals

Radiopharmaceuticals using ^{64}Cu have been studied extensively, as has been discussed for cyclam compounds in section 1.3.1.1.1. The *in vivo* behaviour of copper(II) cyclen complexes bearing *tert*-butyl benzyl and acetate arms has been investigated by Welch and co-workers.[60] Partition coefficient measurements showed an increase in hydrophobic tendencies for copper(II) complexes bearing *tert*-butyl benzyl arms. Conversely, acetate groups caused the complexes to display hydrophilic tendencies. However, the biodistribution of both types of compounds was found to be reliant on the overall charge of the complex. These charged complexes studied were found to have high blood retention times over an initial 15 min period compared with neutral complexes.

The copper(II) complex of the ligand H_2Me_2DO2A has also been investigated as a potential positron emission tomography imaging agent.[61] Protonation studies of the copper(II) complex showed that protonation occurs at the two methyl-substituted amines before protonation of the carboxylate arms, suggesting good stability for the complex *in vivo*. The crystal structure of this complex is shown in Figure 12. In the crystal structure, the copper(II) ion lies in a distorted octahedral geometry with two nitrogens from the ring capping the octahedron. Further evidence for stability at physiological pH was gained from cyclic voltammetry, which displayed only one irreversible peak at -0.81 V, assigned as the reduction of copper(II) to copper(I) with concomitant decomplexation. Biodistribution studies highlighted that the compound was able to cross the blood brain barrier.
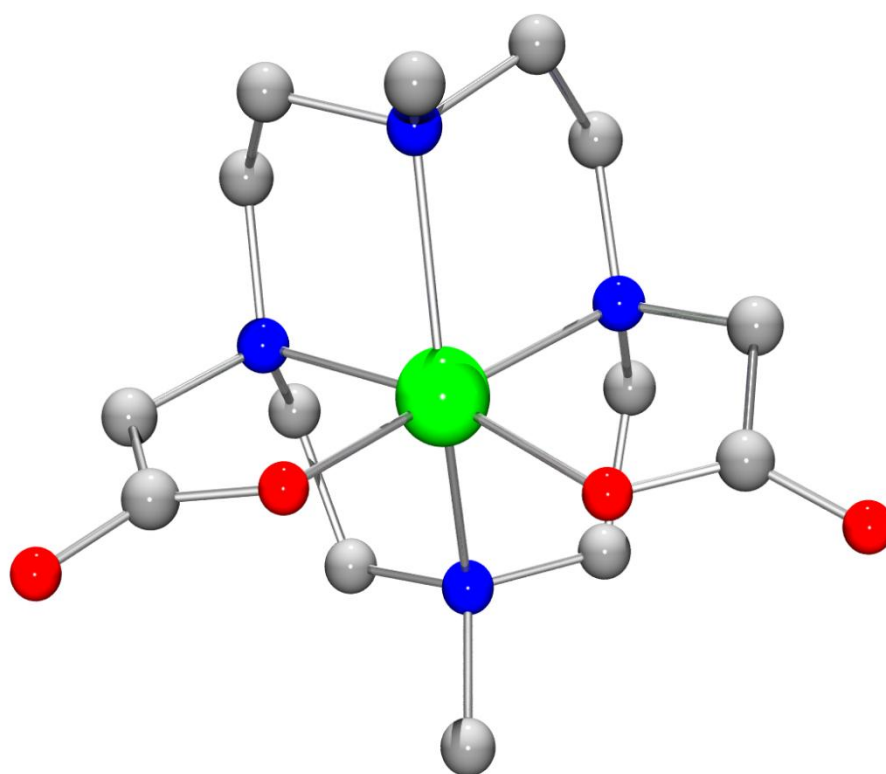
Figure 12: Ball and stick representation of the X-ray crystal structure of the Cu(II) complex of Me₂DO2A. H-atoms have been omitted for clarity (Sun *et al.*).[61]

1.3.2.2.1.2. Bone-seeking radiopharmaceuticals

Another area of radiopharmaceutical design in which cyclen ligands are currently being used is in the development of bone-seeking agents. These ligands typically possess phosphate groups to enable favourable distribution to the bone. Cyclen derivatives with two, three or four methanephosphate pendant arms have been synthesised.[62] All complexes displayed high accumulation in the bone, possibly due to the binding of the methanephosphonate groups to hydroxyapatite. Of the three complexes studied 1,4,7,10-tetraazacyclodecane-1,7-di(methanephosphonic acid) was the most suitable candidate for bone imaging as it was highly stable in rat serum over a period of 24 hr and also showed the best clearance through the blood and liver. A further ligand synthesised with methanephosphate arms attached is shown in Figure 13 (**L¹⁰**). The lanthanum(III), samarium(III) and holmium(III) complexes of the ligand were prepared.[63] These ligands formed highly stable complexes, which

possessed higher thermodynamic stability constants than their acetate counterparts. Biological distribution studies showed that for the [166]Ho 13-membered tetraphosphanote complex a pronounced level of uptake occurred in the bone after 30 min (~6.5%). Because of this, bone/blood and bone/muscle ratios were quite favourable (0.4 and 3.1% ID (injection dose) respectively). [153]Sm labelled compound had less favourable ratios due to a faster decrease of radioactivity, and excretion from main organs being slower.

Another cyclen ligand with phosphate arms attached which was developed for bone palliation is **L**[11] (Figure 13).[64] The bis(phosponate) arm does not coordinate to the metal centre and is protonated at physiological pH. Radioimaging studies using ^{177}Lu were conducted using a large excess of ligand to negate the high affinity of the lutetium(III) ion for bone. The complexes showed high affinity for newly formed bone thus making them suitable candidates as diagnostic agents for bone tumours. Although a single water molecule is still present in the first coordination sphere of the gadolinium complex, the poor clearance from the skeleton probably makes these compounds unsuitable as contrast agents for MRI.
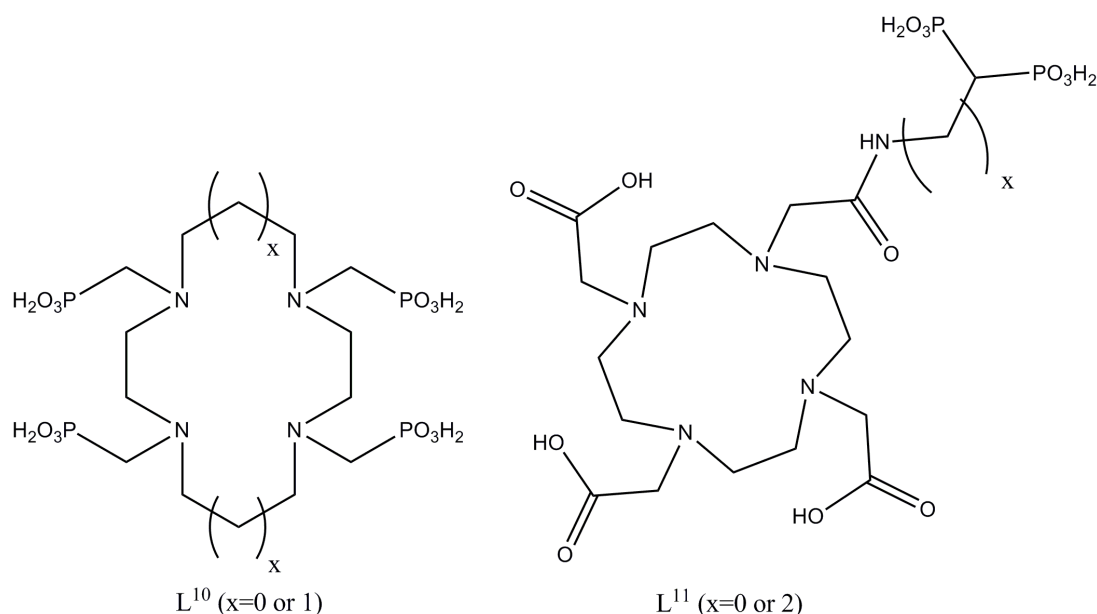
Figure 13: Chemical structures of **L**[10] and **L**[11].

1.3.2.2.1.3. Bioconjugate radiopharmaceuticals

Cyclen ligands can have peptide targeting vectors tethered to them. This enables selective diagnostic imaging of particular cells or tissues. A review on the synthesis and chelation chemistry of DOTA-peptide conjugates has been published recently,[65] as well as a review on the rational design of protein-conjugated MRI contrast agents.[66]

A number of examples of cyclen derived protein- and antibody-conjugates have been produced. Examples of biomolecules used in the formation of protein-conjugates include RGD, octreotate, estradiol and naltrindole. A DOTA-conjugated ^{111}In-labeled RGD-dendrimer has been synthesised.[67] These dendrimers display enhanced uptake in $\alpha_v\beta_3$ integrin expressing tumours *in vivo*. Monomeric, dimeric and tetrameric cyclo(Arg-Gly-Asp-D-Phe-Lys) dendrimers were produced using click chemistry, all consisting of a single gadolinium(III) chelate. *In vivo* studies showed that the tetrameric RGD-dendrimer had better tumour targeting properties than its dimeric and monomeric congeners.

DOTA derived macrocycles were also used to synthesise octreotate conjugates. The synthesis of DOTA-D-Tyr^1-Octreotate enabled both labelling with both radiohalogens and radiometals.[45] The ^{125}I labelled conjugate showed high residual concentration in the tumour 4 hr post injection, suggesting retention of the radioisotope within the tumour mass. The ^{64}Cu conjugate displayed better selectivity for the tumour compared with the ^{125}I conjugate (1.515 ± 0.154 % ID/g and 0.814 ± 0.058% ID/g respectively).

The choice of metal ion chelated to DOTA-D-Tyr^1-Octreotate is of structural significance as it can induce conformation change upon the D-Phe^1 linker.[47] The peptidic part of the conjugate exists in a dynamic equilibrium between a helical and sheetlike structure. NMR data obtained from both yttrium(III) and gallium(III) complexes[46] are comparable for the peptidic moiety meaning that the differences reported in bioavailability[68] must be due to differences found in the D-Phe^1 linker. In the yttrium conjugate, the D-Phe^1 linker is involved in the metal coordination sphere whereas in the gallium conjugate the linker assumes an extended conformation. As the D-Phe^1 residue is important in the binding of the peptide to the somatostatin

receptor, the differences in the coordination sphere of the metal ions leads to the enhanced specificity as observed for the gallium conjugate. The crystal structure of the gallium(III) complex of the ligand is shown in Figure 14.[23] It is worth noting that in the crystal structure one of the acetate arms on the cyclen ring is not coordinated to the metal centre. The gallium ion adopts a *cis*-pseudo-octahedral geometry with a folded macrocyclic unit (2424 conformation). The benzyl amine on the pendent arm provides a convenient point for biomolecule attachment.
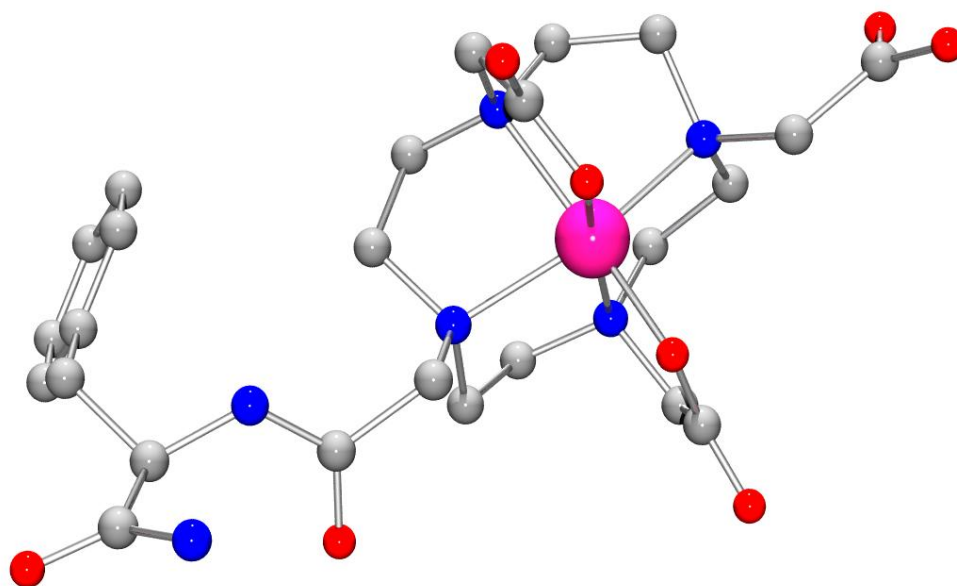
Figure 14: Ball and stick representation of the X-ray crystal structure of gallium(III)-DOTA-D-PheNH$_2$. H-atoms are omitted for clarity (Eisenwiener *et al.*).[23]

Further cancer selective radiopharmaceuticals have been synthesised. Estradiol-conjugates have been reported for use as a radiotherapeutic agent in targeting breast carcinomas. *p*-NCS-benzyl-DOTA conjugated to estradiol with a radioactive ^{177}Lu centre was tested for its binding affinity to MCF-7 cells.[69] A binding of $13.2 \pm 0.8\%$ was observed with 5×10^4 MCF-7 cells for 1 μg of the conjugate. Studies carried out using the radiolabelled bifunctional chelator showed no retention of activity in the cell pellet, thus ruling out carrier mediated uptake. Furthermore, antibody competition binding studies confirmed that there was no change in binding properties after incorporation of the BFC.

Radiopharmaceuticals which can pass the blood brain barrier have been synthesised. These are of interest as they can be used to image brain signalling pathways, for example. Naltrindole (NTI) is currently used in *in vivo* studies for imaging of δ opioid receptors. Radioligands incorporating this moiety have been synthesised for use in PET. These ligands are lipophilic to enable passage across the blood brain barrier, but there is an emerging need for hydrophilic radioligands to be synthesised to enable peripheral δ opioid receptors to be imaged. This is because δ opioid receptors are present in normal heart cells and in primary tumours of the lung and breast. Lever and co-workers have synthesised ^{111}In DOTA and DO3A NTI bioconjugates for exactly this purpose.[70] Both metal complexes displayed high binding affinities (0.1 - 0.2 nM) and excellent selectivities for binding to δ receptors *in vivo*. An alkyl chain ($(CH_2)_n$, where n=3 or 6) was used to attach the NTI to the macrocycle and this also acts as a pharmacokinetic modifier with the log $D_{7.4}$ values ranging from -2.74 (n=3) to -1.79 (n=6). A high level of specific binding (75 - 94%) to δ opioid receptors was observed in mouse gut, heart, spleen and pancreas.

Sugar moieties have also been used to prepare radiopharmaceutical conjugates. For example, lanthanide(III) complexes of DOTA-glycoconjugates have been prepared as a potential new class of lectin-mediated medical imaging agents.[71] Samarium(III), europium(III) and gadolinium(III) mono, di and tetra mono-amide linked glycoconjugates (glucose, lactose and galactose) complexes were prepared. Biodistribution studies of [153]Sm- labelled glycoconjugates of different valancies and sugar type indicated a specific hepatic uptake of the galactose and lactose glycoconjugates through the ASGPR (asialoglycoprotein receptor).

An example of an antibody conjugate has been published by Jurisson and co-workers, who were investigating B72.3 (a bombesin antibody) conjugates of DOTA derivatives.[72] Three analogues were evaluated by Jurisson and co-workers; "NHS-DOTA", "Arm-DOTA" and "Back-DOTA" (chemical structures shown in Figure 15). B72.3 was conjugated to these macrocyclic ligands and complexed with ^{111}In, ^{177}Lu and [90]Y. Overall, the ^{90}Y labelled conjugates were the least stable based on bone uptake (2 - 20% ID/g compared with 2 - 8% ID/g for ^{111}In and ^{177}Lu). In fact for the [90]Y Arm-DOTA conjugate, significant instability of the complex was observed, suggesting possible leaching of the metal from the chelate rather than

metabolism of the radiolabelled conjugate to smaller molecule weight fragments. Further conjugates towards bombesin receptor-positive tumours have been synthesised using the 15-amino-4,7,10,13-tetraoxopentadecanoic acid (PEG4) spacer.[73] IC_{50} values of the lutetium(III) and gadolinium(III) complexes were found to be 6.1 ± 3.0 and 6.6 ± 0.1 nmol/l respectively. Binding studies showed good binding to neuromedin B receptors (NMB-R) and GRPR but no affinity to BB3-R (a bombesin receptor). Rapid blood clearance was observed for both conjugates (0.1-0.47 % ID/g at 4 hr post injection) and, in addition, were quickly washed from GRPR negative tissues except the kidneys.
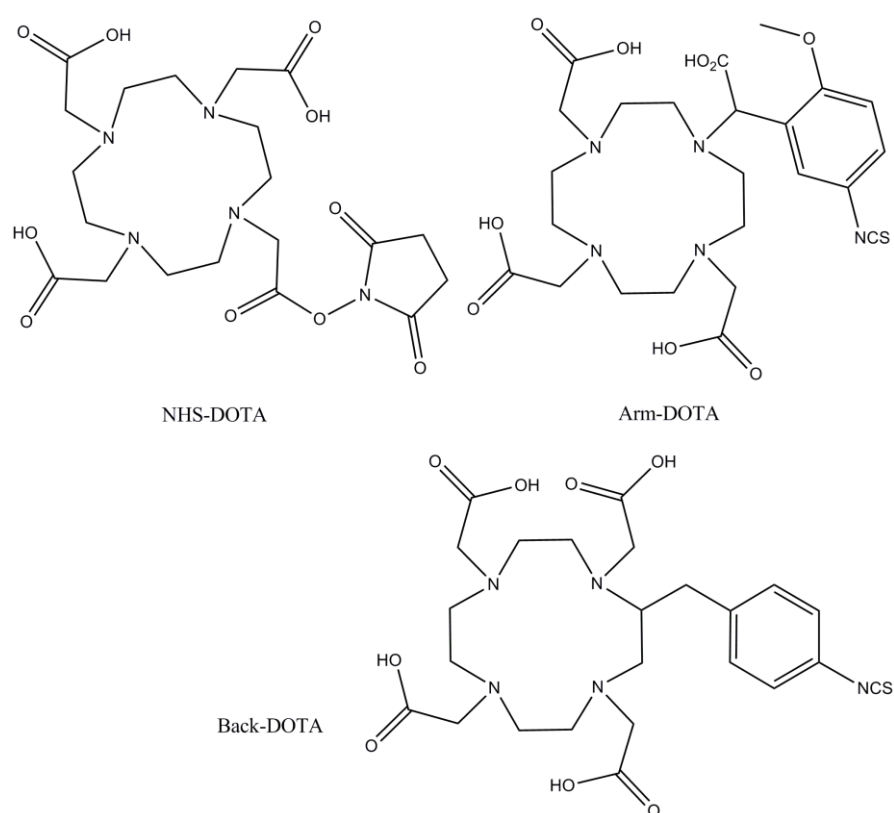
Figure 15: Chemical structures of "NHS-DOTA", "Arm-DOTA" and "Back-DOTA".

1.3.2.2.2. Magnetic resonance imaging contrast agents

Magnetic Resonance Imaging (MRI) is another major area in which cyclen derivatives are used for diagnostic purposes. Gadolinium(III) complexes have been widely investigated as MRI contrast agents.[74] The small cavity size of cyclen and the ability to attach pendent arms through the nitrogen atoms enables gadolinium(III) complexes to be formed which are highly stable. Gadolinium(III) is used in MRI extensively as is paramagnetic. Interaction of the magnetic field with protons in the near vicinity enables an enhanced image to be produced. For image enhancement to occur, water must ideally be able to enter the inner coordination sphere of the metal ion. It is therefore fitting that considerable research effort has been dedicated to the manipulation of the inner coordination sphere through biological and chemical intervention.

An example of how the inner coordination surrounding the gadolinium ion can be altered via a biological process has been reported. Meade and co-workers synthesised a gadolinium(III) 1,4,7,10-tetraazacyclodecane-1,4,7-triacetic acid (DO3A) complex bearing a pendent β-glucuronic acid moiety.[75] This complex is enzymatically processed by bovine liver β-glucuronidase, generating 2-aminoethyl gadolinium(III)DO3A (Scheme 1). The relaxivity differential between glucose-DO3A and non-glucose DO3A was found to be approximately 27% brighter in human serum. This difference is suggested by the authors to be sufficient for *in vivo* imaging. Meade and co-workers have produced another bioactivated MR contrast agent. In this compound a galactopyranose sugar is tethered to a DO3A chelated gadolinium(III) to modulate the hydration state of the metal.[76] A propyl linker was used in between the sugar and macrocyclic scaffold, which possessed a sterochemical centre, enabling the *R* and *S* compounds to be isolated as either the α or β form. The β form was found to have a bidentate carbonate anion to coordinatively saturate the complex (relaxivity measurements showed a dependence on carbonate concentration). Upon cleavage of the sugar, a newly formed hydroxyl group displaces the carbonate enabling water to enter the inner sphere. The α form is entirely different, as the stereochemistry means that the galactopyranose is likely to be positioned directly over the open coordination of the gadolinium(III) and as such prevents water entering the inner sphere (relaxivity measurements showed a

carbonate concentration independence). However, just like the β form, upon cleavage, water is able to enter the coordination sphere.
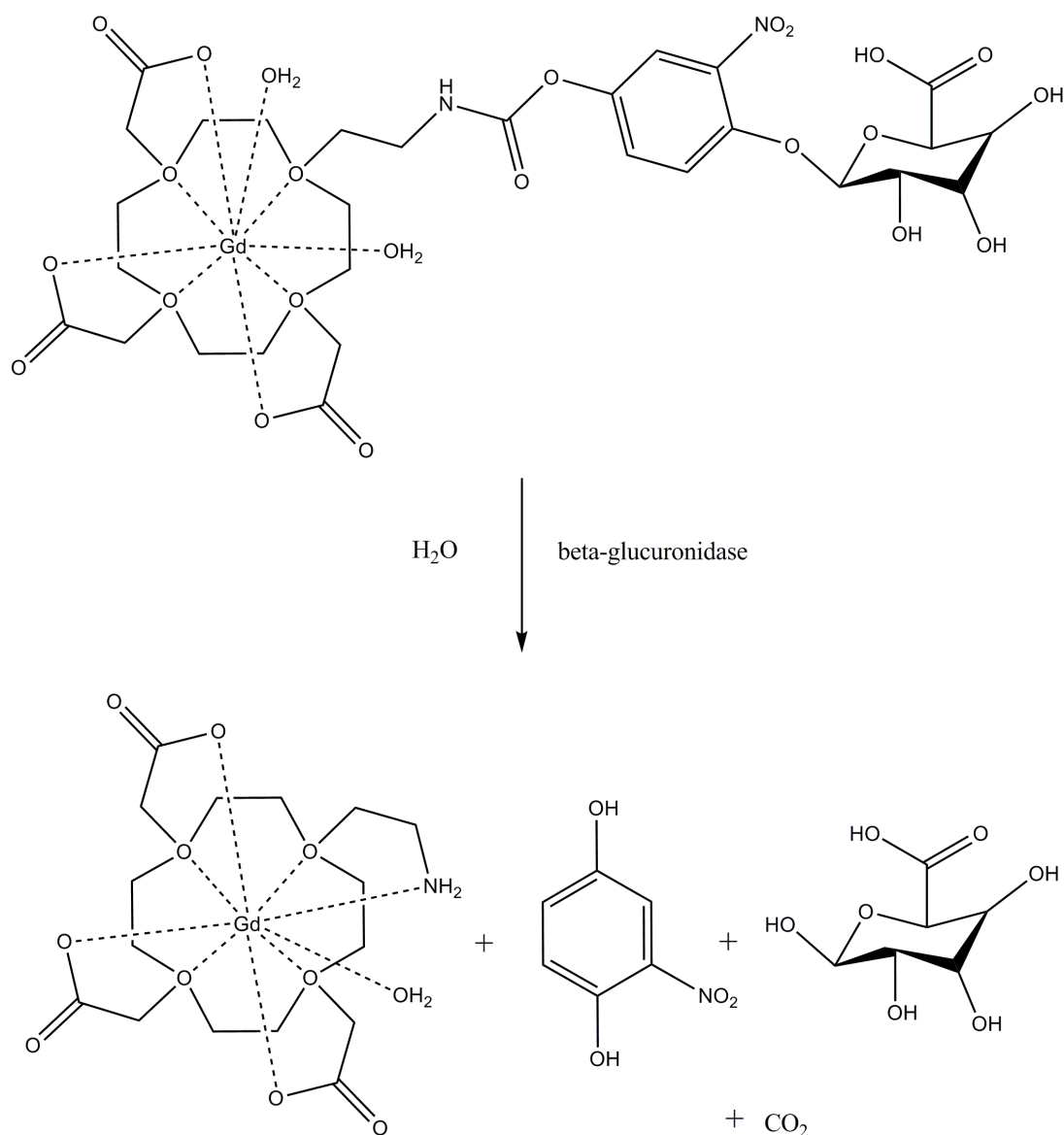
Scheme 1: Hydrolysis of the β-glucuronic acid moiety by β-glucuronidase leading to a change in the hydration state of the gadolinium(III) ion.

The choice of pendent arm attached to the cyclen framework can effect the number of water molecules able to access the inner coordination sphere. For example, heptadentate gadolinium(III) complexes with functionalised propyl or polyethylene glycol (PEG) chains attached show different effects upon interaction with human serum albumin (HSA).[77] The complexes with propyl functionalised pendent arms enable two water molecules to enter the inner coordination sphere whereas

complexes with PEG chains only allow access for one water molecule. However, the expected relaxation enhancement upon binding to HSA was not observed; this was attributed to the displacement of coordinated water molecules by the protein.

R = H or NH$_2$
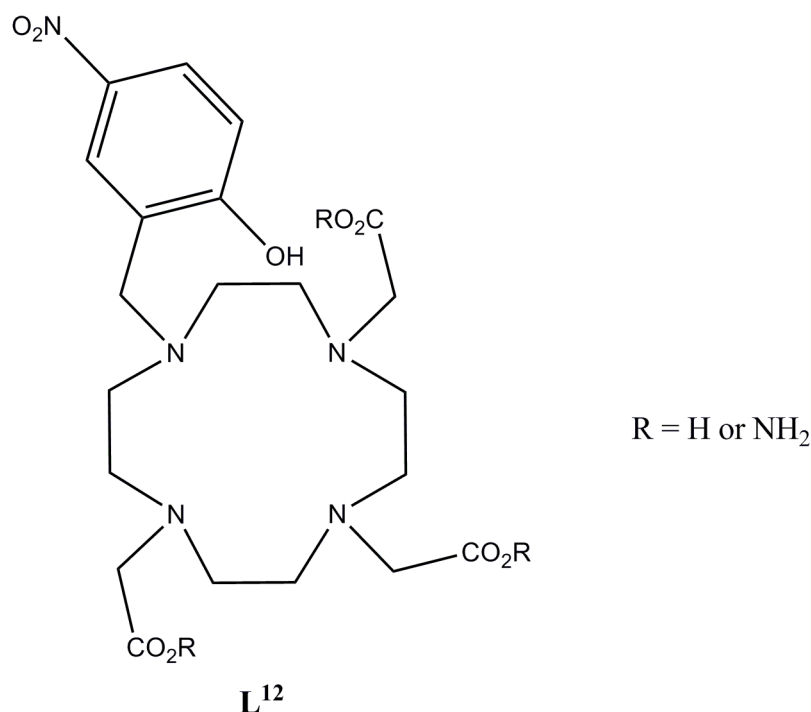
Figure 16: Chemical structure of L^{12}.

Chemical modification of the coordination sphere has also been investigated. This can be achieved by, for example, the inclusion of a pH responsive group. This can allow the modulation of the hydration state, enabling the relaxivity of the complex to be "tuned". This has been explored by Sherry and co-workers, by using a *p*-nitrophenol pendent arm which dissociates at low pH.[78] Two gadolinium(III) chelates were formed based on **L^{12}** (Figure 16), consisting of a nitrophenolic arm plus either three acetates or three amide pendent arms. The crystal structure of the europium(III) complex of **L^{12}** (R = NH$_2$) is shown in Figure 17. The formal charge of the complex was found to be 2+, implying that the phenol is deprotonated. The europium(III) ion sits in a distorted monocapped square antiprismatic geometry with the cyclen ring adopting a [3333] conformation. The relaxivity of the gadolinium(III) complexes were found to differ over a range of pH. At pH 9 the acetate complex has a relaxivity of 4.1 mM^{-1}s^{-1} whereas the amide complex has a relaxivity of ~2.75 mM^{-1}s^{-1}. At pH 5, these values increase to 7 and 3.4 mM^{-1}s^{-1} respectively. For the acetate complex, the change is ascribed to the phenol becoming protonated and

dissociating from the complex, which results in an increase in the hydration state of the metal from 1 to 2. The increase in relaxivity for the amide complex was believed to be due to an increase in prototropic exchange of bound water and/or phenolic protons. Dissociation does not occur due to the reduced electron-donating capacity of the amide-ligating groups rendering the gadolinium(III) ion too electron deficient to enable release of the phenol.
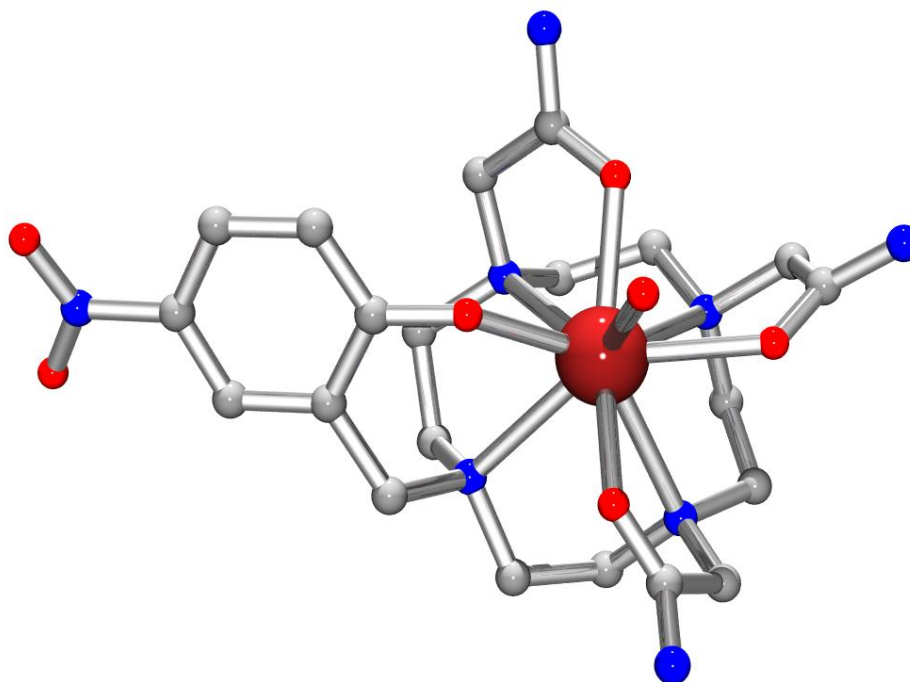
Figure 17: Ball and stick representation of the X-ray crystal structure of the Europium complex of L^{12} (R = NH_2). H-atoms and triflate counter ions have been omitted for clarity (Woods *et al.*).[78]

Sherry and co-workers have also investigated the effect of electronic substituents on the modulation of water exchange.[79] Cyclen was tri-alkylated with ethyl-*N*-bromoacetylglycinate, with the remaining secondary amine being alkylated with various *p*-substituted bromoacetyl aniline derivatives (where X=$CO_2{}^tBu$, CN, F, H, OMe, Me and NO_2/NH_2). Residence lifetimes for electron-withdrawing groups were longer than electron-donating groups, with the opposite being observed for groups considered inductive (see Table 3). The *p*-nitro derivative was chemically reduced to the *p*-amino derivative which showed a difference in intensity of ~30% from chemical exchange saturation transfer (CEST) images.

X substituent	effect	τ_M (µs)	$\Delta\omega$ (ppm)	$1-(M_s/M_0)$
		Mesomeric		
$CO_2{}^tBu$	-M	352±17	47.69	0.415
CN	-M	324±33	47.61	0.477
H	0	269±32	46.72	0.611
OMe	+M	198±19	47.25	0.194
		Inductive		
F	-I	144±8	44.98	0.347
H	0	269±32	46.72	0.611
Me	+1	310±55	46.89	0.113

Table 3: Effects of the X substituent on residence lifetimes in the europium(III) complexes prepared by Sherry and co-workers.[79]

Modification of the ligand framework can be used to allow site specific imaging. This can be approached in a number of ways, including the formation of liposomes. A bimodal fluorescent and paramagnetic liposome has been described by Miller and co-workers.[80] Long alkyl chains were tethered to a DO3A chelator through the use of di-amide small linker. Liposomal formulations of gadolinium(III) complexes were then evaluated by fluorescence microspcopy and MRI. Uptake of the Gd-liposomes into cells (HeLa) showed a marked reduction in their MRI T_1 relaxation times. Formulations were shown to have minimal cytotoxicity and also have a capacity for plasmid DNA transfection. A second neutral bimodal gadolinium(III)-liposome is described for labelling tumours *in vivo*. From MRI images obtained, the imaging agent was clearly localised in the tumour mass and this was verified using fluorescence microscopy.

A tetra-nuclear gadolinium contrast agent which is fibrin-specific has been designed and synthesised for detection of thrombus.[81] The gadolinium(III) ion is bound to a DO3A derived macrocycle with two such entities capping each end of a polypeptide through both C and N termini. Two binding assays were used to assess the viability of these agents for thrombin detection. Plasma clot and dried fibrin assays yielded comparable results in both the number of binding sites (1.9 ± 0.1 and 1.7 ± 0.1 respectively) and the dissociation constant, K_d (0.9 ± 0.3 and 1.6 ± 0.2 respectively). High binding specificity to fibrin was observed in the presence and absence of plasma proteins, indicative of good selectivity. Binding of the polypeptide conjugate to fibrin increases relaxivity to 25 times that of Gd(DOTA) suggesting that this may be a good candidate for detecting blood clots *in vivo*.

Contrast agents which are sensitive towards metal ions are desirable because they can highlight areas of high concentration of certain metallic ions. This is highlighted by either an increase or decrease in image brightness in these areas. Calcium sensitive contrast agents have been produced. One such agent has been reported by Logothetis,[82] which shows ~100% relaxivity enhancement upon addition of calcium(II). This agent is also selective for calcium(II) in the presence of magnesium(II) and zinc(II). Relaxivity enhancement occurs by a water molecule entering the inner sphere of the gadolinium(III) centre upon binding to calcium(II). The hydration numbers obtained are 0.17 in the absence of calcium(II) and 0.88 in the presence of calcium(II).

The development of new synthetic protocols with which to synthesise contrast agents are being developed. For example, click chemistry has been used by Meade and co-workers to produce multimeric MR contrast agents with high relaxivities.[83] Agents synthesised had either three, six, or seven gadolinium(III) centres, with the latter producing a relaxivity of 85.4 ± 3.74 mM^{-1}s^{-1}. Examination of the three agents showed that they were mono-disperse and had good biocompatibility.

Further investigations into using DO3A derived complexes for molecular imaging have focused on using α-amino acids as linkers.[25,84] This enables the tethering of a biomolecule to achieve selectivity for tissue type and also a further acetate group with which to coordinate to the lanthanide metal to give a coordination number of eight.

New imaging techniques based on magnetic resonance are currently in development. Two such examples are Magnetic Resonance Spectrosopy (MRS) of biological systems and paramagnetic chemical exchange saturation transfer (PARACEST). MRS enables the analysis of the chemical content of living tissue to take place *in vivo*. A variety of heptadentate ligands complexed with lanthanide metals have been prepared to act as shift and relaxation agents in MRS.[85] ^{1}H NMR studies for the detection of lactate highlighted that the later lanthanides (terbium(III), dysprosium(III), thulium(III), ytterbium(III)) may exhibit an optimal $\Delta\delta/\Delta v_{\frac{1}{2}}$ ratio. However, the high Lewis acidity of these ions prevents fast exchange conditions from being met. Early lanthanide ions possess opposite characteristics in that they

have a reduced Lewis acidity but spectral analysis is made difficult by line broadening and small spectral range.

Di-peptide PARACEST MRI agents have been developed by Hudson and co-workers.[86] The methodology that they utilised enabled the preparation of tetraalkylated cyclen-oligopeptide conjugates to be produced in yields greater than 90%. Complexation of these oligopeptide conjugates to dysprosium(III), europium(III), neodymium(III), terbium(III), thulium(III) and ytterbium(III) is strongly dependent on the oligopeptide sequence with yields ranging from 42 - 98%. Europium(III) DOTAM complexes displayed the most strongly bound water signal in the CEST spectrum, especially the complex possessing the Gly-Phe-OH oligopeptide sequence (CEST effect ~45% at physiological pH and temperature). Conversely, changing the oligopeptide sequence to Asp-Phe-OH showed only a small CEST effect.

1.3.2.3. Therapeutic agents

Cyclen derived macrocycles have also been investigated with regard to possible therapeutic benefit. For example, macrocyclic ligands formed from the condensation of ethylene diamine or 1,3-dibromopropane with malonic or succinic acid have been synthesised with a view to examining their anti-inflammatory, anti-fertility and anti–microbial properties.[87] Sperm motility and fertilizing capacity of spermatozoa displayed a severe decrease in the presence of manganese(II) complexes. Protein content in the testes, epididymis, ventral prostrate and seminal prostrate decreased by as much as 50% when compared with the control. This decrease in protein content was attributed to androgen deficiency, which was reinforced by data showing a decrease in sialic acid content in rats treated with the manganese complexes. Anti-inflammatory action was shown to increase with the increasing size of the macrocyclic ring, but all compounds tested displayed lower anti-inflammatory activity than phenylbutazone, a known anti-inflammatory.

A further therapeutic use of cyclen macrocycles is in the development of urea-checkpoint kinase inhibitors.[88] Macrocyclic ureas formed using a Grubbs metathesis macrocyclisation were investigated. Amino or ether analogues at the 4-position of a component benzene ring were developed, with IC_{50} values being obtained in the 1 to

10000 nM range. A number of compounds were identified as ideal Chk1 inhibitors, as they exhibited little or no antiproliferative activity alone but significantly potentiated the cytotoxities of DNA-damaging agents.

1.3.2.4. Optical probes

The use of cyclen ligands in the preparation of optical probes for use in a range of different techniques is well documented. A perspective article on emissive europium(III) and terbium(III) complexes discussing their applications for molecular imaging and sensing has been published.[89] Optical probes utilise the luminescence properties of lanthanides. This requires the lanthanide centre to be excited using light of an appropriate wavelength. Excited state lifetimes of the lanthanide(III) ions range from microseconds to milliseconds. This is advantageous as they allow time-resolved spectroscopy and microscopy to be used, in which light scattering and auto-fluorescence can be gated out prior to detection of luminescence from the lanthanide ions. However, excitation of the lanthanide(III) ion is very inefficient, leading to low values of ε (≤ 1 $M^{-1}cm^{-1}$) as the relevant f-f transitions are Laporte forbidden. Lanthanide complexes have therefore been developed which incorporate into the ligand structure a sensitising chromophore, capable of transferring its excited state energy to the encapsulated lanthanide(III) ion.

Chromophores are typically conjugated systems which transfer energy during excitation directly to the metal centre. This increases the quantum yield of luminescence. The evaluation of europium(III) complexes bearing either azaxanthone or azathiaxanthone chromophores has been reported by Parker *et al*.[90] These complexes were assessed as responsive probes for the intracellular environment. The most notable of these were the complexes of **L^{13}** which upon addition of HSA led to a very large decrease in europium(III) emission intensity with concomitant emission lifetime increase from 0.26 ms to 0.35 ms. More interesting was the addition of NaHCO$_3$ causing the hypersensitive and electric-dipole allowed $\Delta J=2$ emission band to become more pronounced. The complexes of both derivatives were found to be non-cytotoxic, and they were found to localise in the mitochondria.

Bi-nuclear optical probes are also of considerable interest. Faulkner and Pope have investigated bis-lanthanide systems using two DO3A chelators to chelate the ions.

These were joined together via the free secondary amine using linker groups ($\mathbf{L^{14}}$). By using a phenol derivative as the linker group, the authors were able to create two environments for which the lanthanide ion could be held.[91] Luminescence studies showed that there were two distinct lanthanide environments co-existing on the luminescence timescale. Luminescence lifetimes measured in D_2O and H_2O fitted to two exponential decay components were obtained, which gave rise to two inner sphere hydration numbers of 0.3 and 1. Given that the two metal centres have coordination numbers of 7 and 8, the low inner sphere hydration numbers were attributed to the lipophilicity of the linking phenolate preventing water molecules approaching the metal centres. The authors have also used xylene as the linker group ($\mathbf{L^{15}}$).[92] This allowed the inner sphere hydration of different metal ions to be probed. The inner sphere solvation (q) of the lanthanide(III) ions under study decreased along the group; for lanthanum(III) q=2, terbium(III) q=1.4 and ytterbium(III) q=0.4.

LnL^{13} (X = S or O)

Yb_2L^{14}

L^{15}
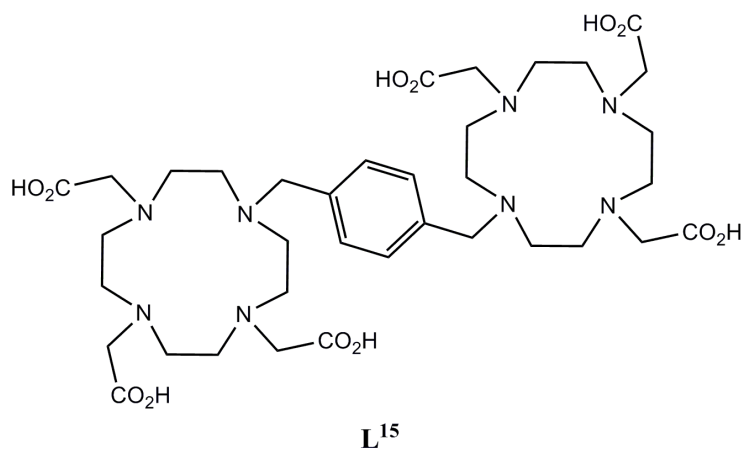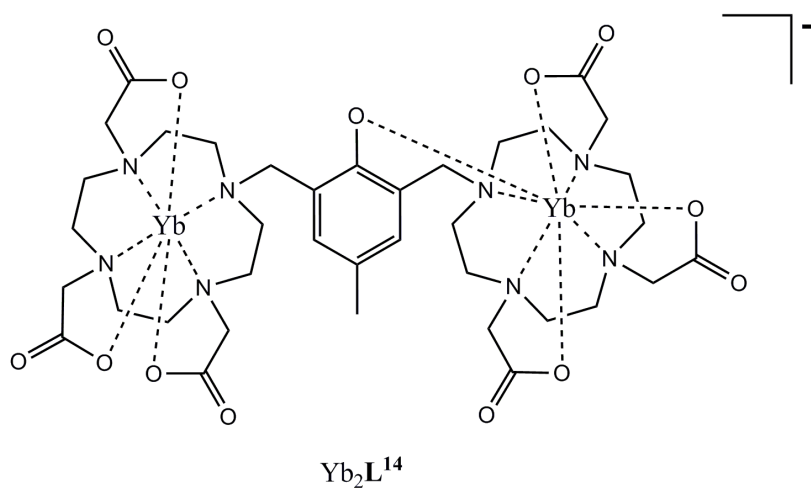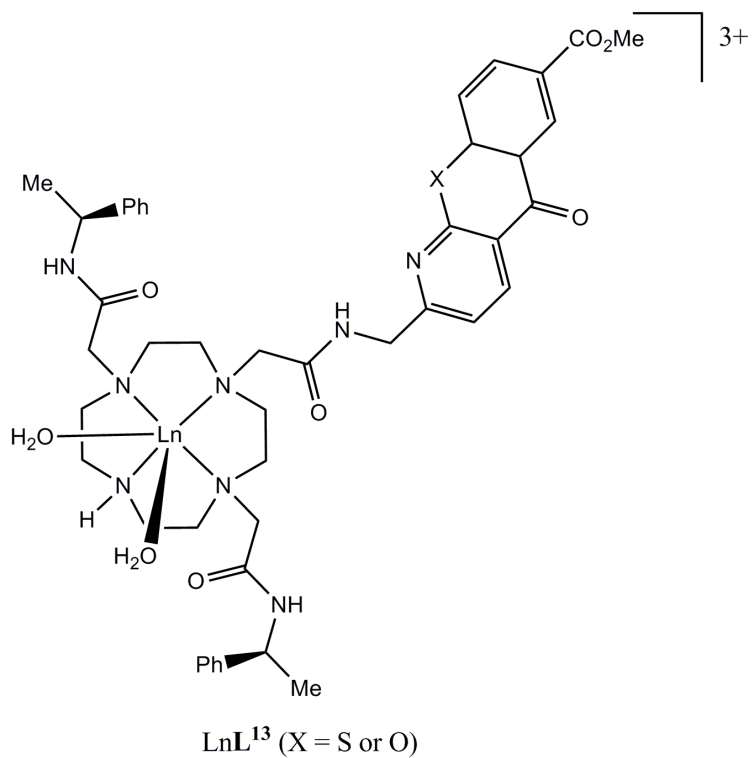
Figure 18: Chemical structures of LnL^{13}, Yb_2L^{14} and L^{15}.

Tri-nuclear optical probes have also been produced. An example of such a probe has been synthesised by Pope and Faulkner.[93] DTPA was used as the linker between two terbium DO3A complexes each with a pendent aminobenzyl arm, before introducing ytterbium(III) into the cleft of the DTPA. The close proximity of the metal ions enabled near-infrared (NIR) emission sensitized by the terbium(III) ions, evidenced by a peak at 980 nm in the ytterbium(III) sensitized emission.

A further area in which optical probes are currently being developed is in the synthesis of metal ion sensitive probes. DOTA complexes and their analogues have been prepared as zinc(II) sensitive probes for biological systems.[94]

EuL^{16} → Zn(II), pH 7.4 → EuZnL^{16}.H$_2$O
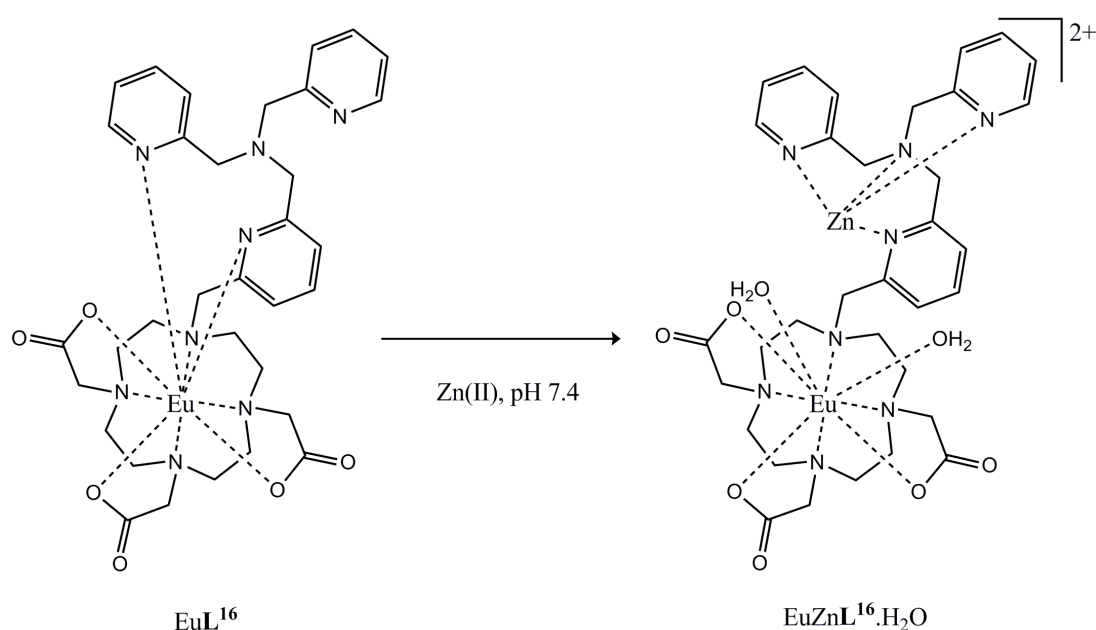
Figure 19: Modulation of the coordination sphere surrounding the europium(III) ion due to coordination of a zinc ion by the bis-picolyl group.

An example of a zinc(II) probe is shown in Figure 19. This example was prepared by Pope and Laye in which the structure incorporates a bis-picolyl unit into a europium DO3A complex (L^{16}). Upon binding of zinc(II), the intensity of ligand fluorescence increased as did the inner sphere hydration of the europium(III) ion (q=0 to q=2).[95] The aqueous environment was designed to replicate physiological conditions; pH 7.4 using 4-(2-hydroxyethyl)-1-piperazineethanesulfonic acid (HEPES) and an ionic buffer solution (140 mM NaCl, 4 mM KCl, 1.16 mM MgCl$_2$, 2.3 mM CaCl$_2$). The crystal structure of the sodium(I) complex of L^{18} is shown in Figure 20. The sodium is eight coordinate; three ester carbonyl groups, four macrocyclic nitrogens and the

nitrogen of the bridging 2,6-pyridyl moiety all coordinate to it. The *bis*-picoyl nitrogens remain uncoordinated.
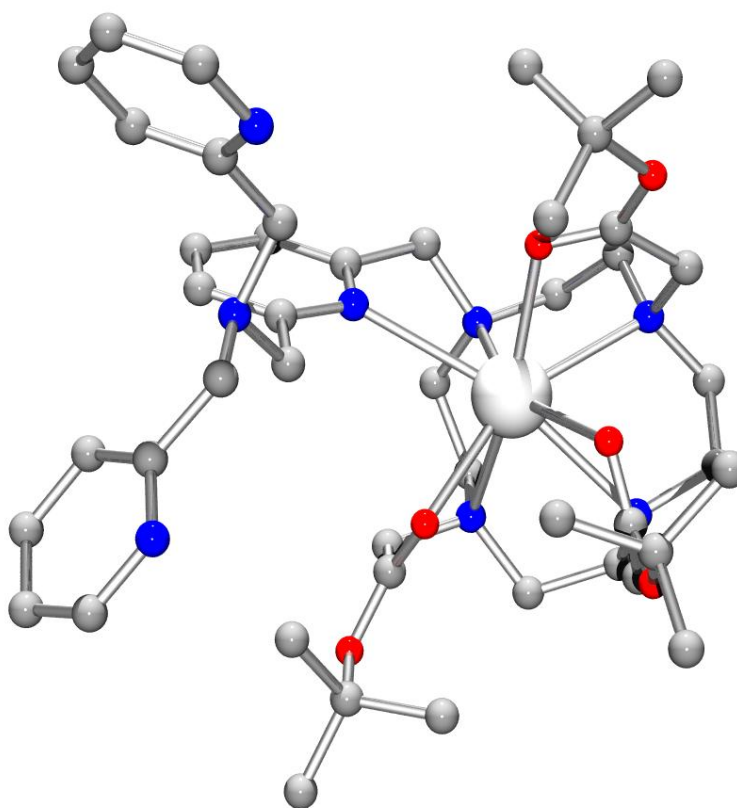
Figure 20: Ball and stick representation of the X-ray crystal structure of the sodium complex of L[16]. H-atoms and two water molecules of crystallisation omitted for clarity (Pope and Laye).[95]

A further zinc(II) sensitive optical probe has been prepared. Aoki and co-workers have recently reported a compound which undergoes hydrolytic uncaging upon complexation with zinc(II).[96] H_2L^{17} possesses negligible fluorescence emission at pH 7.4, but upon the addition of zinc(II) significant fluorescence emission is observed at 512 nm (see Figure 21). The increase in fluorescence is attributed to the hydrolysis of a sulfonamide which is promoted by zinc(II) bound hydroxide.
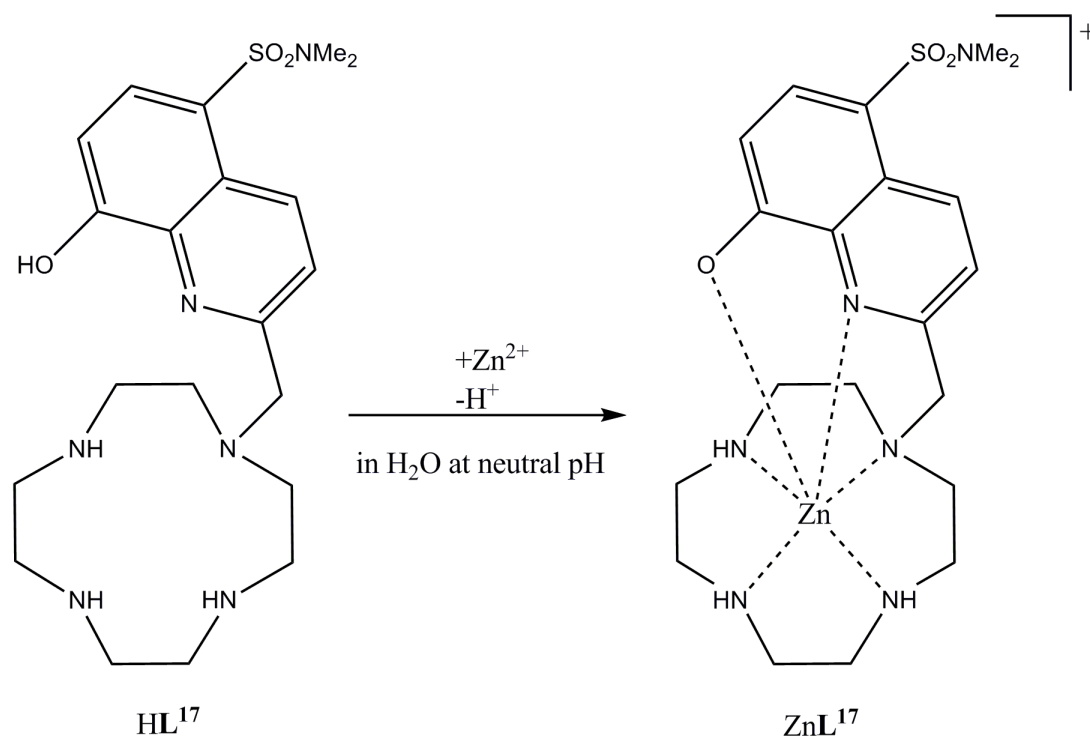
Figure 21: Figure showing conditions for the formation of the zinc(II) complex of L^{17} which occurs at neutral pH.

A further example of fluorescent metal sensitive probes has been published, which can be used in the detection of zinc(II) and cadmium(II) ions.[97] The probe consists of an 8-hydroxy-5-*N*,*N*-dimethylamidosulfonylquinolin-2-ylmethyl pendent arm tethered to a cyclen ring. The cyclen ring quenches the fluorescence emission of the quinolinol moiety. However, when complexed to either zinc(II) or cadmium(II), emission at 512 nm was increased by factor of seventeen and forty-three respectively.

A number of techniques such as luminescence resonant energy-transfer (LRET) and time-resolved long-lived luminescence microscopy (TRLLM) are being developed which use luminescent optical probes. For example, LRET experiments using europium(III) complexes have shown these to be viable potential probes for bioanalysis.[98] The europium(III) centre is held in the cleft of a DOTA derived macrocycle, with a non-coordinated carboxylic acid function as a potential linker to biomolecules (**L^{18}**). LRET was observed when Cy5 dye was added to a solution of the europium(III) complex.
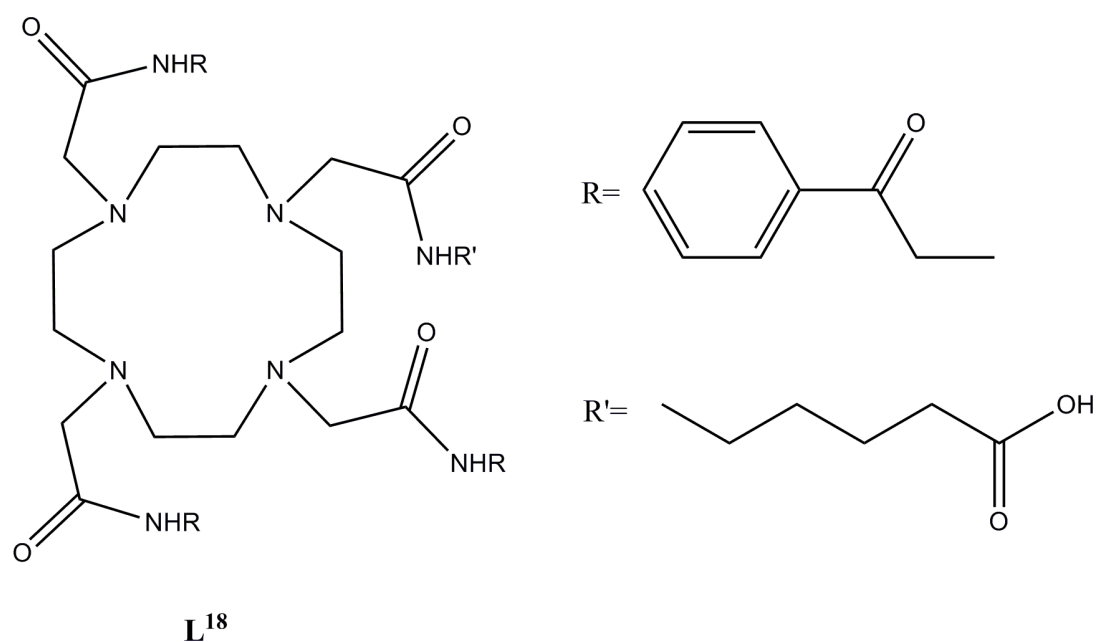
Figure 22: Chemical structure of L^18.

TRLLM can also be used to visualise biomolecules within living biological samples. This technique enables nano-second resolution enabling the interactions of proteins, for example, to be imaged. Nagono and co-workers have developed a new TRLLM system using conventional fluorescence microscopy coupled with an image intensifier and a xenon flash lamp in order to use luminescent europium(III) DOTA derived complexes (**L^19**).[99] The newly developed europium(III) complexes were used to obtain fluorescence images from cells in conjunction with the TRLLM system, with short-lived fluorescence being excluded.

L^19 (R= H, F, CH$_3$, CH$_3$O, NHAc, NH$_2$)
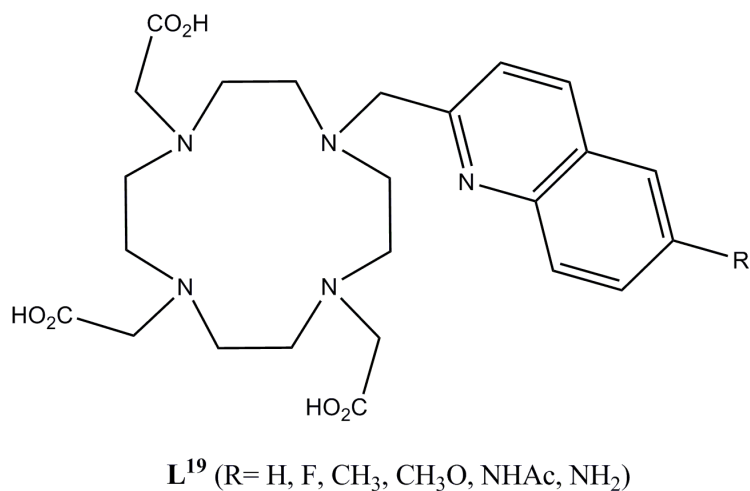
Figure 23: Chemical structure of L^19.

1.4. Penta-, hexa- and octa-aza macrocycles and their analogues

Penta-, hexa- and octa-aza macrocyles have been synthesised towards enzyme mimicry and therapeutic and diagnostic applications. The larger ring size of the macrocycle can be tailored towards the design of cage complexes. A recent review has been published in 2007 on cage complexes of transition metals in biochemistry and medicine.[100] Selected examples for enzyme mimicry and therapeutic and diagnostic applications are now discussed.

1.4.1. Enzyme Mimics

Hydrolytic phosphate-ester cleavage catalysts have been produced using lanthanide and transition metal ions. An example of a lanthanide hydrolytic catalyst has been prepared, with the specific aim of cleaving RNA.[101] A europium(III) ion was complexed to the ligand 1,7-diaza-4,10,13-trioxacyclopentadecane-*N*,*N'*-diacetic acid which exists as a monomer below pH 7. Upon increasing the pH above 7, a dimeric complex is formed, in which the europium(III) centres are bridged by one hydroxide initially, and upon further increase in pH (>10), by two hydroxides. k'_{obsd} plots for both the monomer and dimeric species in the presence of HpPNP show that the dimeric complex is the better catalyst. The monomeric and dimeric transition states involved in the cleavage of HpPNP are stabilised to a similar extent (-7.1 and -7.6 kcal mol^{-1}), suggesting that the europium(III) ion in both complexes only weakly interacts with the substrate.

A further example of a hydrolytic catalyst has been prepared using transition metal ions at the catalytic centre. The di-nuclear copper(II) complexes of the hexaaza macrocycle 2,5,8,17,20,23-hexaaza[9.9]paracyclophane (PEA) has been prepared.[102] The complex catalyses hydrolysis of the phosphotriester 2,4,-dinitrophenyl diethyl phosphate (DNPDEP), where $[Cu_2(PEA)(OH)_2]^{2+}$ and $[Cu_2(PEA)(OH)]^{3+}$ were identified as the active species. Low activity was observed below pH 7 but substantial rate increases above pH 7 are consistent with the active species being a hydroxo species. Two mechanisms for hydrolytic cleavage are suggested; one in which the same copper ion is used for coordination of the substrate and hydrolytic

cleavage, and one where both copper ions are actively involved in coordination and hydrolysis.

Hexaaza copper(II) macrocyles have been synthesised to investigate their interaction with calf thymus DNA.[103] Copper(II) complexes of both cyclam and the di-propyl hexaaza ring were produced. The crystal structure of the former (Figure 24) shows that the copper(II) ion adopts a square planar geometry. Both complexes bind to DNA through electrostatic interactions, whereas the di-benzyl hexaaza ringed complex (crystal structure shown in Figure 24) intercalates with DNA through the two aromatic rings. As such, the side chain plays a key role in determining the mode of binding of the copper complex to DNA. The copper complexes were shown to exhibit nuclease activities, in that circular plasmid DNA was converted to nicked DNA.
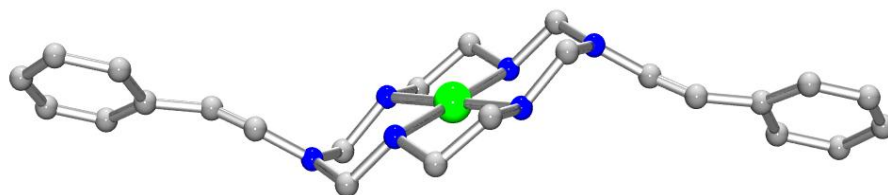
Figure 24: Ball and stick representation of the X-ray crystal structure of the copper(II) dibenzyl hexa-aza ringed complex. H atoms have been omitted for clarity (Liu *et al.*).[103]

1.4.2. Diagnostic agents

MRI contrast agents and radiopharmaceuticals using penta-, hexa- or octa-macrocycles have also been investigated. For example, a macrocyclic ligand formed by the condensation of 2,6-pyridinedimethaneamine (PDA) with diethylenetriamine pentaacetate (DTPA) has been reported by Li *et al.* for the purpose of cell labelling and magnetic resonance imaging applications.[104] Two long alkyl chains rendered the complexes lipophilic with the gadolinium(III) complexes being able to label mammalian cells non-invasively at concentrations in the micromolar range. Cultured cells took up the gadolinium(III) complexes rapidly leading to the production of T1-weighted MR images of increased intensity. From diffusion enhanced fluorescence

resonance energy transfer (DEFRET) studies it was possible for the authors to hypothesise that the complexes labelled the cells by insertion of the two hydrophobic chains into the cell membrane with the hydrophilic binding site facing the extracellular medium.

$$L^{20}$$

$$L^{21}$$
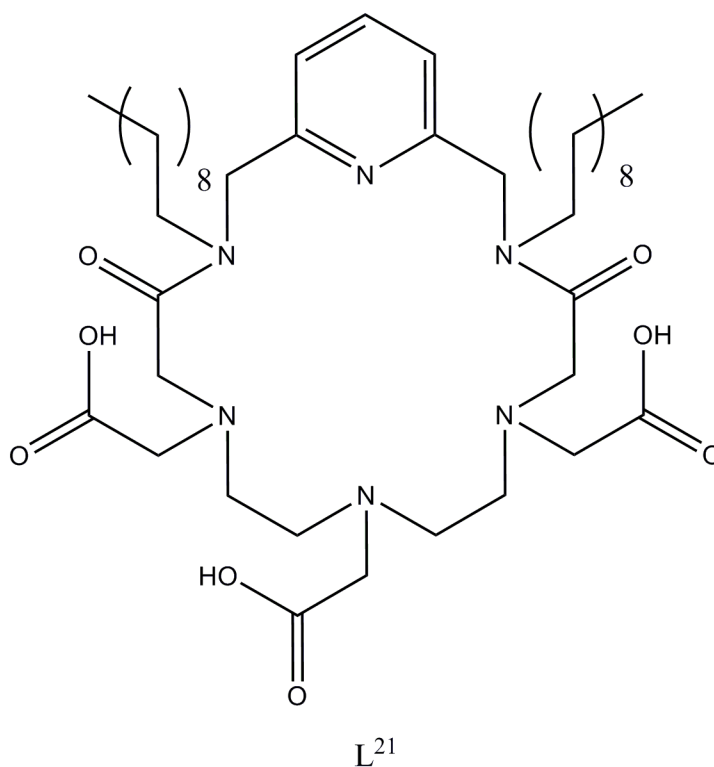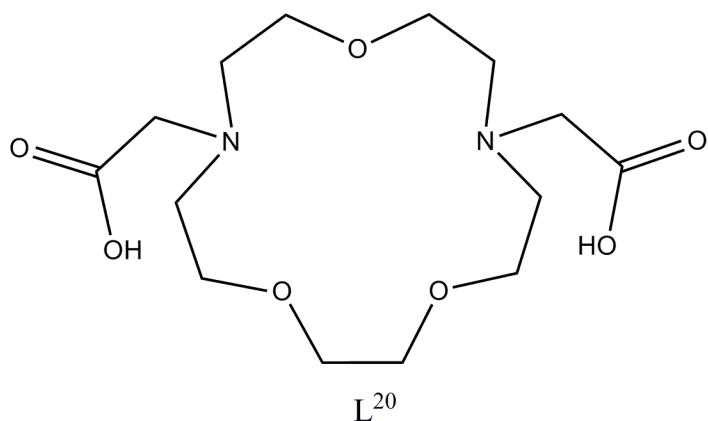
Figure 25: Chemical structures of L[20] and L[21].

Further compounds for diagnostic purposes have been prepared. SarAr, a hexa-aza cage, has recently been used to coordinate ^{64}Cu as a PET emitter.[105] An antibody, B72.3, was tethered to SarAr via a aminobenzyl linker, which meant that the

conjugate would interact with a tumour-associated glycoprotein, TAG-72. Tumour localisation of the bioconjugate to the target site reached 38% ± 5% ID/g within 48 hr. Stability of the ^{64}Cu complex was maintained *in vivo*.

1.4.3. Therapeutic agents

Therapeutic agents have been prepared utilising penta-, hexa- or octa-macrocyclic frameworks. One such example uses a templated synthesis to produce octaaza macrocyles and reports their biological screening.[106] The cadmium(II) bromide complex had desirable anti-microbial properties, with minimum inhibitory concentrations (MICs) of between 2-4 µg ml^{-1} against *S. aureus*, *S. epidermidis*, *S. typhi* and *P. aeruginosa*. These values showed that this compound was more potent than Cefaclor and Linezolid, two standard antibiotics.

1.5. Porphyrin and phthalocyanine based macrocycles

Porphyrins and phthalocyanines are currently being developed as photo-dynamic therapeutic agents. Photodynamic therapy (PDT) is an emerging technique which is used to treat cancer. Porphyrin and phthalocyanine (Pc) compounds and complexes when irradiated with light of an appropriate wave-length produce singlet oxygen, a cytotoxic species. The highly reactive nature of singlet oxygen damages cancerous cells leading to cell death. Both types of compound are currently being developed to increase the quantum yields of singlet oxygen and to also mitigate the innate hydrophobicity of the porphyrins so that they can be used intravenously. Other uses of phthalocyanines and porphyrins include enzyme mimicry and catalytic therapy.

1.5.1. Porphyrin photodynamic therapy agents

The main area in which porphyrins are used is as PDT sensitisers. A variety of different approaches to obtain this goal have been taken. For example, tetra(4-pyridyl)porphyrin (**L**[22]) organometallic ruthenium(II) arene complexes have been produced by Therrien and co-workers.[107] The ruthenium(II) ions coordinate to the nitrogens around the periphery, creating tetra-nuclear species. These compounds also possess chemotherapeutic activity whilst still retaining photodynamic therapeutic properties. Cellular uptake and localization microscopy studies revealed that the compounds accumulated in the melanoma cell cytoplasm in granular structures different from lysosomes. Upon irradiation at 652 nm (5 Jcm^{-2}) cell survival in the presence of the ruthenium(II) compounds ranged from approximately 20 - 45%.

L²²
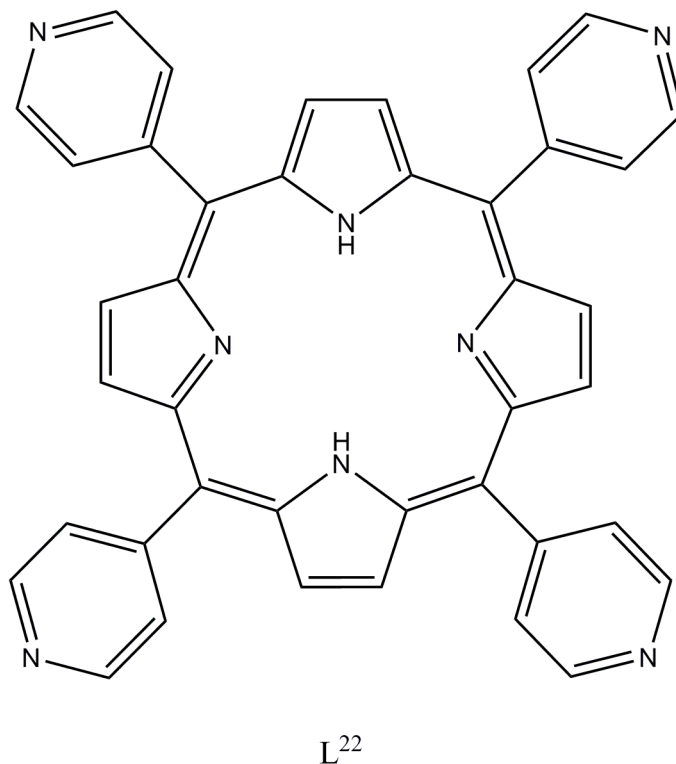
Figure 26: The chemical structure of L²².

Site selective PDT is also a major goal of current research. A meta-tetra(hydroxyphenyl)chlorin-like photosensitiser conjugated to folic acid has been developed to increase the delivery of the agent to tumour sites.[108] A polyethylene glycol chain is used as a spacer between the chlorin and folic acid. The folic acid conjugate and the unconjugated chlorin were incubated with FR-α-positve KB cells or HT-29 cells lacking FR-α. The folic acid conjugate was shown by optical fiber fluorimetry to have enhanced accumulation in KB cells and displayed remarkable selectivity for tumour-to-normal tissue (5:1 ratio) after 4 hr postinjection. The unconjugated chlorin was shown to be taken up by KB and HT-29 cells.

Further research has focused on the delivery of the photosensitiser and its photoactivity. The photodynamic effect of 5-(4-carboxyphenyl)-10,15,20-tris(4-methylphenyl) porphyrin has been compared in homogenous medium and in reverse micelles of n-heptane/sodium bis(2-ethylhexyl)sulfo-succinate (AOT)/water bearing urease as a biological substrate model.[109] In AOT micelles, the high amphiphilic capability of the sensitisers binds the porphyrins to the interfacial region of the reverse micelles. The singlet oxygen generated in these systems was thought not to be distributed evenly across the microheterogenous system as the enzyme activity

51

was much higher than in homogeneous solution. In addition, the presence of azide led to the photo-protection of the enzyme in both systems. Therefore, the authors concluded that singlet oxygen was responsible for the inactivity of the urease.

1.5.2. Phthalocyanine photodynamic therapy agents

Phthalocyanines are also used as sensitisers for PDT. A route to the production of metal-free phthalocyanines for this purpose has been reported. The cyclisation of 1,2,:5,6-di-O-isopropylidine-α-D-glucofuranose or 1,2:3,4-di-O-isopropylidine-α-D-galactopyranose analogues using cerium(III) chloride affords the metal-free phthalocycanines in moderate yield (47% and 58% respectively).[110] Mono-glycosylated Pcs exhibit significantly higher phototoxicity compared with the tetra-α-glycosated analogues. IC_{50} values for the former were reported down to 0.9 μM. The lower phototoxicities of the tetra-α-glycosated Pcs was explained in terms of lower cellular uptake and/or higher aggregation tendency.

Functionalisation of the phthalocyanine periphery can aid water solubility, whilst still retaining light induced phototoxicity. Vicente and co-workers utilised this approach in preparing PEGylated cationic zinc(II) phthalocyanine complexes.[111] Despite high water solubility, the complexes were not present as monomers in solution but as aggregates. Exchange of the zinc(II) ion for silicon incorporating axial substituents was efficient in preventing aggregation. These amphiphilic silicon complexes were highly phototoxic (IC_{50} = 2.2 μM at 1 J cm^{-2} light dose) and also localised in the lysosomes despite their octa-cationic nature.

The preparation of peptide-pthalocyanine conjugate can enable the site selective light induced cytotoxicity. Two zinc(II) phthalocyanine complexes bearing a bifunctional peptide have been reported.[112] The peptide contains sequences for both the bipartite nuclear localisation signals (NLS) of nucleoplasmin and the human immunodeficiency virus I transcriptional activator (HIV-1 Tat). The peptide increases water solubility and these conjugates fluoresce in aqueous solutions (highest quantum yields observed at pH 5.0). Both conjugates were found to have low dark cytotoxicity towards human HEp2 cells (IC_{50} > 77 μM) but were highly phototoxic (IC_{50} < 2 μM at 1 J cm^{-2}). The conjugate utilising a long PEG chain as a

linker accumulated considerably more effectively than the conjugate with a short PEG chain.

1.5.3. Catalytic therapy agents

CT (catalytic therapy) is a cancer treatment modality based on the generation of ROS (reactive oxygen species). Unlike PDT, light of an appropriate wavelength is not required to generate ROS. ROS is instead generated through a catalyst/substrate pair. This technique enables the treatment of cancers which are not accessible by light. The most frequently used substrate and catalyst pair is ascorbate/Co phthalocycanine (PcCo). However, porphyrins are now being explored as a possible alternative to phthalocycanines as they have fewer side effects and are considered to be just as potent.[113] Breast cancer tumour cells were reduced by 20-40% after a single in vitro treatment, using Co(III) hemaotoporphyrin chloride/ascorbate. Apoptosis was stimulated in the cancer cells and the cell cycle disrupted. The number of cells accumulating in the sub G0/G1 stage of the cell cycle increased from 3- to 10-fold, providing evidence for possible DNA induced damage in the tumour cells.

1.5.4. Enzyme mimics

Porphyrins have been synthesised to mimic SOD. A multitude of approaches have been taken to modify porphyrin analogues to obtain the catalytic efficiency shown by the enzyme. One such approach has been reported by Batinić-Haberle and co-workers.[114] Their work led them to synthesise porphyrins with positively charged pendent arms at the *meso* positions. Their findings show that for porphyrins of the same overall cationic charge, the charge placement and distribution within the aryl rings influence dramatically the redox modulation potency of the manganese(III) complexes. Placement of charge closer to the metal centre results in better *in vitro* and *in vivo* activity.

A further example is where tri(ethyleneglycol)-derivatised manganese(III) porphyrins have been synthesised.[115] Use of *ortho* pyridyl or di-*ortho* imidazolyl electron withdrawing groups enabled the metal centre to attain highly positive redox potentials (+250 mV for the tetra PEGylated pyridyl complex and +412 mV for the octa PEGylated imidazolyl complex). The PEG chains aid the water solubility of the complex. SOD-like activity was observed; log k_{cat} of 8.11 (tetra PEGylated pyridyl

complex) and 8.55 (octa PEGylated imidazolyl complex). The former is only a few-fold less potent in disproportionating $O_2^{\bullet-}$ than the SOD enzyme itself.

1.5.5. Therapeutic agents

One aspect of therapeutic research using porphyrins and phthalocyanines has focused on their ability to intercalate with DNA. Tabata and co-workers have reported the use of lead(II), mercury(II) and cadmium(II) porphyrins towards this aim.[116] These complexes were more effective than their free base analogues. The binding mode of the metal complexes relies on the strong intercalation of the ligand to DNA which results in the release of the metal ions. The released metal ions possess strong affinity for the DNA bases or phosphate groups of the DNA. Because of these two factors, the metal complexes were found to be toxic towards protozoan parasites that cause African sleeping sickness in man and livestock.

1.6. Summary

This introduction contains a discussion of selected examples of aza-macrocycles used in enzyme mimicry, diagnostic and therapeutic applications and in the production of optical probes. The different cavity sizes of the macrocycles discussed enable the production of complexes using metal ions from the transition series, lanthanide series and p-block. The tailoring of the cavity can be used to accommodate ions of varying size. The metal ion used to form the complex is chosen based on the properties it possesses. For example, gadolinium(III) ions are used as MRI contrast agents because they are highly paramagnetic and can therefore enhance relaxivity of water protons in the immediate vicinity. Another example is the use of ^{64}Cu in radiopharmaceuticals because it has favourable characteristics for both PET imaging and targeted radiotherapy. The structure of the ligand is designed to maximise the effectiveness of the metallic ion in its role (for example in enabling water molecules to access the coordination sphere of a gadolinium(III) ion in a contrast agent). In addition, the ligand is designed to meet the coordination requirements of the metal centre. This often requires the use of pendent arms which possess additional donor atoms. The macrocycle can be designed to increase the stability of the metal complex. This is an important consideration as decomplexation of the metal centre can lead to *in vivo* toxicity and loss of activity of the complex.

The following chapters of this thesis discuss the design and synthesis of novel aza-macrocyclic complexes bearing pendent arms. In Chapter 2 the design and synthesis of the pendent arms are discussed. In Chapters 3, 4 and 5 the attachment of the pendent arms to form new macrocyclic chelators and their complexes is reported. The properties of these complexes have been investigated with respect to biological applications. These applications include MRI and PDT. In Chapter 6 a summation of the research conducted is given and areas for further work discussed.

2. Design and synthesis of pendent arms

2.1. Introduction

Pendent arms are used in ligand systems for a variety of structural or chemical reasons. The use of pendent arms expands the set of available donors and provides access to a variety of relatively preorganized ligands possessing ligating functionalities that cannot be incorporated into a macrocycle. This is often exploited in the production of complexes with attached biomolecules. The pendent arms themselves can be of chemical importance, possessing for example redox active centres or other desirable properties (such as acting as a photosensitiser).[1]

Two types of pendent arm exist; coordinating pendent arm and non-coordinating pendent arms. Both types are considered, and examples of each type given.

2.1.1. Coordinating pendent arms

Coordinating pendent arms need to possess a donor atom in order to form an interaction with the metal centre. Such groups include ROH, $RCONH_2$ and RCOOH for example. One of the most used pendent arms is the carboxylic group, mainly because it can be deprotonated and thus form an ionic bond with the metal centre. However, many pendent arms can induce metal-ion coordination even though the pendent arm incorporates weaker donors. This is because the donors are held near to the metal, favouring such interactions to occur.

mhpc12   1,4-dhpc12   cyclen
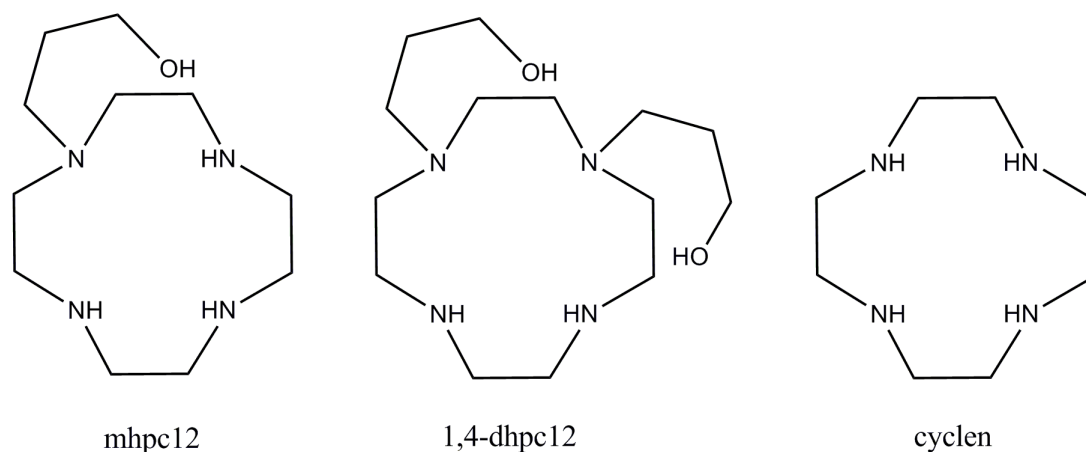
Figure 27: Ligands used in the formation of M(II) complexes in order to study their formation constants.

Table 4 shows the formation constants at 298.2 K for the complexation of cobalt(II), copper(II), zinc(II), cadmium(II) and lead(II) to the ligands as shown in Figure 27.[117] The data shows that the formation constant becomes lower as the number of donor atoms of the ligand increases.

Ligand	Co(II)	Cu(II)	Zn(II)	Cd(II)	Pb(II)
mhpc12	10.5(1)	17.3(1)	13.7(1)	13.0(1)	14.7(1)
1,4-dhpc12	9.7(1)	16.6(1)	12.3(1)	11.8(1)	13.5(1)
Cyclen	13.8	23.3	16.2	14.3	15.9

Table 4: Formation constants at 298.2 K for metal complexes of the ligands displayed in Figure 27.

Parker and co-workers have used a sensitising azaxanthone group in a series of terbium(III) and europium(III) complexes.[118] The azaxanthone group coordinates to the metal centre as well as acting as a sensitiser for the metal centre. It coordinates to the metal centre through a nitrogen atom, see Figure 28.

R = HN–CH(Ph)–Me

X = CO$_2$Me, CO$_2$H, CONHMe, CONHC$_6$H$_{13}$, H or ^{t}Bu
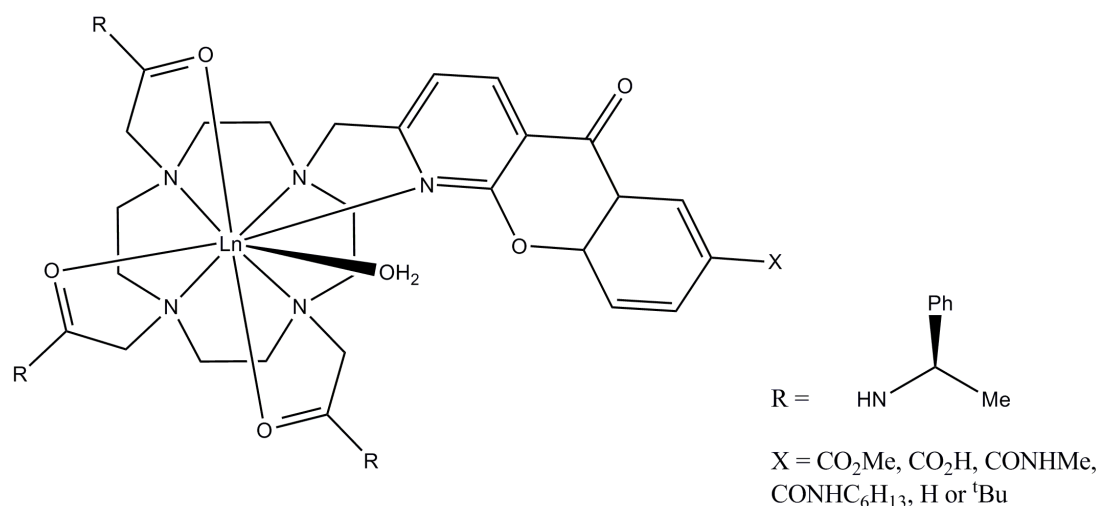
Figure 28: An example of a lanthanide complex with a coordinating sensitiser.

2.1.2. Non-coordinating pendent arms

Non-coordinating pendent arms do not possess donor atoms capable of coordinating to a metal centre. They can instead be used to modify the properties of a ligand. For example, a hydrocarbon chain can be appended to a macrocycle in order to render it lipophilic. Sibert and Cory have used this principle to produce lipophilic cyclam derivatives.[55] Isopropyl and isobutyl chains were N-appended to render the compounds lipophilic but without completely compromising water solubility. Botta

and co-workers utilised polyethylene glycol (PEG) chains to accomplish exactly the opposite.[77] They wanted to increase the water solubility of their complexes in water. In addition the increased molecular weight also served to enhance the inner sphere relaxivity of the resulting MRI contrast agent.

Non-coordinating pendent arms can also be used to append further moieties to the ligand. This route has been explored by Archibald and co-workers who prepared a side-bridged cyclam bearing an aminobenzyl pendent arm.[54] This was used to form an isothiocyanate bond to rhodamine, a fluorescent dye. The structure of the side-bridged ligand is shown in Figure 29.
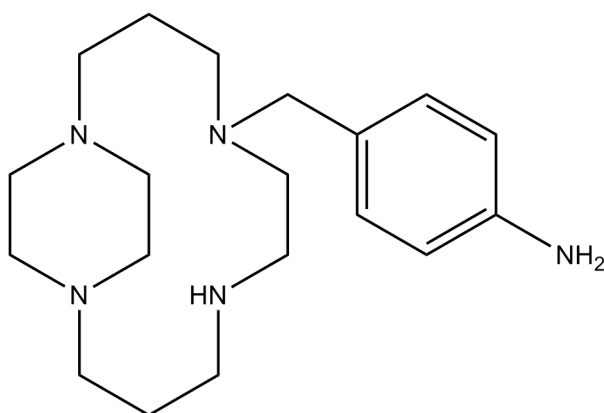
Figure 29: Chemical structure of a side-bridged cyclam bearing an aminobenzyl pendent arm.

The rest of this chapter is concerned with highlighting three different classes of pendent arm and to discuss their design and synthesis, with particular focus on the properties they possess.

2.1.3. Redox active pendent arms

Stabilised di-*tert*-butyl phenyl-X pendent arms (where X = O, NH or S) have been the subject of much focus in the literature. The production of the phenoxyl radical is highly stabilised by the *tert*-butyl groups in the *ortho* and *para* positions and has been reported to be stable for days.[119,120] The same properties were also noted for the anilino radical analogue.[121] The reason for this stability is because the radical can be delocalised throughout the ring system. Density functional theory calculations have shown that the phenoxyl radical possess quinoide character in that the C-O bond length is of apparent double bond character and hence a localised radical.[122] The same is true of the anilino radical,[122] but in the case of the thiyl radical, the C-S bond length would suggest only single bond character.[123] Table 5 gives the bond lengths for X-C_6H_5 radical species, where X = O, NH or S.

	X=O	X=NH	X=S
C1X	1.26	1.34	1.75
C1C2	1.45	1.44	1.39
C2C3	1.38	1.38	1.38
C3C4	1.41	1.41	1.39

Table 5: Bond-lengths (Å) of X-C_6H_5 radicals, where X=O, NH or S.
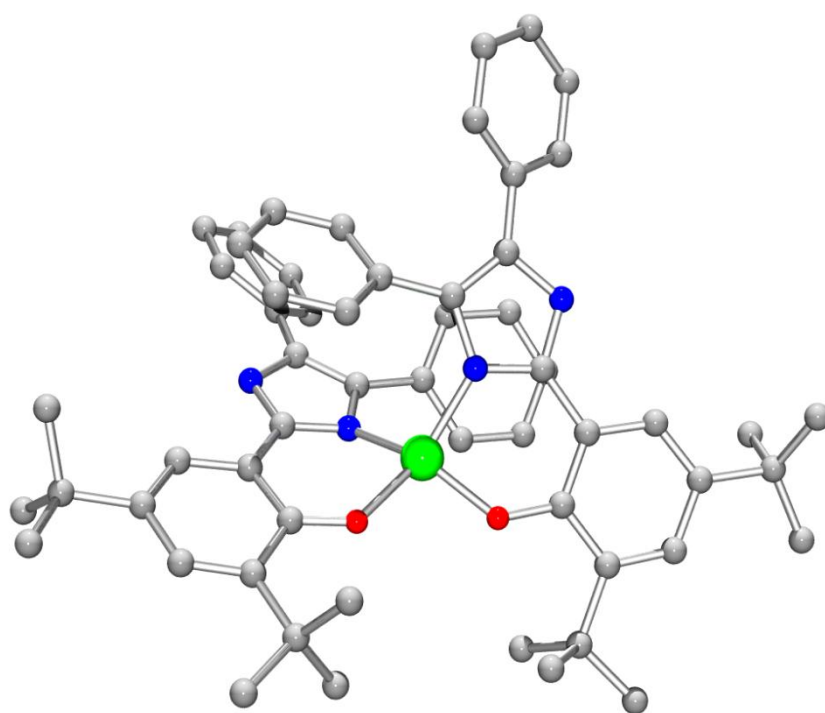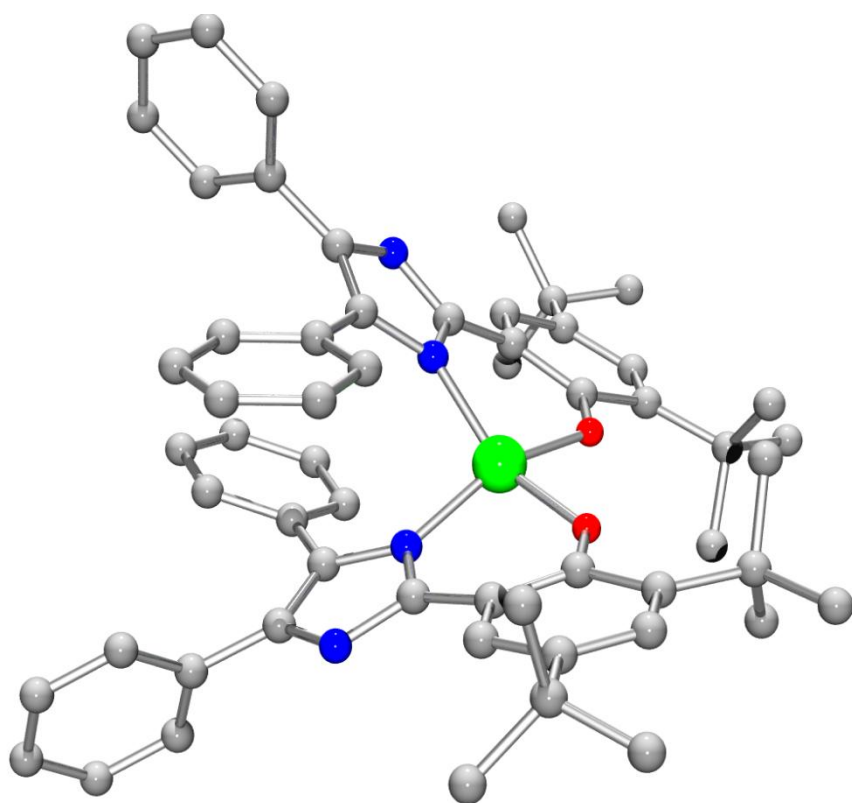
Figure 30: Ball and stick representations of the X-ray crystal structures of two copper complexes prepared by Garner and co-workers.[124]

Only a few examples of the phenoxyl radical have been found in the solid state. Figure 30 shows two crystal structures of copper complexes chelated to two 2-[2'-(4',6'-di-*tert*-butylhydroxyphenyl)]-4,5-diphenylimidazole ligands.[124] Figure 30 shows the ball and stick representations of the copper(II) complexes obtained by reaction of two equivalents of ligand with $Cu(BF_4)_2.H_2O$. The crystal at the top of Figure 30 was grown from a dichloromethane (DCM)-dimethylformamide (DMF) mix. The bottom crystal structure was obtained after oxidation with $Ag[BF_4]$ followed by recrystallisation from DCM-hexane. For the top complex the C-O length is 1.316(2) Å for both ligand units. For the bottom complex, the ligand units are structurally inequivalent- C-O bond lengths were found to be 1.264(5) and 1.322(5) Å. The latter length is in good agreement for one unit existing as a phenolate, but the former suggests that the C-O bond possesses double-bond character as seen in the contraction of the bond length. Therefore the bottom complex consists of both phenolate and phenoxyl radical species.

Phenoxyl radicals are commonplace in nature, being implicated in a number of enzyme active sites where the radical is generated on a tyrosine residue. These are often copper enzymes[125] such as photosystem II[126], ribonucleotide reductase, prostaglandin H synthase and DNA photolyase. Covalent crosslinking of the phenol moiety on the tyrosine residue to another amino acid side chain has also been observed, which leads to the perturbation of its pK_a or redox potential. This is found within galactose oxidase (cysteine side chain)[127] and cytochrome *c* oxidase (histidine side chain). Galactose oxidase is interesting as it oxidises primary alcohols to aldehydes without the need of a redox cofactor present.[128] Oxidation of alcohols occurs through a free radical mechanism, in which the tyrosyl radical, which is directly coordinated to the copper centre, is reduced and oxidised during the catalytic cycle.[129] Formation of the tyrosine-cysteine covalent bond causes a stabilisation of the phenoxyl radical by nearly 0.5 V over the corresponding unsubstituted phenol.[128] The thioether also makes the phenol easier to oxidise, lowering the energy required to generate this species during the catalytic cycle.

Thiyl radicals have also been found in biological systems. They have been found at the active site of all three classes of ribonucleotide reductases (RNR). A cysteine residue located at the active site is converted to the thiyl radical, which is believed to

initiate substrate turnover by abstracting a hydrogen atom from the ribose ring of the substrate.[130] A cysteine radical is also used to mediate the catalytic cycle of pyruvate formate-lyase (PFL), and is believed to be required for homolytic substrate cleavage. Crystal structures of the enzyme reported by Becker and Kabsch provide evidence for how the enzyme uses the thiyl radical for pyruvate cleavage.[131] The crystal structure was obtained of PFL with its two substrates docked (see Figure 31). This scenario is presumed to be the moment prior to pyruvate cleavage. This structure shows that the pyruvate is aligned for radical attack, in conjunction with confining radical migration.
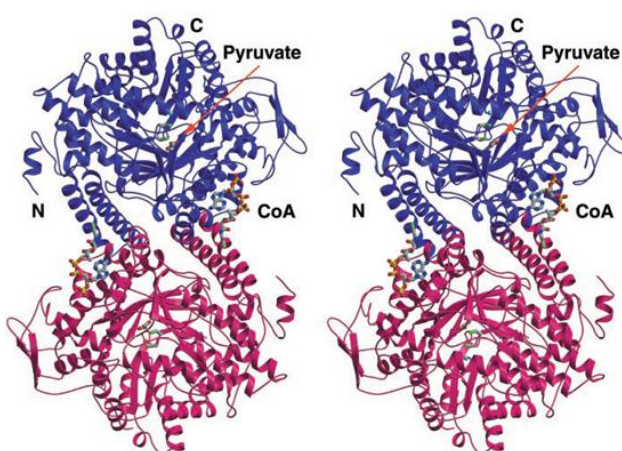
Figure 31: Stereoview of the PFL dimer in complex with pyruvate and CoA.

2.2. Synthesis of di-*tert*-butyl phenol pendent arms

Development of phenolate pendent arms was desirable with respect to the investigation of redox behaviour in conjunction with either transition series or p-block metal ions which are chelated by a macrocycle. They were specifically designed to have a methyl bromide *ortho* to the hydroxyl on the ring system as this could be used to react with an amine and when complexed, a 6-coordinate ring could effectively be formed. In addition, *tert*-butyl groups were used in the other *ortho* position as well as the *para* position to stabilise the radical species once generated. Because of the phenol being acidic, it was decided to produce a range of di-*tert*-butyl-2-hydroxy-benzyl bromide pendent arms of which the phenol was either protected or free. This would enable a suitable coupling strategy to the macrocyclic framework by an S_N2 reaction to be explored whilst also providing several routes to an effective de-protection strategy to be investigated.
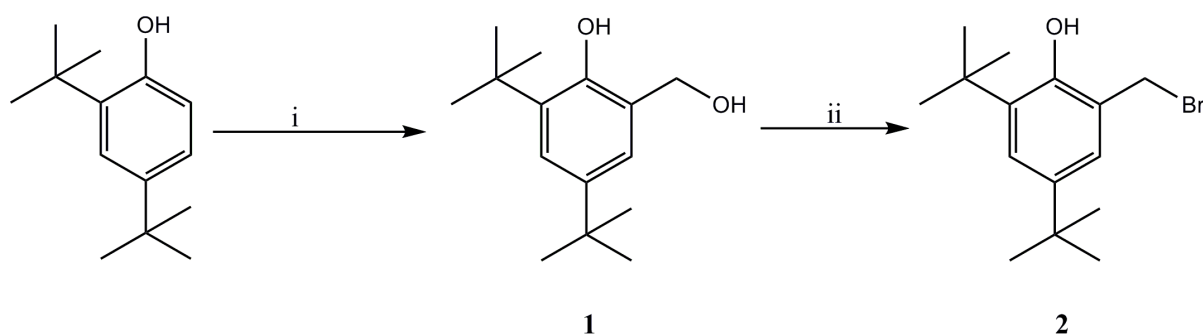
Scheme 2: Synthesis of 2. Conditions; i) paraformaldehyde, LiOH, MeOH, reflux, 24 hr (50%); ii) PBr$_3$, CHCl$_3$, RT, 2 hr (95%).

The first route investigated was the production of the 3,5-di-*tert*-butyl-2-hydroxy benzyl bromide, **2**. The synthesis of the pendent arm (**2**) as shown in Scheme 2 has been published by Wieghardt and co-workers.[132] This route to the un-protected phenol would be advantageous in the latter stages of ligand preparation because there is no need for a further deprotection step. **1** was synthesised from 2,4-di-*tert*-butyl phenol by reacting with paraformaldehyde and LiOH in MeOH for 16 hr at reflux. **1** was isolated from the crude mixture by placing a concentrated hexane solution in a fridge for 3 days after which the crystalline material formed was collected by filtration. **1** was then reacted with PBr$_3$ in CHCl$_3$ at RT to form the viscous oil form of **2**, which solidified when left in a freezer overnight.
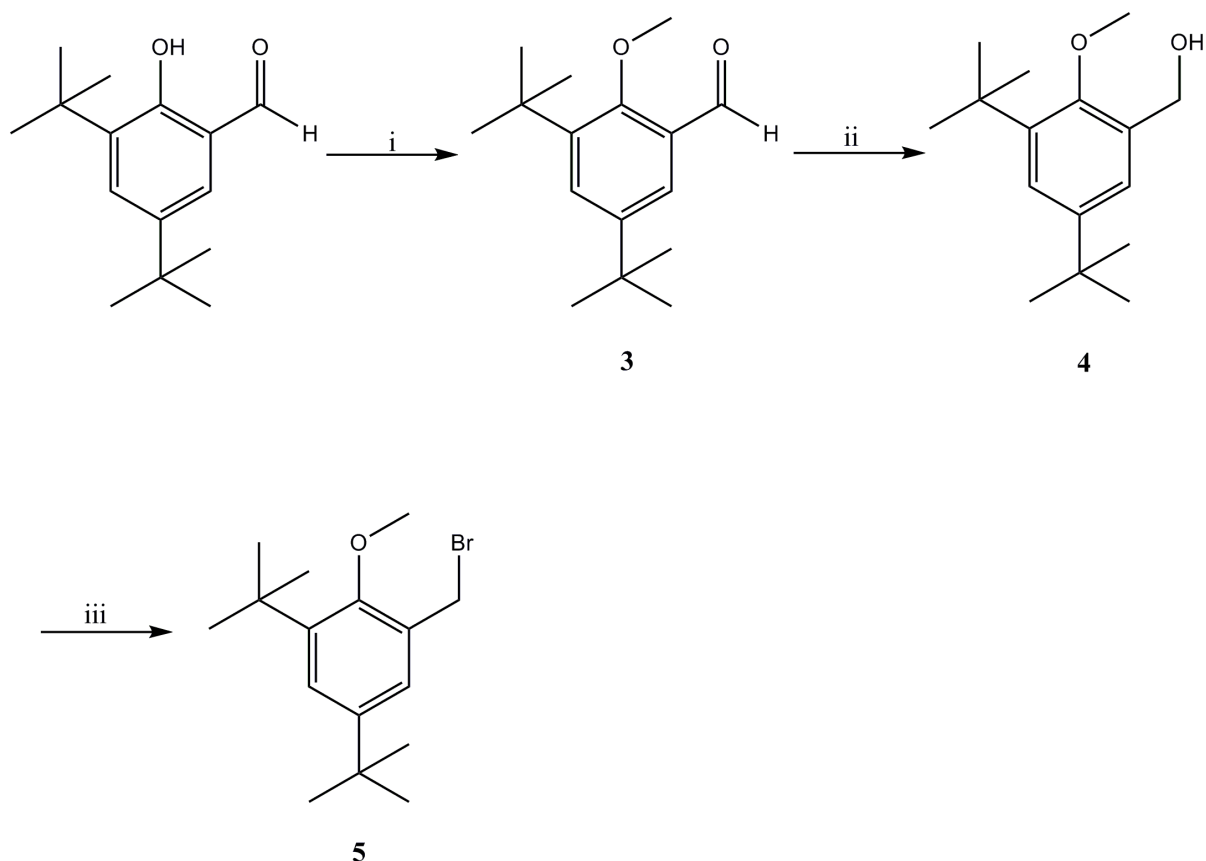
Scheme 3: Synthesis of 5. Conditions; i) MeI, K₂CO₃ acetone, RT, 15 hr (83%); ii) NaBH₄, ethanol, 2.5 hr (100%); iii) PBr₃, CHCl₃, 0°C, 1.5 hr (85%).

Analogues of **2** were now investigated with respect to the introduction of a protecting group for the phenol. This was thought necessary because the phenol is acidic and as such the pendent arm may participate in acid-base reactions as well as nucleophilic substitutions. It was envisaged that a protection-deprotection strategy would be employed, where deprotection would occur once the pendent arm had been appended to the macrocyclic framework. A methyl group was used to produce the first protected phenol pendent arm. The methyl group was introduced on to 2,4-di-*tert*-butyl-2-hydroxy-benzaldehyde using MeI and potassium carbonate. This is shown in Scheme 3. The aldehyde functional group of the molecule is used to form a suitable alkyl halide which can participate in S_N2 reactions involving the macrocycle. This was achieved by firstly reducing the aldehyde using NaBH₄ to form the alcohol. The alcohol was then brominated using PBr₃ in CHCl₃ to give pendent arm **5**.
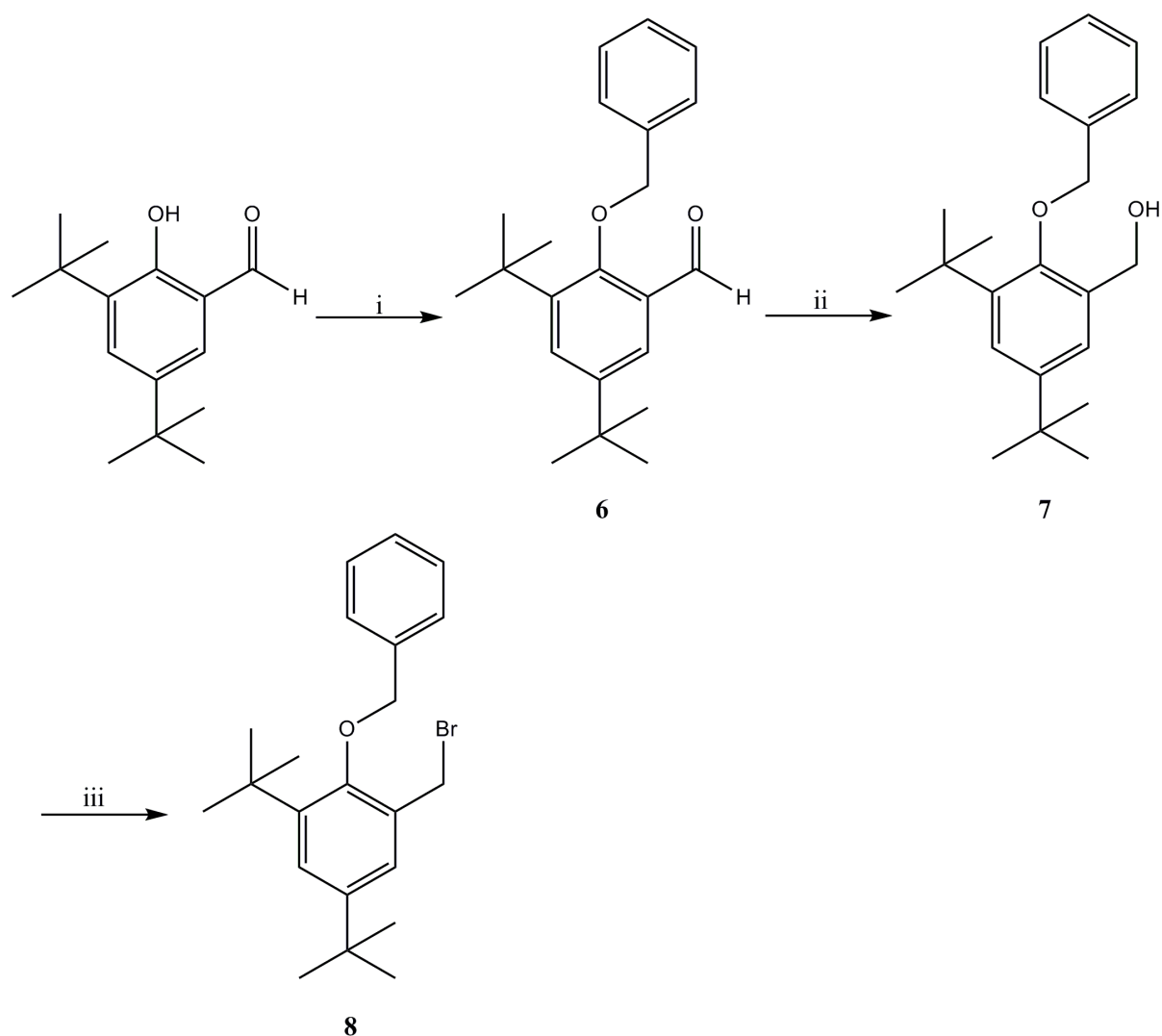
Scheme 4: Synthesis of 8. Conditions; i) benzyl bromide, K₂CO₃, DMF, 75°C, 24 hr (90%); ii) NaBH₄, MeOH, 1 hr, RT (99%); iii) PBr₃, CHCl₃, 0°C, 1 hr (96%).

Having synthesised the methyl protected phenol pendent arm, **5**, further protecting groups for the phenol group were explored. This is because there are limited procedures available for cleaving methyl ethers.[133] In the literature, benzyl protecting groups are used extensively for successful protection-deprotection strategies. There are a large number of ways for deprotecting such groups making them highly versatile. It was because of these reasons that the benzyl group was chosen as a suitable protecting group. Synthetically, the benzyl group was introduced by reaction with 2,4-di-*tert*-butyl-2-hydroxy benzaldehyde in the presence of potassium carbonate using DMF as the solvent. A similar type of reaction had been reported by Counsell and co-workers in the synthesis of di-substituted 1-phenol-2-propanones,[134] and by Belmar and Jiménez for preparing hindered polyanionic chelating ligands.[135]

The desired product was found to precipitate readily when the cooled reaction mixture was poured in to an ice-water mixture, allowing the desired product **6**, to be isolated via filtration. Crystals of **6** were grown from hexane by evaporation; the structure elucidated is shown in Figure 32.
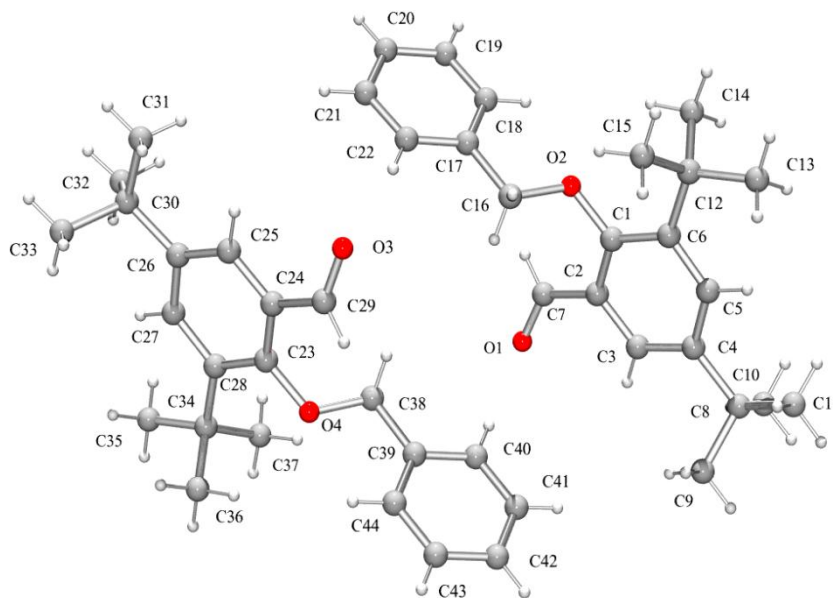
Figure 32: Ball and stick representation of the X-ray crystal structure of 6 with all non-H atoms labelled.

The asymmetric unit of **6** consists of two molecules, rotated through by 180° relative to each other. The benzene rings in each molecule are rotated perpendicular to one another. This is extended to the asymmetric unit where benzene rings opposite each other are again found to be in a perpendicular arrangement.

A similar procedure to the formation of **5** was then used to reduce the aldehyde to form the alcohol which was then brominated using PBr_3 to give **7**.
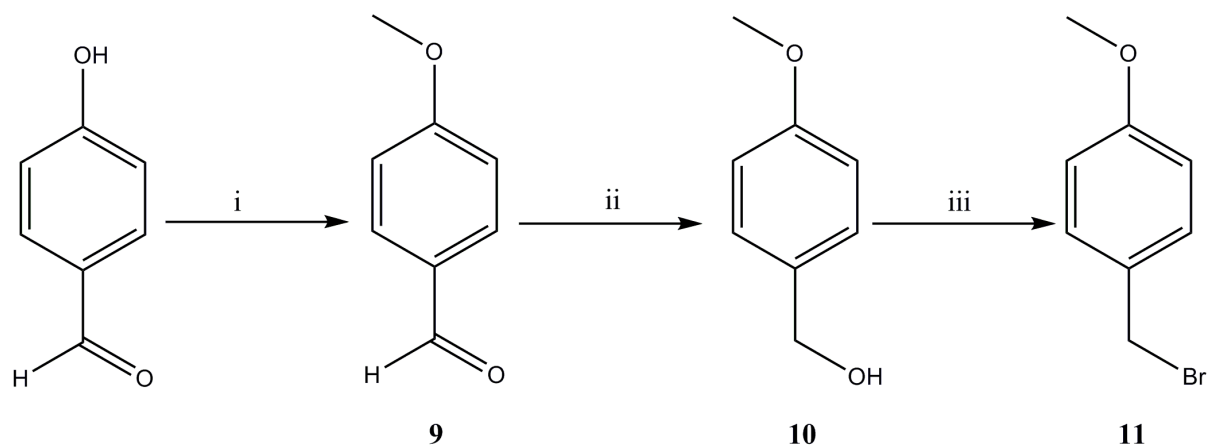
Scheme 5: Synthesis of 11. Conditions; i) MeI, K₂CO₃, acetone, 50°C, 24 hr (100%); ii) NaBH₄, isopropan-2-ol, RT, 4 hr (84%); iii) PBr₃, CHCl₃, 0°C, 1 hr (96%).

The benzyl protecting group can be chemically modified to make deprotection more facile. By introducing a *p*-OMe group, the para position becomes activated towards electrophilic attack. The conditions needed to cleave the protecting group therefore become less harsh than the corresponding benzyl group. This protecting group was synthesised according to Scheme 5.

68
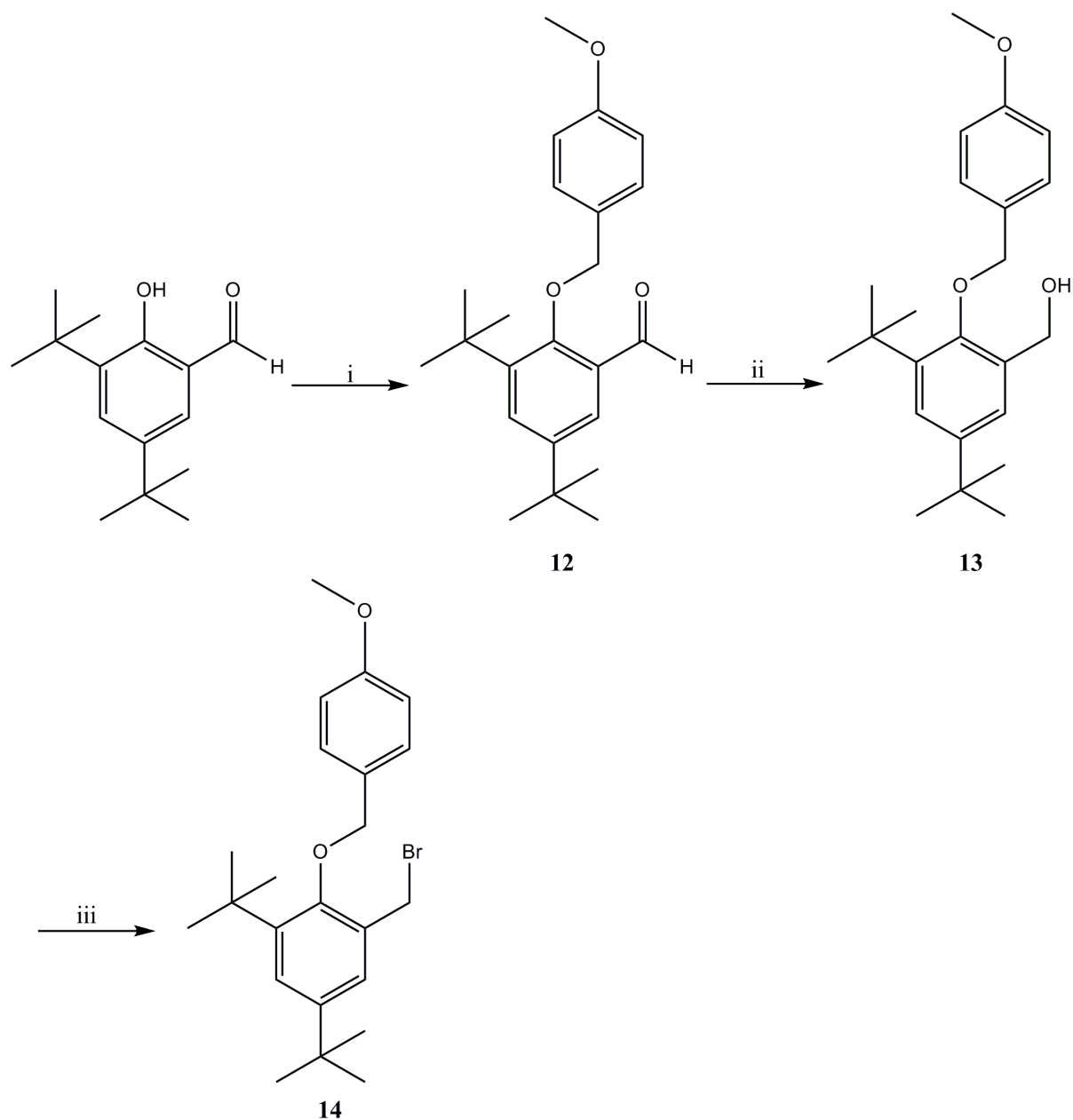
Scheme 6: Synthesis of 14. Conditions; i) 11, K₂CO₃, DMF, 55°C, 24 hr (70%); ii) NaBH₄, ethanol, RT, 3 hr (81%); iii) CBr₄, PPh₃, DCM, RT, 18 hr (68%).

The synthesis of **14** was analogous to the synthesis of **8** apart from the ultimate step where the alcohol is brominated to form the bromide. Considering the literature precedence for *p*-methoxybenzyl cleavage in acidic conditions, bromination using PBr$_3$ was avoided in this case. This is because during bromination using PBr$_3$ small amounts of HBr are formed as a by-product to the reaction. An alternative brominating agent was therefore required. Carbon tetrabromide in conjunction with PPh$_3$ provided such an alternative, producing the desired bromide in 68% yield after column chromatography.
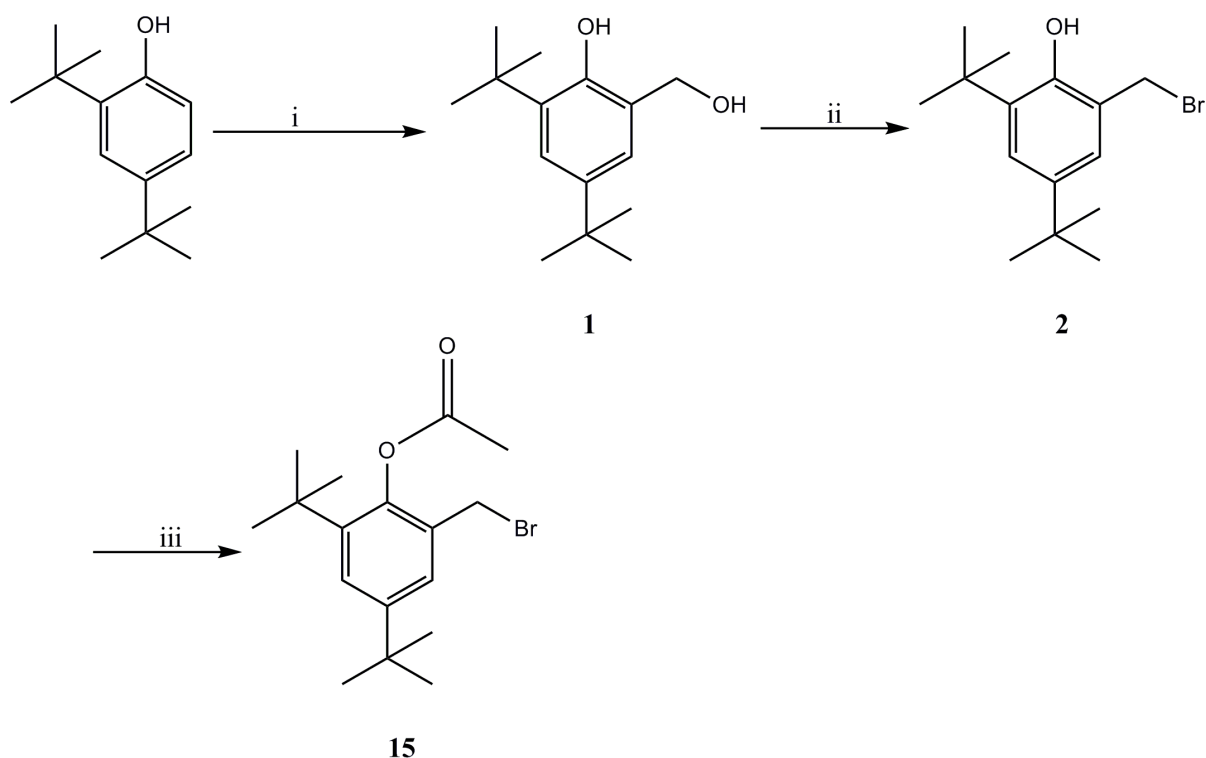
Scheme 7: Synthesis of 15. Conditions; i) paraformaldehyde, LiOH, MeOH, reflux, 24 hr (50%); ii) PBr₃, CHCl₃, RT, 2 hr (95%); iii) acetic anhydride, H₂SO₄ (cat.), RT, 12 hr (100%).

So far, the phenol has been protected using an ether linkage. To extend the library of protected phenol ligands, esters were investigated as a means for protection. Scheme 7 shows the formation of the acetyl protected phenol, **15**. Initial attempts at the formation of an ester to protect the phenol utilised a dimethylamino-pyridine (DMAP) coupling between 2,4,-di-*tert*-butyl-2-hydroxy benzaldehyde and Boc₂O.[136] The reaction was judged complete after 3 hr by TLC (R_f of 0.32 in 5% EtOAc/hexane compared with 0.59 for the starting material). Although this compound was isolated, the reduction of the aldehyde using NaBH₄ accomplished the desired reduction but unfortunately also reduced the ester, reforming the phenol. An alternative reaction pathway to the desired acetyl protected di-*tert*-butyl compound was therefore sought. Wieghardt and co-workers have performed a similar form of protection in protecting 6-*tert*-butyl-*o*-cresol as the acetyl ester using acetic anhydride and H₂SO₄ as a catalyst.[137] Using the conditions these authors reported, compound **2** was reacted with acetic anhydride in the presence of H₂SO₄ as a catalyst at RT. This proved to be a highly efficient way of protecting the phenol, as

after an aqueous work-up **15** was obtained in >95% yield. Crystals of **15** suitable for X-ray crystallography were grown by evaporation of a toluene solution. The structure of **15** is shown in Figure 33.
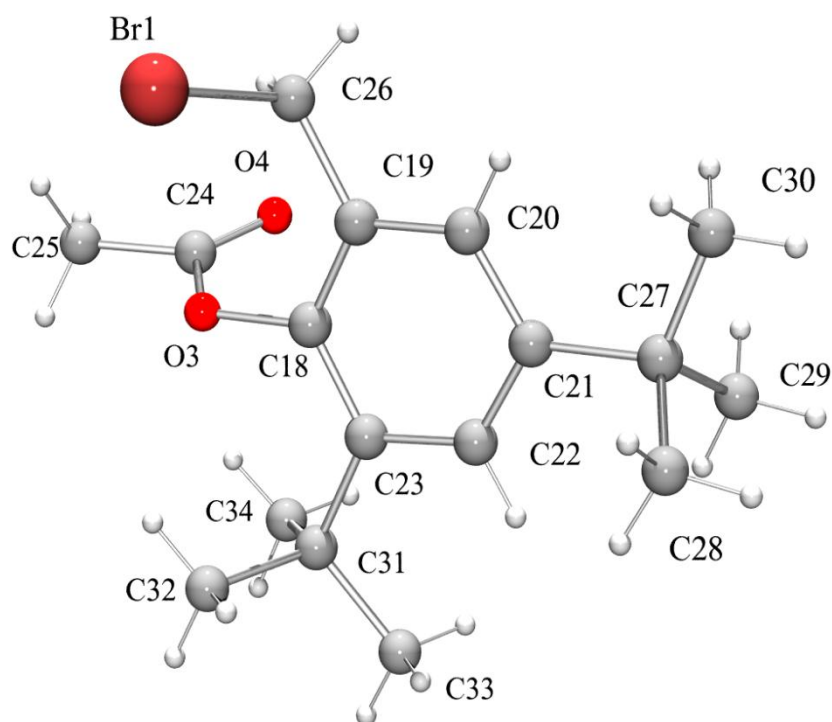
Figure 33: Ball and stick representation of the X-ray crystal structure of 15 with all non-H atoms labelled.

Having established a small library of protected phenolic pendent arms, attention turned to other protecting groups which may be of interest. Extension of the library focused on producing further protecting groups which either utilised one of the existing linkages (ether or ester) or using a previously unexplored one. Despite laborious attempts at synthesis and work-up, none of these groups could be successfully introduced at the phenolic position. These groups will now be discussed and reasons as to why they were not appropriate to be used to protect the phenol highlighted.

Three further ether protecting groups were explored; 3,4-di-hydro-2H-pyrane (THP), bromoacetonitrile and methoxymethyl chloride. THP is well documented in the

literature as being a versatile protecting group for both alcohols and phenols. Because of its lack of selectivity, the reaction between THP and the phenol was only attempted with di-*tert*-butyl-2-hydroxy-benzaldehye and **2**. This ether formation was first investigated using pyridinium *p*-toluenesulfonate (PPTS) as a weak acid to catalyse the reaction.[138] PPTS was freshly prepared by reacting *p*-toluenesulfonic acid monohydrate with pyridine for 20 min at RT. Reaction of THP with **2** using PPTS as a catalyst led to formation of a complex mixture (four spots noticeable on a TLC plate using 5% EtOAc/hexane as an eluent). Reaction of THP with di-*tert*-butyl-2-hydroxy-benzaldehyde resulted in no appreciable product formation. Using copper sulphate pentahydrate, another reported catalyst for tetrahydropyranylation,[139] again no reaction was observed. From both attempts it became apparent that the hydrogen bonding existing between the phenol and the aldehyde at the *ortho* position renders the phenol unavailable for reaction when using an acidic catalyst.

Bromoacetonitrile has been reported as being a robust protecting group as it is reported to be cleaved using a platinum oxide catalyst in a hydrogen atmosphere.[140] Methoxymethyl chloride (MOMCl), was also a suitable candidate, given the ease with which it can be cleaved.[133] Both of these reagents were used in an attempt to form the phenolic ether; they were used in the presence of potassium carbonate and the experiment conducted in either acetone or neat (as in the case for MOMCl). However from the TLC and NMR data collected from these experiments it was apparent that the desired reactions had not occurred.

The sulfonate ester was selected as an alternative protection group which was worthy of study. Two attempts were made at forming the sulfonate ester using either **1** or di-*tert*-butyl-2-hydroxy-benzaldehyde. The reaction of **1** with one equivalent of tosyl chloride resulted in the formation of a mixture. This mixture could not be separated successfully to obtain the desired sulfonate ester. Because of the difficulty in separation, di-*tert*-butyl-2-hydroxy-benzaldehyde presented itself as a better candidate as it only has one hydroxyl group available for reaction. Monitoring this reaction over the course of a week by TLC gave no evidence for the formation of the sulfonate ester. This would seem to suggest that the because of the size of the tosylate group, steric considerations around the phenolic site prevent the formation

of the sulfonate ester. To add further weight to this hypothesis, mesyl was also used in an attempt to protect the phenol. Under similar conditions, TLC again gave no evidence for the formation of the ester. Given the difference in hydrocarbon substituent of the sulfonyl chloride (either toluene or methyl), both sets of experiments would suggest that the steric hindrance originates in the sulfonyl group.

The syntheses of di-*tert*-butyl phenols either masked or unmasked with a methyl bromide in the *ortho* position were attempted. A series of protecting groups have been investigated for their suitability to mask the phenol. Four groups were found to be suited to this role; methyl, benzyl, *p*-methoxybenzyl and acetyl. These four protected species as well as the unmasked phenol analogue can be used to construct macrocyclic species bearing pendent arms. This is reported in Chapters 3 and 4. In these chapters, the redox chemistry of the metal complexes is explored.

2.3. Thiophenol pendent arm synthesis

Production of sulphur analogues of the phenolic systems was also of interest. The reason for this was two fold; firstly that the 2,4,6-tri-*tert*-butyl thiylphenyl radical is not stable when compared with the corresponding phenoxyl radical (half-life of 2.5 min in benzene at 30°C), and also has the propensity to form di-sulphide bonds.[141] This contrasts nicely with the robust nature of the phenoxyl radical. Secondly, sulphur is soft in nature whereas oxygen is hard, therefore providing a means by which analogous complexes can be compared with regard to their coordination preferences.
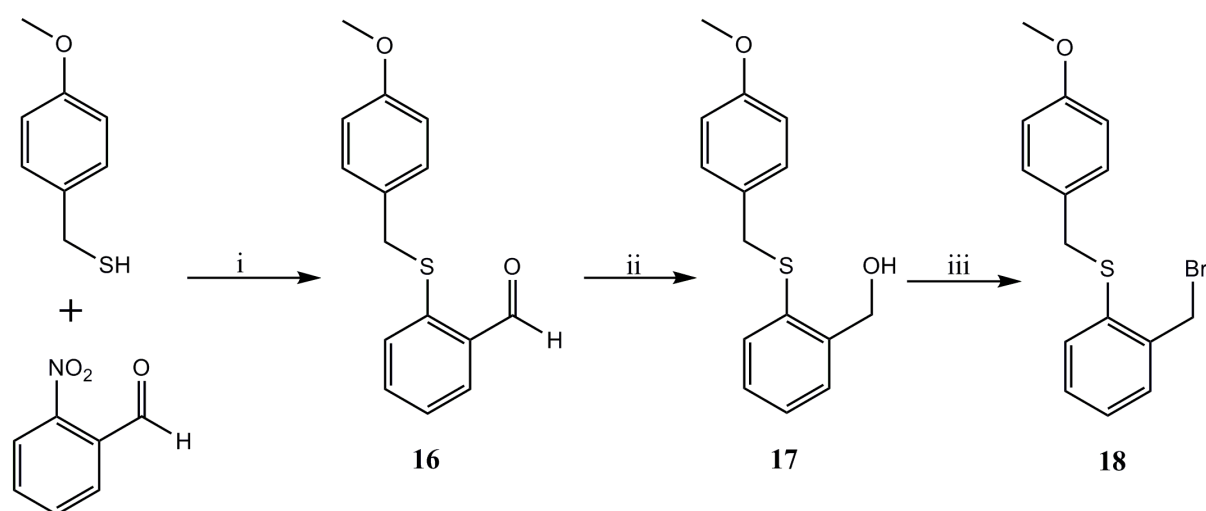
Scheme 8: Synthesis of 18. Conditions; i) K$_2$CO$_3$, DMF, 80°C, 24 hr (89%); ii) NaBH$_4$, propan-2-ol, RT, 1 hr (88%); iii) PBr$_3$, CHCl$_3$, −5°C, 1 hr (68%).

The synthesis of **18** has been reported in the literature to produce triazacyclononane (TACN) metal complexes to study their redox properties.[142] Electrophilic attack by the thiol on the aromatic ring displaces the nitro group as nitrite, leading to the formation of **16**. Crystals isolated from this reaction were suitable for X-ray crystallography. Figure 34 shows the structure of **16** obtained after refinement. Figure 35 shows the packing of **16** within the unit cell.
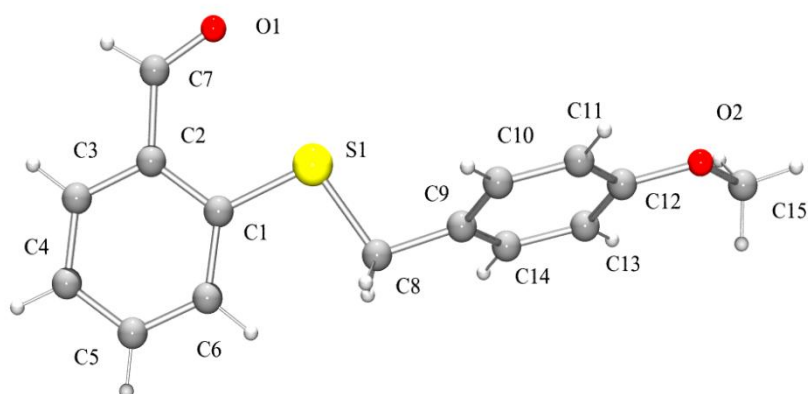
Figure 34: Ball and stick representation of the X-ray crystal structure of 16 with all non-H atoms labelled.
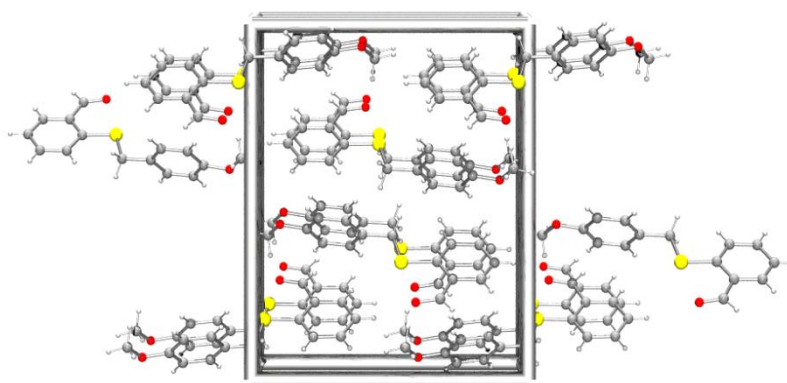
Figure 35: Ball stick representation of the X-ray crystallographic unit cell contents of 16 with H atoms omitted.

17 was synthesised from **16** by reducing the aldehyde with $NaBH_4$ in iso-propanol. Crystals were obtained by evaporation of a toluene solution from which the structure could be elucidated by X-ray analysis. The structure of **17** is shown in Figure 36.
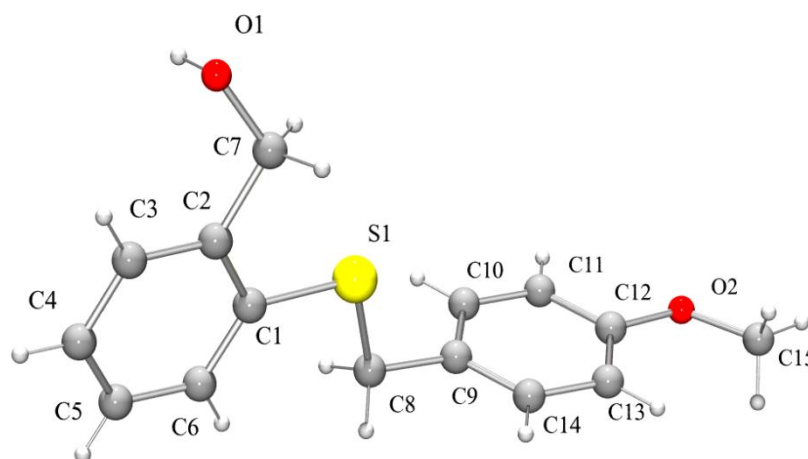
The unit cell of **17** (Figure 37) shows that the molecules are aligned in a co-linear fashion. The distance between phenyl rings is however too large for π-π stacking interactions. However, H-bonding does exist between neighbouring alcohol groups. This is shown in Figure 38. The hydrogen bonding is arranged in a zig-zag fashion between adjacent repeating units. Table 6 shows the hydrogen bond parameters between donor and acceptor atoms in **17**.
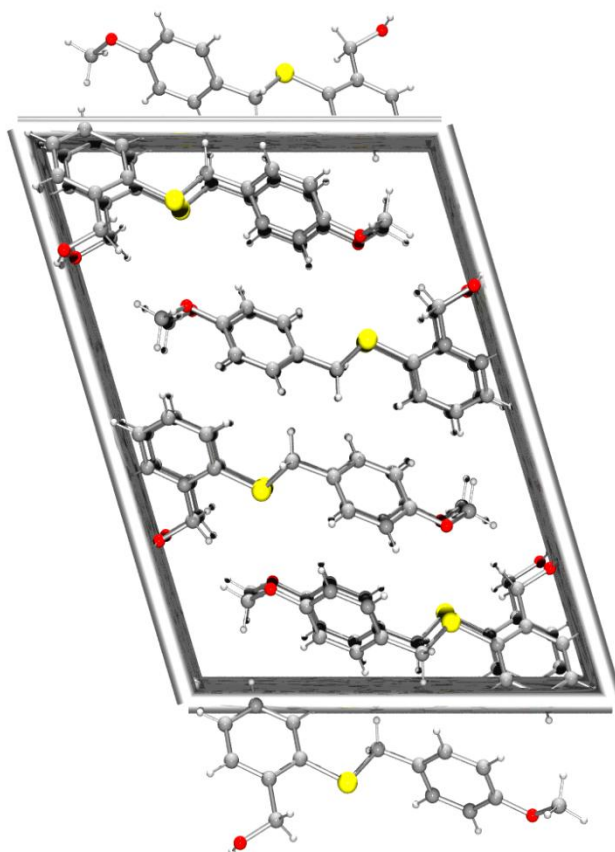
Figure 37: Ball and stick representation of the X-ray crystallographic unit cell contents of 17 with H atoms omitted.
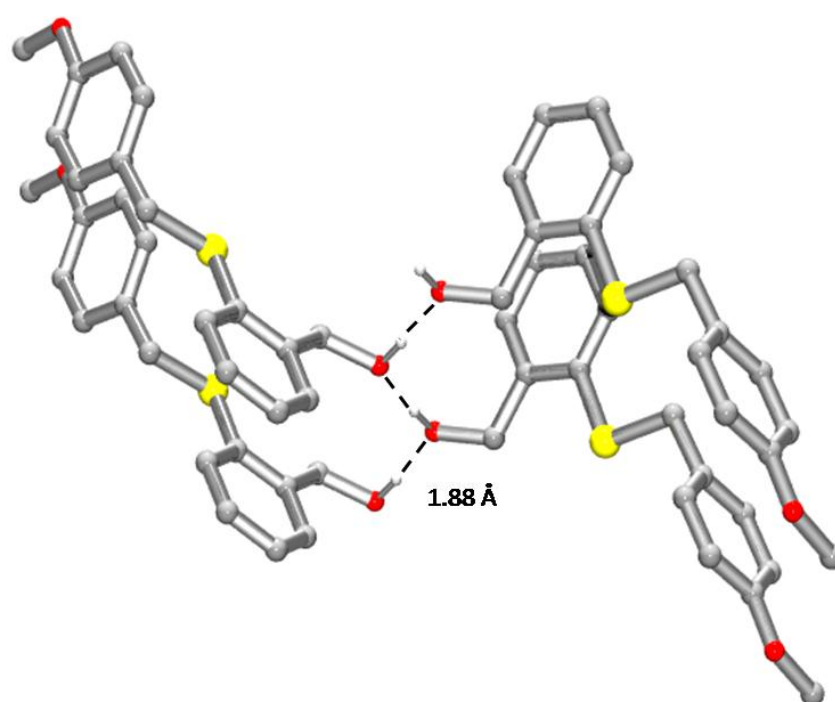
Figure 38: Ball and stick representation of the X-ray crystal structure of 17 showing H-bonding existing between equivalent molecules. A symmetry transformation of -x, y-½, -z+½ was used to generate equivalent atoms.

D-H...A	D(D-H) (Å)	D(H…A) (Å)	d(D…A) (Å)	<(DHA) (°)
O(1)-H(1)…O(1)#1	0.89(2)	1.88(2)	2.7657(10)	174(2)

Table 6: Hydrogen bond parameters for compound 17.

The final step in the preparation of the pendent arm **18**, involved the bromination of the alcohol. The reported procedure for this step was followed, but the product obtained wasn't pure as analysed by NMR. It was believed that the protecting group is slightly acid sensitive and therefore a complex mixture of **18** and the products obtained from cleavage of the thio ether was obtained. The susceptibility of the thio ether to cleavage is not discussed in the original paper and so no purification method was given. After many attempts at recrystallisation, the best method for purification was found to be layering hexane over the oil and allowing it to stand in a freezer overnight. Methanol was then added, and the mixture sonicated at which point a

white solid precipitated. The white precipitate formed by this process was isolated by filtration, and was shown by NMR to be the desired product, **18**.
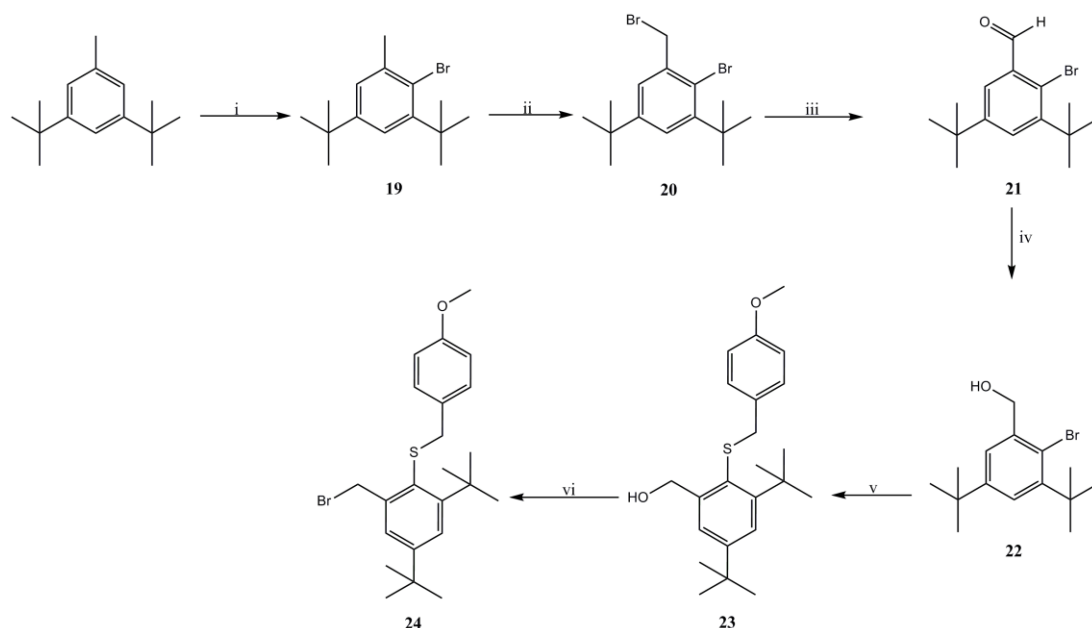
Scheme 9: Synthesis of 24. Conditions; i) trimethylphosphate, Br$_2$, 65 - 70°C, 40 hr (65%); ii) NBS, CCl$_4$, reflux, 1 hr (65%); iii) hexamethylenetetramine, CHCl$_3$, acetic acid, 75°C for 24 hr and then 102°C for 24 hr (30%); iv) NaBH$_4$, propan-2-ol, RT, 2 hr (86%); v) BuLi, thiosulfonic acid S-(4-methoxybenzyl) ester, Et$_2$O, −75°C to −30°C, 5 hr (47%); vi) PBr$_3$, CHCl$_3$,−0°C 1.5 hr (64%).

Focus was then directed to the synthesis of a thiophenolate pendent arm which possessed *tert*-butyl groups for stabilisation of the thiyl radical. Wieghardt and co-workers have reported the synthesis of a thiophenolate which has *tert*-butyl groups in both meta positions[143] or in just one[144], but it was thought prudent to produce pendent arms with the *tert*-butyl groups in the *ortho* and *para* positions which would then be isostructural with the phenol analogues once deprotected. In having a *tert*-butyl group in the *para* position, the propensity of the thiyl radical to form disulfide bonds would also be lowered. This is because the steric bulk surrounding the thiol would inhibit thio radicals reacting with each other to form a disulfide bond. The synthesis of such a compound is shown in Scheme 9, where **24** is the sulphur analogue of **14**. The first step in the preparation of **24** involved the bromination of the aromatic ring, which Wieghardt and co workers reported as being effected using bromine and an iron support in carbon tetrachloride.[142] This step proved difficult to

reproduce despite using very pure bromine (99.999%). A literature search revealed that another route existed for this bromination using the same starting material (2,4-di-*tert*-butyl toluene). Voβ and Edler reported that by using trimethylphosphate and bromine, **19** was isolated after distillation in 65% yield.[145] By using these conditions, **19** was successfully obtained with a yield in direct agreement with the literature. Furthermore, the oil obtained crystallises at RT if left for a week. These crystals were suitable for X-ray diffraction and from the refinement of the X-ray data the structure of **19** was obtained as shown in Figure 39.
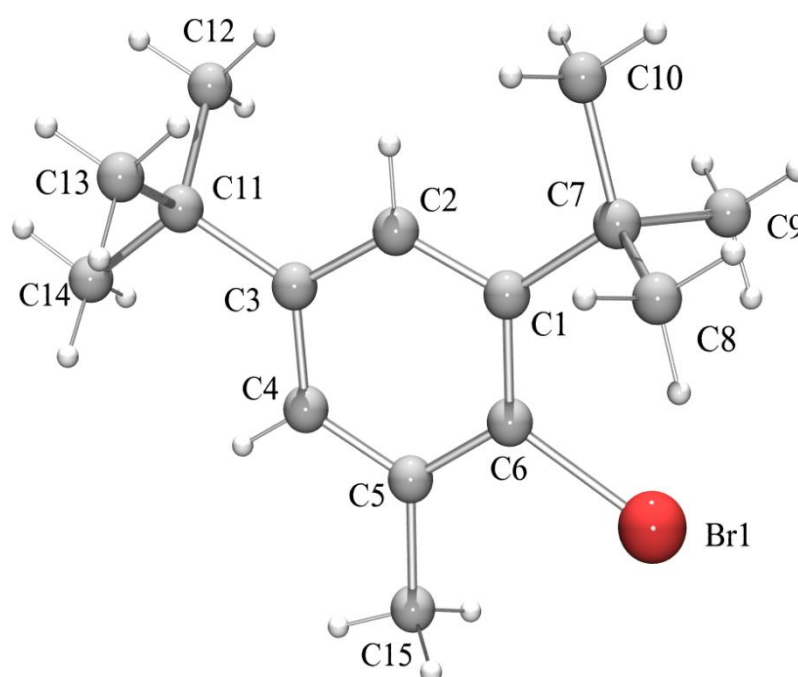
Figure 39: Ball and stick representation of the X-ray crystal structure of 19 with all non-H atoms labelled.

In the next step, the methyl group was brominated using N-bromo succinimide (NBS) in CCl_4. This allowed a Duff type reaction to be used to form the aldehyde. After purification using silica gel chromatography, compound **21** was isolated in 30% yield. Reduction of the aldehyde in the presence of $NaBH_4$ was then carried out, enabling the formation of the lithium salt of **22** by reaction with n-BuLi. The introduction of the sulphur containing moiety via reaction of the lithium salt with toluene-4-thiosulfonic acid S-(4-methoxybenzyl)[146,147] was then performed. This was followed by purification via silica gel chromatography enabling the thio ether, **23**, to

be isolated. From the purification process, the unreacted toluene-4-thiosulfonic acid S-(4-methoxybenzyl) was isolated. Crystals of this material were grown using a hexane/toluene mix. Transparent crystals formed after allowing the mixture to evaporate for 3 days at RT. These crystals were suitable for X-ray analysis, enabling the crystal structure to be obtained. This is shown in Figure 40.
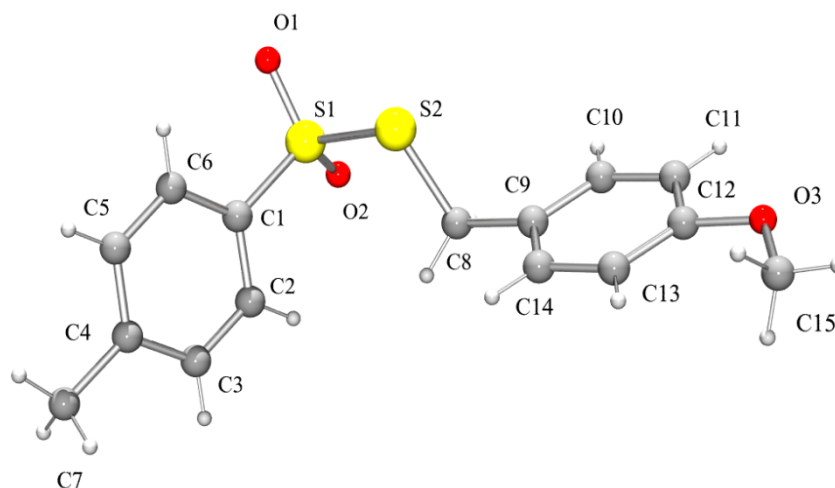
Figure 40: Ball and stick representation of the X-ray crystal structure of toluene-4-thiosulfonic acid S-(4-methoxybenzyl) with all non-H atoms labelled.

The *S*-(4-methoxybenzyl)ester could have been introduced to compound **19**, the methyl group thereby offering a potential site for further functionalisation,[148] such as brominating the methyl group in the same way as **20**.[142] However, with **23** in hand, this was reacted with PBr_3 to give the desired alkyl bromide, which was purified by silica gel column chromatography. The literature stated that this purification was only performed for analytical measurements, although in following this method, purification was found to be required as a substantial amount of by-product was formed. The by-product was believed to be due to the acid cleavage of the thioether, in exactly the same manner as was observed for **18**. Clearly the use of a brominating agent which forms a strong acid is not suitable when preparing these thioether compounds.

The two protected thiol compounds, **24** and **18**, were appended to tetraaza-macrocyclic compounds which are discussed in Chapters 3 and 4. They were then used in a comparative study alongside the phenol analogues already discussed.

2.4. Amino acid derived pendent arm synthesis

Pendent arms which incorporate a reactive group for tethering to the macrocyclic ring as well as providing additional functional groups for coordination to the metal centre and as a point of attachment for further moieties to be chemically joined to the framework are very desirable. Essentially these pendent arms fulfil the role of a pendent arm and linker group. Amino acids have been investigated for this role, as the wide range of side chains affords versatility. The aim of this research was to construct an amino acid capable of providing three functional groups; one for attaching the amino acid derivative to the macrocyclic, a second for acting as a donor group and a third for the attachment of further molecules to the metal complex.

25 (R=CH$_2$COOBn)
26 (R=CH$_2$-pNO$_2$Ph)

27 (R=CH$_2$COOBn)
28 (R=CH$_2$-pNO$_2$Ph)
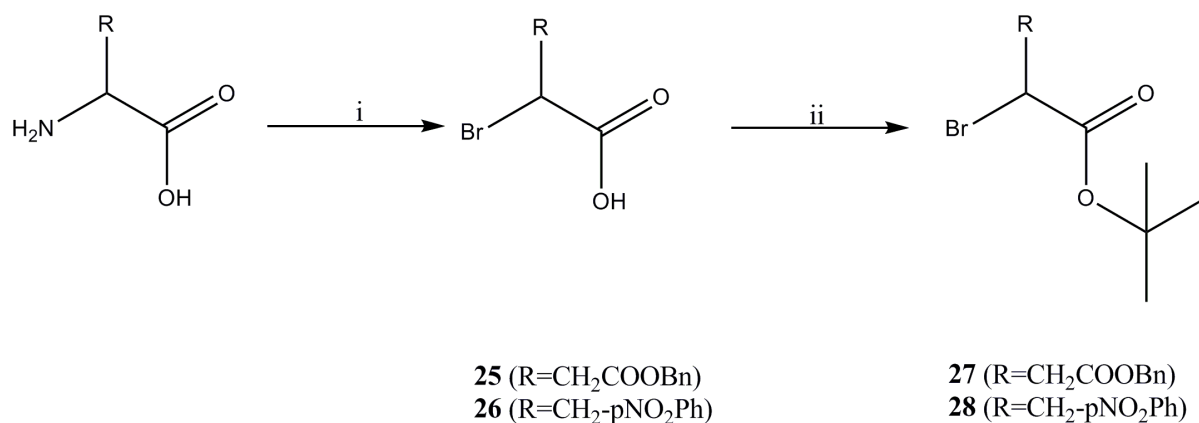
Scheme 10: Synthesis of 25-28. Conditions; i) NaBr, 1 N HBr, NaNO$_2$, H$_2$O, 0°C, 2 hr (25 = 50%, 26 = 86%); ii) TBTA, BF$_3$.OEt$_2$, cyclohexane, DMA, RT, 5 d (27 = 77%, 28 = 41%).

Aspartic acid and 4-nitro-L-phenylalanine were selected as potential amino acids which could then be manipulated to form pendent arms capable of coordinating to a metal centre and also possessing a functional group which can be used as a chemical linker. The amino group of the parent amino acid can be converted to the corresponding secondary bromide by formation of a diazonium salt in the presence of a bromide source. This secondary bromide could then act as the point at which it can be appended to the macrocyclic backbone. A route in which the glutamic and aspartic amino acids have been manipulated in a similar fashion has been published.[149] The respective γ and β benzyl esters of glutamic and aspartic acid can be purchased (Sigma), meaning that the other carboxylic acid can be protected with a different protecting group. The protection of molecules utilising two different

chemical protecting groups which are labile under different conditions are highly desirable, enabling each prospective site to be reacted individually. Another route which utilises an amino acid with two chemically different protecting groups has been reported by Yoo and Pagel.[84] Two routes are presented in this paper to the preparation of α-brominated glycine templates attached to a DO3A backbone. The attachment of the α-brominated glycine templates to DO3A was accomplished in high yield (90% or greater).

The route used in this work to produce such a di-protected amino acid is outlined in Scheme 10. The primary amine was firstly converted to the bromide via an S_N2 reaction of the diazonium salt in the presence of a bromide ion. After column chromatography, both **25** and **26** were isolated in moderate yield. The second step involved the protection of the free carboxylic acid. Use of a *tert*-butyl protecting group, which is acid sensitive, provided a means by which either the benzyl or the *tert*-butyl ester could be selectively deprotected in the latter stages of synthesis when the pendent arm is appended to the macrocycle. Introduction of this *tert*-butyl protecting group was performed under mild conditions using boron trifluoride etherate as a catalyst.[150] Isolation of **27** and **28** was achieved after aqueous extraction to remove any dimethylacetamide (DMA) that remained. Crystals suitable for X-ray crystallography were produced from which the structure of **28** was obtained as shown in Figure 41.
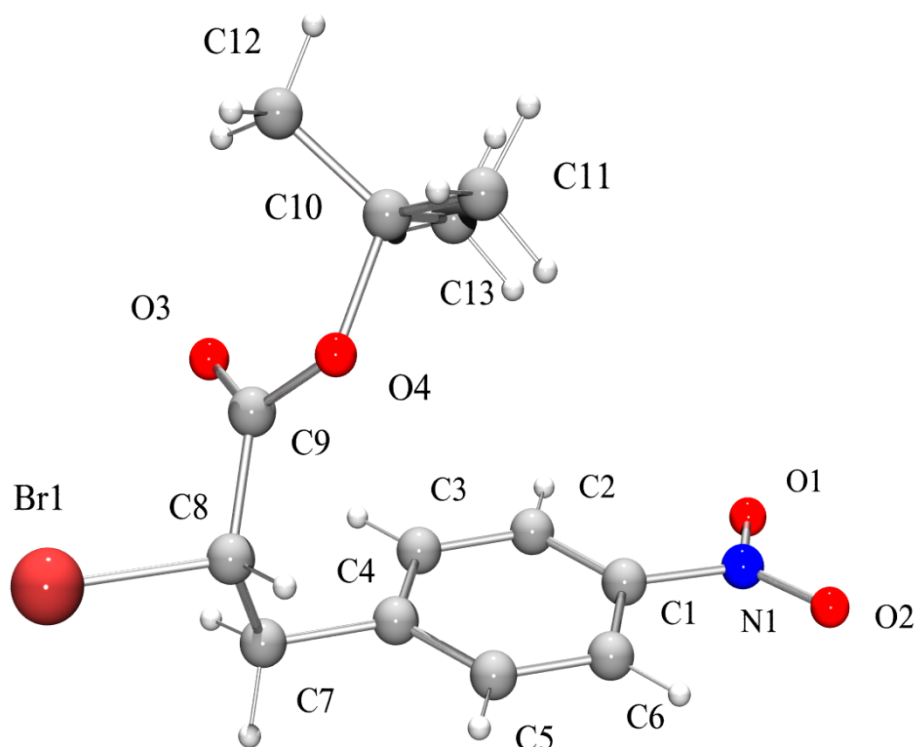
Figure 41: Ball and stick representation of the X-ray crystal structure of 28 with all non-H atoms labelled.

The unit cell of **28** consists of both the R and S forms. This is because two possible reaction mechanisms exist for the S_N2 reaction which occurs at the chiral carbon. A bromide could displace the diazonium ion, which would leave as dinitrogen. This reaction mechanism would cause a Walden inversion at the chiral centre leading to the formation of the R product. The second possible reaction mechanism incurs via internal nucleophilic attack by the carboxylic group, leading to the formation of an epoxide. Again this would lead to the R form being obtained. However, the epoxide ring can then undergo nucleophilic attack by a bromide ion, leading to the epoxide ring breaking. This would result in the S product being formed (as two Walden inversions have occurred at the chiral centre). The presence of both R and S forms in the crystal structure would suggest that both reaction mechanisms are equally as likely. In the unit cell these stereo-isomers are orientated so that π-π stacking is observed. This π-π stacking occurs in a face-to-face arrangement with a ring centre-ring centre distance of around 3.79 Å. This is shown in Figure 42. Data obtained

from optimised structures for the related benzene dimer are in good agreement, reporting this interplane separation distance as 3.8 Å.[151]
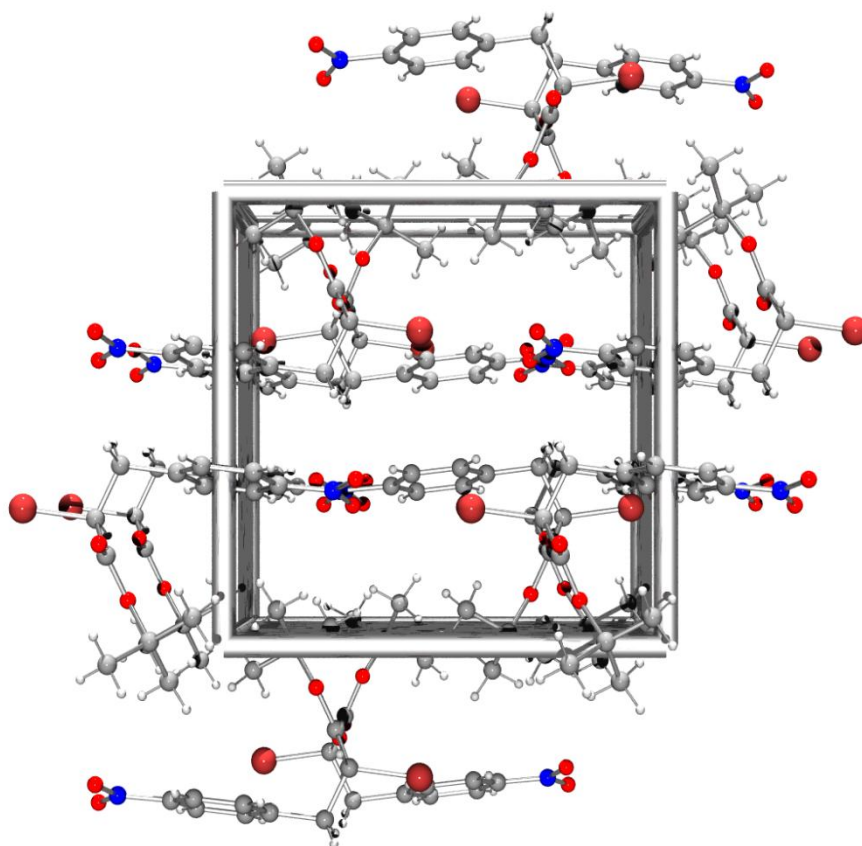
Figure 42: Ball and stick representation of the X-ray crystallographic unit cell contents of 28 with H atoms omitted for clarity. A C$_2$ axis is present which runs through the centre of the cell.

2.5. Polyethylene glycol pendent arm synthesis

Water solubilising pendent arms are useful for macrocyclic systems which are designed towards a biological application but possess hydrophobic properties. Polyethylene glycol (PEG) chains are used for this purpose by increasing water solubility and as such, development of pendent arms of this nature was highly desirable. The synthesis of mono-methoxy capped PEGs was of interest as this gave the possibility of functionalising the remaining hydroxyl group selectively. The length of the PEG chain affects the level of solubilisation and so multiple chain lengths were investigated. These PEG chains were to be used to solubilise porphyrin macrocyclic systems, which are very hydrophobic in nature. Therefore, it was decided to investigate two methoxy capped PEG chains with average molecular weights of 550 and 750 each and triethylene monomethoxy alcohol. The latter could be characterised fully and therefore provided the bench mark for the synthesis and analysis of the two other PEG chains. The synthesis of these PEG chains is outlined in Scheme 11.

29 and **30**

n = 11 (average) for **29** and 15 (average) for **30**

31

n = 2
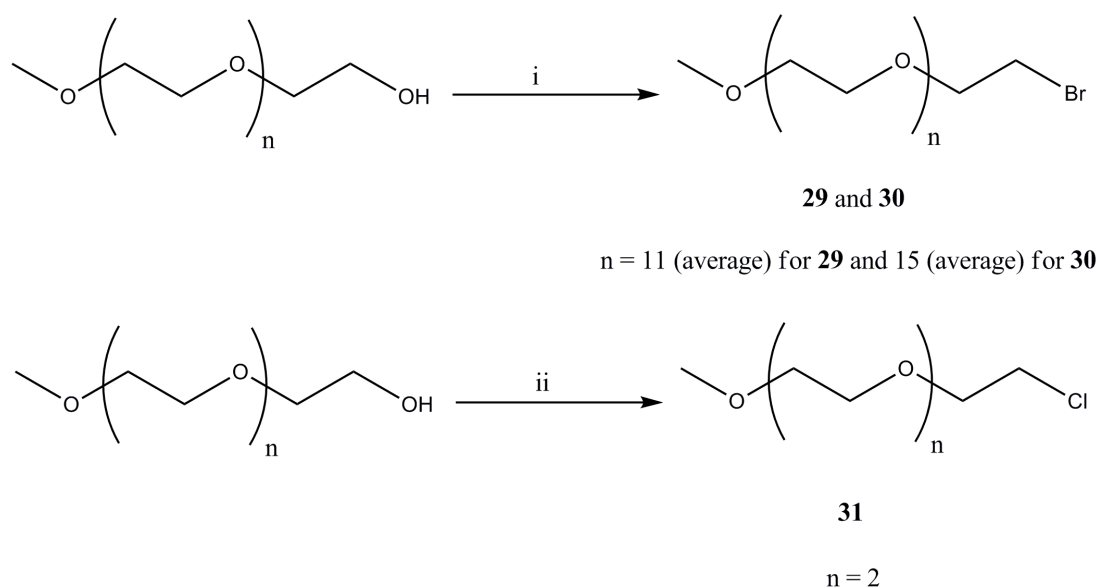
Scheme 11: Synthesis of 29-31. Conditions; i) PBr$_3$, DCM, 0°C, 1.5 hr (40-76%); ii) SOCl$_2$, pyridine, reflux, 3 hr (89%).

The synthesis of these PEG chains was convenient given the fact that the mono-methoxy derivatives could be purchased from Sigma. The alcohol could then be functionalised selectively given the robust nature of the methoxy group (with little

concern for cleaving the methyl ether). PEG chains **29** and **30** were synthesised by reaction with PBr$_3$ followed by an extensive extraction of the aqueous layer to enable full recovery of the product. However, this procedure was not compatible for brominating the alcohol of the triethylene monomethoxy analogue. Because of this, a literature search was performed to investigate other potential routes to producing the alkyl halide. The alcohol was converted to the chloride using thionyl chloride to prepare **31**.[152]

2.6. Conclusion

This chapter has discussed the design and synthesis of primary and secondary alkyl halides which were used as pendent arms in macrocyclic systems. Three different types of pendent arm have been synthesised; redox active pendent arms, amino acid pendent arms and PEG arms. Phenol and thiophenol pendent arms have been synthesised in which the phenol or thiophenol is protected. Phenol pendent arms have been synthesised either as the unmasked phenol or as the methyl, benzyl and *p*-methoxybenzyl ethers or as the acetyl ester. A wide range of deprotection methods can therefore be trialled when coupled to a macrocyclic system. The thiophenol pendent arms were all synthesised as the *p*-methoxybenzyl thioethers. Thiophenol and phenol pendent arms were synthesised with *tert*-butyl groups in the *ortho* and *para* positions. This is to stabilise the radical species once formed by preventing radical coupling.

The amino acid pendent arms were synthesised from 4-nitro-L-phenylalanine and β-benzyl-aspartic acid. Conversion of the amine group to the corresponding secondary bromide formed the tethering point. Both amino acids were synthesised with two other functional groups which can be selectively deprotected to enable a further moiety to be introduced. The remaining donor can be used to coordinate to the metal centre.

The PEG chains were synthesised as either the bromide or chloride derivatives. The triethylene glycol chain, **31**, was synthesised to act as a model for the other two PEG chains which have average molecular weights of 550 (**29**) and 750 (**30**) prior to bromination. These chains possess water solubilising properties which were investigated and are reported in Chapter 5.

3. Synthesis of cyclam derivatives with *N*-appended phenolates or thiophenolates

3.1. Introduction

This chapter reports the synthesis and characterisation of side-bridged cyclam (Figure 43) macrocyclic frameworks with pendent thiophenolate and phenolate arms. Side-bridged cyclam is a laterally reinforced macrocycle, in which two amines are linked by an ethyl chain. This gives rise to a piperazine ring, which can adopt four different conformations (similar to cyclohexane). Of the four conformations (chair, half-boat, boat and twist), the chair is the most stable.[51] Pendent arms can be appended to the macrocyclic ring through the nitrogen atoms. Previous work on side-bridged cyclam derivatives is limited, with only eleven such compounds found within the literature. Of these eleven compounds, only three possess functional groups in the pendent arm. Carboxylic, nitro and amine groups all provide the additional functionality, and all three have been reported by Archibald and co-workers.[41,54]

3.1.1. Side-bridged cyclam compounds

Yamamoto and Maruoka have reported the formation of the side-bridged cyclam directly from the glyoxal condensate of cyclam.[153] This was achieved through the use of diisobutyl aluminium hydride (DIBAL). An adapted procedure has also been reported by Fabbrizzi *et al.*[154] This compound has two secondary amines which can then be further reacted. However, this does mean that selective mono-alkylation is difficult as both sites are, theoretically, equally reactive. A synthetic protocol that circumvents this problem was published by Koliński in 1995.[155] This paper reported the mono alkylation of a bisaminal species, formed by reaction of glyoxal with cyclam. Cross-bridged cyclam derivatives synthesised using this methodology had been published prior to this by Weisman and Wong.[156] The mono-alkylated bisaminal species can then be reduced to give the side-bridged species. Methyl and benzyl arms were both reported as pendent arms in this asymmetric approach.

Archibald and co-workers have synthesised the copper(II) complexes of side-bridged cyclams bearing either a *tert*-butyl acetate or an acetic acid (HSBTE1A, see Figure 43) pendent arm. The copper(II) ion is five coordinate bound in a distorted square-based pyramidal geometry with considerable distortion towards trigonal bipyramidal (τ parameter of 0.37).[41]

Side-bridged cyclam   HSBTE1A
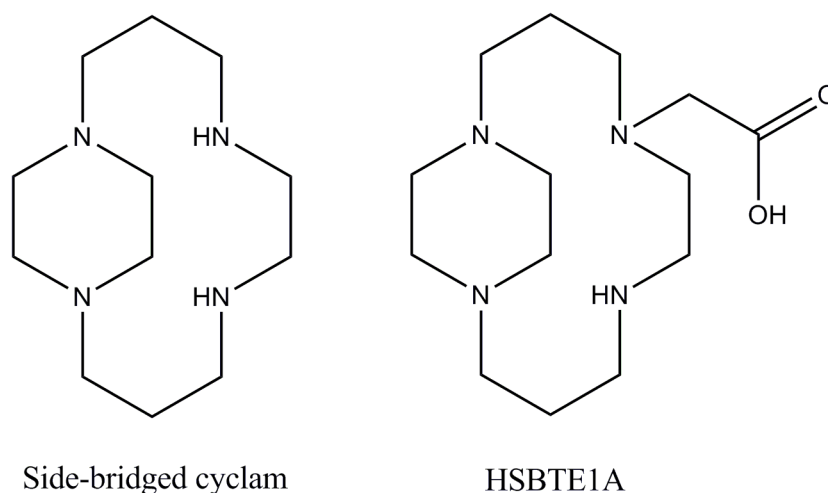
Figure 43: Structures of side-bridged cyclam and HSBTE1A.

Plutnar *et al.* have probed the reaction of mono-alkylated side-bridged cyclams with respect to further alkylation reactions.[157] The compound that they chose to study was one which had been synthesised previously by Archibald and co-workers.[54] Their results, which include X-ray structural data (Figure 44), show that the addition of a carboxylic acid occurs at one of the nitrogens on the piperazine ring and not at the secondary amine.
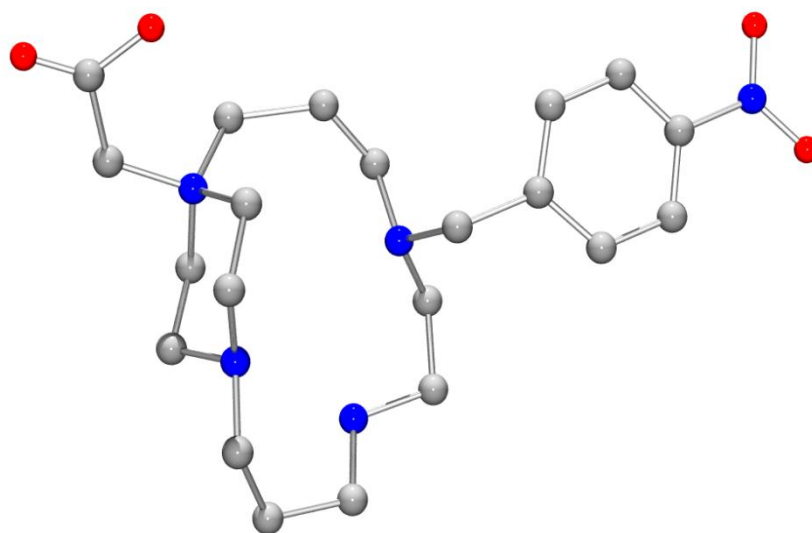
Figure 44: Ball and stick representation of the X-ray crystal structure of a side-bridged cyclam with a *p*-nitrobenzyl arm and an acetate arm. Non H-atoms and a bromide counter ion have been omitted for clarity (Plutnar *et al.*).[157]

3.1.2. Side-bridged cyclen compounds

Similar side-bridged macrocyclic species have been synthesised using cyclen, the [12]aneN$_4$ macrocycle. For this type of configurationally restricted macrocycle there are only three published examples. The synthesis of the side-bridged species first published by Wainwright and co-workers in 1982 was carried out using 1,2-dibromo-ethane.[158] The main product isolated from this process is the mono-side bridged cyclen although the di-bridged species is also formed in small quantities. Further examples have been published by Handel and co-workers.[159] Two side-bridged cyclens are attached together by a xylene ring, with the macrocycle units being tethered through either the 1,2, 1,3 or 1,4 positions. Another derivative, whereby the central linker is exchanged for a pyridyl group is also detailed in the same paper by Handel. The macrocyclic units are attached to this central unit in the *ortho* positions.

3.1.3. Examples of known phenolate complexes

Kimura and co-workers have published the crystal structure of a phenol containing cyclam ligand as well as its copper complex. The ligand was synthesised from coumarin and the corresponding tetraamine via Michael addition followed by intramolecular lactamization in a yield of 20% after a period of two weeks.[160] It was found that a nitro group in the 4 position reduced the cyclisation time to 3 days with a similar yield (19%). Reduction of the lactam formed in both instances was performed using B$_2$H$_6$ to afford the free ligand. The crystal structure of the ligand shows that it possesses three H-bonds; two between nitrogen atoms in the macrocycle, and a third between the phenol OH and the nearest nitrogen atom.[161]
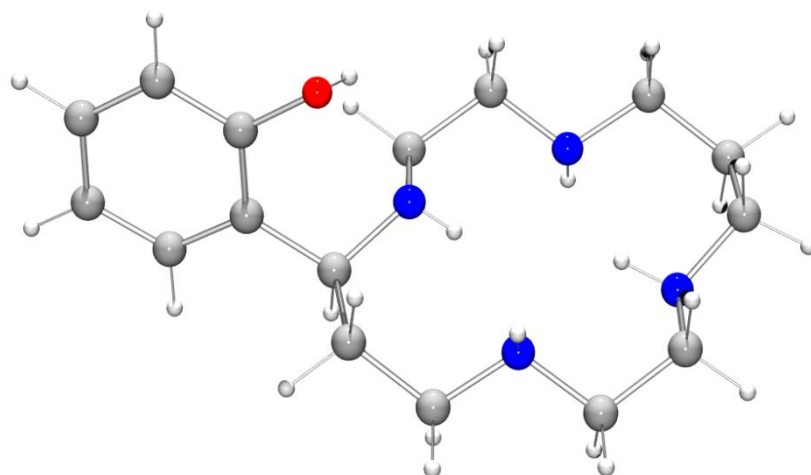
Figure 45: Ball and stick representation of the X-ray crystal structure of phenolate appended cyclam (Kimura *et al*).[161]

The phenol moiety is attached to the macrocyclic ring system through the carbon backbone, and when complexed to a metal, forms a six-membered chelate ring. The complexation of the couramin derived macrocycle with various transition metal ions was then carried out. Analysis of the copper(II) complex shows that the phenolic oxygen forms an axial interaction with the copper centre which adopts a five coordinate geometry (Figure 46).[161] An unusually large thermal motion exists between C(9) and C(10) in conjunction with a very short C(9)-C(10) distance (1.25 Å) suggesting the ligand has some flexibility on coordination.
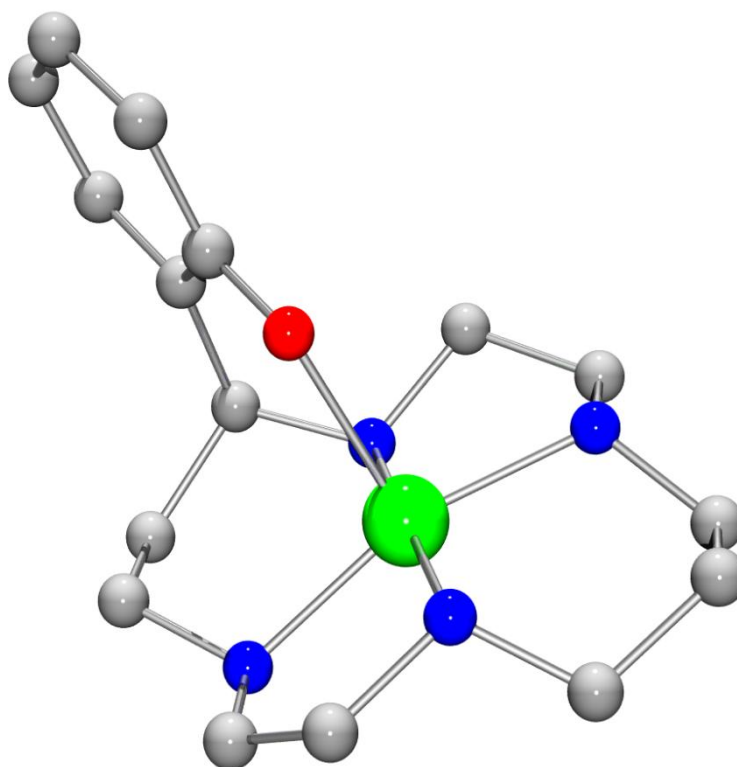
It is interesting to note that $Fe(OH)_3$ is taken into solution by this ligand to form a stable 1:1 red complex.[162] The stabilisation of the iron(III) state with respect to the iron(II) state was evidenced from cyclic voltammetry. The redox potential observed in phenolate free macrocyclic systems such as the 16-membered saturated penta-amine macrocyclic complex (-0.04 V) or haemoglobin (-0.07 V), is significantly lower than the redox potential observed for the iron(III) cyclam complex with appended phenol (-0.16 V). However this value is still higher than Fe(III) carriers such as mugineic acid (-0.34 V) and enterobactin (-0.99 V).

The nickel(II) complex of the ligand shown in Figure 45 shows a significantly lowered redox potential of +0.35 V vs SCE (0.5 M Na_2SO_4, pH 7.5, 25 °C) for $Ni^{III/II}$ with respect to that of nickel(II)-cyclam (+0.50 V vs. SCE).[160] The phenol moiety also becomes harder to oxidise upon coordination to nickel(II) (~+0.5 V uncoordinated, ~+0.9 V coordinated). An explanation of these redox potential shifts

is suggested by the data obtained from the crystal structure. The nickel(II) ion adopts an octahedral geometry with the nickel(II) ion lying in the same plane as the four nitrogen atoms.[163] The oxygen of the phenolate fills one apical site with a Ni-O bond length of 2.015 Å. This distance is shorter than the four Ni-N bond lengths (2.072, 2.051, 2.085 and 2.078 Å) and far shorter than apical bond lengths in octahedral nickel(II)-cyclam complexes (2.492 Å for X = Cl, 2.169 Å for X = NO$_3$). The other apical site is filled by an oxygen of a perchlorate anion, which has a bond length of 2.402 Å.
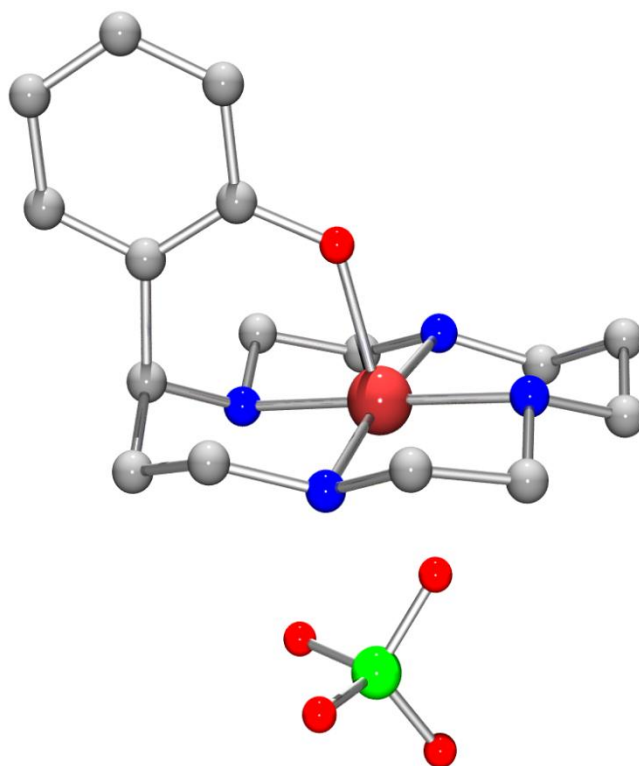
Figure 47: Ball and stick representation of the X-ray crystal structure of the nickel(II) complex with phenolate appended cyclam. Non-hydrogen atoms have been omitted for clarity (Kimura _et al._).[163]

3.1.4.   Examples of known thiophenolate complexes

Thiol and thiophenolate pendent armed azaamacrocycles have also been studied. A bis(μ-thiolato)dicopper(II) complex has been synthesised using thiirane to introduce the mercaptoethyl group on to a TACN backbone.[164] The crystal structure of the dicopper(II) complex (Figure 48) shows that each sulphur atom bridges the two copper centres.
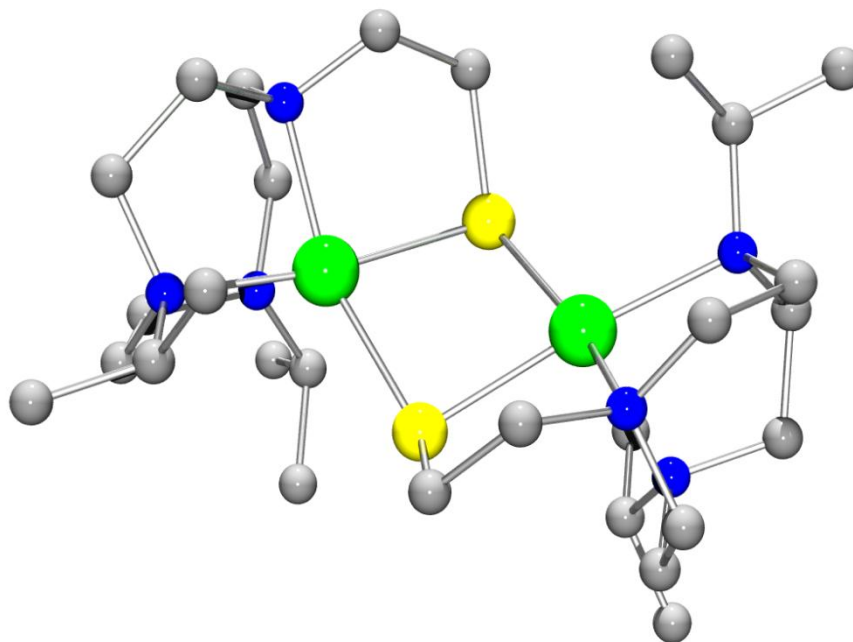
Figure 48: Ball and stick representation of the X-ray crystal structure of the bis(μ-thiolato)dicopper(II) complex. H atoms and perchlorate ions omitted for clarity (Tolman *et al.*).[164]

Welch and co-workers have also studied mercaptoethyl complexes. They have reported the synthesis of a tris-mercaptoethyl TACN ligand.[165] The mercaptoethyl group was this time introduced using ethylene sulphide. The indium and gallium radiolabelled complexes were prepared and found to be stable *in vivo*. The complexes were less lipophilic than expected, which is believed to be due to the facial arrangement of the thiolates around the metal centre, resulting in a substantial dipole moment.
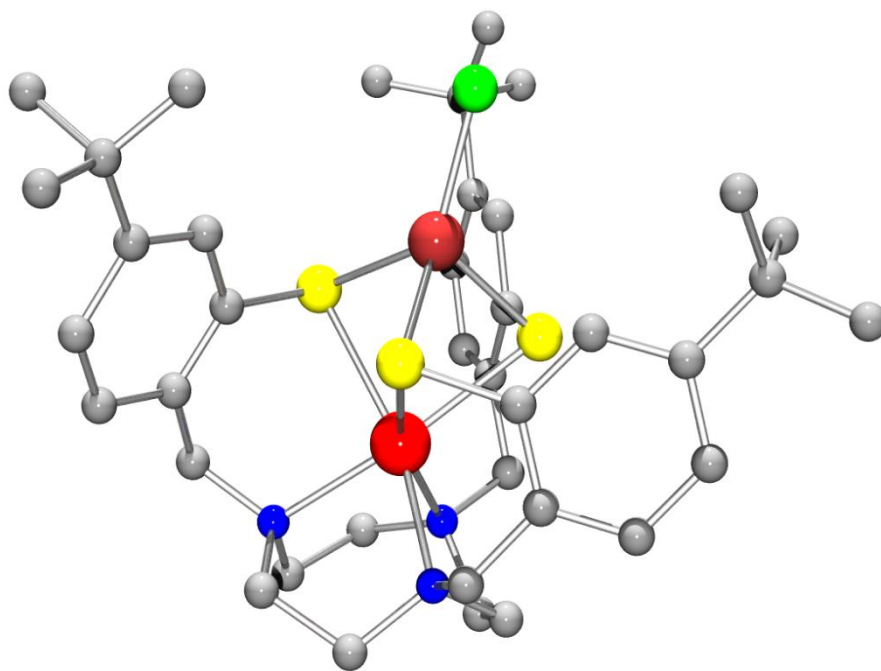
Figure 49: Ball and stick representation of the X-ray crystal structure of the tris(thiophenolate) zinc(II)-nickel(II) dinuclear complex. H atoms omitted for clarity (Weighardt *et al.*).[144]

Example of complexes incorporating thiophenolate moieties have been reported by Weighardt and co-workers. They have produced TACN ligands bearing derivatised aromatic thiols which possess *tert*-butyl groups. Species have been produced with *tert*-butyl groups in the *meta*[144] or *ortho* and *para*[142] positions. Hetero dinuclear complexes have been produced of a tris(thiophenolate) derivative with a *tert*-butyl group in the *meta* position. A crystal structure (Figure 49) of a complex of this type was obtained where a zinc(II) ion is coordinated by the three nitrogen and sulphur atoms in an intermediate octahedral trigonal prismatic arrangement. The sulphur atoms also coordinate to a second metal ion (nickel(II)), bridging the two metal centres. The nickel(II) ion occupies a tetrahedral geometry with a chloride ion capping the tetrahedron.

3.2. Synthesis of side-bridged cyclam complexes with phenolate pendent arms

The design of the phenolate systems incorporating phenolate arms synthesised in this work was based on the tetraaza macrocycle, cyclam (**32**). The aim was to attach one pendent arm, providing a coordination set of N_4O_1 for the metal centre. Scheme 12 shows a synthetic scheme in which the reactivity of the amines can be controlled by rigidifying the macrocyclic backbone.

32   **33**
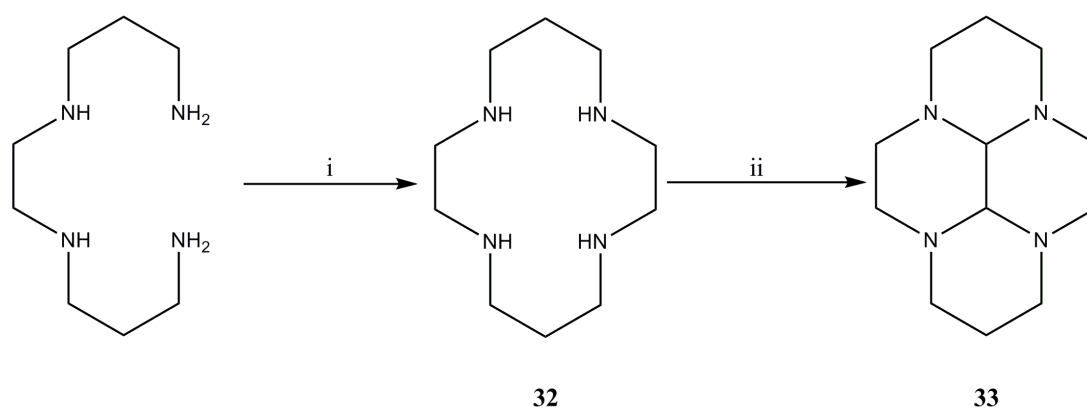
Scheme 12: Synthesis of 33. Conditions; i) Nickel(II) perchlorate hexahydrate, glyoxal overnight then NaBH₄ at 90°C for 1 hr followed by NaCN at reflux for 2 hr; ii) MeOH, glyoxal, −10°C to RT (100%).

Cyclam can be synthesised using either a nickel(II) template reaction[166,167] or by using a method reported by Handel and co-workers.[168] Alternatively it can be purchased from Strem Chemicals. The introduction of glyoxal at -10°C forms a glyoxal bridge. This has the effect of rigidifying the macrocycle, allowing the reactivity of the secondary amines to be controlled. On first inspection of **33**, it would seem that all four nitrogen atoms are in the same environment and should react in a similar fashion. However, this is not the case. Because of the rigidified nature of the macrocycle, the lone pairs on the nitrogens fall into two chemically different groups. The first is where the lone pair is pointing directly into the macrocyclic cleft. The steric hindrance prevents prospective reagents for nucleophilic attack from approaching the lone pair. This renders these two sites unreactive. The second group where the nitrogen lone pair is pointing away from the cleft, can easily participate in nucleophilic attack of appropriate reagents. The possibility of both nitrogens reacting in this way is reduced when considering the

product formed; an ammonium salt. Reactions using non-polar solvents cause this product to precipitate, therefore preventing further reaction from occurring. This methodology can be used to selectively alkylate one tertiary amine site, resulting in the attachment of only one pendent arm.
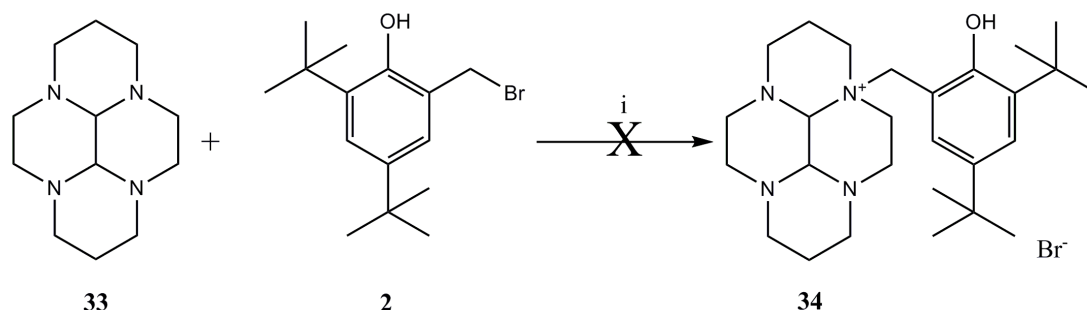
Scheme 13: Synthesis of 34. Conditions; i) dry MeCN, RT, (product not isolated).

An attempt was made to attach di-*tert*-butyl-2-hydroxy-benzylbromide, (**2**), to glyoxal cyclam (**33**) using this methodology. Upon the addition of dry MeCN to a mixture of **2** and **33**, an immediate precipitate formed. After three days at RT, the reaction mixture was concentrated under reduced pressure before ether was added. The material that was insoluble in ether was then collected by filtration. Two important points were noted from observations regarding reaction work-up. Firstly the amount of recovered solid was approximately the same amount of **33** that was used initially. Secondly, the filtrate was UV-active whereas the solid was not. The proton and carbon NMR of both products were analysed, and revealed that the desired reaction had not occurred. The data for the solid suggested recovery of starting material **33**. The fact that it was collected as a solid and is ether insoluble would suggest that it was protonated. NMR analysis of the filtrate was complicated as the number of signals made any structural assignment difficult. However, it was evident that no attachment of **2** to **33** had occurred. Instead, it is suggested that glyoxal cyclam (**33**) had acted as a base instead of a nucleophile. By deprotonating the phenol, this created a nucleophile which attacked a further molecule of **2** at the benzylic position followed by displacement of the bromide. This process creates a dimer. Evidence for dimerisation was obtained from mass spectrometry analysis, which indicated the presence of di-, tri- and tetramers of **2**.
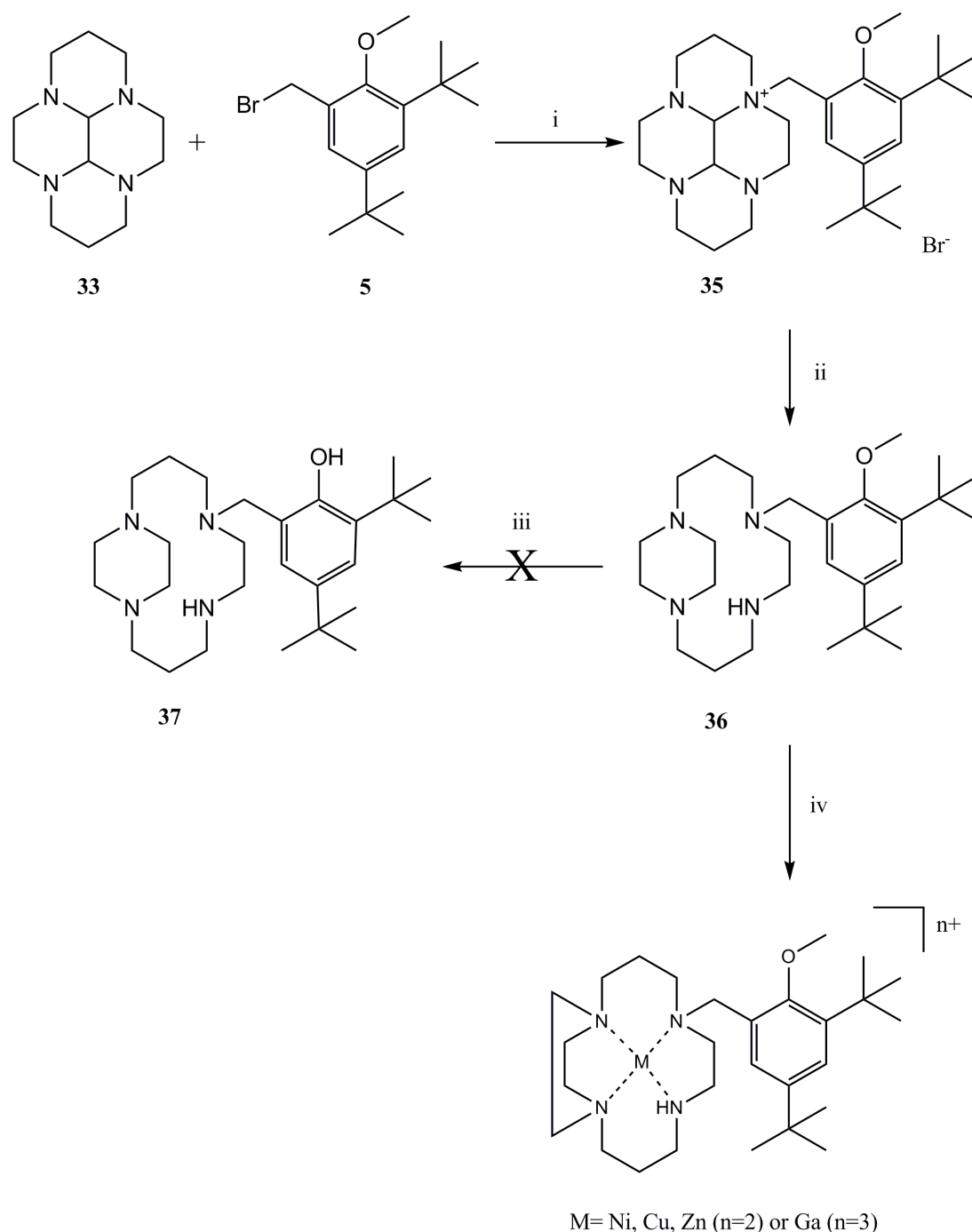
Scheme 14: Synthesis of 36 and its complexation to Ni(II), Cu(II), Zn(II) and Ga(III). Conditions; i) dry MeCN, RT, 5 days (64%); ii) ethanol, NaBH₄, RT, 7 days (89%); iii) see text; iv) Metal salt, MeOH, reflux, 2 hr - 2 d (Cu=98%, Zn=95%, Ni=98%, Ga complex not isolated).

After the unsuccessful reaction using the unprotected phenolic species, focus was switched to protected analogues. Firstly the methyl ether derivative, **5**, was investigated. The attachment of **5** to glyoxal cyclam, **33**, was attempted in a similar

fashion to that detailed in Scheme 13 (see Scheme 14). Unlike the previous reaction, no precipitate formed. After three days the reaction was worked-up and analysis of the solid collected showed that the reaction of **5** with **33** had occurred. In the next step the glyoxal bridge was reduced to form the piperazine ring, forming the side-bridged cyclam species **36**. This was achieved using $NaBH_4$ in alcoholic media. In an attempt to unmask the phenol, BBr_3 was then used. This reagent has been previously used to deprotect 3,3'-dihydroxyphenyl,[169] which although not as sterically hindered as **36**, still highlighted the conditions required to cleave the methyl ether. The conditions reported for this deprotection were used in various attempts to effect the desired deprotection step. The temperature was initially held at -80°C, and the reaction time was varied, between 2 and 4 hours, before allowing the reaction mixture to warm to RT o/n. Unfortunately, the desired ether cleavage reaction was unsuccessful, the methyl peak was present in the ^{13}C NMR after each attempt. The steric hindrance surrounding the ether moiety may be the reason for the lack of cleavage. A subsequent reaction using the boron-trifluoride ethyl etherate and sodium iodide reagent system[170] was also unsuccessful. However, complex formation was still of interest.

The complexation of **35** was performed using transition and p-block metals. Nickel(II), copper(II) and zinc(II) were chosen from the transition elements, and gallium(III) was chosen from the p-block. Nickel(II) and copper(II) were of interest because they possess a variety of stable oxidation states whereas zinc(II) and gallium(III) are redox inactive. The latter are both d^{10} and hence diamagnetic enabling NMR data to be collected. Gallium(III) complexes are of particular interest because only two related complexes of configurationally restricted tetraazamacrocycles have been reported previously. Weisman and Wong have reported the synthesis of cross-bridged cyclen[171] and cyclam[172] complexes using either the gallium nitrate or chloride salts respectively. The complexes were isolated by centrifugation after heating at reflux for 2 days. Yields obtained from recrystallisation were in the range of 50-60%. These conditions were used when synthesising the gallium(III) chloride complex of **36**. However, they seemed to be unsuitable for the side bridged compound as it was difficult to isolate the metal complex. Therefore, a different method for gallium(III) complexation was sought, and an alternative method has been reported by Sharma and co-workers. Their

investigations into metalloantimalarials lead to them to synthesise an amine phenol ligand and study its complexes with gallium(III).[173] To insert the gallium into the acyclic cleft, Ga(acac)$_3$ in MeOH was heated to reflux in the presence of the ligand. Then, KClO$_4$ in hot water was added and reflux continued for a further 30 min. Crystals could then be collected after recrystallisation from ethanol/acetonitrile (9:1). However, this method also proved to be incompatible with this ligand system and the gallium(III) complex was not isolated.

All the metal complexation reactions were carried out in MeOH. Metal perchlorate salts were used to maximise the potential for the complexes to crystallise to enable structural characterisation. Transition metal complexation reactions were heated to reflux for 1.5 to 2 hours whereas attempts at forming the gallium(III) complexes were left for 2 days. Products were purified by size exclusion chromatography on a Sephadex LH-20 column. Yields for the transition metal complexes of **36** were in the range of 95 - 98%.

Orange crystals of the nickel(II) complex of **36** were grown by evaporating an acetone-ether solution at RT. Orange crystals suitable for X-ray analysis were obtained. The oxygen atom from the methoxy group of the pendent arm is not used in the coordination of the nickel(II) centre, which adopts a distorted square planar geometry with the four nitrogen atoms of the macrocyclic ring (bond lengths for the nickel(II) ion are given in Table 7). There is disorder in the *tert*-butyl group *para* to the methoxy group, with each atom occupying two sites ~50% of the time (only one site shown in Figure 50).

The electronic spectrum of [Ni**36**]$^{2+}$ would also suggest that the ion is square planar as a single d-d transition was observed at 477 nm. Lindoy and co-workers[174] observed only one band for their N-benzylated cyclam complexes in the region of 474-488 nm, all of which were square planar. The copper(II) complex of **36** also possesses one d-d band in the UV, which is diagnostic of a copper(II)-N$_4$ chromophore, in which solvent or anion may occupy axial positions.[175] However, the featureless nature of the spectrum results in it being of little use for the assignment of a detailed coordination geometry around the copper(II) ion.
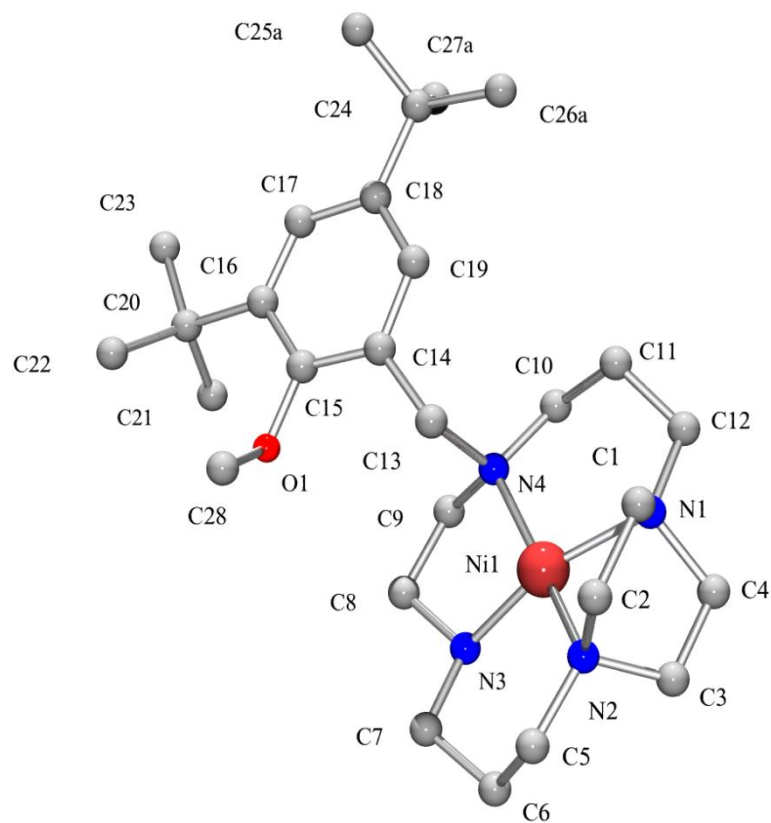
Figure 50: Ball and stick representation of the X-ray crystal structure of [Ni36][(ClO$_4$)$_2$]. Water molecules and perchlorate anions omitted for clarity.

	Bond length (Å)
Ni(1)-N(1)	1.941(5)
Ni(1)-N(2)	1.922(6)
Ni(1)-N(3)	1.921(5)
Ni(1)-N(4)	1.953(5)

Table 7: Selected bond lengths from the X-ray crystal structure of [Ni36][(ClO$_4$)$_2$].
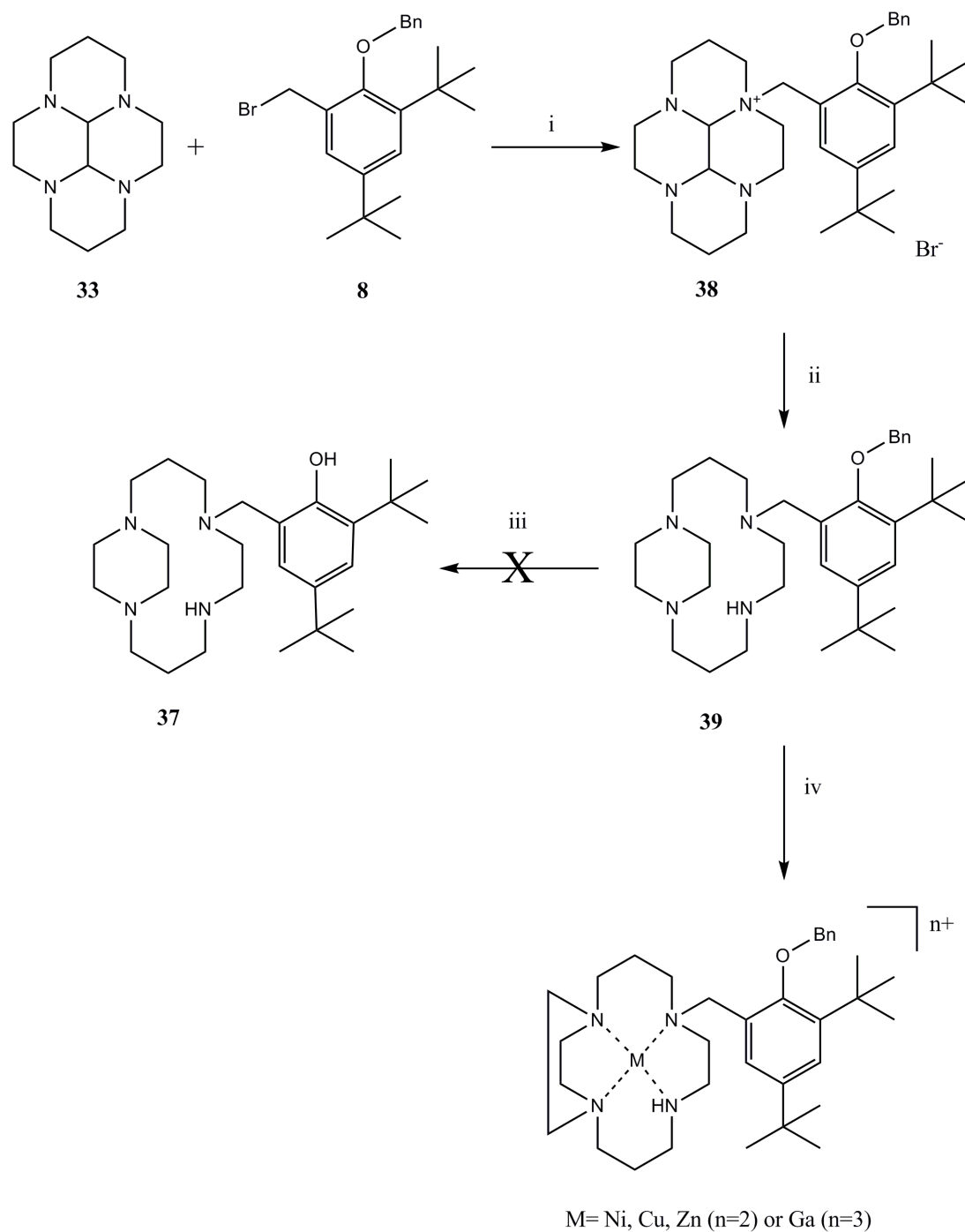
Scheme 15: Synthesis of 39 and its complexation to Ni(II), Cu(II), Zn(II) and Ga(III). Conditions; i) MeCN, RT, 3 d (66%); ii) MeOH, NaBH₄, RT, 2 d (80%); iii) see text; iv) metal salt, MeOH, reflux, 2 hr - 2 d (Cu=87%, Ni=42%, Zn=47%, Ga complex not isolated).

Because of the stability of the methyl phenol to cleavage, focus switched to the benzylic derivatives. The large number of ways in which these groups can be cleaved makes them highly versatile.[133] The synthesis of the side-bridged cyclam species

bearing the benzyl protecting group is outlined in Scheme 15. The synthesis of **39** is directly analogous to that of **36**. However, problems were again encountered in the deprotection step. A range of conditions were used in attempts to cleave the protecting group and unmask the phenol. In general, conditions employed for aromatic debenzylation fall into categories of (1) catalytic hydrogenolysis, (2) reductive cleavage, (3) iodide-mediated debenzylation, (4) metal mediated debenzylation, (5) Lewis-acid-mediated debenzylation and (6) acid-mediated cleavage. Initial attempts at cleaving the benzyl ether were directed towards catalytic hydrogenolysis (1). The problem with this type of deprotection lay in the presence of both *N*-benzylic and *O*-benzylic moieties in these molecules, with potential for both to be cleaved under similar conditions. Belmar and Jiménez, in their pursuit of highly hindered polyanionic chelating ligands, used a benzyl group to protect 2,4-di-*tert*-butyl phenol which was linked to an aromatic amine by an amide bond. Palladium on carbon (10% w/w) in the presence of hydrogen was sufficient to cleave the protecting group.[135] The conditions outlined in this paper were used in an attempt to deprotect the phenol in **39**. However, only starting material was recovered and so a number of further conditions were explored. Firstly, the reaction was attempted at a higher pressure using a Parr apparatus. Three different pressures were used in an attempt to effect the desired debenzylation; 10, 20 and 40 psi were all used, but starting material or a multiple component mixture was always recovered after work-up. After this laborious process, the catalyst was changed. Several different catalysts were used in attempts to cleave the benzyl ether. Firstly, 5% Pd/C was used. This was used to circumvent possible *N*-debenzylation by lowering the amount of active catalyst. However, the material recovered after each attempt was either recovered starting material or a multi-component mixture. This was also the case when a lead poisoned catalyst was used, or Pd 10% on activated carbon, wet, Degussa type E101 NE/W which is specifically for debenzylation purposes. Following these results, the literature was consulted for alternative options.

Of particular interest was the work reported by Binkley and Hehemann,[176] which has been further developed by Riley and Grindley.[177] The procedure described is for a light-initiated process for the rapid debenzylation of sterically hindered benzyl ethers. Given the steric bulk surrounding the benzyl ether in **39**, this looked promising. Both sets of authors report that the use of $CaCO_3$ and NBS in a biphasic

mixture of CCl_4 and water can cleave benzyl ethers in greater than 70% yield in the presence of light. This set of conditions causes α-bromination of the benzyl ether, therefore promoting subsequent cleavage of the ether bond. On reproduction of these experimental conditions however, the desired product was not isolated.

The use of boron trifluoride ethyl etherate in conjunction with NaI has been reported as being a suitable reagent system for cleavage of benzyl and methyl ethers.[170] Debenzylation of cyclohexanyl benzyl ether using this reagent system gave a 75% yield of the corresponding alcohol in just over an hour. The phenol benzyl ether was obtained in 84% after 21 hr. Alcohols are therefore more readily cleaved than phenols using this reagent system. Using the conditions described, this reagent system was used in an attempt to debenzylate **39**. The reaction was allowed to proceed for 48 hours given the hindered nature of the benzyl ether. However, after reaction work-up only the starting material was recovered.

The use of solid-supported acids has been reported for the debenzylation of aryl benzyl ethers.[178] The use of Amberlyst-15 was reported as being selective towards benzyl ethers whilst methyl ethers were left intact. This gave yields of greater than 70% for debenzylation, but was highly dependent on the stoichiometry of the reaction. The authors reported that a 1:1 ratio of reactant to Amberlyst-15 afforded the best yield, for 2 hr at a temperature of below 120°C (chosen arbitrarily because Amberlyst-15 degrades at temperatures above this). However, it was found that Amberlyst-15 did not cleave the benzyl ether in **39**.

Debenzylation has also been reported to occur using $Pd(OH)_2/C$ in MeOH in the absence of hydrogen. This process is believed to occur via the oxidative cleavage of the ether although transfer hydrogenation is a possible competing reaction, with MeOH serving as the hydrogen donor. Molar equivalents of the catalyst are used because if MeOH does indeed act as a hydrogen donor, then the formaldehyde produced will effectively poison the catalyst. However, this reagent system did not cleave the benzyl group either.

Other routes exist for deprotecting this group. One such way is to use ferric chloride. This has been reported by the groups of Fraser-Reid and Takeda where they investigated the deprotection of a series of benzyl protected oligosaccharides[179] and

monosaccharides.[180] Using Takeda's conditions (RT, dry DCM, 2 equivalents of FeCl$_3$) however did not yield the desired deprotected species. It is stated that the end point of the reaction is reached when the colour of the mixture is green-blue.[180] This was not observed when reproducing this deprotection method; in fact no colour change occurred.

Acetyl bromide in alcoholic media has been found to be an efficient system for the facile removal of various protective groups which are stable to acetyl chloride in alcoholic media.[181] The deprotection of a benzyl ether to give the corresponding phenol is reported in greater than 80% yield. However, once again this reaction was unsuccessful.

As a result of being unable to deprotect the phenolic ether, attention turned to the complexation of this prochelator to metal ions. Complexation of **39** to the transition metals of interest (nickel(II), copper(II) and zinc(II)) was performed in the same way as those to **36**. However, the gallium(III) complex was not isolated. The nickel(II) and copper(II) complexes were analysed by cyclic voltammetry, the data for which is reported in section 3.4. Electronic spectra of the copper(II) and nickel(II) complexes of **39** were similar to those of **36**. Two single d-d bands were observed at 550 and 481 nm for the copper(II) and nickel(II) complexes respectively. The nickel(II) complex is therefore square planar whereas it is again difficult to ambiguously assign the coordination around the copper(II) ion.
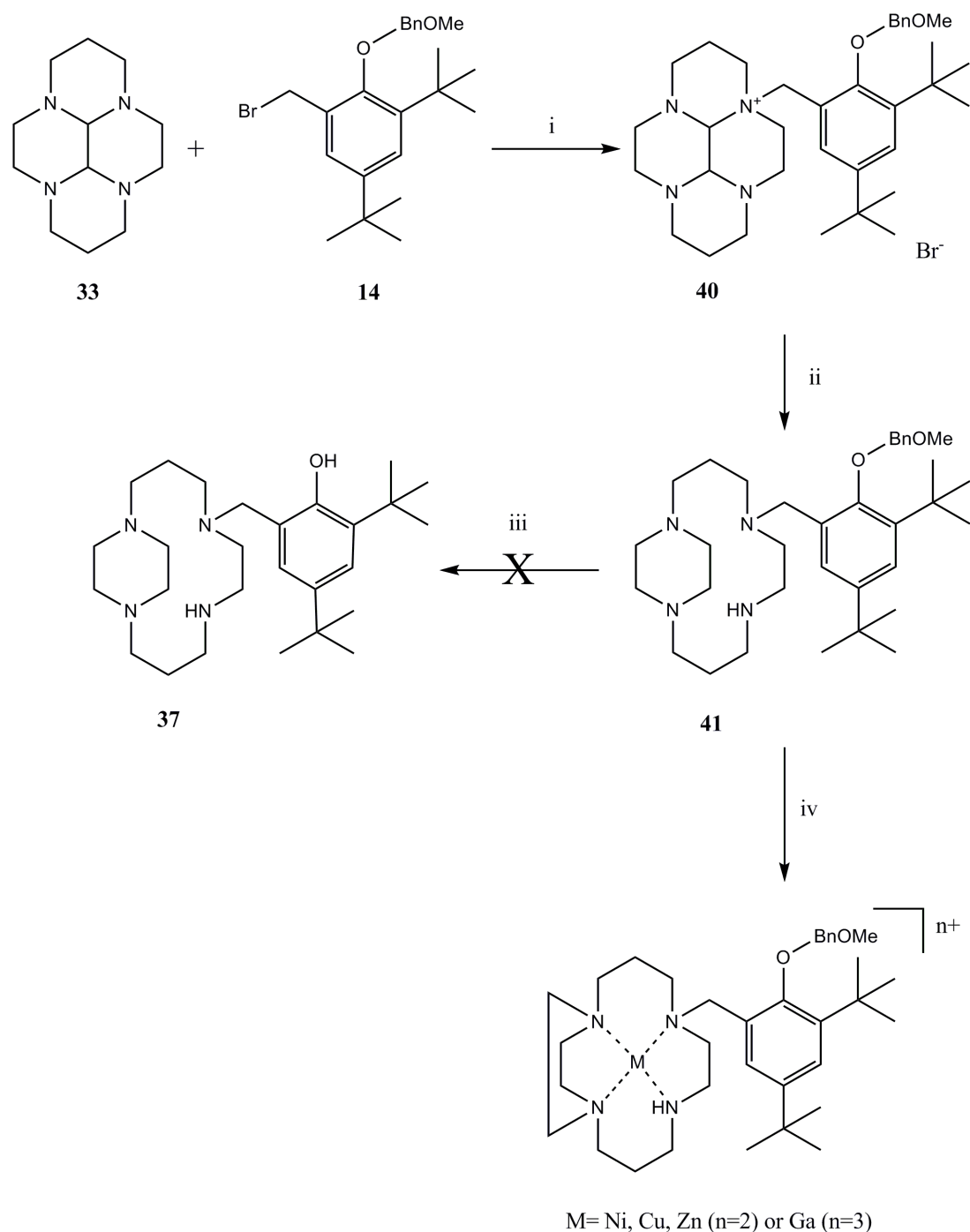
Scheme 16: Synthesis of 41 and its complexation to Ni(II), Cu(II), Zn(II) and Ga(III). Conditions; i) MeCN, RT, 4 d (88%); ii) EtOH, NaBH₄, 2 weeks, RT (97%); iii) see text; iv) metal salt, MeOH, 2 hr - 2 d (Cu=29%, Ni=44%, Zn=49%, Ga complex not isolated).

The *p*-methoxybenzyl derivatives offered alternative reactions for the deprotection step. The synthesis of the protected species was again via the bisaminal intermediate, and was directly analogous to the synthesis of previous side-bridged compounds **36**

and **39**. However, the deprotection of the phenol protecting group was again problematic.

Hodgetts and Wallace have reported that *p*-methoxybenzyl ethers are unstable in acetic acid.[182] The conditions they employed (heating to 90°C in acetic acid for between 4 and 72 hr, followed by an aqueous work-up) seemed appropriate for unmasking the phenol. Compound **41** was therefore dissolved in acetic acid and heated to 90°C for 72 hr. The work-up was modified given that the product is zwitterionic in nature and therefore water soluble. The reaction mixture was concentrated and the oily residue triturated with ether. The precipitate was then collected by filtration. NMR data collected on the precipitate showed that the ether functionality was still intact. The reaction was performed again, this time heating to reflux but this was also unsuccessful.

Cerium chloride heptahydrate in conjunction with sodium iodide has been found to be an excellent reagent system for deprotection of *p*-methoxybenzyl ethers.[183] When used to deprotect the *p*-methoxybenzyl ethers of phenol and *p*-nitrophenol, yields of 86 and 89% were obtained respectively. This seemed to be an ideal system for the deprotection of compound **41**. In using this reagent system, an additional equivalent of cerium chloride heptahydrate was used. This was because it was envisaged that the cerium could coordinate with the tetraazamacrocyclic ring, and thus would not be available for activating the ether bond. Therefore 2.5 equivalents of cerium chloride heptahydrate were used, along with one equivalent of sodium iodide. The reaction was conducted in MeCN and heated at reflux for 24 hr. The reaction mixture was then concentrated and the resulting hygroscopic solid re-dissolved in 6M HCl. The reaction mixture was then heated to 55°C for 3 hours. This last step should ensure that any formed phenol was protonated and that the cerium chelated by the macrocyclic ring was subsequently removed from the cavity. The product obtained from this treatment was then transferred to a Sephadex LH-20 column. Two bands were obtained; one orange, which eluted first, and one yellow, eluting shortly afterwards. Analysis by proton and carbon NMR and mass spectrometry showed that neither of these fractions contained the desired deprotected compound.

The nickel(II), copper(II) and zinc(II) complexes of this chelator (**41**) were prepared but the gallium(III) complex again proved to be problematic and could not be

isolated. The cyclic voltammetry data for the nickel(II) and copper(II) complexes are reported in section 3.6. Electronic spectra of the copper(II) and nickel(II) complexes of **41** were similar to those of **36** and **39**. Two single d-d bands were observed at 529 and 478 nm for the copper(II) and nickel(II) complexes respectively. The nickel(II) complex is therefore square planar whereas it is again difficult to ambiguously assign the coordination around the copper(II) ion. The different phenolic ethers produced would therefore appear to have no effect on the coordination around the metal centre; the same geometry is observed for both the nickel(II) and copper(II) complexes of **36**, **39** and **41**.
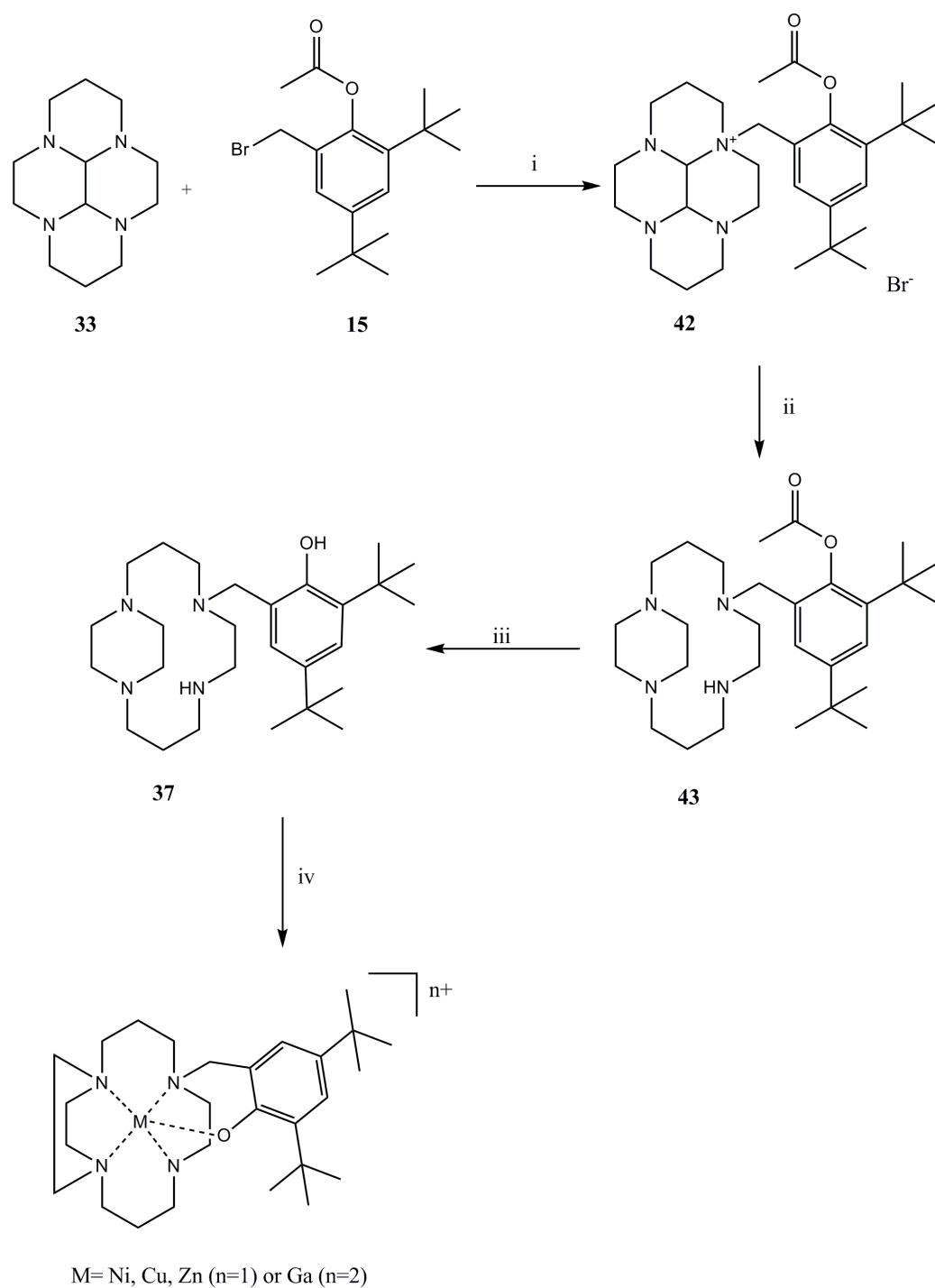
Scheme 17: Synthesis of 37 and its subsequent complexation to Ni(II), Cu(II), Zn(II) and Ga(III). Conditions; i) dry MeCN, RT, 3 d (75%); ii) EtOH, NaBH₄, RT, o/n (98%); iii) 6M HCl, MeOH, o/n (79%); iv) metal salt, MeOH, reflux, 2 hr - 2 d (Cu=40%, Ni=30%, Zn=29%, Ga complex not isolated).

The synthesis of the phenol ester compound, **43**, was approached in exactly the same way as the methyl and benzylic ether derivatives. Unlike the previous derivatives,

the acetyl group could be successfully removed to unmask the phenol. As the acetyl group is acid labile, deprotection strategies focussed on acid hydrolysis. 2M HCl in MeOH was initially used in an attempt to cleave the protecting group under reflux conditions overnight. Analysis of the proton and carbon NMR showed that the ester was still intact. 3M and 4M HCl in MeOH under the same conditions were also ineffective. However, when using 6M HCl, the acetyl group was absent from the NMR, showing the phenol had been deprotected. Complexation reactions with the ligand were performed in basic media; this was to ensure that both the phenol and amines functionalities were deprotonated. Upon addition of triethylamine to a methanolic solution of **37**, an instant colour change was observable from light yellow to a straw colour. It was assumed that this colour change was because of the change in delocalisation around the aromatic system due to the formation of the phenolate anion. Copper(II), nickel(II) and zinc(II) perchlorate salts were used to form the metal complexes. These complexes are very hygroscopic, and were isolated as oils.

The synthesis of copper(I) complexes was also attempted as these complexes would be neutral in terms of charge and hence would not require a counter anion. Two attempts at synthesising the copper(I) complexes were made using Schlenk line techniques and [Cu(NCMe)$_4$][BF$_4$]. Despite efforts to prevent getting oxygen into the reaction vessel, both products were isolated as dark blue solids which quickly oiled, implying that the copper(I) had been oxidised to copper(II).

The cyclic voltammetry for the nickel(II) and copper(II) complexes of **37** are reported in section 3.6. These complexes are of interest because they should have both ligand and metal centred redox processes. The electronic spectrum of the copper(II) complex displayed only a single band due to d-d transitions at 641 nm. The shift observed for the copper(II) complex of **37** is indicative of a five-coordinate geometry (either distorted square based pyramidal or trigonal bipyramidal) being formed around the metal ion.[41] This would imply that the phenolate tethered to the macrocyclic ring is bound to the metal centre in solution. The electronic spectrum of the nickel(II) complex of **37** possesses one strong d-d transition at 441 nm. In the nickel(II) complex of a phenolate cyclam ligand produced by Kimura and co-workers,[184] different absorptions are observed dependent on pH. At acidic and basic pH absorptions of 424 and 559 nm were observed respectively, corresponding to a

transition from low spin to high spin.[185] This data suggests that in the nickel(II) complex of **37**, the nickel(II) ion adopts a square planar geometry with the phenol not bound to the metal centre. Support for the presence of a high spin nickel(II), in which the phenol is bound to the metal in the axial site, is evidenced by a very weak peak at 581 nm.

3.3. Synthesis of side-bridged cyclams with thiophenolate pendent arms

The synthesis of the side-bridged cyclam bearing a thiophenol and its subsequent complexation is outlined in Scheme 18. The attachment of the thiophenol **18** to glyoxal bridged cyclam **33** was achieved in 94%. This ammonium salt was then converted to the side-bridged species by use of $NaBH_4$ in alcoholic media. The *p*-methoxybenzyl protecting group was then cleaved using mercury(II) acetate and H_2S under deoxygenated conditions. Because of the propensity of this ligand to form disulfide bridged dimers, the ligand was used as quickly as possible and all solvents degassed prior to use. Metal insertion was also performed under an inert atmosphere. The nickel(II) and zinc(II) complexes were all isolated in this manner and purified by collecting the appropriate fraction after loading on to a Sephadex LH-20 column. These complexes had a tendency to oil after a few minutes of exposure to air and so cyclic voltammetry studies were conducted as soon as possible. The data obtained or the nickel(II) complex of **46** is reported in section 3.7. The electronic spectrum of the nickel(II) complex of **46** possess two d-d transition bands at 367 and 464 nm. This could possibly imply that the nickel(II) centre oscillates between square planar and octahedral in solution. It is difficult to ascertain whether or not the thiophenolate pendent arm is always bound to the nickel(II) centre.
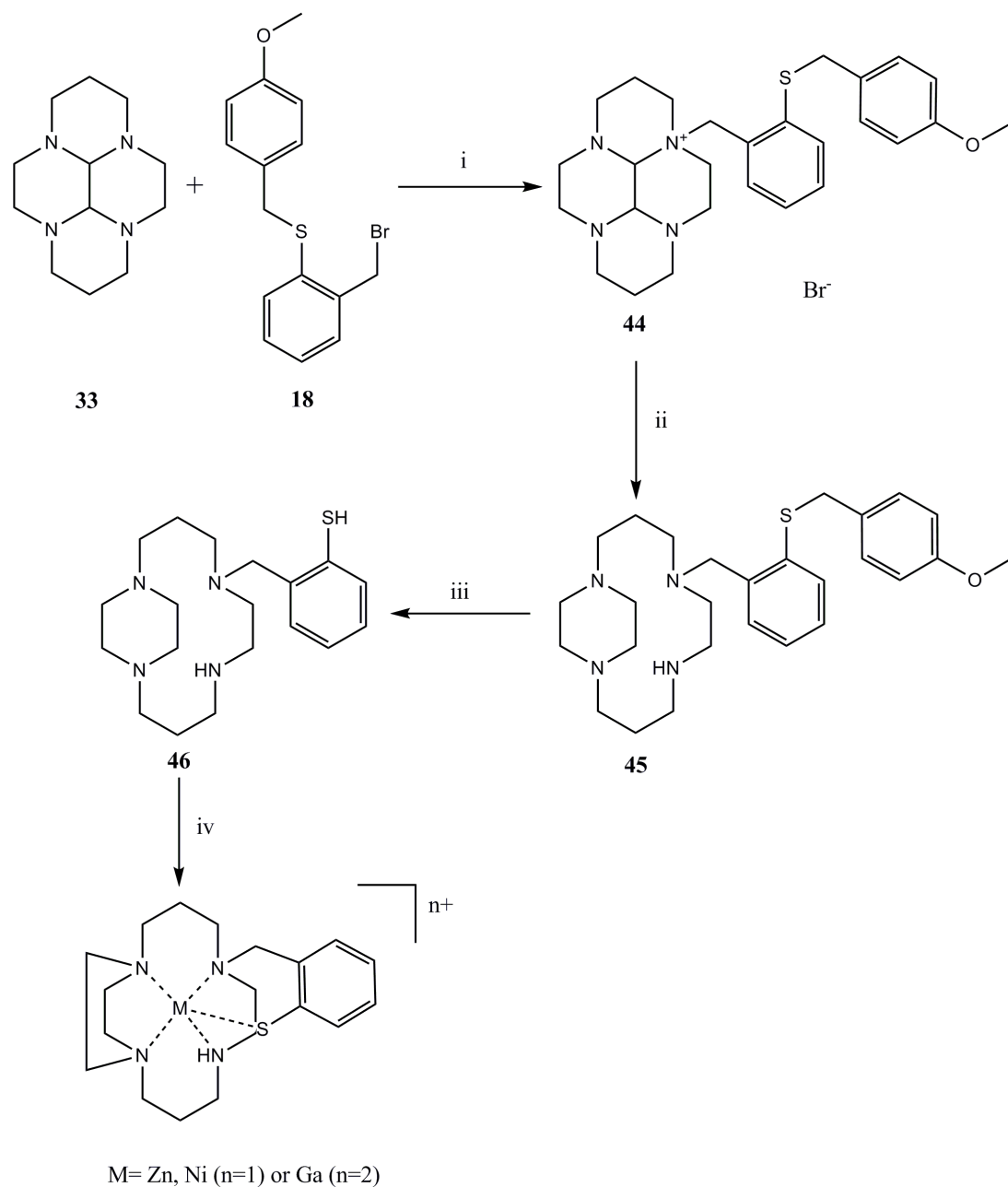
Scheme 18: Synthesis of 46 and complexation with Zn(II), Ni(II) and Ga(III). Conditions: i) dry MeCN, RT, 1 week (94%); ii) MeOH, NaBH₄, RT, 1 week (82%); iii) MeOH, Hg(OAc)₂, reflux, 16 hr then H₂S bubbled through the solution for 20 min (93%); iv) metal salt, reflux 2 hr - 2 d (Ni=92%, Zn=50%, Ga complex not isolated).

The synthesis of the di-*tert*-butyl thiophenol ligand, **49**, was approached in the same manner as the thiophenol ligand. **33** was reacted with **24** forming the ammonium salt in 95% yield. The glyoxal bridge was then reduced using NaBH₄ in alcoholic media. The sulphur protecting group was then removed using Hg(OAc)₂ in MeOH. As

before, because of the propensity of the unprotected thiophenolate species to dimerise, the metal complexes of the salt were synthesised as quickly as possible. These complexation reactions were performed using degassed solvents and under an inert atmosphere. The nickel(II), zinc(II) and copper(II) complexes of **48** were all isolated as solids, whereas the gallium(III) complex once again proved to be elusive. The nickel(II) and copper(II) complexes were both analysed by cyclic voltammetry, the data from which is reported in section 3.7. The electronic spectra of the copper(II) and nickel(II) complexes of **48** possess a single d-d band each at 550 and 550 nm respectively. In the case of the nickel(II) complex this would suggest that the ion is square planar; similar values have been reported for nickel(II) complexes of cyclam derivatives with a pendent pyridyl arm.[186] The d-d band for the copper(II) complex means that a geometry cannot be ambiguously assigned for the ion.
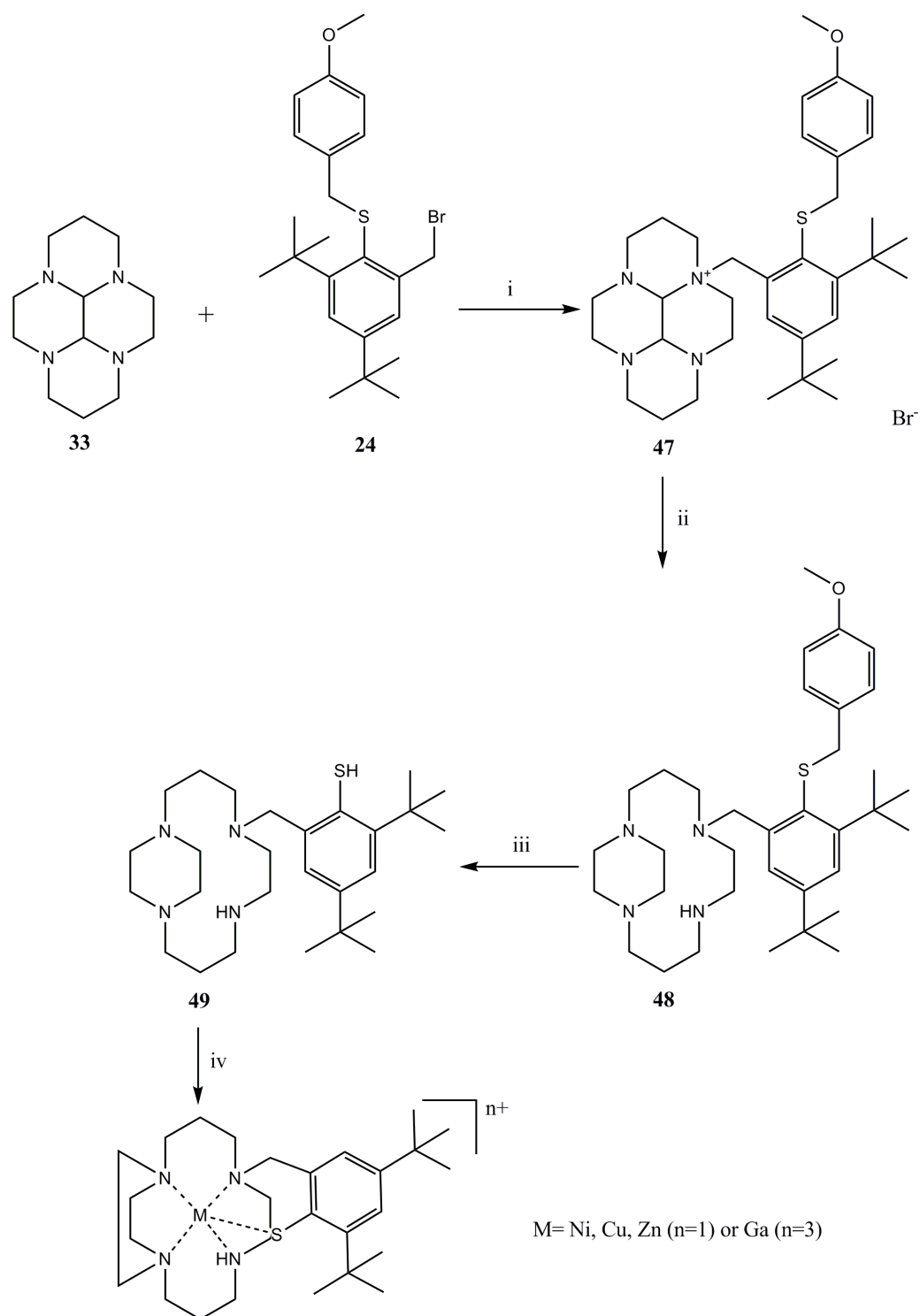
Scheme 19: Synthesis of 49 and complexation with nickel(II), copper(II), zinc(II) and gallium(III). Conditions; i) dry MeCN, RT, 3 days (95%); ii) MeOH, NaBH₄, 5 days, RT (49%); iii) MeOH, Hg(OAc)₂, 60°C o/n then H₂S bubbled through the solution for 20 min (97%); iv) metal salt, MeOH, reflux, 2 hr - 2 d (Cu=70%, Ni=94%, Zn=87%, Ga complex not isolated).

3.4. Cyclic voltammetry data for side-bridged cyclam phenolate complexes

Cyclic voltammetry was conducted on both phenolate and thiophenolate complexes. The purpose of these experiments was to probe the redox behaviour of the metal and the ligand. The generation of the phenoxyl and thiyl radical can be observed under these conditions. The redox potentials for these processes can be compared to other known examples to provide an insight into the stability of the complexes formed.
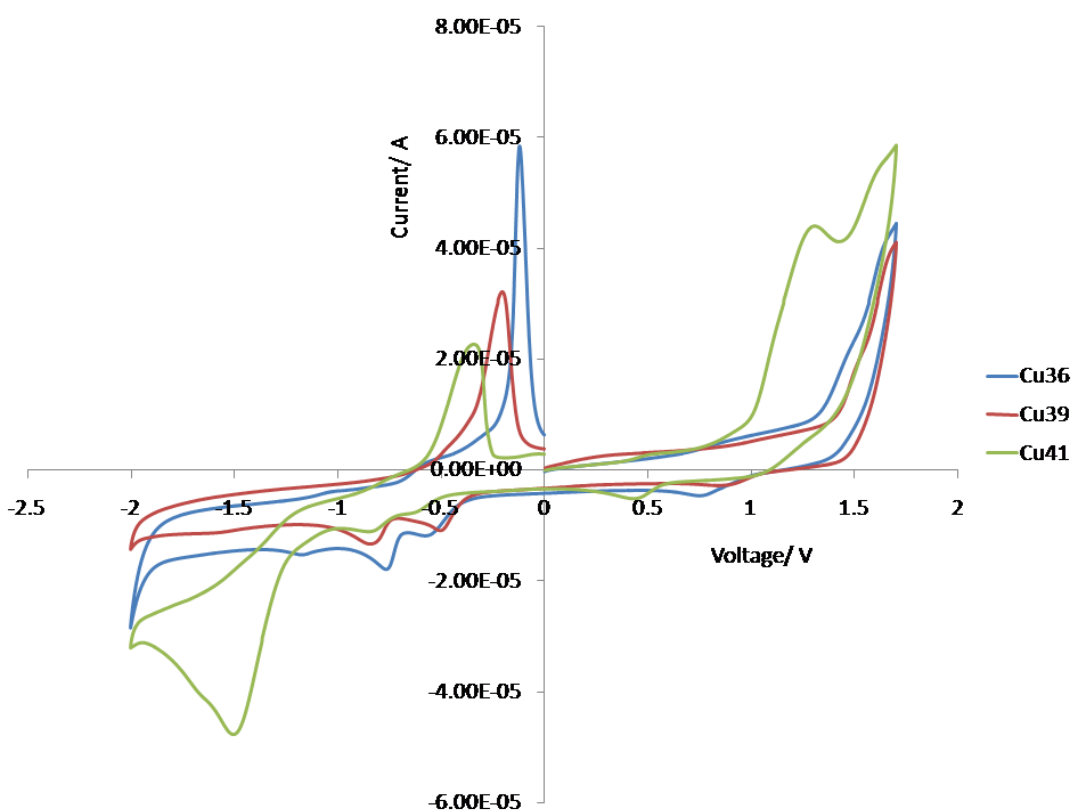
Figure 51: Cyclic voltammograms of [Cu36]$^{2+}$, [Cu39]$^{2+}$ and [Cu41]$^{2+}$ at 0.2 V/s. Data collected in acetonitrile with tetra-butyl ammonium perchlorate as a supporting electrolyte at RT using a platinum reference electrode.

Figure 51 shows the cyclic voltammograms for the copper(II) complexes of **36**, **39** and **41**. The copper(II) complex of **41** displays different behaviour to the other two complexes. This complex possesses a Cu(II)/Cu(III) wave at +1.26 V, whereas for the other two complexes this is not observed. The copper(II) reduction consists of two species; adsorbed and free. This is evidenced for all three complexes by the presence of two small peaks in the cathodic region at −0.79 and −0.56 V. The free

118

and adsorbed species are re-oxidised simultaneously given the presence of one oxidation peak at −0.38 V, −0.23 V and −0.13 V for [Cu**41**]$^{2+}$, [Cu**39**]$^{2+}$, and [Cu**36**]$^{2+}$ respectively. This peak therefore appears to be sensitive to the protecting group at the phenolic site. The shift towards anodic potentials occurs in the order *p*-methoxybenzyl < benzyl < methyl. The peak at -1.48 V is ascribed to the reduction of the copper(II) to copper(0), which is irreversible. Further evidence to support this was obtained by performing repetitive scans; the spectra became more inconsistent with time as the electrode became fouled by the deposition of copper on the surface.
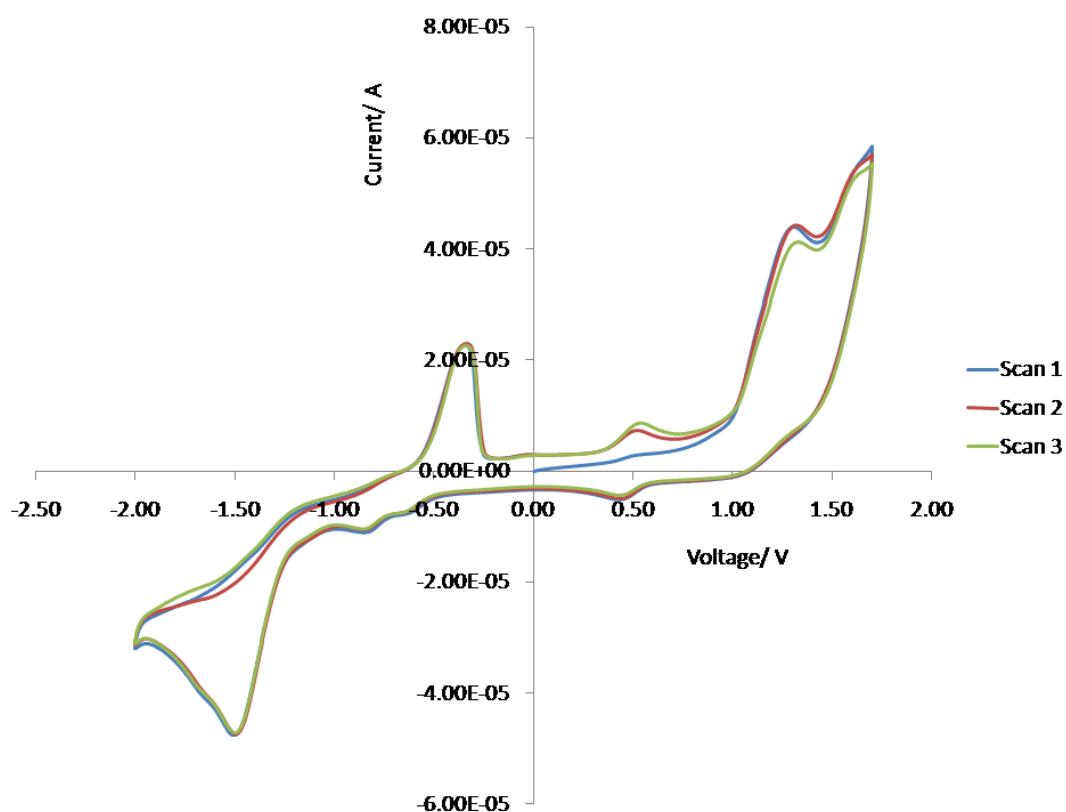
Figure 52: Consecutive cyclic voltammograms of [Cu37]$^{+}$ at 0.2 V/s. Data collected in acetonitrile with tetra-butyl ammonium perchlorate as a supporting electrolyte at RT using a platinum reference electrode.

Figure 52 shows the cyclic voltammagram of the copper(II) complex of **37**. At +0.48 V a fully reversible peak is observed, which is assigned to the formation of the phenoxyl radical and subsequent reduction back to the phenolate. Reversibility of this wave was tested by plotting the peak current verses the square root of the scan rate. This plot gave a straight line; indicative of a reversible process. Previous work by Wieghardt and co-workers has been focused on the study of numerous metal

complexes with phenolate pendent arms. Their studies have shown that the redox potential for the phenoxyl radical/phenolate couple can vary depending on the metal centre. For a TACN zinc(II) complex with a di-*tert*-butyl phenolate and two methyl pendent arms, the redox potential for the reversible formation of the phenoxyl radical is between -0.09 V and -0.32 V.[132] When the methyl pendent arms are exchanged for acetates, values of 0.63, 0.73 and 0.36 V are obtained for the gallium(III), iron(III) and cobalt(III) metal complexes respectively.[142] The irreversible peak at +1.27 V is believed to be metal centred and is due to the formation of copper(III). In the cathodic region there are two small reduction peaks at -0.82 and -0.60 V and an oxidation peak at -0.37 V. The two reduction peaks are believed to be due to the redox couple Cu(II)/Cu(I) for both adsorbed and free species. The oxidation peak corresponds to the re-oxidation of both the adsorbed and free species back to copper(II). Examples in the literature for cyclam copper complexes which have been examined by cyclic voltammetry would seem to support this assignment. For example, cyclam copper(II) complexes bearing *N*-benzyl pendent arms have been shown to possess redox potentials of +1.37 to +1.63 V for the Cu(III)/Cu(II) redox couple (all irreversible) and potentials of -0.18 to -0.85 V for the Cu(II)/Cu(I) redox couple.[174] Similar values have been obtained for the tris-copper(II) cyclam complexes (+1.38 to +1.58 V and -0.64 to -0.85 V respectively).[185]
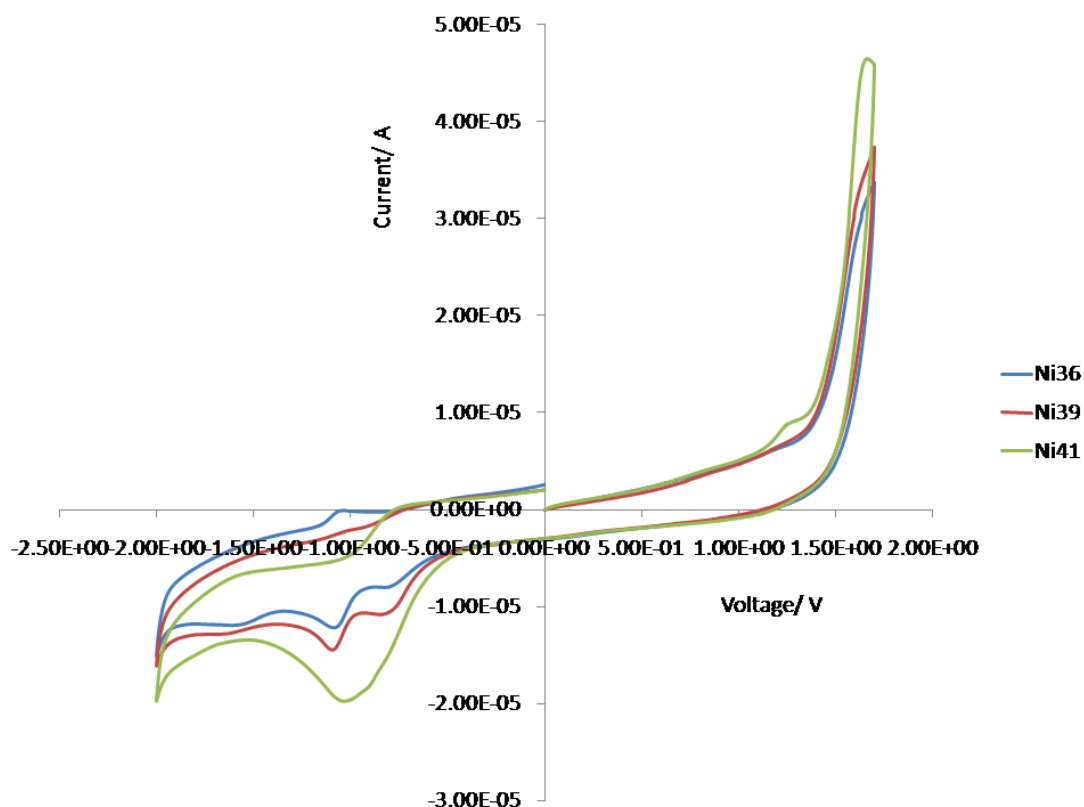
Figure 53: Cyclic voltammograms of [Ni36]$^{2+}$, [Ni39]$^{2+}$ and [Ni41]$^{2+}$ recorded at 0.2 V/s. Data collected in acetonitrile with tetra-butyl ammonium perchlorate as a supporting electrolyte at RT using a platinum reference electrode..

Figure 53 shows the cyclic voltammograms of the three nickel(II) complexes of **36**, **39** and **41**. The nickel(II) complex of **41** is again different, which is consistent with the trends observed for the analogous copper complex. It displays a small oxidation peak at +1.22 V which is assigned to Ni(II)/Ni(III) redox couple. All three complexes display a Ni(II)/Ni(I) reduction peak between −0.6 and −1.2 V. The peak is split between adsorbed and free species, and only the nickel(II) complex of **41** complex seems to display any reversibility.
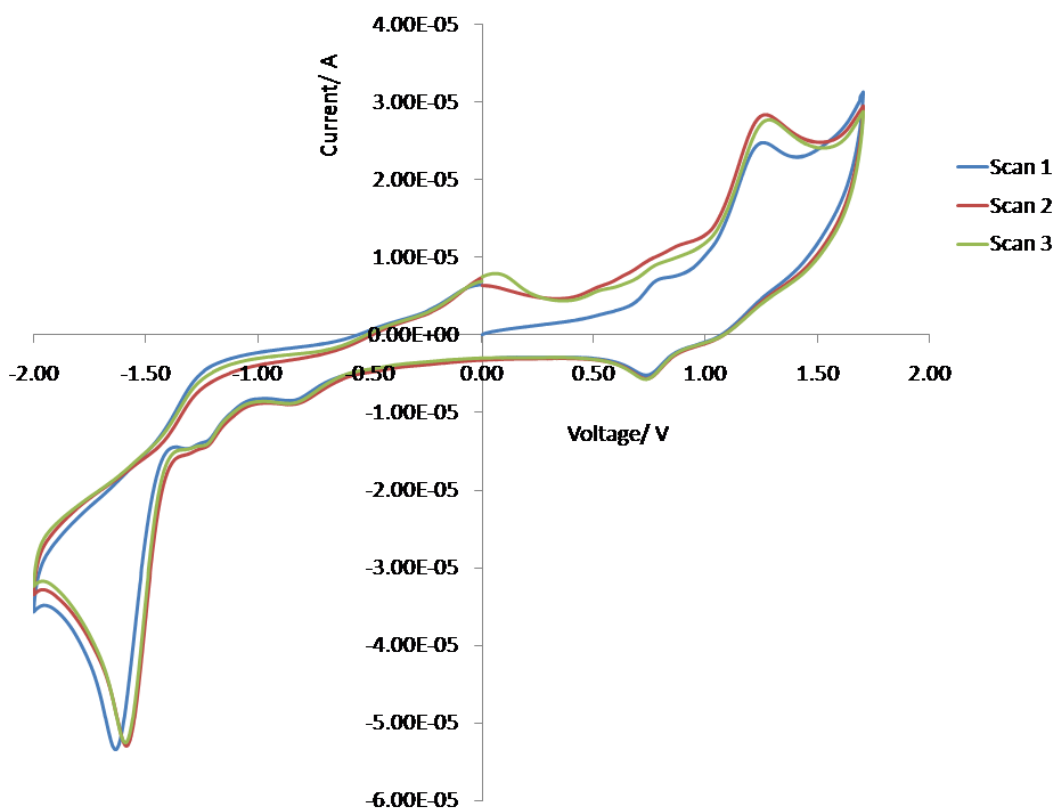
Figure 54: Consecutive cyclic voltammograms of [Ni37]$^+$ 0.2 V/s. Data collected in acetonitrile with tetra-butyl ammonium perchlorate as a supporting electrolyte at RT using a platinum reference electrode..

Figure 54 shows the cyclic voltammograms at 0.2 V/s for three consecutive scans. The reversible formation of the phenoxyl radical is observed at +0.74 V (reversibility of this wave was tested by plotting peak current verses the square root of scan rate; a straight line, indicative of a reversible process, was obtained). This is significantly more positive than for the copper(II) complex, meaning that the nickel(II) ion must be stabilising this redox process to a greater extent (i.e. a more positive potential is required to generate the radical species). Kimura and co-workers reported that the phenol undergoes oxidation at +0.5V for their nickel(II) complex of phenolate appended cyclam.[161] Therefore the phenol in complex [Ni**37**]$^+$ is more stable to oxidation than the corresponding phenol in the non-configurationally restricted complex. The oxidative peak at +1.24 V is believed to be due to the formation of nickel(III) from nickel(II). Literature values for this transition from other cyclam complexes vary between +1.07 and +1.52 V,[174] and +1.07 to +1.16 V.[185] An interesting feature of the cyclic voltammogram arises in the second and third scans in

122

that the initial oxidation of the phenolate to the phenoxyl radical is no longer clearly defined. Previously nickel(II) complexes have been observed to possess two sets of quasi-reversible waves which are both part of the Ni(II)/Ni(III) process.[174,185] The relative size of these pairs of waves can vary considerably with the nature of the ligand, solvent and electrode. Oxidation potentials for the second set of waves occur between ~+0.5 to +1 V. It is therefore possible that a second set of waves for the Ni(II)/Ni(III) couple is formed after the initial scan near to the reversible wave of the phenoxyl radical. This may well lead to the distortion of the peak shape of the latter wave to a slope that is observed in scans two and three.

3.5. Cyclic voltammetry data for side-bridged cyclam thiophenolate complexes
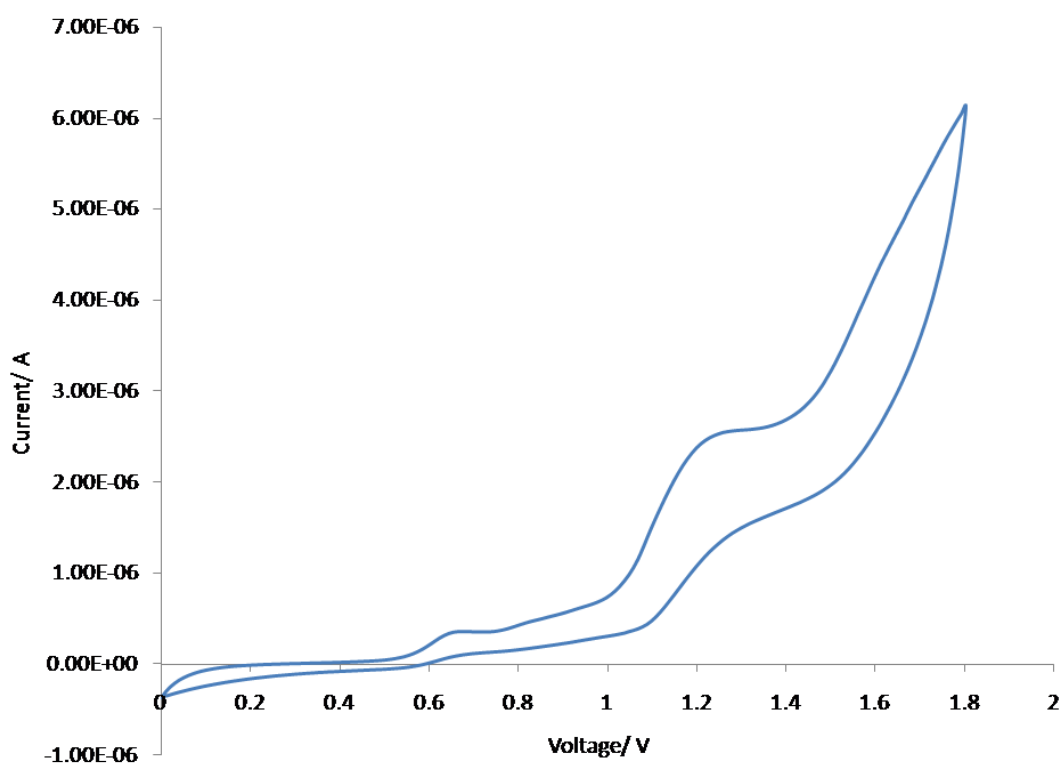
Figure 55: Cyclic voltammogram of [Ni46]$^+$ at 0.01 V/s. Data collected in acetonitrile with tetra-butyl ammonium tetrafluoroborate as a supporting electrolyte at RT using a platinum reference electrode.

Figure 55 shows the cyclic voltammogram of [Ni**46**]$^+$ recorded at 0.01 V/s. Two peaks are observable. The peak at +0.60 V is assigned to the formation of the thiyl radical. Literature data for the formation of this species in other systems has been reported as +0.90, +0.65 and +0.60 V respectively for the gallium(III), iron(III) and cobalt(III) complexes of TACN ligands bearing a single thiophenolate and two acetate pendant arms.[142] The peak therefore at +1.18 V is not ligand centred but due to the Ni(II)/Ni(III) redox couple. This peak appears to be quasi-reversible with there being a small back wave present at +1.1 V which could correspond to the reduction of nickel(III).
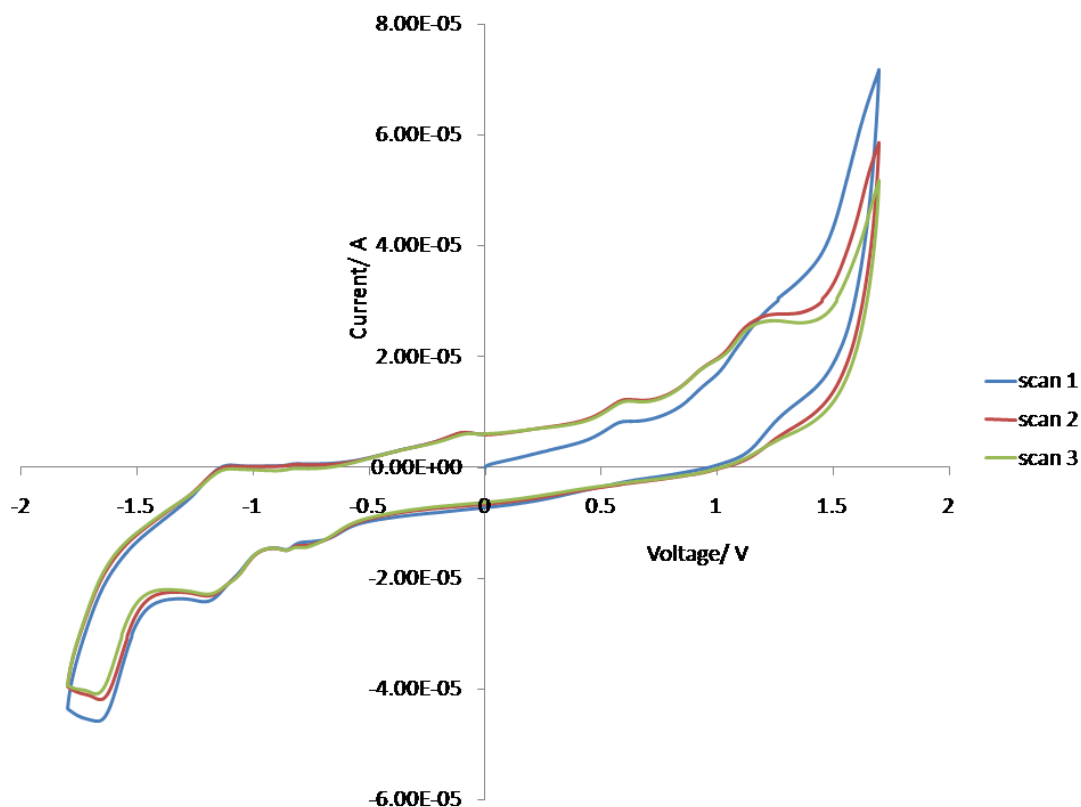
Figure 56: Consecutive cyclic voltammograms of [Ni49]$^+$ at 0.2 V/s. Data collected in MeCN with tetra-butyl ammonium perchlorate as a supporting electrolyte at RT using a platinum reference electrode.

Figure 56 shows three consecutive cyclic voltammograms of [Ni**49**]$^+$ at 0.2 V/s. This data can again be compared with other complexes. Gallium(III) and cobalt(III) complexes have been reported with TACN ligands bearing one di-*tert*-butyl thiophenolate and two acetate pendent arms. Irreversible waves at +0.82 V and +0.53 V were assigned to the formation of the thiyl radical. It is thought that after formation of the radical species M-SR scission occurs followed by reaction to form a disulfide linked dimer. The cyclic voltammograms in Figure 56 display two peaks in the anodic region; one at +0.53 V and the other at +1.11 V. From this data, it is difficult to make a full assignment, but the waves are due to the formation of the thiyl radical and Ni(II)/Ni(III) redox couple. At +1.12 V there is a quasi-reversible wave due to the Ni(II)/Ni(I) redox couple. The irreversible peak at −0.2 V only appears after the anodic region is scanned first. Wieghardt and co-workers reported a similar observation for their cobalt(III) complex. They found that after scanning through the oxidation wave, that upon re-reduction, a small wave at −0.5 V was

observed. This wave was assigned to the reduction of a disulfide complex. It is reasonable to suggest therefore that the wave at −0.2 V in Figure 56 can be similarly assigned.
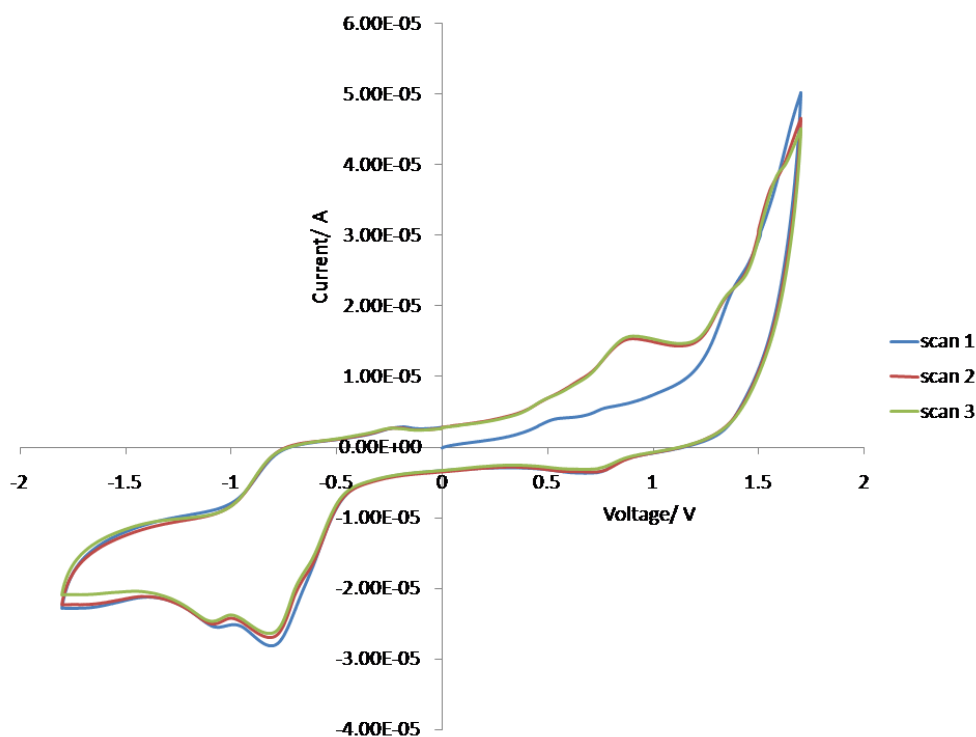
Figure 57: Consecutive cyclic voltammograms of [Cu49]$^+$ recorded at 0.2 V/s. Data collected in acetonitrile with tetra-butyl ammonium perchlorate as a supporting electrolyte at RT using a platinum reference electrode.

Figure 57 shows three consecutive cyclic voltammograms for [Cu**49**]$^+$ at 0.2 V/s. Two waves are observed in the anodic region; one at +0.50 V and the other at +0.8 V. By comparison with the nickel(II) thiophenolate species and also because the wave at higher potential shows quasi-reversibility, the waves are assigned to the formation of the thiyl radical and oxidation of copper(II) to copper(III) respectively. The wave in the cathodic region at −0.76 V is assigned to the reduction of copper(II) to copper(I). This is again split, most likely through the production of adsorbed and free species. A further wave is observed in the cathodic region. This peak is not observed if the cathodic region is scanned first, suggesting that this species may be formed after thiyl radical generation and reaction. As discussed, the homolytic coupling between two such species would result in the production of a dimeric complex. This wave at −0.25 V could be an oxidation of this dimeric species.

3.6. Conclusion

In this chapter the synthesis of side-bridged cyclam complexes with pendent thiophenolate or phenolate arms has been examined. The side-bridged cyclam compound bearing an unmasked phenol could not be synthesised directly due to a competing reaction. The side-bridged cyclam compounds bearing protected phenol pendent arms were synthesised successfully but it was difficult to unmask the phenol. The only suitable deprotection strategy for unmasking the phenol was found to be using 6M HCl in conjunction with the acetyl protected compound, **43**. Nickel(II), copper(II) and zinc(II) complexes were produced for the phenolate and protected phenol side-bridged cyclam compounds. Gallium(III) complex formation was also attempted but was unsuccessful. The crystal structure of the nickel(II) complex of **36** was obtained in which the nickel(II) centre adopts a square-planar geometry. Cyclic voltammetry of the nickel(II) and copper(II) complexes was performed. For the copper complexes, the Cu(II)/Cu(III) redox couple was shifted towards anodic potentials in the order *p*-methoxybenzyl < benzyl < methyl. For [Cu**37**]$^+$ a wave corresponding to the formation of the phenoxyl radical was observed at +0.48V (reversible). The phenoxyl radical was also observed to form in [Ni**37**]$^+$ at +0.74V.

Metal complexes of the thiophenol side-bridged cyclams were also produced. Again, gallium(III) complexes were desired but were not isolated. The thiophenol was unmasked by cleaving the *p*-methoxybenzyl protecting group using mercury acetate and hydrogen sulphide. Cyclic voltammetry was performed on the copper(II) and nickel(II) complexes. The CV of [Ni**46**]$^+$ possesses a wave at +0.60 V which is assigned to the formation of the thiyl radical. In the copper(II) and nickel(II) complexes of **49**, the formation of the thiyl radical was assigned to peaks at +0.50 and +0.53 V respectively. These complexes also display evidence for dimerisation occurring in solution. Oxidation waves at −0.25 and −0.2 V are assigned to the oxidation of the dimer for the copper(II) and nickel(II) complexes of **49** respectively.

4. Synthesis of cyclen derived macrocyclic systems with phenolate, thiophenolate and amino-acid pendent arms

4.1. Introduction

This chapter contains a report of the synthesis of cyclen derived macrocyclic lanthanide complexes bearing either phenol, thiophenolate or amino-acid pendent arms. The cavity size of cyclen means that it is suited towards lanthanide metal ions with the metal centre sitting above the plane of the four nitrogen donors. The ligands were designed to provide the lanthanide centre with either a N_4O_4 or $N_4O_3S_1$ donor set. As lanthanides typically prefer coordination numbers of seven to nine, this meant that there was possibly a ninth coordination site available. As the compounds could have application as MRI contrast agents, the availability of a ninth site would enable a water molecule to enter the inner coordination sphere. When complexed to a paramagnetic metal centre this would enable the perturbation of the surrounding proton nuclei by the paramagnetic centre, thus leading to the enhancement of images produced. Specifically, it is the interaction with the proton nuclei of water molecules that leads to an enhancement of the image.

4.1.1. Magnetic resonance contrast agents

The use of MRI as a worldwide imaging modality has promoted the need for better enhancement of the images obtained. Currently, about 40% of MRI scans worldwide are performed using contrast agents. The function of the contrast agent is to accelerate the relaxation of water protons in the surrounding tissue. This objective can be achieved by using paramagnetic substances. This effect was first reported by Bloch *et al* by using ferric nitrate salt to enhance the relaxation of water protons.[187] Currently gadolinium(III) complexes are by far the most widely used in contrast agents in clinical practice. Some of these contrast agents are shown in Figure 58.
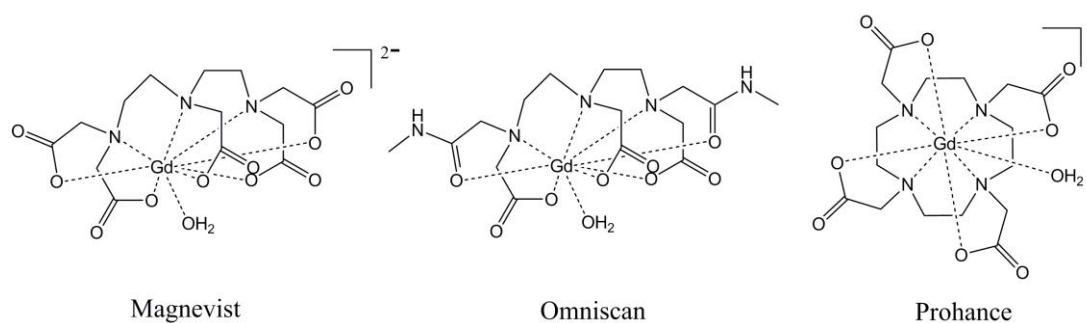
Figure 58: Chemical structures of some of the contrast agents currently used in clinical practice.

Performing an MR scan requires the use of a strong magnetic field. This has the effect of causing the majority of proton nuclei to align in the direction of which the magnetic field is applied (see Figure 59). A radio-frequency (RF) pulse, perpendicular to the magnetic field, causes the proton nuclei to flip into a transverse plane. This can be thought of as a high energy state as the magnetisation of the proton nuclei is in a plane perpendicular to that of the external magnetic field. After the RF pulse is switched off, the proton nuclei begin to re-align with the external magnetic field. As the proton nuclei relax from a high energy state to a low energy state, a further RF pulse is emitted as a result. This RF pulse can be detected and interpreted in order to produce images of the local area.
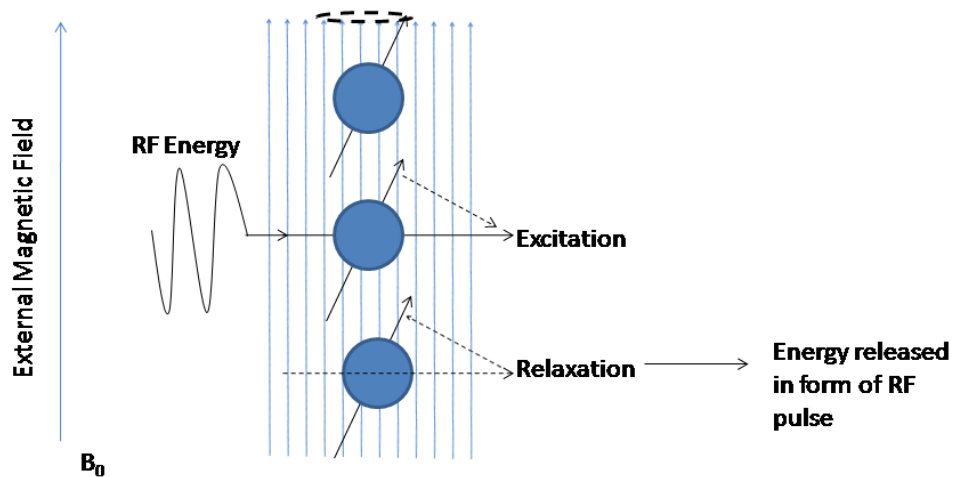
Figure 59: Diagram showing the effect on the proton nuclei caused by the external magnetic field and RF pulse.

Relaxation of the nuclei occurs through two relaxation processes; T1 and T2. T1 relaxation arises because of the longitudinal relaxation of the proton nuclei. This is also known as spin-lattice relaxation. This relaxation process is responsible for the dissipation of energy from radiofrequency-excited protons into their molecular environment or "lattice". T1 is a measure of time required for the magnetisation in the longitudinal direction to return to 63% of its equilibrium magnetisation.

T2 is responsible for the dissipation of the transverse magnetisation. This is also known as spin-spin relaxation. Unlike T1, the T2 process reduces order after an excitation pulse. This is because individual components of the magnetisation lose their alignment and rotate at various rates in the transverse plane. The T2 relaxation

time is a measure of the time required for 63% of the initial magnetisation to dissipate.

T1 contrast agents utilise a paramagnetic metal ion to reduce the time taken for proton nuclei to return to their equilibrium magnetisation. This leads to image enhancement because of a reduction of line broadening. The paramagnetic relaxation of the water protons originates from the dipole-dipole interactions between the nuclear spins and the fluctuating local magnetic field caused by the unpaired electron spins. This magnetic field around the paramagnetic centre diminishes rapidly with distance. Therefore, chemical interactions that bring water protons into the immediate proximity of the metal ion play an important role in transmitting the paramagnetic effect towards the bulk solvent. For gadolinium(III) complexes, this specific interaction corresponds to the binding of the water molecules in the first coordination sphere of the metal ion. These inner water-sphere water protons then exchange with bulk solvent protons (k_{ex} represents the exchange constant for this process in Figure 60) and in this way the paramagnetic influence is propagated to the bulk.
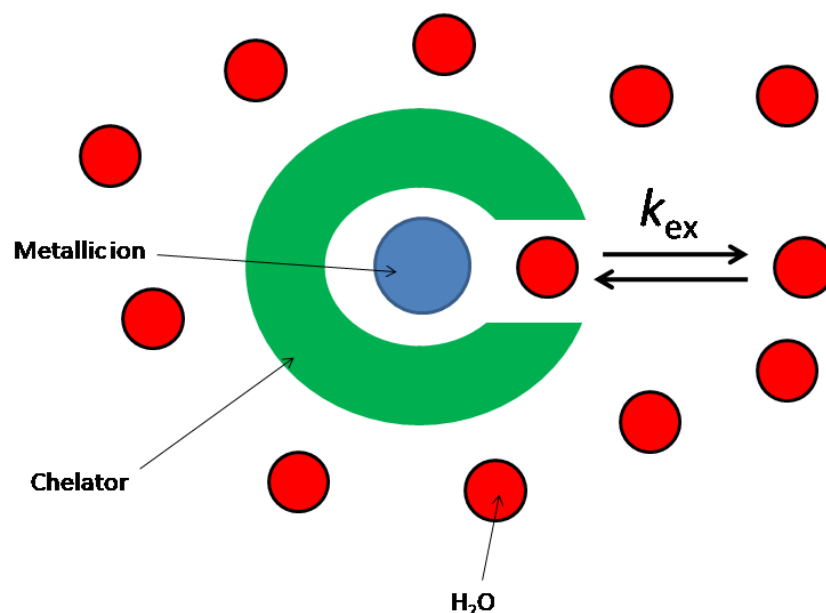
Figure 60: Diagram showing the exchange of water molecules in the inner sphere of a contrast agent complex.

4.1.2. Examples of known phenolate complexes

A Beilstein database search highlights that only two previous examples have been reported in which phenol moieties are incorporated into the pendent arms of cyclen derived macrocycles. The first example was reported by Heath, Faulkner and co-workers.[91] Their paper is concerned with the synthesis of a dinuclear ytterbium(III) complex. The ytterbium(III) ions are held in two DO3A macrocyclic units which are bound together using a phenol bridging group. The way in which the phenol is positioned means that it can be involved in the coordination of either metal centre, but the bulk of the DO3A unit prevents both lanthanides from sharing the phenolate oxygen donor. Hydration numbers of 1 and 0.3 were obtained, inferring that the ytterbium(III) metal centres are eight and seven coordinate respectively. The reason for the apparently low hydration numbers was attributed to the lipophilicity of the linking phenolate which prevented water molecules from approaching the metal centres. The phenol linker group was introduced by reacting 2,6-bis(chloromethyl)-4-methylphenol with two equivalents of DO3A in the presence of potassium carbonate.

The other example has been reported by Sherry and co-workers.[78] Their study focused on the effect of ligating groups on dissociation of a *p*-nitrophenolic pendent arm. This *p*-nitrophenolic pendent arm was introduced by reacting 2-hydroxyl-5-nitrobenzyl bromide with two equivalents of cyclen in dioxane. This gave the mono-alkylated derivative in 55% yield. Acetate groups were then introduced at the remaining three secondary amine sites using bromoacetic acid at pH 8.5 in 49% yield. This gave the formation of the chelator in 27% yield. An alternative procedure was used in the formation of the triamide derivative. This procedure involved the use of six steps to synthesis the chelator in 48% yield. The *p*-nitrophenolic arm was introduced in the ultimate step by reacting it with a stoichometric amount of DO3AM in the presence of K_2CO_3. Recrystallisation from methanol/acetonitrile afforded the chelator in 65% from this step.

Further fourteen membered macrocycles have been synthesised with phenolic pendent arms. Much of this work has been focused on monoazacrown macrocycles with a pendent spirobenzopyran moiety. A reported synthesis to give a spirobenzopyran attached to a monoaza-12-crown has been published by Kimura.[188]

This was synthesised by reacting 2-(3-(chloromethyl)-2-hydroxy-5-nitrophenyl)acetaldehyde with 1,4,7-trioxa-10-azacyclododecane in the presence of triethylamine. This was then further reacted with 1,3,3-trimethyl-2-methyleneindoline to form the spirobenzyopyran 12-monoazacrown, which can be converted to the zwitterionic merocyanine isomer by UV irradiation. In addition, for those spirobenzopyran derivatives possessing a piperidinomethyl group at the 8-position, isomerisation has been shown to proceed in the presence of metal ions such as zinc(II) even under dark conditions. This arises because the merocyanine form is stabilised to some extent by chelate formation with the metal cation (Scheme 20).
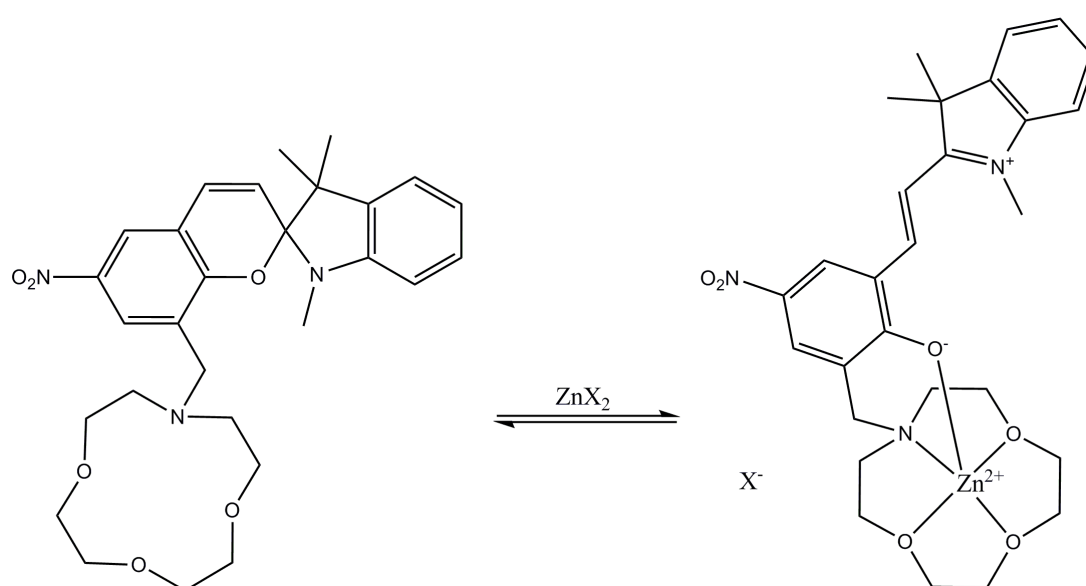
Scheme 20: Equilibrium between the spirobenzopyran and merocyanine isomers perturbed by the addition of a zinc(II) salt.

Kimura and co-workers have also used monoazacrown macrocycles bearing spirobenozopyran pendent arms to investigate cation specific isomerisation.[189] Selectivity for lithium(I) and sodium(I) was found to be dependent on the ring size; a twelve membered ring being selective for the former whilst a fourteen membered ring selective for the latter. This was reflected in the isomerisation of the spirobenzopyran to the merocyanine form. For the twelve-membered macrocycle, lithium(I) selectivity reflected the degree of isomerisation whereas for the fourteen membered ring, isomerisation decreased in the order lithium(I) $\geq$ sodium(I) > potassium(I). This would suggest that the complexation of lithium(I) by the crown

moieties stabilises the merocyanine isomers significantly more than other group I metals.

Kimura and co-workers have also reported further applications for this ligand type with regard to studying the photoresponse profile of poly(vinyl chloride) (PVC) membranes.[190] A lipophilic chain was appended to the spirobenzopran moiety, which was then incorporated into the PVC membrane. Upon UV-irradiation, the potential was found to increase and then decrease. The photoresponse profile was affected considerably by the nature of the metal ion in the monoazacrown cavity and also the pH of the aqueous phase. The change in potential was believed to be brought about by fast proton exchange, followed by subsequent slow metal–ion exchange into the merocyanine form. Further work by Kimura and co-workers in this area has focused on incorporating the crowned spirobenzopyran moiety at the side chain of the PVC either as one component or being split into its two representative parts.[191]

Toğrul and co-workers have synthesised borocrytands which bear two 4-*tert*-butyl saligenin units.[192] Previous borocrytands which utilised catechol pendent arms were found to be very oxygen sensitive. This is because of the strong basicity of the macrocyclic core, resulting in intramolecular proton transfer from the catechol group to the tertiary amines thus generating the catecholate ammonium zwitterion.[193] The propensity to oxidation can be reduced by forming boron complexes and also by converting the catechol to saligenine. The boron is complexed by the two saligenine units leaving the macrocyclic cavity available to complex a further metal ion.

Work by Shinkai and Linnane has produced calix-tetra-aza-crowns ether bearing phenol pendent arms with the aim of studying interactions with group I metals and diammonium cations.[194] A monoaza-12-crown incorporating an *o*-methyl phenol pendent arm was also synthesised. Both compounds were found to have selectivity for potassium(I) and rubidium(I). The increased selectivity of the calix-tetra-aza-crown-ether is due to the four aza crowns acting in a cooperative manner.

4.1.3. Examples of known thiophenolate complexes

A Beilstein database search reveals, that at present, there is no literature in which a thiophenolate pendent arm is appended to a cyclen macrocyclic unit. Examples do exist, however, which use monoazacrowns. Kimura's group, have reported the synthesis and evaluation of two spirobenzothiapyran 12-monoazacrowns similar to the ligands already discussed.[195,196] As a result, when the merocyanine isomer is formed, a thiophenolate coordinates to the metal ion instead of a phenolate. The spirobenzothiapyran unit is introduced using an analogous methodology to the spirobenzopyran. 2-(3-(chloromethyl)-2-hydroxy-5-nitrophenyl)acetaldehyde was reacted with 1,4,7-trioxa-10-azacyclododecane in the presence of triethylamine. Conversion of the phenol to the thiophenol was achieved by using $(CH_3)_2NCSCl$ in the presence of triethylamine, by treatment with toluene and finally by hydrolysis with KOH in H_2O-EtOH. The crowned thiosalicyl aldehyde is then reacted with 2-methylene-1,3,3,trimethylindoline to complete the spirobenzothiapyran unit (see Scheme 21).
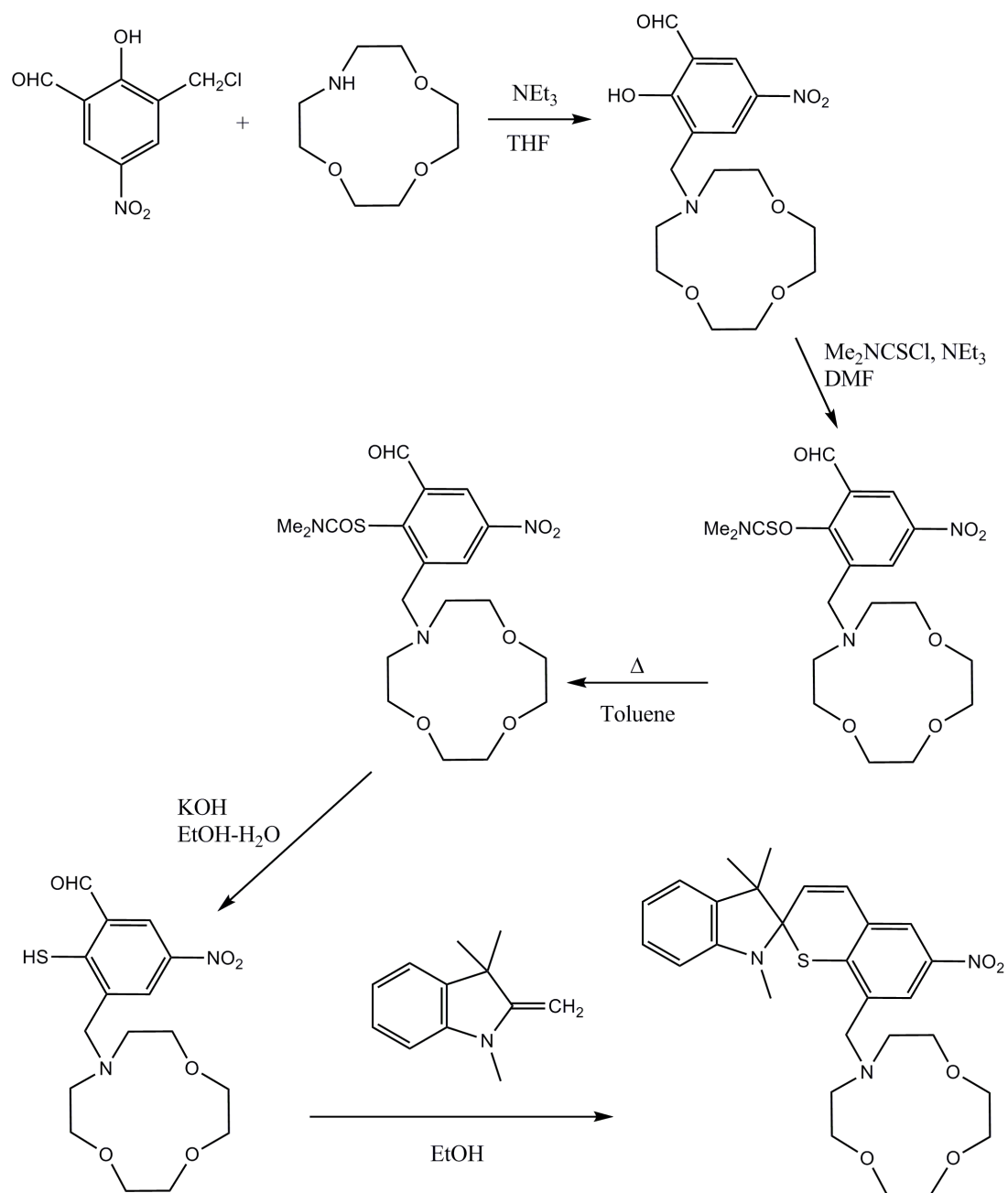
Scheme 21: Synthesis of crowned spirobenzothiapyran[195].

4.2. Synthesis of cyclen ligands with thiophenolate and phenolate pendent arms and their lanthanide complexes

The synthetic methodology used in this work to form chelators and lanthanide complexes bearing either a phenolate or thiophenolate pendent arm was designed so that complexes of type seen in Figure 61 could be produced (where X = O or S). The macrocyclic chelator along with the pendent arms provides the lanthanide centre with a coordination number of eight. This leaves the possibility of a ninth coordination site which can be filled by a water molecule.
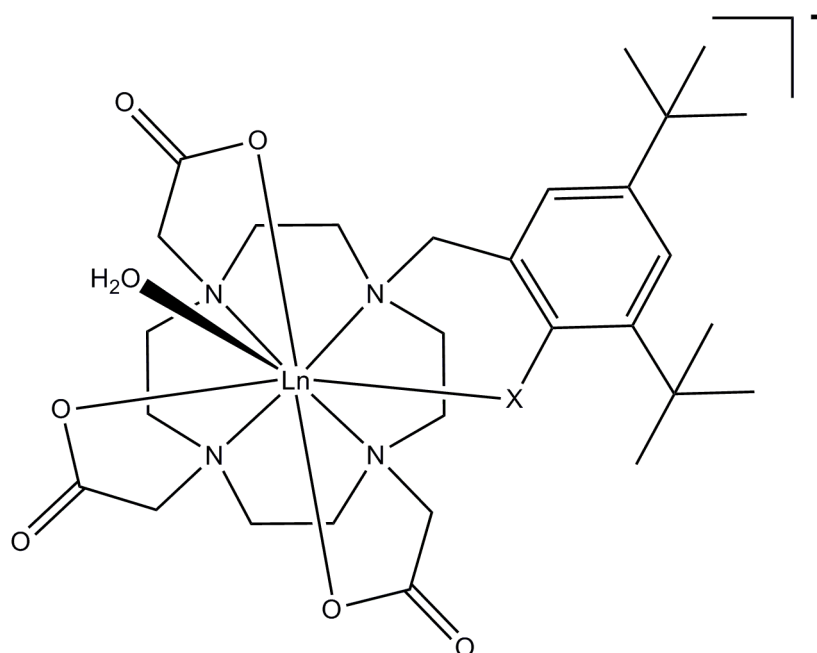
Figure 61: Chemical structure of target lanthanide complexes bearing either a thiophenolate or phenolate pendent arm (X = O or S).

These complexes were designed to have potential as contrast agents for MRI, and so the availability of a coordination site which can be filled by a water molecule is important. This is because the transmission of the paramagnetic effect towards the bulk solvent is more effective when an inner sphere water molecule is present. It was proposed that the thiophenolate or phenolate arm could be oxidised, to generate the phenoxyl or thiyl radicals respectively. By doing so, the pendent arm would become a poor donor for the lanthanide centre and enable a further coordination site to become vacant. This could be filled by a further water molecule and as such the

effect of the lanthanide ion on the relaxation of proton nuclei on water molecules in the vicinity would be increased. This change in the coordination environment of the lanthanide can be detected through comparison with the unoxidised complex. In the following two sections, the synthesis of the phenolate and thiophenolate ligand systems and their complexes will be discussed, which is followed by an analysis of their physical and image enhancing properties.

4.2.1. Synthesis of phenolate bearing macrocyclic ligands and their complexes

The first synthetic strategy that was attempted to prepare the phenolate bearing macrocycle is outlined in Scheme 22. This route makes use of the previously synthesised *tert*-butyl ester of 1,4,7,10-tetraazacyclododecane-1,4,7-triacetic acid (DO3A-TB).[197] This compound possesses a single secondary amine which can be used to attach a further pendent arm by nucleophilic attack. DO3A-TB was reacted with the unmasked phenol pendent arm, **2**, which had been synthesised as outlined in Chapter 2. However, the desired reaction did not occur. Changing the base from potassium carbonate to sodium hydrogen carbonate was not effective, therefore, alternative routes were sought.

Wieghardt and co-workers have published a procedure for the attaching of 2-hydroxy-3,5-di-tert-butyl-benzyl bromide to 1,4-dimethyl-1,4,7-triazacyclononane.[132] This was accomplished by using KOH in dry toluene and heating to 70°C for 6 hr. The product from this reaction was suitable for the formation of metal complexes without the need for purification. This seemed to be very well suited towards the reaction of the same pendent arm with DO3A-TB. Using these conditions, however, did not give the target compound
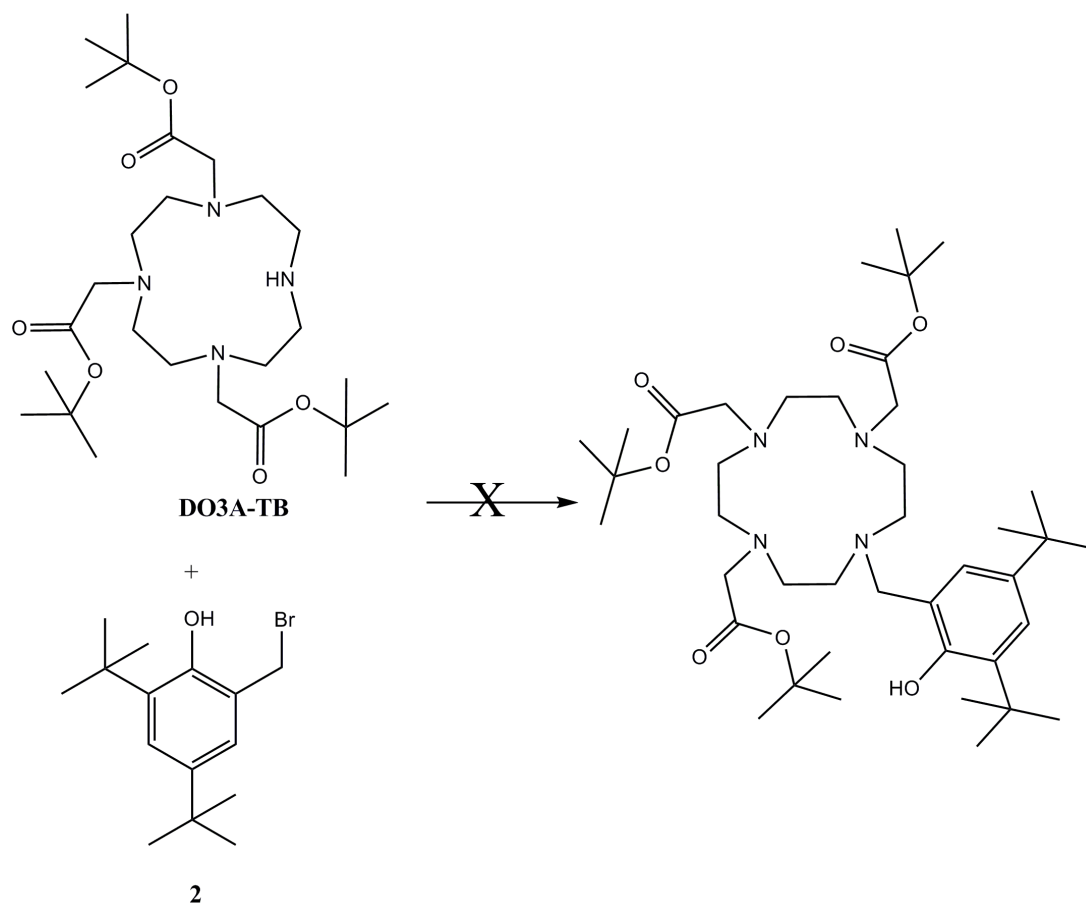
Scheme 22: Attempted reaction of 2 with DO3A-TB.

Mannich condensations have been used for the formation of salicylidene(amine)diaminoethane (salen) and substituted salens previously. Secondary amines have been reacted with various *tert*-butyl substituted phenol pendent arms to form di-substituted species by Kol *et al.*[198] Yields of 71-100% were obtained. Another example has been prepared by Gibson and co-workers. An acyclic ligand was produced which possessed two 2,4-di-methyl-phenol moieties separated by an ethylenediamine chain.[199] Gibson and co-workers have reported further complexes, this time focusing on 2,4-di-*tert*-butyl phenols.[200] The ligands bearing one phenol pendent arm were obtained in good to excellent yields.

The literature precedence for the use of Mannich type condensation for attaching substituted pendent arms to secondary amines suggested that this could be used for producing the target ligand as shown in Scheme 23. DO3A-TB was used for attempting such condensations because it only possesses one secondary amine which

is available for reaction. Despite the literature precedence for this reaction, it was unsuccessful and so alternatives were again sought.
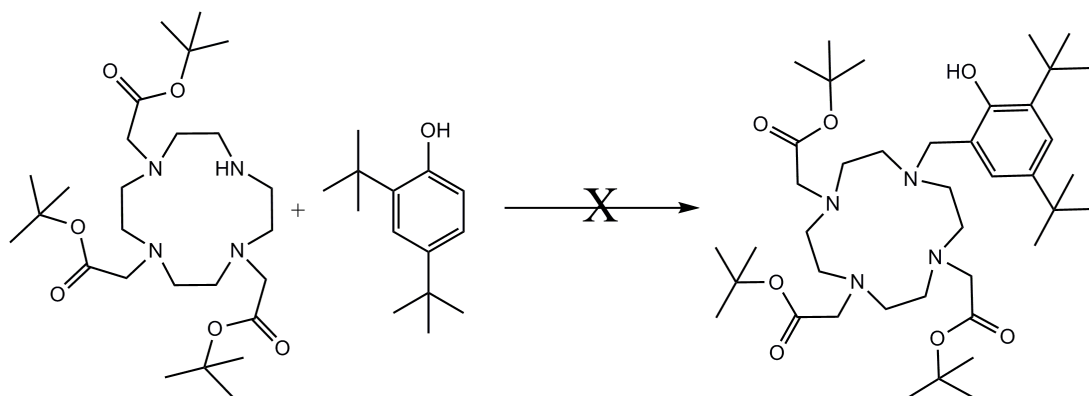
Scheme 23: Attempted Mannich reaction between DO3A-TB and 2,4-di-tert-butyl-phenol.

Welch and co-workers have reported the synthesis of cyclen derivatives bearing one, two, three or four *tert*-butyl benzyl pendent arms.[60] Di-iso-propyl amine was used as the base to promote the reaction. This reaction was used in an attempt to mono-alkylate the cyclen ring with one pendent arm. This was carried out with the unmasked phenol compound, **2**, but was unsuccessful. The reason for this may lie in the formation of the phenolate anion which can form oligomers with other molecules of **2**, as was observed when performing the same reaction using glyoxal cyclam, **33**, in Chapter 3.
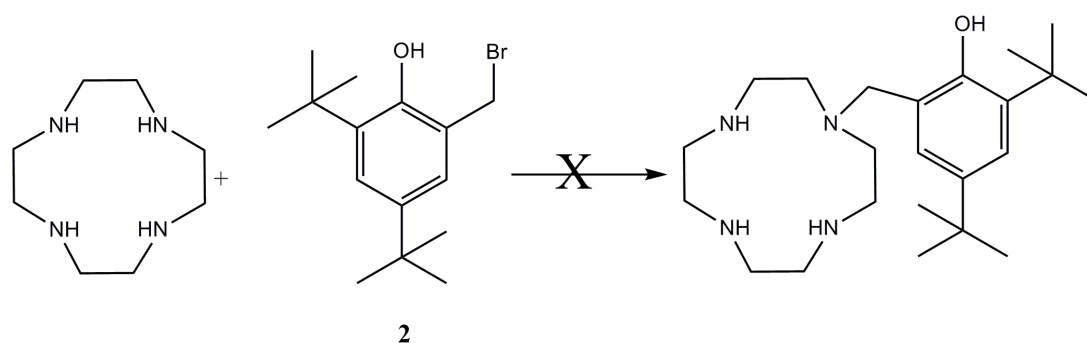
Scheme 24: Attempted reaction between cyclen and 2.

Further routes to mono-alkylated cyclen compounds have been reported in the literature. Gunnlaugsson and co-workers have reported yields of 60 to 75% for the mono-alkylation of cyclen with a variety of alkyl halides.[201] This route uses four equivalents of cyclen to one equivalent of alkyl halide and affords the mono-alkylated product without the need for purification. The excess cyclen can also be recovered from the alkaline aqueous layer by firstly concentrating it under reduced pressure and then neutralising it. This route was therefore applicable to the production of a cyclen species bearing one phenol protected pendent arm. Within the Archibald group this approach has been used previously, leading to the synthesis of a cyclen bearing a *tert*-butyl carbamate (BOC) protected ethyl amine (compound prepared by Chris Welch).

The desired reaction proceeded in good yield (89%). It was found that by triturating the oily residue with pentane, a yellow solid could be obtained. Interestingly, use of this methodology in attaching the same pendent arm to DO3A was not successful. Meade and co-workers have reported a similar observation when they were investigating the problematic attachment of a glucoronic containing pendent arm.[75] In trying to attach the pendent arm, two different reaction pathways were attempted. In the first approach, DO3A was used, which gave an incomplete reaction but by using cyclen the desired reaction was achieved. The reason for the difference in reactivity arises because the nucleophilicity of the macrocyclic units differ. The macrocyclic free base is more nucleophilic towards the unactivated alkyl bromide electrophile than the DO3A compound.

Having now appended the phenolate pendent arm, the resulting acetate arms could then be tethered as shown in Scheme 25. The attachment of the *tert*-butyl acetate

arms to compound **50** was performed in the presence of potassium carbonate. After extraction of the crude product, column chromatography was required to isolate the desired product.

The next step involved the hydrolysis of both types of ester. Wieghardt has reported the simultaneous hydrolysis of an acetyl *p-tert*-butyl phenol pendent arm and an ethyl ester using LiOH.H$_2$O in 61% yield.[137] *tert*-Butyl esters, however, are resistant to basic hydrolysis and so using this methodology would require a further step. Using acidic hydrolysis to cleave both types of ester simultaneously was the more suitable option. Having previously performed a similar deprotection on compound **42** using 6M HCl to promote hydrolysis, the same conditions were again employed. After heating compound **51** in 6M HCl at reflux overnight, the desired chelator, **52**, was obtained as the tetra-hydrochloride salt in 94% yield.
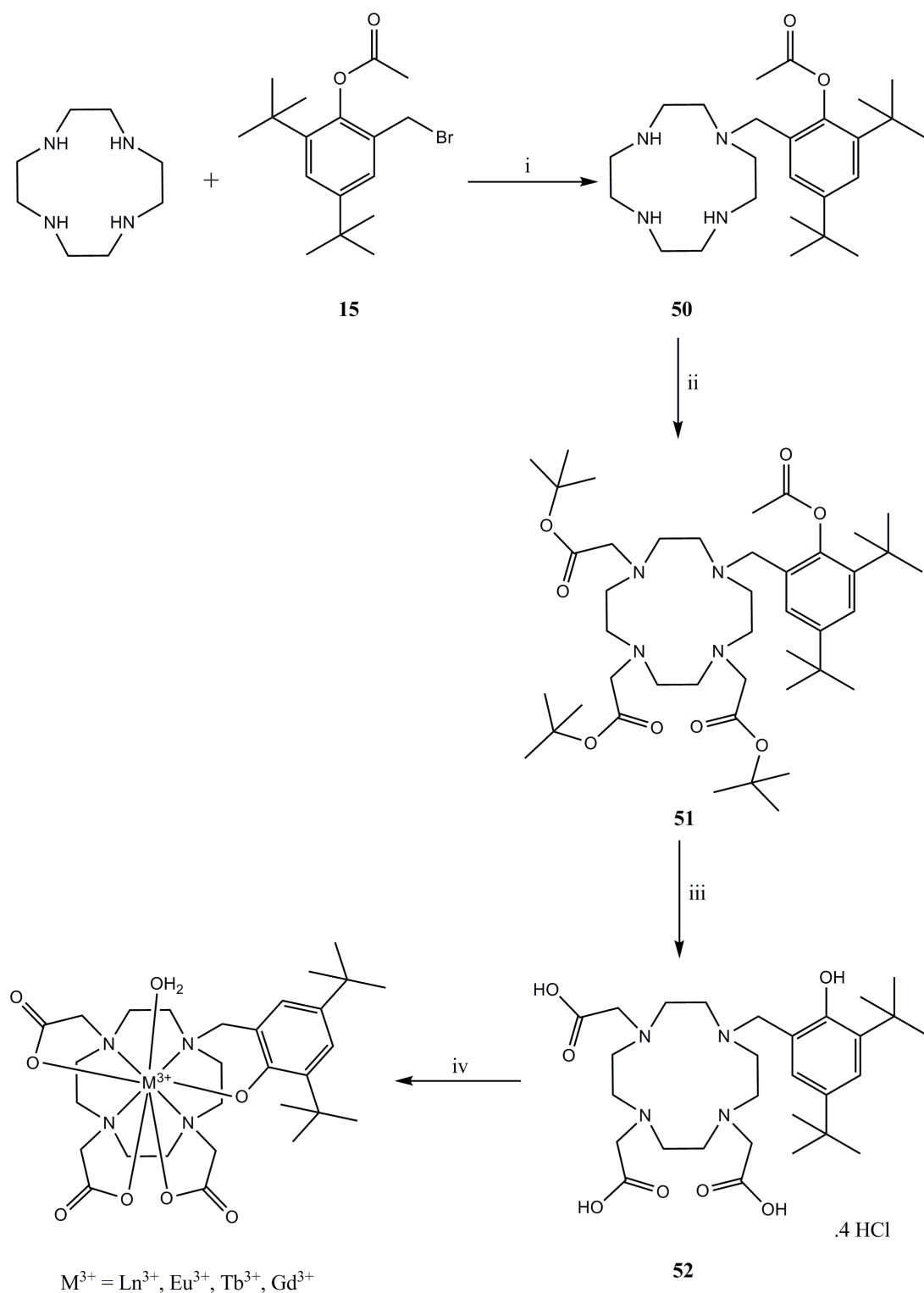
Scheme 25: Synthesis of 51. Conditions; i) CHCl₃, NEt₃, reflux, 16hr (89%); ii) BrCH₂COOᵗBu, K₂CO₃, dry MeCN, RT, 48 hr (71%); iii) 6 M HCl, reflux, o/n (94%); iv) metal salt, NEt₃, MeOH, reflux, 2 hr (La=76%, Eu=83%, Tb=90% and Gd=96%).

Four metals ions were identified for investigation; lanthanum(III), europium(III), gadolinium(III) and terbium(III). Lanthanum(III) was chosen because it is diamagnetic and thus the complexes can be used to obtain unshifted ^{1}H NMR data. Europium(III) and terbium(III) both possess luminescent properties, which were thought to be of interest because the phenolate could possibly act as a sensitiser for the metal centre. Europium and terbium also flank gadolinium in the periodic table and as such can be used to gain further information about the properties of the gadolinium complex. Finally, gadolinium(III) was chosen because it possesses seven unpaired electrons. Any complexes produced will therefore be highly paramagnetic, which is vital to the application of these complexes as contrast agents for use in MRI.

Metal complexation was performed in methanol using a 1:1 ratio of metal salt to ligand **51**. NEt$_3$, was used to ensure the deprotonation of the eight coordination donor atoms. After heating the solution to reflux for 2 hr, the solutions were filtered once cool. After evaporation of the filtrate, the oily residue was dissolved in methanol and eluted down a Sephadex column with MeOH. The desired fraction was collected and concentrated under reduced pressure. The oil collected was triturated with diethyl ether to produce the metal complexes as off-white solids. A variety of physical techniques were then used to study the properties of the metal complexes.

4.2.2. Synthesis of thiophenolate bearing macrocyclic ligands and their complexes

With the successful synthesis of cyclen bearing a phenol and three acetate pendent arms, attention now turned to its thiophenolate analogue. The same methodology was employed for the synthesis of the thiophenolate analogue. Thus four equivalents of cyclen and one equivalent of the thiophenol pendent arm were reacted in the presence of triethylamine. The desired compound, **53**, was isolated in 83% yield. The acetate arms could then be attached to the remaining secondary amine sites to complete the synthesis of the fully protected chelator. This step required column chromatography to purify the product. The thiol protecting group, *p*-methoxy benzyl, could now be removed by cleaving the thioether bond. This was achieved by the use of mercury acetate and hydrogen sulphide. The *tert*-butyl esters were then cleaved by heating a solution of **55** in 6 M HCl to reflux overnight. Performing the deprotection steps in this order would also cleave any disulphide bridged dimers formed.
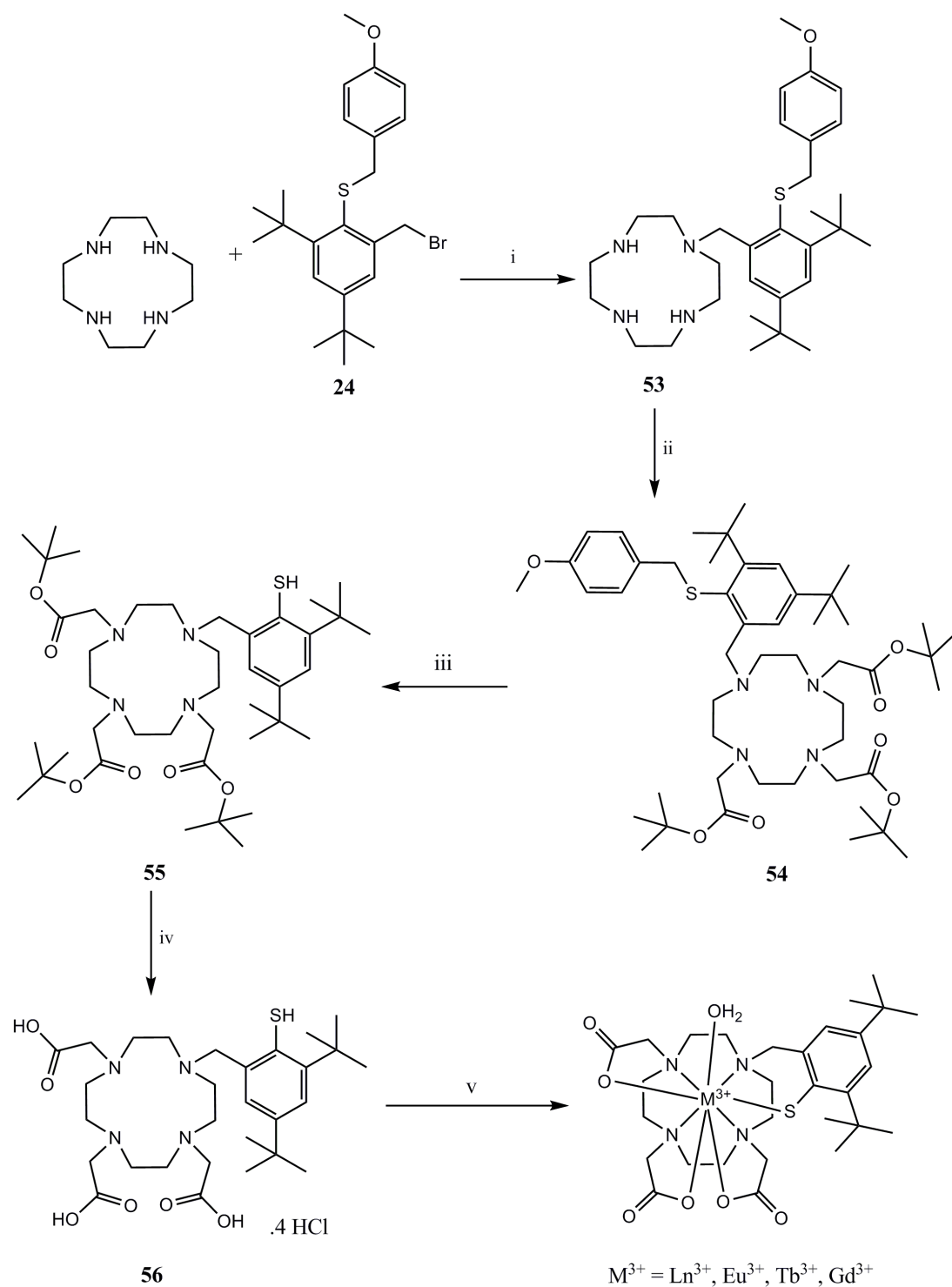
Scheme 26: Synthesis of 56. Conditions; i) CHCl₃, NEt₃, reflux, 15 hr (83%); ii) BrCH₂COOᵗBu, K₂CO₃, dry MeCN, RT, 24 hr (64%); iii) MeOH, Hg(OAc)₂, H₂S, MeOH, (100%); iv) 6 M HCl, reflux, o/n (100%); v) metal salt, NEt₃, MeOH, reflux, 2 hr (La=76%, Eu=100%, Tb=90%, Gd=87%).

The complexation of this prochelator to the four lanthanide ions lanthanum(III), europium(III), gadolinium(III) and terbium(III) was performed under an argon atmosphere. Triethylamine was used to deprotonate the acetate, tertiary amines and thiol functionalities to enable coordination to all eight donors. All solvents used in the preparation and work-up were degassed prior to use. The same work-up procedure as for the phenolate complexes was used.

4.2.3.Images obtained from magnetic resonance imaging T1 experiments

Figure 62 shows T1 weighted images produced from gadolinium(III) complexes of **52** and **56**. Images were collected using a flash scan which collected 8 slices of 1 mm thickness with a repetition time of 100 ms. The experiments were conducted using a small NMR tube inside a larger NMR tube. For A and C, the inner tube contained the gadolinium(III) complex of **52** and **56** dissolved in water respectively, with water in the outside tube. These images clearly show an enhancement of the image in the inner tube compared to the outer tube. The paramagnetic centre accelerates the relaxation time of the surrounding water molecules, so that it takes less time for water molecules to realign with the external magnetic field. For images B and D, the inner tube contains an aqueous solution of [Gd**52**]$^{\bullet}$ and [Gd**56**]$^{\bullet}$ respectively, with the unoxidised corresponding metal complex in the outer tube. By oxidising the phenol or thiophenol bond cleavage between the metal centre and the pendent arm is likely to occur enabling a further water molecule to enter the inner coordination sphere. An extra water molecule in the coordination sphere, enables the effect of the paramagnetic metal centre to be further propagated through to the bulk. However, upon oxidation using potassium ferric cyanide , there is no apparent difference in voxel intensity between the inner and outer tubes. This may be because although an extra coordination site is being made available, the hydrophobic nature surrounding this site prevents a water molecule from entering in to it. A similar example has been described by Faulkner.[91] The hydrophobic effect of a bridging phenol between two DO3A components each chelating a ytterbium(III) ion meant that coordination numbers of only eight and seven were observed.
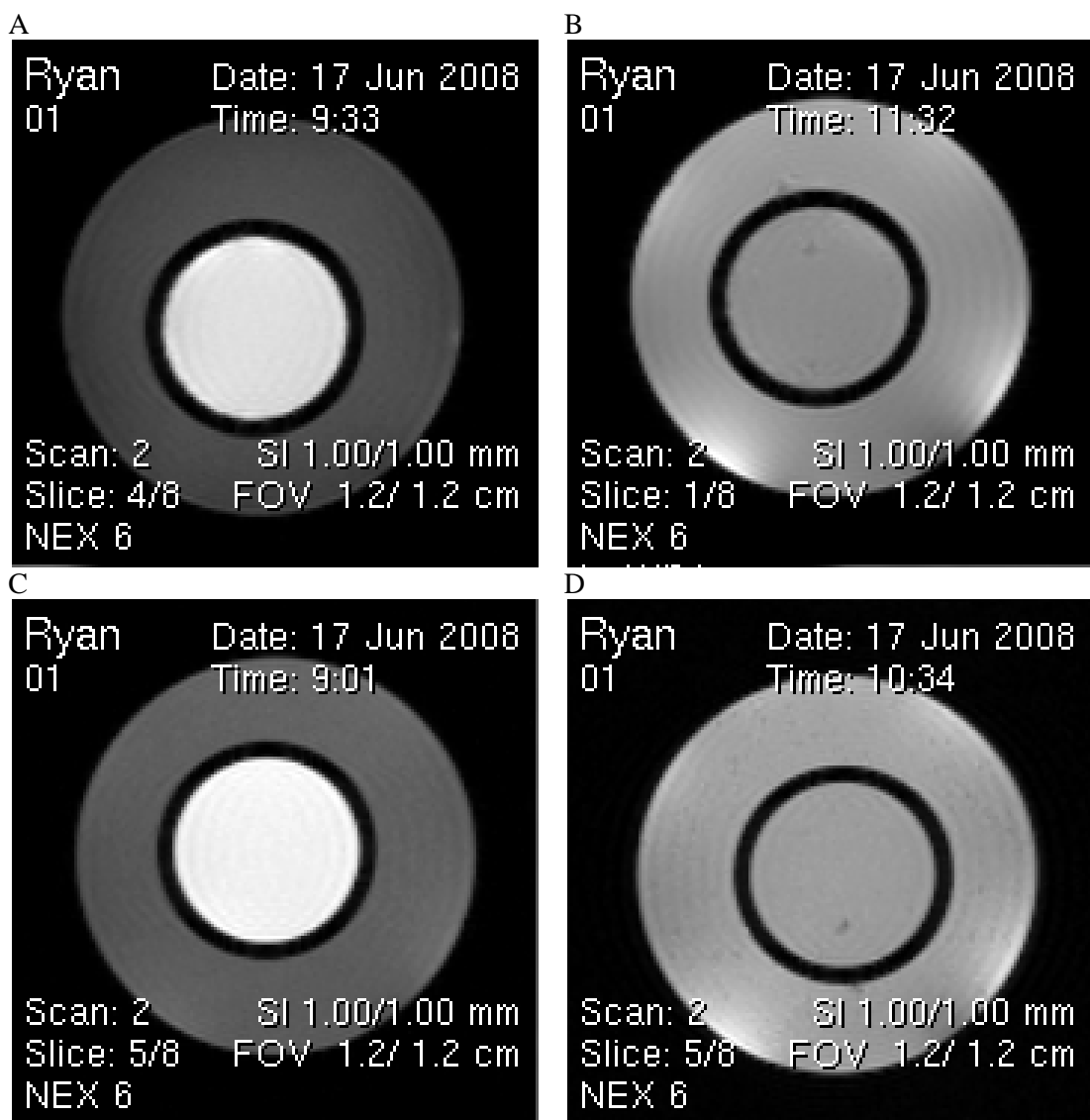
Figure 62: T1 weighted images of [Gd52]⁻ and [Gd56]⁻ relative to water (A and C) and relative to their oxidised species (B and D).

4.2.4. UV-visible spectra of [Eu52][NHEt$_3$]
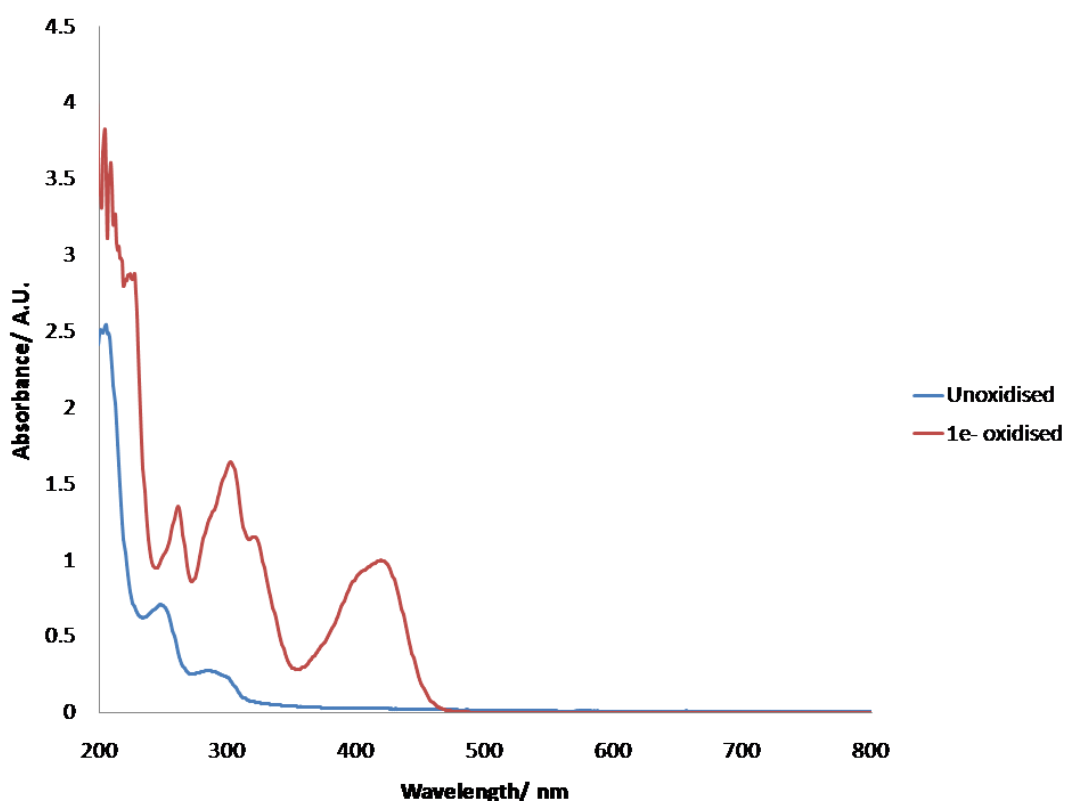
Graph 1: UV-visible spectra of [Eu52]⁻ (shown in blue) and [Eu52]• (shown in red).

Graph 1 shows the spectra for [Eu**52**]⁻ and [Eu**52**]•. The [Eu**52**]⁻ species possess π-π* transitions in the 250 – 300 nm range. To oxidise this complex, an aqueous solution of potassium ferric cyanide was used. The UV-visible spectrum for the oxidised species shows characteristic bands to suggest the presence of the phenoxyl radical. The phenoxyl radical is typified by the presence of a fairly weak absorption maximum at 500-800 nm and two intense maxima at 380-440 nm.[202] These features have also been identified in proteins such as ribonucleotide reductase and in the active form of galactose oxidase.[128]

4.2.5. Fluorescence spectra of the europium(III) and terbium(III) complexes of 52 and 56
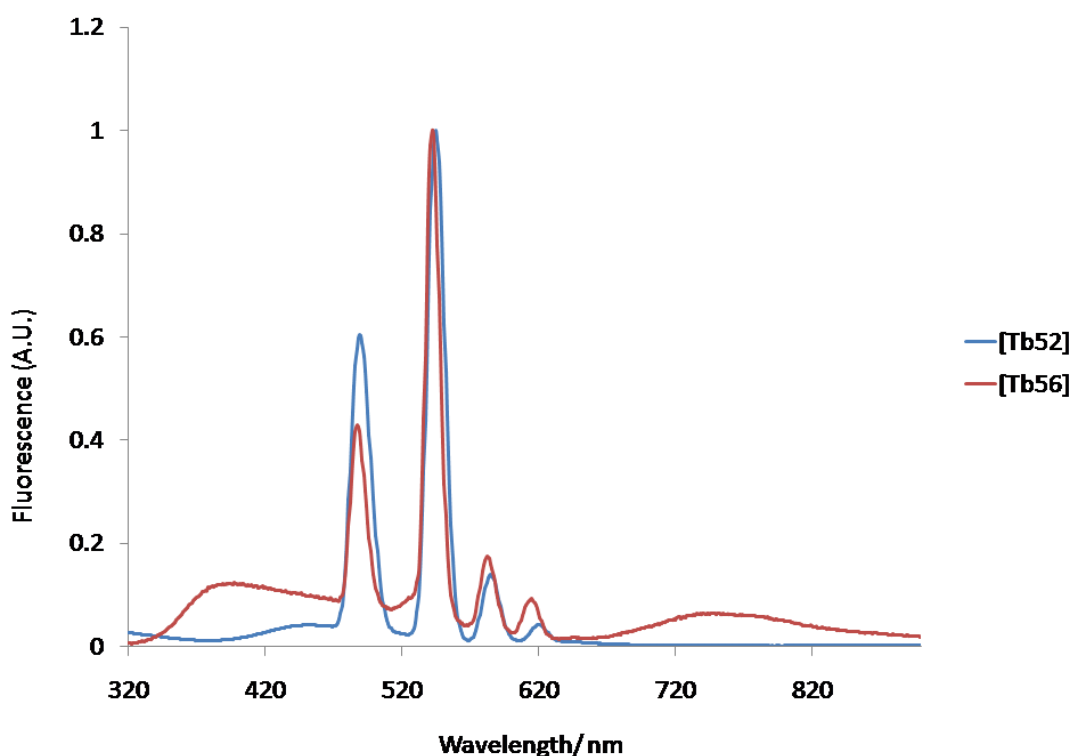
Graph 2: Graph showing the normalised fluorescence spectra of [Tb52]⁻ and [Tb56]⁻.

Graph 2 shows the normalised fluorescence spectra of [Tb**52**]⁻ and [Tb**56**]⁻ excited at 250 and 260 nm respectively (spectra normalised to the most intense peak). Comparison of the two spectra highlights that both complexes possess four emission peaks, with the thiophenolate complex ([Tb**56**]⁻) being slightly blue shifted compared with the phenolate complex ([Tb**52**]⁻). The four peaks are centred at 490, 545, 587 and 623 nm for [Tb**52**]⁻ and 498, 543, 585 and 617 nm for [Tb**56**]⁻. These peaks can be assigned to the following transitions; $^5D_4{\rightarrow}^7F_6$ (~620 nm), $^5D_4{\rightarrow}^7F_5$ (~598 nm), $^5D_4{\rightarrow}^7F_4$ (~544 nm) and $^5D_4{\rightarrow}^7F_3$ (~491 nm). The broad peaks centred around approximately 390 and 750 nm in [Tb**56**]⁻ are most likely due to solvent effects.
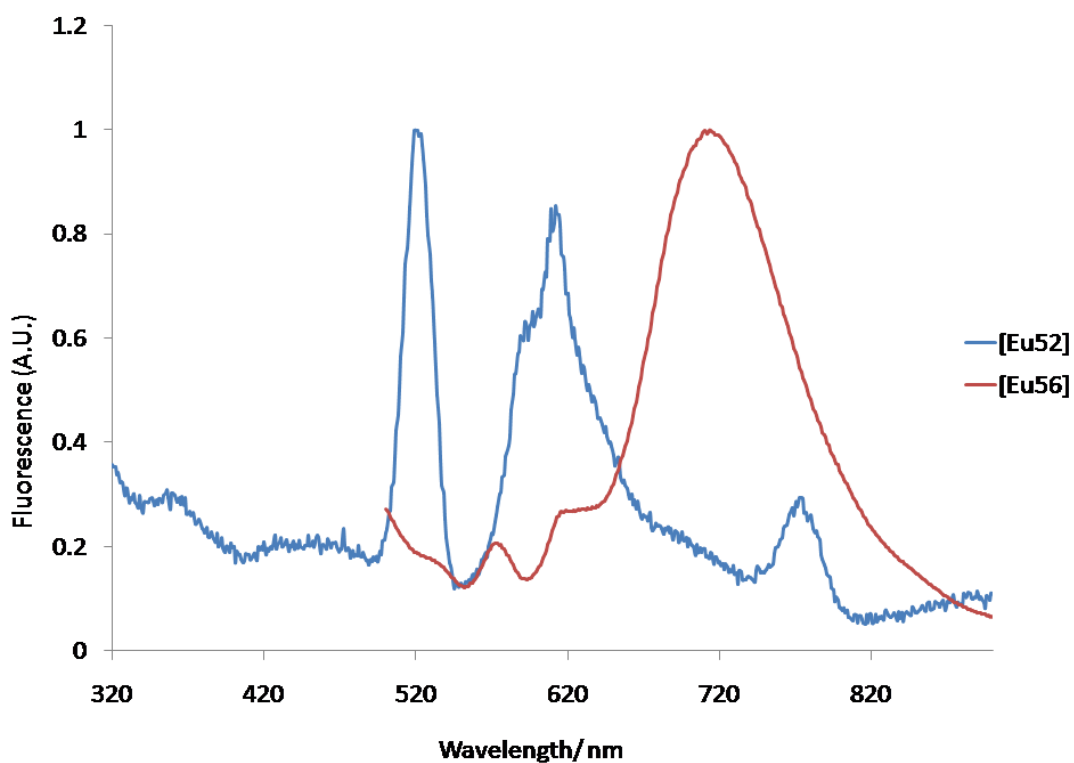
Graph 3: Graph showing the normalised fluorescence spectra of [Eu52]⁻ and [Eu56]⁻.

Graph 3 shows the normalised fluorescence spectra of [Eu**52**]⁻ and [Eu**56**]⁻ excited at 255 and 280 nm respectively (spectra normalised to the most intense peak). Compared with the terbium(III) complexes of **52** and **56**, the europium(III) complexes possess significantly different emission spectra. The europium(III) complex of **52** possesses four peaks centred at 521, 595, 612 and 775 nm. The peaks at 595 and 612 nm are due to $^5D_0 \rightarrow {}^7F_1$ and $^5D_0 \rightarrow {}^7F_2$ transitions respectively. The other two peaks are probably due to solvent effects. The emission spectrum of [Eu**56**]⁻ was collected from 500 nm due to the spectrum being overshadowed by a large emission peak centred around 460 nm. The spectrum possesses three peaks at 573, 619 and 714 nm. The peak at 573 nm is due to a $^5D_0 \rightarrow {}^7F_0$ transition whereas the peak at 619 nm is due to a $^5D_0 \rightarrow {}^7F_2$. The peak at 714 nm is most likely again due to solvent effects.

4.2.6. Cyclic voltammetry of the thiophenolate and phenolate europium complexes
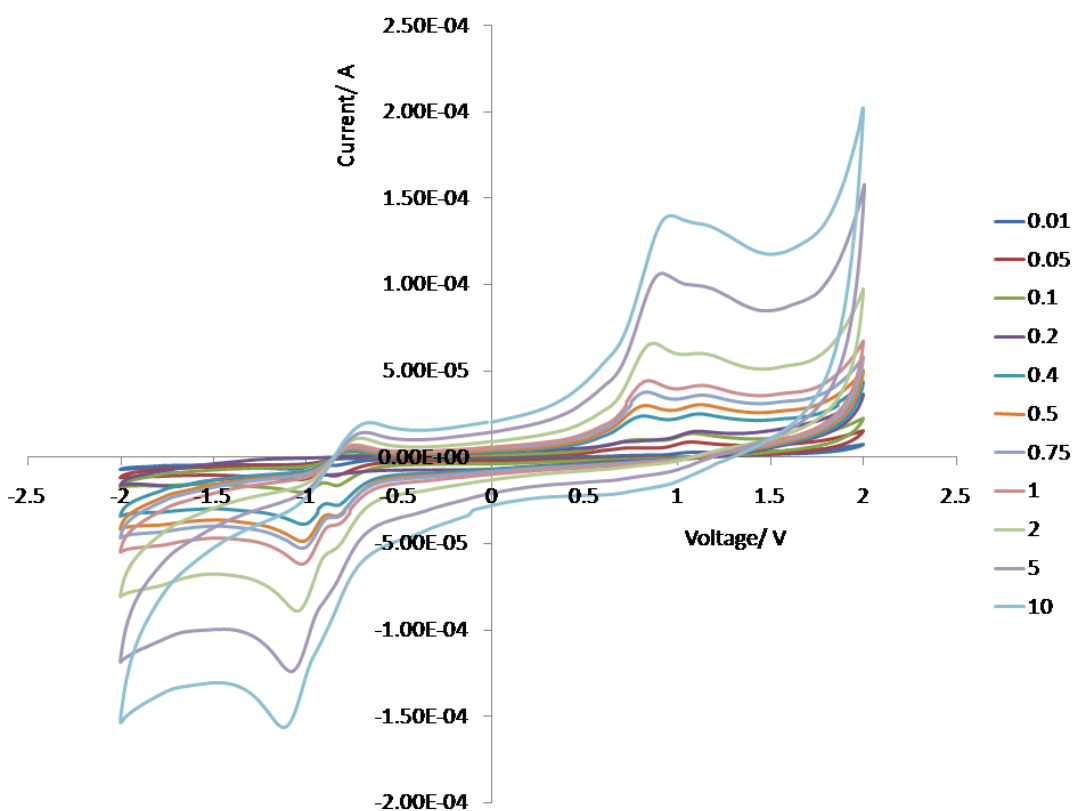
Figure 63: Cyclic voltammograms of [Eu52]⁻ measured at various scan rates (0.01 – 10 V/s) in acetonitrile using tetrabutylammonium tetrafluoroborate as a supporting electrolyte.

Figure 63 shows cyclic voltammograms for [Eu**52**]⁻ at scans of 0.01 – 10 V/s. In the anodic region there is a set of waves which shows some reversibility. This is believed to be ligand centred and is formed because of an oxidative process whereby the phenolate is oxidised to the phenoxyl radical. The most likely reason why this wave is split is because of adsorbed and free species being oxidised at slightly different potentials. In the cathodic region there is only one wave at −1.10 V. This wave is quasi-reversible (as shown by a plot of peak current verses the square root of scan rate) in nature with the back-wave displaced by 0.38 V. In previous examples where the cyclic voltammetry of europium(III) complexes of either macrocyclic and linear chelators have been reported,[203] redox potentials for the europium(III)/europium(II) redox couple were given as −1135 mV, −996 mV, −1340 mV and −585 mV for DOTA, TETA, DTPA and the hydrated ion complexes

respectively. Therefore, the wave at −1.10 V is in good agreement with that of other literature complexes for the europium(III)/europium(II) couple. It is worth noting that the this redox couple is stabilised by 515 mV relative to that of the hydrated europium(III) ion.
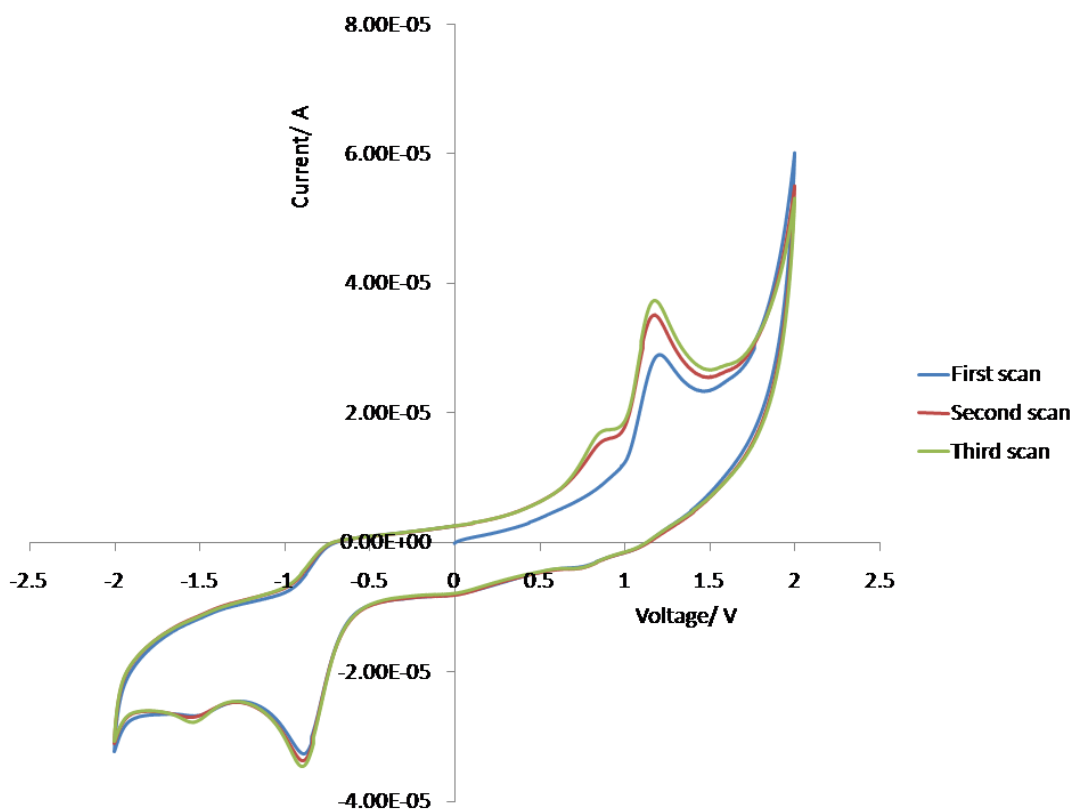
Figure 64: Consecutive cyclic voltammograms of [Eu56]⁻ measured at 0.2 V/s in acetonitrile using tetrabutylammonium tetrafluoroborate as a supporting electrolyte at RT.

Figure 64 shows the consecutive cyclic voltammograms of [Eu**56**]⁻ at a scan rate of 0.2 V/s. In the anodic region for the first scan there is one wave which is irreversible at +1.14 V. This wave is formed because of the oxidation of the thiophenolate generating the thiyl radical. In the cathodic region there is one wave present. This is the reduction of the europium(III) to europium(II). Compared with [Eu**52**]⁻, this reduction occurs more readily, being 0.23 V more positively shifted. The reason for this may be due to the type of donors that the europium ion prefers. Europium is a hard acid and therefore prefers hard donors. A phenolate fulfils this role whereas a thiophenolate, being a soft donor does not. The reduction of the europium ion is therefore easier to perform using soft donors to the metal centre compared with hard

donors. On the second and third scans there is a new wave formed in the anodic region. This is believed to arise because of head-to-head coupling between two thiyl radical species. The resulting di-sulfide product can participate in an oxidative process giving rise to the wave at +0.83 V. The production of the di-sulfide species may also explain the small peak at −1.49 V. This could be due to the simultaneous reduction of both europium metal ions in the di-sulfide product.
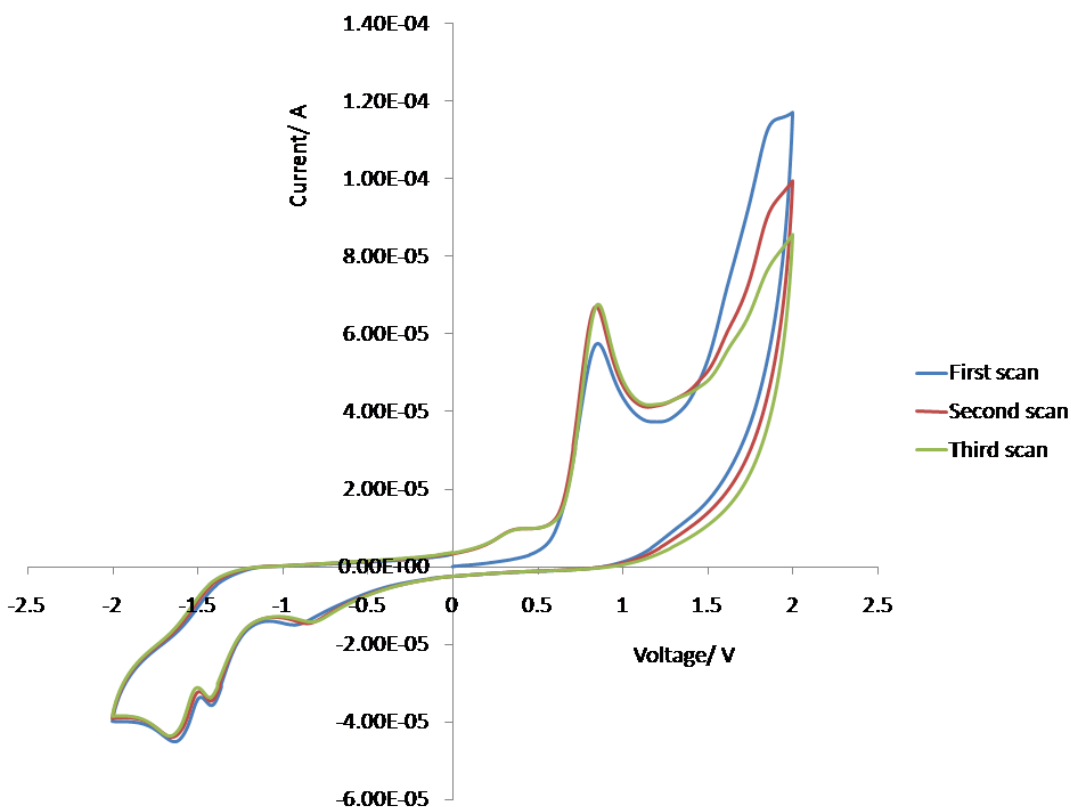
Figure 65: Consecutive cyclic voltammograms of [Eu56]⁻ measured at 0.2 V/s in acetonitrile using tetrabutylammonium tetrafluoroborate as a supporting electrolyte at −40°C.

Figure 65 shows consecutive cyclic voltammograms of [Eu**56**]⁻ with a scan rate of 0.2 V/s at −40°C. Compared with the same scan at RT, there are notable differences. Firstly the oxidation of thiyl radical is shifted to +0.83 V compared with +1.14 V at RT. The oxidation of the di-sulfide species is also shifted to a less positive potential of +0.32 V, a shift of 0.50 V. The reason for these shifts may be due to the complex existing in two isomeric forms which are temperature dependent. DOTA like lanthanide complexes are known to exist as four isomers (each isomer exists as a pair of enantiomers). The donor atoms are arranged into two parallel planes; one of which

is formed from the four nitrogen atoms of the macrocyclic ring and the other being formed from the four donor atoms of the pendent arms. In solution four isomers (i.e. two pairs of enantiomers) arise from the combination of two chiralities. The first one is related to the conformation of the ethylene groups of the macrocyclic ring (λ/δ) and the second one is caused by the mutual twist between the two planes arising from the orientation of the pendent arms (Λ/Δ).[204] The $\Lambda\delta\delta\delta\delta/\Delta\lambda\lambda\lambda\lambda$ isomer pair is called square-antiprismatic (SAP) whereas the $\Lambda\lambda\lambda\lambda\lambda/\Delta\delta\delta\delta$ pair is called twisted square-antiprismatic (TSAP). These two diastereoisomers differ by the sign and magnitude of the antiprism tilt angle. Smaller angles are indicative of TSAP structures, whilst SAP structures possess larger tilt angles.[205] The interconversion between the two diastereoisomeric forms is believed to occur via two simultaneous intramolecular exchanges: ring inversion and rotation of the pendent arms around the N-CH$_2$ bond. This is thought to occur through either a concerted twisting process or by the detachment of one or more arms.[206]
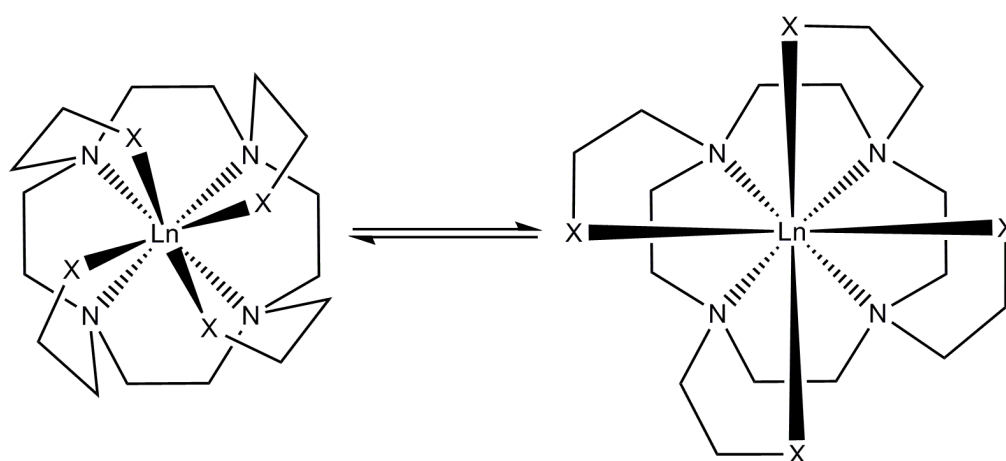
Twisted square-antiprismatic isomer   Square-antiprismatic isomer

Scheme 27: Structures of the twisted square-antiprismatic and square-antiprismatic isomers.

Comparison of the two cyclic voltammograms at RT and at $-40°C$, supports the presence of two isomeric forms. It is clear that at each temperature, one isomer dominates. This is true of other europium(III) complexes, such as [Eu(DOTA)(H$_2$O)$_x$]$^-$ which exists in an approximate 1:4 ratio of TSAP to SAP diastereoisomers at 298 K.[207] It is also notable that the isomers possess different redox potentials caused because of their structural arrangements. For example, the

thiyl radical is easier to oxidise at −40°C than at RT. This is further reinforced after consulting the cathodic region. In the cathodic region, there are three waves at −0.81, −1.40 and −1.64 V. All three waves are irreversible waves. Compared with the scans performed at RT, the waves at +0.81 and −1.40 V can be assigned to the reduction of the mono-nuclear and di-nuclear species respectively. Both are shifted to more positive values compared with those at RT. The remaining wave at −1.64 V is more difficult to assign. This may be a component of the wave at −1.40 V, implying that this wave comprises of free and adsorbed species. It is unlikely that this wave is ligand centred.

4.3. Attempted attachment of cyclen derivatives bearing amino acid pendent arms to a side-bridged cyclam compound

The cyclen macrocycles synthesised thus far do not possess functional groups for the attachment of other units to the complex. The ability to attach further moieties is of great interest as biological vectors (such as proteins and antibodies) can be incorporated in to the ligand structure, enabling site specific imaging or therapeutic action. The pendent arms synthesised in Chapter 2 possess functional groups for the attachment of further moieties. In addition, once the pendent arm is attached to the macrocycle, the coordination set provided to the metal centre is N_4O_4. For example, **27**, possesses two carboxylic acid groups which are protected as the *tert*-butyl and benzyl esters. Each carboxylic acid group can be unmasked separately, enabling the sites to be reacted in turn. The carboxylic acid group located α to the chiral centre can participate in coordination to a metal centre, thus forming a five-membered chelate ring. However, the carboxylic acid group in the β position is not orientated for coordination to a metal centre and as such, can be used to append further moieties, e.g. by forming amide linkages between the pendent arm and other molecules. Figure 66 shows the structure of a hetero-dinuclear complex utilising fully the amino acid pendent arm **27**. In Figure 66, **27** acts as a coordination donor to a lanthanide centre and is also used to form a covalent bond with another macrocyclic component via the formation of an amide bond.
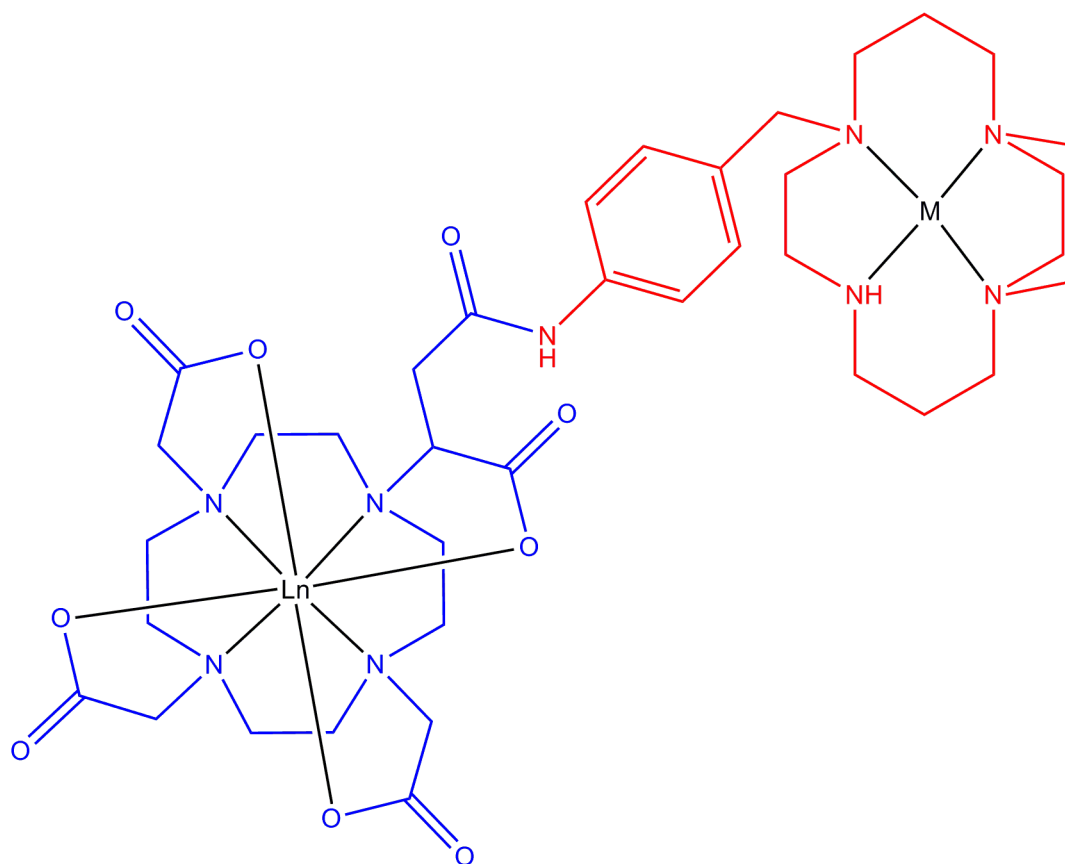
Figure 66: The proposed structure of the hetero-di-nuclear complex.

In the structure in Figure 66, there are two macrocyclic tetra-aza rings; cyclen and cyclam. Cyclam is more suited towards coordination of transition metals whereas cyclen is more suited towards coordination of lanthanide metals. This is advantageous given that lanthanide and transition metals have a variety of uses for biological applications. For example transition metals are used in PET imaging, whereas lanthanide metal complexes can be used in MRI as contrast agents and in the production of fluorescent complexes. This methodology identified two components which would need to be synthesised. Each component contained a different macrocyclic element. The side-bridged cyclam complex with a *p*-nitro benzyl arm was supplied by Graeme McRobbie[208] (compound **60**, shown in red in Figure 66) and thus only the cyclen containing component (shown in blue in Figure 66) needed to be synthesised. The cyclen component consists of a DO3A fragment which is attached to the amino acid pendent arm, **27**. The structure of this ligand is therefore analogous to the structures of the phenolate and thiophenolate ligand systems already discussed within this chapter.
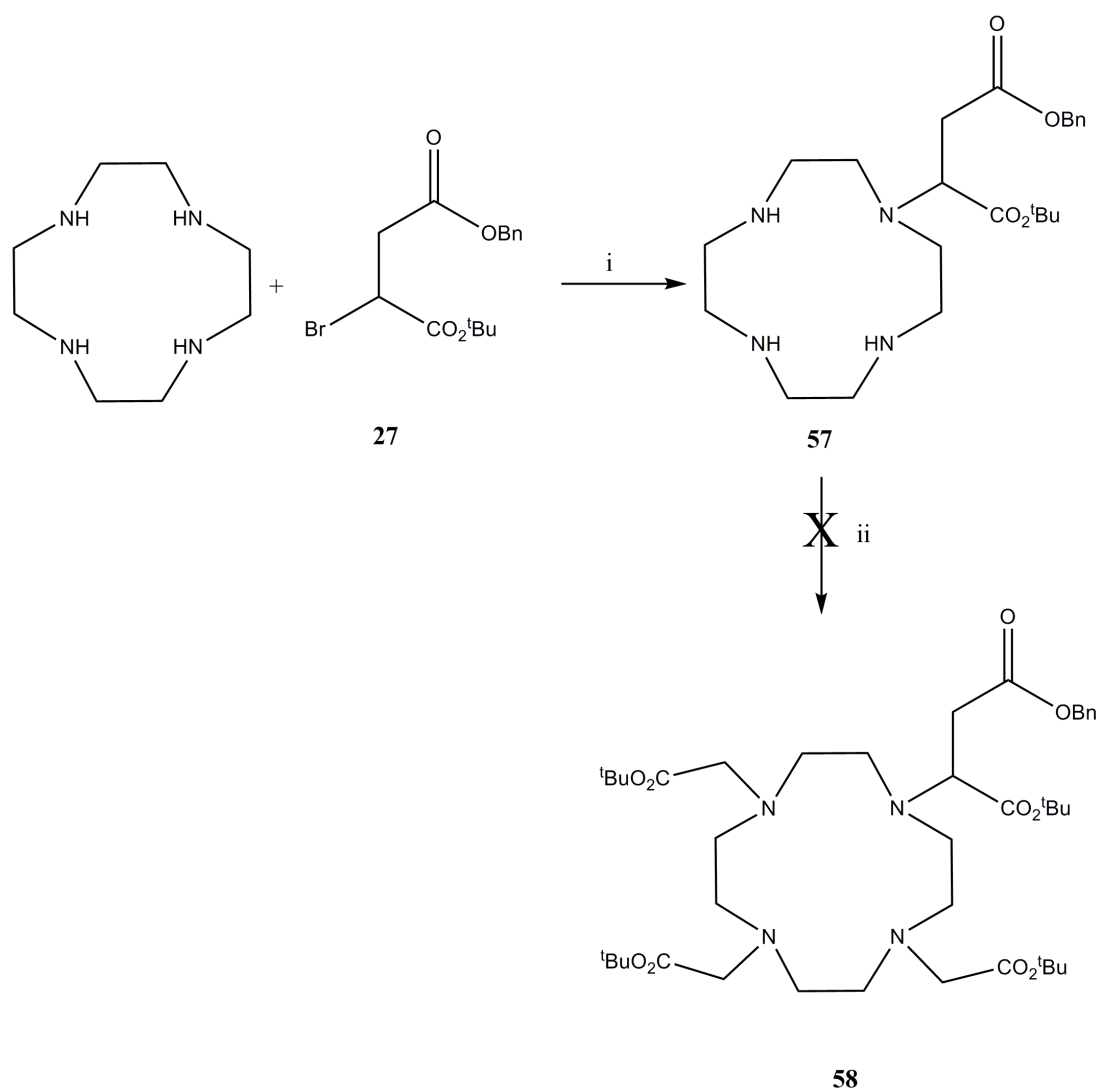
Scheme 28: Attempted synthesis of 58. Conditions; i) CHCl$_3$, 44 hr, RT (32%); ii) dry MeCN, K$_2$CO$_3$ (10 equiv), BrCH$_2$COO^{t}Bu, 24 hr, RT.

The first synthetic step would be to either append the *tert*-butyl acetate arms or the amino acid arms. At this point the literature was consulted to see if there were any examples of secondary halides being used in this manner. Pagel and Yoo[84] have reported the synthesis of an α-amino-DOTA compound. The α-amino group was introduced using α-brominated glycine templates. These were reacted with DO3A in the presence of six equivalents of K$_2$CO$_3$ and isolated in excellent yield (90-95%). t*ert*-Butyl and benzyl groups were used as protecting groups during the synthesis of the glycine templates. After the glycine template was attached to the secondary amine site of DO3A, these protecting groups were cleaved in excellent yields, to afford the fully deprotected chelator. Another example has been reported by Mäcke,

using pendent arm **27**.[25] Considering this literature precedence, it was decided to append the amino acid pendent arm first, followed by the addition of the *tert*-butyl acetate arms. Mäcke reports only a 21% mono-alkylation yield of cyclen using pendent arm **27**. Their previous efforts to introduce succinic acid-di-*tert*-butylester gave yields below 5% for monoalkylation with the elimination product fumaric acid-di-*tert*-butylester dominating. Using the di-phenylmethyl ester derivative gave a high yield of mono-alkylation (79%), although this cannot be used in a selective deprotection strategy. Use of 2-bromoglutaric-1-tert-butyl-5-benzylester gave 83% yield of mono-alkylation, with no elimantion product being isolated. The reason therefore for low yields of the succinic ester was due to the formation of a conjugated π-system formed through an elimination pathway. The yield obtained for the attachment of pendent arm **27** to cyclen was reported as being only 21%. In reproducing this reaction, the conditions (dropwise addition of **27** to two equivalents of cyclen dissolved in $CHCl_3$) were modified. To maximise yield, a syringe pump was used, which delivered **27** at a rate of 2 ml per hr (1.99 g of **27** dissolved in 40 ml of $CHCl_3$). After stirring at RT for a further 24 hr, the reaction was stopped and the crude material subjected to silica gel column chromatography using an eluent of $EtOH/NH_3$ (95:5). The desired fraction was isolated giving the mono-alkylated product in 32% yield, a 11% increase from the reported yield for this reaction. The next step was to react the three secondary amine sites by introducing *tert*-butyl acetate pendent arms at these sites. However, this proved problematic; a chromatographic separation could not be found which lead to the clean isolation of the desired compound.
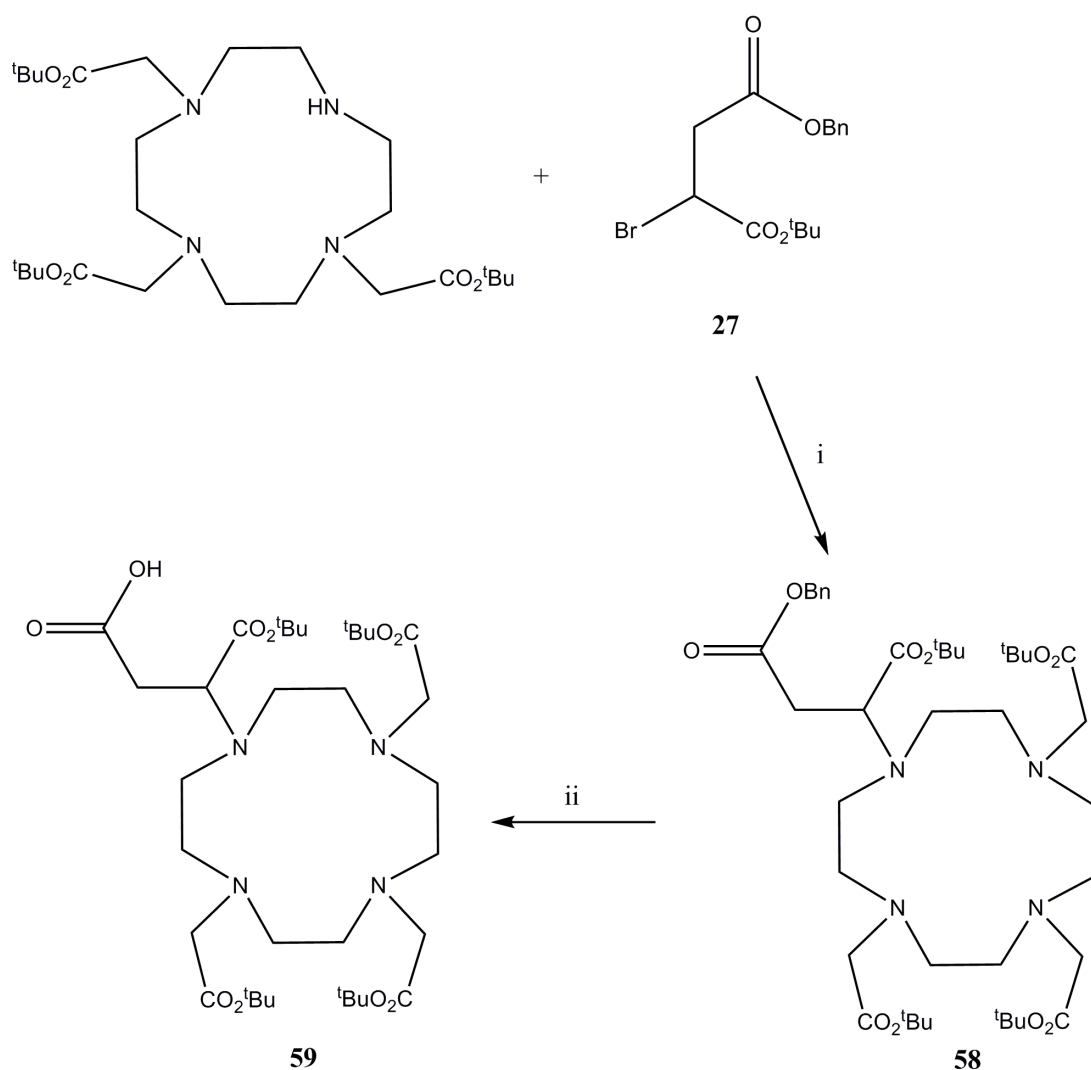
Scheme 29: Synthesis of 58. Conditions; i) K₂CO₃ (6 equiv.), dry MeCN, 65°C, 5 hr (76%); ii) 10% Pd/C, 25 psi, H₂, 24 hr, RT (57%).

The alternative pathway to the production of **59** was to react **27** with DO3A-TB. This reaction was performed according to the conditions of Yoo and Pagel.[84] After silica gel column chromatography using an eluent of DCM/MeOH (97:3 (v/v)), **58** was isolated in 76% yield. The benzyl group was then selectively cleaved in the presence of Pd/C in a hydrogen saturated atmosphere at 25 psi over 24 hr and **59** was obtained in a yield of 57%. The carboxylic acid group was now unmasked, enabling it to be used in a coupling reaction with compound **60**.
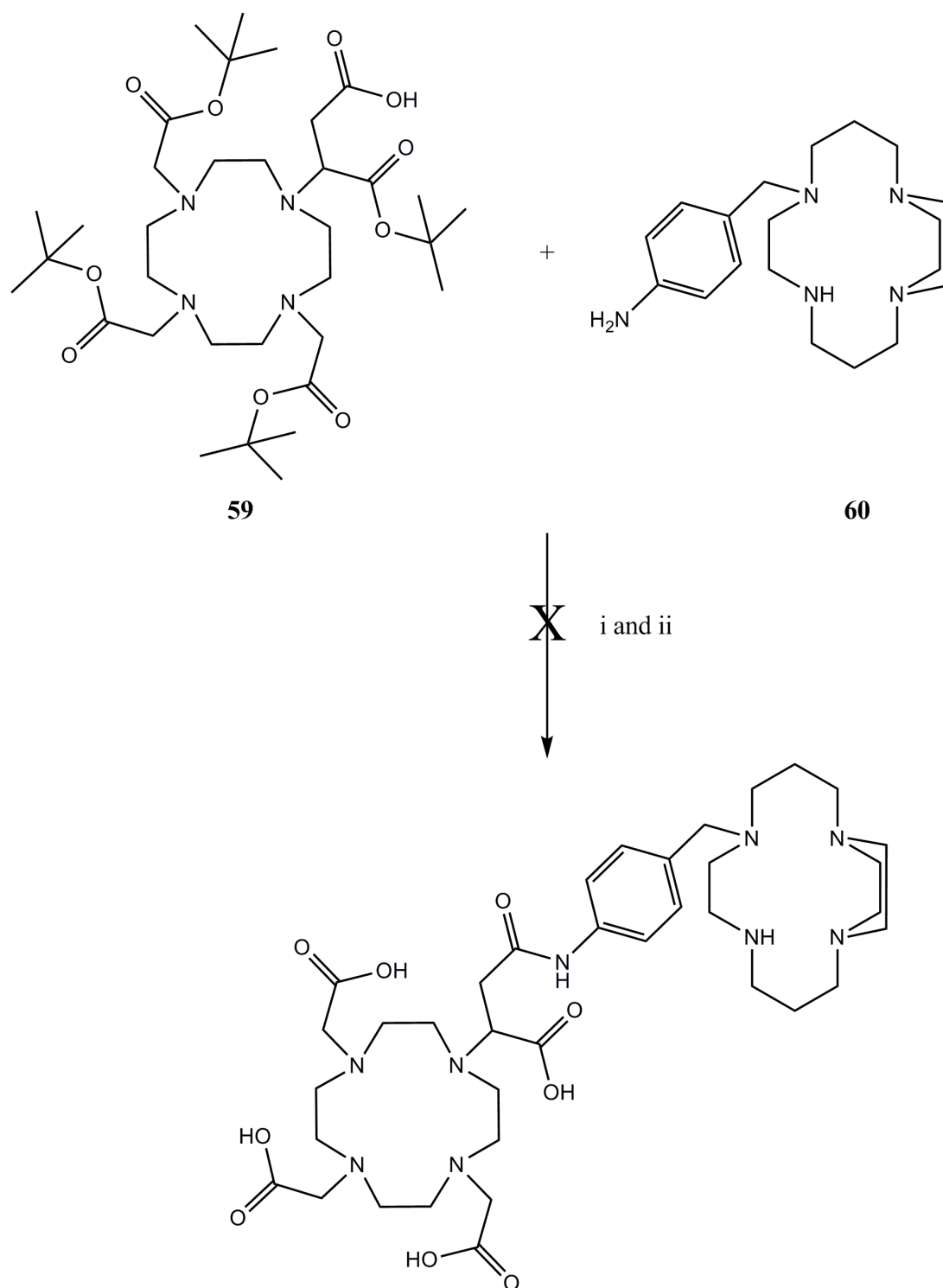
Scheme 30: Attempted coupling of 59 and 60. Conditions; i) DCC, HOBt, dry DCM, RT 10 days; ii) 6 M HCl, MeOH, reflux, o/n.

Couplings between aromatic amines and carboxylic acids have been used in several coupling strategies. Zhao and co-workers have produced potent and selective 2-azepanone inhibitors of human tryptase.[209] To synthesise such inhibitors, it was

necessary to couple a 2-azapanone derivative with biphenyl-4-carboxylic acid to form an amide. This coupling reaction was achieved by the use of 1-ethyl-3-(3-dimethylaminopropyl) carbodiimide hydrochloride (EDC), hydroxybenzotriazole (HOBT) and di-isopropyl-ethyl amine in DCM. A yield of 85% was obtained. Seto and Xie in their pursuit of bidentate protein tyrosine phosphatase inhibitors produced a library of compounds which used diamine benzyl linker groups coupled to two identical aryl α-ketocarboxylic acids.[210] Coupling of the two different components with EDC and DMAP formed the di-amide compounds in yields of between 47 and 76% after column chromatography. A further example in which aromatic amines are involved in the formation of amides has been published by Nagata and co-workers.[211] Their investigations into tricyclic indole-2-carboxylic acids required a coupling reaction between a di-substituted benzyl amine and a tricyclic component with a carboxylic acid. Two different approaches were used; one which used bis(2-oxo-3-oxazolidinyl)phosphonic chloride (BopCl) and triethylamine, and another which used water-soluble carbodiimide (WSC) and HOBt. Yields of 79-88% were obtained respectively.

To couple **58** to **59**, dicyclohexylcarbodiimide (DCC) was used as coupling reagent in the presence of HOBt. The reaction was allowed to proceed for 10 days before concentrating under reduced pressure. Silica and alumina chromatographic conditions were found to be unsuitable for the purification of the resulting coupled product and because of this, size exclusion chromatography was used. From the resulting column, two fractions were produced, which were analysed by NMR spectroscopy. This analysis proved inconclusive as to which fraction contained the desired product. The two bands were eluted close together and therefore a certain degree of overlap could have arisen.

To obtain better separation using size exclusion chromatography, both fractions from the previous step were combined and treated with 6M HCl at reflux to cleave the *tert*-butyl esters. Size exclusion chromatography was performed on the product isolated, leading to the collection of three bands. Analysis of all three samples again proved inconclusive. It is therefore possible that the desired coupling reaction had not occurred. The steric bulk surrounding the two coupling sites could have prevented them from being suitably activated by the coupling reagent to enable

amide formation. Degradation of **59** could also have occurred. Intramolecular cyclisation of the asparatic acid moiety is possible, leading to the formation of a five-membered ring (a succinic ester). This compound would not be able to participate in amide coupling reactions.

4.4. Conclusion

In this chapter the preparation of cyclen derived complexes bearing phenolate, thiophenolate and amino acid arms has been described. Ligands were produced bearing three acetate arms and either one phenol/ thiophenol pendent arm. The phenolate ligand, **52**, was synthesised using the acetyl protected di-*tert*-butyl pendent arm, **15**. This circumvented previous deprotection problems highlighted in Chapter 3. The thiophenolate ligand, **56**, was produced using pendent arm **24**. Lanthanide complexes of the ligands were synthesised. For the gadolinium(III) complexes, T1 weighted images were collected. These images showed that the complexes [Gd**52**]⁻ and [Gd**56**]⁻ enhanced the image relative to water. The oxidised species [Gd**52**]• and [Gd**56**]• were found to not enhance the image relative to the unoxidised complexes. The lipophilic nature surrounding the metal ion is believed to prevent further water molecules entering the inner coordination sphere after oxidation, and therefore no enhancement of the image is observed.

Analysis of the europium(III) complexes was conducted using UV-visible spectroscopy, CV and fluorescence spectroscopy. The UV-visible spectrum of [Eu**52**]⁻ displays only π-π* transitions, but upon one electron oxidation, the characteristic fingerprint of a phenoxyl radical was observed. This was further observed in the cyclic voltammogram (peak at ~+0.75 V due to formation of the phenoxyl radical). The thiyl radical was also observed in the cyclic voltammogram of [Eu**56**]⁻ (wave at +1.14 V). When cooled to −40°C, this peak shifts to +0.83 V. The existence of different isomers was suggested for the ease of this oxidation at lower temperatures. Fluorescence spectra for the europium(III) complexes of **52** and **56** possess two emission peaks each whereas the terbium(III) complexes possess four emission peaks each.

Macrocyclic ligands based on a cyclen framework were also produced with pendent arm **27** attached. Subsequent debenzylation, afforded a possible point for a further moiety to be attached. This ligand was used in an attempt to couple a further macrocycle, a side-bridged cyclam compound with a pendent *p*-aminobenzyl arm (**60**). Although unsuccessful, this route does highlight a possible synthetic strategy for the production of dual-imaging probes using amino acid linker moieties.

5. Porphyrin complexes bearing hydroxyl and polyethylene glycol chains towards photodynamic therapy

5.1. Introduction

In this chapter, the design and synthesis of porphyrins bearing hydroxyl or polyethylene glycol (PEG) pendent arms for photodynamic therapy (PDT) is described. PDT is an emerging anticancer therapy which uses light to stimulate a photosensitiser in order to generate singlet oxygen, a highly potent cytotoxic agent. Porphyrins are commonly used in this role.[212,213] In the pursuit of PDT agents, the design of the porphyrin sensitisers was centred upon maximising their water solubility whilst still retaining their therapeutic effect.

The introduction will focus on PDT and also cover target molecule design.

5.1.1. Photodynamic therapy

PDT is based on the accumulation of a photosensitiser in malignant tissue after the administration of the photosensitiser. Subsequent illumination with light of an appropriate wavelength creates a photochemical reaction, the so-called photodynamic effect, which produces singlet oxygen. The process whereby singlet oxygen is generated is shown in the Jablonski diagram in Figure 67.
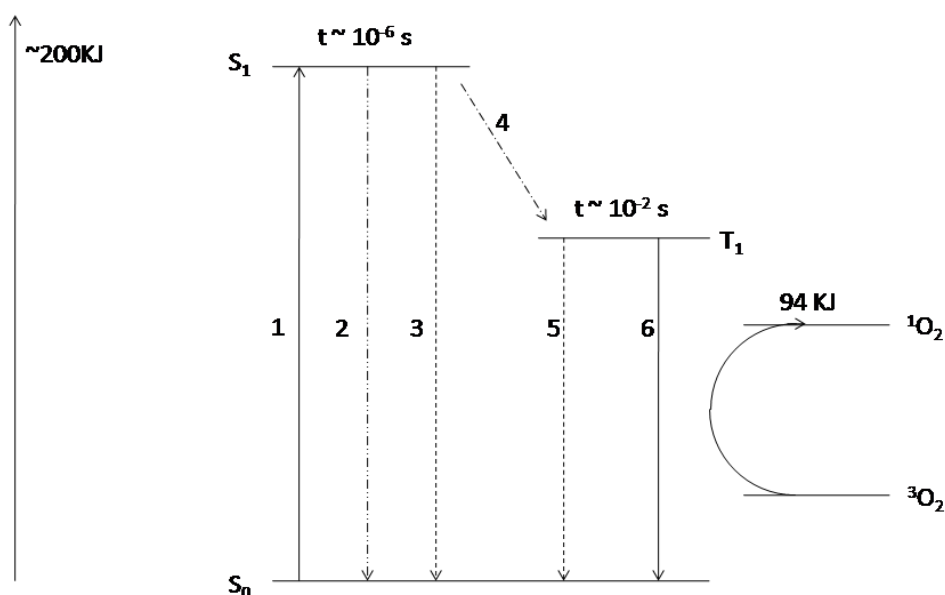
Figure 67: Jablonski diagram showing the process whereby singlet oxygen is generated.

The first step in the generation of singlet oxygen is where the sensitiser is transformed from its ground singlet state (S_0) into a short-lived excited singlet state [(S_1, ($\sim 10^{-6}$s)] by illumination with light of an appropriate wavelength (1 in Figure 67).[212] The sensitiser can then relax to the ground state through either nonradiative decay (2) or fluorescence (3). Alternatively the sensitiser can undergo intersystem crossing (4) to the longer lived triplet state [(T_1, ($\sim 10^{-2}$s)]. A sensitiser in the triplet state can still relax to the ground state by either phosphorescence (5) or internal conversion (6). Alternatively the excited triplet state can undergo two types of reaction. Firstly, it can participate in an electron-transfer process with a biological substrate to form radicals and radical ions which, after interaction with oxygen, can produce oxygenated products such as the superoxide ion, O_2^- (type I reaction). Alternatively it can undergo a photochemical process known as a type II reaction, which results in the conversion of stable triplet oxygen ($^3O_2$) to the short lived but highly reactive singlet oxygen ($^1O_2$), the putative cytotoxic agent.[213] In water the lifetime of $^1O_2$ is approximately 1-3 μs, whereas in most organic solvents the lifetime is 4-50 times longer. However, the lifetime of $^1O_2$ is considerably shorter in cellular systems, ranging from 100 ns in the lipid regions of membranes to 250 ns in the cytoplasm. The diffusion range of $^1O_2$ is predicted to be limited to approximately 45 nm in cellular media. Because of the diameter of human cells (10 to 100 μm), they cannot diffuse more than a single cell length. Thus, the site of the primary generation of $^1O_2$ determines which subcellular structures may be accessed and subject to free radical attack. Singlet oxygen is a powerful, fairly indiscriminate oxidant that reacts with a variety of biological molecules and assemblies. For this reason, the Type II reaction predominates over Type I, although there is some indication that the superoxide ion may also be involved in some aspects of PDT damage.

5.1.2. Synthetic targets

The structures of the two synthetic targets are shown in Figure 68. Both are designed to give water solubility of the compound and its complexes. Hydroxy and polyethylene glycol (PEG) chains are both used for this purpose. Both types of compound can form metal complexes. For the hydroxy compound (Figure 68, left compound), it was decided to focus on the production of gallium(III) complexes, whereas for the PEGylated porphyrins (Figure 68, right compound), gallium(III), nickel(II) and zinc(II) complexes were all synthesised. Gallium(III) complexes of tetaphenylporphyrin (TPP) is discussed. This is followed by a discussion of the literature on tetra(pentafluorophenyl)porphyrins, which can be used for the synthesis of PEGylated porphyrin derivatives. The synthesis of both target molecules is then presented.
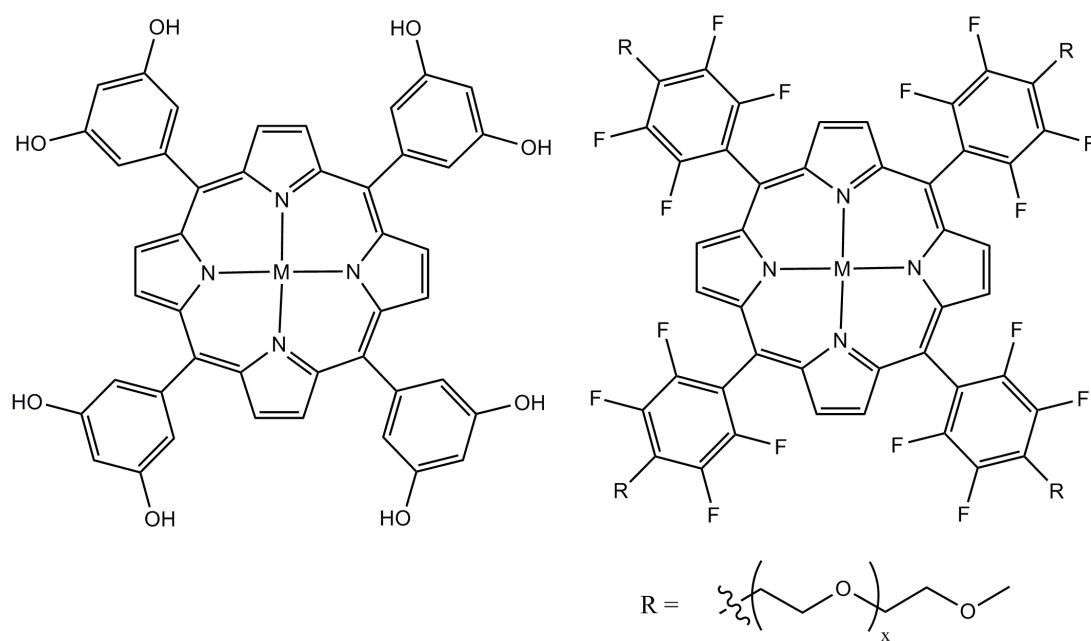
Figure 68: Target molecules that are potential PDT agents.

5.1.3. Tetraphenylporphyrin gallium complexes

Gallium(III) complexes of tetraphenylporphyrin (TPP) possess interesting properties which make them appealing to study. Firstly, gallium(III) typically adopts square based pyramidal geometries within the porphyrin cleft, with an anion occupying the axial position. This anion can be readily substituted or reacted enabling complexes with different anions or organometallic complexes to be produced. The electrochemistry and photolysis properties of compounds of this type have been studied. Incorporation of gallium can result in an increase in quantum yields of singlet oxygen due to the "heavy atom effect".[214] This property is desirable in the production of PDT agents.

The synthesis of [Ga(TPP)Cl] has been reported by Guilard and co-workers.[215] The gallium(III) is inserted into the macrocyclic cleft using the chloride salt dissolved in acetic acid and heating to reflux for 12 hr in the presence of sodium acetate. A yield of 71% was obtained whilst insertion into 2,3,7,8,12,13,17,18-octaethylpoprhyrin (OEP) and 2,3,7,8,12,13,17,18-octamethylpoprhyrin (OMP) gave yields of 75 and 86% respectively. Single crystals of [Ga(TPP)]Cl were grown via recrystallisation from toluene. The crystal structure is shown in Figure 69.[215] Other halogen complexes were synthesised by reacting the chloride complex with either hydrofluoric or hydroiodic acid in toluene yielding the fluoride and iodide complexes respectively.
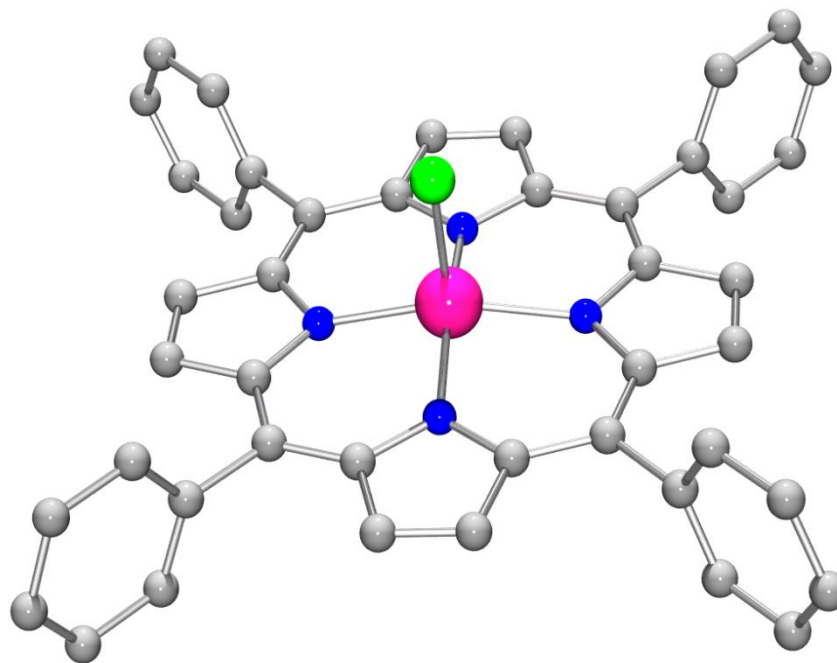
Figure 69: Ball and stick representation of the X-ray crystal structure of [Ga(TPP)Cl] (Guilard and Coutsolelos).[215]

A further two methods are reported for the insertion of gallium(III) into the porphyrin cleft. Eaton and co-workers investigated ring rotation in gallium complexes of *para*-substituted tetraphenylporphyrins.[216] The use of $(NH_4)Ga(SO_4)_2.12H_2O$ in refluxing acetic acid containing excess sodium acetate affords the gallium complex with a single axial hydroxyl group in 75 to 84% yield. The hydroxyl can be exchanged for a chloride by boiling in either tetrachloroethane or trichloroethene. Yields obtained for this conversion were in the range of 57 to 100%. The other method, reported by Buchler and co-workers uses the gallium(III) acetylacetonate salt in refluxing phenol.[217] This produces a gallium-porphyrin complex in which the gallium bears an axial phenoxide substituent. A yield of 92% was achieved when using this methodology to complex OEP with gallium(III).

Feng and co-workers have synthesised a gallium(III) TPP complex with an axially coordinated hydride.[218] This was synthesised by the reaction of the gallium(III) chloride complex with $NaBH_4$. The presence of the hydride coordinated to gallium was confirmed by IR, NMR and crystallographic data. The electronic spectrum of the complex shows that the complex belongs to the 'hyperclass' of porphyrins as the Soret is split into two peaks. Other axial substituents have also been investigated. For

example Guilard and co-workers have reported the synthesis and characterisation of gallium porphyrin complexes with thiocyanate or azide substituents.[219] Acetylide complexes have been prepared by Balch and co-workers.[220]

DiPasquale and Mayer investigated the interaction of TPP gallium(III) complexes with hydrogen peroxide.[221] The TPP gallium complex was used as a model for iron-heme. The hydrogen peroxide-iron-heme complex is a suggested intermediate in the following reaction

$$[\text{Fe}^{III}(H_2O_2)]^+ + \text{RH} \rightarrow [Fe^{III}(\text{OH})] + \text{RO}H_2^+$$
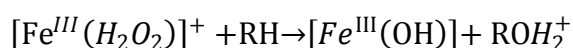
Gallium(III) was used as a substitute for iron in these model complexes as it is redox inactive and has a similar size to iron(III). TPP gallium(III) complexes, with weakly coordinating anions, were produced. Those synthesised included gallium complexes with triflate, hydroxide, methyl or perchlorate as axial donors. Hydrogen peroxide was found to be a very poor ligand to the gallium in the TPP complex. An excess of hydrogen peroxide in deuterated DCM did not displace water or perchlorate from the gallium centre.

The electrochemistry of gallium(III) tetraphenyl and octaethyl porphyrin complexes has been investigated.[222] Each gallium(III) complex shows two reversible oxidations and two reversible reductions (see Table 8). Thin layer spectra recorded during the first reduction and first oxidation reveal spectra that are characteristic of anion and cation radicals.

Porphyrin	Anion	Oxidation		Reduction	
		1st	2nd	1st	2nd
TPP	Cl⁻	1.16	1.40	-1.12	-1.52
	OAc⁻	1.17	1.41	-1.14	-1.53
	F⁻	1.18	1.42	-1.15	-1.54
	OH⁻	1.17		-1.16	-1.54
OEP	Cl⁻	1.00	1.44	-1.38	-1.81
	OAc⁻	1.01	1.44	-1.36	-1.87
	F⁻	1.00	1.45	-1.38	-1.82
	OH⁻	1.01	1.44	-1.37	-1.88

Table 8: Oxidation and redox potentials of gallium(III) TPP and OEP complexes with different anions.

Further research has been conducted again by Kadish and co-workers, this time focusing on five coordinate ionic and σ-bonded gallium complexes.[223] The oxidation and reduction potentials for the OEP complexes are shown in Table 9.

Axial ligand	Oxidation			Reduction	
	1st	2nd	3rd	1st	2nd
$C(CH_3)_3$	0.76	1.20	1.47	-1.31	-1.74
C_4H_9	0.79	1.19	1.47	-1.29	-1.73
C_2H_5	0.80	1.20	1.46	-1.27	-1.70
CH_3	0.86	1.19	1.46	-1.29	-1.71
$C_2H_2C_6H_5$	0.99	1.21	1.48	-1.24	-1.67
C_6H_5	1.05	1.22	1.48	-1.22	-1.66
$C_2C_6H_5$	1.27	1.47		-1.19	-1.59

Table 9: Oxidation and redox potentials of gallium(III) TPP complexes with different hydrocarbon axial ligands.

Subsequent research has involved the laser-flash photolysis of the σ-bonded gallium complexes.[224] Steady-state photolysis was shown to lead to the photodissociation of the metal-carbon-bond. This occurs when the axial group is CH_3, C_2H_5, C_4H_9, $CH(CH_2)_2$ or $C(CH_3)_3$. However, when the axial group is $CH=CHC_6H_5$ or $C≡CC_6H_5$, photodissociation does not occur. The difference in the photoreactivity arises because of the nature of the metal-carbon bond. The compounds which undergo photodissociation display purely σ–bond character, whereas those that didn't photodissociate possess ionic character. Laser photolysis studies conducted in the presence and absence of ferrocene indicate that the reaction proceeds through a triplet state originating from the porphyrin macrocycle.

Balch and co-workers have prepared gallium complexes of TPP with both 5-hexenyl and cyclopentylmethyl axial ligands in order to study the cyclization of the 5-

hexenyl radical.[225] When the reaction was performed in the presence of nitrosobenzene, a radical trap, no cyclization was observed. The ESR spectrum of the 5-hexenyl complex and nitrosobenzene after irradiation for 2 hr is typical for that of a nitroxide Ph(R)NO$^\bullet$.

A novel cyclic trimer of a gallium(III) porphyrin has been reported.[226] To prepare this complex, TPP was benzoylated in the β position. The gallium(III) was then readily inserted to form the monomer complex. Cleavage of the benzoyl ester using a basic hydrolysis resulted in the formation of the cyclic trimer. In this complex, each gallium ion is square-based pyramidal, with the four nitrogens of the porphyrin ring forming the base and the hydroxyl group of a neighbouring porphyrin filling the apical position. Addition of the acids HCl, HBr and trifluoroacetic acid (TFA) cleaved the trimer to form the monomeric species (2-OH-TPP)GaX, where X = Cl, Br or triflate). This process can be reversed by the addition of a proton scavenger, 2,4,6-collidine.

To summarise, the published work on gallium(III) TPP complexes and their derivatives includes at least three routes of metal insertion. On complete formation, the gallium ion prefers to adopt a square-based pyramidal geometry in all the examples discussed. The anion filling the apical position can be substituted enabling, for example, the formation of organometallic compounds. The gallium(III) porphyrin complexes have also been shown to possess electrochemical behaviour which is dependent on the nature of the anion in the apical position.

5.1.4. Tetra(pentafluorophenyl)porphyrin compounds

Tetra(pentafluorophenyl)porphyrins have been studied widely because of the readily substituted *p*-fluoride on the pentafluorophenyl rings. This enables a range of substituents to be incorporated into the porphyrin backbone and its resulting complexes. Furthermore, all of the fluorine atoms can be substituted by adjusting the reaction conditions. Examples of these reactions are now discussed along with the synthesis of tetra(pentafluorophenyl)porphyrin.

The synthesis of 5,10,15,30-tetrakis(pentafluorophenyl)porphine (TF_5PP), **62**, was first reported in 1969 by Longo and co-workers.[227] Subsequent complexation studies were also conducted. The attempted preparation of silver(II) complexes using the nitrate salt in acetic acid does not result in the formation of the expected (TF_5PP)Ag product but instead forms the porpholactone deriviative.[228] Copper and nickel porpholactone deriviatives have also been produced in a similar fashion. Further investigation in to the metallation of TF_5PP, also demonstrated that DMF was not a suitable solvent.[229] Use of DMF led to the formation of *meso*-tetrakis(*o,o,m,m*-tetra-fluoro-*p*-(dimethylamino)phenylporphinato complexes. The proposed pathway for this was via the degradation of DMF at reflux to form dimethylamine. This amine can substituent a *p*-fluorine atom on one or more of the phenyl rings via an activated aromatic substitution reaction. This reaction is known to occur under-mild conditions when a phenyl ring bears both strongly electron withdrawing groups and good leaving groups such as fluorine anions. Substitution of the *p*-fluorine was shown to be almost quantitative from experimental data. Interestingly, when heating the free base porphyrin, one or two of the four *p*-fluorine atoms are substituted. Clearly the reaction mechanism for this substitution differs from when there is a metal residing in the cavity.

Nickel(II) *meso*-tetrakis(polyfluorophenyl)porphyrins have been synthesised with pyrrole groups in order to form electropolymerized films.[230] From the reaction of 1-(3-hydroxypropyl)pyrrole in THF with sodium followed by subsequent reaction with (TF_5TP)Ni, resulted in a five component mixture from which mono-, di-, tri- and tetra-substituted products were obtained along with starting material. The electropolymerisation of these compounds led to the isolation of films which

exhibited the regular electroactivity of *N*-substituted polypyrroles as well as the spectroscopic and electrochemical features of the nickel(II) porphyrins.

Drain and co-workers have developed an efficient microwave-assisted synthesis of amine-substituted tetra(pentafluorophenyl)porphyrin.[231] The porphyrin and ten equivalents of the relevant amine are irradiated with 1100 W microwaves for between 10 and 30 minutes to afford the tetra-substituted porphyrin in 72 to 96% yield. The reaction uses *N*-methylpyrrolidone as a solvent to avoid problems with the decomposition of DMF. The crystal structure of the tetra-substituted tetraethylenediamine mono-*N*-t-Boc (Por-EDA$_4$) was also reported (Figure 70). In this structure the ethylenediamine chains are arranged into two different conformations; bent and extended. The bent conformation is organised by an intramolecular bond.
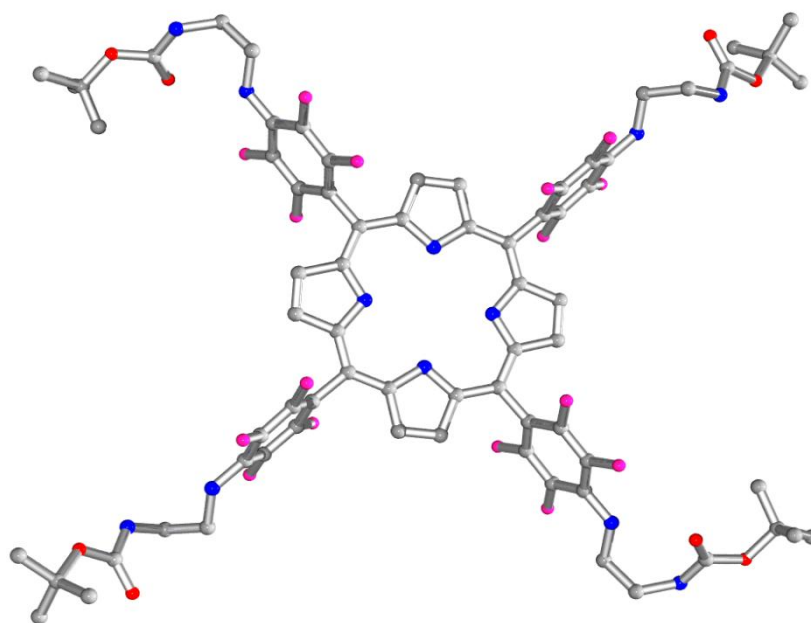
Figure 70: Ball and stick representation of the X-ray crystal structure of Por-EDA$_4$ (Drain and co-workers).[231]

Weiss and co-workers have prepared porphyrin derivatives with cationic pendent arms by substituting all of the fluorine atoms in

tetra(pentafluorophenyl)porphyrin.[232] The pendent arms, DMAP and triethylphosphane, were introduced using self-activated silyl-assisted polyonio substitution (SASAPOS) type reactions. Yields of 99 and 97% were obtained respectively.

Tetra(pentafluorophenyl) porphyrin was used to form the PEGylated target molecule as shown in Figure 68. The ability to displace the *p*-fluoride atom selectively was utilised to attach PEG chains to the porphyrin backbone. Addition of these PEG chains will aid solubility of the resulting compound and its complexes.

5.2. Synthesis of tetra(3,5-di-hydroxyphenyl)porphyrin and its gallium complex
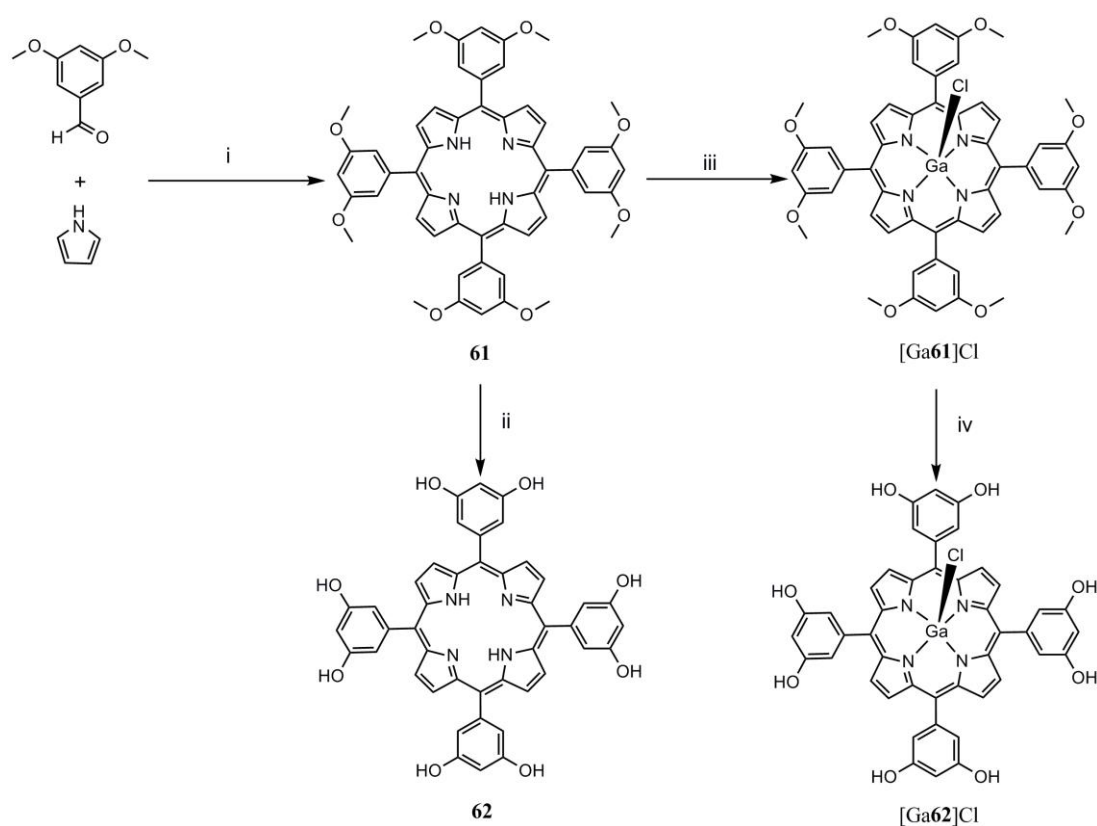
Scheme 31: Synthesis of 61 and 62. Conditions; i) propionic acid, reflux, 30 min, 19%; ii) BBr₃, DCM, RT, 72 hr, 84%; iii) gallium(III) chloride, sodium acetate, acetic acid, reflux, 81%; iv) BBr₃, DCM, RT, 24 hr, 100%

Scheme 31 shows the synthesis of the tetra(3,5-di-methoxyphenyl)porphyrin, **61**, and tetra(3,5-di-hydroxyphenyl)porphyrin, **62**, and their gallium(III) complexes. The first step in the synthesis was to produce the porphyrin ring system from pyrrole and 3,5-di-methoxy-benzaldehyde in propionic acid. This reaction has been reported previously by Nolte and co-workers[233] using a modified methodology developed by Tsuchida and co-workers.[234] The product can be obtained from the crude mixture by filtration, resulting in the isolation of the desired material in 19% yield as a purple crystalline material.

Crystals of **61** suitable for X-ray crystallographic analysis were grown from a toluene solution left to evaporate at RT and the structure was determined as shown in

Figure 71. The porphyrin core is planar with the dimethoxyphenyl rings arranged in a perpendicular fashion (see Figure 72).
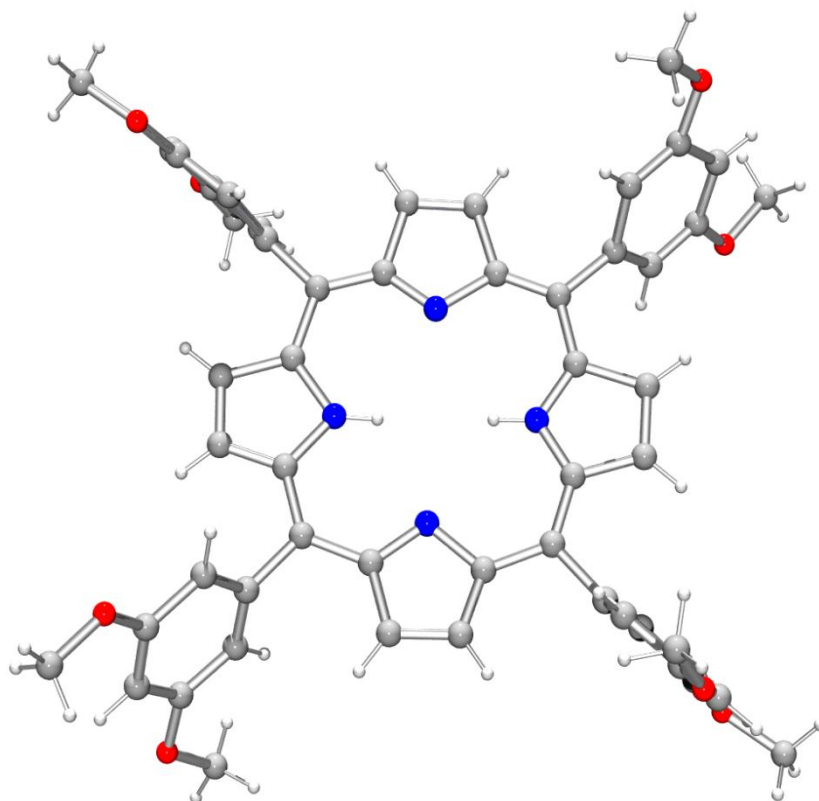
Figure 71: Ball and stick representation of the X-ray crystal structure of 61. Water molecules are omitted for clarity.
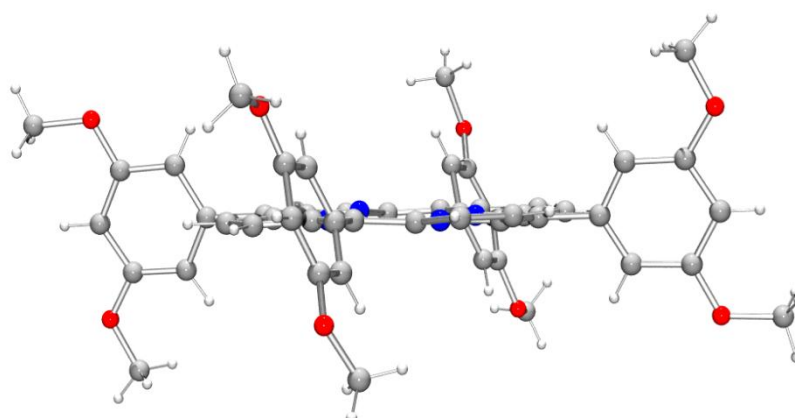
Figure 72: Ball and stick representation of the X-ray crystal structure of 61 viewed along the horizontal axis.

The next step in the synthesis of the free base porphyrin involves the cleavage of the methoxy ethers. This deprotection has been reported previously, using boron tribromide.[233,234] This reaction was carried out with asymmetric porphyrin derivatives which have three 3,5-dimethoxybenzene rings decorating the periphery, affording the hexa-hydroxy porphyrin in 75% yield after column chromatography.[235] Using boron tribromide to cleave the methyl ethers gave **62** as a dark purple solid in 84% yield.

Synthesis of the gallium(III) complexes was performed using **61** by Guilard's method of gallium insertion,[215] to give the gallium complex in 81% yield as a violet solid. **62** was not used for this complexation reaction because it was thought that the hydroxyl groups on the periphery of the porphyrin may act as coordination donors to the gallium(III). This could possibly lead to the formation of porphyrin complexes were molecules of **62** are bridged by a single gallium(III) ion. Crystals of [Ga**61**]Cl were grown from a toluene solution which was left to evaporate at RT. The X-ray structure was determined as shown in Figure 73. The gallium(III) ion adopts a square-based pyramidal geometry, with a chloride in the apical position (bond lengths shown in Table 10). The gallium ion is elevated out of the porphyrin cleft by an angle of 10° as determined by the angle between two adjacent nitrogen atoms and the gallium ion.
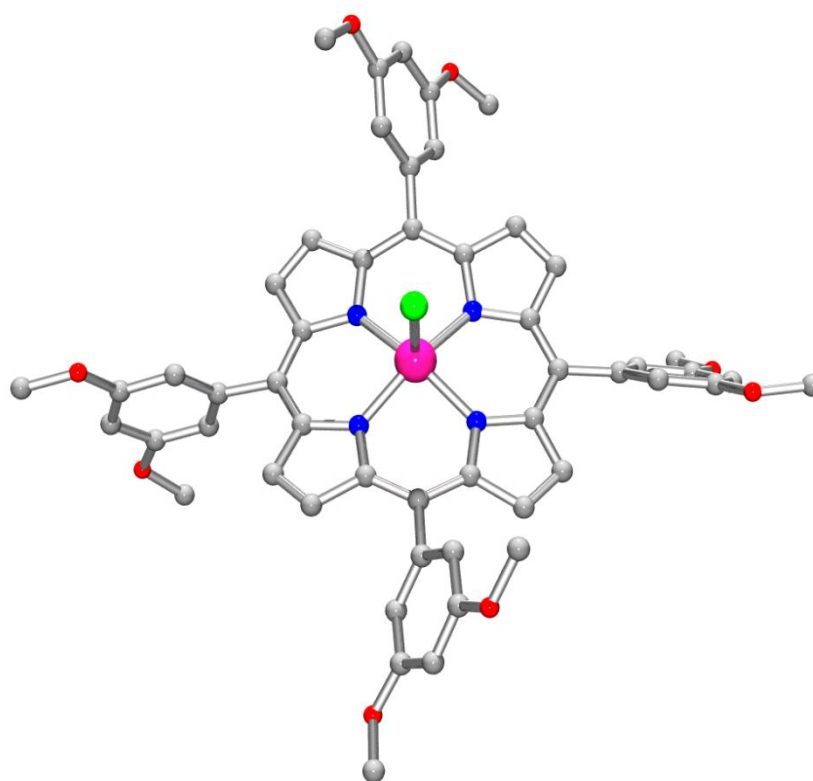
Figure 73: Ball and stick representation of the X-ray crystal structure of [Ga61]Cl. Water molecule and H-atoms omitted for clarity.

Of particular note is the deformation from planarity shown in this structure which is clearly noticeable when viewing along the horizontal axis, with the porphyrin core in the plane (Figure 74). Compared with the free-base derivative there is considerable saddle strain. This coincides with the dimethoxyphenyl rings becoming further distorted from being perpendicular to the porphyrin ring system. The insertion of the gallium ion into the porphyrin cleft is the most likely cause for this distortion.
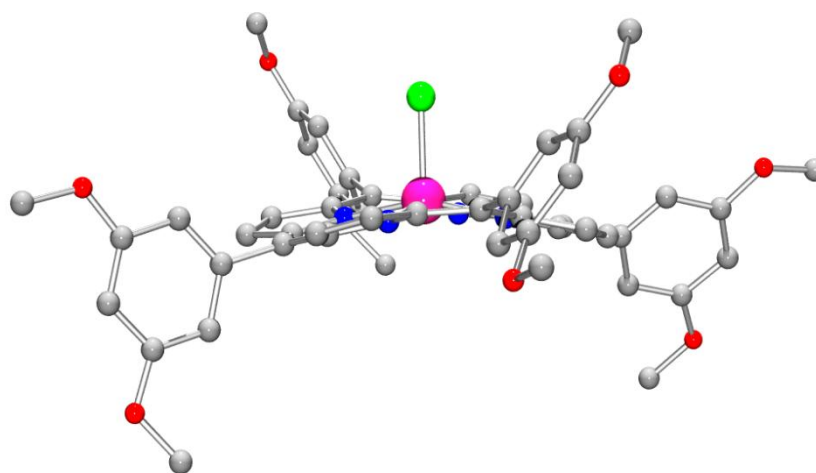
Figure 74: Ball and stick representation of the X-ray crystal structure of [Ga61]Cl viewing along the horizontal axis.

	Bond length (Å)
Ga(1)-N(1)	2.0213(18)
Ga(1)-N(2)	2.0144(17)
Ga(1)-N(3)	2.0316(18)
Ga(1)-N(4)	2.0217(17)
Ga(1)-Cl(1)	2.2067(9)

Table 10: Selected bond lengths from the X-ray crystal structure of [Ga61]Cl.

The next step was to cleave the methyl ethers. This cleavage was performed using boron tribromide in an analogous way to the preparation of **62**, and [Ga**62**]Cl was isolated as a very dark purple powder in quantitative yield.

5.2.1. Electrochemistry
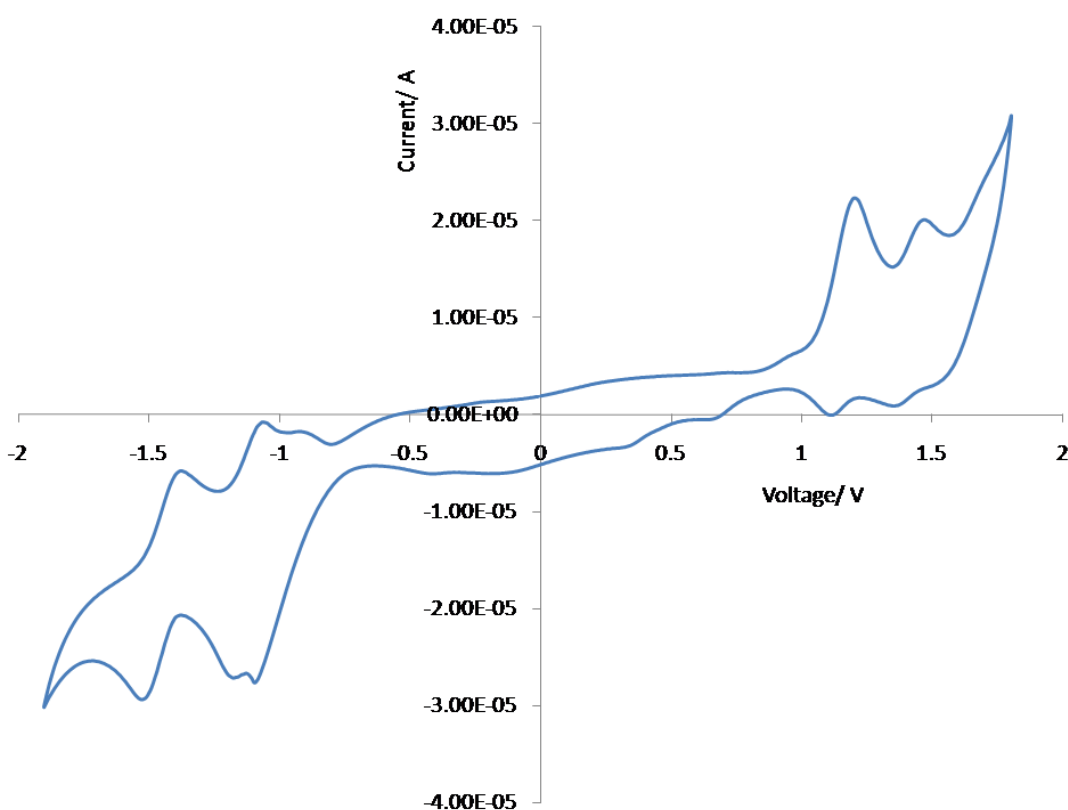
Figure 75: Cyclic voltammogram of 61 at a scan rate of 0.2 V/s in dichloromethane with tetrabutylammonium tetrafluoroborate as a supporting electrolyte.

Figure 75 shows the cyclic voltammogram of **61**. In the anodic region there are two waves at +1.19 V and +1.44 V, which are both reversible. These waves correspond to the formation of the radical cation and cation species respectively. In the anodic region there are also two waves, which appear at −1.12 and −1.51 V. These waves indicate the formation of the radical anion and anion species respectively. Both waves are again reversible. A plot of peak current verses the square root of scan rate gives a straight line which passes through the origin for all four waves; this is indicative that each wave is reversible in nature. The wave at −1.12 V appears to consist of two components; this is ascribed to the presence of both adsorbed and free species. Diagnostic criteria for metal complexes of porphyrins have been developed by Fuhrhop *et al.*[236] These criteria are as follows; i) the difference in $E_{½}$'s for the first ring oxidation and the first ring reduction is equal to 2.25 ± 0.15 V; ii) $\Delta E_{½}$ (reduction) = 0.42 ± 0.05 V; and iii) $\Delta E_{½}$ (oxidation) = 0.29 ± 0.05 V. Values

184

obtained for **61** for these criteria are i) 2.26 V, ii) 0.39 V and iii) 0.24 V. Compound **61** therefore fulfils all criteria, and therefore the four redox waves can be assigned as porphyrin ring centred.
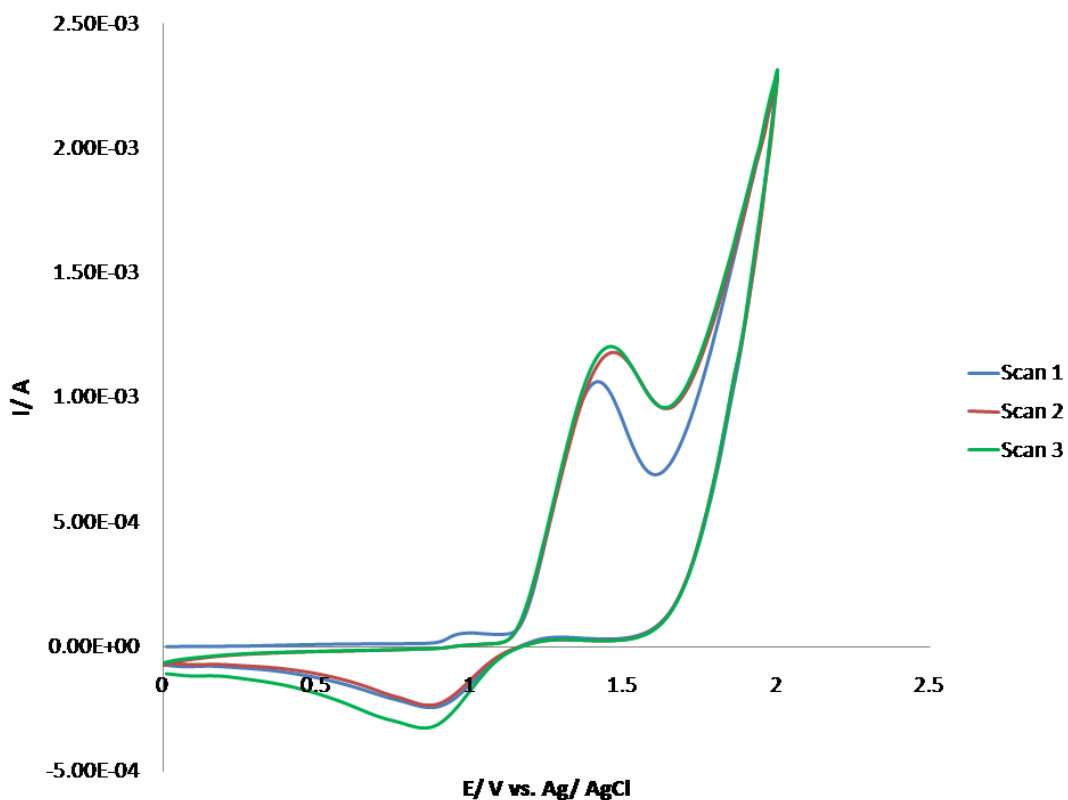
Figure 76: Repetitive cyclic voltammograms of 62 in water using potassium chloride as a supporting electrolyte at a scan rate of 0.1 V/s

Figure 76 shows the successive cyclic voltammograms of **62** measured in water at 0.1 V/s. Compared with **61**, the porphyrin possesses different behaviour. Only the anodic region is shown as the cathodic region is featureless. In the first scan a small broad peak is observable at ~+1 V. This peak is not present in further scans. It is interesting to note that after the first scan, the height of the peak at 1.39 V increases. This coincides with a complete disappearance of the peak at +1 V. It is proposed that the peak at ~+1 V is the formation of a radical species; a phenoxyl radical. The phenoxyl radical could result in dimerisation as shown in Scheme 32.
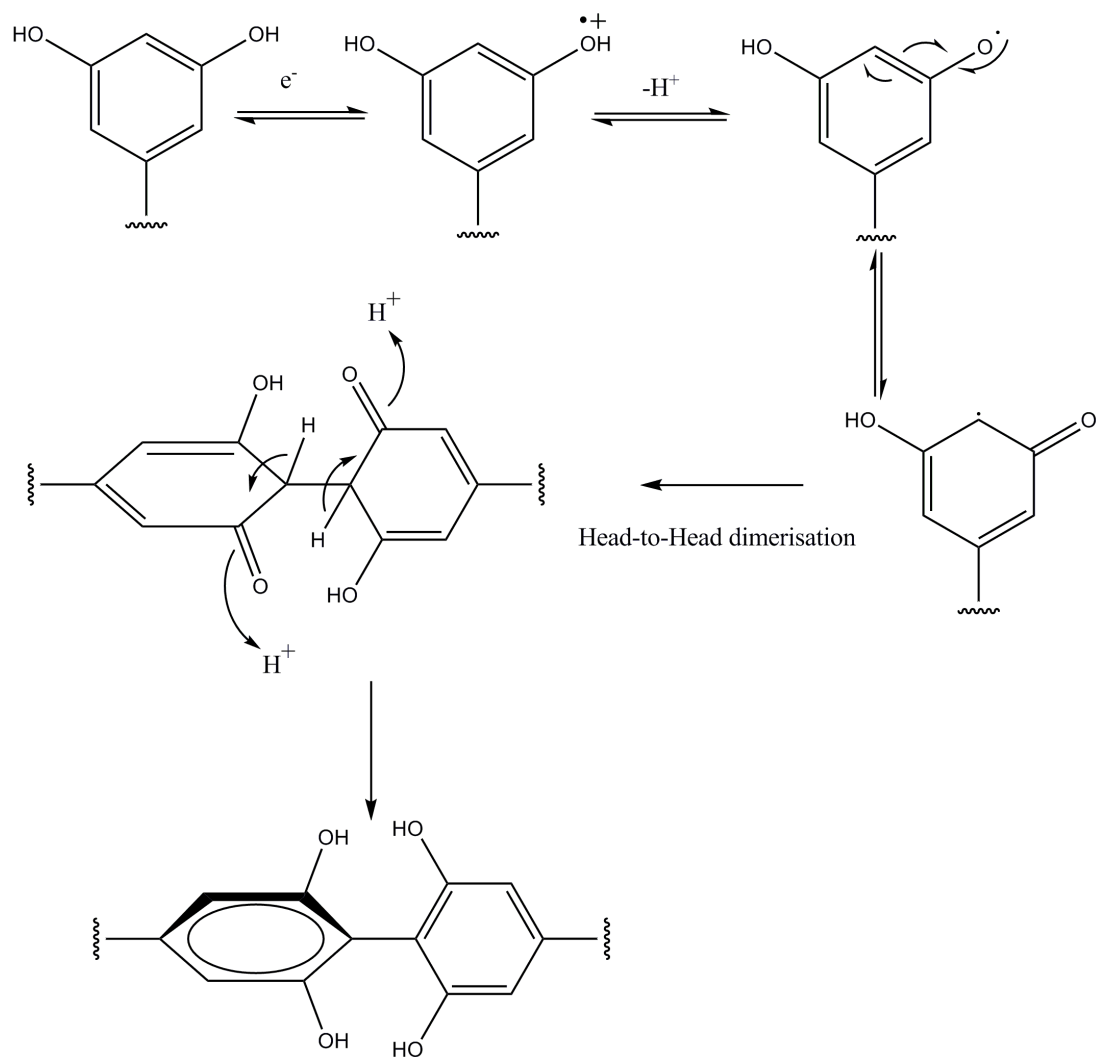
Scheme 32: Proposed reaction pathway for the formation of the porphyrin polymer formed from 62.

Scheme 32 shows the proposed pathway to form the porphyrin polymer of **62**. In the first step, one of the hydroxyl groups undergoes oxidation, generating the radical cation. Subsequent lose of a proton leaves a phenoxyl radical species. Through resonance, the radical can move through the conjugated π system, and by doing so, the radical can reside at the *para* position on the ring. Two such radicals can react with one another to form a dimer by forming a new C-C bond via radical fusion. The resulting dimer then regains its aromaticity by intermolecular hydrogen transfer. This same reaction can proceed at the other three di-hydroxy-phenyl positions on **62** therefore resulting in a polymer that extends both vertically and horizontally. Reaction of 3,5-dihydroxy-toluene in the presence of potassium ferricyanide is known to lead to the formation of 2,2',6,6'-tetrahydroxy-4,4'-

dimethylbiphenyl.[237,238] The dimerisation was shown to occur through a radical mechanism caused by one electron oxidation by potassium ferricyanide. This lends support to the notion of the porphyrin polymer being formed as outlined in Scheme 32.

The formation of the poprhyrin polymer is further evidenced by the presence of a large amount of adsorbed species on the platinum electrode. Also, from Figure 76, the peak at +1.39 V in the first scan shifts to +1.46 V on subsequent scans. This may suggest that on scans 2 and 3, a different species is responsible for this oxidative wave. This peak may originate from the oxidation of the polymerised porphyrin.

To further probe this reaction, the platinum working electrode was exchanged for a 1 cm wide 190 μm thick strip of Toray™ Carbon Paper. The experiment was then conducted again using the same conditions. The cyclic voltammogram recorded at the new electrode surface is shown in Figure 77. If repetitive cyclic voltammograms are collected, a deposit can be seen to form on the graphite surface which coincides with the solution gradually becoming clearer. The porphyrin polymer being formed must therefore become impregnated into the carbon paper. A similar type of procedure has been reported by Mosinger and co-workers.[239] They report the synthesis of immobilised TPP photosensitisers into polymeric nanofibres. These nanofibres were placed in bacterial cultures of *E. coli*. Upon irradiation, the bactericidal effect is clearly observable due to the absence of bacterial colonies. The generation of singlet oxygen by illumination with red light provided the cyctotoxic species. To investigate further the composition of material on the surface of the carbon paper, SEM coupled with X-ray emission spectroscopy was used.
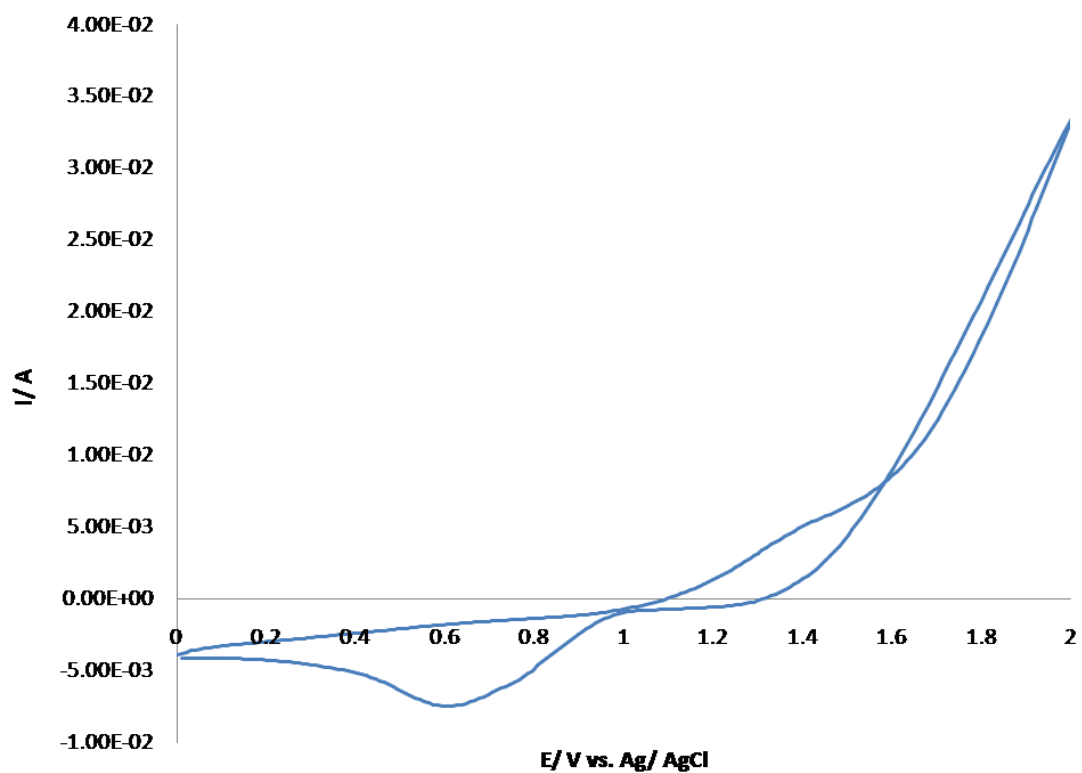
Figure 77: Cyclic voltammogram of 62 recorded at a graphite electrode at a scan rate of 0.2 V/s.

5.2.2. Scanning electron microscopy studies
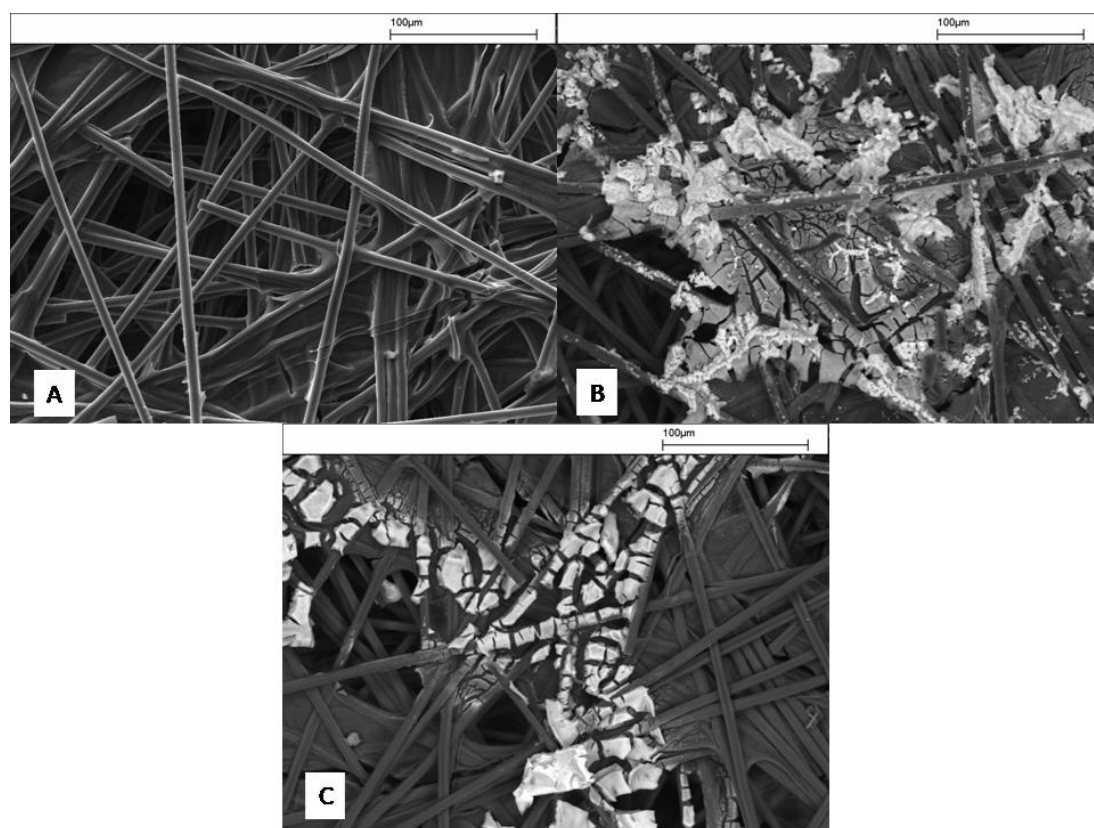
Figure 78: SEM images of the carbon paper and of the carbon paper impregnated with the porphyrin polymer formed from 62.

Scanning electron microscopy (SEM) was used to analyse the surface of the electrode impregnated with material produced from cyclic voltammetry experiments. Figure 78 shows the images of the carbon paper material (A), the carbon paper coated with material produced from cyclic voltammetry (B) and the carbon paper with material produced from cyclic voltammetry after washing with water (C). The SEM image of the clean electrode (A) was collected using a secondary electron detector. This enabled the tomography of the surface of the substrate to be observed. Electrodes with material impregnated into the graphite sheets (B and C) were analysed by using a backscattered electron detector. This enabled elemental contrast to be obtained. There is a clear difference between B and C in terms of the material impregnated into the carbon paper. B possesses both crystalline and powder phases, whereas C just has a powder phase. The chemical composition of the treated and non-treated carbon paper was probed by X-ray emission spectroscopy.
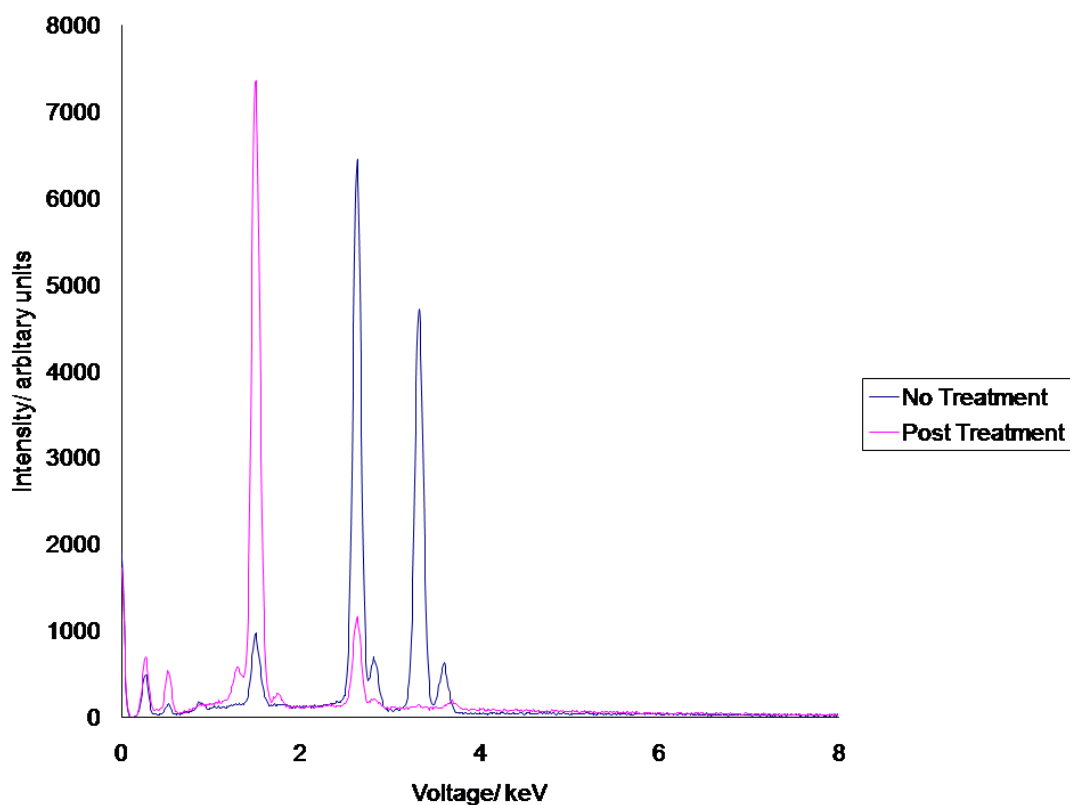
Graph 4: X-ray emission lines of the carbon paper impregnated with the porphyrin polymer formed from 62 before and after treatment.

Graph 4 shows the difference in the composition of the material deposited on the surface of the carbon graphite. Pre-washing, the surface is contaminated with large quantities of KCl, which was used as the supporting electrolyte during cylic voltammetry studies. This is evidenced by the presence of peaks at 2.63 and 3.32 keV. These are both generated due to chlorine (K_α emission line with a K_β emission line as shoulder to this peak) and potassium (K_α emission line with a K_β emission line as shoulder to this peak) respectively. A further smaller peak is present at 1.5 keV which is due to the presence of bromine (L_α emission line). The carbon paper was treated by leaving it in distilled water overnight. After washing, the spectrum now only possessed one major peak, which corresponds to bromine at 1.5 keV. The presence of this peak would suggest that during the cleavage of the methyl ethers using boron tribromide, the chloride axially attached to the gallium ion is exchanged for a bromide ion. This is not quantitative as there is still a small peak for chloride in the spectrum whilst there is a complete absence of a potassium peak. Gallium possesses K and L lines at around 10 keV and 1.1 keV respectively. The K line was

not detected and the L line is not clearly observable. Due to the presence of the other elemental emission lines in this area, it is possible that the gallium L line is masked.

5.2.3. Cytotoxicity studies

Cytotoxicity studies were conducted on **62** and [Ga**62**]Cl. These studies are used to measure the light induced toxicity of each complex by determining the percentage of cells killed after irradiation. The porphyrin compound is incubated in the cells for a small amount of time prior to being irradiated with red light. The percentage number of cells killed is then calculated. A control is used, whereby the cells are incubated with the porphyrin but kept in the dark. A high percentage of cell kill for the control is known as "dark toxicity" and has no therapeutic potential. Only the percentage number of cells killed upon irradiation with light is a useful measure of how effective a compound will be for PDT.
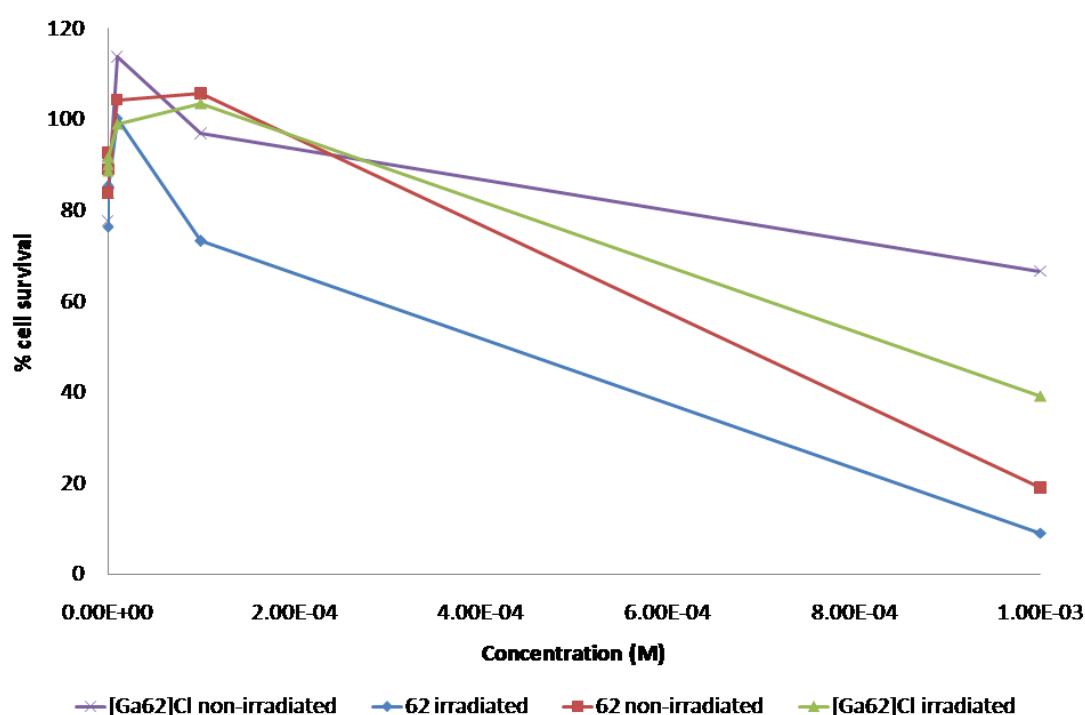
Graph 5: Percentage cell survival of human Caco2 cells in the presence of 62 and [Ga62]Cl.

Graph 5 shows the percentage survival of human Caco2 cells in the presence of either **62** or [Ga**62**]Cl. It is clear from the graph that both compounds display the

similar cytotoxic effects when non-irradiated and irradiated. **62** and its gallium complex are therefore not vey suitable as PDT agents because they possess high levels of dark toxicity.

5.3. Synthesis of tetra(pentafluorophenyl)porphyrin PEGylated derivatives and their nickel(II), zinc(II) and gallium(III) complexes

The synthesis of the PEGylated tetra(pentafluorophenyl)porphyrin derivatives, **64-66**, are shown in Scheme 33. Tetra(pentafluorophenyl)porphyrin, **63**, was synthesised according to the literature procedure by Longo and co-workers.[227] This involves the heating to reflux of pyrrole and pentafluorobenzaldehyde in propionic acid for 6 hr. When made in this way, there are considerable amounts of chlorin impurity present, which is difficult to separate by column chromatography. A purification method reported by Gouterman and co-workers was therefore used.[228,240] The purification they describe utilises a metallation of the free base porphyrin in order to separate it from the chlorin impurity. In order to extract the porphyrin from the crude material, the product was first put onto a wet-packed neutral alumina column. Using an eluent mixture of petroleum ether and hexane (5:8), both green (chlorin) and red (porphyrin) bands were collected, whilst a black band remained at the top. The green and red bands were then combined and the porphyrin/chlorin mix reacted with zinc(II) acetate in refluxing chloroform/methanol. The complex was then purified by column chromatography, using a basic alumina column. The green chlorin band was then eluted using hexane/DCM (1:1). After the column was clear, the desired porphyrin band was brought down using DCM. The porphyrin was then demetallated using concentrated HCl, and the free base porphyrin extracted using an aqueous work-up.

$R = $

64, x = 2
65, x = 11 (average)
66, x = 15 (average)
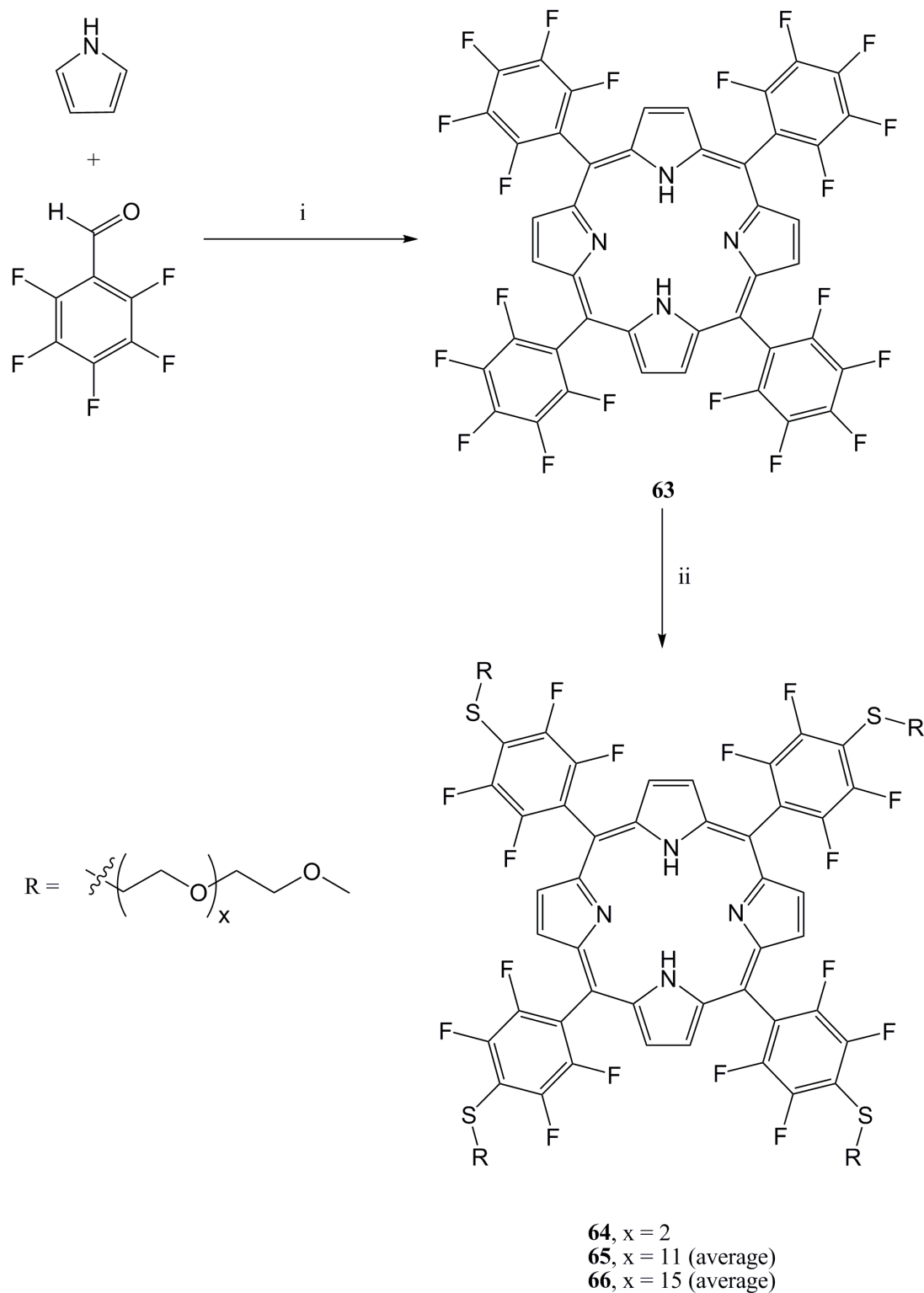
Scheme 33: Synthesis of 63-66. Conditions; i) propionic acid, reflux, 6 hr (4%); DMF, 10 equivalents of 29, 30, or 31, RT, 3 d (64=75%, 65=100%, 66=100%).

Complex formation of porphyrin **63** was accomplished using three different metals; nickel(II), zinc(II) and gallium(III). Complexation with zinc(II) and nickel(II)

involved dissolving the porphyrin in chloroform or acetic acid respectively, followed by the addition of the appropriate metal salt. Complexation with gallium(III) proved more difficult however. Initially the methodology developed by Guilard and co-workers was used.[215] The porphyrin was dissolved in dry acetic acid and the gallium chloride added in the presence sodium acetate. The reaction was heated to reflux and allowed to proceed for 12 hr. After this time, TLC showed that the reaction was not complete. The mixture was subjected to column chromatography and the desired fraction which had a R_f of 0.44 (ethyl acetate/hexane 5/95) was isolated. Using this methodology, the gallium complex was obtained in only 5% yield. One possible reason for this was the low solubility of porphyrin in acetic acid.

63

[M**63**]Y where M= Ni, Zn, or Ga
Y= OPh when X= Ga

R =

[M**64**] M= Ni or Ga. R=R'. x=2.
Y=OPh when M=Ga.
[M**65**] M=Ni, Zn or Ga. R=R'.
x=11.Y=OPh when M= Ga.
[M**66**] M= Ni, Zn or Ga. R=R'.
x=15.Y=OPh when M=Ga.
[M**67**] M=Zn. R'=F. x=3.
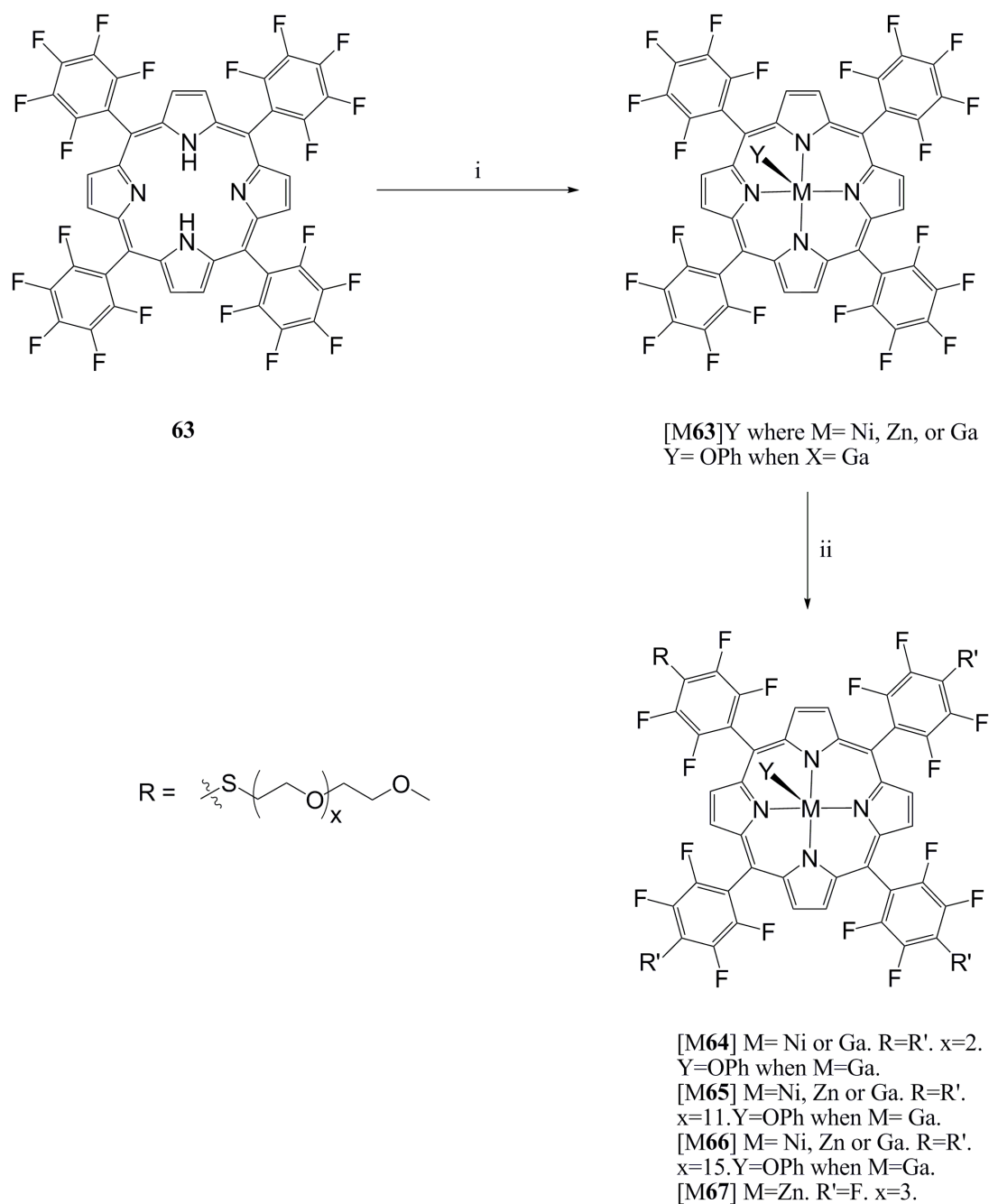
Scheme 34: Synthesis of Ni(II), Zn(II) and Ga(III) metal complexes of 63-67. Conditions; i) when M=Zn: Zn(II) acetate, DCM, reflux, 4 hr (92%); when M=Ni: Ni(II) acetate, acetic acid, reflux, 24 hr (95%); when M=Ga: GaCl$_3$, sodium acetate, acetic acid, reflux, 24 hr (6%) or Ga(acac)$_3$, PhOH, 220°C, 30 min (92%); ii) DMF, 10 equivalents of 29, 30, or 31, RT, 3 d ([M64]=62-94%, [M65]=58-94%, [M66]=72-95%, [Zn67]=8%).

Figure 79 shows the crystal structure of [Ga**63**]C$_4$H$_4$N obtained from crystallographic refinement. Crystals were grown from a toluene solution left to

evaporate at RT. The unit cell contains a single molecule of toluene and a pyrrolic anion. The pyrrolic anion is not coordinated to the gallium centre. The presence of a pyrrolic anion in the unit cell is unlikely due to its high basicity; better quality data is needed to ambiguously assign the chemical nature of the anion. The toluene molecule is disordered over four sites; the molecule is present either above or below the porphyrin plane in which it occupies two different site positions. Figure 79 shows all four positions for the toluene molecule. The gallium ion sits in the plane of the porphyrin and adopts a square planar geometry (bond lengths for the gallium(III) ion are shown in Table 11). Figure 80 shows [Ga**63**]C_4H_4N viewing perpendicular to the horizontal plane. This shows the toluene molecule is directly centred above/below the gallium ion. The distance between the gallium centre and the centre of toluene molecule is 3.29 Å. The pyrrolic anion could be generated from the decomposition of **62** during complexation due to its insolubility in acetic acid, or having been carried through from the previous step.
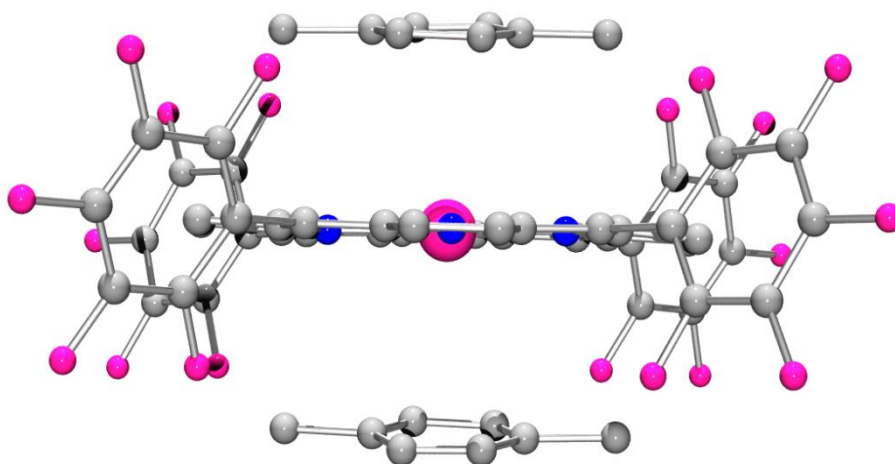
Figure 79: Ball and stick representation of the X-ray crystal structure of [Ga63]C_4H_4N viewed along the horizontal axis. The pyrrolic anion is omitted for clarity.
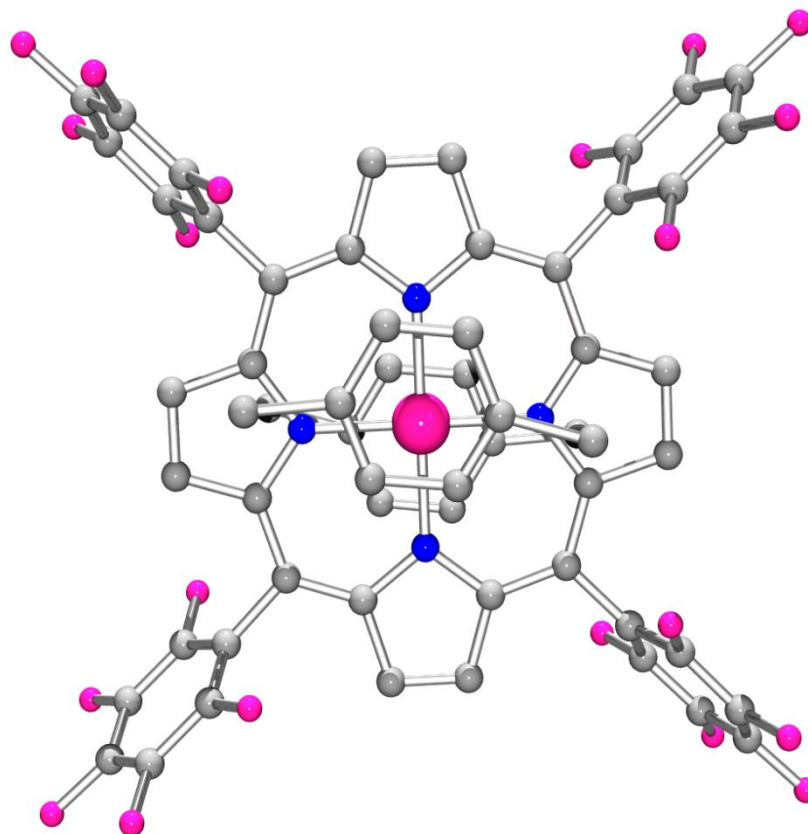
Figure 80: Ball and stick representation of the X-ray crystal structure of [Ga63]C₄H₄N viewed along the vertical axis. H-atoms and the pyrrolic anion have been omitted for clarity.

	Bond lengths (Å) for [Ga**63**]C₄H₄N	Bond lengths (Å) for [Ga**63**]OPh
Ga(1)-N(1)	2.038(5)	2.109(7)
Ga(1)-N(1)#1	2.038(5)	2.108(7)
Ga(1)-N(2)	2.046(5)	2.086(8)
Ga(1)-N(2)#1	2.046(5)	2.059(7)
Ga(1)-O(1)		1.796(11)

Table 11: Selected bond lengths from the X-ray crystal structures of [Ga63]C₄H₄N and [Ga63]OPh.

The second metallation procedure used for the insertion of gallium into porphyrin **63** was that developed by Buchler.[217] The porphyrin and gallium acetylacetonate were dissolved in phenol and heated to 220°C for 20 min. The crude material was then purified by column chromatography to remove the excess phenol. This was performed using a neutral alumina column, with the red band containing the metal

complex being eluted with benzene. Crystals of this material were grown from a toluene solution left to evaporate at RT.
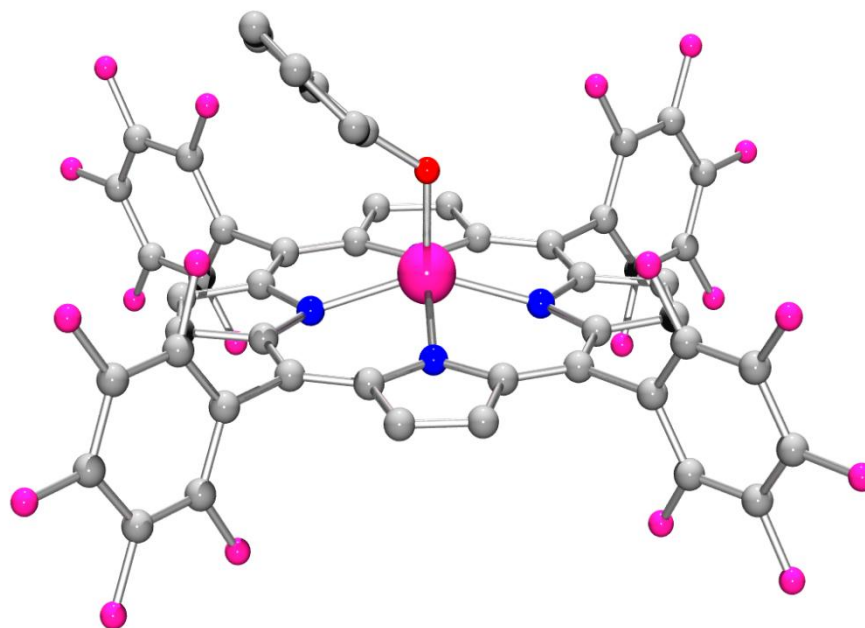
Figure 81: Ball and stick representation of the X-ray crystal structure of [Ga63]OPh with hydrogen atoms omitted for clarity.

Figure 81 shows the X-ray structure of [Ga**63**]OPh. The gallium ion adopts a five coordinate geometry, with the oxygen of the bound phenolate anion capping the apex of a square based pyramid. The bond lengths of the gallium(III) ion are shown in Table 11.

To PEGylate the porphyrin, a methodology developed by Boyle and co-workers was used.[241] They describe the regio-selective synthesis of monofunctionalised porphyrins via the displacement of a *p*-fluorine atom. These porphyrin derivatives possess a single pentafluorophenyl ring. Reactions were conducted in DMF at RT using sodium sulphide in the presence of an electrophile. Yields of 57-82% of mono-functionalised products were obtained after being left to react for 12 hr. This route therefore appeared to be applicable to the synthesis of the target compound.

Using this methodology, the PEGylated porphyrin complexes were prepared by attaching the PEG chains. This was performed by dissolving the complex in DMF and adding ten equivalents of the relevant PEG (either **29**, **30** or **31**) chain in the presence of ten equivalents of sodium sulphide. After three days the reaction was

judged complete by TLC (absence of starting material and also a new single spot with an R_f of 0.37) except for the zinc(II) complex of **66**. Analysis showed that the reaction had not occurred (only one spot visible by TLC which had the same R_f as the starting material). The most likely reason for no reaction occurring is the aggregation of [Zn**62**]. Aggregation of [Zn**62**] is likely to be deterred by longer PEG chains (such as **29** and **30**), but with **31**, the chain length is much shorter and therefore unable to disrupt the aggregation. To disrupt aggregation, the reaction mixture was heated to 60°C and left for three weeks. Analysis now showed a multi-component mixture in which starting material was still present but another intense spot with an R_f of 0.45 was also present. Other less intense spots were present at lower R_f values. The various fractions were isolated using column chromatography using a wet packed silica gel column. The starting material was eluted from the column using DCM and the remaining products eluted with MeOH/DCM (10/90 (v/v)). The first spot removed in this way was the major component but it was only isolated in 8% yield. Analysis of this component by NMR showed that this was the mono-substituted product, [Zn**67**]. Analysis of the other spots was made difficult by the poor separation but these are believed to be the di-, tri- and tetra-substituted products. Combined yield of all three of these fractions was less than 5%.

Clean up of the other metallated tetra-PEGylated porphyrins, [M**64**]-[M**66**] (Scheme 33) was necessary to remove the excess PEG. Column chromatography was found to be laborious and in the case of longer PEG chains (**29** and **30**), particularly challenging. Therefore an alternative method for removing the excess PEG was sought. One method which appeared appropriate was to use dialysis. Spectrum Laboratories Inc. produce a product called a Float-A-Lyzer, which is basically dialysis tubing incorporated into a device which floats. This type of device could be purchased with a molecular weight cut-off (MWCO) of 1000 Da. This was ideal as the PEG chains all weighed less than this and the PEGylated porphyrin complexes all weighed considerably more. This appeared to be a very attractive method. The Float-A-Lyzers purchased had an internal diameter of 10 mm and a volume of 3ml. The tetra-PEGylated porphyrins were then dissolved in water/MeOH and placed within the Float-A-Lyzer and left for a period of one week immersed in water to enable the excess PEG to diffuse from the internal cavity. The tetra-PEGylated

porphyrin was then removed and re-analysed by NMR. This showed that the excess PEG had been removed from the samples.
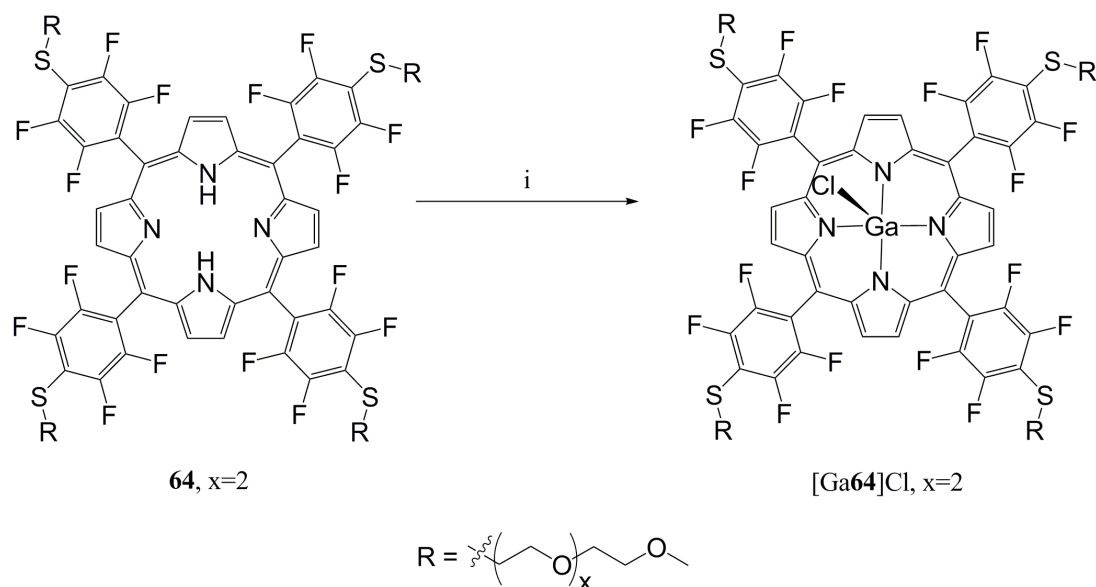
Scheme 35: Synthesis of [Ga63]Cl. Conditions; GaCl₃, dry acetic acid, sodium acetate, reflux, 18 hr, 100%.

The problematic insertion of gallium(III) into the porphyrin cleft of **62** was investigated further by seeing if the same problems were encountered when using the tetra-PEGylated porphyrin **63**. The porphyrin was again dissolved in acetic acid and the gallium chloride salt added to it in the presence of sodium acetate (see Scheme 35 for further conditions). After refluxing the mixture for 18 hr, it was analysed by TLC which showed that complex formation had proceeded as intended. Subsequent silica gel column chromatography (eluent DCM/MeOH 95/5 (v/v)) gave the gallium(III) complex in quantitative yield. This implies that **63** is more soluble in acetic acid than its analogue **62**, thus increasing the yield of the product.

5.3.1. Cytotoxicity studies

Cytotoxcity studies were conducted on the PEGylated porphyrins and their metal complexes. The aim of these studies was to ascertain if the light induced cyctotoxity was dependent on the length of the PEG chain. A second aim was to see if the metal ion had an influence on these properties. Experiments were conducted in the same way as those in section 5.2.3.
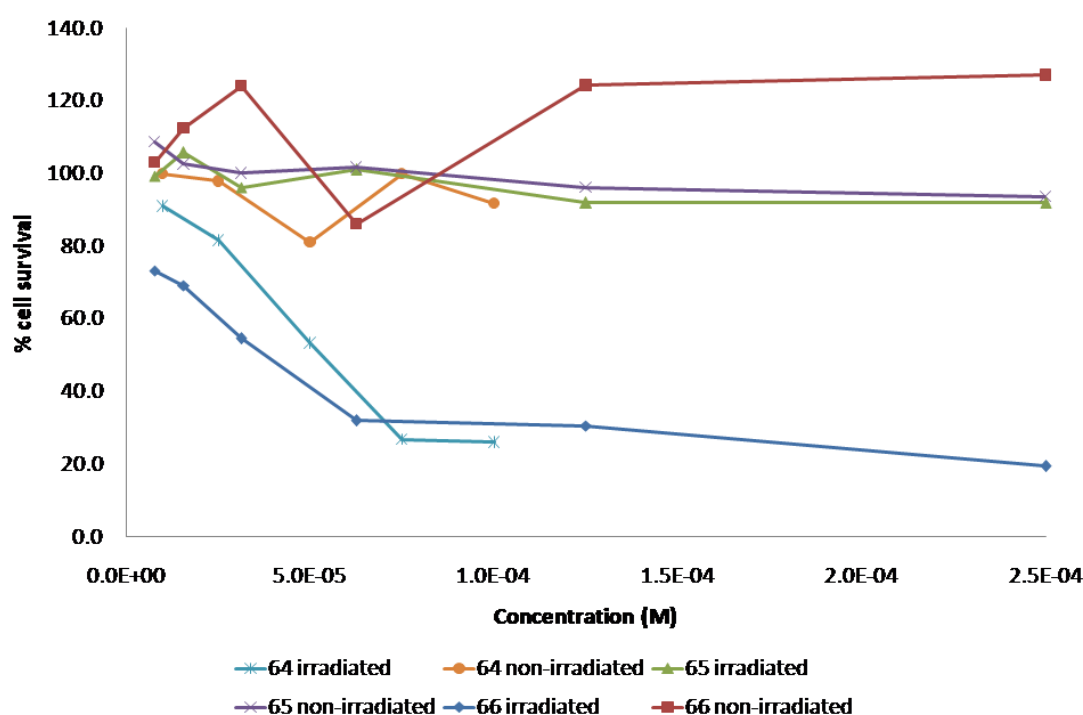
Graph 6: Percentage cell survival of human Caco2 cells in the presence of 64, 65 and 66.

Graph 6 shows the percentage cell survival of human Caco2 cells when exposed to differing concentrations of **64**, **65** and **66** after irradiation with red light or when kept in the dark (non-irradiated). From the graph, one noticeable trend is observable. When the PEG chain has an average molecular weight of 550 (**65**), there is negligible effect upon cell survival when either irradiated or non-irradiated. However, compared with compounds **64** and **66**, a clear difference is noticeable. Compounds **64** and **66** have no appreciable effect on cell survival when not irradiated but when irradiated, the percentage of cells surviving decreases rapidly

with increasing concentration. It is possible that compounds **64** and **66** are able to cross the cell membrane using membrane channels, leading to intracellular singlet oxygen generation. Within the cell, the singlet oxygen generated can damage cell organelles leading to cell kill. The lack of cell kill for compound **65** suggests that this may not be able to internalise within the cell. Singlet oxygen is therefore generated outside of the cell leading to low levels of cell kill.

These results differ to the trend observed by Ng and co-workers.[242] They produced 1,4-diPEGylated zinc(II) phthalocyanines $(ZnPc[O(CH_2CH_2O)_nMe]_2)$. The chain length was found to be important with regard to light induced cytotoxicity. When n = 2, or 8 and above, high IC_{50} values were obtained (> 0.1 μM against HT29). Conversely, those compounds where n = 4 or 6 possessed IC_{50} values of less than 0.1 μM. The reason for the differences in these values is that when n = 2 the compounds are not very water soluble, and at high values of n (greater than 8), the compounds aggregated in the culture medium, probably due to strong dipole-dipole interactions among the side chains. Aggregation provides an efficient non-radiative relaxation pathway, thereby reducing the population of the triplet state and the singlet oxygen generation efficiency.

The nickel(II) complexes of **64**, **65** and **66** were all found to have negligible light induced cytotoxicity and high levels of dark toxicity. The same was found for the zinc(II) complexes of **65**, **66** and **67**. In all of these complexes, the metal sits in either the plane of the porphyrin ring (zinc) or slightly sitting out of the plane (nickel). These complexes can therefore aggregate. This leads to ineffective singlet oxygen generation and would also account for the high dark toxicity observed.

The gallium(III) phenoxide complexes, however, were found to possess light induced cytotoxicity (see Graph 7). Compared with the unmetallated derivatives (**64**, **65** and **66**), a different trend was observed. For the gallium phenoxide complexes, the longer length chains are both cytotoxic on exposure to light, whereas the complex with the smallest PEG chain (**31**), were found to be inactive. All three complexes possess low levels of dark toxicity. The differences in light induced toxicity, suggests that these complexes internalise or localise differently compared with the free porphyrins.
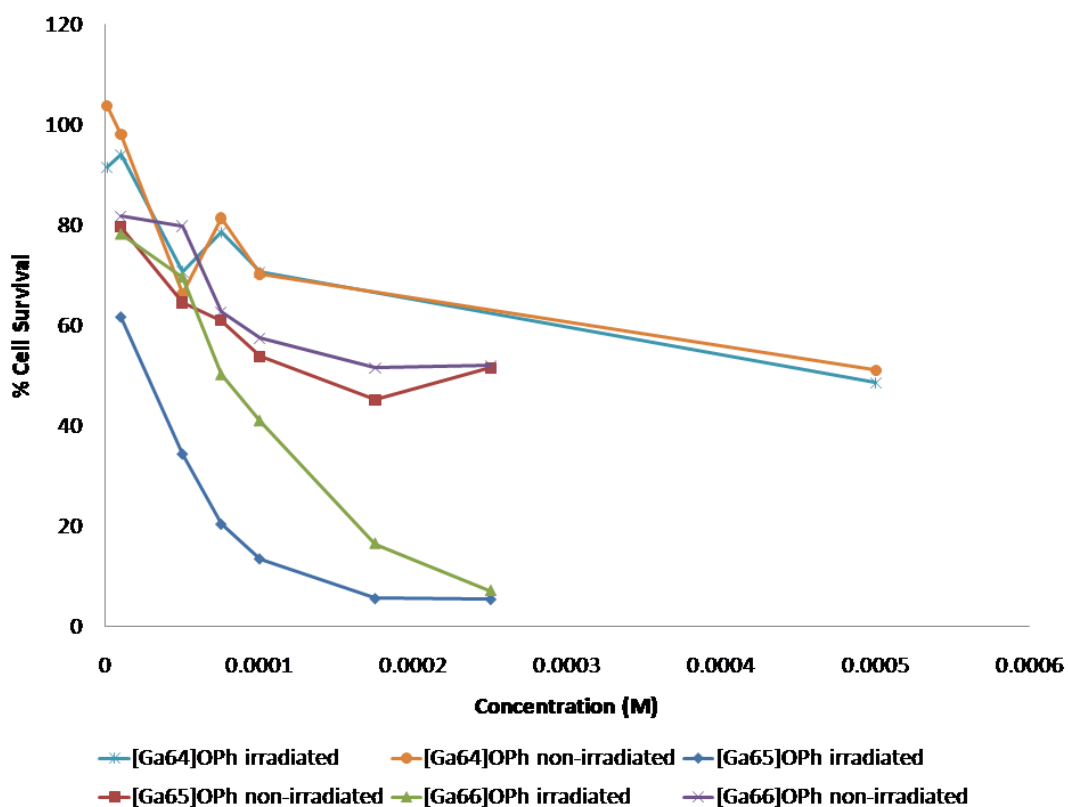
Graph 7: Percentage cell survival of human Caco2 cells in the presence of the gallium(III) phenoxide complexes of 64, 65 and 66.

Changing the anion in the gallium(III) complexes was found to have a profound effect on the light induced toxicity. The percentage cell survival of human Caco2 cells in the presence of [Ga**64**]Cl is shown in Graph 8. Compared with [Ga**64**]OPh, the compound exhibits light induced cytotoxicity, which becomes greater with each successive experiment. Each experiment was performed using the same stock solution of [Ga**64**]Cl in DMSO. This infers that a more cytotoxic species is being generated over time. This could occur by displacement of the chloride attached to the gallium(III) centre by a DMSO molecule.
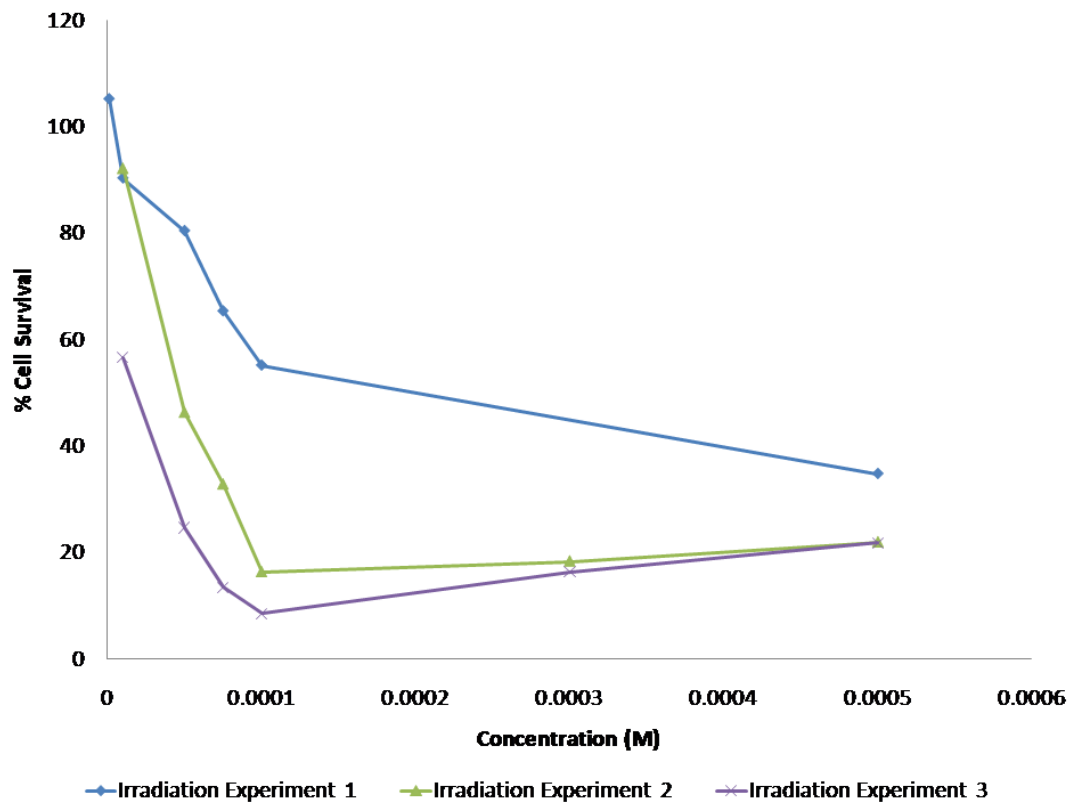
Graph 8: Percentage cell survival of human Caco2 cells in the presence of the [Ga64]Cl from experiments conducted in triplicate.

5.4. Conclusion

In this chapter, the focus has been on the production of water soluble PDT agents. PDT agent design has been based around porphyrin molecules, and two such compounds have been synthesised for this purpose. The first porphyrin synthesised was based on TPP, and has eight hydroxyl groups decorating the periphery. Insertion of gallium(III) into the porphyrin cleft induces saddle strain on the porphyrin which is readily seen from the crystal structures obtained. Electrochemistry of the free base, **61**, fulfils the rules outlined by Fuhrlop[236] whereas compound **62** underwent an electrochemical reaction. **62** and its gallium complex are believed to undergo head-to-head dimerisation, thus forming a polymer. It was possible to coat the surface of a carbon paper electrode with this material and study it using SEM. Investigations into the cytotoxicity profiles of both the metallated and free base porphyrin of compound **62** showed that dark toxicity almost mirrored the light induced toxicity. These compounds are therefore not suitable as PDT agents but may be suitable as antibacterial agents incorporated into fibrous materials.

The second porphyrin derivative investigated was tetra(pentafluorophenyl)porphyrin and its complexes with gallium(III), zinc(II) and nickel(II). The porphyrin was synthesised by an Adler method and required a metallation-demetallation procedure to isolate the free-base. Insertion of zinc(II) and nickel(II) into the porphyrin gave satisfactory yields whereas gallium insertion proved problematic; use of Guilard and co-workers method[215] resulted in only 5% of the desired metal complex being isolated. Much more satisfactory yields were obtained by using the method reported by Buchler and co-workers.[217] Compound **63** and its complexes were used to produce porphyrins bearing four PEG chains. Each of these chains was attached via a thioether linkage following displacement of the *para*-fluoride. Yields for this PEGylation reaction were typically high although one exception was for the zinc(II) complex of **67**. PEGylation for this complex proved difficult to carry out, a possible reason being that the porphyrin was forming aggregates. Heating this reaction encouraged the PEGylation reaction to proceed as desired. Cytotoxity studies of the free-bases **64**, **65** and **66** revealed an interesting trend. **64** and **66** were light induced toxic whereas **66** was not. This suggests that **64** and **66** might be able to cross the cell membrane whereas **65** cannot. Zinc(II) and nickel(II) complexes were found to be ineffective light induced cyctotoxic agents. The gallium(III) phenoxide complexes

of **65** and **66** were found to be light induced cytotoxic whereas the complex of **64** was not. This suggests a different mechanism of cell kill compared with the unmetallated tetra-PEGylated compounds. [Ga**64**]Cl was found to be light induced cytotoxic, however, and became more cytotoxic over time when left in solution. Displacement of the chloride from the gallium(III) centre in the stock solution by a DMSO molecule is believed to form the more potent cytotoxic agent.

6. Conclusions and further work

6.1. Conclusions

The goal of this research was to synthesise macrocyclic ligand systems bearing pendent arms for potential use in diagnostic and therapeutic applications such as magnetic resonance imaging (MRI) and photodynamic therapy (PDT). Tetraaza macrocyclic complexes of 1,4,7,10-tetraazacylcododecane (cyclen), 1,4,8,11-tetraazacyclotetradecane (cyclam) and porphyrins incorporating transition, lanthanide and p-block metal ions have been synthesised towards this aim. Novel redox active macrocyclic systems with attached pendent arms have been produced which has provided insight into the stability of the complexes produced.

In Chapter 2, the design and synthesis of the pendent arms which were used to attach to the macrocycles was discussed. Redox active, amino acid and PEG pendent arms were all successfully synthesised. Phenol and thiophenol pendent arms were synthesised with the aim of investigating their redox properties when incorporated into macrocyclic complexes of cyclen and cyclam. Phenol pendent arms were synthesised with methyl, benzyl, *p*-methoxybenzyl and acetyl protecting groups. In addition, an unmasked phenol derivative was also synthesised. Two thiophenol pendent arms were synthesised, both utilising a *p*-methoxybenxyl group to protect the thiol. These were synthesised according to a procedure detailed by Wieghardt and co-workers.[142] The phenol and thiophenol pendent arms were synthesised with *tert*-butyl groups in the *ortho* and *para* positions of the aromatic ring. These were required to stabilise the radical species once generated. A thiophenol derivative was synthesised without *tert*-butyl groups for comparison.

Amino acid pendent arms were synthesised based on the two amino acids aspartic acid and 4-nitro-L-phenylalanine. The amino group of each amino acid was converted to a bromide via a diazonium salt intermediate. This gave a point of possible attachment to a tetraaza macrocycle. The remaining carboxylic acid groups were protected to enable selective deprotection once attached. Finally, polyethylene glycol (PEG) chains were synthesised. These chains are of varying length with one end of the chain capped as a methoxy group whilst the other is an alcohol. The synthesis of the PEG pendent arms uses commercially available materials and involves either a bromination or chlorination of the alcohol functional group. This activates the PEG chain towards nucleophilic attack. These chains were subsequently

used to increase the water solubility of tetra(pentafluorophenyl)porphyrin complexes by displacement of a *p*-fluoride on each phenyl ring.

In Chapter 3, the preparation of side-bridged cyclam complexes with thiophenolate or phenolate pendent arms was discussed. Use of the phenol pendent arms as discussed in Chapter 2 led to a library of side-bridged cyclams being produced. There were a number of issues with the protecting group strategy and after attempting different variations, use of the acetyl protected phenol was identified as the most appropriate. This was cleaved using 6M HCl in conjunction with the acetyl protected compound, **43**. Nickel(II), copper(II) and zinc(II) complexes were produced for the phenolate and protected phenol side-bridged cyclam compounds. Gallium(III) complexes were also desired but were not isolated for either the phenolate or thiophenolate compounds. Cyclic voltammetry of the nickel(II) and copper(II) complexes was performed to obtain evidence of the phenoxyl radical being generated. For the copper complexes, the Cu(II)/Cu(III) redox couple was shifted towards anodic potentials in the order *p*-methoxybenzyl < benzyl < methyl. For [Cu**37**]$^+$, the side-bridged cyclam di-*tert*-butyl-phenolate copper(II) complex, a wave corresponding to the formation of the phenoxyl radical was observed at +0.48 V (reversible). The phenoxyl radical was also observed to form in [Ni**37**]$^+$ at +0.74 V.

Nickel(II) complexes of the thiophenol side-bridged cyclams were produced. The thiophenol was unmasked by cleaving the *p*-methoxybenzyl protecting group using mercury acetate and hydrogen sulphide. Cyclic voltammetry was performed on the copper(II) and nickel(II) complexes. The cyclic voltammogram (CV) of the nickel(II) complex of the side-bridged cyclam with attached thiophenolate arm ([Ni**46**]$^+$) possesses a wave at +0.60 V which is assigned to the formation of the thiyl radical. In the copper(II) and nickel(II) complexes of the side-bridged cyclam complex with a di-*tert*-butyl-thiophenolate arm attached (**49)**, the formation of the thiyl radical was assigned to peaks at +0.50 and +0.53 V respectively. These complexes also display evidence for dimerisation occurring in solution. Dimerisation occurs between two radical species to form a di-sulphide bond. Oxidation waves at −0.25 and −0.2 V are assigned to the oxidation of the dimer for the copper(II) and nickel(II) complexes of **49** respectively.

Chapter 4 details the production of lanthanide macrocyclic complexes using cyclen as the tetraazamacrocyclic scaffold. Ligands were produced bearing three acetate arms and either one phenol/thiophenol pendent arm or an amino acid pendent arm. The phenolate ligand, **52**, was synthesised using the acetyl protected di-*tert*-butyl pendent arm, **15**. The thiophenolate ligand, **56**, was produced using the di-*tert*-butyl thiophenolate pendent arm, **24**. Lanthanide complexes of the ligands were synthesised. For the gadolinium(III) complexes, T1 weighted images were collected. These images showed that the complexes [Gd**52**]$^-$ and [Gd**56**]$^-$ enhanced the image relative to water. The oxidised species [Gd**52**]$^\bullet$ and [Gd**56**]$^\bullet$ did not enhance the image relative to the starting complexes. The lipophilic nature surrounding the metal ion is believed to prevent further water molecules entering the inner coordination sphere after oxidation, and therefore no enhancement of the image is observed.

The UV-visible spectrum of [Eu**52**]$^-$ displays only a π-π* transition, but upon one electron oxidation, the characteristic fingerprint of a phenoxyl radical was observed. This was further observed in the cyclic voltammogram (peak at ~+0.75 V due to formation of the phenoxyl radical). The thiyl radical was also observed in the cyclic voltammogram of [Eu**56**]$^-$ (wave at +1.14 V). When cooled to −40°C, this peak shifts to +0.83 V. The existence of different isomers was suggested for the ease of this oxidation at lower temperatures. Fluorescence spectra of [Eu**52**]$^-$ and [Eu**56**]$^-$ possess two emission peaks each. For [Eu**52**]$^-$ the peaks are centred at 595 and 612 nm which corresponds to $^5D_0\rightarrow{}^7F_1$ and $^5D_0\rightarrow{}^7F_2$ transitions respectively. The emission peaks for [Eu**56**]$^-$ are at 573 and 614 nm and correspond to $^5D_0\rightarrow{}^7F_0$ and $^5D_0\rightarrow{}^7F_2$ transitions. In contrast, the terbium(III) complexes of **52** and **56** possess four emission peaks each. These peaks correspond to the following transitions; $^5D_4\rightarrow{}^7F_6$ (~620 nm), $^5D_4\rightarrow{}^7F_5$ (~598 nm), $^5D_4\rightarrow{}^7F_4$ (~544 nm) and $^5D_4\rightarrow{}^7F_3$ (~491 nm).

Macrocyclic ligands based on a cyclen framework were also produced with the aspartic acid pendent arm, **27,** attached. This ligand was used in an attempt to couple a further macrocycle, a side-bridged cyclam compound with a pendent *p*-aminobenzyl arm (**60**). Although unsuccessful, this route does highlight a possible synthetic strategy for the production of dual-imaging probes using amino acid linker moieties.

In Chapter 5, the synthesis of porphyrin complexes with either hydroxyl or PEG chains on the periphery as potential PDT agents is detailed. The octa-hydroxyl porphyrin (**62**) was synthesised using an Adler condensation of 3,5-dimethoxy-benzaldehyde and pyrrole. Cleavage of the methoxy ethers was achieved using boron tribromide. Gallium(III) complexes were produced of tetra(3,5-dimethoxyphenyl)porphyrin (**61)** and **62**. Comparison of **61** and [Ga**61**]Cl compounds highlighted that the inclusion of gallium into the cleft of the porphyrin induces severe saddle strain, causing the sp^2 hybridised porphyrin planar core to deviate from planarity. An intriguing property arose when analysing **62** and [Ga**62**]Cl by cyclic voltammetry. These compounds do not possess characteristic porphyrin behaviour. The cyclic voltammagram for **62** has a broad peak at ~+1 V. This is assigned to the formation of a radical species. This radical can react with an equivalent radical species, leading to the formation of dimer. Subsequent reaction of the porphyrin dimer results in the formation of a porphyrin polymer. Evidence to support the porphyrin polymer being formed was gained by performing cyclic voltammetry using carbon paper. This resulted in a purple coating being deposited on the surface. Analysis using SEM and X-ray emission spectroscopy revealed that the surface was heavily contaminated with KCl. A washing procedure was sufficient to remove this excess potassium salt but leave the porphyrin polymer intact on the surface of the carbon paper. Cytotoxicity of the porphyrins showed that light induced cytotoxicity mirrored that of the dark toxicity. No selective PDT effect was observed. However, the ability to coat a porphyrin polymer onto the surface of carbon paper might suggest a possible use of these compounds as anti-bacterial agents. Mosinger and co-workers has reported such an application of a porphyrin sensitiser previously.[239]

Tetra(pentafluorophenyl)porphyrin (**63**) derivatives whereby the four *p*-fluorine atoms are substituted for polyethylene glycol chains were also synthesised. Crystal structures of gallium(III) complexes of **63** were obtained. In one structure the gallium(III) ion is in a square based pyramidal geometry with an apical phenolate. In the other structure, the gallium(III) ion is square planar; the pyrrolic anion does not directly coordinate to the metal centre. Such a geometry with a gallium(III) ion in a porphyrin cleft is rare. The attachment of PEG chains (**29-31**) via displacement of the *p*-fluorines of **63** led to the synthesis of compounds possessing differing light

induced cytotoxicity (**64-67**). Light induced cytotoxicity was examined by using *in vitro* cellular studies with Caco2 cells. The free base porphyrins, **64-66**, showed a size related light induced cytotoxicity. **64** and **66** were both induced light cytotoxic whereas **65** was not. All three were not dark toxic. The nickel(II) and zinc(II) complexes of **64-67** were all found to be light and dark toxic, which is believed to be caused by aggregation. Light induced cytotoxicity of the gallium(III) phenoxide complexes showed that if longer chains were attached to the porphyrin then the resulting compounds were light induced cytotoxic. However, if the shortest chain is attached to the porphyrin then the resulting compound ([Ga**66**]OPh) exhibits no light induced cytotoxicity. These compounds therefore result in cell death using a different mechanism to that of the free ligands. Compared with [Ga**64**]OPh, which possesses both light and dark toxicity, [Ga**64**]Cl has light induced cytotoxity with only minor associated dark toxicity. This suggests that the anion within the complex can also affect the light induced cytotoxicity. [Ga**64**]Cl also becomes increasingly more light induced cytotoxic with time when left in solution, suggesting the formation of more a cytotoxic species whilst it is stored in DMSO. Dark toxicity of this compound also increases with time.

To summarise, this research has been focused on the design and synthesis of tetraaza macrocycles bearing pendent arms towards biological applications. Three different macrocycles have been investigated; cyclam, cyclen and porphyrin. These macrocycles have been used to form metal complexes of different types of transition, lanthanide and p-block metal ions.

6.2. Further work

This research has scope for further development. Several of the key areas highlighted within this thesis provide avenues for future research. In this section each area of work is discussed relevant to its future research potential.

6.2.1. Side-bridged cyclams bearing redox active pendent arms

The research detailed within has covered ligand systems in which the redox pendent arm is attached through one of the nitrogen atoms. A further way to incorporate this moiety would be through the carbon network. Examples of this type have been reported previously by Kimura and co-workers,[160,161] however, they have not been synthesised with *tert*-butyl groups to stabilise the radical species. Furthermore, this type of route would still leave the nitrogen atoms available for attaching further moieties. This could again be exploited via the use of a bis-aminal intermediate, enabling the reactivity of the nitrogens to be controlled. In addition, side-bridged cyclens bearing redox pendent arms could also be developed. This would provide a comparison for the side-bridged cyclam complexes already produced, while varying the geometric parameters around the metal ion.

A different approach to the synthesis of the phenol pendent arm could also be taken. In this work, the phenol has been protected as either an ether or an ester. An alternative way could be to use a boronic ester, which can be subsequently cleaved to form the phenol when desired. This type of methodology has been used previously by Franz and co-workers to produce triggered pro-chelators for iron sequestration.[243]

6.2.2. Lanthanide complexes bearing redox active pendent arms

The drawback of the lanthanide complexes bearing redox pendent arms already synthesised is that upon one electron oxidation, no further water molecules appear to access the inner coordination sphere. For these complexes to be effective MRI agents, this will need to be improved upon. The current hypothesis is that the lipophilic nature of the ligand prevents more than one water molecule from accessing the metal centre. To circumvent this problem, it could be possible to introduce

hydrophilic groups in close proximity to the metal centre by modification of the ligand structure. This would hopefully enable further water molecules to access the metal centre when the phenoxyl or thiyl radical is formed. Image enhancement could also be achieved by the formation of a disulfide bound between [Gd**56**]⁻ and a protein which has accessible thiol groups on its surface. The resulting protein conjugate would have a much longer rotational correlation time which can enhance the relaxivity considerably.

The production of mixed phenol/thiophenol ligand systems would be of interest. Having characterised the phenolate and thiophenolate metal systems independently, investigations using cyclic voltammetry would highlight the effect on the ease of oxidation of the metal centre as well as the pendent arms. It would also be interesting to see the effect on the redox properties of the phenolate pendent arms when a dimer is formed because of thiyl radical-radical coupling.

6.2.3. Water soluble porphyrin sensitisers

Compound **62** and its gallium(III) complex have been shown to be electrochemically deposited on to carbon paper. To provide further evidence for the mechanism suggested, the synthesis of an asymmetric porphyrin is proposed. This porphyrin will possess only one 3,5-di-hydroxy-phenyl ring, and as such, only dimers can be formed by the head-to-head coupling pathway. Bulk electrolysis or reactions using potassium ferricyanide could be used to form this dimeric product, which could then be isolated and characterised.

PEGylation reactions of **63** deserve further attention. The compounds synthesised already possess differing light toxicity dependent on the type of metal ion and also the number and length of the PEG chains. This area can be easily expanded upon by investigation of further metal centres to attenuate the light induced cytotoxic effect. The isolation of [Zn**67**] as the mono-PEGylated complex warrants further research, as this suggests a possible route to producing asymmetric systems from a symmetrical porphyrin.

7. Experimental

7.1. Chemicals

All materials for synthetic procedures were purchased from Lancaster, Aldrich or Strem Chemicals. Exceptions to this were the Toray™ Carbon Paper which was purchased from fuelstore.com and the Float-A-Lyzers which were purchased from Spectrum Laboratories Inc. All materials were used as received unless otherwise stated. The solvents used were of general purpose or HPLC grade and were purchased from Fisher Scientific. TLC analysis was performed using aluminium-backed silica gel 60 F_{254}, 0.2 (Merck plates) or aluminium-backed aluminium oxide 60 F_{254}, (Merck plates). Silica gel chromatography was performed with silica gel 60 (Davisil). Alumina gel chromatography was performed using aluminium oxide 150 (Aldrich). When required diethyl ether, dichloromethane, acetonitrile and acetic acid were dried as follows; diethyl ether was dried over sodium metal and benzophenone followed by distillation; dichloromethane and acetonitrile were dried over calcium hydride for 24 h followed by distillation; acetic acid was dried by adding acetic anhydride (3% w/v) and distilling (b.p. 118°C).

7.2. Instrumentation

Evaporation of solvents was preformed on a Buchi RE 111 rotary evaporator at 35-60°C equipped with a diaphragm vacuum pump. All NMR spectra were acquired in the solvent indicated with chemicals shifts (δ) quoted as parts per million values (ppm) and coupling constants (J) quoted in hertz (Hz). NMR spectra were recorded using a JOEL JNM-LA400 FT NMR spectrometer at a frequency of 400 MHz for ^{1}H spectra, 100 MHz for ^{13}C spectra and 376 MHz for ^{19}F spectra. Mass spectrometry was performed using either a Finnegan MAT 900 XLT system to collect electrospray ionization (ES-MS) spectra or matrix assisted laser desorption ionization (MALDI). Accurate mass spectrometry measurements were obtained using a LTQ Orbitrap XL. UV/visible spectra were obtained using an Agilent8453E UV-VIS diode array spectrometer using 1 cm^3 quartz cells.

Single crystal X-ray diffraction data were collected on a Stöe IPDS-II imaging plate diffractometer, using MoKα X-rays of λ=0.71073 Å. Crystals were cooled to 150 K during data collection, with the temperature controlled by an Oxford Systems Cryostream Cooler. Diffraction data were solved using direct methods (SHELXS),

and the refinement was by full-matrix least squares against F^2 (SHELXL-97) method. The WinGX program[244] was used for refinement and production of data tables, and the ORTEP-3 program[245] was used for structural visualisation. Hydrogen atoms were fixed in idealised positions and refined using a riding model, with C-H distances of 0.97 Å, N-H distances of 0.91 Å, and U_{iso} 1.5 times U_{eq} of the carrier atom. All ORTEP representations show ellipsoids at the 50% probability level. Ortep representations and crystal data and structure tables are included within this chapter. Torsion and bond length tables are included in the appendix on the CD.

Cyclic voltammetry was performed using a standard three-electrode configuration with platinum working (0.2 mm diameter disk) and counter electrodes and a Ag/AgCl reference which gave the FeCp/ FeCp+ couple at 0.55 V using an Autolab II PGSTAT 30 system. All measurements were made in an argon/nitrogen purged solution of either MeCN/ 0.2 mol dm^{-3} [n-Bu$_4$N][BF$_4$] or MeCN/ 0.2 mol dm^{-3} [n-Bu$_4$N][ClO$_4$] or H$_2$O/ 0.2 mol dm^{-3} KCl over the scan rates of 0.01 V s^{-1} to 10 V s^{-1}.

Cytotoxicity testing was conducted using the following protocol. Each porphyrin compound formulated in DMSO and diluted in medium (DMEM+ 4.5 g/L Glucose + NEAA + 2 mM L-glutamine) to give concentrations ranging from 1×10^{-4} to 1×10^{-6}M was added to Caco 2 cells (Human Caucasian colon adenocarcinoma) adjusted to a concentration of 1×10^6 cells /ml. The cells were then incubated in the dark for an hour at 37°C and 5% CO$_2$ after which they were washed in a 3 fold excess of medium to eliminate any unbound porphyrin. The pellets of cells and porphyrin were re-suspended in 1 ml medium and 4x100 μl of each concentration was put in two 96 wells plates. One plate was irradiated with red light to a dose of 3.6 J/cm^2 while the other served as dark control. After irradiation, 5 μl of Fetal Bovine Serum was added to each well and the plates were returned to the incubator overnight. After 18 to 24 hours, an MTT cell viability assay was performed and the results expressed as a percentage of cell viability versus porphyrin concentration; an LD 90 (lethal dose where 90% of the cells are killed) was determined from the resulting curves. Each experiment was repeated in triplicate (minimum).

7.3. Pendent arm synthesis

7.3.1. Synthesis of 2,4-di-*tert*-butyl-6-(hydroxymethyl)phenol (1)
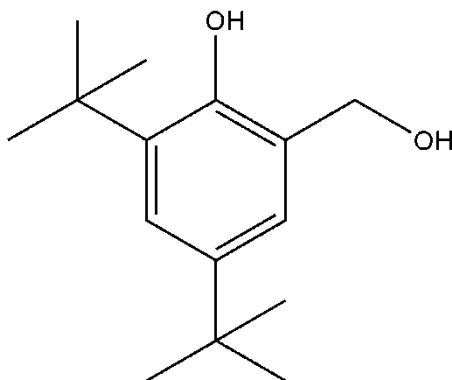
2,4-di-*tert*-butyl-phenol (20 g, 0.097 mol) was dissolved in methanol (30 ml). To this solution was added $LiOH.H_2O$ (0.33 g, 0.008 mol) and paraformaldehyde (3 g, 0.1 mol) in methanol (40 ml) dropwise. After addition was complete, the solution was then heated to reflux for 24 hr, before allowing it to cool and concentrating in vacuo. The residue was then taken up in ethyl acetate (20 ml) and the inorganic salts filtered off. The filtrate was then concentrated and redissolved in hexane and placed in a fridge o/n. A crystalline solid formed and was collected to give **1** as fine white needles (11.39 g, 50%); ^{1}H NMR [$CDCl_3$] δ 7.54 (br s, 1H, PhOH), 7.29 (d, 1H, J=2.5 Hz, ArH), 6.90 (d, 1H, J=2.5 Hz, ArH), 4.83 (s, 2H, CH_2OH), 1.44 (s, 9H, ^{t}Bu), 1.30 (s, 9H, ^{t}Bu); ^{13}C NMR [$CDCl_3$] δ 153.10, 141.61, 136.52, 124.09, 123.94, 122.59 (C_{arom}), 65.90 (CH_2), 34.93, 34.19 (C(^{t}Bu)), 31.59, 29.67 (Me(^{t}Bu)). CHN data not collected.

7.3.2. Synthesis of 2-(bromomethyl)-4,6-di-*tert*-butylphenol (2)
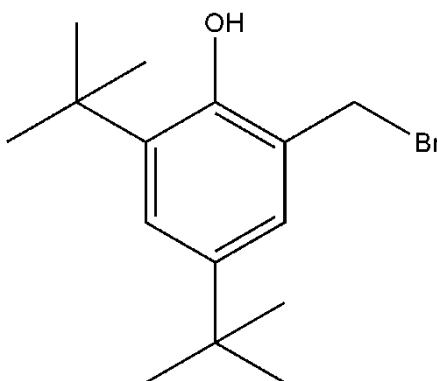
To a solution of **1** (4.98 g, 0.0211 mol) in CHCl$_3$ (60 ml) at 0°C and under a nitrogen atmosphere, was added PBr$_3$ (5.71 g, 0.0211 mol) in CHCl$_3$ (20 ml) over the course of 30 min. After addition was completed, stirring was continued at 0°C for a further hour. The solution was then poured into brine (200 ml), and the organic layer separated. The organic layer was further washed with brine (3 x 200 ml) and then dried over MgSO$_4$ and concentrated under reduced pressure to give a yellow oil (6.0 g, 95%); ^{1}H NMR [CDCl$_3$] δ 7.37 (d, 1H, J=2.53 Hz, ArH), 7.14 (d, 1H, J=2.53 Hz, ArH), 5.2 (br s, 1H, PhOH), 4.61 (s, 2H, CH$_2$), 1.47 (s, 9H, ^{t}Bu), 1.34 (s, 9H, ^{t}Bu); ^{13}C NMR [CDCl$_3$] δ 153.10, 141.61, 136.52, 124.09, 123.94, 122.59 (C$_{arom}$), 65.90 (CH$_2$), 34.93, 34.19 (C(^{t}Bu)), 31.59, 29.67 (Me(^{t}Bu)); MS (ES-MS): *m/z* 300 (M$^+$), 219 ((M-Br)$^+$); Calcd. for C$_{15}$O$_1$H$_{23}$Br$_1$: C, 60.20; H, 7.69. Found: C, 59.76; H, 8.27.

7.3.3. Synthesis of 3,5-di-*tert*-butyl-2-methoxybenzaldehyde (3)
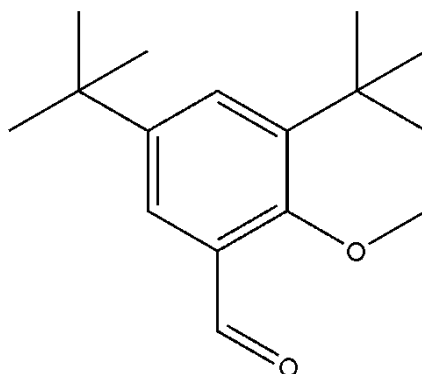
K$_2$CO$_3$ (1.5 g, 0.011 mol) was suspended in acetone (30 ml) and stirred at RT for 5 min before adding 3,5-di-*tert*-butyl-2-hydroxybenzaldehyde (0.5 g, 0.00214 mol) and MeI (1.3 ml, 0.0214 mol). This yellow mixture was then stirred at RT for 15 hr, by which time the reaction was judged to be complete by TLC (5 % ethyl acetate in hexane). The solution was concentrated in vacuo and the white solid redissolved in hexane. The potassium carbonate was then removed by filtration and the filtrate concentrated to give **3** as a yellow oil (0.44 g, 83%): R$_f$=0.5 (5% ethyl acetate in hexane); ^{1}H NMR [CDCl$_3$] δ 10.22 (s, 1H, CHO), 7.61 (d, 1H, J=2.5 Hz, ArH), 7.51 (d, 1H, J=2.5 Hz, ArH), 3.82 (s, 3H, OMe), 1.32 (s, 9H, ^{t}Bu), 1.22 (s, 9H, ^{t}Bu); ^{13}C NMR [CDCl$_3$] δ 190.66 (CHO), 166.19, 146.16, 142.76, 130.60, 128.97, 124.22 (C$_{arom}$), 65.88 (OMe), 35.22, 34.58 (C(^{t}Bu)), 31.23, 30.76 (CH$_3$(^{t}Bu)). CHN data not collected.

7.3.4. Synthesis of (3,5-di-*tert*-butyl-2-methoxyphenyl) methanol (4)
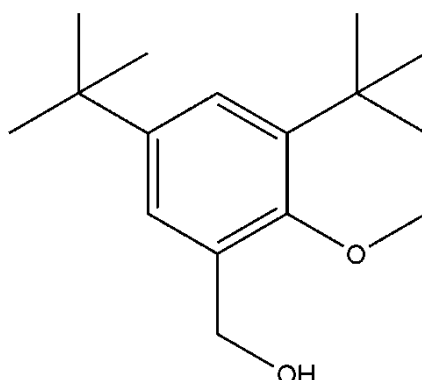
3 (0.44 g, 1.77 mmol) was dissolved in ethanol (30 ml) to which was added $NaBH_4$ (0.1 g, 2.63 mmol) portionwise. This yellow solution was then stirred at RT for 2.5 hr before stripping off the solvent and partitioning between DCM (60 ml) and brine (200 ml). The organic layer was collected and dried over $MgSO_4$ before removing the solvent in vacuo to give a yellow oil. This was placed in a fridge o/n whereby the oil solidified to give a white solid (0.44 g, 100%); ^{1}H NMR [$CDCl_3$] δ 7.30 (d, 1H, J=2.5 Hz, ArH), 7.29 (d, 1H, J=2.5 Hz, ArH), 5.26 (s, 1H, OH), 4.74 (s, 2H, CH_2), 3.78 (s, 3H, OMe), 1.40 (s, 9H, ^{t}Bu), 1.31 (s, 9H, ^{t}Bu); ^{13}C NMR [$CDCl_3$] δ 155.30, 145.99, 141.83, 133.43, 124.40, 123.88 (C_{arom}), 61.94 (OMe), 61.82 (CH_2OH), 35.26, 34.51 (C(^{t}Bu)), 31.47, 31.07 (CH_3(^{t}Bu)). CHN data not collected.

7.3.5. Synthesis of 1-(bromomethyl)-3,5-di-*tert*-butyl-2-methoxybenzene (5)
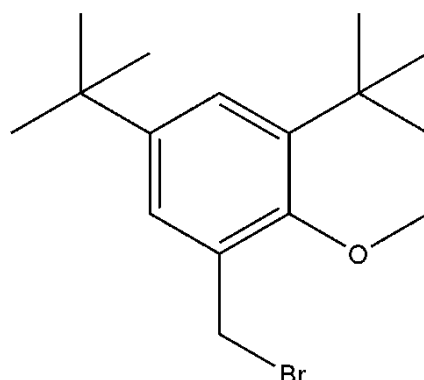
4 (0.44 g, 1.41 mmol) was dissolved in CHCl$_3$ (25 ml) at 0°C. PBr$_3$ (0.38 g, 1.41 mmol) dissolved in CHCl$_3$ (15 ml) was then added dropwise over 30 min under a nitrogen atmosphere. The yellow solution was then stirred at 0°C for a further 1 hr before the organic layer was washed with brine (3 x 200 ml). The organic layer was collected, dried over Na$_2$SO$_4$ and concentrated in vacuo to give **5** as a yellow oil (0.47, 85%); ^{1}H NMR [CDCl$_3$] δ 7.36 (d, 1H, J=2.5 Hz, ArH), 7.34 (d, 1H, J=2.5 Hz, ArH), 4.63 (s, 2H, CH$_2$), 3.90 (s, 3H, OMe), 1.45 (s, 9H, ^{t}Bu), 1.36 (s, 9H, ^{t}Bu); ^{13}C NMR [CDCl$_3$] δ 155.69, 146.26, 142.27, 130.65, 127.13, 125.11 (C$_{arom}$), 62.18 (OMe), 35.39, 34.50 (C(^{t}Bu)), 31.40, 31.07 (CH$_3$(^{t}Bu)), 29.96 (CH$_2$Br); MS (ES-MS): *m/z* 312 (M$^+$), 233(M-Br$^+$). Satisfactory CHN data not obtained.

7.3.6. Synthesis of 2-(benzyloxy)-3,5-di-*tert*-butylbenzaldehyde (6)
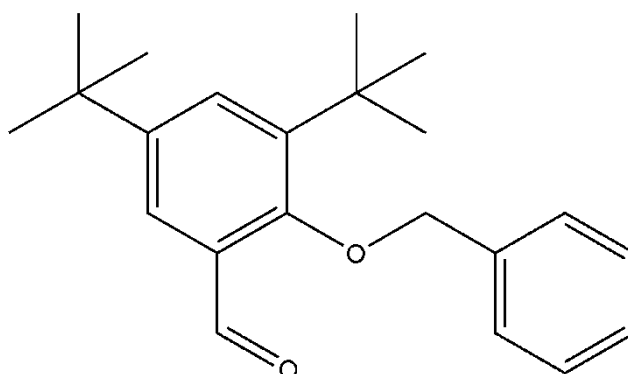
3,5-di-*tert*-butyl-2-hydroxybenzaldehyde (4.0 g, 0.0171 mol) and potassium carbonate (2.1 g, 0.0171 mol) were dissolved in DMF (25 ml) at 0°C and stirred for 5 min. To the yellow solution was added benzyl bromidde (2.89 g, 0.0168 mol) and the resulting mixture was heated to 75°C for 24 hr before cooling and pouring into ice-water (200 ml). The precipitate formed by this process was then collected by filtration and washed with water (2 x 10 ml) to give **6** as fine crystals (5.0 g, 90%): ^{1}H NMR [CDCl$_3$] δ 10.34 (s, 1H, CHO), 7.75 (d, 1H, J=2.5 Hz, ArH), 7.66 (d, 1H, J=2.5 Hz, ArH), 7.51-7.36 (m, 5H, Bn), 5.04 (s, 2H, CH$_2$), 1.46 (s, 9H, ^{t}Bu), 1.34 (s, 9H, ^{t}Bu); ^{13}C NMR [CDCl$_3$] δ 190.81 (CHO), 159.71, 146.64, 143.08, 136.57, 130.95, 129.3276, 128.63, 128.13, 127.00, 124.03 (C$_{arom}$), 80.39 (CH$_2$), 35.40, 34.73 (C(^{t}Bu)), 31.31, 30.94 (Me(^{t}Bu)). CHN data not collected.
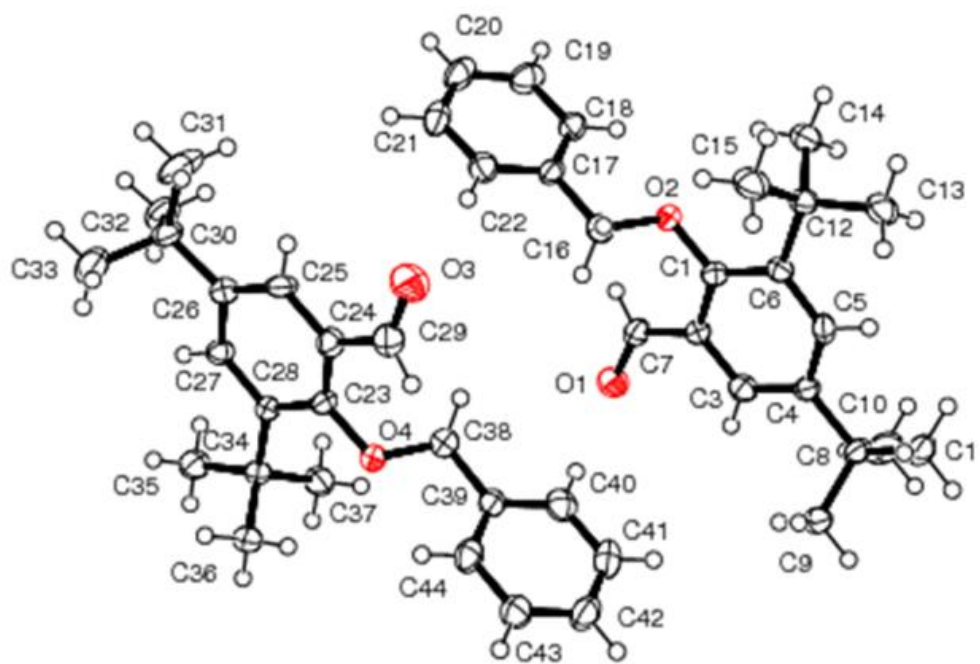
Figure 82: ORTEP representation of the X-ray crystal structure of 6 with all non-H atoms labelled.

Table 12: Crystal data for the structural refinement of 6.

Identification code	sja55_06
Empirical formula	$C_{22} H_{28} O_2$
Formula weight	324.44
Temperature	150(2) K
Wavelength	0.71073 Å
Crystal system	Triclinic
Space group	P-1
Unit cell dimensions	a = 10.735(3) Å $\quad$ α= 80.06(2)°.
	b = 11.234(3) Å $\quad$ β= 85.55(2)°.
	c = 16.555(4) Å $\quad$ γ = 73.12(2)°.
Volume	1881.2(8) Å^3
Z	4
Density (calculated)	1.146 Mg/m^3
Absorption coefficient	0.071 mm^{-1}
F(000)	704
Crystal size	0.46 x 0.25 x 0.22 mm^3
Theta range for data collection	2.82 to 34.79°.
Index ranges	-17<=h<=12, -17<=k<=17, -26<=l<=26
Reflections collected	43609
Independent reflections	15941 [R(int) = 0.1899]
Completeness to theta = 34.79°	97.9 %
Absorption correction	None
Refinement method	Full-matrix least-squares on F^2
Data / restraints / parameters	15941 / 0 / 434
Goodness-of-fit on F^2	0.638
Final R indices [I>2sigma(I)]	R1 = 0.0571, wR2 = 0.0909
R indices (all data)	R1 = 0.3237, wR2 = 0.1414
Extinction coefficient	0.00044(18)
Largest diff. peak and hole	0.307 and -0.256 e.Å^{-3}

7.3.7. Synthesis of (2-(benzyloxy)-3,5-di-*tert*-butylphenyl)methanol (7)
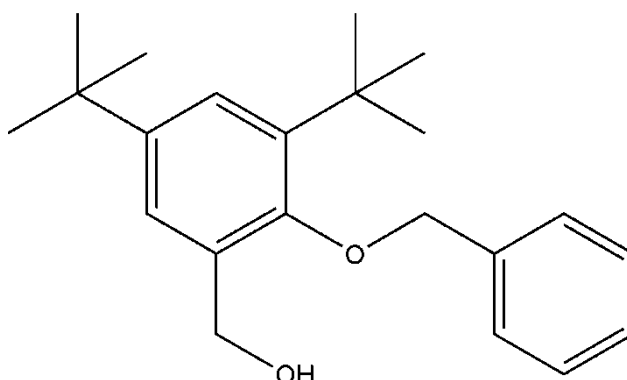
To a solution of **6** (4.50 g, 0.0139 mol) dissolved in methanol (50 ml) was added NaBH$_4$ (1.05 g, 0.0278 mol) portion wise over 5 min. After addition was complete, the yellow solution was stirred at RT for an hour before removing the solvent in vacuo. The white solid formed was then partitioned between CHCl$_3$ (50 ml) and brine (200 ml). The organic layer was collected and further washed with brine (2 x 200 ml). The organic extracts were then combined, dried over MgSO$_4$ and concentrated in vacuo to give **7** as a pale yellow oil (4.50 g, 99%); ^{1}H NMR [CDCl$_3$] δ 7.50-7.30 (m, 7H, ArH), 4.97 (s, 2H, CH$_2$, CH$_2$Bn), 4.74 (s, 2H, CH$_2$OH), 1.43 (s, 9H, ^{t}Bu), 1.32 (s, 9H, ^{t}Bu); ^{13}C NMR [CDCl$_3$] δ 153.81, 146.23, 142.06, 137.64, 133.67, 128.46, 127.64, 126.82, 124.78, 124.14 (C$_{arom}$), 75.84 (CH$_2$Bn), 61.50 (CH$_2$OH), 35.41, 34.51 (C(^{t}Bu)), 31.46, 31.22 (Me(^{t}Bu)). CHN not collected.

7.3.8. Synthesis of 2-(benzyloxy)-1-(bromomethyl)-3,5-di-*tert*-butylbenzene (8)
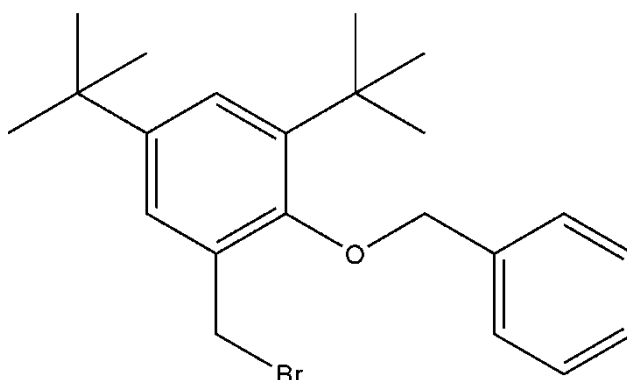
To **7** (2.07 g, 0.00635 mol) in CHCl$_3$ (50 ml) at 0°C under nitrogen was added PBr$_3$ (1.72 g, 1.5 ml, 0.00635 mol) in CHCl$_3$ (30 ml) over 30 min. The solution was then stirred at 0°C for 1 hr before pouring into brine (200 ml). The organic layer was extracted and then washed further with brine (3 x 200 ml). The organic extracts were combined, dried over Na$_2$SO$_4$ and then concentrated in vacuo to give **8** as a white solid (2.36 g, 96%); ^{1}H NMR [CDCl$_3$] δ 7.56-7.34 (m, 7H, ArH), 5.12 (s, 2H, CH$_2$Bn), 4.58 (s, 2H, CH$_2$Br), 1.43 (s, 9H, ^{t}Bu), 1.32 (s, 9H, ^{t}Bu); ^{13}C NMR [CDCl$_3$] δ 154.15, 146.53, 142.50, 137.61, 130.88, 128.52, 127.73, 127.32, 126.76, 125.31 (C$_{arom}$), 75.21 (CH$_2$Bn), 35.57, 34.54 (C(^{t}Bu)), 31.41, 31.23 (Me(^{t}Bu)), 30.09 (CH$_2$Br); MS (ES-MS): *m/z* 388 (M$^+$); Calcd for C$_{14}$H$_{27}$Br$_1$O$_1$: C, 67.90; H, 7.40. Found: C, 68.03; H, 7.63.

7.3.9. Synthesis of 4-methoxybenzaldehyde (9)
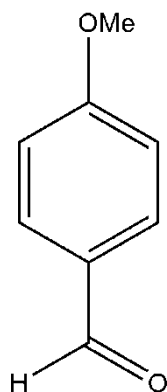
4-Hydroxybenzaldehyde (5 g, 0.041 mol) and K_2CO_3 (5.66 g, 0.041 mol) were dissolved in acetone (35 ml) and the mixture stirred at RT for 5 min. MeI (29 g, 0.2 mol) was then added and the reaction heated to 50°C for 24 hr. The solution was then allowed to cool and concentrated in vacuo before being taken up into DCM (30 ml). The suspension was then filtered and the filtrate concentrated to give a yellow oil (5.57 g, 100%): ^{1}H NMR [CDCl$_3$] δ 9.74 (s, 1H, CHO), 6.85 (d, 2H, J=8.70 Hz, ArH),7.68 (d, 2H, J=8.70 Hz, ArH), 3.73 (s, 3H, OMe); ^{13}C NMR [CDCl$_3$] δ 190.38 (CHO), 164.27, 131.90, 131.58, 129.60, 113.97 (C$_{arom}$), 55.18 (OMe). CHN data not collected.

7.3.10. Synthesis of (4-methoxyphenyl)methyl alcohol (10)
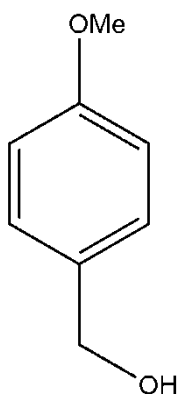
To a solution of **9** (5.57 g, 0.041 mol) in propan-2-ol (30 ml) was added $NaBH_4$ (1.57 g, 0.041 mol) portionwise with stirring. The reaction was then stirred at RT for a further 4 hr before removing the solvent in vacuo. The white solid was then dissolved in DCM (30 ml) and washed with brine (100 ml). The organic layer was separated and dried over $MgSO_4$. It was then filtered and concentrated to give a light yellow oil (4.71 g, 84%); ^{1}H NMR [$CDCl_3$] δ 7.16 (d, 2H, J=8.5 Hz, ArH), 6.79 (d, 2H, J=8.5 Hz, ArH), 4.44 (s, 2H, CH_2), 3.85 (s, 1H, OH), 3.68 (s, 3H, OMe); ^{13}C NMR [$CDCl_3$] δ 158.46, 132.95, 128.14, 113.65, 113.34 (C_{arom}), 63.80 (CH_2), 54.72 (OMe). CHN data not collected.

7.3.11. Synthesis of 1-(bromomethyl)-4-methoxybenzene (11)
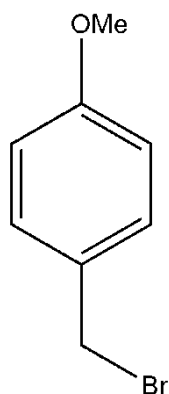
To a solution of **10** (4.71 g, 0.0341 mol) in $CHCl_3$ (30 ml) at 0°C under a nitrogen atmosphere was added PBr_3 (9.25g, 0.0341 mol) in $CHCl_3$ (20 ml) dropwise over 0.5 hr. Stirring was then continued for 1 hr at 0°C. The solution was then washed with brine (4 x 100 ml) before drying over $MgSO_4$ and removing the solvent in vacuo to give a light orange oil (6.6 g, 96%); ^1H NMR [$CDCl_3$] δ 7.55 (d, 2H, J=8.7 Hz, ArH), 7.43 (d, 2H, J=8.7 Hz, ArH), 5.12 (s, 2H, CH_2Br), 4.58 (s, 3H, OMe); ^{13}C NMR [$CDCl_3$] δ 159.36, 130.19, 129.64, 113.90 (C_{arom}), 54.98, (OMe), 33.86 (CH_2); MS (ES-MS): *m/z* 202 (M$^+$), 121 ((M-Br)$^+$). CHN data not collected.

7.3.12. Synthesis of 3,5-di-*tert*-butyl-2-(4-methoxybenzyloxy)benzaldehyde (12)
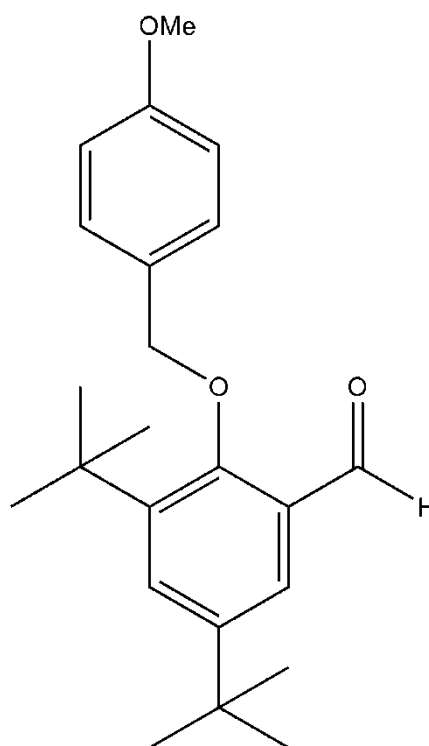
3,5-Di-*tert*-butyl-2-hydroxy benzaldehyde (2 g, 0.0085 mol) and K_2CO_3 (1.18 g, 0.0085 mol) in DMF (40 ml) were stirred together for 5 min. **11** (1.89 g, 0.0094 mol) was then added and the solution heated to 55°C for 24 hr. The reaction mixture was allowed to cool before pouring in to ice-water (60 ml). A precipitate formed which was removed by filtration. The crude solid was then subjected to hot pentane washes (4 x 10 ml). The resulting white solid was then recrystallised from hexane. This gave **12** as transparent crystals (2.11 g, 70%); ^{1}H NMR [CDCl$_3$] δ 10.35 (CHO), 7.75 (d, 1H, J=2.67 Hz, ArH), 7.67 (d, 1H, J=2.67 Hz, ArH), 7.43 (d, 2 H, J=8.7, ArH), 6.95 (d, 2 H, J=8.7, ArH), 4.96 (s, 2H, CH$_2$Bn), 3.83 (s, 3H, OMe), 1.46 (s, 9H, ^{t}Bu), 1.34 (s, 9H, ^{t}Bu); ^{13}C NMR [CDCl$_3$] δ 190.79 (CHO), 159.69, 159.54, 146.44, 143.02, 130.86, 129.34, 128.66, 128.62, 123.94, 113.98 (C$_{arom}$), 80.26 (CH$_2$Bn), 55.21 (OMe), 35.32, 34.65 (C(^{t}Bu)), 31.26, 30.91 (Me(^{t}Bu)); MS (ES-MS): *m/z* 354 (M$^+$). CHN data not collected.
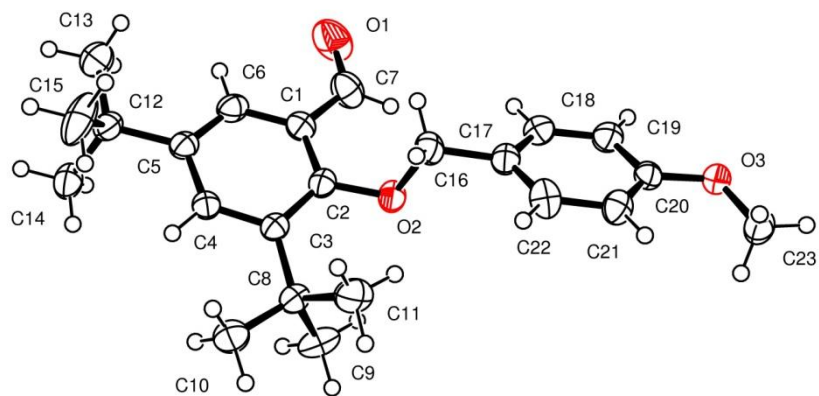
Figure 83: ORTEP representation of the X-ray crystal structure of 12 with all non-H atoms labelled.

Table 13: Crystal data for the structural refinement of 12.

Identification code	sja19_07
Empirical formula	$C_{23} H_{30} O_3$
Formula weight	354.47
Temperature	150(2) K
Wavelength	0.71073 Å
Crystal system	Monoclinic
Space group	P21/a
Unit cell dimensions	a = 9.0804(17) Å α= 90°.
	b = 24.181(6) Å β= 105.627(15)°.
	c = 9.5998(18) Å γ = 90°.
Volume	2030.0(7) Å^3
Z	4
Density (calculated)	1.160 Mg/m^3
Absorption coefficient	0.075 mm^{-1}
F(000)	768
Crystal size	0.35 x 0.30 x 0.20 mm^3
Theta range for data collection	2.36 to 35.02°.
Index ranges	-12<=h<=14, -37<=k<=38, -15<=l<=15
Reflections collected	27544
Independent reflections	8771 [R(int) = 0.2187]
Completeness to theta = 35.02°	97.9 %
Absorption correction	None
Refinement method	Full-matrix least-squares on F^2
Data / restraints / parameters	8771 / 0 / 236
Goodness-of-fit on F^2	0.632
Final R indices [I>2sigma(I)]	R1 = 0.0574, wR2 = 0.1166
R indices (all data)	R1 = 0.2552, wR2 = 0.1569
Extinction coefficient	0.0009(4)
Largest diff. peak and hole	0.261 and -0.296 e.Å^{-3}

7.3.13. Synthesis of (3,5-di-*tert*-butyl-2-(4-methoxybenzyloxy)phenyl)methanol (13)
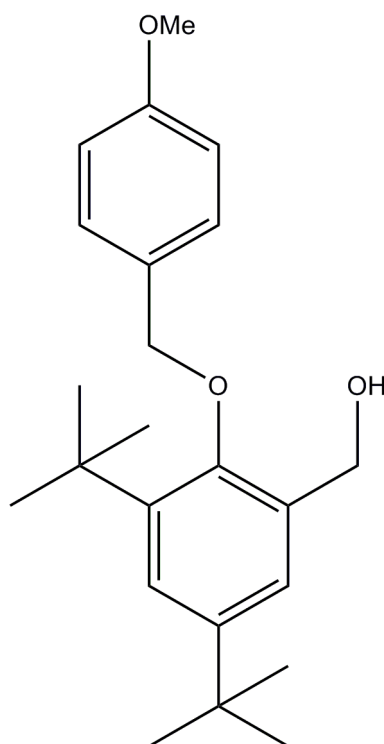
To a solution of **12** (1.5 g, 0.0042 mol) in ethanol (40 ml) was added $NaBH_4$ (0.16 g, 0.0042 mol) portionwise with stirring. The solution was stirred for 3 hours at RT before concentrating the mixture under reduced pressure. The residue was then partitioned between DCM (100 ml) and water (100 ml). The organic layer was collected, dried over $MgSO_4$ and concentrated under reduced pressure. This gave **13** as a white solid (1.21 g, 81%); ^1H NMR [$CDCl_3$] δ 7.45 (d, 2H, J=8.42 Hz, ArH), 7.37 (d, 1H, J=2.53 Hz, ArH), 7.32 (d, 1H, J=2.53 Hz, ArH), 6.95 (d, 2H, J=8.42 Hz, ArH), 4.91 (s, 2H, CH_2Bn), 4.79 (s, 2H, CH_2OH), 3.82 (s, 3H, OMe), 1.45 (s, 9H, ^tBu), 1.34 (s, 9H, ^tBu); ^{13}C NMR [$CDCl_3$] δ 159.22, 153.87, 146.20, 142.14, 133.74, 129.74, 128.67, 124.73, 124.20, 113.92 (C_{arom}), 75.65 (CH_2Bn), 61.83 (CH_2OH), 55.21 (OMe), 35.43, 34.52, (C(^tBu)), 31.47, 31.28, (Me(^tBu)); MS (ES-MS): *m/z* 356 (M$^+$); Calcd for $C_{23}O_3H_{32}$: C, 77.53; H 8.99. Found C, 77.54; H, 8.73.

7.3.14. Synthesis of 1-(bromomethyl)-3,5-di-*tert*-butyl-2-(4-methoxybenzyloxy)benzene (14)
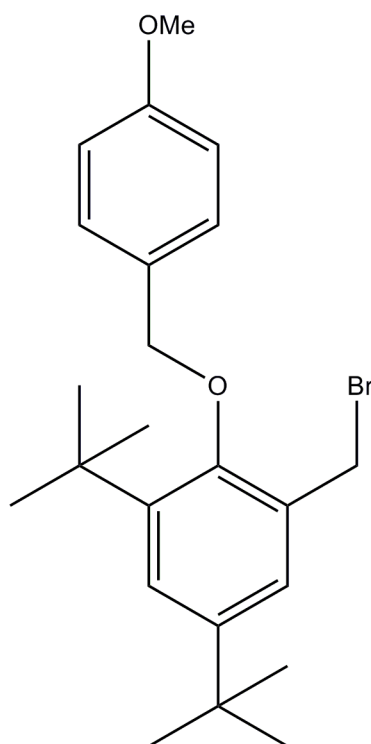
13 (1 g, 0.00281 mol) and CBr_4 (1.4 g, 0.00421 mol) were dissolved in dry DCM (20 ml) to which was added triphenylphosphine (1.11 g, 0.00421 mol) in dry DCM (10 ml) over 5 min. A yellow solution formed which was then stirred at RT for 18 hr. Water (150 ml) was then added and the organic layer was extracted. The aqueous layer was further extracted with DCM (2 x 50 ml). All the organic extracts were combined and dried over $MgSO_4$. The crude product was then purified by silica gel chromatography (1:1 DCM/hexane v/v). The fractions containing the desired compound were then combined and concentrated under reduced pressure to give a light pink solid (0.80 g, 68%); R_f=0.58 (1:1 hexane/DCM v/v); ^1H NMR [$CDCl_3$] δ 7.52 (d, 2H, J=8.56 Hz, ArH), 7.38 (s, 2H, ArH), 6.89 (d, 2H, J=8.56 Hz, ArH), 5.18 (s, 2H, CH_2Bn), 4.63 (s, 2H, CH_2Br), 3.86 (s, 3H, OMe), 1.47 (s, 9H, ^tBu), 1.36 (s, 9H, ^tBu); ^{13}C NMR [$CDCl_3$] δ 159.30, 154.24, 146.43, 142.50, 130.90, 129.75, 128.52, 127.31, 125.98, 113.96 (C_{arom}), 75.05 (CH_2Bn), 55.28 (OMe), 35.58, 34.54 (C(^tBu)), 31.59 (CH_2Br), 31.41, 31.27 (Me(^tBu)); MS (ES-MS) m/z 339 ((M-Br)$^+$), 219 ((MH-$C_8H_9O_1$, Br)$^+$). Satisfactory CHN not obtained.

7.3.15.   Synthesis   of   2-(bromomethyl)-4,6-di-*tert*-butylphenyl acetate (15)
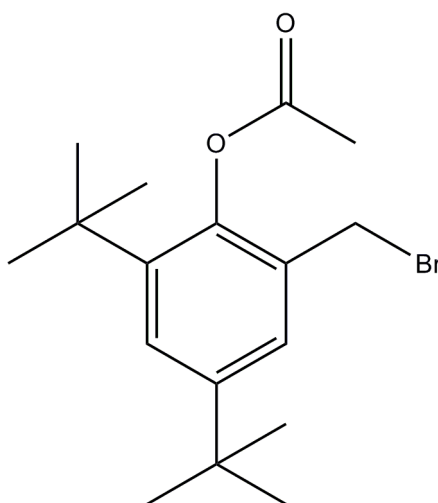
To solution of **2** (3.0 g, 0.0100 mol) in acetic anhydride (2.05 g, 0.0201 mol) was added H_2SO_4 (5 drops). The reaction mixture was stirred for 12 hr at which time the TLC showed complete consumption of the starting material (silica plate using 5% EtOAc in hexane as the eluent). DCM (50 ml) was then added and the mixture washed with brine (2 x 100 ml). The organic layer was collected and dried over $MgSO_4$ before filtering under reduced pressure. The resulting yellow oil was placed in a freezer whereby a solid formed o/n (3.41 g, 100%); ^{1}H NMR [CDCl$_3$] δ 7.42 (s, 1H, ArH), 7.32 (s, 1H, ArH), 4.34 (s, 2H, CH$_2$Br), 2.42 (s, 3H, COMe), 1.37 (s, 9H, [t]Bu), 1.33 (s, 9H, [t]Bu); ^{13}C NMR [CDCl$_3$] δ 169.75 (COMe), 148.70, 145.52, 141.39, 130.10, 126.40, 125.59 (C$_{arom}$), 35.12, 34.80 (C([t]Bu)), 31.50, 30.73 (Me([t]Bu)), 29.68 (CH$_2$Br), 21.57 (COCH$_3$); Calcd. for $C_{17}O_2Br_1H_{25}$: C, 59.82; H, 7.33. Found: C, 60.11; H, 7.52; MS (ES-MS): *m/z* 261 (M[+]), 219.2 ((MH-BrOAc)[+]).
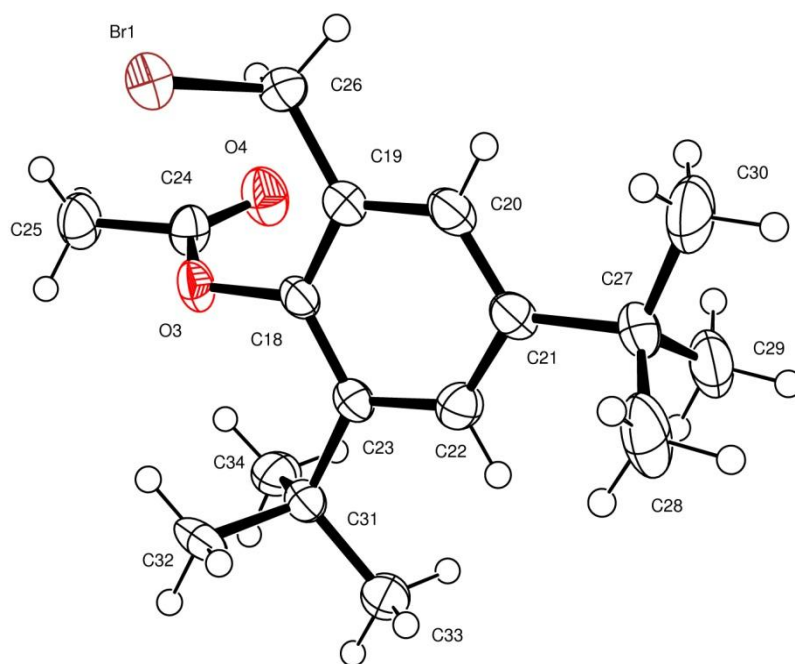
Figure 84: ORTEP representation of the X-ray crystal structure of 15.

Table 14: Crystal data for the structural refinement of 15.

Identification code	sja9_08
Empirical formula	$C_{17} H_{25} Br O_2$
Formula weight	341.27
Temperature	150(2) K
Wavelength	0.71073 Å
Crystal system	Orthorhombic
Space group	Pbca
Unit cell dimensions	a = 9.8366(12) Å $\alpha = 90°$.
	b = 18.441(3) Å $\beta = 90°$.
	c = 18.750(3) Å $\gamma = 90°$.
Volume	3401.2(9) $Å^3$
Z	8
Density (calculated)	1.333 Mg/m^3
Absorption coefficient	2.417 mm^{-1}
F(000)	1424
Crystal size	0.29 x 0.26 x 0.16 mm^3
Theta range for data collection	2.21 to 29.53°.
Index ranges	-13<=h<=11, -25<=k<=25, -20<=l<=25
Reflections collected	18419
Independent reflections	4716 [R(int) = 0.2836]
Completeness to theta = 29.53°	99.3 %
Absorption correction	None
Refinement method	Full-matrix least-squares on F^2
Data / restraints / parameters	4716 / 0 / 188
Goodness-of-fit on F^2	0.619
Final R indices [I>2sigma(I)]	R1 = 0.0551, wR2 = 0.1123
R indices (all data)	R1 = 0.2412, wR2 = 0.1459
Largest diff. peak and hole	0.482 and -1.421 e.$Å^{-3}$

7.3.16. Synthesis of 2-(4-methoxybenzylthio)benzaldehyde (16)
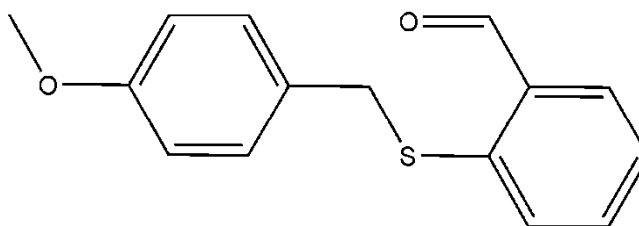
2-Nitro-benzaldehyde (4.56 g, 0.03 mol) was dissolved in DMF (40 ml) at 0°C and 4-methoxyphenylmethanethiol (4.89 g, 0.035 mol) and K_2CO_3 (5.43 g, 0.039 mol) were added. The mixture was then heated to 80°C for 24 hr. After this time, the mixture was allowed to cool before pouring it into ice-water (60 ml) which resulted in the formation of a yellow precipitate. This was collected via filtration and then recrystallised from petroleum ether 60-80 and chloroform (1:1 v/v), giving **16** as yellow crystals (6.89 g, 89%); ^{1}H NMR [CDCl$_3$] δ 10.19 (s, 1H, CHO), 7.74 (dd, 1H, J=1.3 Hz, 7.6 Hz, ArH), 7.42-7.43 (m, 7H, ArH), 4.01 (s, 2H, CH$_2$), 3.69 (s, 3H, OMe); ^{13}C NMR [CDCl$_3$] δ 191.44 (CHO), 158.97, 141.36, 134.59, 133.88, 131.41, 130.01, 129.86, 127.96, 126.01, 114.00 (C$_{arom}$), 55.21 (CH$_2$), 38.34 (OMe); Calcd. for $C_{15}H_{14}O_2S_1$: C, 69.77; H, 5.43; S, 12.40. Found: C, 69.84; H, 5.51; S, 13.49; MS (ES-MS): *m/z* 258 (M$^+$).
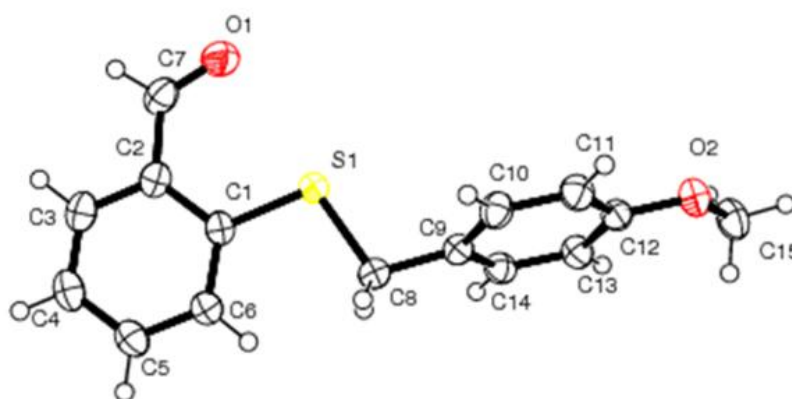
Figure 85: ORTEP representation of the X-ray crystal structure of 16 with all non-H atoms labelled.

Table 15: Crystal data for the structural refinement of 16.

Identification code	sja46_06
Empirical formula	$C_{15} H_{14} O_2 S$
Formula weight	258.32
Temperature	150(2) K
Wavelength	0.71073 Å
Crystal system	Monoclinic
Space group	P21/c
Unit cell dimensions	a = 5.5375(6) Å α= 90°.
	b = 13.7647(12) Å β= 95.596(8)°.
	c = 16.6308(18) Å γ = 90°.
Volume	1261.6(2) Å^3
Z	4
Density (calculated)	1.360 Mg/m^3
Absorption coefficient	0.247 mm^{-1}
F(000)	544
Crystal size	0.42 x 0.22 x 0.19 mm^3
Theta range for data collection	2.46 to 34.83°.
Index ranges	-8<=h<=8, -22<=k<=17, -26<=l<=26
Reflections collected	15809
Independent reflections	5339 [R(int) = 0.0621]
Completeness to theta = 34.83°	97.4 %
Absorption correction	None
Refinement method	Full-matrix least-squares on F^2
Data / restraints / parameters	5339 / 0 / 164
Goodness-of-fit on F^2	0.933
Final R indices [I>2sigma(I)]	R1 = 0.0529, wR2 = 0.1381
R indices (all data)	R1 = 0.1150, wR2 = 0.1703
Extinction coefficient	0.022(3)
Largest diff. peak and hole	0.677 and -0.664 e.Å^{-3}

7.3.17. Synthesis of (2-(4-methoxybenzylthio)phenyl)methanol (17)
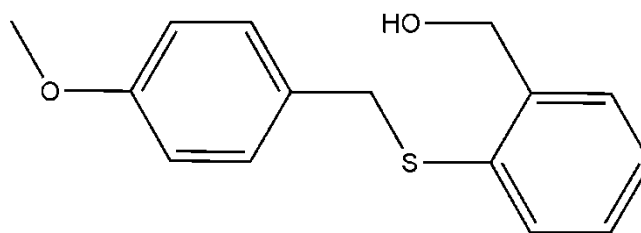
16 (11.3 g, 0.044 mol) was suspended in propan-2-ol (30 ml) to which NaBH$_4$ (1.6 g, 0.044 mol) was added portionwise. This was stirred at RT under a nitrogen atmosphere for 1 hr and then heated to 80°C for a further 1 hr. The solution was then allowed to cool to RT resulting in the formation of a white crystalline product. The propan-2-ol was then removed in vacuo and the white solid dissolved in DCM (50 ml) and washed with brine (200 ml). The organic layer was collected and further washed with brine (2 x 200 ml). The combined organic extracts were then dried over Na$_2$SO$_4$ before being concentrated in vacuo to yield **17** as a white solid (10.04 g, 88%); ^{1}H NMR [CDCl$_3$] δ 7.31-7.26 (m, 2H, ArH), 7.17-7.14 (m, 2H, ArH), 7.03 (d, 2H, J=8.7 Hz, ArH), 6.71 (d, 2H, J=8.7 Hz, ArH), 4.51 (s, 2H, CH$_2$OH), 3.95 (s, 2H, CH$_2$S), 3.72 (s, 3H, OMe); ^{13}C NMR [CDCl$_3$] δ 158.84, 141.59, 134.26, 131.67, 129.89, 129.24, 128.41, 128.27, 127.21, 113.92 (C$_{arom}$), 63.67 (CH$_2$OH), 55.24 (SCH$_2$), 39.25 (OMe); MS (ES-MS): *m/z* 260 (M$^+$). Satisfactory CHN data not obtained.
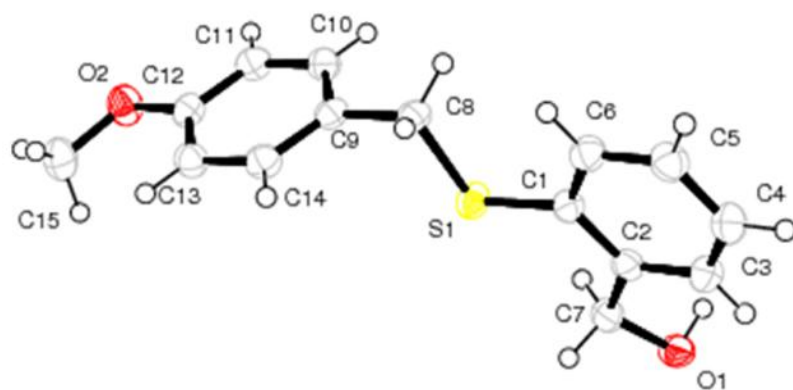
Figure 86: ORTEP representation of the X-ray crystal structure of 17 with all non-H atoms labelled.

Table 16: Crystal data for the structural refinement of 17.

Identification code	sja54_06
Empirical formula	$C_{15} H_{16} O_2 S$
Formula weight	260.35
Temperature	150(2) K
Wavelength	0.71073 Å
Crystal system	Monoclinic
Space group	P21/c
Unit cell dimensions	a = 14.5448(18) Å α= 90°.
	b = 4.8986(3) Å β= 107.532(10)°.
	c = 19.419(2) Å γ= 90°.
Volume	1319.3(2) $Å^3$
Z	4
Density (calculated)	1.311 Mg/m^3
Absorption coefficient	0.236 mm^{-1}
F(000)	552
Crystal size	0.6 x 0.24 x 0.19 mm^3
Theta range for data collection	2.94 to 34.86°.
Index ranges	-23<=h<=16, -7<=k<=6, -30<=l<=30
Reflections collected	20507
Independent reflections	5667 [R(int) = 0.0835]
Completeness to theta = 34.86°	98.7 %
Absorption correction	None
Refinement method	Full-matrix least-squares on F^2
Data / restraints / parameters	5667 / 0 / 167
Goodness-of-fit on F^2	0.785
Final R indices [I>2sigma(I)]	R1 = 0.0405, wR2 = 0.0914
R indices (all data)	R1 = 0.1238, wR2 = 0.1143
Extinction coefficient	0.0082(13)
Largest diff. peak and hole	0.372 and -0.712 $e.Å^{-3}$

7.3.18. Synthesis of (2-(bromomethyl)phenyl)(4-methoxybenzyl)sulfane (18)
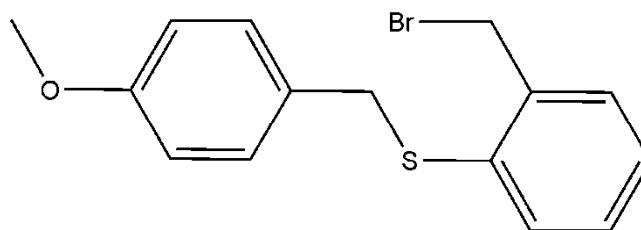
17 (8.16 g, 0.0314 mol) was dissolved in $CHCl_3$ (100 ml) and stirred under a nitrogen atmosphere at $-5°C$. To this was added PBr_3 (5.75 g, 0.02123 mol) dissolved in $CHCl_3$ (50 ml) over a period of 25 min. After the addition was complete stirring continued for a period of 30 min before warming to RT and washing the $CHCl_3$ layer with brine (4 x 500 ml). The organic layer was collected and dried over Na_2SO_4 before removing the solvent under reduced pressure to yield a yellow oil. Hexane (100 ml) was layered over the top of this oil and it was placed in a freezer for 48 hr. After this time methanol (20 ml) was added and the mixture sonicated. The milky white suspension formed by this process was then filtered, yielding **18** as a white powder (6.86g, 68%); ^1H NMR [$CDCl_3$] δ 7.29-7.09 (m, 6H, ArH), 6.73 (d, 2H, J=8.4 Hz, ArH), 4.53 (s, 2H, CH_2), 3.98 (s, 2H, CH_2), 3.69 (s, 3H, OMe); ^{13}C [$CDCl_3$] δ 158.95, 138.62, 136.28, 132.09, 130.68, 130.17, 129.24, 129.12, 127.38, 114.01 (C_{arom}), 55.37 (CH_2S), 39.16 (OMe), 32.29 (CH_2OH); MS (ES-MS): m/z 324 (MH^+). Satisfactory CHN data not obtained.

7.3.19. Synthesis of 2-bromo-3,5-di-*tert*-butyltoluene (19)
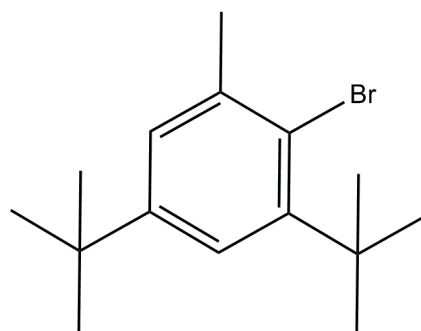
3,5-Di-tert-butyltoluene (20.15 g, 0.0986 mol) was dissolved in trimethylphosphate (150 ml) and heated to 65-70°C. Bromine (19.2 g, 0.12 mol) was then added in trimethylphosphate (100 ml). Heating continued for a further 16 hr before adding further bromine (9.6 g, 0.06 mol). Heating was continued for a further 24 hr before extracting the product with petroleum ether (bp 60-80°C, 150 ml). The ether layer was then washed with saturated NaHCO$_3$ solution (100 ml) followed by water (200 ml). It was separated, dried over MgSO$_4$ and concentrated under reduced pressure. The crude product was then purified by distillation under reduced pressure with the distillate with a bp of 112-114°C being collected. This gave the title compound as a transparent oil which crystallised after a week at RT (18.27 g, 65%); ^{1}H NMR [CDCl$_3$] δ 7.37 (d, 1H, J=1.76 Hz, ArH), 7.17 (d, 1H, J=1.76 Hz, ArH), 2.47 (s, 3H, CH$_3$), 1.58 (s, 9H, CH$_3$(^{t}Bu)), 1.34 (s, 9H, CH$_3$(^{t}Bu); ^{13}C NMR [CDCl$_3$] δ 139.18, 138.11, 126.45, 125.92, 122.87, 122.59 (C$_{arom}$), 36.78, 36.70 (C(^{t}Bu)), 31.19, 29.99 (Me(^{t}Bu)), 25.66 (CH$_3$); MS (ES-MS): *m/z* 282 (M$^+$), 267 (M-Me)$^+$). CHN data not collected.
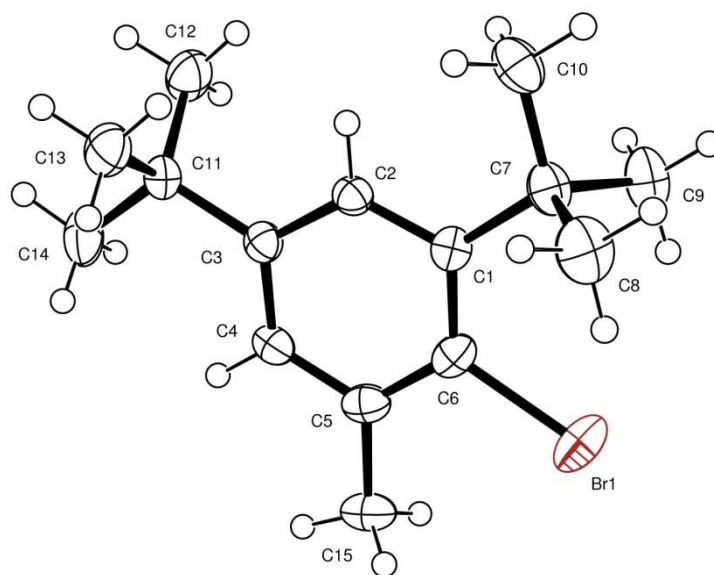
Figure 87: ORTEP representation of the X-ray crystal structure of 19 with all non-atoms labelled.

Table 17: Crystal data for the structural refinement of 19.

Identification code	sja_02
Empirical formula	$C_{15} H_{23} Br$
Formula weight	283.24
Temperature	150(2) K
Wavelength	0.71073 Å
Crystal system	Monoclinic
Space group	P21/n
Unit cell dimensions	a = 9.8553(12) Å $\alpha = 90°$.
	b = 11.6024(13) Å $\beta = 104.440(8)°$.
	c = 13.1040(13) Å $\gamma = 90°$.
Volume	1451.0(3) $Å^3$
Z	4
Density (calculated)	1.945 Mg/m^3
Absorption coefficient	4.212 mm^{-1}
F(000)	888
Crystal size	0.26 x 0.18 x 0.15 mm^3
Theta range for data collection	2.76 to 34.74°.
Index ranges	-15<=h<=15, -17<=k<=18, -19<=l<=20
Reflections collected	16678
Independent reflections	6110 [R(int) = 0.0907]
Completeness to theta = 34.74°	97.5 %
Absorption correction	None
Refinement method	Full-matrix least-squares on F^2
Data / restraints / parameters	6110 / 0 / 146
Goodness-of-fit on F^2	0.879
Final R indices [I>2sigma(I)]	R1 = 0.0581, wR2 = 0.1482
R indices (all data)	R1 = 0.1159, wR2 = 0.1751
Extinction coefficient	0.0047(16)
Largest diff. peak and hole	2.411 and -1.453 e.$Å^{-3}$

7.3.21. Synthesis of 2-bromo-3,5-di-*tert*-butylbenzyl bromide (20)
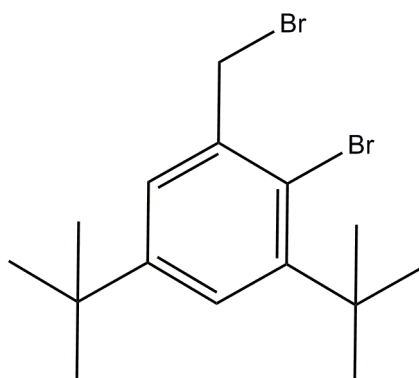
19 (37.40 g, 0.132 mol), NBS (0.147 mol, 26.1 mol) and AIBN (0.87 g, 5.3 mmol) were dissolved in CCl_4 (375 ml) with stirring. The solution was heated gently to reflux and left for 1 hr. The solution was then allowed to cool before filtering at $-10°C$. The filtrate was concentrated to give **20** as a yellow oil (45.24 g, 95%); ^1H NMR [$CDCl_3$] δ 7.44 (d, 1H, J=1.89 Hz, ArH), 7.25 (d, 1H, J=1.89 Hz, ArH), 4.69 (s, 2H, CH_2Br), 1.53 (s, 9H, CH_3(^tBu)), 1.34 (s, 9H, CH_3(^tBu)); ^{13}C NMR [$CDCl_3$] δ 146.84, 137.73, 126.89, 126.47, 122.98 (C_{arom}), 36.81 (CH_2Br), 36.98, 34.42 (C(^tBu)), 31.15, 30.12 (CH_3(^tBu)); MS (ES-MS): *m/z* 362 (M^+), 282 (($M-Br)^+$), 267 (($M-CH_2Br)^+$). CHN data not obtained.

7.3.22. Synthesis of 2-bromo-3,5-di-tert-butylbenzaldeyde (21)
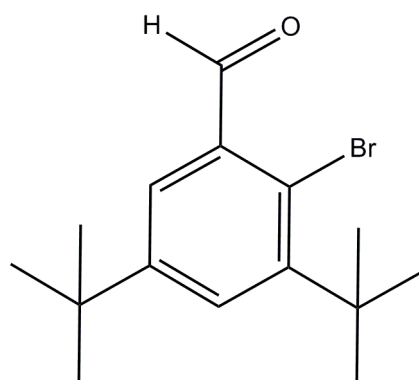
20 (47.84 g, 0.132 mol) and hexamethylenetetramine (52.57 g, 0.375 ml) were dissolved in $CHCl_3$ (400 ml) and heated to 75°C for 24 hr. The yellow oil was then concentrated in vacuo and the liquid taken up in 50% acetic acid (400 ml) and more hexamethylenetetramine (52.57 g, 0.375 mol) added. The solution was heated to 102°C for 24 hr before adding concentrated HCl (60 ml). Heating was continued for a further 15 min before allowing to cool. Ether (200 ml) was then added to the solution, and the organic layer was extracted. The aqueous layer was further washed with ether (2 x 200 ml) before combining the organic extracts which were then washed with 2M HCl (3 x 500 ml) and saturated $NaHCO_3$ solution (3 x 500 ml). The organic phase was then dried over Na_2SO_4 before concentrating under reduced pressure. The crude product was purified by silica column chromatography (using 100:1 n-hexane: ether (v/v) as the eluent). This gave the desired compound as a yellow oil (11.79 g, 30%); R_f=0.32 (100:1 n-hexane: ether (v/v)); ^{1}H NMR [$CDCl_3$] δ 10.54 (s, 1H, CHO), 7.24 (quasi-d, 2H, ArH), 1.51 (s, 9H, CH_3(^{t}Bu)), 1.31 (s, 9H, CH_3(^{t}Bu)); ^{13}C NMR [$CDCl_3$] δ 194.17 (CHO), 150.36, 148.42, 135.28, 131.07, 124.92, 124.62 (C_{arom}), 37.50, 34.89 (C(^{t}Bu)), 30.90, 30.08 (Me(^{t}Bu); MS (ES-MS): m/z 296 (M$^+$). CHN data not obtained.

7.3.23. Synthesis of (2-bromo-3,5-di-*tert*-butylphenyl)methanol (22)
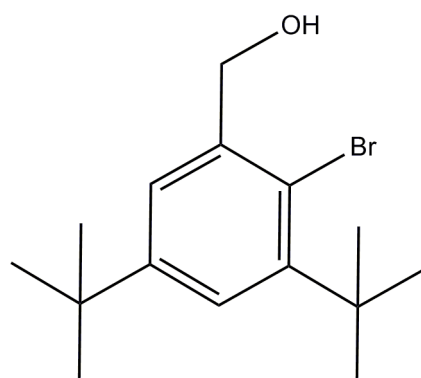
To a solution of **21** (4.23 g, 14.2 mmol) in propan-2-ol (80 ml) was added $NaBH_4$ (0.44 g, 11.6 mmol) portion wise at RT. Stirring continued for 2 hr before concentrating under reduced pressure. The residue was extracted with Et_2O (120 ml) and washed with brine (3 x 100 ml). The resulting solution was dried over $MgSO_4$ and the filtrate concentrated in vacuo to afford a white powder (3.68 g, 86%); ^1H NMR [$CDCl_3$] 7.44 (d, 1H, J=2.39 Hz, ArH), 7.36 (d, 1H, J=2.39 Hz, ArH), 4.76 (br, 2H, CH_2), 2.37 (s, 1H, OH), 1.54 (s, 9H, CH_3(^{t}Bu)), 1.32 (s, 9H, CH_3(^{t}Bu)); ^{13}C NMR [$CDCl_3$] 149.99, 147.51, 140.83, 124.76, 124.38, 120.41 (C_{arom}), 66.92 (CH_2), 37.31, 34.82 (C(^{t}Bu)), 31.34, 30.13 (CH_3(^{t}Bu)); MS (ES-MS): *m/z* 298 (M$^+$). CHN data not obtained.

7.3.24. Synthesis of (3,5-di-*tert*-butyl-2-(4-methoxybenzylthio)phenyl)methanol (23)
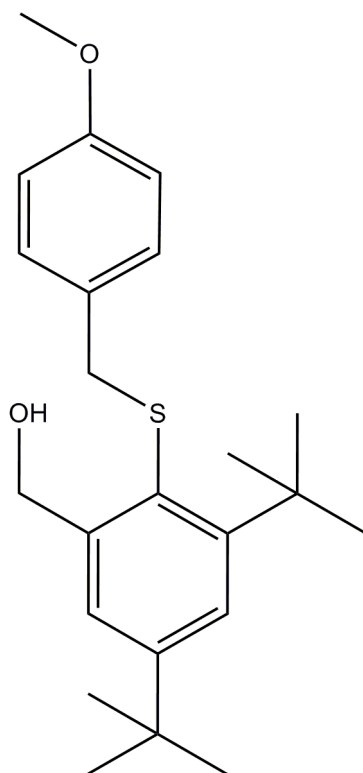
To a solution of **22** (3.68 g, 12.3 mmol) in dry Et$_2$O (25 ml) was added 2.5 M BuLi in n-hexane (10.6 ml, 17.0 mmol) under an argon atmosphere with ice cooling. The solution was stirred at 0°C for 10 mins and then at RT for 3 hrs. Toluene-4-thiosulfonic acid S-(4-methoxybenzyl) ester (3.92 g, 12.7 mmol) in dry Et$_2$O (45 ml) was then added at −75°C. The solution was stirred at −75°C for 1 hr, and then at −30°C for a further 4 hr. To this mixture was then added 2M HCl$_{(aq)}$ (105 ml), and the organic layer was collected. The aqueous layer was then extracted with Et$_2$O (2 x 50 ml). The organic layers were then combined and washed with 2M HCl$_{(aq)}$ (2 x 100 ml) followed by saturated NaCl$_{(aq)}$ (3 x 100 ml). The organic layer was again collected and then dried over MgSO$_4$. The solution was then filtered to remove solids and the filtrate concentrated under reduced pressure to give a crude oil (7.31 g). The crude oil was subjected to silica gel chromatography (eluting with toluene/Et$_2$O 20/1 (v/v)). The fractions containing the desired compound were collected and concentrated in vacuo to give a pale yellow oil (2.13 g, 47%); ^{1}H NMR [CDCl$_3$] δ 7.25 (d, 1H, J=2.27 Hz, ArH), 7.22 (d, 1H, J=2.27 Hz, ArH), 7.21 (m, 2H, ArH), 6.84 (m, 2H, ArH), 4.97 (d, 2H, CH$_2$OH, J=6.48 Hz), 3.87 (s, 2H, CH$_2$), 3.80

(s, 3H, OCH$_3$), 2.69 (t, 1H, OH, J=6.48 Hz), 1.59 (s, 9H, CH$_3$(^{t}Bu)), 1.33 (s, 9H, CH$_3$(^{t}Bu)); ^{13}C NMR [CDCl$_3$] δ 158.94, 153.80, 151.73, 146.75, 130.11, 129.02, 124.54, 123.91, 114.06 (C$_{arom}$), 65.52 (CH$_2$OH), 55.29 (OCH$_3$), 42.86 (SCH$_2$), 37.69, 34.85 (C(^{t}Bu)), 31.64, 31.25 (CH$_3$(^{t}Bu)); MS (ES-MS): *m/z* 372 (M$^+$). CHN data not obtained.

7.3.25. Synthesis of (2-(bromomethyl)-4,6-di-*tert*-butylphenyl)(4-methoxybenzyl)sulfane (24)
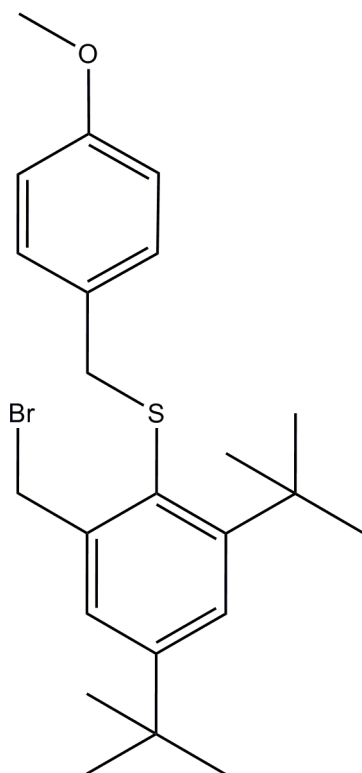
To a solution of **23** (2.13g, 5.72 mmol) in CHCl$_3$ (25 ml) was added PBr$_3$ (3.52 ml, 3.81 mmol) in CHCl$_3$ (10 ml) over a period of 10 min. The solution was stirred at 0°C for 90 min and then washed with brine (4 x 200 ml). The organic layer was collected and dried over MgSO$_4$ before concentrating under reduced pressure. The crude material obtained by this process was then purified by column chromatography (silica gel 60, eluent: n-hexane/ ether 5/1 (v/v)). This gave **24** as a yellow oil (1.60 g, 64%); R$_f$=0.69 (n-hexane/ ether 5/1 (v/v)); ^{1}H NMR [CDCl$_3$] δ 7.45 (m, 2H, ArH), 7.23 (m, 2H, ArH), 6.84 (m, 2H, ArH), 5.03 (s, 2H, CH$_2$Br), 3.98 (s, 2H, SCH$_2$), 3.80 (s, 3H, OCH$_3$), 1.58 (s, 9H, CH$_3$(^{t}Bu)), 1.32 (s, 9H, CH$_3$(^{t}Bu)); ^{13}C NMR [CDCl$_3$] δ158.89, 153.84, 151.28, 143.92, 130.80, 130.21, 129.14, 126.86, 124.86, 113.99, (C$_{arom}$), 55.27 (OCH$_3$), 42.47 (SCH$_2$), 37.92, 34.84 (C(^{t}Bu)), 34.64(CH$_2$Br), 31.59, 31.16 (CH$_3$(^{t}Bu)); MS (ES-MS): *m/z* 434 (M$^+$). CHN data not collected.

7.3.26. Synthesis of 5-(benzyloxy)-2-bromo-5-oxobutanoic acid (25)
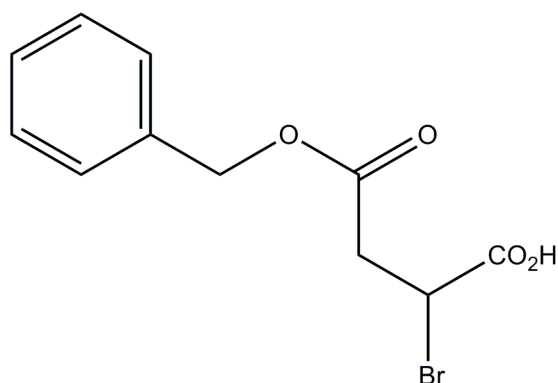
L-Aspartic acid β benzyl ester (4.59 g, 20.56 mmol) and NaBr (7.4 g, 71.96 mmol) in 1N HBr (45 ml) was cooled to 0°C under a blanket of N_2. To this was added $NaNO_2$ (2.41 g, 34.95 mmol) portion wise. The reaction was then stirred for a further 2 hr at 0°C before H_2SO_4 (1.7 ml) was added followed by diethyl ether (50 ml). The organic layer was extracted using portions of diethyl ether (3 x 50 ml), which were combined and then washed with brine (4 x 50 ml). The ether layer was then dried over $NaSO_4$ before filtering and concentrating in vacuo to give a yellow oil. Purification of the crude product by silica gel chromatography (hexane: ethyl acetate 75:25 to 25:75 v/v) gave **25** as a yellow oil (2.93 g, 50%); ^{1}H NMR [CDCl$_3$] δ 9.00 (br s, 1H, COOH), 7.31-7.25 (m, 5H, ArH), 5.09 (s, 2H, CH$_2$Ph), 4.54 (dd, 1H, ^{3}J=6.17, 8.71 Hz, CH), 3.24 (dd, 1H, ^{3}J=8.71, ^{2}J=17.27 Hz, CH$_2$), 2.97 (dd, 1H, ^{3}J=6.17, ^{2}J=17.27, CH$_2$); ^{13}C NMR [CDCl$_3$] δ 168.69, 167.42 (COOH and COOBz), 135.19, 128.68, 128.34, 128.02 (C$_{arom}$), 65.87 (CH$_2$Ph), 51.71 (CH), 38.62 (CH$_2$); MS (MALDI): *m/z* 286 (M$^+$). Satisfactory CHN not obtained.

7.3.27. Synthesis of 2-bromo-3-(4-nitrophenyl)propanoic acid (26)
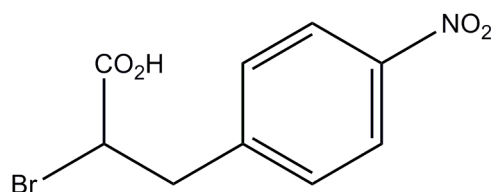
4-Nitro-L-phenylalanine (5.18 g, 22.69 mmol) and NaBr (8.2 g, 79 mmol) in 1N HBr (45 ml) was cooled to 0°C under a blanket of nitrogen. To this was added NaNO$_2$ (2.66 g, 38.6 mmol) portion wise. The reaction was then stirred for a further 2 hr at 0°C before H$_2$SO$_4$ (2 ml) was added followed by diethyl ether (50 ml). The organic layer was extracted using diethyl ether (3 x 50 ml), which were combined and then washed with water (4 x 50 ml). The ether layer was then dried over MgSO$_4$ before filtering and concentrating in vacuo to give a yellow oil, from which a crystalline product formed (5.71 g, 86%); R$_f$=0.36 (1:1 ethyl acetate/hexane v/v), R$_f$=0.36 (5:95 MeOH/DCM v/v); ^{1}H NMR [CDCl$_3$] δ 8.11 (d, 2H, J=8.70 Hz, ArH), 7.34 (d, 2H, J=8.70 Hz, ArH), 4.38 (t, 1H, J=7.58, CH), 3.58 (dd, 1H, ^{3}J=7.58, ^{2}J=14.32 Hz, CH$_2$), 3.36 (dd, 1H, ^{3}J=7.58, ^{2}J=14.32 Hz, CH$_2$); ^{13}C NMR [CDCl$_3$] δ 169.64 (COOH), 146.87, 144.32, 132.67, 124.43 (C$_{arom}$), 46.09 (CH$_2$), 41.36 (CH); MS (ES-MS): *m/z* 258 (M$^+$). Satisfactory CHN not obtained.

7.3.28. Synthesis of 4-benzyl 1-*tert*-butyl 2-bromosuccinate (27)
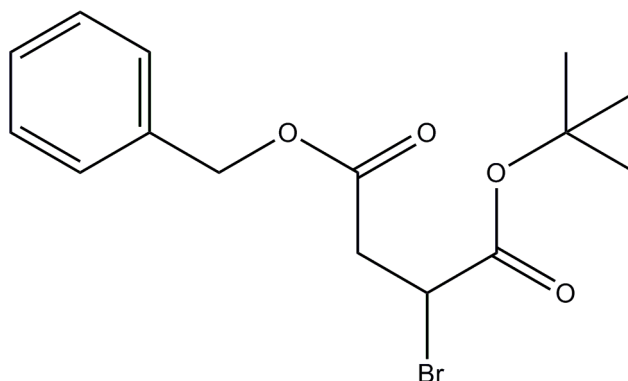
25 (2.93 g, 0.01 mol) was dissolved in chloroform (20 ml) to which was added a solution of *tert*-butyltrichloroacetimidate (4.47 g, 0.02 mol) in cyclohexane (20 ml) drop wise over a period 20 min. During this addition a white precipitate formed which was dissolved by the drop wise addition of DMA (~3 ml). Boron trifluoride ethyl etherate (320 µL) was then added as a catalyst and the solution stirred at RT for a period of 5 d. The mixture was then concentrated and hexane (30 ml) and water (50 ml) were then added. The hexane layer was collected and the solvent removed under reduced pressure to afford a light yellow oil (2.63 g, 77%); R_f=0.42 (20:1 hexane/ethylacetate (v/v)); ^{1}H NMR [CDCl$_3$] δ 7.38-7.30 (m, 5H, ArH), 5.14 (s, 2H, CH$_2$), 4.48 (dd, 1H, ^{3}J=6.18, 8.84 Hz, CH), 3.26 (dd, 1H, ^{3}J=8.84, ^{2}J=17.12 Hz, CH$_2$), 2.98 (dd, 1H, ^{3}J=6.18, ^{2}J=17.12 Hz, CH$_2$), 1.40 (s, 9H, ^{t}Bu); ^{13}C NMR [CDCl$_3$] δ 169.39, 167.69 (COO^{t}Bu and COOBz), 135.17, 128.43, 128.27, 128.16 (C$_{arom}$), 82.57 (C(^{t}Bu)), 66.46 (CH$_2$Ph), 52.31 (CH), 39.72 (CH$_2$), 27.63 (Me(^{t}Bu)); MS (ES-MS): *m/z* 343 (M$^+$), 287 ((M-^{t}Bu)$^+$). Satisfactory CHN not obtained due to trace DMA impurity.

7.3.29. Synthesis of *tert*-butyl 2-bromo-3-(4-nitrophenyl)propanoate (28)
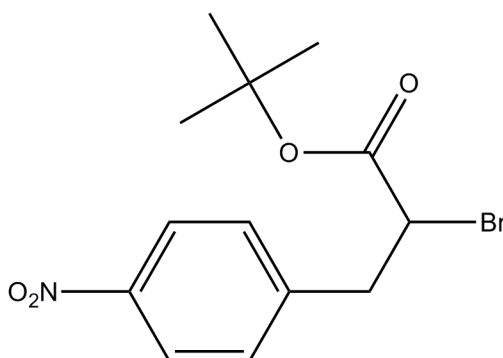
26 (5.71 g, 0.021 mol) was dissolved in chloroform (20 ml) to which was added a solution of *tert*-butyltrichloroacetimidate (8.53 g, 0.039 mol) in cyclohexane (20 ml) drop wise over a period 20 min. During this addition a white precipitate formed which was dissolved by the drop wise addition of DMA (~4 ml). Boron trifluoride ethyl etherate (320 µL) was then added as a catalyst and the solution stirred at RT for a period of 5 d. The mixture was then concentrated and hexane (50 ml) and water (50 ml) were then added. The hexane layer was collected and the solvent removed under reduced pressure to afford a dark yellow crystalline solid (2.86 g, 41%); ^{1}H NMR [CDCl$_3$] δ 8.16 (d, 2H, J=7.88 Hz, ArH), 7.40 (d, 2H, J=7.88 Hz, ArH), 4.31 (t, 1H, ^{3}J=7.52 Hz, CH), 3.51 (dd, 1H, ^{3}J=7.52 Hz, ^{2}J=14.30 Hz, CH$_2$), 3.29 (dd, 1 H, ^{3}J=7.52 Hz, ^{2}J=14.30 Hz, CH$_2$), 1.41 (s, 9H, ^{t}Bu); ^{13}C NMR [CDCl$_3$] δ 167.78 (COO^{t}Bu), 147.14, 144.41, 130.15, 123.70 (C$_{arom}$), 83.07 (C(^{t}Bu)), 45.72 (CH$_2$), 40.49 (CH), 27.61 (Me(^{t}Bu)); MS (ES-MS): *m/z* 347 ((M+NH$_4$)$^{+}$). Satisfactory CHN not obtained due to trace DMA impurity.
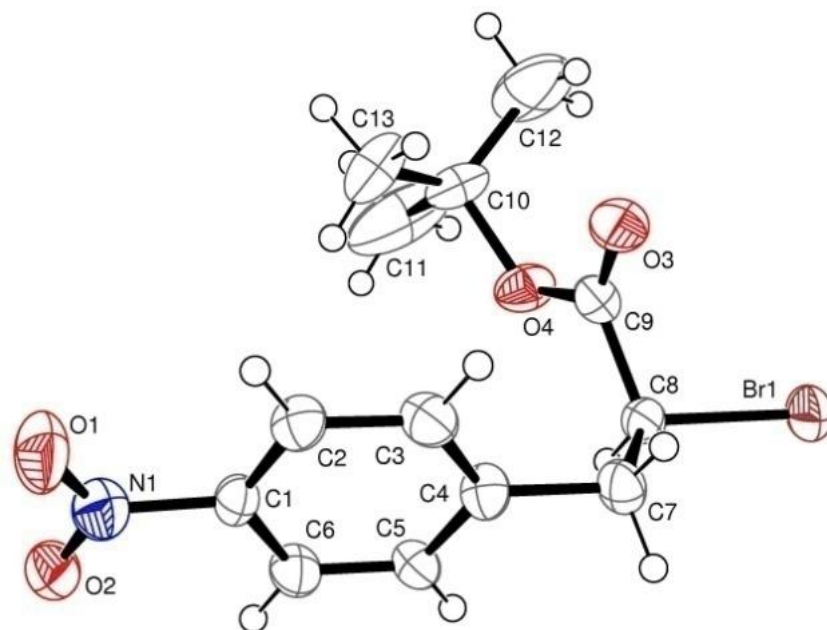
Figure 88: ORTEP representation of the X-ray crystal structure of 28 with all non H-atoms labelled.

## Table 18: Crystal data for the structural refinement of 28.

Identification code	sja9_06
Empirical formula	$C_{13} H_{16} Br_1 N_1 O_4$
Formula weight	430.19
Temperature	150(2) K
Wavelength	0.71073 Å
Crystal system	monoclinic
Space group	$P\,2_1/c$
Unit cell dimensions	a = 11.578(5) Å $\quad\alpha = 90°$.
	b = 12.033(4) Å $\quad\beta = 91.24(3)°$.
	c = 10.686(4) Å $\quad\gamma = 90°$.
Volume	1488.4(10) Å^3
Z	4
Density (calculated)	1.473 Mg/m^3
Absorption coefficient	2.771 mm^{-1}
F(000)	672
Crystal size	0.61 x 0.12 x 0.05 mm^3
Theta range for data collection	3.07 to 34.83°.
Index ranges	-18<=h<=18, -19<=k<=19, -14<=l<=17
Reflections collected	35589
Independent reflections	6382 [R(int) = 0.5047]
Completeness to theta = 34.83°	98.5 %
Refinement method	Full-matrix least-squares on F^2
Data / restraints / parameters	6382 / 0 / 189
Goodness-of-fit on F^2	0.728
Final R indices [I>2sigma(I)]	R1 = 0.0632, wR2 = 0.0741
R indices (all data)	R1 = 0.3576, wR2 = 0.1235
Extinction coefficient	0.00084(16)
Largest diff. peak and hole	0.903 and -1.376 e.Å^{-3}

7.3.30. Synthesis of mono-methoxy PEG (average MW=550) chains with a primary bromide (29)
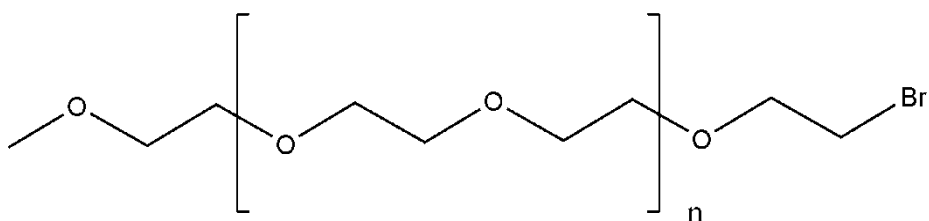
Mono methoxy capped PEG (10 g, ~0.013 mol) with an average MW of 550 was dissolved in DCM (30 ml) at 0°C under nitrogen, to which was added PBr$_3$ (14.4 g, 0.053 mol) in DCM (10 ml) over 30 min. Stirring was then continued for a further hour at 0°C before adding brine (200 ml). The organic layer was separated, further washed with brine (2 x 200 ml) and concentrated to give **29** as a yellow oil (4g, ~40%); ^{1}H NMR [CDCl$_3$] δ 3.63 (t, J=7.87 Hz, nH), 3.57-3.41 (m, 8nH), 3.32 (t, J=9.64 Hz, nH). CHN data not obtainable.

7.3.31. Synthesis of mono-methoxy PEG (average MW=750) chains with a primary bromide (30)
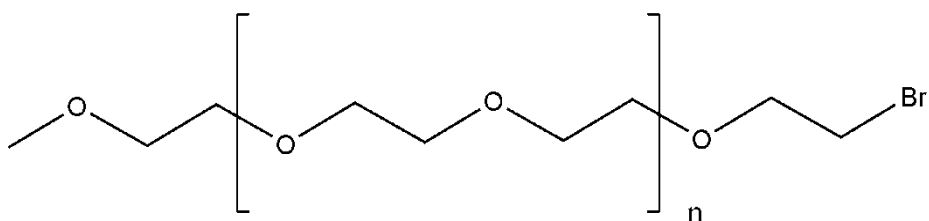
Mono methoxy capped PEG (10g, ~0.018 mol) with an average MW of 750 was dissolved in DCM (30 ml) at 0°C under nitrogen, to which was added PBr$_3$ (19.69 g, 0.072 mol) in DCM (10 ml) over 30 min. Stirring was then continued for a further hour at 0°C before adding brine (200 ml). The organic layer was separated, further washed with brine (2 x 200 ml) and concentrated in vacuo to give **30** as a yellow oil (8.44g, ~76%); ^{1}H NMR [CDCl$_3$] δ 3.65 (t, J=7.58 Hz, nH), 3.56-3.47 (m, 11nH), 3.35 (t, J=6.32 Hz, nH). CHN data not obtainable.

7.3.32. Synthesis of 1-[2-(2-chloro-ethoxy)-ethoxy]-2-methoxy-ethane (31)
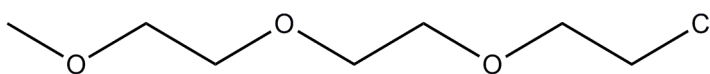
Monomethoxy triethylene PEG (2 g, 12.2 mmol) was dissolved in pyridine (0.98 ml, 12.2 mol) under nitrogen. To this was added thionyl chloride (1.74 g, 14.6 mmol) over 10 min. The slightly yellow solution was then heated to reflux for 3 hr. The solution was allowed to cool before washing with water (100 ml). The organic layer was collected and dried over magnesium sulphate before concentrating the filtrate in vacuo. This gave the compound as a yellow oil (1.98 g, 89%); ^{1}H NMR [CDCl$_3$] δ 3.57 (t, 2H, J=5.88 Hz, CH$_2$), 3.51-3.44 (m, 8H, CH$_2$), 3.38-3.35 (m, 2H, CH$_2$), 3.19 (s, 3H, OMe); ^{13}C NMR [CDCl$_3$] δ 71.40, 70.81, 70.09, 70.06, 70.03 (CH$_2$), 58.41 (OMe), 42.25 (CH$_2$Cl); MS (ES-MS): m/z 59 (MeOCH$_2$CH$_2$$^+$) [no higher fragments observed due to heavy fragmentation of PEG chain]. CHN data not collected.

7.4. Cyclam compounds and complexes

7.4.1. Synthesis of cyclam (32)

Nickel(II) perchlorate hexahydrate (54.7 g, 0.15 mol) was dissolved in water (400 ml). 1,5,8,12-tetraazadodecane (24 g, 0.15 mol) was added with stirring before cooling to 5°C and adding glyoxal (22.5 ml). The dark purple solution was left to stir o/n. The solution was then cooled to 5°C, and NaBH$_4$ (11 g, 0.3 mol) was added portionwise over 1 hr with rapid stirring. The solution was then heated to 90°C and filtered whilst still hot. To the filtrate was added NaCN (29 g, 0.6 mol) and the solution heated to reflux for 2 hr. The orange solution was concentrated under reduced pressure until the volume was ~100 ml. NaOH (15 g, 0.38 mol) was then added and the aqueous layer washed repeatedly with CHCl$_3$ (5 x 100 ml). The organic fractions were collected and dried over MgSO$_4$. The solution was filtered and the filtrate concentrated under reduced pressure to give the crude product (17.07 g). The crude product was recrystallised from chlorobenzene to afford **32** as thin white needles (10.89 g, 36%); ^{1}H NMR [CDCl$_3$] δ 2.73 (t, 8H, J=5.19 Hz, NC$\underline{H_2}$CH$_2$C$\underline{H_2}$N), 2.66 (s, 8H, NC$\underline{H_2}$C$\underline{H_2}$N), 2.51 (br s, 4H, NH), 1.71 (quin, 4H, J=5.19 Hz, NCH$_2$C$\underline{H_2}$CH$_2$N). CHN data not collected.

7.4.2. Synthesis of *cis*-3a,5a,8a,10a-tetraazaperhydropyrene (33)

Cyclam (1.08 g, 5 mmol) in methanol (40 ml) was cooled to −10°C and glyoxal (0.78 g, 5 mmol) in methanol (30 ml) was added dropwise over a period of 1.5 hr. The solution was stirred for a further 30 min at −10°C before stirring at RT for 4 hr. The methanol was then removed under reduced pressure before treating the product using diethyl ether (30 ml). The diethyl ether extracts were collected and combined and the solvent removed under reduced pressure. This afforded a yellow oil which, on drying in vacuo, yielded a cream solid (1.11 g, 100%); ^{1}H NMR [CDCl$_3$] δ 3.46 (t, 2H, J=11 Hz, NC$\underline{H}$N), 3.01 (s, 2H, CH$_2$), 2.92-2.83 (m, 6H, CH$_2$), 2.66 (d, 2H, J=11 Hz, CH$_2$), 2.26 (d, 2H, J=11 Hz, CH$_2$), 2.20-2.04 (m, 6H, CH$_2$), 1.14 (dquin, 2H, J=2.25 Hz, 13 Hz, CH$_2$); ^{13}C NMR [CDCl$_3$] δ 55.69 (NC$\underline{H}$N), 53.98, 52.11, 44.39 (CH$_2$), 19.22 (NCH$_2$C$\underline{H_2}$CH$_2$N); MS (ES-MS): *m/z* 222 (M$^+$). CHN data not collected.

7.4.3. Synthesis of *N*-3,5-di-*tert*-butyl-2-methoxy-benzyl-*cis*-3a,5a,8a,10a-tetraazaperhydropyrene bromide (35)

33 (0.21g, 0.959 mmol) and **5** (0.3g, 0.958 mmol) were dissolved in dry MeCN (20 ml) and stirred at RT for 5 days. The solvent was removed in vacuo and the residue washed with diethyl ether (30 ml). A precipitate formed which was collected by filtration and washed with further ether (3 x 10 ml). This gave the product as a white solid (0.33 g, 64%); ^{1}H NMR [CD$_3$OD] δ 7.52 (d, 1H, J=2.2 Hz, ArH), 7.33 (d, 1H, J=2.2 Hz, ArH), 4.76 (s, 5H, CH$_2$), 4.21-4.15 (m, 2H, CH$_2$), 3.72-3.49 (m, 1H, CH$_2$), 3.40-3.33 (m, 1H, CH$_2$), 3.21-2.87 (m, 12H, CH$_2$ and OMe), 2.55-2.15 (m, 6H, CH$_2$), 1.33 (s, 9H, ^{t}Bu), 1.24 (s, 9H, ^{t}Bu); ^{13}C NMR [CD$_3$OD] δ 155.07, 143.81, 140.55, 126.73, 124.85, 117.05 (C$_{arom}$), 80.13, 73.10 (NC**H**N), 67.33 (O**Me**), 60.02 (NC**H$_2$**Ph), 55.89, 55.56, 51.47, 50.92, 49.09, 48.91, 45.93, 39.27 (CH$_2$), 31.96, 30.98 (C(^{t}Bu)), 27.16, 27.13 (Me(^{t}Bu)), 15.66, 15.56 (NCH$_2$**CH$_2$**CH$_2$N). CHN data not satisfactory.

7.4.4. Synthesis of 5-(3,5-di-*tert*-butyl-2-methoxybenzyl)-1,5,8,12-tetraazabicyclo[10.2.2]hexadecane (36)

35 (250 mg, 0.467 mmol) was dissolved in ethanol (100 ml) to which was added NaBH$_4$ (0.36 g, 9.3 mmol) portionwise. The solution was then stirred for 7 days at RT before removing the solvent in vacuo. The white solid formed was partitioned between DCM (60 ml) and water (pH 14, 200 ml). The organic layer was collected and dried over Na$_2$SO$_4$. The solution was then filtered and the filtrate concentrated under reduced pressure to give **36** as a yellow oil (190 mg, 89%); ^{1}H NMR [CDCl$_3$] δ 7.16 (d, 1H, J=2.5 Hz, ArH), 7.11 (d, 1H, J=2.5 Hz, ArH), 3.65 (s, 3H, OMe), 3.00-2.13 (m, 26H, CH$_2$), 1.32 (s, 9H, ^{t}Bu), 1.23 (s, 9H, ^{t}Bu); ^{13}C NMR [CDCl$_3$] δ 156.65, 145.04, 141.78, 126.61, 123.10 (C$_{arom}$), 62.39 (O$\underline{Me}$), 57.08 (N$\underline{CH_2}$Ph), 56.96, 54.52, 54.34, 53.70, 53.38, 51.66, 51.14, 49.80, 48.57, 48.12 (CH$_2$), 35.27, 34.44 (C(^{t}Bu)), 31.64, 31.29 (Me(^{t}Bu)), 24.04, 19.56 (NCH$_2$$\underline{CH_2}CH_2$N); MS (ES-MS): *m/z* 460.5 (M$^+$). CHN data not satisfactory.
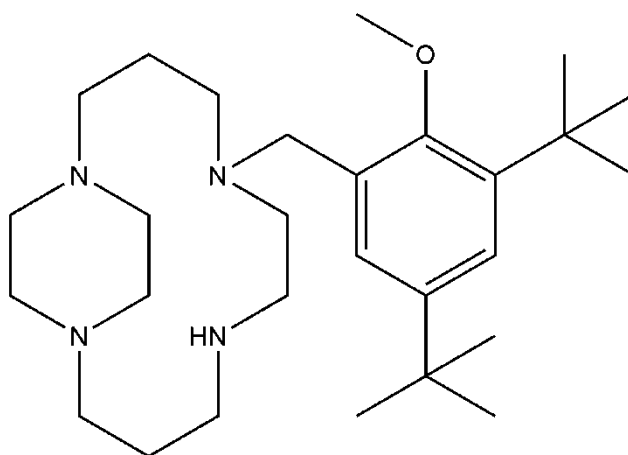
7.4.5. Synthesis of copper(II) 5-(3,5-di-*tert*-butyl-2-methoxybenzyl)-1,5,8,12-tetraazabicyclo[10.2.2]hexadecane perchlorate ([Cu36][(ClO$_4$)$_2$]
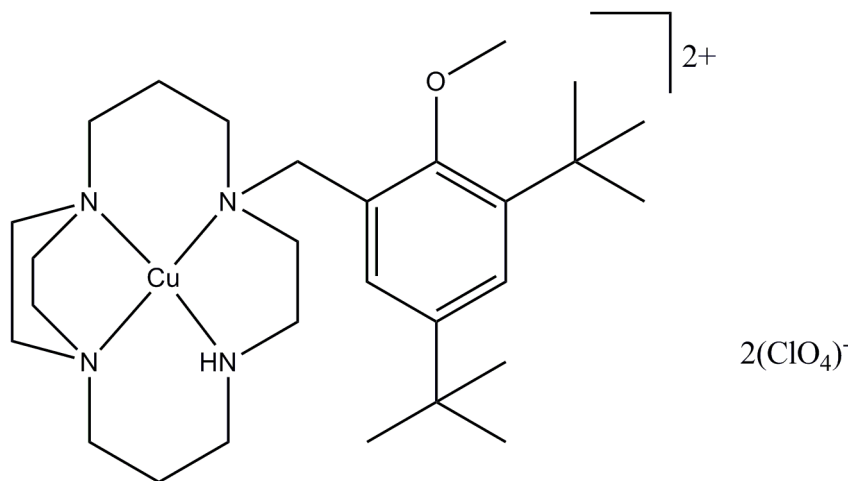
To a solution of **36** (100 mg, 0.218 mmol) in MeOH (10 ml) was added copper(II) perchlorate hexahydrate (0.08 g, 0.218 mmol) in MeOH (3 ml). The blue solution was then heated to reflux for 2 hr. After this time the solution was allowed to cool, filtered and concentrated under reduced pressure to give a blue-purple crystalline solid (154 mg, 98%); HRMS (ES-MS) expected for $C_{28}N_4H_{50}O_5Cl_1Cu_1$: 620.2760, found 620.2767; ε (MeOH): 547 nm (331 mol^{-1}dm^{3}cm^{-1}). CHN not collected due to risk of explosion.

7.4.6. Synthesis of zinc(II) 5-(3,5-di-*tert*-butyl-2-methoxybenzyl)-1,5,8,12-tetraazabicyclo[10.2.2]hexadecane perchlorate ([Zn36][(ClO$_4$)$_2$]
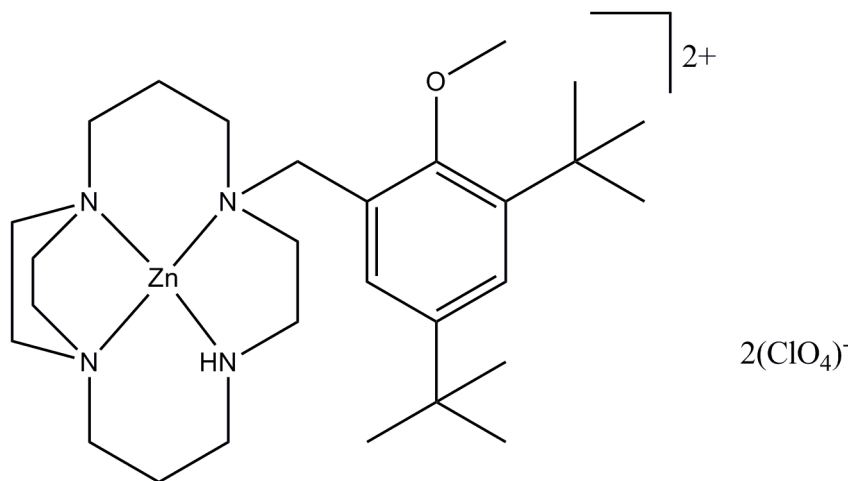
To a solution of **36** (100 mg, 0.218 mmol) in MeOH (10 ml) was added zinc(II) perchlorate hexahydrate (0.08 g, 0.218 mmol) in MeOH (3 ml). The yellow solution was then heated to reflux for 2 hr. After this time the solution was allowed to cool, filtered and concentrated under reduced pressure to give a white crystalline solid (150 mg, 95%); ^{1}H NMR [CD$_3$CN] δ 7.14 (d, 1H, J=2.52 Hz, ArH), 7.10 (d, 1H, J=2.52 Hz, ArH), 3.64 (s, 3H, OMe), 2.99-2.11 (m, 26H, CH$_2$), 1.33 (s, 9H, ^{t}Bu), 1.25 (s, 9H, ^{t}Bu); ^{13}C NMR [CD$_3$CN] δ 157.45, 145.09, 141.48, 125.71, 124.30 (C$_{arom}$), 62.89 (OMe), 57.78 (NCH$_2$Ph), 56.54, 54.44, 54.27, 53.65, 53.34, 51.58, 51.18, 49.75, 48.67, 48.13 (CH$_2$), 35.45, 34.65 (C(^{t}Bu)), 31.62, 31.56 (Me(^{t}Bu)), 24.12, 19.64 (NCH$_2$CH$_2$CH$_2$N); HRMS (ES-MS) expected for C$_{28}$H$_{50}$O$_5$N$_4$Cl$_1$Zn$_1$: 621.2756, found 621.2763. CHN not collected due to risk of explosion.

7.4.7. Synthesis of nickel(II) 5-(3,5-di-*tert*-butyl-2-methoxybenzyl)-1,5,8,12-tetraazabicyclo[10.2.2]hexadecane perchlorate ([Ni36][(ClO$_4$)$_2$])
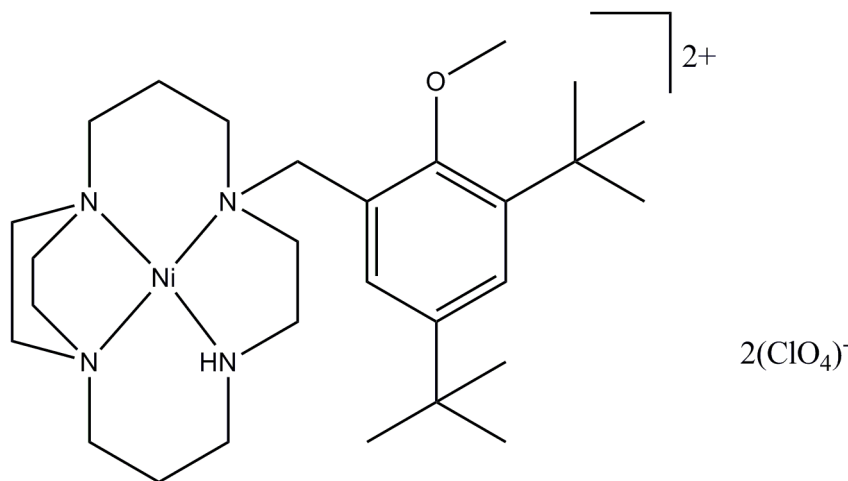
To a solution of **36** (100 mg, 0.218 mmol) in MeOH (10 ml) was added nickel(II) perchlorate hexahydrate (0.08 g, 0.218 mmol) in MeOH (3 ml). The orange solution was then heated to reflux for 2 hr. After this time the solution was allowed to cool, filtered and concentrated under reduced pressure to give a orange crystalline solid (152 mg, 98%); HRMS (ES-MS) expected for C$_{28}$H$_{50}$N$_4$ONi: 258.1664 (M^{2+}) found 258.1665; HRMS (ES-MS) expected for C$_{28}$H$_{50}$N$_4$ONi: 615.2818 (M$^+$) found 615.2808; ε (MeOH): 477 nm (197 mol^{-1}dm^{3}cm^{-1}). CHN not collected due to risk of explosion.
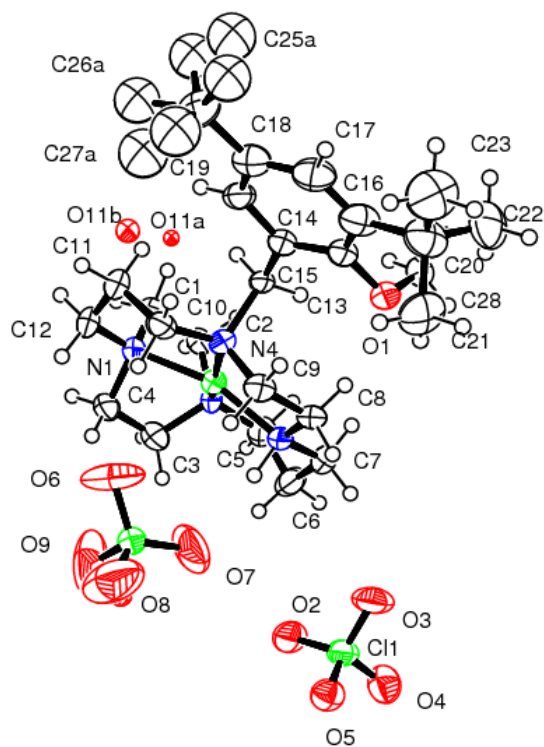
Figure 89: ORTEP representation of the X-ray structure of [Ni36][(ClO$_4$)$_2$] with all non-H atoms labelled.

Table 19: Crystal data for the structural refinement of [Ni36][(ClO₄)₂].

Identification code	sja38_08
Empirical formula	$C_{120} H_{164} Cl_{l8} N_{16} N_{i4} O_{39}$
Formula weight	2973.03
Temperature	150(2) K
Wavelength	0.71073 Å
Crystal system	Monoclinic
Space group	P21/c
Unit cell dimensions	a = 25.066(4) Å α= 90°.
	b = 11.2561(17) Å β= 96.911(14)°
	c = 12.752(2) Å γ = 90°.
Volume	3571.8(10) Å^3
Z	1
Density (calculated)	1.378 Mg/m^3
Absorption coefficient	0.752 mm^{-1}
F(000)	1556
Crystal size	0.39 x 0.36 x 0.27 mm^3
Theta range for data collection	2.49 to 34.90°.
Index ranges	-40<=h<=40, -17<=k<=18, -20<=l<=20
Reflections collected	103581
Independent reflections	15376 [R(int) = 0.2890]
Completeness to theta = 34.90°	98.4 %
Absorption correction	None
Refinement method	Full-matrix least-squares on F^2
Data / restraints / parameters	15376 / 3 / 421
Goodness-of-fit on F^2	0.903
Final R indices [I>2sigma(I)]	R1 = 0.1256, wR2 = 0.3045
R indices (all data)	R1 = 0.2736, wR2 = 0.3472
Extinction coefficient	0.0028(8)
Largest diff. peak and hole	1.633 and -0.963 e.Å^{-3}

7.4.8. Synthesis of *N*-3,5-di-*tert*-butyl-2-benzyl ether-benzyl-cis 3a,5a,8a,10a-tetraazaperhydropyrene (38)
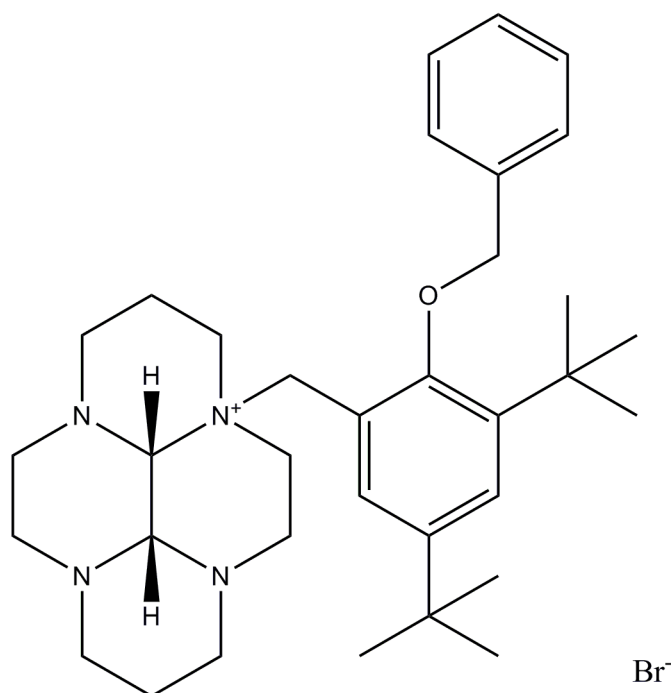
33 (0.45 g, 0.002 mmol) and **8** (0.78 g, 0.002 mmol) were dissolved in MeCN (30 ml) and stirred at RT for 3 days. The MeCN was then removed in vacuo and the isolated oil was triturated diethyl ether (30 ml) to yield a white solid. This white solid was then filtered off and further washed with ether (2 x 30 ml) to give **38** as a white solid (0.38 g, 66%); ^{1}H NMR [CD$_3$OD] δ 7.67-7.35 (m, 7H, ArH), 4.13-4.05 (m, 1H, CH$_2$), 3.59-2.80 (m, 12H, CH$_2$), 3.04-2.80 (m, 9H, CH$_2$), 2.52-2.03 (m, 4H, CH$_2$), 1.34 (s, 9H, ^{t}Bu), 1.26 (s, 9H, ^{t}Bu); ^{13}C NMR [CD$_3$OD] δ 153.22, 143.92, 140.43, 133.41, 126.91, 125.32, 124.91, 124.83, 123.88, 117.04 (C$_{arom}$), 80.32, 74.66 (N$\underline{C}$HN), 72.91 (O$\underline{C}$H$_2$Ph), 66.93 (N$\underline{C}$H$_2$Ph), 56.13, 55.88, 50.80, 50.70, 49.00, 48.43, 38.96 (CH$_2$), 31.98, 30.86 (C(^{t}Bu)), 27.25, 26.98 (Me(^{t}Bu)), 15.48, 15.15 (NCH$_2$$\underline{C}H_2CH_2$N); MS (ES-MS): *m/z* 532.4 (M$^+$). CHN not satisfactory.

7.4.9. Synthesis of 5-(2-(benzyloxy)-3,5-di-*tert*-butylbenzyl)-1,5,8,12-tetraazabicyclo[10.2.2]hexadecane (39)

38 (1.09 g, 0.00178 mol) was dissolved in methanol (40 ml) to which $NaBH_4$ (1.36 g, 0.03568 mol) was added portionwise over 5 min. The mixture was then stirred at RT for 2 days before heating to reflux for 2 hr. The solvent was removed under reduced pressure and $KOH_{(aq)}$ (pH 14, 200 ml) added. DCM (100 ml) was used to extract the organic product which was then dried over $MgSO_4$ and evaporated in vacuo to afford **39** as a yellow oil (0.76 g, 80%); ^1H NMR [$CDCl_3$] δ 7.44-7.20 (m, 7H, ArH), 5.19 (s, 2H, NCH_2Bn), 4.82 (s, 2H, OCH_2Bn), 3.70-3.68 (m, 2H, CH_2), 3.28-3.24 (m, 7H, CH_2), 3.12-2.84 (m, 5H, CH_2), 2.56-2.39 (m, 11H, CH_2), 1.36 (s, 9H, ^tBu), 1.23 (s, 9H, ^tBu); ^{13}C NMR [$CDCl_3$] 155.04, 145.35, 141.97, 137.87, 129.86, 128.47, 127.62, 126.72, 126.63, 123.34 (C_{arom}), 77.00 (O$\underline{C}H_2$Ph), 56.86 (N$\underline{C}H_2$Ph), 54.50, 53.95, 53.63, 50.99, 50.66, 49.73, 48.15, 47.83 (CH_2), 35.41, 34.45 (C(^tBu)), 31.64, 31.32 (Me(^tBu)), 25.64, 23.84 (N$CH_2\underline{C}H_2CH_2$N); MS (ES-MS): *m/z* 536.4 (MH^+). CHN not satisfactory.

7.4.10. Synthesis of copper(II) 5-(2-(benzyloxy)-3,5-di-*tert*-butylbenzyl)-1,5,8,12-tetraazabicyclo[10.2.2]hexadecane perchlorate ([Cu39][(ClO$_4$)$_2$])

To **39** (100 mg, 0.187 mmol) dissolved in MeOH (10 ml) was added copper(II) perchlorate hexahydrate (0.07 g, 0.187 mmol) in MeOH (3 ml). The blue solution was then heated to reflux for 2 hr. After this time the solution was allowed to cool, filtered and concentrated under reduced pressure to give a purple crystalline solid (130 mg, 87%); HRMS (ES-MS) expected for $C_{34}H_{54}O_5N_4Cl_1Cu_1$: 696.3073, found 696.3075; ε (MeOH): 550 nm (286 mol^{-1}dm^{3}cm^{-1}). CHN not collected due to risk of explosion.

7.4.11. Synthesis of zinc(II) 5-(2-(benzyloxy)-3,5-di-*tert*-butylbenzyl)-1,5,8,12-tetraazabicyclo[10.2.2]hexadecane perchlorate ([Zn39][(ClO$_4$)$_2$])

To **39** (100 mg, 0.187 mmol) dissolved in MeOH (10 ml) was added zinc(II) perchlorate hexahydrate (0.0822 g, 0.187 mmol) in MeOH (3 ml). The yellow solution was then heated to reflux for 2 hr. After this time the solution was allowed to cool, filtered and concentrated under reduced pressure to give a white crystalline solid (0.0702 mg, 47%); ^{1}H NMR [CD$_3$CN] δ 7.46-7.22 (m, 7H, ArH), 5.21 (s, 2H, NCH$_2$Bn), 4.79 (s, 2H, OCH$_2$Bn), 3.72-3.66 (m, 2H, CH$_2$), 3.29-3.22 (m, 7H, CH$_2$), 3.13-2.82 (m, 5H, CH$_2$), 2.57-2.33 (m, 11H, CH$_2$), 1.34 (s, 9H, ^{t}Bu), 1.26 (s, 9H, ^{t}Bu); ^{13}C NMR [CD$_3$CN] 156.13, 144.39, 142.04, 137.62, 129.56, 128.82, 127.54, 126.59, 126.36, 123.28 (C$_{arom}$), 77.13 (OCH$_2$Ph), 56.44 (NCH$_2$Ph), 54.47, 53.82, 53.59, 51.07, 50.68, 49.57, 48.21, 47.91 (CH$_2$), 35.26, 34.67 (C(^{t}Bu)), 31.56, 31.29 (Me(^{t}Bu)), 25.58, 23.78 (NCH$_2$CH$_2$CH$_2$N); HRMS (ES-MS) expected for C$_{34}$H$_{54}$N$_4$O$_5$ZnCl: 697.3069, found 697.3060. CHN not collected due to risk of explosion.

7.4.12.   Synthesis of nickel(II) 5-(2-(benzyloxy)-3,5-di-*tert*-butylbenzyl)-1,5,8,12-tetraazabicyclo[10.2.2]hexadecane perchlorate ([Ni39][(ClO₄)₂])

To **39** (150mg, 0.281 mmol) dissolved in MeOH (10 ml) was added nickel(II) perchlorate hexahydrate (102 mg, 0.281 mmol) in MeOH (3 ml). The yellow/brown solution was then heated to reflux for 2 hr. After this time the solution was allowed to cool, filtered and concentrated under reduced pressure to give an orange crystalline solid (0.0925 g, 42%); HRMS (ES-MS) expected for $C_{34}H_{54}N_4O_5NiCl$: 691.3131 (M^+), found 691.3122; ε (MeOH): 481 nm (100 $mol^{-1}dm^3cm^{-1}$). CHN not collected due to risk of explosion.

7.4.13. Synthesis of 3a-3,5-di-*tert*-butyl-2-(4-methoxy-benzyloxy)-benzyl-decahyro-5a, 8a, 10a-triaaza-3a-azonia-pyrene bromide (40)

33 (0.53 g, 2.4 mmol) and **14** (1 g, 2.4 mmol) were dissolved in dry MeCN (20 ml) and stirred for 4 days at RT. After this time, a precipitate had formed. The reaction mixture was then concentrated under reduced pressure and filtered. The solid was then washed with pentane (3 x 20 ml), and the product was isolated as a orange solid (1.35g, 88%); ^{1}H NMR [CD$_3$OD] δ 7.57 (d, 1H, J=2.38 Hz, ArH), 7.42 (d, 2H, J=8.56 Hz, ArH), 7.39 (d, 1H, J=2.38 Hz, ArH), 6.94 (d, 2H, J=8.56 Hz, ArH), 4.78 (s, 2H, NCH$_2$Phen); 3.73 (s, 3H, OMe), 3.50-3.20 (m, 6H, CH$_2$), 3.01- 2.66 (m, 12H, CH$_2$), 2.37-1.94 (m, 6H, CH$_2$), 1.41 (s, 9H, ^{t}Bu), 1.26 (s, 9H, ^{t}Bu);^{13}C NMR [CD$_3$OD] δ 161.52, 158.18, 148.52, 131.4105, 130.59, 130.16, 129.63, 121.76, 115.51 (C$_{arom}$), 85.13, 79.53 (NCHN), 77.69 (OCH$_2$Phen), 71.63 (NCH$_2$Phen), 60.64, 55.92, 55.41, 53.72, 53.14, 52.77, 44.79, 43.68 (CH$_2$ and OMe), 36.70, 35.56 (C(^{t}Bu)), 31.92, 31.71 (Me(^{t}Bu)), 20.18, 19.90 (CH$_2$CH$_2$CH$_2$); MS (ES-MS): *m/z* 562.4 (M$^+$), 222 ((macrocycle)$^+$). CHN not collected.

7.4.14. Synthesis of 5-[3,5-di-*tert*-butyl-2-(4-methoxy-benzyloxy)-benzyl]-1,5,8,12-tetraaza-bicyclo[10.2.2]hexadecane (41)

To **40** (1 g, 1.56 mmol) dissolved in EtOH (50 ml) was added NaBH$_4$ (1.18 g, 31.20 mmol) portionwise. A colour change from yellow to colourless occurred during this addition. The mixture was then left for 2 weeks stirring at RT, before concentrating under reduced pressure. The residual solid was then partitioned between DCM (50 ml) and water (200 ml). The pH of the aqueous layer was adjusted to 14 by the addition of KOH. The organic layer was then collected and dried over MgSO$_4$ before concentrating under reduced pressure. The product was obtained as a yellow oil (0.85 g, 97%); ^{1}H NMR [CDCl$_3$] δ 7.37 (d, 2H, J=8.42 Hz, ArH), 7.32 (s, 1H, ArH), 7.23 (s, 1H, ArH), 6.86 (d, 2H, J=8.42 Hz, ArH), 4.73 (s, 2H, OC$\underline{H}_2$Phen), 3.70 (s, 3H, OMe), 3.65 (s, 2H, NC$\underline{H}_2$Phen), 3.05-2.99 (m, 1H, CH$_2$), 2.78 (br s, 6H, CH$_2$), 2.56-2.35 (m, 12H, CH$_2$), 2.21-1.94 (m, 6H, CH$_2$), 1.37 (s, 9H, ^{t}Bu), 1.29 (s, 9H, ^{t}Bu); ^{13}C NMR [CDCl$_3$] δ 163.56, 159.21, 149.49, 145.88, 135.55, 134.29, 132.75, 130.64, 127.14, 117.83 (C$_{arom}$), 81.47 (OC$\underline{H}_2$Phen), 61.36, 59.44, 58.19, 58.07, 57.79, 57.52, 55.56, 53.64, 52.44, 49.27 (CH$_2$ and OMe), 39.58, 38.71 (C(^{t}Bu)), 35.83, 35.52 (Me(^{t}Bu)), 24.28, 23.01 (CH$_2$C$\underline{H}_2$CH$_2$); MS (ES-MS): *m/z* 566.3 (MH$^+$). CHN not collected.

7.4.15. Synthesis of copper(II) 5-[3,5-di-*tert*-butyl-2-(4-methoxy-benzyloxy)-benzyl]-1,5,8,12-tetraaza-bicyclo[10.2.2]hexadecane perchlorate ([Cu41][(ClO$_4$)$_2$]


To **41** (0.1 g, 0.1773 mmol) dissolved in MeOH (8 ml) was added copper(II) perchlorate hexahydrate (0.657g, 0.1773 mmol) in MeOH (2 ml). The blue solution was heated to reflux for 2 hr before allowing to cool to RT. The solution was then concentrated under reduced pressure before redissolving in the minimal amount of MeOH. This solution was then eluted down a Sephadex LH-20 column with MeOH. The blue fraction was isolated and concentrated under reduced pressure. The oily residue was triturated with ether (3 x 5 ml) to afford the title compound as a blue solid (0.0430 g, 29%); HRMS (ES-MS) expected for C$_{35}$H$_{56}$O$_2$N$_4$CuClO$_4$: 726.3179, found 726.3183; ε (MeOH): 529 nm (154 mol^{-1}dm^{3}cm^{-1}). CHN not collected due to risk of explosion.

7.4.16. Synthesis of nickel(II) 5-[3,5-di-*tert*-butyl-2-(4-methoxy-benzyloxy)-benzyl]-1,5,8,12-tetraaza-bicyclo[10.2.2]hexadecane perchlorate ([Ni41][(ClO₄)₂])

To **41** (0.1 g, 0.1773 mmol) dissolved in MeOH (8 ml) was added nickel(II) hexahydrate (0.0648 g, 0.1773 mmol) in MeOH (2 ml). The orange solution was heated to reflux for 2 hr before allowing to cool to RT. The solution was then concentrated under reduced pressure before redissolving in the minimal amount of MeOH. This solution was then eluted on a Sephadex LH-20 column with MeOH. The orange fraction was isolated and concentrated under reduced pressure. The oily residue was triturated with ether (3 x 5 ml) to afford the title compound as an orange solid (0.0640g, 44%); HRMS (ES-MS) expected for $C_{35}H_{56}O_2N_4NiClO_4$: 721.3236, found 721.3237; ε (MeOH): 478 nm (96 mol⁻¹dm³cm⁻¹). CHN not collected due to risk of explosion.

7.4.17. Synthesis of zinc(II) 5-[3,5-di-*tert*-butyl-2-(4-methoxy-benzyloxy)-benzyl]-1,5,8,12-tetraaza-bicyclo[10.2.2]hexadecane perchlorate ([Zn41][(ClO₄)₂])

To **41** (0.1 g, 0.1773 mmol) dissolved in MeOH (8 ml) was added zinc(II) hexahydrate (0.066 g, 0.1773 mmol) in MeOH (2 ml). The yellow solution was heated to reflux for 2 hr before allowing to cool to RT. The solution was then concentrated under reduced pressure before re-dissolving in the minimal amount of MeOH. This solution was then eluted on a Sephadex LH-20 column with MeOH. The light yellow fraction was isolated and concentrated under reduced pressure. The oily residue was triturated with ether (3 x 5 ml) to afford the title compound as a white solid (0.0720g, 49%); ^{1}H NMR [CD$_3$CN] δ 7.35 (d, 2H, J=8.67 Hz, ArH), 7.29 (s, 1H, ArH), 7.21 (br s, 1H, ArH), 6.86 (d, 2H, J=8.67 Hz, ArH), 4.77 (s, 2H, OC$\underline{H}_2$Phen), 3.69 (s, 3H, OMe), 3.63 (s, 2H, NC$\underline{H}_2$Phen), 3.11-3.01 (m, 1H, CH$_2$), 2.78 (br s, 6H, CH$_2$), 2.56-1.92 (m, 18H, CH$_2$), 1.34 (s, 9H, ^{t}Bu), 1.26 (s, 9H, ^{t}Bu); ^{13}C NMR [CDCl$_3$] δ 164.01, 158.87, 149.24, 146.13, 135.77, 134.34, 132.68, 130.23, 127.35, 117.57 (C$_{arom}$), 81.51 (OC$\underline{H}_2$Phen), 60.49, 59.29, 58.23, 58.01, 57.81, 56.26, 55.78, 54.57, 52.81, 49.37 (CH$_2$ and OMe), 39.46, 38.58 (C(^{t}Bu)), 35.71, 35.46 (Me(^{t}Bu)), 24.67, 23.19 (CH$_2$C$\underline{H}_2$CH$_2$); HRMS (ES) expected for C$_{34}$H$_{54}$O$_2$N$_4$ZnO$_4$Cl: 713.3804, found 713.3807. CHN not collected due to risk of explosion.

7.4.18. Synthesis of 3a-(2-acetoxy-3,5-di-*tert*-butyl-benzyl)-decahydro-5a,8a,10a-triaza-3a-azonia-pyrene bromide (42)

33 (1.36 g, 6.13 mmol) and **15** (2.09 g, 6.13 mmol) were dissolved in dry MeCN (15 ml) and stirred at RT for 3 days. After this period, the reaction mixture was concentrated under reduced pressure and the residue taken up in to diethyl ether (40 ml). A white solid formed which was collected by filtration (2.60 g, 75%); ^{1}H NMR [CD$_3$OD] δ 7.70 (d, 1H, J=2.52 Hz, ArH), 7.48 (br s, 1H, ArH), 4.85 (s, 2H, NC$\underline{H}_2$Ph), 4.30 (br s, 2H, CH$_2$), 3.65-3.59 (m, 2H, CH$_2$), 3.15-2.96 (br m, 8H, CH$_2$), 2.69-2.47 (m, 6H, CH$_2$), 2.38-2.25 (m, 4H, CH$_2$), 2.02 (s, 3H, COMe), 1.23 (s, 9H, ^{t}Bu), 1.22 (s, 9H, ^{t}Bu); ^{13}C NMR [CD$_3$OD] δ 170.53 (CO), 149.69, 147.94, 143.19, 128.38, 120.87, 117.15 (C$_{arom}$), 70.84 (NC$\underline{H}$N), 59.71 (NC$\underline{H}_2$Ph), 54.83, 54.56, 52.66, 52.53, 42.90 (CH$_2$), 35.29, 34.85 (C(^{t}Bu)), 30.71, 30.15 (Me(^{t}Bu)), 21.35 (COO$\underline{Me}$), 19.32, 19.16 (CH$_2$C$\underline{H}_2$CH$_2$); MS (ES-MS): *m/z* 483.3 (M$^+$). CHN not satisfactory.

7.4.19. Synthesis of acetic acid 2,4-di-*tert*-butyl-6-(1,5,8,12-tetraaza-bicyclo[10.2.2]hexadec-5-ylmethyl)phenyl ester (43)

42 (2.6 g, 4.62 mmol) was dissolved in ethanol (150 ml) to which was added NaBH$_4$ (3.51 g, 92.4 mmol) portion wise. The reaction mixture was stirred at RT o/n at which time hydrogen evolution had ceased. The reaction mixture was then concentrated under reduced pressure and the residue partitioned between DCM (100 ml) and water (250 ml). The pH of the aqueous layer was then adjusted to 14 with the addition of KOH. The organic layer was then collected and dried over MgSO$_4$. The filtrate was then concentrated under reduced pressure before dissolving in the minimal amount of acetone (~10 ml) which was triturated with pentane (150 ml) to give a cream solid which was collected by filtration (2.20 g, 98%); ^{1}H NMR [CDCl$_3$] δ 7.37 (d, 2H, J=2.50 Hz, ArH), 7.24 (d, 2H, J=2.50 Hz, ArH), 5.23 (s, 2H, CH$_2$), 3.33-2.37 (m, 28H, CH$_2$ and NH), 2.25 (s, 3H, COOMe), 1.27 (s, 9H, ^{t}Bu), 1.25 (s, 9H, ^{t}Bu); ^{13}C NMR [CDCl$_3$] δ 166.07 (<u>C</u>O), 144.12, 142.26, 136.81, 127.90, 122.03, 119.27 (C$_{arom}$), 53.80, 53.39, 51.38, 49.94, 48.25, 47.86, 46.99, 45.95, 45.47, 44.78, 43.52 (CH$_2$), 31.16, 31.05 (C(^{t}Bu)), 27.74, 26.78 (Me(^{t}Bu)), 23.09, 22.78, (CH$_2$<u>CH$_2$</u>CH$_2$), 20.83 (COO<u>Me</u>); HRMS (ES-MS) expected for C$_{29}$H$_{50}$N$_4$O$_2$H: 487.4007, found 487.3996. CHN not satisfactory.

7.4.20. Synthesis of 2,4-di-*tert*-butyl-6-(1,5,8,12-tetraaza-bicyclo[10.2.2]hexadec-5-ylmethyl)-phenol hydrochloride salt (37)

To **43** (1.5 g, 3.09 mmol) dissolved in MeOH (10 ml) was added 6M HCl(aq) (10 ml). This induced a colour change from yellow to colourless. The solution was then heated to reflux for 24 hr before cooling to room temperature. The solution was concentrated under reduced pressure, and the addition of acetone (30 ml) caused a yellow precipitate to form. This was collected by filtration and dried in vacuo (1.44 g, 79%); ^{1}H NMR [D$_2$O] δ 7.24 (s, 1H, ArH), 7.16 (s, 1H, ArH), 3.40-3.14 (m, 15H, CH$_2$ and NH), 2.02-1.80 (m, 10H, CH$_2$), 1.11 (s, 9H, ^{t}Bu), 1.01 (s, 9H, ^{t}Bu); ^{13}C NMR [D$_2$O] δ 151.65, 144.37, 140.08, 127.67, 125.56, 120.51 (C$_{arom}$), 74.31 (N$\underline{C}$H$_2$Phen), 49.16, 48.81, 48.18, 47.97, 47.76, 46.83, 45.95 (CH$_2$), 34.55, 33.92 (C(^{t}Bu)), 30.67, 29.47 (Me(^{t}Bu)), 21.49, 20.72 (CH$_2$$\underline{C}H_2CH_2$); HRMS (ES-MS) expected for C$_{27}$H$_{48}$N$_4$OH: 445.3901, found 445.3891. CHN not collected.
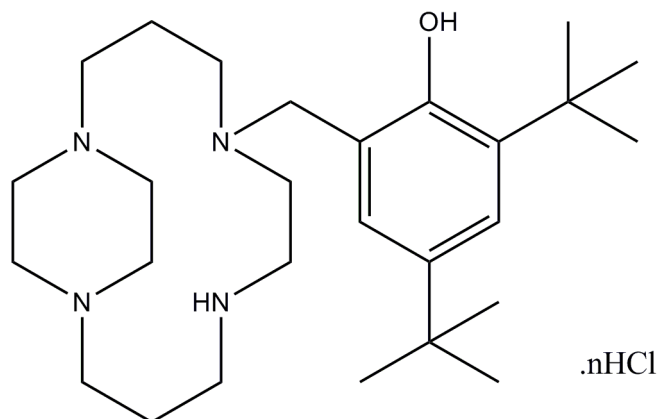
7.4.21. Synthesis of copper(II) 2,4-di-*tert*-butyl-6-(1,5,8,12-tetraaza-bicyclo[10.2.2]hexadec-5-ylmethyl)-phenolate perchlorate ([Cu37]ClO$_4$)
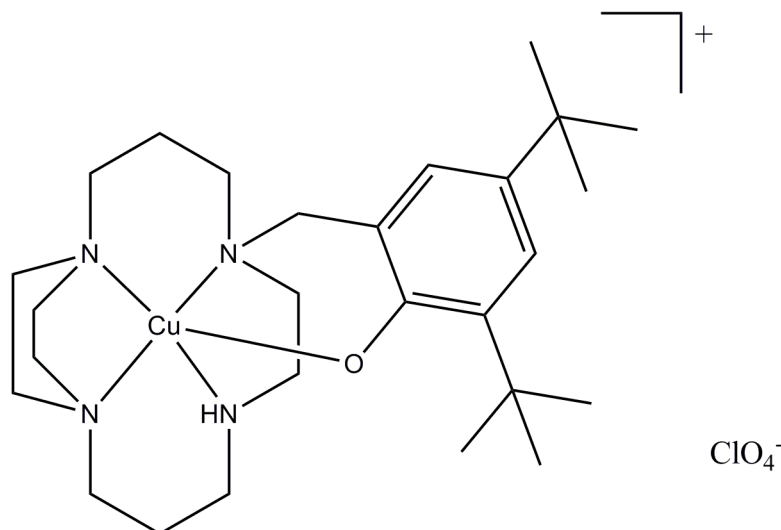
To **37** (180 mg, 0.305 mmol) in MeOH (8 ml) was added NEt$_3$ (150 mg, 1.5 mmol). The reaction mixture was stirred for 5 min, by which time the colour of the solution had changed from yellow to straw colour. To this solution was then added copper(II) perchlorate hexahydrate (113 mg, 0.305 mmol) in MeOH (3 ml). The royal blue solution was then heated to reflux for 2 hr before allowing to cool. The reaction mixture was concentrated under reduced pressure to the minimal volume before eluting down a Sephadex LH-20 column using MeOH. The blue fraction was collected and concentrated under reduced pressure. The oil obtained was triturated with ether (3 x 5 ml) to give a hygroscopic blue solid (0.0737 g, 40%); HRMS (ES-MS) expected for (cation-2H)$^+$ C$_{27}$H$_{45}$N$_4$O$_1$Cu$_1$: 504.2884 found 504.2875; ε (MeOH): 641 nm (27 mol^{-1}dm^{3}cm^{-1}). CHN not collected due to risk of explosion.

7.4.22. Synthesis of nickel(II) 2,4-di-*tert*-butyl-6-(1,5,8,12-tetraaza-bicyclo[10.2.2]hexadec-5-ylmethyl)-phenolate perchlorate ([Ni37]ClO$_4$)
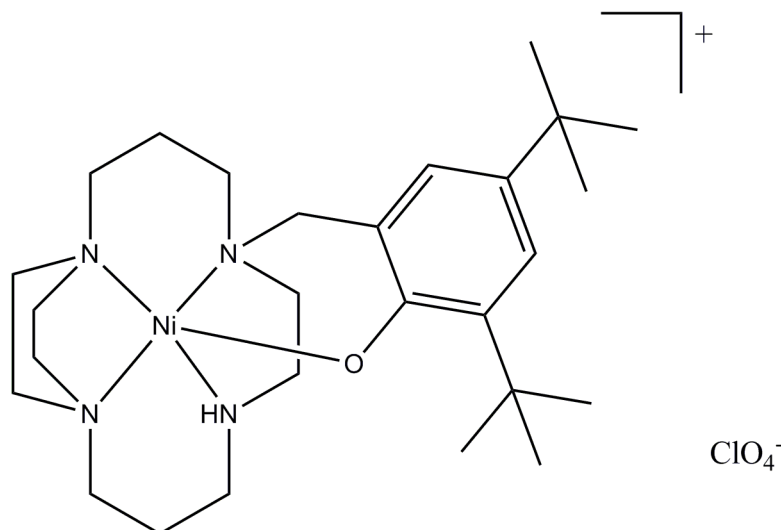
To **37** (180 mg, 0.305 mmol) in MeOH (8 ml) was added NEt$_3$ (150 mg, 1.5 mmol). The reaction mixture was stirred for 5 min, by which time the colour of the solution had changed from yellow to straw colour. To this solution was then added nickel(II) perchlorate hexahydrate (112 mg, 0.305 mmol) in MeOH (3 ml). The orange solution was then heated to reflux for 2 hr before allowing to cool. The reaction mixture was concentrated under reduced pressure to the minimal volume before eluting down a Sephadex LH-20 column using MeOH. The orange fraction was collected and concentrated under reduced pressure. The oil obtained was triturated with ether (3 x 5 ml) to give a hygroscopic orange solid (0.0541 g, 30%); HRMS (ES) expected for C$_{27}$H$_{47}$N$_4$ONi: 501.3098, found 501.3093; ε (MeOH): 441 nm (12 mol^{-1}dm^{3}cm^{-1}). CHN not collected due to risk of explosion.

7.4.23. Synthesis of zinc(II) 2,4-di-*tert*-butyl-6-(1,5,8,12-tetraaza-bicyclo[10.2.2]hexadec-5-ylmethyl)-phenolate perchlorate ([Zn37]ClO₄)
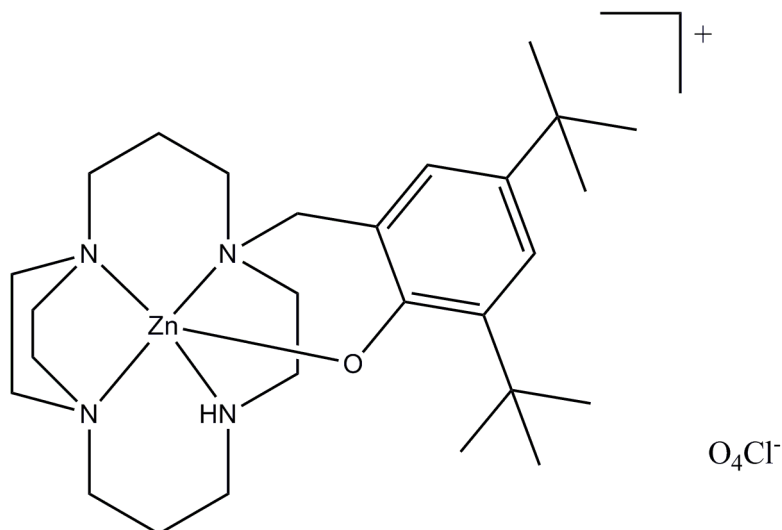
To **37** (180 mg, 0.305 mmol) in MeOH (8 ml) was added NEt₃ (150 mg, 1.5 mmol). The reaction mixture was stirred for 5 min, by which time the colour of the solution had changed from yellow to straw colour. To this solution was then added zinc(II) perchlorate hexahydrate (113 mg, 0.305 mmol) in MeOH (3 ml). The straw coloured solution was then heated to reflux for 2 hr before allowing to cool. The reaction mixture was concentrated under reduced pressure to the minimal volume before eluting down a Sephadex LH-20 column using MeOH as the eluent. The yellow fraction was collected and concentrated under reduced pressure. The oil obtained was triturated with ether (3 x 5 ml) to give a hygroscopic white solid (0.0530 g, 29%); ^{1}H NMR [CD₃CN] δ 7.63 (s, 1H, ArH), 7.53 (s, 1H, ArH), 4.10-4.09 (m, 2H, C$\underline{H}_2$Ph), 3.26-2.09 (m, 25H, NH and CH₂), 1.31 (s, 9H, ^{t}Bu), 1.22 (s, 9H, ^{t}Bu); ^{13}C NMR [CD₃CN] δ 152.43, 138.58, 138.03, 136.39, 132.56, 129.65 (C$_{arom}$), 68.76 (CH₂Ph), 51.17, 50.35, 48.26, 48.21, 48.18, 48.11, 47.93 (CH₂), 31.57, 31.03 (C(^{t}Bu)), 30.30, 29.94 (Me(^{t}Bu)); HRMS (ES) expected for C₂₇H₄₇N₄OZn: 507.3036, found 507.3036. CHN not collected due to risk of explosion.

7.4.24. Synthesis of *N*-2-(4-methoxybenzylsulphonyl)-benzyl-*cis* 3a,5a,8a,10a-tetraazaperhydropyrene (44)
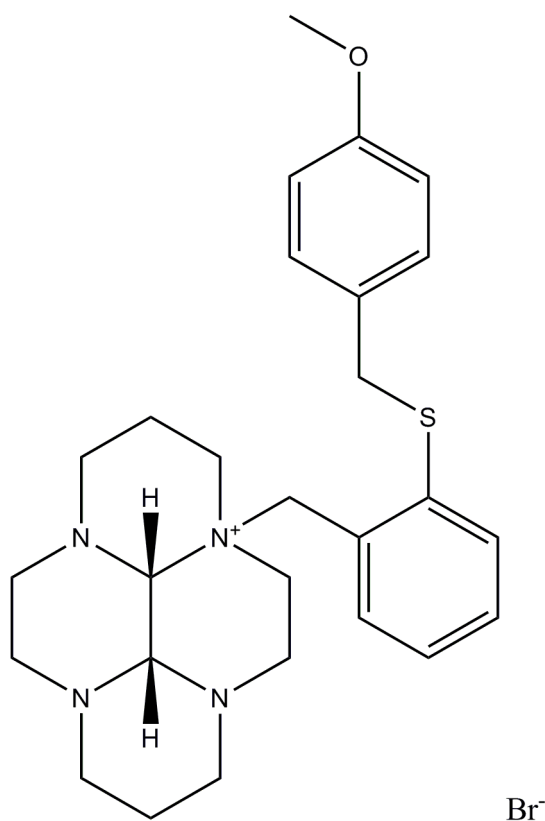
33 (0.2 g, 0.901 mmol) and **18** (290 mg, 0.901 mmol) were dissolved in dry MeCN (20 ml). The resulting yellow solution was then stirred at RT for 1 week before removing the solvent in vacuo and washing with ether (30 ml). The solid formed by this process was then further washed with ether (2 x 30 ml) to give the desired product as a yellow solid (0.46 g, 94%); ^{1}H NMR [CDCl$_3$] δ 7.83 (d, 1H, J=7.8 Hz, ArH), 7.56 (t, 1H, J=7.6 Hz, ArH), 7.43 (t, 1H, J=7.6 Hz, ArH), 7.36 (d, 1H, J=7.8 Hz, ArH), 6.93 (d, 2H, J=8.6 Hz, Ar), 6.83 (d, 2H, J=8.6 Hz, Ar), 4.30-3.93 (m, 6H, CH$_2$), 3.76 (s, 3H, OMe), 3.03-2.89 (m, 14H, CH$_2$), 2.44-2.37 (m, 4H, CH$_2$), 2.11-2.08 (m, 2H, CH$_2$); ^{13}C NMR [CDCl$_3$] δ 158.45, 137.74, 136.74, 134.30, 132.25, 130.70, 130.47, 130.03, 129.25, 114.35 (C$_{arom}$), 82.50, 75.56 (NC$\underline{H}$N), 59.76 (OMe), 59.25, 55.63, 54.36, 53.35, 51.89, 51.60, 49.75, 46.79 (CH$_2$), 40.92 (SCH$_2$), 18.46, 18.15 (NCH$_2$C$\underline{H_2}$CH$_2$N); MS (ES-MS): *m/z* 465.3 (M$^+$), 224 ((macrocycle)$^+$). CHN not collected.

7.4.25. Synthesis of 5-(2-(4-methoxybenzylthio)benzyl)-1,5,8,12-tetraazabicyclo[10.2.2]hexadecane (45)
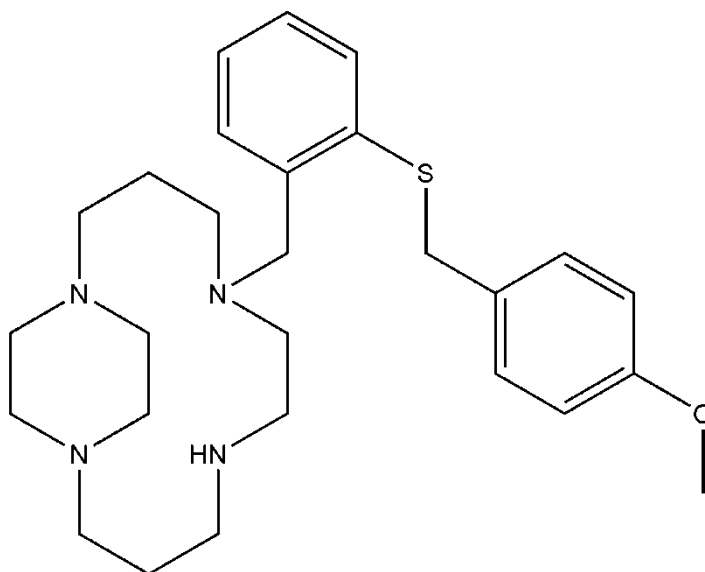
To **44** (0.2 g, 0.367 mmol) dissolved in MeOH (40 ml) was added $NaBH_4$ (280 mg, 7.368 mmol) portionwise. The solution was then stirred at RT for a week before removing the solvent in vacuo. The residue was taken up into DCM (100 ml) and washed with $KOH_{(aq)}$ (pH 14, 200 ml). The organic layer was collected, dried and evaporated to dryness to afford **45** as a light yellow oil (0.14 g, 82%); ^{1}H NMR [CDCl$_3$] δ 7.38-7.08 (m, 6H, ArH), 6.77-6.69 (m, 2H, ArH), 5.23 (s, 2H, CH$_2$), 4.04-3.32 (m, 13H, CH$_2$ and OMe), 3.03-2.74 (m, 8H, CH$_2$), 2.55-1.93 (m, 8H, CH$_2$); ^{13}C NMR [CDCl$_3$] δ 159.20, 137.32, 131.38, 130.37, 130.24, 128.73, 128.68, 125.92, 114.04, 113.82 (C$_{arom}$), 67.58, 59.46 (CH$_2$), 57.89 (NCH$_2$Ph), 56.50 (OMe), 55.57, 55.39, 50.28, 50.18, 48.24, 47.17 (CH$_2$), 38.44 (SCH$_2$), 19.66, 18.51 (NCH$_2$CH$_2$CH$_2$N); MS (ES-MS): *m/z* 469.4 (MH$^+$). CHN not collected.

7.4.26. Synthesis of 2-(1,5,8,12-tetraazabicyclo[10.2.2]hexadecane-5-ylmethyl)benzenethiol (46)
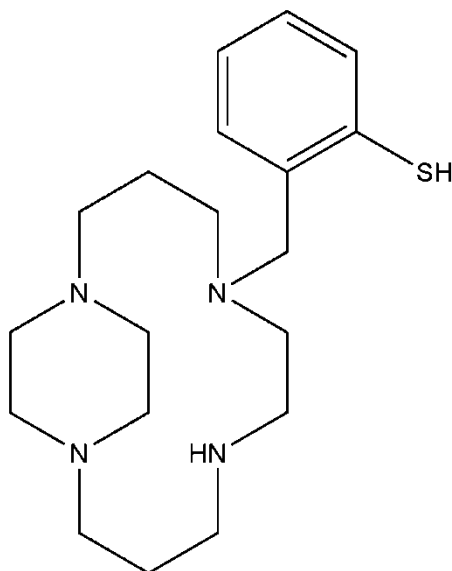
To **45** (0.14 g, 0.299 mmol) dissolved in methanol (10 ml) was added mercury acetate (0.19 g, 0.598 mmol) in methanol (5 ml). The suspension was then heated to 60°C for 14 hr. After this period a white precipitate had formed and the solvent was removed under reduced pressure. The white powder obtained was washed with pentane (2 x 10 ml) and then redissolved in methanol (20 ml). The solution was bubbled with nitrogen for 10 min followed by passing hydrogen sulphide through the solution for 20 min. The solution was then bubbled with nitrogen for a further 30 min. The black mercury sulphide was filtered off and the yellow solution was concentrated in vacuo. The crude product was used without further purification and used immediately for complexation reactions (100 mg, 93%). CHN not collected.

7.4.27. Synthesis of nickel(II) 2-(1,5,8,12-tetraazabicyclo[10.2.2]hexadecane-5-ylmethyl)benzenethiol perchlorate ([Ni46]ClO₄)
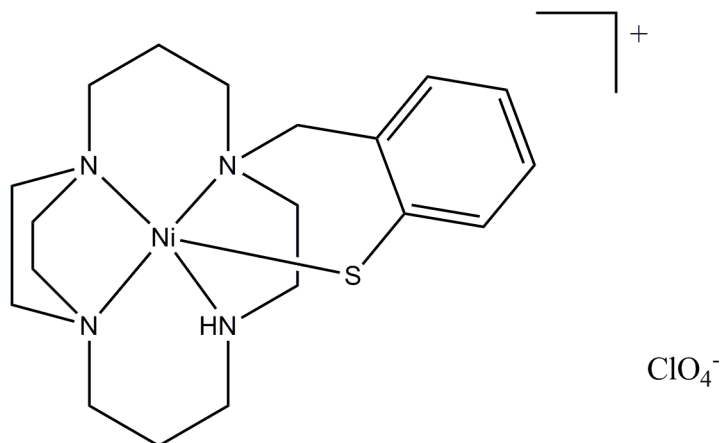
46 (0.034 g, 0.0996 mmol) was dissolved in degassed methanol (5 ml) to which was added [Ni(ClO$_4$)$_2$].6H$_2$O (0.05 g, 0.1296 mmol) in degassed methanol (2 ml) with stirring. The clear solution was heated to reflux under argon for 2 hr and then stirred at RT for 14 hr. The solution was removed in vacuo and the brown solid redissolved in acetone (2 ml). This was then passed down a short Sephadex LH-20 column, eluting with acetone to remove remaining inorganic salts, and the eluent concentrated in vacuo. This gave the product as a brown powder (37 mg, 92%); HRMS (ES-MS) expected for Ni$_1$C$_{19}$N$_4$S$_1$H$_{33}$: 405.1617, found 405.1610, ε (acetone): 367 nm (149 mol^{-1}dm^{3}cm^{-1}), 464 nm (68 mol^{-1} dm^3 cm^{-1}). CHN not collected due to risk of explosion.

7.4.28. Synthesis of zinc(II) 2-(1,5,8,12-tetraazabicyclo[10.2.2]hexadecane-5-ylmethyl)benzenethiol perchlorate ([Zn46]ClO$_4$)
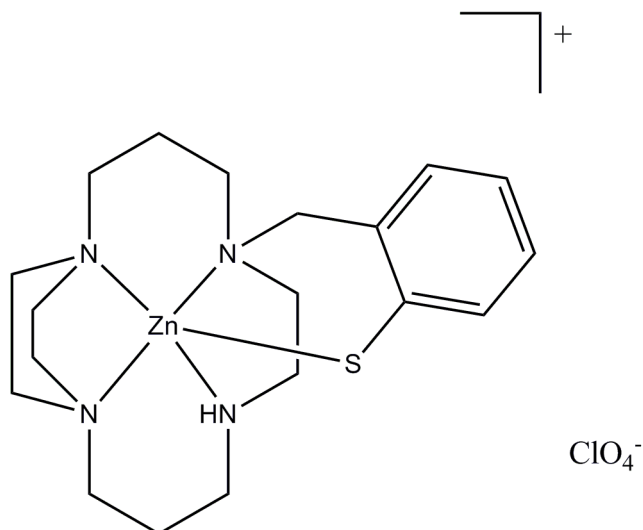
46 (0.034 g, 0.0996 mmol) was dissolved in degassed methanol (5 ml) to which was added [Zn(ClO$_4$)$_2$].8H$_2$O (0.05 g, 0.1295 mmol) in degassed methanol (1 ml) with stirring. The clear solution was then heated to reflux under argon for 2 hr and then stirred at RT for 14 hr. The solution was then removed in vacuo and the white solid redissolved in acetone (2ml). This was passed down a short Sephadex LH-20 column, eluting with acetone to remove remaining inorganic salts, and the eluent concentrated in vacuo. This gave the product as a white powder (20 mg, 50%); ^{1}H NMR [CDCl$_3$] δ 7.05-6.80 (m, 4H, Ar), 3.91-2.17 (m, 27H, CH$_2$ and NH); ^{13}C NMR [CDCl$_3$] δ 134.74, 132.43, 130.84, 128.52, 123.14, 114.17 (C$_{arom}$), 67.94, 60.79 (CH$_2$), 58.49 (NCH$_2$Ph), 56.64, 55.87, 54.02, 53.71, 53.64, 53.10, 51.49, 50.49 (CH$_2$), 24.11 (NCH$_2$CH$_2$CH$_2$N); HRMS (ES-MS) expected for Zn$_1$C$_{19}$N$_4$S$_1$H$_{33}$: 411.1554, found 411.1555. CHN not collected due to risk of explosion.

7.4.29. Synthesis of 3a-[3,5-di-*tert*-butyl-2-(4-methoxy-benzylsulfanyl)-benzyl-decahyro-5a, 8a, 10a-triaaza-3a-azonia-pyrene bromide (47)
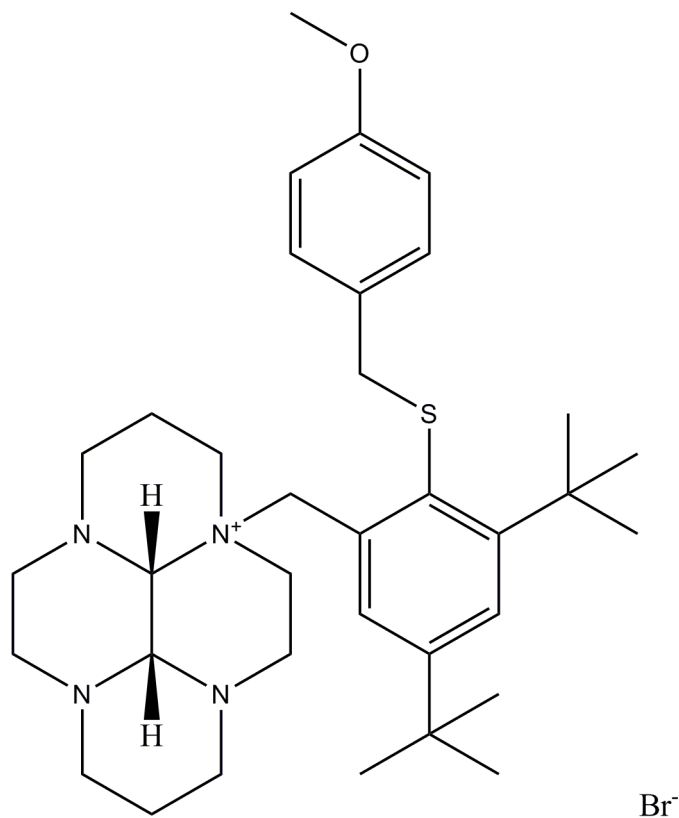
33 (0.39 g, 1.77 mmol) and **24** (0.72 g, 1.77 mmol) were dissolved in dry MeCN (15 ml) and stirred at RT for 3 days. After this period of time a precipitate had formed. The mixture was concentrated under reduced pressure, before suspending in ether. The yellow/ cream solid was then collected by filtration and washed repeatedly with ether (4 x 5 ml) to afford the title compound (1.10g, 95%); ^{1}H NMR [D$_2$O] δ 7.58 (br s, 1H, ArH), 7.27 (br s, 4H, ArH), 6.73 (br s, 1H, ArH), 4.21 (s, 2H, NCH$_2$Ph), 3.56-1.98 (m, 27H, CH$_2$, NC<u>H</u>N and OMe), 1.39 (s, 9H, ^{t}Bu), 1.20 (s, 9H, ^{t}Bu); ^{13}C NMR [D$_2$O] δ 169.64, 158.97, 152.74, 136.89, 133.04, 131.35, 127.69, 125.79, 125.01, 114.33 (C$_{arom}$), 83.15, 75.71 (NC<u>H</u>N), 69.88 (NC<u>H$_2$</u>Phen), 63.09, 60.18 (CH$_2$), 55.77 (OMe), 54.20, 52.99, 52.22, 51.31, 48.09, 46.75, 43.71, 42.13 (CH$_2$), 37.91 (SC<u>H$_2$</u>Phen), 34.85, 34.63 (C(^{t}Bu)), 31.74, 30.74 (Me(^{t}Bu)), 18.81, 18.19 (CH$_2$C<u>H$_2$</u>CH$_2$); MS (ES-MS): *m/z* 577 (M$^+$), 222 ((macrocycle)$^+$). CHN not satisfactory.

7.4.30. Synthesis of 5-[3,5-di-*tert*-butyl-2-(4-methoxy-benzylsulfanyl)-benzyl]-1,5,8,12-tetraaza-bicyclo[10.2.2]hexadecane (48)
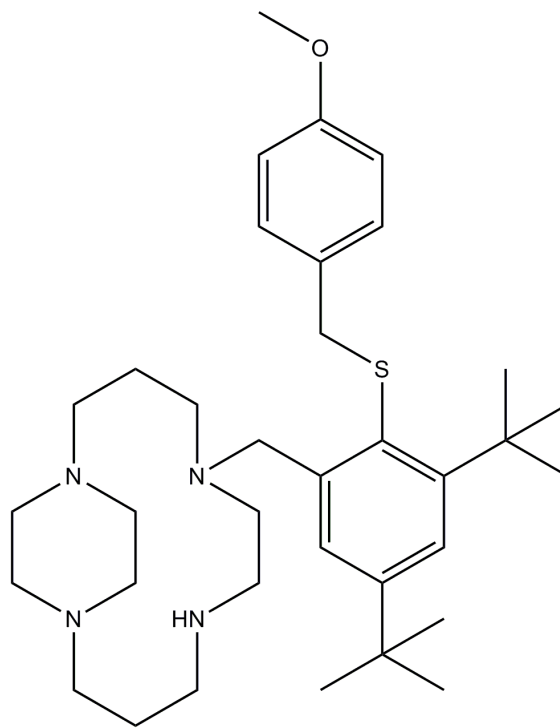
To **47** (1.10 g, 16 .7 mmol) dissolved in MeOH (50 ml) was added NaBH$_4$ (1.34 g, 35.3 mmol) portion wise with stirring. Stirring continued for 5 days before concentrating under reduced pressure. The residue was then partitioned between DCM (100 ml) and water (200 ml). The pH of the aqueous layer was adjusted to 14 by addition of KOH. The organic layer was separated and dried over MgSO$_4$. The solid was then removed by filtration and the filtrate concentrated in vacuo to afford a yellow oil (0.52 g, 49%); ^{1}H NMR [CDCl$_3$] δ 7.68 (d, 1H, J=2.02 Hz, ArH), 7.61 (d, 1H, J=2.02 Hz, ArH), 7.38 (d, 2H, J=8.76 Hz, ArH), 7.03 (d, 2H, J=8.76 Hz, ArH), 3.98 (s, 2H, SCH$_2$Phen), 3.87 (s, 3H, OMe), 3.46-3.13 (m, 8H, CH$_2$), 2.87-2.73 (m, 12H, CH$_2$), 2.46-2.36 (m, 5H, CH$_2$), 1.99-1.89 (m, 2H, CH$_2$), ^{13}C NMR [CDCl$_3$] δ 158.52, 152.77, 149.98, 144.34, 135.80, 130.52, 125.40, 122.48, 120.41, 113.58 (C$_{arom}$), 56.63 (NCH$_2$Phen), 56.26 (OMe), 54.72, 54.10, 53.39, 53.12, 50.88, 49.88, 47.92, 47.77 (CH$_2$), 37.34 (SCH$_2$Phen), 34.49, 34.34 (C(^{t}Bu)), 31.37, 31.23 (Me(^{t}Bu)), 26.03, 23.43 (CH$_2$CH$_2$CH$_2$); HRMS (ES-MS) expected for C$_{35}$H$_{57}$O$_1$N$_4$S$_1$: 581.4248 found 581.4248. CHN not satisfactory.

7.4.31. Synthesis of 2,4-di-*tert*-butyl-6-(1,5,8,12-tetraaza-bicyclo[10.2.2]hexadec-5-ylmethyl-benzenethiol (49)
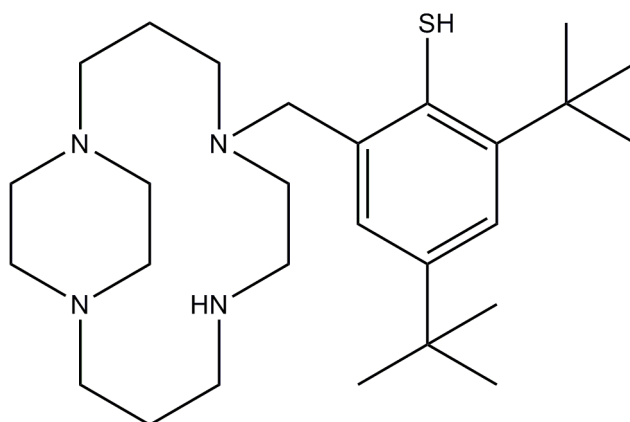
To **48** (0.40 g, 0.69 mmol) dissolved in MeOH (7 ml) was added Hg(OAc)$_2$ (0.44 g, 1.38 mmol). The solution was then heated to 60°C o/n before allowing to cool. The mixture was then concentrated under reduced pressure and the resulting white solid washed twice with pentane (2 x 10 ml). The solid was then redissolved in MeOH (10 ml) and the solution purged with nitrogen for 10 min. H$_2$S was then bubbled through the solution for 20 min before re-purging the solution with nitrogen again for 1 hr. The black HgS was then filtered off using a bed of celite, which was washed with degassed MeOH (20 ml). The filtrate was concentrated affording a dark yellow oil (0.31 g, 97%). This was used without any further purification for the immediate preparation of the metal complexes. HRMS (ES-MS) expected for C$_{27}$H$_{48}$N$_4$H: 429.3952 found 429.3944 (M-S$^+$). CHN not collected to likelihood of oxidising thiolphenol group.

7.4.32. Synthesis of copper(II) 2,4-di-*tert*-butyl-6-(1,5,8,12-tetraaza-bicyclo[10.2.2]hexadec-5-ylmethyl-benzenethiolate perchlorate ([Cu49]ClO₄)
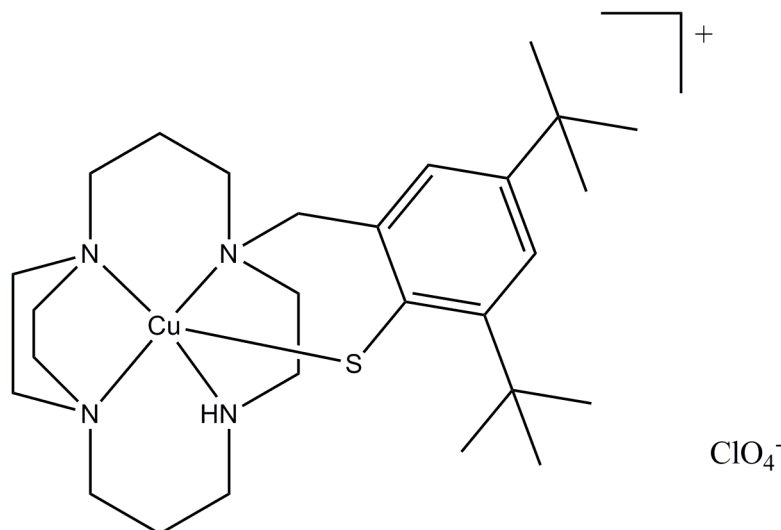

To **49** (0.06 g, 0.13 mmol) dissolved in degassed MeOH (8 ml) under a nitrogen atmosphere was added NEt₃ (50 μl) at RT with stirring. After 5 min, a solution of copper(II) perchlorate hexahydrate (0.05 g, 0.13 mmol) in degassed MeOH (3 ml) was added. This resulted in an instant violet colour forming in solution. The solution was then heated to reflux for 1.5 hr before allowing to cool. The solution was reduced in volume under reduced pressure before eluting down a Sephadex LH-20 column with MeOH. The blue fraction was collected and concentrated under reduced pressure to give a blue powder (0.0563g, 70%); HRMS (ES-MS) expected for $C_{27}H_{47}N_4SCu$: 522.2812, found 522.2815; ε (MeOH): 550 nm (185 mol⁻¹dm³cm⁻¹). CHN not collected due to risk of explosion.

7.4.33.   Synthesis of nickel(II) 2,4-di-*tert*-butyl-6-(1,5,8,12-tetraaza-bicyclo[10.2.2]hexadec-5-ylmethyl-benzenethiolate perchlorate ([Ni49]ClO₄)
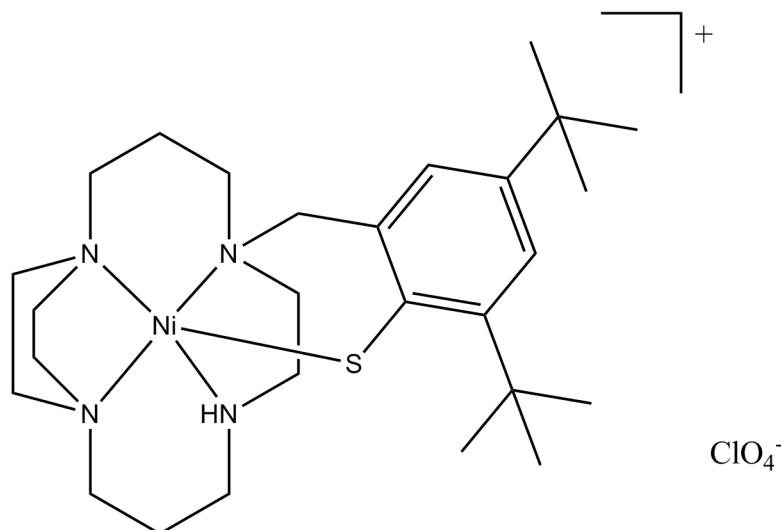
To **49** (0.06 g, 0.13 mmol) dissolved in degassed MeOH (8 ml) under a nitrogen atmosphere was added NEt₃ (50 µl) at RT with stirring. After 5 min, a solution of nickel(II) perchlorate hexahydrate (0.049 g, 0.13 mmol) in degassed MeOH (3 ml) was added. This resulted in an instant yellow colour forming in solution. The solution was then heated to reflux for 1.5 hr before allowing to cool. The solution was reduced in volume under reduced pressure before eluting down a Sephadex LH-20 column with MeOH. The orange fraction was collected and concentrated under reduced pressure to give a orange powder (0.0765g, 94%); HRMS (ES-MS) expected for $C_{27}H_{47}N_4SNi$: 517.2869, found 517.2859; ε (MeOH): 550 (91 mol⁻¹ dm³ cm⁻¹). CHN not collected due to risk of explosion.

7.4.34. Synthesis of zinc(II) 2,4-di-*tert*-butyl-6-(1,5,8,12-tetraaza-bicyclo[10.2.2]hexadec-5-ylmethyl-benzenethiolate perchlorate ([Zn49]ClO$_4$)
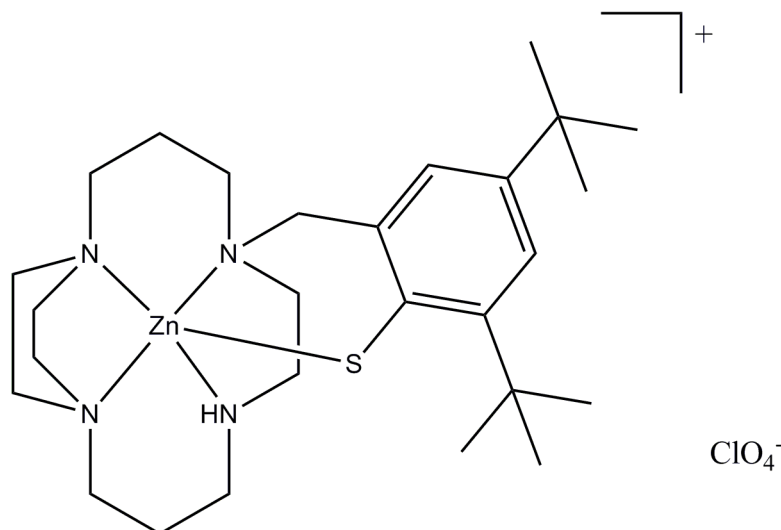
To **49** (0.06 g, 0.13 mmol) dissolved in degassed MeOH (8 ml) under a nitrogen atmosphere was added NEt$_3$ (50 μl) at RT with stirring. After 5 min, zinc(II) perchlorate hexahydrate (0.047 g, 0.13 mmol) in degassed MeOH (3 ml) was added. This resulted in an instant yellow colour forming in solution. The solution was then heated to reflux for 1.5 hr before allowing to cool. The solution was reduced in volume under reduced pressure before eluting down a Sephadex LH-20 column, eluting with MeOH. The light yellow fraction was collected and concentrated under reduced pressure to give a white powder (0.0705g, 87%); ^{1}H NMR [CD$_3$CN] 7.43 (s, 1H, ArH), 7.05 (s, 1H, ArH), 4.11 (s, 2H, NCH$_2$Ph), 3.79-3.27 (m, 6H, CH$_2$), 2.98-2.04 (m, 13H, CH$_2$ and NH), 1.94-1.54 (m, 6H, CH$_2$), 1.29 (s, 9H, ^{t}Bu), 1.24 (s, 9H, ^{t}Bu); ^{13}C NMR [CD$_3$CN] δ 131.39, 130.86, 129.40, 128.48, 125.42, 124.96 (C$_{arom}$), 58.86 (CH$_2$), 57.50 (NCH$_2$Ph), 53.17, 52.42, 50.41, 48.77, 47.16, 45.51 (CH$_2$), 35.63, 35.42 (C(^{t}Bu)), 31.75, 31.64 (Me(^{t}Bu)), 25.30, 22.28 (CH$_2$CH$_2$CH$_2$); HRMS (ES-MS) expected for C$_{27}$H$_{47}$N$_4$SZn: 523.2807, found 523.2798. CHN not collected due to risk of explosion.

7.5. Cyclen compounds and complexes

7.5.1. Synthesis of 1,4,7,tris(*tert*-butoxycarboxymethyl)-1,4,7,10-tetraazacyclododecane (DO3A-TB)
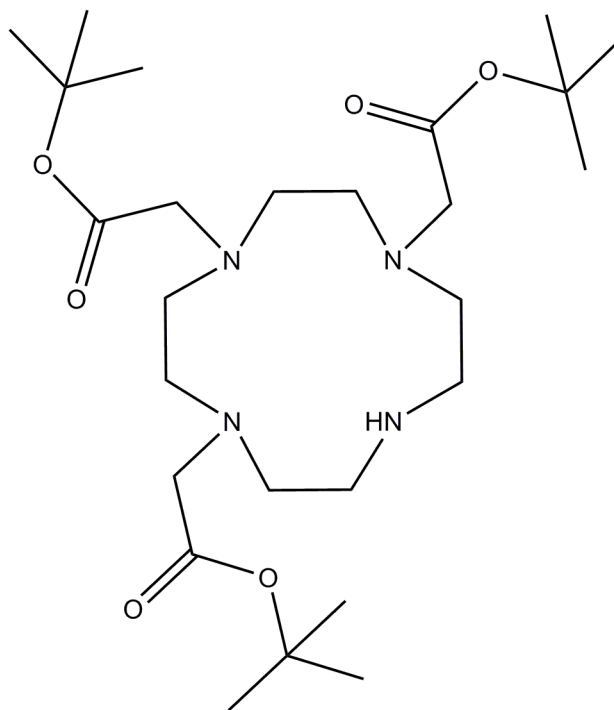
Cyclen (3.07 g, 0.0178 mol) and $NaHCO_3$ (4.49 g, 0.0535 mol) was dissolved in MeCN (900 ml) to which was added *tert*-butylbromoacetate (10.43 g, 0.0535 mol) in MeCN (300 ml) over 5 hours at RT with vigorous stirring. Stirring was then continued for a further 72 hr. The solution was then filtered and the filtrate concentrated under reduced pressure. The crude mixture was then purified via silica column chromatography using DCM rising to 2% MeOH in DCM. The fractions containing the desired product were combined and concentrated under reduced pressure. This gave DO3A-TB as a cream solid (5.22 g, 57%); R_f=0.2 (2% MeOH in DCM); ^{1}H NMR [CDCl$_3$] δ 3.29 (4H, N$\underline{CH_2}$COO^{t}Bu) 3.20 (s, 2H, N$\underline{CH_2}$COO^{t}Bu), 3.01 (s, 4H, $\underline{CH_2}$NH$\underline{CH_2}$), 2.83 (m, 12H, N$\underline{CH_2CH_2}$N); ^{13}C NMR [CDCl$_3$] δ 170.35, 169.46 ($\underline{C}$OO^{t}Bu), 81.63, 81.47 (C(^{t}Bu)), 57.98, 51.15, 49.01, 47.33 (CH$_2$), 28.05, 28.01 (CH$_3$(^{t}Bu)); MS (ES-MS): *m/z* 515 (MH$^+$). CHN not collected.

7.5.2. Synthesis of 2-((1,4,7,10-tetraazacyclodecane-1-yl)methyl)-4,6-di-*tert*-butylphenyl acetate (50)
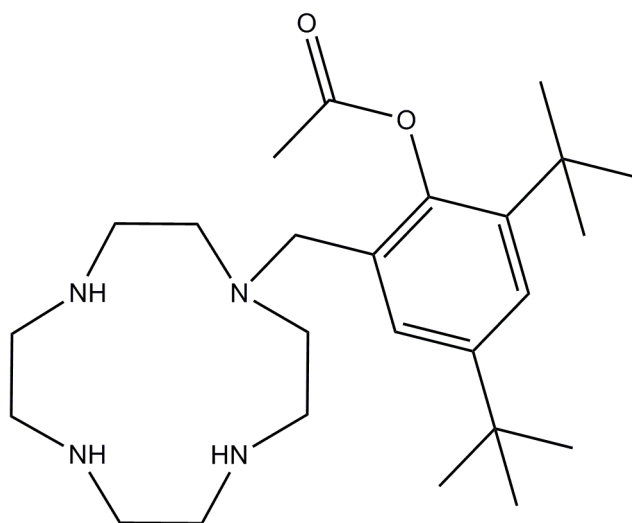
Cyclen (5 g, 0.0289 mol) and NEt$_3$ (0.88 g, 8.72 mmol) were dissolved in CHCl$_3$ (80 ml). To this solution was added **15** (2.48 g, 7.3 mmol). The yellow solution was heated to a gentle reflux for 16 hr. At this point, TLC analysis showed complete consumption of the starting material. The solution was then washed with 1M NaOH (4 x 100 ml) before the organic layer was collected and dried over MgSO$_4$. The solution was then filtered and the filtrate concentrated under reduced pressure. The yellow oil obtained was then triturated with pentane (50 ml) affording a yellow solid (2.78 g, 89% based on starting moles of **15**); ^{1}H NMR [CDCl$_3$] δ 7.40 (d, 1H, J=2.10 Hz, ArH), 7.20 (d, 1H, J=2.10 Hz, ArH), 2.75-2.36 (m, 18H, CH$_2$), 2.29 (s, 3H, OMe), 1.25 (s, 9H, ^{t}Bu), 1.24 (s, 9H, ^{t}Bu); ^{13}C NMR [CDCl$_3$] 169.63 (<u>C</u>OAc), 147.73, 145.45, 139.89, 131.52, 125.46, 123.03 (C$_{arom}$), 54.14 (NCH$_2$Ph), 47.04, 46.44, 46.24, 45.10 (CH$_2$), 34.74, 34.63 (C(^{t}Bu)), 31.42, 30.51 (Me(^{t}Bu)), 21.47 (COO<u>Me</u>); MS (ES-MS): *m/z*= 433.3 (MH$^+$). CHN not satisfactory.

7.5.3. Synthesis of *tert*-butyl 2,2',2"-(10-(2-acetoxy-3,5-di-*tert*-butylbenzyl)-1,4,7,10-tetraazacyclododecane-1,4,7-triyl)triacetate (51)
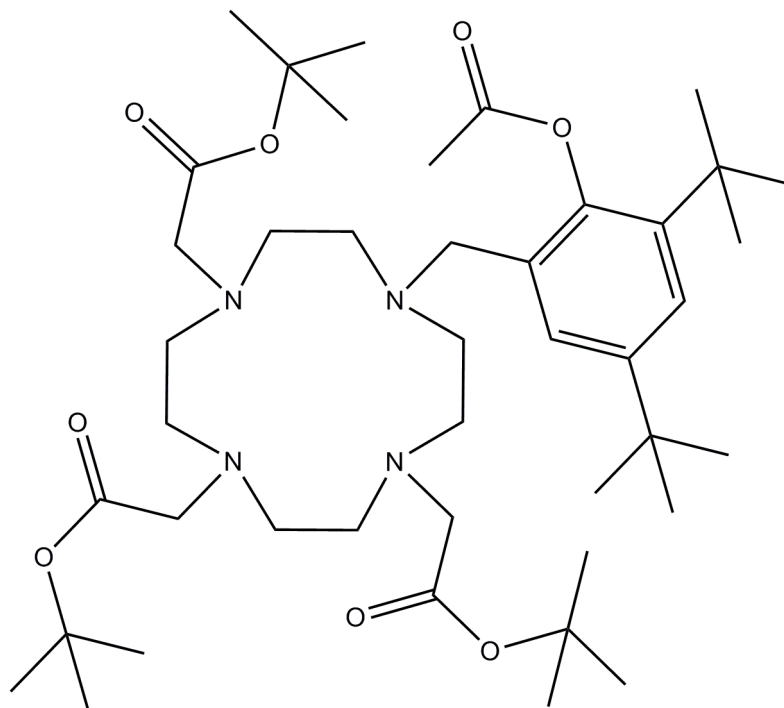
50 (0.5 g, 1.16 mmol) was dissolved in dry MeCN (20 ml) to which was added K_2CO_3 (1.60 g, 11.56 mmol). After stirring for 5 min, *tert*-butyl-bromo acetate (0.56 g, 2.89 mmol) was added dropwise over 5 min with stirring. The solution was then stirred for a further 48 hrs before concentrating under reduced pressure. The residue was taken up into DCM (40 ml) and the remaining solids filtered off. The filtrate was reduced and the residue purified on activated alumina (eluent 5% MeOH in DCM). The fractions containing the desired product were combined and concentrated under reduced pressure to give a yellow oil (0.64 g, 71%); R_f=0.34 (5% MeOH in DCM); ^{1}H NMR [CDCl$_3$] δ 7.45 (d, 1H, J=2.58 Hz, ArH), 7.42 (d, 1H, J=2.58 Hz, ArH), 3.59-3.13 (m, 8H, CH$_2$), 2.95-2.48 (m, 16H, NCH$_2$CH$_2$N), 2.23 (s, 3H, OMe), 1.39 (s, 9H, ^{t}Bu), 1.38 (s, 18H, ^{t}Bu), 1.37 (s, 9H, ^{t}Bu), 1.34 (s, 9H, ^{t}Bu); ^{13}C NMR [CDCl$_3$] δ 170.86, 170.55 (COO^{t}Bu), 150.39, 145.48, 139.78, 137.94, 137.17, 136.40 (C$_{arom}$), 80.88, 80.79 (COOC(Me$_3$)), 58.56, 57.10, 56.06, 55.54, 54.78, 54.25 (NCH$_2$CH$_2$N), 34.84, 34.04 (C(^{t}Bu)), 31.65, 31.44, 30.59, 29.63 (Me(^{t}Bu)), 21.51 (OMe); HRMS (ES-MS) expected for C$_{43}$H$_{75}$O$_8$N$_4$: 775.5579 found 775.5586. CHN not satisfactory.

7.5.4. Synthesis of 2,2',2"-(10-(2-acetoxy-3,5-di-*tert*-butylbenzyl)-1,4,7,10-tetraazacyclododecane-1,4,7-triyl)triacetic acid (52)
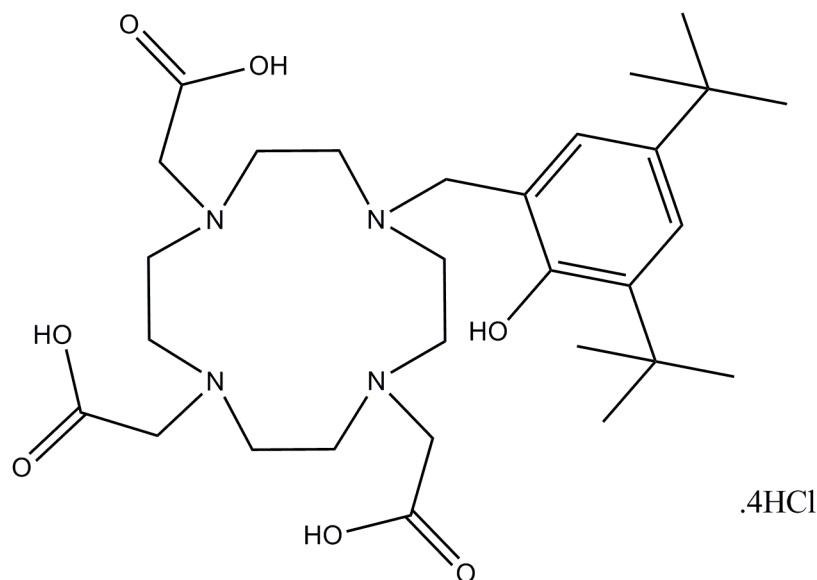
To **51** (0.64 g, 0.827 mmol) dissolved in MeOH (10 ml) was added 6M HCl (15 ml). The yellow/ orange solution was then heated to reflux for 24 hr. The solution was then allowed to cool before concentrating under reduced pressure. The residue was then triturated with acetone (3 x 10 ml) to afford a light orange solid (0.55 g, 94%); ^{1}H NMR [D$_2$O] 7.35 (br s, 2H, ArH), 3.78-3.02 (m, 24H, CH$_2$); ^{13}C NMR [D$_2$O] 173.69, 167.86 (COOH), 151.24, 146.10, 145.61, 140.37, 139.42, 126.87 (C$_{arom}$), 52.54 (NCH$_2$Ph), 52.11, 48.28, 47.46 (CH$_2$), 34.52, 34.25 (C(^{t}Bu)), 31.03, 30.00 (Me(^{t}Bu)). CHN not collected. Mass spec obtained but no peaks discernable from spectrum. Peaks at 500 and 149.

7.5.5. Synthesis of lanthanum(III) 2,2',2''-(10-(2-acetoxy-3,5-di-*tert*-butylbenzyl)-1,4,7,10-tetraazacyclododecane-1,4,7-triyl)triacetic acid triethylammonium ([La52][NHEt₃])

$[NHEt_3]^+$
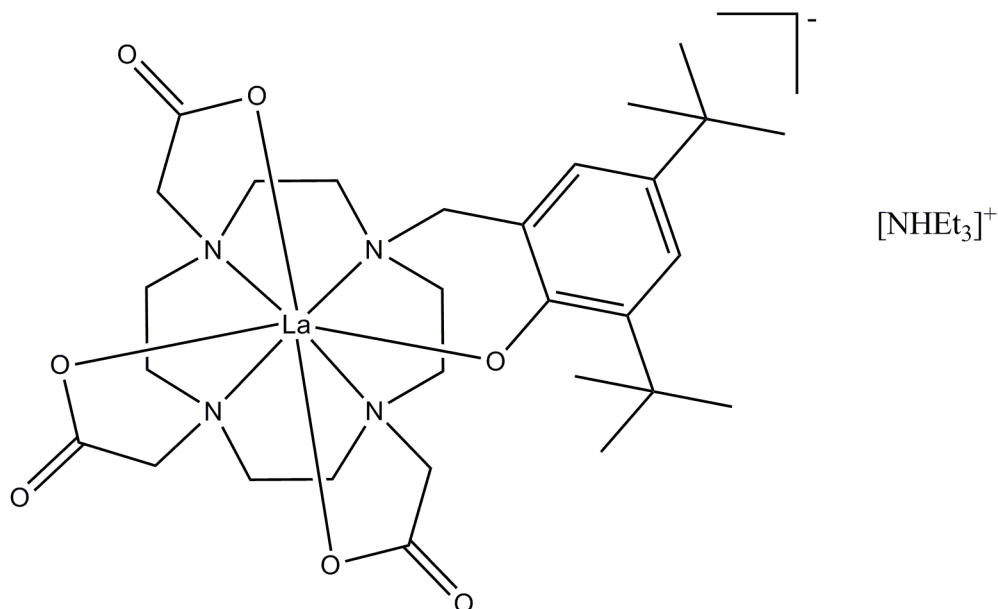
To **52** (0.10 g, 0.141 mmol) dissolved in degassed MeOH (5 ml) was added NEt₃ (0.11 g, 1.13 mmol) and the solution was stirred at RT for 5 min. After this time lanthanum(III) trifluoromethanesulfonate hydrate (0.0823 g, 0.141 mmol) in MeOH (1 ml) was added and the solution was heated to reflux for 2 hr. Allowed to cool to RT before concentrating under reduced pressure to the minimal volume. The solution was then eluted down a Sephadex LH-20 column with MeOH. The orange band was collected and concentrated under reduced pressure. The oily residue was washed with ether (3 x 5 ml) to give a white solid (0.06 g, 76%); ^{1}H NMR [D$_2$O] 7.37-7.28 (m, 2H, ArH), 3.84-3.08 (m, 24H, CH$_2$); ^{13}C NMR [D$_2$O] 174.31, 166.98 (COOH), 152.07, 147.38, 145.87, 141.67, 140.57, 131.67 (C$_{arom}$), 53.01 (NC$\underline{H}_2$Ph), 54.56, 49.69, 48.62, 48.59 (CH$_2$), 34.73, 33.94 (C(^{t}Bu)), 31.17, 30.48 (Me(^{t}Bu)); HRMS (ES-MS) expected for C$_{29}$H$_{44}$O$_7$N$_4$La: 699.2279, found 699.2268. CHN not collected.

7.5.6. Synthesis of europium(III) 2,2',2"-(10-(2-acetoxy-3,5-di-*tert*-butylbenzyl)-1,4,7,10-tetraazacyclododecane-1,4,7-triyl)triacetic acid triethylammonium ([Eu52][NHEt₃])

$[NHEt_3]^+$
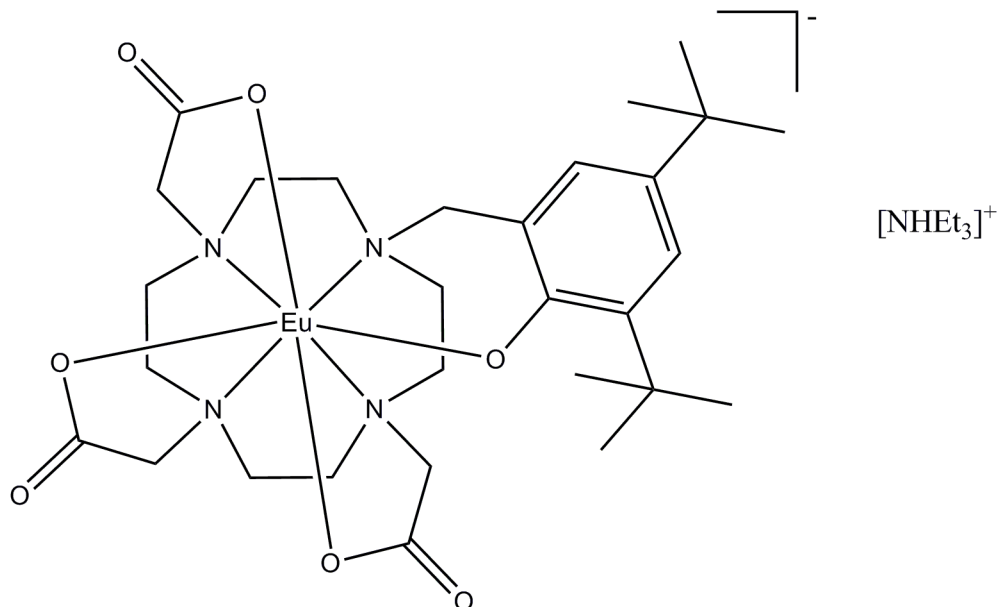
To **52** (50 mg, 0.0705 mmol) dissolved in MeOH (5 ml) was added NEt₃ (0.06 g, 0. 564 mmol). The orange solution was stirred for 5 min before adding europium(III) trifluoromethane sulfonate hydrate (0.04 g, 0.0705 mmol). The solution was then heated to reflux for 2 hr before allowing to cool to RT and then concentrated under pressure. The oily residue was redissolved in the minimium amount of MeOH (~1ml) and eluted down a Sephadex LH-20 column with MeOH. The yellow fraction was collected and concentrated under reduced pressure. The oily residue was triturated with ether (3 x 5 ml) to afford a white solid (0.497g, 82%), HRMS (ES-MS) expected for $C_{29}H_{44}O_7N_4{}^{151}Eu_1$: 711.2412, found 711.2422; Fluoresence (MeOH): 521 nm, 595 nm ($^5D_0 \rightarrow ^7F_1$), 612 nm ($^5D_0 \rightarrow ^7F_2$), 775 nm; UV-Vis (MeOH): 250-300 nm (π-π*); UV-Vis (MeOH) after oxidation with ferric cyanide: 250-300 nm (π-π*), 380-440 nm (phenoxyl radical). CHN not collected.

7.5.7. Synthesis of terbium(III) 2,2',2''-(10-(2-acetoxy-3,5-di-*tert*-butylbenzyl)-1,4,7,10-tetraazacyclododecane-1,4,7-triyl)triacetic acid triethylammonium ([Tb52][NHEt₃])
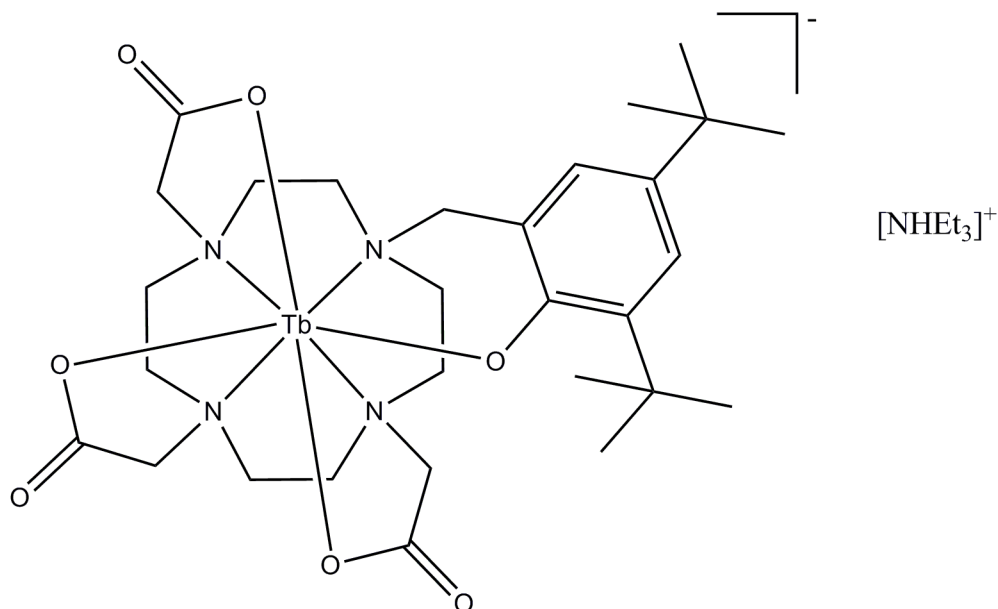
To **52** (0.085 g, 0.141 mmol) dissolved in MeOH (5 ml) was added NEt_3 (0.11 g, 1.13 mmol) and the solution was stirred at RT for 5 min. After this time, terbium(III) trifluoromethanesulfonate hydrate (0.085 g, 0.141 mmol) in MeOH (1 ml) was added and the resulting solution was heated to reflux for 2 hr. The solution was allowed to cool to RT before concentrating under reduced pressure to the minimium volume. The solution was then eluted down a Sephadex LH-20 column with MeOH. The orange band was collected and concentrated under reduced pressure. The oily residue was washed with ether (3 x 5 ml) to give a white solid (0.07 g, 90%); HRMS (ES-MS) expected for $C_{29}H_{44}O_7N_4Tb$: 719.2469 found 719.2455; Fluoresence (MeOH): 490 nm ($^5D_4 \rightarrow ^7F_3$), 545 nm ($^5D_4 \rightarrow ^7F_4$), 587 nm ($^5D_4 \rightarrow ^7F_5$), 623 nm ($^5D_4 \rightarrow ^7F_6$). CHN not collected.

7.5.8. Synthesis of gadolinium(III) 2,2',2"-(10-(2-acetoxy-3,5-di-*tert*-butylbenzyl)-1,4,7,10-tetraazacyclododecane-1,4,7-triyl)triacetic acid triethylammonium ([Gd52][NHEt₃])
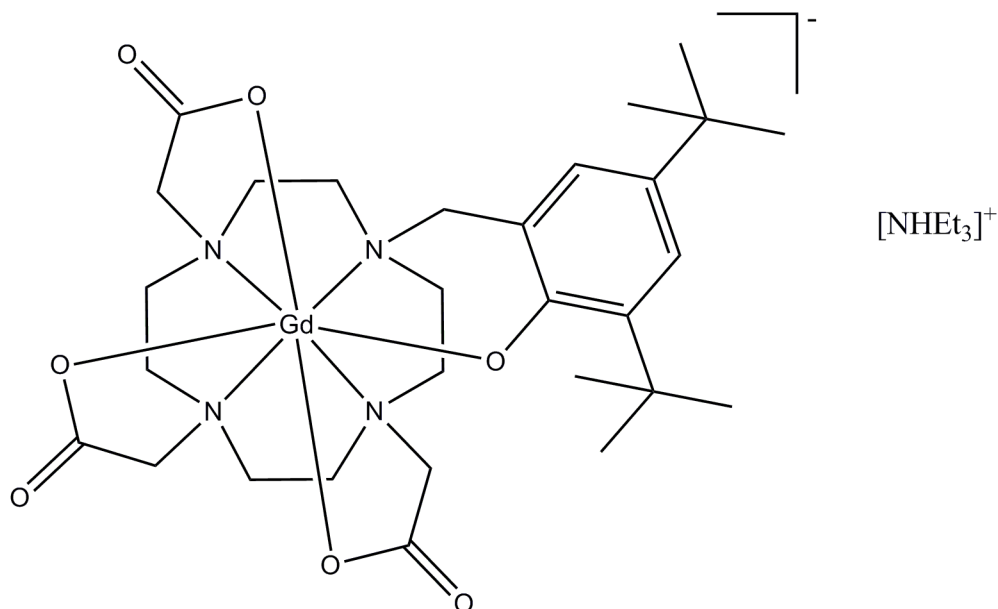
To **52** (70 mg, 0.0985 mmol) in MeOH (10 ml) was added NEt_3 (0.11 ml, 0.787 mmol). The dark orange solution was allowed to stir for 5 min before the addition of gadolinium(III) nitrate hexahydrate (0.0454 g, 0.0985 mmol) in MeOH (1 ml). The solution was heated to reflux with stirring for 2 hr. The solution was allowed to cool before concentrating under reduced pressure. The oily residue was redissolvd in the minimium amount of MeOH (~1ml) and eluted down a Sephadex LH-20 column with MeOH. The yellow fraction was collected and concentrated under reduced pressure. The oily residue was triturated with ether (3 x 5ml) to give a white powder (0.0775 g, 96%); MS (MS-ES): m/z 718.3 ((M-[NHEt₃])⁺). CHN not collected.

7.5.9. Synthesis of 1-[3,5-di-*tert*-butyl-2-(4-methoxy-benzylsulfanyl)-benzyl]-1,4,7,10-tetraaza-cyclodecane (53)
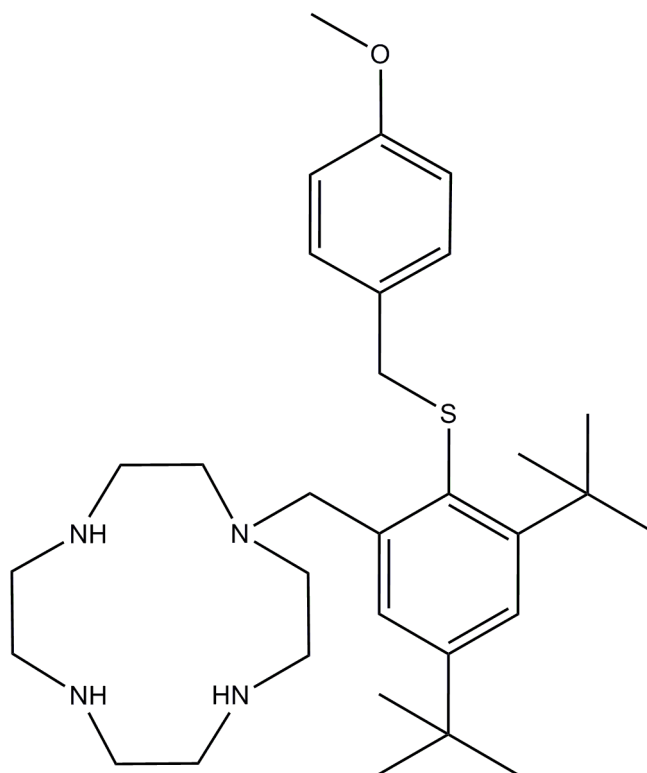
To cyclen (0.80 g, 1.84 mmol) in $CHCl_3$ (10 ml) was added a solution of **24** (1.26 g, 7.35 mmol) and triethylamine (0.22 g, 2.20 mmol) in $CHCl_3$ (40 ml). The resulting solution was then heated to a gentle reflux for 15 hrs before being allowed to cool to RT. The solution was then washed with 1 M $NaOH_{(aq)}$ (3 x 15 ml), followed by water (3 x 15 ml). The organic layer was collected and dried over $MgSO_4$ before being concentrated under reduced pressure to give **53** as a viscous yellow oil (0.80 g, 83%); ^1H NMR [$CDCl_3$] δ 7.51 (m, 2H, ArH), 7.08 (m, 2H, ArH), 6.71 (m, 2H, ArH), 3.67 (s, 2H, $PhCH_2N$), 3.60 (s, 2H, SCH_2), 3.48 (s, 3H, OCH_3), 2.71 (s, 4H, $HNCH_2$), 2.58 (s, 4H, NCH_2), 2.47 (s, 8H, $HNCH_2$), 1.47 (s, 9H, $CH_3(^tBu)$), 1.24 (s, 9H, $CH_3(^tBu)$)); ^{13}C NMR [$CDCl_3$] 158.49, 152.27, 150.07, 144.77, 138.19, 129.76, 124.95, 122.49, 120.52, 113.58 (C_{arom}), 54.89 (OCH_3), 51.12, 46.86, 46.23 ($HNCH_2$), 44.81 (NCH_2), 42.14 (SCH_2), 34.43 ($PhCH_2N$), 37.42, 34.41 ($C(^tBu)$), 31.23, 31.05 ($CH_3(^tBu)$). CHN not collected.

7.5.10. Synthesis of *tert*-butyl 2,2',2''-(10-(3,5-di-*tert*-butyl-2-(4-methoxybenzylthio)benzyl)-1,4,7,10-tetraazacyclododecane-1,4,7-triyl)triacetate (54)
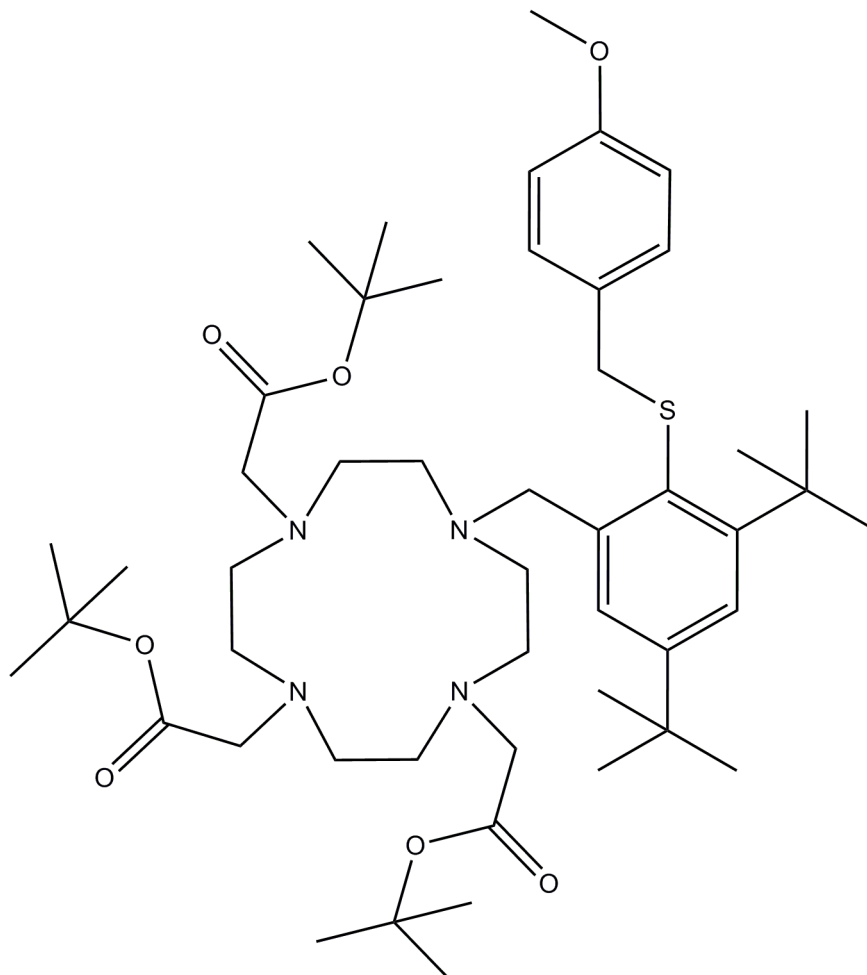
53 (0.80 g, 1.52 mmol) and potassium carbonate (2.10 g, 15.03 mmol) were dissolved in dry MeCN (30 ml). *Tert*-butyl bromo acetate was then added to this solution over a period of 5 min with stirring. The solution was then stirred at RT for a further 24 hr. The mixture was then concentrated under reduced pressure, redissolved in DCM and then filtered to remove any undissolved solids. The organic layer was concentrated under reduced pressure to give the crude material. The crude material was purified by column chromatography (silica 60, eluent DCM/ MeOH 10/1 (v/v)). The fraction with an R_f=0.43 was collected, concentrated under reduced pressure and triturated with ether (3 x 10 ml) to give a pale yellow powder (0.70 g 64%); R_f=0.43 (DCM/ MeOH 10/1 (v/v)); ^{1}H NMR [CDCl$_3$] δ 7.32 (d, 1H, J=2.11 Hz, ArH), 7.24 (d, 1H, J=2.11 Hz, ArH), 6.98 (d, 2H, J=8.91 Hz, ArH), 6.72 (d, 2H,

J=8.91 Hz, ArH), 5.24 (s, 2H, PhCH$_2$N), 3.73-2.11 (m, 24H, CH$_2$) 1.41 (s, 9H, CH$_3$(^{t}Bu)), 1.38 (s, 9H, CH$_3$(^{t}Bu)), 1.37 (s, 9H, CH$_3$(^{t}Bu)), 1.35 (s, 9H, CH$_3$(^{t}Bu)), 1.25, (s, 9H, CH$_3$(^{t}Bu)); ^{13}C NMR [CDCl$_3$] δ 173.09, 172.60 (CO), 151.18, 142.73, 136.02, 130.22, 129.96, 124.55, 123.32, 121.06, 113.95, 113.75 (C$_{arom}$), 82.45, 82.25 (COO$\underline{C}$(Me)$_3$), 55.16 (OC$\underline{H_3}$), 51.12, 50.97, 49.62 (HNC$\underline{H_2}$), 43.41 (NC$\underline{H_2}$), 37.60 (SC$\underline{H_2}$), 34.72 (PhC$\underline{H_2}$N), 34.85, 31.34, (Ph$\underline{C}$(^{t}Bu)), 27.98, 27.94, 27.92, 27.72, 27.52 (C$\underline{H_3}$(^{t}Bu)); HRMS (ES-MS) expected for C$_{49}$H$_{81}$O$_7$N$_4$S$_1$ 869.5820, found 869.5818. CHN not collected.

7.5.11. Synthesis of *tert*-butyl 2,2',2"-(10-(3,5-di-*tert*-butyl-2-mercaptobenzyl)-1,4,7,10-tetraazacyclododecane-1,4,7-triyl)triacetate (55)
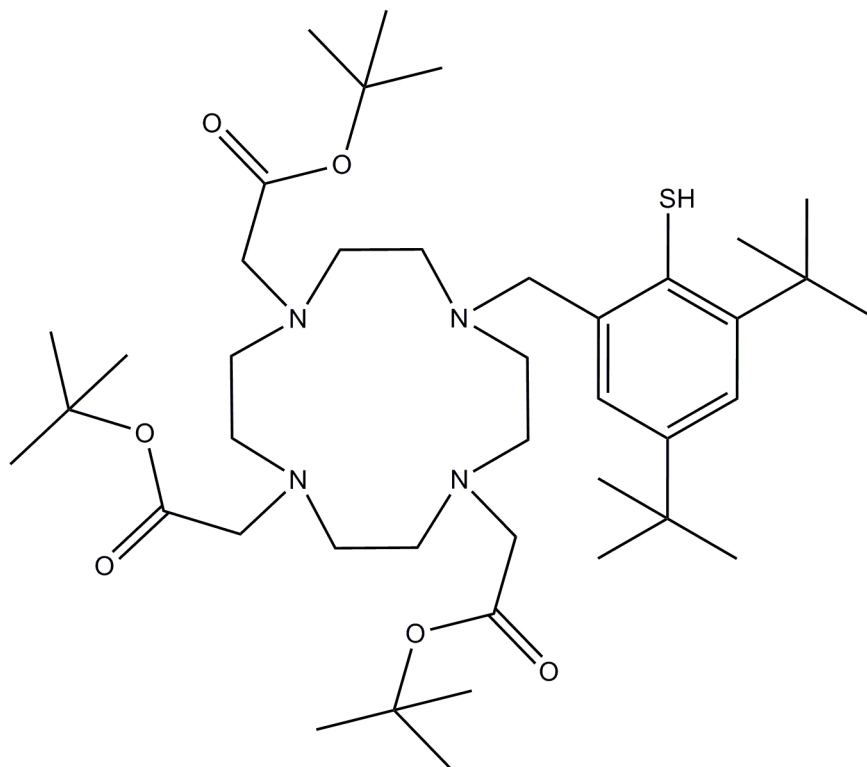
To **54** (0.35 g, 0.40 mmol) dissolved in methanol (12 ml) was added mercury acetate (0.26 g, 0.80 mmol) under a nitrogen atmosphere. The resulting solution was stirred at 60°C for 6 hr and then concentrated under reduced pressure. The residue was then washed with n-pentane (2 x 10 ml) and concentrated under reduced pressure to yield a yellow oil. To this oil was added methanol (12 ml) and the resulting mixture degassed for 5 min. H_2S was then bubbled through the solution for 20 mins before purging the solution with nitrogen for 25 min. The solution was then filtered through celite and the filtrate concentrated under reduced pressure to yield a yellow oil (0.30 g, 100%); ^1H NMR [CDCl$_3$] δ 7.42 (d, 1H, J=1.88 Hz, ArH), 7.31 (d, 1H, J=1.88 Hz ArH), 4.50 (s, 1H, SH), 3.74-2.56 (m, 24H, CH$_2$), 1.44 (s, 9H, CH$_3$(^{t}Bu)), 1.38 (s, 9H, CH$_3$(^{t}Bu)), 1.36 (s, 9H, CH$_3$(^{t}Bu)), 1.27 (s, 9H, CH$_3$(^{t}Bu)), 1.25 (s, 9H, CH$_3$(^{t}Bu)); ^{13}C NMR [CDCl$_3$] δ 169.72, 169.64 (CO), 151.95, 151.83, 130.16, 129.34, 125.85, 124.01 (C$_{arom}$), 83.85, 81.94, 77.32 (COO$\underline{C}$(Me)$_3$), 56.15, 54.37, 52.08, 51.02 (NCH$_2$), 34.91, 31.48 (Ph$\underline{C}$(^{t}Bu)), 31.41, 28.17, 28.06 (CH$_3$(^{t}Bu)). CHN not collected due to oxidisable thiophenol.

7.5.12. Synthesis of 2,2',2''-(10-(3,5-di-*tert*-butyl-2-mercaptobenzyl)-1,4,7,10-tetraazacyclododecane-1,4,7-triyl)triacetic acid (56)
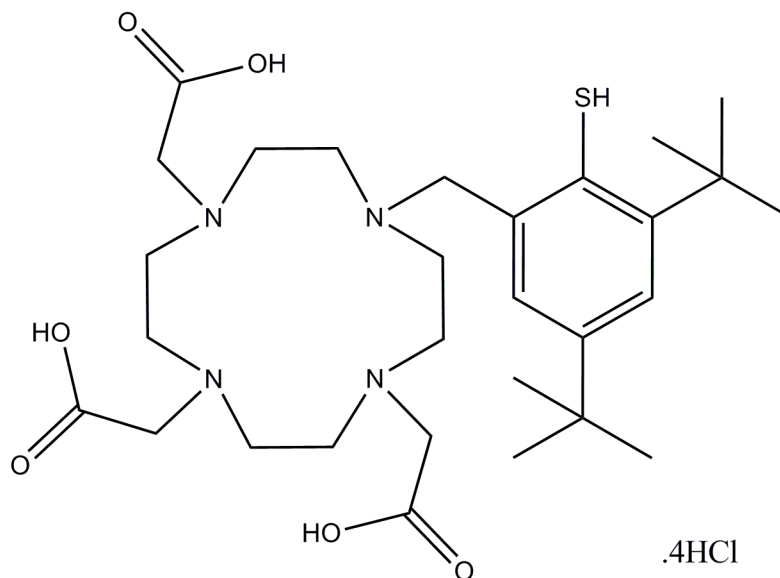
To **55** (0.30 g, 0.40 mmol) in methanol (12 ml) was added 6M HCl (15 ml). The resulting solution was heated to 95°C with stirring for 18 hr, before allowing to cool. The resulting solution was then concentrated, and the residue washed with acetone (3 x 25 ml) to afford a white solid (0.29 g, 100%); ^{1}H NMR [CDCl$_3$] δ 7.45-7.40 (m, 2H, ArH), 3.68-2.86 (m, 24H, CH$_2$), 1.12 (br s, 18H, CH$_3$(^{t}Bu)); ^{13}C NMR [CDCl$_3$] 173.19, 168.73 (CO), 158.19, 153.32, 138.00, 128.92, 125.75, 124.93 (C$_{arom}$) 52.98, 49.22, 48.51, 48.11 (NCH$_2$), 34.24, 33.98 (C(^{t}Bu)), 31.60, 30.57 (CH$_3$(^{t}Bu)). CHN not collected due to oxidisable thiophenol.

7.5.13. Synthesis of lanthanum(III) 2,2',2''-(10-(3,5-di-*tert*-butyl-2-mercaptobenzyl)-1,4,7,10-tetraazacyclododecane-1,4,7-triyl)triacetic acid ammonium ([La56][NHEt₃])
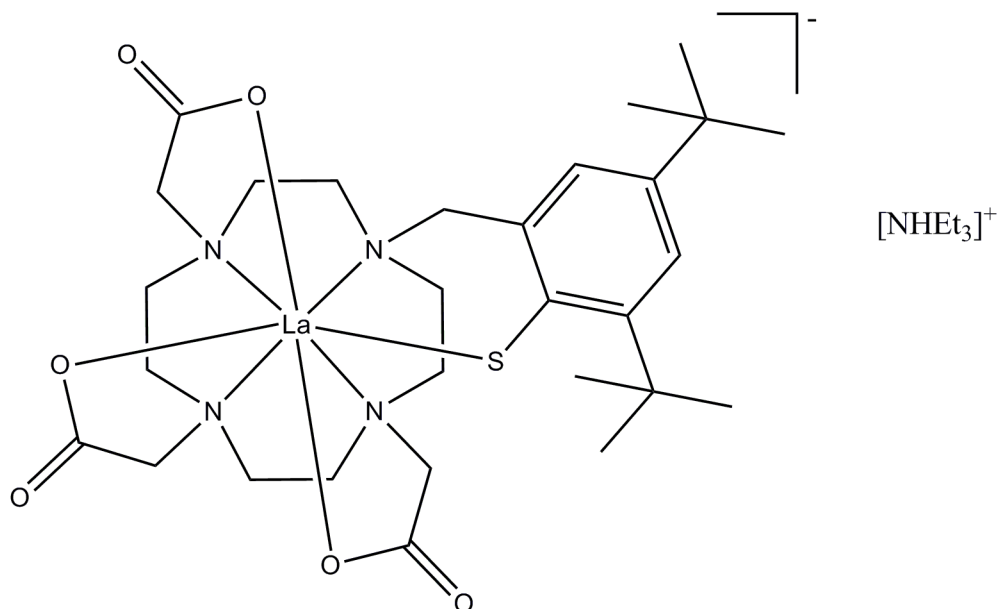

To **56** (0.07 g, 96 µmol) dissolved in degassed MeOH (5 ml) was added NEt₃ (0.1 ml, 0.77 mmol) and the solution was stirred at RT for 5 min. After this time lanthanum(III) trifluoromethanesulfonate hydrate (0.0564 g, 96 µmol) in MeOH (1 ml) was added and the resulting solution was heated to reflux for 2 hr. It was allowed to cool to RT before concentrating under reduced pressure. The concentrated solution was then eluted down a Sephadex LH-20 column with MeOH. The orange band was collected and concentrated under reduced pressure. The oily residue was washed with ether (3 x 5 ml) to give a white solid (0.06 g, 76%); ^{1}H NMR [CDCl₃] δ 7.44-7.39 (m, 2H, ArH), 3.67 (s, 2H, PhCH₂N), 3.49-2.77 (m, 22H, CH₂), 1.24 (s, 9H, CH₃(ᵗBu)), 1.16 (s, 9H, CH₃(ᵗBu)); ^{13}C NMR [CDCl₃] 174.42, 169.32 (CO), 157.65, 154.44, 141.53, 139.81, 126.67, 124.87 (C$_{arom}$) 53.09, 50.65, 48.97, 48.19 (NCH₂), 35.57, 34.08 (C(ᵗBu)), 31.54, 31.12 (CH₃(ᵗBu)); MS (MS-ES): *m/z* 715.2 ((M-[NHEt₃])⁺). CHN not collected due to oxidisable thiophenol.

7.5.14. Synthesis of europium(III) 2,2',2"-(10-(3,5-di-*tert*-butyl-2-mercaptobenzyl)-1,4,7,10-tetraazacyclododecane-1,4,7-triyl)triacetic acid ammonium ([Eu56][NHEt₃])
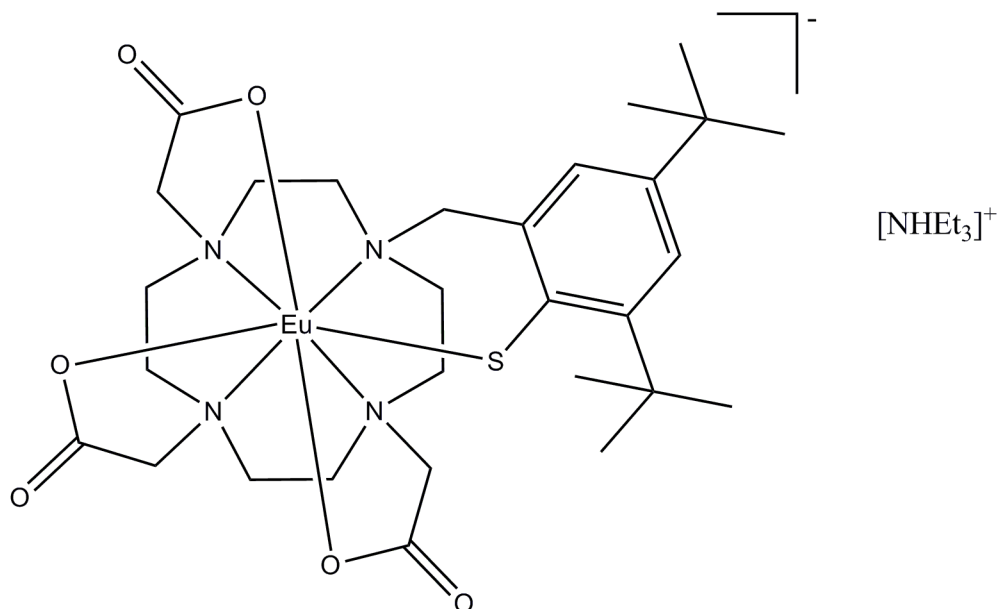
To **56** (0.0413 g, 57 μmol) in degassed methanol (5 ml) was added europium(III) trifluoromethanesulfonate (0.0379 g, 63 μmol) in MeOH (1 ml) with stirring. To this mixture was added triethylamine (0.0489 g, 0.48 mmol) dropwise over 5 min. The resulting solution was then heated to 80°C for 2 hr. The resulting solution was then concentrated under reduced pressure before re-dissolving in the minimal amount of degassed MeOH. This solution was then eluted down a Sephadex LH-20 column. The yellow fraction was collected and concentrated under reduced pressure. The oily product was then triturated with ether (3 x 5 ml) to afford a brown powder (0.0471g, 100%); MS (ES-MS): *m/z* 729.1 ((M-[NHEt₃])$^+$); Fluoresence (MeOH): 573 nm ($^5D_0{\rightarrow}^7F_0$), 619 nm ($^5D_0{\rightarrow}^7F_2$), 714 nm. CHN not collected due to oxidisable thiophenol.

7.5.15. Synthesis of terbium(III) 2,2',2''-(10-(3,5-di-*tert*-butyl-2-mercaptobenzyl)-1,4,7,10-tetraazacyclododecane-1,4,7-triyl)triacetic acid ammonium ([Tb56][NHEt₃])
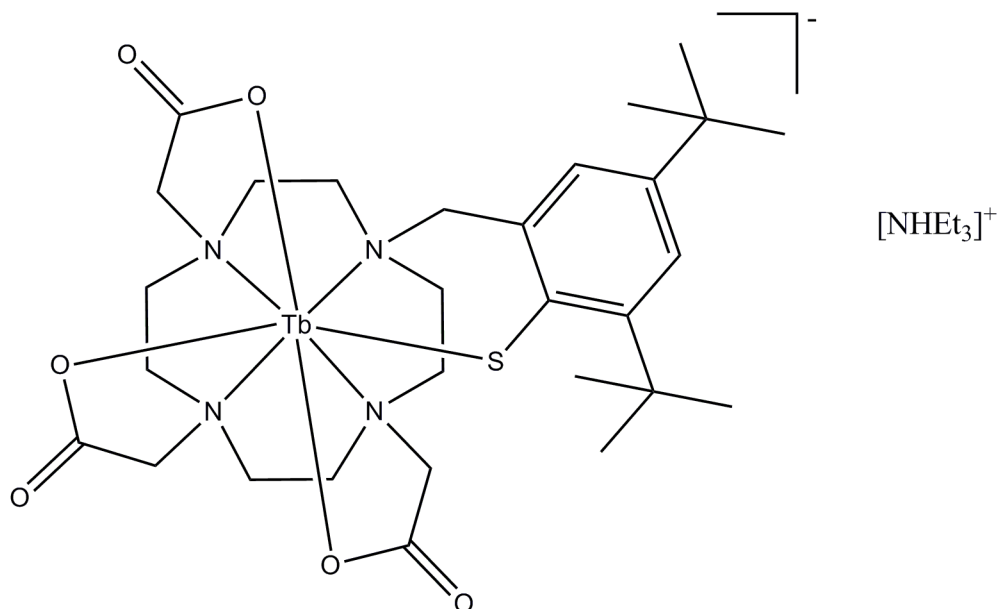

To **56** (0.07 g, 96 µmol) dissolved in degassed MeOH (5 ml) was added NEt$_3$ (0.1 ml, 0.77 mmol) and the solution was stirred at RT for 5 min. After this time terbium(III) trifluoromethanesulfonate hydrate (0.0584, 96 µmol) in degassed MeOH (1 ml) was added and the resulting solution was heated to reflux for 2 hr. Allowed to cool to RT before concentrating under reduced pressure to the minimal volume. The solution was then eluted down a Sephadex LH-20 column with MeOH. The orange band was collected and concentrated under reduced pressure. The oily residue was washed with ether (3 x 5 ml) to give a white solid (0.07 g, 90%); MS (MS-ES): *m/z* 735.2 ((M-[NHEt$_3$])$^+$); Fluoresence (MeOH): 498 nm ($^5D_4 \rightarrow {}^7F_3$), 543 nm ($^5D_4 \rightarrow {}^7F_4$), 585 nm ($^5D_4 \rightarrow {}^7F_5$), 617 nm ($^5D_4 \rightarrow {}^7F_6$). CHN not collected due to oxidisable thiophenol.

7.5.16. Synthesis of gadolinium(III) 2,2',2''-(10-(3,5-di-*tert*-butyl-2-mercaptobenzyl)-1,4,7,10-tetraazacyclododecane-1,4,7-triyl)triacetic acid ammonium ([Gd56][NHEt₃])
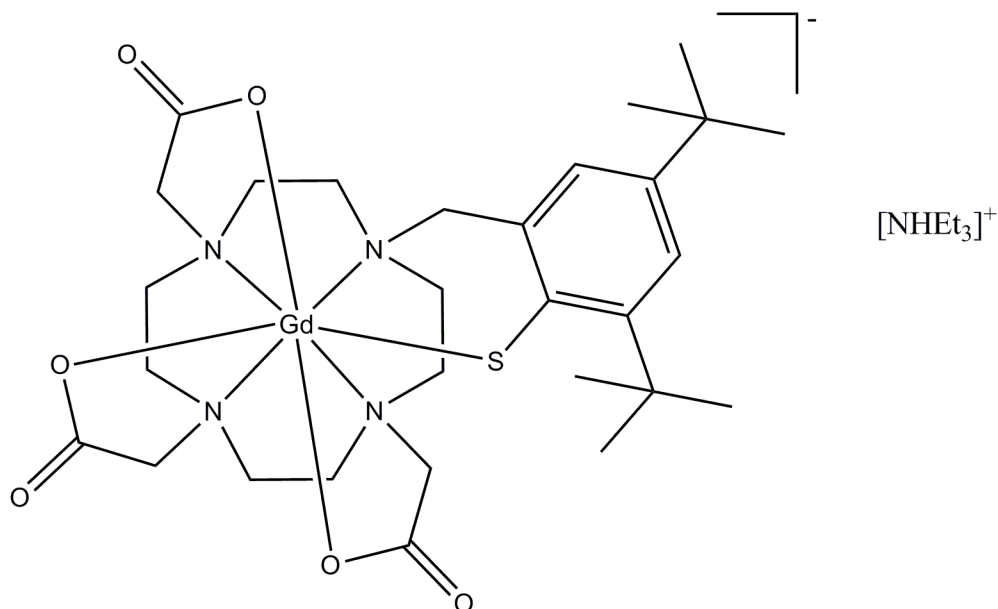
To **56** in degassed methanol was added gadolinium(III) nitrate hexahydrate (0.0372 g, 0.0825 mmol) with stirring. To this mixture was added triethylamine (0.1 ml, 0.77 mmol) dropwise over 5 min. The resulting solution was then heated to 80°C for 2 hr. The resulting solution was then concentrated under reduced pressure before re-dissolving in the minimal amount of degassed MeOH. This solution was then eluted down a Sephadex LH-20 column with MeOH. The yellow fraction was collected and concentrated under reduced pressure. The oily product obtained was triturated with ether (3 x 5 ml) to afford a cream powder (0.0602 g, 87%); MS (MS-ES): *m/z* 734.2 ((M-[NHEt₃])⁺). CHN not collected due to oxidisable thiophenol.

7.5.17. Synthesis of 1-benzyl 3-*tert*-butyl 2-((1,4,7,10-tetraazacyclododecane-1-yl)methyl)malonate (57)
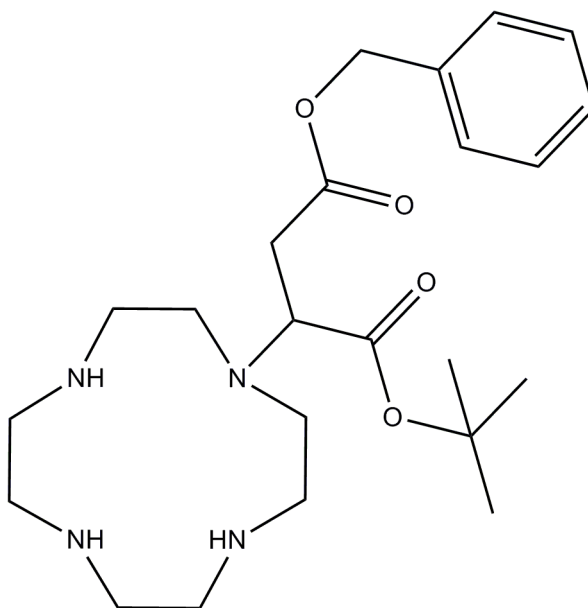
Cyclen (1 g, 5.80 mmol) was dissolved in $CHCl_3$ (100 ml) to which was added **27** (1.99 g, 5.80 mmol) in $CHCl_3$ (40 ml) with stirring over 20 hr using a syringe pump set to deliver 2 ml/ hr. Stirring continued for a further 24 hr before the reaction mixture was concentrated under reduced pressure. The crude product was purified by silica gel chromatography (eluent EtOH/ NH_3 (95/5)). The fractions containing the desired product were combined and concentrated under reduced pressure to afford a colourless oil (0.81 g, 32%); R_f=0.2 (EtOH/NH_3 (95/5)); ^{1}H NMR [$CDCl_3$] δ 7.13-7.04 (m, 5H, Ph), 4.93 (s, 2H, C$\underline{H}_2$Ph), 3.63-3.57 (m, 2H, NC$\underline{H}_2$CH), 3.23-3.21 (m, 1H, CH), 2.60-2.44 (m, 19H, NCH$_2$CH$_2$N and NH), 1.21 (s, 9H, ^{t}Bu); ^{13}C NMR [$CDCl_3$] 172.17, 168.66 ($\underline{C}$OO^{t}Bu), 137.66, 131.06, 123.72, 123.23 (C_{arom}), 77.06 ($\underline{C}$(Me)$_3$), 61.68 (N$\underline{C}$HCOO^{t}Bu), 60.99 (COO$\underline{C}$H$_2$Ph), 56.24, 44.09, 42.89, 40.75 (CH$_2$),30.31 (CH$\underline{C}$H$_2$COOBn), 23.41 (Me(^{t}Bu)); HRMS (ES-MS) expected for $C_{23}H_{39}O_4N_4$: 435.2966 found 435.2962. CHN not satisfactory.

7.5.18. Synthesis of 1-benzyl 3-*tert*-butyl 2-((4,7,10-tris(2-*tert*-butoxy-2-oxoethyl)-1,4,7,10-tetraazacyclododecane-1-yl)methyl)malonate (58)
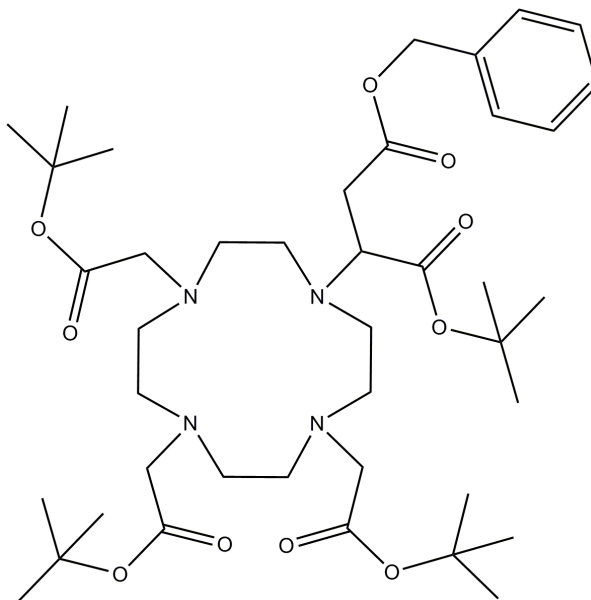
To DO3A-TB (0.82 g, 1.6 mmol) and potassium carbonate (1.21 g, 8.75 mmol) in MeCN (100 ml) was added **27** (0.50 g, 1.46 mmol) dropwise over 5 min. The solution was then heated to 65°C for 5 hr before allowing to cool. The solution was then concentrated and re-dissolved in DCM (40 ml) before filtering off any insoluble solids. The filtrate was again concentrated in vacuo before purifying using a short silica plug (eluent DCM/MeOH 97/3). The fractions containing the desired product were combined and concentrated under reduced pressure to afford a golden yellow oil (0.86 g, 76%); R_f=0.19 (hexane/EtOAc 20/1); R_f=0.54 (DCM/MeOH 95/5); ^{1}H NMR [CDCl$_3$] δ 7.31-7.21 (m, 5H, Ph), 5.22 (s, 2H, COOC$\underline{H}_2$Ph), 4.09-4.06 (m, 1H NC$\underline{H}$COOtBu), 3.35-3.08 (m, 8H, CH$_2$), 2.78-2.02 (m, 16H, CH$_2$), 1.41 (s, 9H, ^{t}Bu), 1.40 (s, 27H, ^{t}Bu); ^{13}C NMR [CDCl$_3$] 172.69, 172.17, 168.66 ($\underline{C}$O), 141.37, 135.16, 128.27, 126.65 (C$_{arom}$), 82.48, 81.44 (COO^{t}Bu), 68.14 (NC$\underline{H}$COO^{t}Bu), 66.46 (COO$\underline{C}$H$_2$Ph), 58.43, 55.46, 53.24, 52.19 (CH$_2$), 47.37 (CH$_2$), 44.53 (NCHC$\underline{H}_2$COOBn), 29.30, 28.79 (C(^{t}Bu)), 27.73, 27.56 (Me(^{t}Bu)); HRMS (ES-MS) expected for C$_{41}$H$_{66}$N$_4$O$_{10}$H: 775.4852 found 775.4851. CHN not satisfactory.

7.5.19. Synthesis of 2-(4,7,10-tris-*tert*-butoxycarbonyl-1,4,7,10-tetraaza-cyclododec-1-yl)-succinic acid 1-*tert*-butyl ester (59)
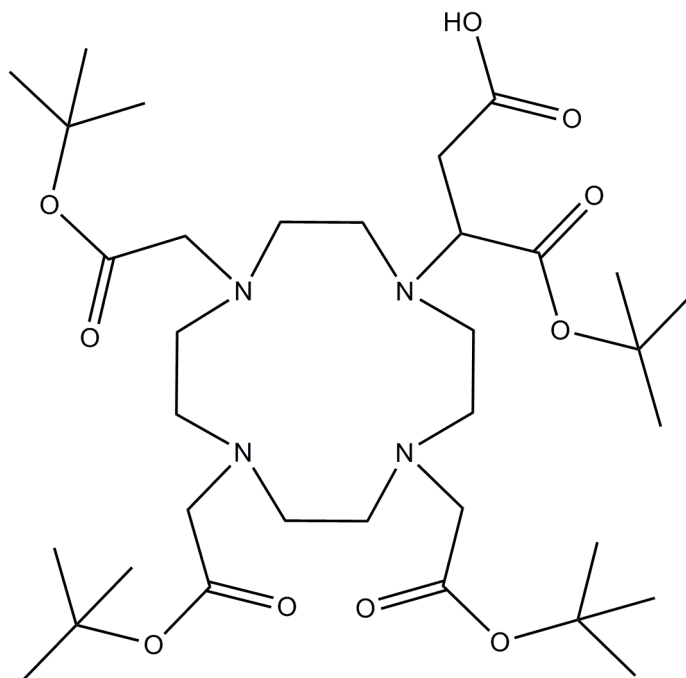
58 (0.28 g, 0.361 mmol) in MeOH (40 ml) was added 10% Pd/C (0.02 g) in H_2O (1 ml). The solution was transferred to a Parr shaker bottle where it was shaken under a hydrogen atmosphere at 25 psi for 1 d. The solution was filtered through celite, washing with MeOH (20 ml). The filtrate was collected and concentrated under reduced pressure. The oily residue was triturated with pentane (3 x 10 ml) to afford a white solid (0.14 g, 57%); ^{1}H NMR [CDCl$_3$] δ 3.38-2.10 (m, 25H), 1.38 (s, 21H, ^{t}Bu), 1.35 (s, 9H, ^{t}Bu); ^{13}C NMR [CDCl$_3$] δ 168.40, 166.20, 165.48 (COO^{t}Bu), 77.44, 75.19 (C(^{t}Bu)), 53.29 (NCHCO$_2$^{t}Bu), 51.16, 48.07, 46.86, 46.70, 44.92, 44.03 (CH$_2$), 42.54 (NCHCH$_2$COOH), 23.67, 23.38 (Me(^{t}Bu)); HRMS (ES-MS) for C$_{34}$H$_{58}$N$_4$O$_8$H: 651.4327 found 651.4321 ((M-2H$_2$O+H)$^+$). CHN not satisfactory.

7.5.20. 4-(1,5,8,12-tetraaza-bicyclo[10.2.2]hexadec-5-ylmethyl)-phenylamine (60)
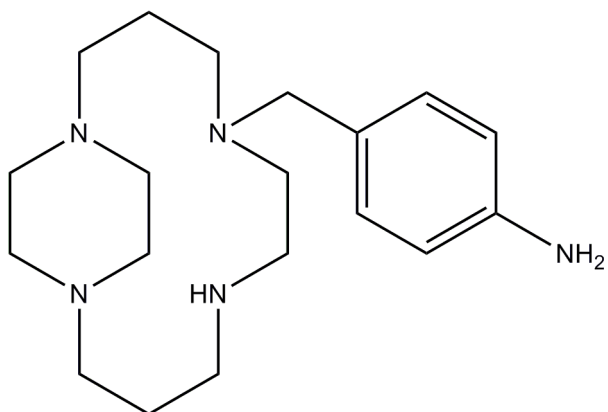
Compound 60 was supplied by Graeme McRobbie, The University of Hull.[208]

7.6. Porphyrin derivative synthesis

7.6.1. Synthesis of 5,10,15,20-tetrakis(3,5-dimethoxy-phenyl)-porphyrin (61)
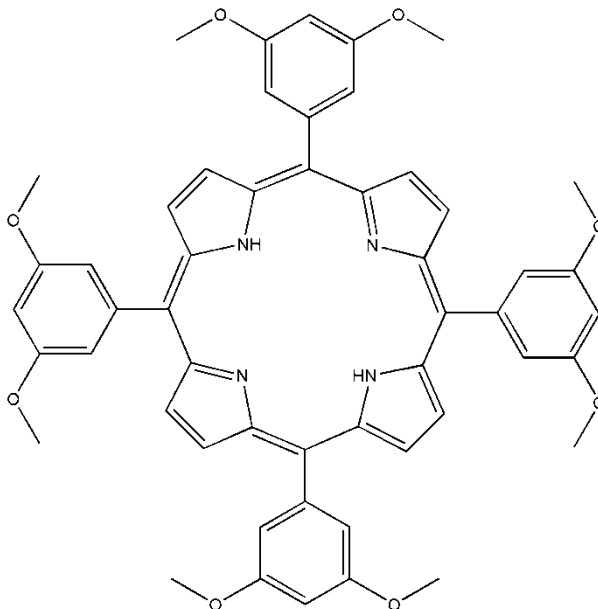
3,5-Dimethoxybenzaldehyde (2.5 g, 0.025 mol) and propionic acid (50 ml) were heated to reflux. To this solution was added pyrrole (1.01 g, 0.015 mol) over 5 min, which caused a colour change in the reaction mixture from light yellow to dark purple. The solution was allowed to reflux for a further 30 min before cooling to RT. The resulting black tarry solution was then filtered and a purple solid was collected. The solid was washed with methanol (25 ml) and hot water (60 ml). The compound was then dissolved in CHCl$_3$ (10 ml) and eluted down a basic alumina column. The fraction containing **61** was collected and concentrated under reduced pressure to afford a purple solid (0.60 g, 19%); R$_f$=0.50 (50% hexane in ethyl acetate), R$_f$=0.29 (DCM); ^{1}H NMR [CDCl$_3$] δ 8.93 (s, 8H, βH), 7.41 (d, 8H, J=2.18 Hz, ArH), 6.91 (t, 4 H, J=2.18 Hz, ArH), 3.96 (s, 24H, OMe), −2.84 (s, 2H, NH); ^{13}C NMR [CDCl$_3$] δ 158.84, 144.01, 131.01, 113.83, 100.16 (C$_{arom}$), 55.63 (OMe); MS (MALDI): *m/z* 855 (MH$^+$); UV-Vis (DCM): 419 nm, 514 nm, 549 nm, 588 nm, 645 nm. CHN not collected.
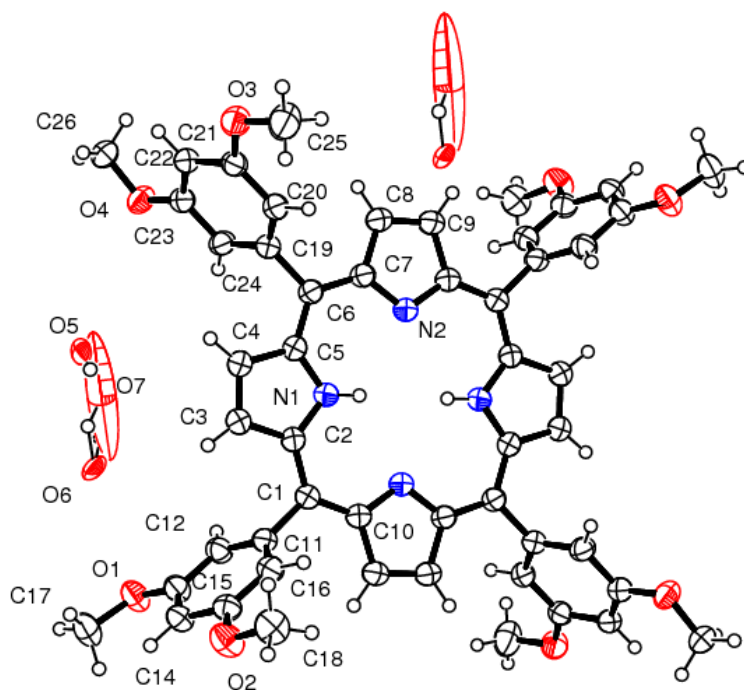
Figure 90: ORTEP representation of the X-ray structure of 61 with all atoms labelled.

Table 20: Crystal data for the structural refinement of 61.

Identification code	sja35_06
Empirical formula	$C_{26} H_{26} N_2 O_7$
Formula weight	478.49
Temperature	150(2) K
Wavelength	0.71073 Å
Crystal system	Triclinic
Space group	P-1
Unit cell dimensions	a = 11.2795(17) Å α= 109.310(11)°.
	b = 11.3173(17) Å β= 100.963(12)°.
	c = 11.8705(17) Å γ = 110.976(11)°.
Volume	1250.8(3) $Å^3$
Z	2
Density (calculated)	1.203 Mg/m^3
Absorption coefficient	0.085 mm^{-1}
F(000)	477
Crystal size	1.00 x 0.52 x 0.17 mm^3
Theta range for data collection	2.79 to 34.80°.
Index ranges	-18<=h<=18, -18<=k<=17, -19<=l<=18
Reflections collected	29275
Independent reflections	10670 [R(int) = 0.0773]
Completeness to theta = 34.80°	98.4 %
Absorption correction	None
Refinement method	Full-matrix least-squares on F^2
Data / restraints / parameters	10670 / 0 / 312
Goodness-of-fit on F^2	1.745
Final R indices [I>2sigma(I)]	R1 = 0.1519, wR2 = 0.4313
R indices (all data)	R1 = 0.1923, wR2 = 0.4723
Extinction coefficient	0.21(4)
Largest diff. peak and hole	3.016 and -0.659 e.$Å^{-3}$

7.6.2. Synthesis of gallium(III) 5,10,15,20-tetrakis(3,5-dimethoxy-phenyl)-porphyrin chloride ([Ga61]Cl)
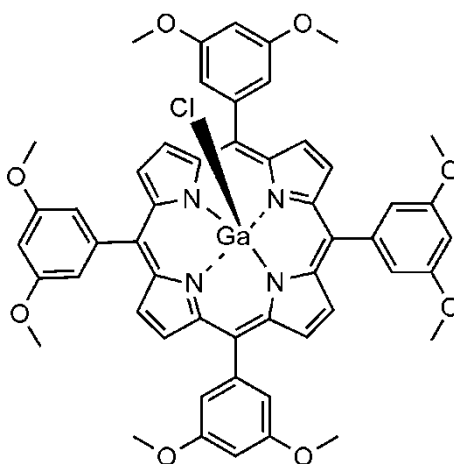
61 (0.35 g, 0.41 mmol), GaCl$_3$ (108 mg, 0.62 mmol) and sodium acetate (200mg, 2.44 mol) were mixed and placed under a nitrogen atmosphere. To this was added dry acetic acid (40 ml) and the resulting solution heated to reflux for 24 hr. The solution was then concentrated in vacuo and redissolved in toluene (10 ml). This solution was placed in a freezer for 14 hr which resulted in crystallization of the product. Crystals were collected by filtration to give [Ga**61**]Cl as purple crystals (0.32 g, 81%); ^{1}H NMR [CDCl$_3$] δ 9.18 (s, 8H, βH), 7.47 (s, 4H, ArH), 7.31 (s, 4H, ArH), 6.91 (t, 4H, J=2.1 Hz, Ar), 3.95 (s, 24H, OMe); ^{13}C NMR [CDCl$_3$] δ 158.84, 148.87, 143.25, 132.07, 120.23, 113.33, 100.62 (C$_{arom}$), 55.75 (OMe); MS (MALDI): *m/z* 921 (M-Cl$^+$); UV-Vis (DCM): 419 nm, 513 nm, 550 nm, 587 nm, 645 nm. CHN not collected.

Figure 91: ORTEP representation of the X-ray crystal structure of [Ga61]Cl with all non-H atoms labelled.

Table 21: Crystal data for the structural refinement of [Ga61]Cl.

Identification code	sja45_06
Empirical formula	$C_{52} H_{46} Cl Ga N_4 O_{8.20}$
Formula weight	963.27
Temperature	150(2) K
Wavelength	0.71073 Å
Crystal system	Monoclinic
Space group	P21/c
Unit cell dimensions	a = 17.2983(11) Å $\quad$ α= 90°.
	b = 13.7726(7) Å $\quad$ β= 128.990(4)°.
	c = 25.3585(17) Å $\quad$ γ = 90°.
Volume	4695.8(5) Å^3
Z	4
Density (calculated)	1.381 Mg/m^3
Absorption coefficient	0.705 mm^{-1}
F(000)	2024
Crystal size	0.24 x 0.22 x 0.18 mm^3
Theta range for data collection	2.74 to 34.95°.
Index ranges	-26<=h<=26, -22<=k<=18, -40<=l<=40
Reflections collected	57592
Independent reflections	19072 [R(int) = 0.0697]
Completeness to theta = 34.95°	92.6 %
Absorption correction	None
Refinement method	Full-matrix least-squares on F^2
Data / restraints / parameters	19072 / 2 / 618
Goodness-of-fit on F^2	0.857
Final R indices [I>2sigma(I)]	R1 = 0.0536, wR2 = 0.1332
R indices (all data)	R1 = 0.1080, wR2 = 0.1518
Extinction coefficient	0.00032(19)
Largest diff. peak and hole	0.786 and -1.844 e.Å^{-3}

7.6.3. Synthesis of 5,10,15,20-tetrakis(3,5-dihydroxy-phenyl)-porphyrin (62)
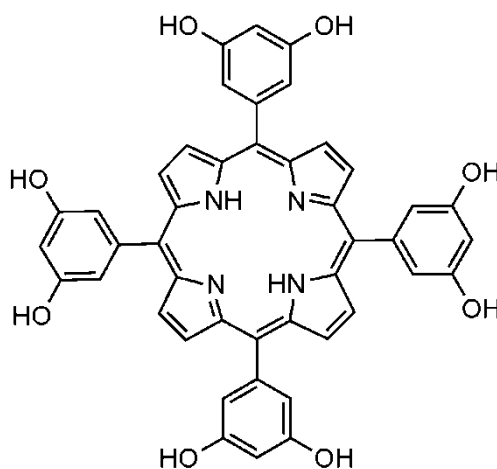
To **61** (0.76g, 0.88 mmol) in DCM (150 ml) was added BBr_3 (1 M solution in hexane, 20 ml). The solution was stirred for 20 hr at RT before adding further BBr_3 (1 M solution in hexane, 20 ml). After stirring the solution for a further 72 hours, saturated $NaHCO_{3(aq)}$ (200 ml) was added slowly and the DCM layer separated. This solution was dried over $MgSO_4$ to give **62** as a purple solid (0.65 g, 84%); ^{1}H NMR [$CDCl_3$] δ 8.88 (s, 16H, βH and OH), 7.80 (m, 4H, Ar), 6.63 (m, 8H, Ar), −2.63 (s, 2H, NH); MS (MALDI): *m/z* 743 (M[+]); HRMS (ES-MS) calculated for $C_{44}H_{30}N_4O_8$ 743.2136, found 743.2132; UV-Vis (MeOH): 418 nm, 513 nm, 547 nm, 587 nm, 645 nm; UV-Vis (H_2O): 417 nm, 522 nm, 558 nm, 581 nm, 636 nm. CHN not collected.

7.6.4. Synthesis of gallium(III) 5,10,15,20-tetrakis(3,5-dihydroxy-phenyl)-porphyrin chloride (Ga62Cl)
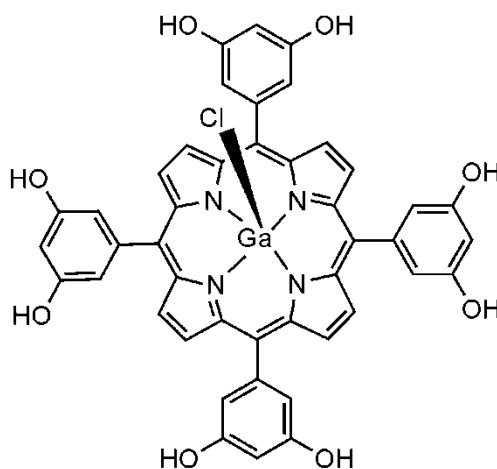
To [Ga**61**]Cl (100 mg, 0.1 mmol) dissolved in DCM (80 ml) was added BBr_3 (6 ml, 1 M in hexanes). The resulting green solution was stirred at RT for 72 hr before adding saturated $NaHCO_{3(aq)}$ (100 ml). The DCM layer was extracted, dried over $MgSO_4$, concentrated in vacuo to give the product as a deep purple solid (0.1g, 100%); ^{1}H NMR δ [CDCl$_3$] 9.1 (s, 8H, βH), 8.93 (br s, 8H, OH), 6.91 (m, 8H, ArH), 6.50 (m, 4H, ArH); MS (MALDI): *m/z* 810 (M-Cl$^+$); UV-Vis (MeOH): 418 nm, 515 nm, 546 nm, 588 nm, 646 nm. CHN not collected.

7.6.5. Synthesis of tetra(pentafluorophenyl) porphyrin (63)

Pentafluorobenzaldehyde (5.32 g, 0.02713 mol) was dissolved in propionic acid and the resulting solution heated to reflux. Pyrrole (1.82 g, 0.02713 mol) was then added over 5 min. Heating at reflux was continued for 6 hr before cooling and concentrating under reduced pressure. The black solid that remained was then adsorbed onto Hyflo and transferred to a short silica plug. The chlorin and porphyrin bands were then eluted with petroleum ether and hexane (5:8 respectively) leaving the polymeric products behind. The chlorin and porphyrin bands were combined and concentrated in vacuo to give the crude product (1.67 g). The crude product was then dissolved in $CHCl_3$ (100 ml) to which was added zinc acetate (3.76 g, 0.0171 mol) in methanol (20 ml) and left to stir for 14 hr. The reaction mixture was concentrated in vacuo and purified by column chromatography (DCM/hexane (1:1) raising to DCM (100%)). The red fraction was collected and dissolved in concentrated HCl (10 ml) and the solution was stirred for an hour. The solution was then diluted with water (100 ml) and the organic layer separated. The organic layer was then repeatedly washed with water until the aqueous layer was neutral. The organic layer was then dried over $MgSO_4$ and concentrated in vacuo to give **63** as a purple solid (0.25g, 4%); ^{1}H NMR [$CDCl_3$] δ 8.92 (s, 8H, βH), −2.93 (s, 2H, NH); ^{19}F NMR [$CDCl_3$] δ −161.19 (m, 2 F, *m*-F), −151.09 (t, 1F, J=20.8 Hz, *p*-F), −136.39 (dd, 2F, J= 6.9, 23.1 Hz, *o*-F); MS (MALDI): *m/z* 975 (M$^+$); ε (DMF): 410 nm (345680 mol^{-1}dm^{3}cm^{-1}), 504 nm nm (22922 mol^{-1}dm^{3}cm^{-1}), 533 nm (1946 mol^{-1}dm^{3}cm^{-1}), 580 nm (6956 mol^{-1}dm^{3}cm^{-1}), 655 nm (225 mol^{-1}dm^{3}cm^{-1}). CHN not collected.

7.6.6. Synthesis of zinc(II) tetra(pentafluorophenyl) porphyrin ([Zn63])
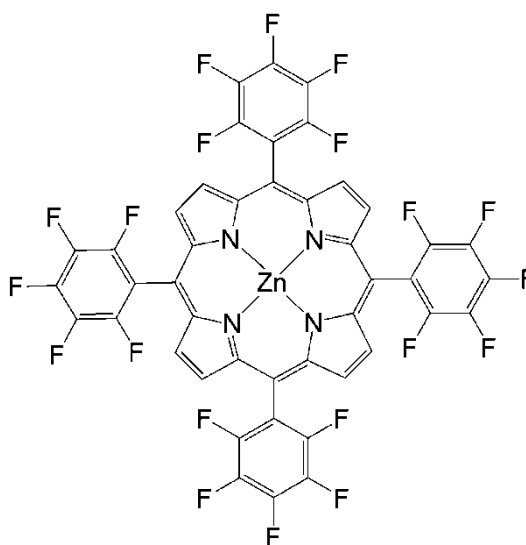
Method 1

Pentafluorobenzaldehyde (5.32 g, 0.02713 mol) was dissolved in propionic acid and the resulting solution heated to reflux. Pyrrole (1.82 g, 0.02713 mol) was then added over 5 min. Heating at reflux was continued for 6 hr before cooling and concentrating under reduced pressure. The black solid that remained was then adsorbed onto Hyflo and transferred to a short silica plug. The chlorin and porphyrin bands were then eluted with petroleum ether and hexane (5:8 respectively) leaving the polymeric products behind. The chlorin and porphyrin bands were combined and concentrated in vacuo to give the crude product (1.67 g). The crude product was then dissolved in $CHCl_3$ (100 ml) to which was added zinc acetate (3.76 g, 0.0171 mol) in methanol (20 ml) and left to stir for 14 hr. The reaction mixture was concentrated in vacuo and purified by column chromatography (DCM/hexane (1:1) raising to DCM (100%)) to give **34** as a red solid (0.8 g, 11%); ^1H NMR [$CDCl_3$] δ 8.99 (s, 8H, βH); ^{19}F NMR [$CDCl_3$] δ −161.61 (m, 2F, m-F), −151.82 (t, 1F, J=24.2 Hz, p-F), −136.69 (dd, 2F, J=16.2, 39.0 Hz, o-F); MS (MALDI): m/z 1038 (M$^+$); ε (DMF): 419 nm (514063 mol^{-1}dm^{3}cm^{-1}), 551 nm nm (24431 mol^{-1}dm^{3}cm^{-1}), 626 nm (3690 mol^{-1}dm^{3}cm^{-1}). CHN not collected.

Method 2

63 (0.1 g, 0.1 mmol) was dissolved in DCM (10 ml) and heated to reflux. A solution of zinc(II) acetate (230 mg, 0.00125 mol) was then added dropwise over 30 min. The solution was heated at reflux for a further 4 hr before allowing to cool. Analysis by TLC showed complete consumption of the starting material. The solution was then concentrated in vacuo and redissolved in DCM (10 ml). The solution was filtered and the filtrate collected. Evaporation of the filtrate under reduced pressure gave a purple crystalline material (0.0980 g, 92%); R_f=0.7 (1/1 hexane/DCM v/v); ^{1}H NMR [CDCl$_3$] δ 8.99 (s, 8H, βH); ^{19}F NMR [CDCl$_3$] δ −161.61 (m, 2F, *m*-F), −151.82 (t, 1F, J=24.2 Hz, *p*-F), −136.69 (dd, 2F, J=16.2, 39.0 Hz, *o*-F); MS (MALDI): *m/z* 1038 (M$^+$); ε (DMF): 419 nm (514063 mol^{-1}dm^{3}cm^{-1}), 551 nm nm (24431 mol^{-1}dm^{3}cm^{-1}), 626 nm (3690 mol^{-1}dm^{3}cm^{-1}). CHN not collected.

7.6.7. Synthesis of Gallium tetra-pentafluorophenyl-poprhyrin phenoxide or chloride ([Ga63]X, where X=OPh or Cl)

X= OPh or Cl
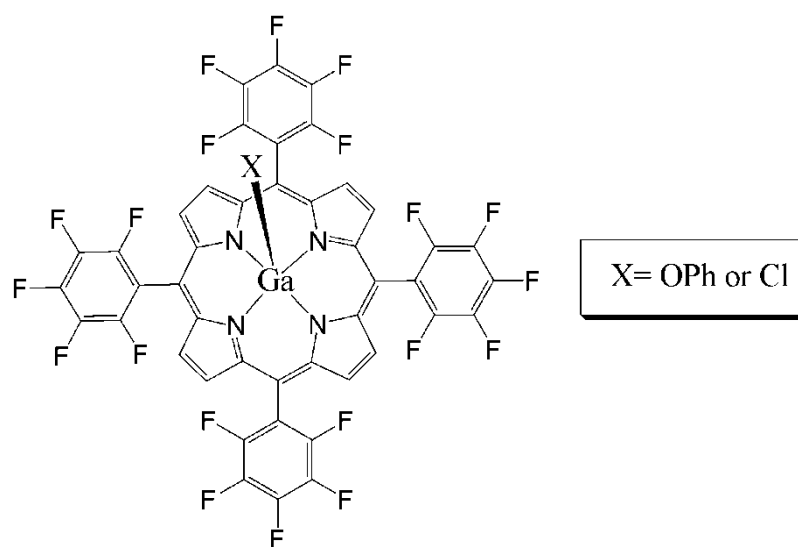
Method 1 (X= Cl)

63 (0.15 g, 0.15 mmol), sodium acetate (0.08 g, 0.98 mmol) and GaCl$_3$ (0.04 g, 0.21 mmol) were mixed and placed under a nitrogen atmosphere to which was added dry acetic acid (25 ml) and the resulting purple solution then heated to reflux for 12 hr. After this time the solution was allowed to cool before removing the solvent in vacuo. The product was then purified by silica gel column chromatography (eluting with 5% ethyl acetate in hexane). The fractions were combined and concentrated in vacuo to give [Ga**63**]Cl as red needles (10 mg, 6%); ^{1}H NMR [CDCl$_3$] δ 8.95 (s, 8H, βH); MS (MALDI): *m/z* 1042 ((M-Cl)$^+$); ε (DMF): 417 nm (595063 mol^{-1}dm^{3}cm^{-1}), 485 nm nm (3416 mol^{-1}dm^{3}cm^{-1}), 549 nm (26949 mol^{-1}dm^{3}cm^{-1}). CHN not collected.
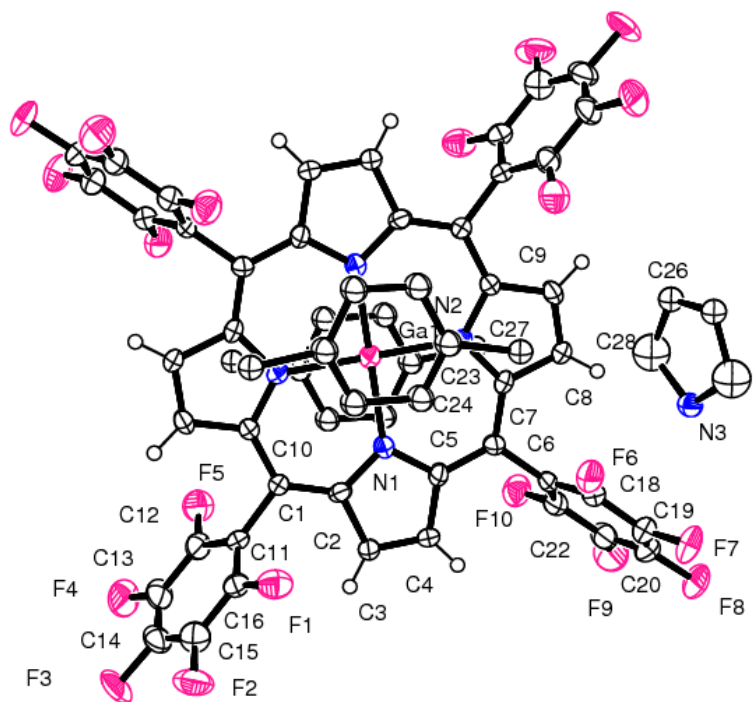
Figure 92: ORTEP representation of the X-ray crystal structure [Ga63]NC$_4$H$_4$ with all non-H atoms labelled.

Table 22: Crystal data for the structural refinement of [Ga63]NC$_4$H$_4$.

Identification code	rem_02
Empirical formula	C$_{96}$ H$_{16}$ F$_{40}$ Ga$_4$ N$_{10}$
Formula weight	2208.63
Temperature	150(2) K
Wavelength	0.71073 Å
Crystal system	Monoclinic
Space group	C2/c
Unit cell dimensions	a = 15.349(3) Å $\quad$ α= 90°.
	b = 25.690(4) Å $\quad$ β= 102.074(15)°.
	c = 12.609(2) Å $\quad$ γ = 90°.
Volume	4861.9(14) Å^3
Z	2
Density (calculated)	1.749 Mg/m^3
Absorption coefficient	0.702 mm^{-1}
F(000)	2548
Crystal size	0.20 x 0.15 x 0.10 mm^3
Theta range for data collection	2.71 to 34.93°.
Index ranges	-24<=h<=24, -40<=k<=40, -19<=l<=20
Reflections collected	33475
Independent reflections	10326 [R(int) = 0.3511]
Completeness to theta = 34.93°	96.9 %
Absorption correction	None
Refinement method	Full-matrix least-squares on F^2
Data / restraints / parameters	10326 / 0 / 353
Goodness-of-fit on F^2	0.694
Final R indices [I>2sigma(I)]	R1 = 0.1051, wR2 = 0.2432
R indices (all data)	R1 = 0.3553, wR2 = 0.3249
Extinction coefficient	0.0037(4)
Largest diff. peak and hole	1.999 and -0.849 e.Å^{-3}

Method 2 (X=OPh)

63 (20 mg, 0.02 mmol), Ga(acac)$_3$ (10 mg, 0.03 mmol) and phenol (0.75 g) were heated to 220°C for 30 min before allowing to cool to RT. The crude product was then dissolved in benzene and eluted down a short silica column. The red fraction was collected and concentrated in vacuo to give [Ga**63**]OPh as a violet powder (21 mg, 92%); ^{1}H NMR [CDCl$_3$] δ 9.12 (s, 8H, βH), 5.75-5.62 (m, 2H, OPh), 1.81-1.84 (m, 3H, OPh); MS (MALDI): m/z 1042 ((M-OPh)$^+$); ε (DMF): 418 nm (33805 mol$^-$^{1}dm^{3}cm^{-1}), 485 nm nm (178 mol^{-1}dm^{3}cm^{-1}), 550 nm (895 mol^{-1}dm^{3}cm^{-1}). CHN not collected.
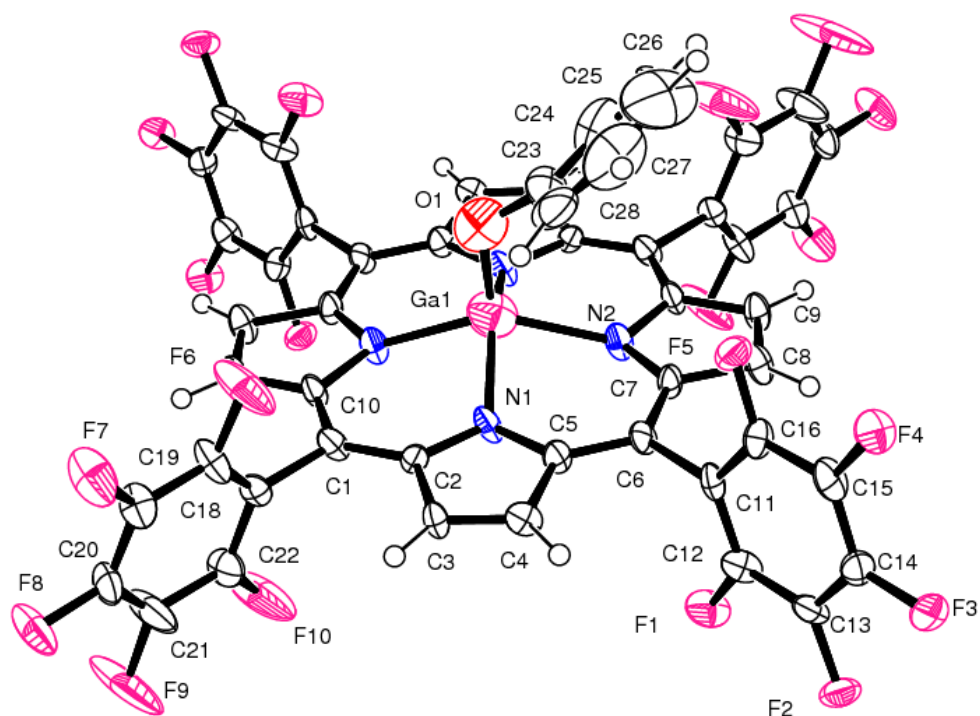
Figure 93: ORTEP representation of the X-ray crystal structure of [Ga63]OPh with all non-H atoms labelled.

Table 23: Crystal data for the structural refinement of [Ga63]OPh.

Identification code	sja21_08
Empirical formula	$C_{56} H_{17} F_{20} Ga_2 N_4 O_2$
Formula weight	1297.18
Temperature	150(2) K
Wavelength	0.71073 Å
Crystal system	Triclinic
Space group	P-1
Unit cell dimensions	a = 8.4379(13) Å $\quad$ α= 81.408(13)°.
	b = 14.743(2) Å $\quad$ β= 78.497(13)°.
	c = 20.582(3) Å $\quad$ γ = 75.383(12)°.
Volume	2414.5(6) Å^3
Z	2
Density (calculated)	1.240 Mg/m^3
Absorption coefficient	0.405 mm^{-1}
F(000)	884
Crystal size	0.31 x 0.25 x 0.16 mm^3
Theta range for data collection	2.87 to 34.80°.
Index ranges	-13<=h<=13, -23<=k<=23, -33<=l<=29
Reflections collected	63466
Independent reflections	20737 [R(int) = 0.1905]
Completeness to theta = 34.80°	99.0 %
Absorption correction	None
Refinement method	Full-matrix least-squares on F^2
Data / restraints / parameters	20737 / 0 / 758
Goodness-of-fit on F^2	0.936
Final R indices [I>2sigma(I)]	R1 = 0.1603, wR2 = 0.4049
R indices (all data)	R1 = 0.3470, wR2 = 0.4577
Extinction coefficient	0.048(4)
Largest diff. peak and hole	1.556 and -2.641 e.Å^{-3}

7.6.8. Synthesis of nickel(II) tetra(pentafluorophenyl) porphyrin [Ni63]
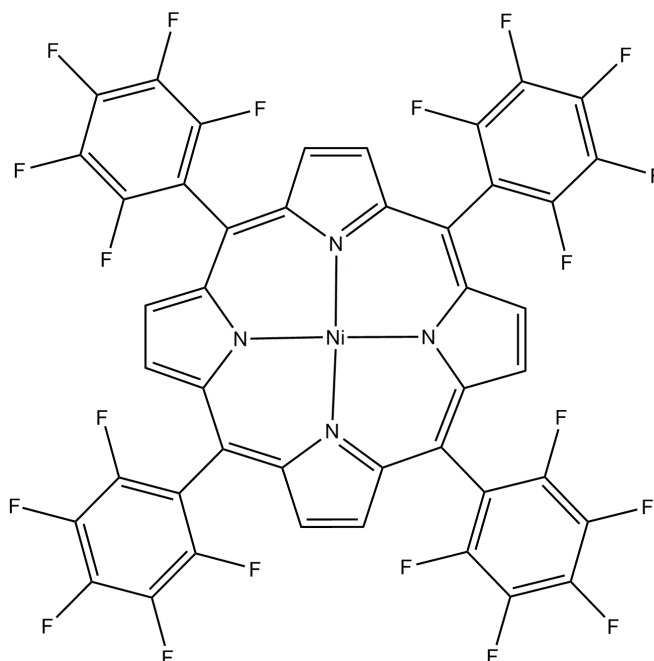
63 (0.08 g, 0.082 mmol) was dissolved in acetic acid (10 ml) to which was added nickel(II) acetate.4H$_2$O (0.02 g, 0.082 mmol). The solution was then heated to reflux for 24 hr. Analysis by TLC showed complete consumption of the starting material. The solution was then concentrated in vacuo to give a purple crystalline material (0.08 g, 95%); R$_f$=0.7 (1/1 hexane/DCM (v/v)); ^{1}H NMR [CDCl$_3$] δ 8.72 (s, 8H, βH); ^{19}F NMR [CDCl$_3$] δ −161.07 (m, 2F, *m*-F), −151.19 (t, 1F, J=20.7 Hz, *p*-F), −136.54 (dd, 2F, J= 6.9, 23.1 Hz, *o*-F); MS (MALDI): *m/z* 1028 (M$^+$); UV-Vis (DCM): 405 nm, 520 nm, 557 nm. CHN not collected.

7.6.9. Synthesis of 5,10,15,20-tetrakis(2,3,5,6-tetrafluoro-4-{2-[2-(2-methoxy-ethoxy)-ethoxy]-ethylsulfanyl}-phenyl)-porphyrin (64)
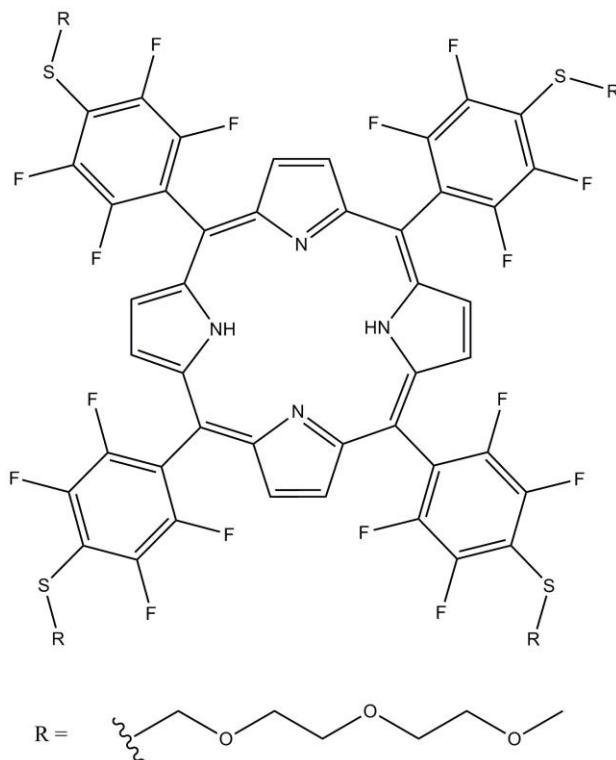
To **63** (200 mg, 0.21 mmol), **31** (0.37 g, 2.1 mmol) and Na_2S (0.16 g, 2.1 mmol) was added DMF (5 ml). The reaction mixture was stirred for 3 days after which, the reaction was judged complete by TLC (absence of starting material). The reaction mixture was then concentrated under reduced pressure before re-dissolving in 50/50 DCM/hexane (50 ml). This solution was then washed with a saturated brine solution from which the organic layer was collected and dried over $MgSO_4$. The purple solution was concentrated in vacuo and the oily residue was washed repeatedly with hexane under the washings were clear to give the title product as a purple oil (240 mg, 75%); ^{1}H NMR [$CDCl_3$] δ 8.92 (s, 8H, βH), 3.85-3.27 (m, 60H, PEG), −2.97 (s, 2H, NH); ^{19}F NMR [$CDCl_3$] δ −133.64 (s, 2F, o-F), −137.03 (s, 2F, m-F); MS (MALDI): m/z= 1615.518 (M$^+$); ε (DMF): 401 nm (264000 mol^{-1}dm^{3}cm^{-1}), 505 nm, 532 nm, 580 nm, 650 nm. CHN not collected.

7.6.10. Synthesis of tetraPEGylated 63 with PEG chains of an average weight of 550 (65)
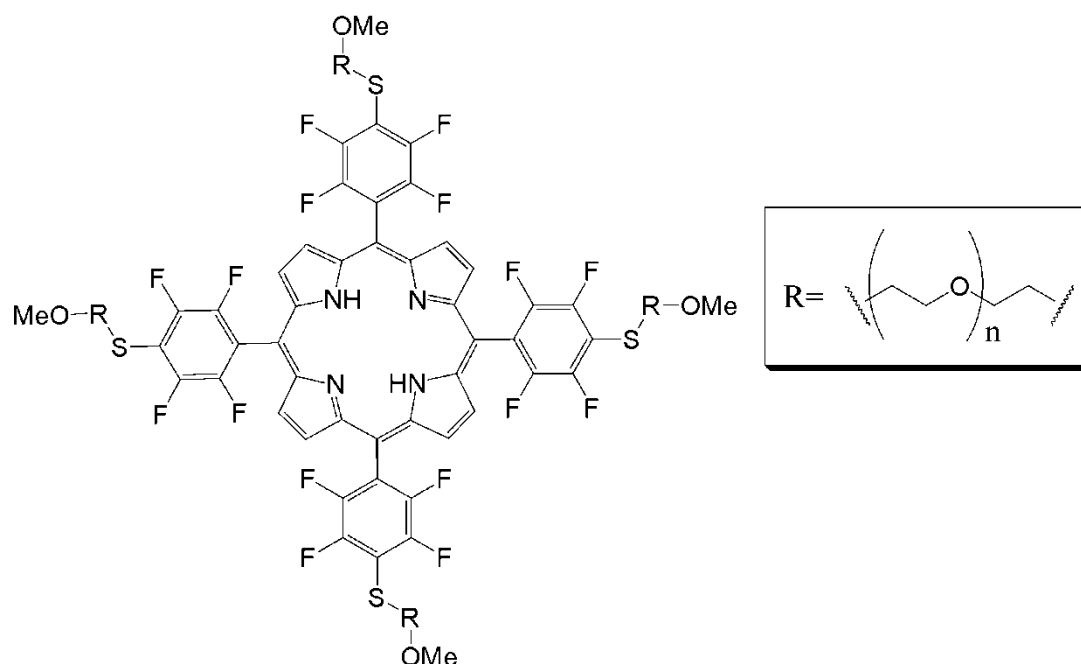
63 (20 mg, 0.021 mmol) and **29** (0.13g, 0.21 mmol) were dissolved in DMF (5 ml). Na_2S (18 mg, 0.21 mmol) was then added and solution stirred at RT for 72 hr. Saturated $NaHCO_{3(aq)}$ (10 ml) was then added and the precipitate that formed was removed by filtration. The filtrate was then concentrated under reduced pressure and the isolated violet oil was then washed repeatedly with hexane until the washings were clear. This gave **65** as a purple solid (0.06 g, 100%): ^{1}H NMR [$CDCl_3$] δ 8.85 (s, 8H, βH), 3.73 (t, xH, J=6.32 Hz), 3.68-3.34 (m, xH, PEG chain), −2.13 (br s, 2H, NH); UV-Vis (DMF): 417 nm, 505 nm, 535 nm, 580 nm, 634 nm. CHN not collected.

7.6.11. Synthesis of PEGylated 63 with PEG chains of an average weight of 750 (66)
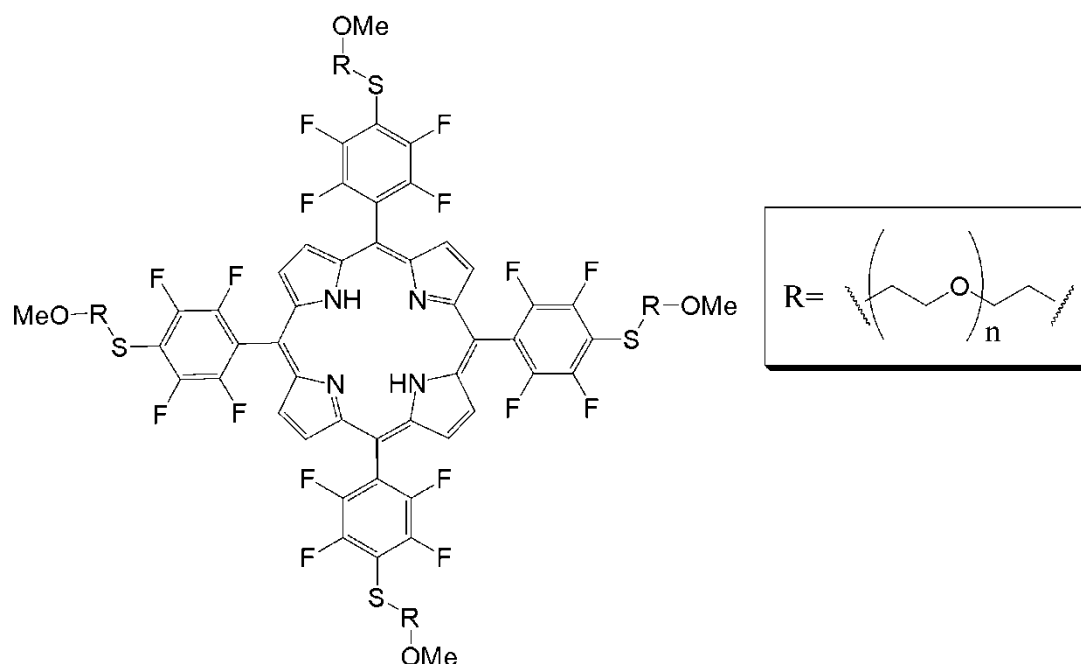
63 (20 mg, 0.021 mmol) and **30** (0.13g, 0.21 mmol) were dissolved in DMF (5 ml). Na_2S (18 mg, 0.21 mmol) was then added and solution stirred at RT for 72 hr. Saturated $NaHCO_{3(aq)}$ (10 ml) was then added and the precipitate that formed was removed by filtration. The filtrate was then concentrated under reduced pressure and the isolated violet oil was then washed repeatedly with hexane until the washings were clear. This gave **66** as a purple solid (110 mg, 87%): ^{1}H NMR [$CDCl_3$] δ 8.89 (s, 8 H, βH), 3.75 (t, J=6.32 Hz, xH, PEG), 3.71-3.45 (m, xH, PEG), 3.41 (t, J=6.32 Hz, xH, PEG), −2.04 (br s, 2H, NH); UV-Vis (DMF): 411 nm, 505 nm, 532 nm, 581 nm, 649 nm. CHN not collected.

7.6.12. Synthesis of nickel(II) 5,10,15,20-tetrakis(2,3,5,6-tetrafluoro-4-{2-[2-(2-methoxy-ethoxy)-ethoxy]-ethylsulfanyl}-phenyl)-porphyrin ([Ni64])

R =
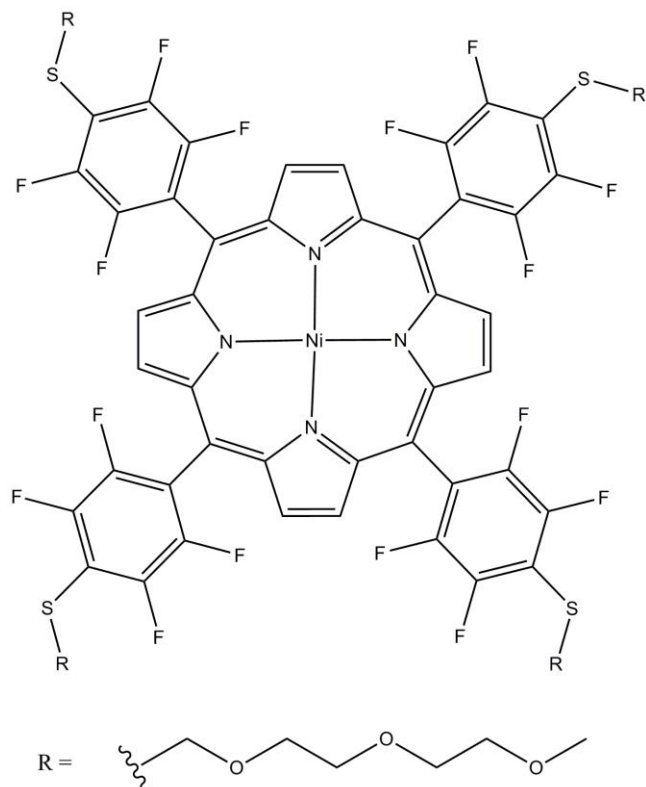
To [Ni**63**] (110 mg, 0.11 mmol), **31** (0.19 g, 1.1 mmol) and Na_2S (0.08 g, 1.1 mmol) was added DMF (5 ml). The reaction mixture was stirred for 3 days after which, the reaction was judged complete by TLC (absence of starting material). The reaction mixture was then concentrated under reduced vacuum before re-dissolving in 50/50 DCM/hexane (50 ml). This solution was then washed with a saturated brine solution from which the organic layer was collected and dried over MgSO4. The purple solution was concentrated in vacuo and the oily residue was washed repeatedly with hexane under the washings were clear to give the title product as a purple oil (110 mg, 62%); ^{1}H NMR [CDCl$_3$] δ 8.74 (s, 8H, βH), 3.87-3.29 (m, 60H, PEG); ^{19}F NMR [CDCl$_3$] δ −133.49 (s, 2F, o-F), −137.14 (s, 2F, m-F); MS (MALDI): m/z = 1087 (MH$_4$-(CH$_2$CH$_2$OCH$_2$CH$_2$OCH$_2$CH$_2$OCH$_3$)$_4$$^+$); ε (DMF): 405 nm (297280 mol^{-1}dm^{3}cm^{-1}), 523 nm (21652 mol^{-1}dm^{3}cm^{-1}), 557 nm (17115 mol^{-1}dm^{3}cm^{-1}). CHN not collected.

7.6.13. Synthesis of gallium(III) 5,10,15,20-tetrakis(2,3,5,6-tetrafluoro-4-{2-[2-(2-methoxy-ethoxy)-ethoxy]-ethylsulfanyl}-phenyl)-porphyrin phenoxide or chloride ([Ga64]X where X= OPh or Cl)

R =

X = OPh or Cl
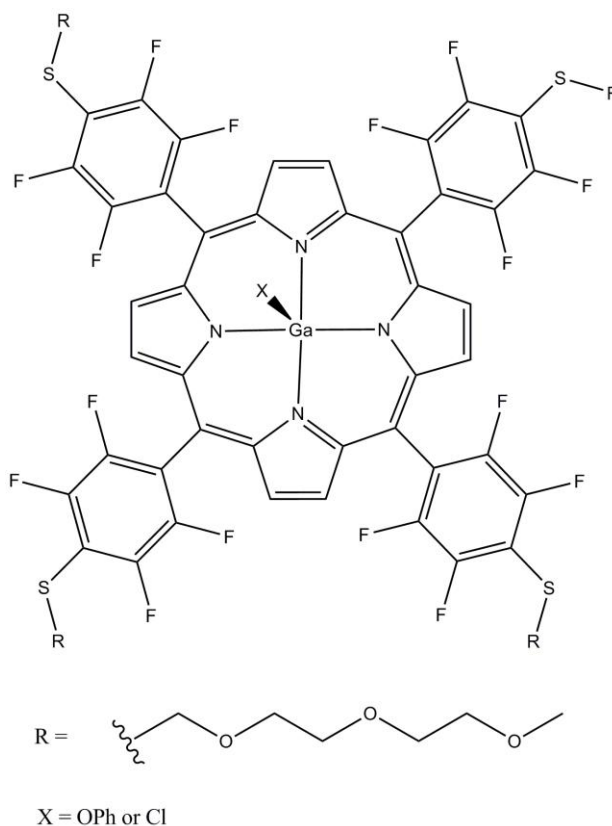
X=OPh

[Ga**63**]OPh (0.1 g, 0.088 mmol), **31** (0.16 g, 0.88 mmol) and Na$_2$S (0.07 g, 0.88 mmol) were dissolved in DMF (5 ml) and stirred at RT for 3 days. TLC (silica, 5/95 MeOH/DCM (v/v)) at this point showed compete consumption of the starting material. The solution was then concentrated under reduced pressure and the resulting material partitioned between DCM (50 ml) and water (100 ml). The organic layer was collected and further washed with brine (100 ml). The organic layer was then dried over MgSO$_4$ and filtered. The filtrate was collected and concentrated under reduced pressure. The oily residue was then repeatedly washed with hexane (~5 x 5 ml) until the washings were clear. The desired compound was isolated as a red oil (0.13 g, 83%); ^{1}H NMR [CDCl$_3$] 9.09 (s, 8H, βH), 3.09-3.24 (m, 60H, PEG), 5.11 (s, 2H, OPh), 1.80 (br s, 3H, OPh); ^{19}F NMR [CDCl$_3$] δ -133.62 (dq, 2F,

J=11.56 and 13.87, *o*-F), -136.54 (dq, 2F, J=11.56, *m*-F), MS (MALDI): *m/z* = 1684 (M-OPh$^+$); ε (DMF): 421 nm (135597 mol^{-1}dm^{3}cm^{-1}), 509 nm (1198 mol^{-1}dm^{3}cm^{-1}), 551 nm (6964 mol^{-1}dm^{3}cm^{-1}). CHN not collected.

X=Cl

64 (150 mg, 0.0924 mmol), sodium acetate (0.04 g, 0.465 mmol) and GaCl$_3$ (0.02 g, 0.124 mmol) were dissolved in dry acetic acid (15 ml). The resulting purple solution was then heated to reflux for 18 hr. The solution was then allowed to cool before filtering off any solids and concentrating under reduced pressure. The crude product was purified by column chromatography (silica, 5/95 MeOH/ DCM (v/v)). The violet/red band was collected and concentrated under reduced pressure to afford a violet solid (0.15 g, 94%); R$_f$=0.35 (5/95 MeOH/ DCM v/v); ^{1}H NMR [CDCl$_3$] δ 9.10 (br s, 8H, βH), 3.81-3.10 (m, 60H, PEG); ^{19}F NMR [CDCl$_3$] δ −133.59 (s, 2F, *o*-F), −137.43 (s, 2F, *m*-F); MS (MALDI): *m/z* = 1684 (M-Cl$^+$); ε (DMF): 420 nm (287972 mol^{-1}dm^{3}cm^{-1}), 508 nm (4250 mol^{-1}dm^{3}cm^{-1}), 551 nm (12559 mol^{-1}dm^{3}cm^{-1}). CHN not collected.

7.6.14. Synthesis of tetraPEGylated [Ga63]OPh with PEG chains of an average weight of 550 ([Ga65]OPh)

[Ga**63**]OPh (0.0076 g, 0.00667 mmol), **29** (0.04 g, 0.0667 mmol) and Na_2S (0.005 g, 0.0668 mmol) were dissolved in DMF (6 ml) and stirred at RT for 72 hr. The solution was then concentrated under reduced pressure and the resulting material partitioned between DCM (50 ml) and water (100 ml). The organic layer was collected and further washed with brine (100 ml). The organic layer was then dried over $MgSO_4$ and filtered. The filtrate was collected and concentrated under reduced pressure. The oily residue was then repeatedly washed with hexane (~5 x 10 ml) until the washings were clear. The desired compound was isolated as a purple oil (0.0197 g, ~94%); ^{1}H NMR [CDCl$_3$] δ 8.88-8.92 (m, 8H, β H), 5.07 (m, 2H, OPh), 3.76 (t, J=6.26 Hz, xH, PEG), 3.72-3.43 (m, xH, PEG), 3.29 (t, J= 6.26 Hz, xH, PEG), 1.73 (m, 3H, OPh); UV-Vis (DMF): 418 nm, 550 nm, 619 nm. CHN not collected.

7.6.15. Synthesis of the tetraPEGylated [Ga63]OPh with PEG chains of an average weight of 750 ([Ga66]OPh)

[Ga**63**]OPh (0.0076 g, 0.00667 mmol), **30** (0.0541 g, 0.0667 mmol) and Na_2S (0.005 g, 0.0668 mmol) were dissolved in DMF (6 ml) and stirred at RT for 72 hr. The solution was then concentrated under reduced pressure and the resulting material partitioned between DCM (50 ml) and water (100 ml). The organic layer was collected and further washed with brine (100 ml). The organic layer was then dried over $MgSO_4$ and filtered. The filtrate was collected and concentrated under reduced pressure. The oily residue was then repeatedly washed with hexane (~5 x 10 ml) until the washings were clear. The desired compound was isolated as a purple oil (0.0257 g, ~93%); ^{1}H NMR [CDCl$_3$] δ 8.91-8.94 (m, 8H, β H), 5.09 (m, 2H, OPh), 3.79 (t, J=6.24 Hz, xH, PEG), 3.74-3.45 (m, xH, PEG), 3.31 (t, J=6.24 Hz, xH, PEG), 1.74 (m, 3H, OPh); ; UV-Vis (DMF): 419 nm, 550 nm, 623 nm. CHN not collected.

7.6.16. Synthesis of tetraPEGylated [Ni63] with PEG chains of an average weight of 550 ([Ni65])

[Ni**63**] (40 mg, 0.0388 mmol), **29** (0.24 g, 0.388 mmol) and Na_2S (0.03 g, 0.388 mmol) were dissolved in DMF (6 ml) and stirred at RT for 72 hr. The solution was then concentrated under reduced pressure and the resulting material partitioned between DCM (50 ml) and water (100 ml). The organic layer was collected and further washed with brine (100 ml). The organic layer was then dried over $MgSO_4$ and filtered. The filtrate was collected and concentrated under reduced pressure. The oil formed by this process was then dissolved in MeOH/ water (3 ml) and transferred to a Float-A-Lyzer. The Float-A-Lyzer was left in distilled water for a week. The solution was then removed from the Float-A-Lyzer and concentrated under reduced pressure. The desired compound was isolated as a purple oil (0.1012 g, ~79%); ^{1}H NMR [$CDCl_3$] δ 8.91 (br s, 8H, βH), 3.81 (t, J=6.26 Hz, xH, PEG), 3.78-3.47 (m, xH PEG), 3.35 (t, J= 6.26 Hz, xH, PEG); UV-Vis (DMF): 404 nm, 523 nm, 556 nm. CHN not collected.

7.6.17. Synthesis of tetraPEGylated [Ni63] with PEG chains of an average weight of 750 ([Ni66])

[Ni**63**] (40 mg, 0.0388 mmol), **30** (0.32 g, 0.388 mmol) and Na_2S (0.03 g, 0.388 mmol) were dissolved in DMF (6 ml) and stirred at RT for 72 hr. The solution was then concentrated under reduced pressure and the resulting material partitioned between DCM (50 ml) and water (100 ml). The organic layer was collected and further washed with brine (100 ml). The organic layer was then dried over $MgSO_4$ and filtered. The filtrate was collected and concentrated under reduced pressure. The oil formed by this process was then dissolved in MeOH/ water (3 ml) and transferred to a Float-A-Lyzer. The Float-A-Lyzer was left in distilled water for a week. The solution was then removed from the Float-A-Lyzer and concentrated under reduced pressure. The desired compound was isolated as a purple oil (0.1478 g, ~95%); ^{1}H NMR [$CDCl_3$] δ 8.83 (br s, 8H, βH), 3.79 (t, J=6.31 Hz, xH, PEG), 3.77-3.43 (m, xH, PEG), 3.34 (t, J= 6.31 Hz, xH, PEG); UV-Vis (DMF): 403 nm, 522 nm, 556 nm. CHN not collected.

7.6.18. Synthesis of tetraPEGylated [Zn63] with PEG chains of an average weight of 550 ([Zn65])

[Zn**63**] (0.1 g, 0.0963 mmol), **29** (0.59 g, 0.963 mmol) and Na$_2$S (0.08 g, 0.963 mmol) were dissolved in DMF (6 ml) and stirred at RT for 72 hr. The solution was then concentrated under reduced pressure and the resulting material partitioned between DCM (50 ml) and water (100 ml). The organic layer was collected and further washed with brine (100 ml). The organic layer was then dried over MgSO$_4$ and filtered. The filtrate was collected and concentrated under reduced pressure. The oil formed by this process was then dissolved in MeOH/ water (3 ml) and transferred to a Float-A-Lyzer. The Float-A-Lyzer was left in distilled water for a week. The solution was then removed from the Float-A-Lyzer and concentrated under reduced pressure. The desired compound was isolated as a purple oil (0.18 g, ~58%); ^{1}H NMR [CDCl$_3$] δ 8.85 (s, 8H, βH), 3.83 (t, J=6.19 Hz, xH, PEG), 3.74-3.49 (m, xH, PEG), 3.36 (t, J= 6.19 Hz, xH, PEG); UV-Vis (DMF): 421 nm, 552 nm, 623 nm. CHN not collected.

7.6.19. Synthesis of tetraPEGylated [Zn63] with PEG chains of an average molecular weight of 750 ([Zn66])

[Zn**63**] (0.1 g, 0.0963 mmol), **30** (0.78 g, 0.963 mmol) and Na$_2$S (0.08 g, 0.963 mmol) were dissolved in DMF (6 ml) and stirred at RT for 72 hr. The solution was then concentrated under reduced pressure and the resulting material partitioned between DCM (50 ml) and water (100 ml). The organic layer was collected and further washed with brine (100 ml). The organic layer was then dried over MgSO$_4$ and filtered. The filtrate was collected and concentrated under reduced pressure. The oil formed by this process was then dissolved in MeOH/ water (3 ml) and transferred to a Float-A-Lyzer. The Float-A-Lyzer was left in distilled water for a week. The solution was then removed from the Float-A-Lyzer and concentrated under reduced pressure. The desired compound was isolated as a purple oil (0.28 g, ~72%); ^{1}H NMR [CDCl$_3$] δ 8.98 (br s, 8 H, β H), 3.88 (t, J=6.27 Hz, xH, PEG), 3.79-3.44 (m, xH, PEG), 3.34 (t, J=6.27 Hz, xH, PEG); UV-Vis (DMF): 420 nm, 552 nm, 623 nm. CHN not collected.

7.6.20. Synthesis of zinc(II)5,10-15-tris-pentafluorophenyl-20-(2,3,5,6-tetrafluoro-4-{2-[2-(2-methoxy-ethoxy)-ethoxy]-ethylsulfanyl}-phenyl)-porphyrin ([Zn67])
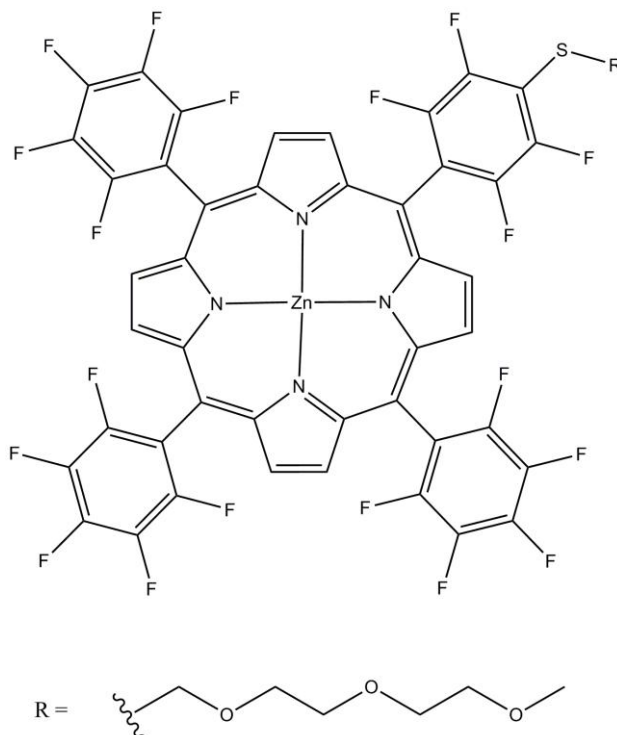
[Zn**63**] (110 mg, 0.106 mmol), **31** (0.19 g, 1.06 mmol) and Na$_2$S (0.08 g, 1.06 mmol) were dissolved in DMF and heated to 60°C for three weeks. The solution was then allowed to cool to RT and the resulting solution concentrated under reduced pressure. The oily residue was partitioned between DCM (50 ml) and water (100 ml). The organic layer was then dried over MgSO$_4$ and filtered. The filtrate was collected and concentrated under reduced pressure. The crude material was purified by column chromatography (silica, eluent: DCM initially followed by 10/90 MeOH/DCM (v/v)). The fractions containing the product were isolated and concentrated under reduced pressure to yield the desired compound as a red oil (0.01 g, 8%); R$_f$=0.45 (10/90 MeOH/DCM (v/v)); ^{1}H NMR [CDCl$_3$] δ 8.86 (br s, 8H, βH), 3.58-3.24 (m, 15H, PEG); ^{19}F NMR [CDCl$_3$] −134.04 to −137.60 (m, 12F, *o-* and *m*-F), −152.23 to −152.28 (m, 3F, *p*-F); MS (MALDI): *m/z*= 1197.95 (M$^+$); UV-Vis (DMF): 419 nm, 552 nm, 585 nm. CHN not collected.

8. References

(1)   Lindoy, L. F. *The Chemistry of Macrocyclic Ligand Complexes*; Cambridge University press: Cambridge, **1989**.

(2)   Yatsimirskii, K. B. *Theo. Exp. Chem.* **1980**, *16*, 28-33.

(3)   Cabbiness, D. K.; Margerum, D. W. *J. Am. Chem. Soc.* **1969**, *91*, 6540-6542.

(4)   Cabbiness, D. K.; Margerum, D. W. *J. Am. Chem. Soc.* **1970**, *92*, 2151-2153.

(5)   Pletnev, I. V. In *Macrocyclic Compounds in Analytical Chemistry*; Zolotov, Y. A., Ed.; John Wiley & Sons Inc: New York, **1997**; *Vol. 143*.

(6)   Micheloni, M.; Paoletti, P.; Sabatini, A. *J. Chem. Soc., Dalton Trans.* **1983**, 1169-72.

(7)   Costamagna, J.; Ferraudi, G.; Matsuhiro, B.; Campos-Vallette, M.; Canales, J.; Villagrán, M.; Vargas, J.; Aguirre, M. J. *Coord. Chem. Rev.* **2000**, *196*, 125-164.

(8)   Liang, F.; Wan, S.; Li, Z.; Xiong, X.; Yang, L.; Zhou, X.; Wu, C. *Curr. Med. Chem.* **2006**, *13*, 711-727.

(9)   Mancin, F.; Tecilla, P. *New J. Chem.* **2007**, *31*, 800-817.

(10)   Bunn, S. E.; Liu, C. T.; Lu, Z.-L.; Neverov, A. A.; Brown, R. S. *J. Am. Chem. Soc.* **2007**, *129*, 16238-16248.

(11)   Lu, Z.-L.; Liu, C. T.; Neverov, A. A.; Brown, R. S. *J. Am. Chem. Soc.* **2007**, *129*, 11642-11652.

(12)   Qian, J.; Gu, W.; Liu, H.; Gao, F.; Feng, L.; Yan, S.; Liao, D.; Cheng, P. *Dalton Trans.* **2007**, 1060-1066.

(13)   Addison, A. W.; Rao, T. W.; van Reedijk, J.; Verschoor, G. C. *J. Chem. Soc., Dalton Trans.* **1984**, 1349-1356.

(14)   Bai, S. Q.; Gao, E. Q.; Z., H.; Fabg, C. F.; Yan, C. H. *New J. Chem.* **2005**, *29*, 935-941.

(15)   Sheng, X.; Guo, X.; Lu, X.-M.; Lu, G.-Y.; Shao, Y.; Liu, F.; Xu, Q. *Bioconjugate Chem.* **2008**, *19*, 490-498.

(16)   Burdinski, D.; Bothe, E.; Wieghardt, K. *Inorg. Chem.* **2000**, *39*, 105-116.

(17)   Fernandes, A. S.; Gasper, J.; Cabral, M. F.; Caneiras, C.; Guedes, R.; Rueff, J.; Castro, M.; Costa, J.; Oliveira, N. G. *J. Inorg. Biochem.* **2007**, *101*, 849-858.

(18)   Chong, H.-S.; Garmestani, K.; Ma, D.; Milenic, D. E.; Overstreet, T.; Brechbiel, M. W. *J. Med. Chem.* **2002**, *45*, 2458-3464.

(19)   Blower, P. J.; Lewis, J. S.; Zweit, J. *Nucl. Med. Bio.* **1996**, *23*, 957-980.

(20)   Chong, H.-S.; Mhaske, S.; Lin, M.; Bhuniya, S.; Song, H. A.; Brechbiel, M. W.; Sun, X. *Bioorg. Med. Chem. Lett.* **2007**, *17*, 6107-6110.

(21)   Chong, H.-S.; Song, H. A.; Ma, X.; Milenic, D. E.; Brady, E. D.; Lim, S.; Lee, H.; Baidoo, K. E.; Cheng, D.; Brechbiel, M. W. *Bioconjugate Chem.* **2008**, *19*, 1439-1447.

(22)   Chong, H.-S.; Ma, X.; Lee, H.; Bui, P.; Song, H. A.; Birch, N. *J. Med. Chem.* **2008**, *51*, 2208-2215.

(23)   Eisenwiener, K.-P.; Prata, M. I. M.; Buschmann, J.; Zhang, H.-W.; Santos, A. C.; Wenger, S.; Reubi, J. C.; Mäcke, H. R. *Bioconjugate Chem.* **2002**, *13*, 530-541.

(24)   Morelein, S. M.; Welch, M. J. *Int. J. Nucl. Med. Biol.* **1981**, *8*, 277-287.

(25)   Eisenwiener, K.-P.; Powell, P.; Mäcke, H. R. *Bioorg. Med. Chem. Lett.* **2000**, *10*, 2133-2135.

(26)   Gasser, G.; Tjioe, L.; Graham, B.; Belousoff, M. J.; Juran, S.; Walther, M.; Künstler, J.-U.; Bergmann, R.; Stephan, H.; Spiccia, L. *Bioconjugate Chem.* **2008**, *19*, 719-730.

(27)   Yang, C.-T.; Sreerama, S. G.; Hsieh, W.-Y.; Liu, S. *Inorg. Chem.* **2008**, *47*, 2719-2727.

(28)   Stavila, V.; Allali, M.; Canaple, L.; Stortz, Y.; Franc, C.; Maurin, P.; Beuf, O.; Dufay, O.; Samarut, J.; Janier, M.; Hasserodt, J. *New J. Chem.* **2008**, *32*, 428-435.

(29)   Wieghardt, K.; Schoffmann, E.; Nuber, B.; Weiss, J. *Inorg. Chem.* **1986**, *25*, 4877-4883.

(30)   Christiansen, L.; Hendrickson, D. N.; Toftlund, H.; Wilson, S. R.; Xie, C. L. *Inorg. Chem.* **1986**, *25*, 2813-2818.

(31)   Spiccia, L.; Fallon, G. D.; Grannas, M. J.; Nichols, P. J.; Tiekink, E. R. T. *Inorg. Chim. Acta* **1998**, *279*, 192-199.

(32)   Delgado, R.; Félix, V.; Lima, L. M. P.; Price, D. W. *Dalton Trans.* **2007**, 2734-2745.

(33)   Liang, X.; Sadler, P. J. *Chem. Soc. Rev.* **2004**, *33*, 246-266.

(34)   Hubin, T. J. *Coord. Chem. Rev.* **2003**, *241*, 27-46.

(35)   Boswell, C. A.; Sun, X.; Niu, W.; Weisman, G. R.; Wong, E. H.; Rheingold, A. L.; Anderson, C. J. *J. Med. Chem.* **2004**, *47*, 1465-1474.

(36)   Liu, S.; Edwards, D. S. *Bioconjugate Chem.* **2001**, *12*, 7-34.

(37)   Sprague, J. E.; Peng, Y.; Fiamengo, A. L.; Woodin, K. S.; Southwick, E. A.; Weisman, G. R.; Wong, E. H.; Golen, J. A.; Rheingold, A. L.; Anderson, C. J. *J. Med. Chem.* **2007**, *50*, 2527-2535.

(38)   Heroux, K. J.; Woodin, K. S.; Tranchemontagne, D. J.; Widger, P. C. B.; Southwick, E. A.; Wong, E. H.; Weisman, G. R.; Tomellini, S. A.; Wadas, T. J.; Anderson, C. J.; Kassel, S.; Golen, J. A.; Rheingold, A. L. *Dalton Trans.* **2007**, 2150-2162.

(39)   Sun, X.; Wuest, M.; Weisman, G. R.; Wong, E. H.; Reed, D. P.; Boswell, C. A.; Motekaitis, R.; Martell, A. E.; Welch, M. J.; Anderson, C. J. *J. Med. Chem.* **2002**, *45*, 469-477.

(40)   Bass, L. A.; Wang, M.; Welch, M. J.; Anderson, C. J. *Bioconjugate Chem.* **2000**, *11*, 527-532.

(41)   Silversides, J. D.; Allan, C. C.; Archibald, S. J. *Dalton Trans.* **2007**, 971-978.

(42)   Sun, X.; Kim, J.; Martell, A. E.; Welch, M. J.; Anderson, C. J. *Nucl. Med. Bio.* **2004**, *31*, 1051-1059.

(43)   Kaden, T. A. *Dalton Trans.* **2006**, 3617-3623.

(44)   Sprague, J. E.; Peng, Y.; Sun, X.; Weisman, G. R.; Wong, E. H.; Achilefu, S.; Anderson, C. J. *Clin. Cancer Res.* **2004**, *10*, 8674-8682.

(45)   Li, W. P.; Lewis, J. S.; Kim, J.; Bugaj, J. E.; Johnson, M. A.; Erion, J. L.; Anderson, C. J. *Bioconjugate Chem.* **2002**, *13*, 721-728.

(46)   Ugur, Ö.; Kothari, P. J.; Finn, R. D.; Zanzonico, P.; Ruan, S.; Guehther, I.; Maecke, H. R.; Larson, S. M. *Nucl. Med. Bio.* **2002**, *29*, 147-157.

(47)   Deshmukh, M. V.; Voll, G.; Kühlewein, A.; Mäcke, H.; Schmitt, J.; Kessler, H.; Gemmecker, G. *J. Med. Chem.* **2005**, *48*, 1506-1514.

(48)   Boswell, C. A.; Regino, C. A. S.; Baidoo, K. E.; Wong, K. J.; Bumb, A.; Xu, H.; Milenic, D. E.; Kelley, J. A.; Lai, C. C.; Brechbiel, M. W. *Bioconjugate Chem.* **2008**, *19*, 1476-1484.

(49)   Liang, X.; Parkinson, J. A.; Weishäupl, M.; Gould, R. O.; Paisey, S. J.; Park, H.-s.; Hunter, T. M.; Blindauer, C. A.; Parsons, S.; Sadler, P. J. *J. Am. Chem. Soc.* **2002**, *124*, 9105-9112.

(50)   Hunter, T. M.; McNae, I. W.; Simpson, D. P.; Smith, A. M.; Moggach, S.; White, F.; Walkinshaw, M. D.; Parsons, S.; Sadler, P. J. *Chem. Eur. J.* **2007**, *13*, 40-50.

(51)   Bosnich, B.; Poon, C. K.; Tobe, M. L. *Inorg. Chem.* **1965**, *4*, 1102-1108.

(52)   McRobbie, G.; Valks, G. C.; Empson, C. J.; Khan, A.; Silversides, J. D.; Pannecouque, C.; De Clerq, E.; Fiddy, S. G.; Bridgeman, A. J.; Young, N. A.; Archibald, S. J. *Dalton Trans.* **2007**, 5008-5018.

(53)   Valks, G. C.; McRobbie, G.; Lewis, E. A.; Hubin, T. J.; Hunter, T. M.; Sadler, P. J.; Pannecouque, C.; De Clerq, E.; Archibald, S. J. *J. Med. Chem.* **2006**, *49*, 6162-6165.

(54)   Khan, A.; Silversides, J. D.; Madden, L.; Greenman, J.; Archibald, S. J. *Chem. Commun.* **2006**, 416-418.

(55)   Sibert, J. W.; Cory, A. H.; Cory, J. G. *Chem. Commun.* **2002**, 154-155.

(56)   Epstein, D. M.; Chappell, L. L.; Khalili, H.; Supkowski, R. M.; Horrocks, W. D.; Morrow, J. R. *Inorg. Chem.* **2000**, *39*, 2130-2134.

(57)   Baker, B. F.; Khalili, H.; Wei, N.; Morrow, J. R. *J. Am. Chem. Soc.* **1997** *119*, 8749-8755.

(58)   Rossiter, C. S.; Mathews, R. A.; Morrow, J. R. *J. Inorg. Biochem.* **2007**, *101*, 925-934.

(59)   Bazzicalupi, C.; Bencini, A.; Berni, E.; Giorgi, C.; Maoggi, S.; Valtancoli, B. *Dalton Trans.* **2003**, 3574-3580.

(60)   Yoo, J.; Reichert, D. E.; Welch, M. J. *J. Med. Chem.* **2004**, *47*, 6625-6637.

(61)   Barbaro, P.; Bianchini, C.; Capannesi, G.; Di Luca, L.; Laschi, F.; Petroni, D.; Salvadori, P. A.; Vacca, A.; Vizza, F. *J. Chem. Soc., Dalton Trans.* **2000**, 2393-2401.

(62)   Sun, X.; Wuest, M.; Kovács, Z.; Sherry, A. D.; Motekaitis, R.; Zheng, W.; Martell, A. E.; Welch, M. J.; Anderson, C. J. *J. Biol. Inorg. Chem.* **2003**, *8*, 217-225.

(63)   Marques, F.; Gano, L.; Campello, M. P.; Lacerda, S.; Santos, I.; Lima, L. M. P.; Costa, J.; Antunes, P.; Delgado, R. *J. Inorg. Biochem.* **2006**, *100*, 270-280.

(64)   Vitha, T.; Kubicek, V.; Hermann, P.; Vander Elst, L.; Muller, R. N.; Kolar, Z. I.; Wolterbeck, H. T.; Breeman, W. A. P.; Lukes, I.; Peters, J. A. *J. Med. Chem.* **2008**, *51*, 677-683.

(65)   De León-Rodríguez, L. M.; Kovács, Z. *Bioconjugate Chem.* **2008**, *19*, 391-402.

(66)   Yang, J. J.; Yang, J.; Wei, L.; Zurkiya, O.; Yang, W.; Li, S.; Zou, Y.; Wilkins Maniccia, A. L.; Mao, H.; Zhao, F.; Malchow, R.; Zhao, S.; Johnson, J.; Hu, X.; Krogstad, E.; Liu, Z.-R. *J. Am. Chem. Soc.* **2008**, *130*, 9260-9267.

(67)   Dijkagraaf, I.; Rijnders, A. Y.; Soede, A.; Dechesne, A. C.; Wima von Esse, G.; Brouwer, A. J.; Corstens, F. H. M.; Boerman, O. C.; Rijkers, D. T. S.; Liskamp, R. M. J. *Org. Biomol. Chem.* **2007**, *5*, 935-944.

(68)   Heppeler, A.; Froidevaux, S.; Macke, H. R.; Jermann, E.; Béhé, M.; Powell, P.; Hennig, M. *Chem. Eur. J.* **1999**, *5*, 1974-1981.

(69)   Banerjee, S.; Das, T.; Chakraborty, S.; Samuel, G.; Korde, A.; Venkatesh, M.; Pillai, M. R. A. *Bioorg. Med. Chem.* **2005**, *13*, 4315-4322.

(70)   Duval, R. A.; Allmon, R. L.; Lever, J. R. *J. Med. Chem.* **2007**, *50*, 2144-2156.

(71)   André, J. P.; Geraldes, C. F. G. C.; Martins, J. A.; Merbach, A. E.; Prata, M. I. M.; Santos, A. C.; de Lima, J. J. P.; Tóth, É. *Chem. Eur. J.* **2004**, *10*, 5804-5816.

(72)   Moshin, H.; Fitzsimmons, J.; Shelton, T.; Hoffman, T. J.; Cutler, C. S.; Lewis, M. R.; Athey, P. S.; Gulyas, G.; Kiefer, G. E.; Frank, R. K.; Simon, J.; Lever, S. Z.; Jurisson, S. S. *Nucl. Med. Bio.* **2007**, *34*, 493-502.

(73)   Zhang, H.; Schuhmacher, J.; Waser, B.; Wild, D.; Eisenhut, M.; Reubi, J. C.; Maecke, H. R. *Eur. J. Nucl. Med. Mol. Imaging* **2007**, *34*, 1198-1208.

(74)   Hermann, P.; Kotek, J.; Kubíček, V.; Lukeš, I. *Dalton Trans.* **2008**, 3027-3047.

(75)   Duimistra, J. A.; Femia, F. J.; Meade, T. J. *J. Am. Chem. Soc.* **2005**, *127*, 12847-12855.

(76)   Urbanczyk-Pearson, L. M.; Femia, F. J.; Smith, J.; Parigi, G.; Duimistra, J. A.; Eckermann, A. L.; Luichnat, C.; Meade, T. J. *Inorg. Chem.* **2008**, *47*, 56-68.

(77)   Botta, M.; Quici, S.; Pozzi, G.; Marzanni, G.; Pagliarin, R.; Barra, S.; Geminatti Crich, S. *Org. Biomol. Chem.* **2004**, *2*, 570-577.

(78)   Woods, M.; Kiefer, G. E.; Bott, S.; Castillo-Muzquiz, A.; Eshelbrenner, C.; Michaudet, L.; McMillan, K.; Mudigunda, S. D. K.; Ogrin, D.; Tircsó, G.; Zhang, S.; Zhao, P.; Sherry, A. D. *J. Am. Chem. Soc.* **2004**, *126*, 9248-9256.

(79)   Ratnaker, S. J.; Woods, M.; Lubag, A. J. M.; Kovács, Z.; Sherry, A. D. *J. Am. Chem. Soc.* **2007**, *130*, 6-7.

(80)   Kamaly, N.; Kalber, T.; Ahmad, A.; Oliver, M. H.; So, P.-W.; Herlihy, A. H.; Bell, J. D.; Jorgensen, M. R.; Miller, A. D. *Bioconjugate Chem.* **2008**, *19*, 118-129.

(81)   Overoye-Chan, K.; Koemer, S.; Looby, R. J.; Kolodziej, A. F.; Zech, S. G.; Deng, Q.; Chasse, J. M.; McMurry, T. J.; Caravan, P. *J. Am. Chem. Soc.* **2008**, *130*, 6025-6039.

(82)   Dhingra, K.; Maier, M. E.; Beyerlein, M.; Angelovski, G.; Logothetis, N. K. *Chem. Commun.* **2008**, *2008*, 3444-3446.

(83)   Song, Y.; Kohlmeir, E. K.; Meade, T. J. *J. Am. Chem. Soc.* **2008**, *130*, 6662-6663.

(84)   Yoo, B.; Pagel, M. D. *Tetrahedron Lett.* **2006**, *47*, 7327-7330.

(85)   Dickins, R. S.; Badari, A. *Dalton Trans.* **2007**, 3661-3668.

(86)   Wojciechowski, F.; Suchy, M.; Li, A. X.; Azab, H. A.; Bartha, R.; Hudson, R. H. E. *Bioconjugate Chem.* **2007**, *18*, 1625-1636.

(87)   Singh, R. V.; Chaudhary, A. *J. Inorg. Biochem.* **2004**, *98*, 1712-1721.

(88)   Tao, Z.-F.; Wang, L.; Stewart, K. D.; Chen, Z.; Gu, W.; Bui, M.-H.; Merta, P.; Zhang, H.; Kovar, P.; Johnson, E.; Park, C.; Judge, R.; Rosenberg, S.; Sowin, T.; Lin, N.-H. *J. Med. Chem.* **2007**, *50*, 1514-1527.

(89)   Pandya, S.; Yu, J.; Parker, D. *Dalton Trans.* **2006**, 2757-2766.

(90)   Murray, B. S.; New, E. J.; Pal, R.; Parker, D. *Org. Biomol. Chem.* **2008**, *6*, 2085-2094.

(91)   Pope, S. J. A.; Kenwright, A. M.; Heath, S. L.; Faulkner, S. *Chem. Commun.* **2003**, 1550-1551.

(92)   Pope, S. J. A.; Kenwright, A. M.; Boote, V. A.; Faulkner, S. *Dalton Trans.* **2003**, 3780-3784.

(93)   Faulkner, S.; Pope, S. J. A. *J. Am. Chem. Soc.* **2003**, *125*, 10526-10527.

(94)   Kimura, E.; Kikuta, E. *J. Biol. Inorg. Chem.* **2000**, *5*, 139-155.

(95)   Pope, S. J. A.; Laye, R. H. *Dalton Trans.* **2006**, 3108-3113.

(96)   Aoki, S.; Sakurama, K.; Ohshima, R.; Matsuo, N.; Yamada, Y.; Takasawa, R.; Tanuma, S.; Takeda, K.; Kimura, E. *Inorg. Chem.* **2008**, *47*, 2747-2754.

(97)   Aoki, S.; Sakurama, K.; Matsuo, N.; Yamada, Y.; Takasawa, R.; Tanuma, S.; Shiro, M.; Takeda, K.; Kimura, E. *Chem. Eur. J.* **2006**, *12*, 9066-9080.

(98)   Ferrand, A.-C.; Imbert, D.; Chauvin, A.-S.; Vandevyver, C. D. B.; Bünzli, J.-C. G. *Chem. Eur. J.* **2007**, *13*, 8678-8687.

(99)   Hanaoka, K.; Kikuchi, K.; Kobayashi, S.; Nagano, T. *J. Am. Chem. Soc.* **2007**, *129*, 13502-13509.

(100)   Voloshin, Y. Z.; Varzatskii, O. A.; Bubnov, Y. N. *Russ. Chem. Bull.* **2007**, *56*, 577-605.

(101)   Farquhar, E. R.; Richard, J. P.; Morrow, J. R. *Inorg. Chem.* **2007**, *46*, 7169-7177.

(102)   Clifford, T.; Danby, A. M.; Lightfoot, P.; Richens, D. T.; Hay, R. W. *J. Chem. Soc., Dalton Trans.* **2001**, 240-246.

(103)   Liu, J.; Zhang, H.; Chen, C.; Deng, H.; Lu, T.; Ji, L. *Dalton Trans.* **2003**, 114-119.

(104)   Zheng, Q.; Dai, H.; Merrit, M. E.; Malloy, C.; Pan, C. Y.; Li, W.-H. *J. Am. Chem. Soc.* **2005**, *127*, 16178-16188.

(105)   Di Bartolo, N.; Sargeson, A. M.; Smith, S. V. *Org. Biomol. Chem.* **2006**, *4*, 3350-3357.

(106)   Singh, D. P.; Kumar, R.; Malik, V. *Transition Met. Chem.* **2007**, *32*, 1051-1055.

(107)   Schmitt, F.; Govindaswamy, P.; Süss-Fink, G.; Han Ang, W.; Dyson, P. J.; Juillerat-Jeanneret, L.; Therrien, B. *J. Med. Chem.* **2008**, *51*, 1811-1816.

(108)   Gravier, J.; Schneider, R.; Frochot, C.; Bastogne, T.; Schmitt, F.; Didelon, J.; Guillemin, F.; Barberi-Heyob, M. *J. Med. Chem.* **2008**, *51*, 3867-3877.

(109)   Scalise, I.; Durantini, E. N. *J. Photochem. Photobiol., A* **2004**, *162*, 105-113.

(110)   Choi, C.-F.; Huang, J.-D.; Lo, P.-C.; Fong, W.-P.; Ng, D. K. P. *Org. Biomol. Chem.* **2008**, *6*, 2173-2181.

(111)   Li, H.; Jensen, T. J.; Fronczek, F. R.; Vicente, M. G. H. *J. Med. Chem.* **2008**, *51*, 502-511.

(112)   Sibrian-Vazquez, M.; Ortiz, J.; Nesterova, I. V.; Fernández-Lázaro, F.; Sastre-Santos, A.; Soper, S. A.; Vicente, M. G. H. *Bioconjugate Chem.* **2007**, *2007*, 410-420.

(113)   Rozanova, N.; Zhang, J. Z.; Heck, D. E. *Cancer Lett.* **2007**, *252*, 216-224.

(114)   Rebouças, J. S.; Spasojević, I.; Tjahjono, D. H.; Richaud, A.; Méndez, F.; Benov, L.; Batinić-Haberle, I. *Dalton Trans.* **2007**, 1233-1242.

(115)   Batinić-Haberle, I.; Spasojević, I.; Stevens, R. D.; Bondurant, B.; Okado-Matsumoto, A.; Fridovich, I.; Vujašković, Ž.; Dewhirst, M. W. *Dalton Trans.* **2006**, 617-624.

(116)   Tabata, M.; Sarker, A. K.; Nyarko, E. *J. Inorg. Biochem.* **2003**, *94*, 50-58.

(117)   Davies, P. J.; Wainwright, K. P. *Inorg. Chim. Acta* **1999**, *294*, 103-108.

(118)   Kielar, F.; Law, G.-L.; New, E. J.; Parker, D. *Org. Biomol. Chem.* **2008**, *6*, 2256-2258.

(119)   Griller, D.; Barclay, L. R. C.; Ingold, K. U. *J. Am. Chem. Soc.* **1975**, *97*, 6151-6154.

(120)   Altwicker, E. R. *Chem. Rev.* **1967**, *67*, 475-531.

(121)   Land, E. J.; Porter, G. *J. Chem. Soc.* **1961**, 3540-3542.

(122)   Adamo, C.; Subra, R.; Di Matteo, A.; Barone, V. *J. Chem. Phys.* **1998**, *109*, 10244-10254.

(123)   Tripathi, G. N. R.; Sun, Q.; Armstrong, D. A.; Chipman, D. M.; Schuler, R. H. *J. Phys. Chem.* **1992**, *96*, 5344-5350.

(124)   Benisvy, L.; Blake, A. J.; Collison, D.; Davies, E. S.; Garner, C. D.; McInnes, E. J. L.; McMaster, J.; Whittaker, G.; Wilson, C. *Chem. Commun.* **2001**, 1824-1825.

(125)   Rogers, M. S.; Dooley, D. M. *Curr. Opin. Chem. Biol.* **2003**, *7*, 189-196.

(126)   Pujols-Ayala, I.; Barry, B. A. *Biochim. Biophys. Acta* **2004**, *1655*, 205-216.

(127)   Ito, N.; Phillips, S. E. V.; Stevens, C.; Ogel, Z. B.; McPherson, M. J.; Keen, J. N.; Yadav, K. D. S.; Knowles, P. F. *Nature* **1991**, *350*, 87-90.

(128)   Whittaker, J. W. *Arch. Biochem. Biophys.* **2005**, *433*, 227-239.

(129)   McPherson, M. J.; Parsons, M. R.; Spooner, R. K.; Wilmot, C. M. *Handbook of Metalloproteins*; John Wiley and Sons Ltd.: New York, **2001**; *Vol. 2*.

(130)   Kolberg, M.; Strand, K. R.; Graff, P.; Andersson, K. K. *Biochim. Biophys. Acta* **2004**, *1699*, 1-34.

(131)   Becker, A.; Kabsch, W. *J. Biol. Chem.* **2002**, *277*, 40036-40042.

(132)   Sokolowski, A.; Müller, J.; Weyhermüller, T.; Schnepf, R.; Hildebrandt, P.; Hildenbrand, K.; Bothe, E.; Wieghardt, K. *J. Am. Chem. Soc.* **1997**, *119*, 8889-8900.

(133)   Weissman, S. A.; Zewge, D. *Tetrahedron* **2005**, *61*, 7833-7863.

(134)   Counsell, R. E.; Desai, P.; Kulkarni, P. G. *J. Med. Chem.* **1971**, *14*, 789-792.

(135)   Jiménez, C. A.; Belmar, J. B. *Tetrahedron* **2005**, *61*, 3933-3938.

(136)   Hansen, M. H.; Riggs, J. R. *Tetrahedron Lett.* **1998**, *39*, 2705-2706.

(137)   Stockheim, C.; Hoster, L.; Weyhermüller, T.; Wieghardt, K.; Nuber, B. *J. Chem. Soc., Dalton Trans.* **1996**, 4409-4416.

(138)   Miyashita, N.; Yoshikoshi, A.; Grieco, P. A. *J. Org. Chem.* **1977**, *42*, 3772-3774.

(139)   Khan, A. T.; Choudhury, L. H.; Ghosh, S. *Tetrahedron Lett.* **2004**, *45*, 7891-7894.

(140)   Benarab, A.; Boyé, S.; Savelon, L.; Guillaumet, G. *Tetrahedron Lett.* **1993**, *34*, 7567-7568.

(141)   Rundel, W. *Chem. Ber.* **1969**, *102*, 359-370.

(142)   Kimura, S.; Bill, E.; Bothe, E.; Weyhermüller, T.; Wieghardt, K. *J. Am. Chem. Soc.* **2001**, *123*, 6025-6039.

(143)   Kruse, T.; Weyhermüller, T.; Wieghardt, K. *Inorg. Chim. Acta* **2002**, *331*, 81-89.

(144)   Beissel, T.; Glaser, T.; Kesting, F.; Wieghardt, K.; Nuber, B. *Inorg. Chem.* **1996**, *35*, 3936-3947.

(145)   Edler, R.; Voβ, J. *Chem. Ber.* **1989**, *122*, 187-191.

(146)   Field, L.; Clark, R. D. *Org. Synth.* **1958**, *38*, 62.

(147)   Harman, J. P.; Field, L. *J. Org. Chem.* **1986**, *51*, 5235-5244.

(148)   Nicholson, G.; Silversides, J. D.; Archibald, S. J. *Tetrahedron Lett.* **2006**, *47*, 6541-6544.

(149)   Eisenwiener, K.-P.; Powell, P.; Mäcke, H. R. *Bioorg. Med. Chem. Lett.* **2000**, *10*, 2133-2135.

(150)   Armstrong, A.; Brackenridge, I.; Jackson, R. F. W.; Kirk, J. M. *Tetrahedron Lett.* **1988**, *29*, 2483-2486.

(151)   Jorgensen, W. L.; Severance, D. L. *J. Am. Chem. Soc.* **1990**, *112*, 4768-4774.

(152)   Gudipati, V.; Curran, D. P.; Wilcox, C. S. *J. Org. Chem.* **2006**, *71*, 3599-3607.

(153)   Yamamoto, H.; Maruoka, K. *J. Am. Chem. Soc.* **1981**, *103*, 4186-4194.

(154)   Boiocchi, M.; Bonizzoni, M.; Fabbrizzi, L.; Foti, F.; Licchelli, M.; Poggi, A.; Taglietti, A.; Zema, M. *Chem. Eur. J.* **2004**, *10*, 3209-3216.

(155)   Kolinski, R. A. *Pol. J. Chem.* **1995**, *69*, 1039-1045.

(156)   Weisman, G. R.; Rogers, M. E.; Wong, E. H.; Jasinski, J. P.; Paight, E. S. *J. Am. Chem. Soc.* **1990**, *112*, 8604-8605.

(157)   Plutnar, J.; Havlíčková, J.; Kotek, J.; Hermann, P.; Lukeš, I. *New J. Chem.* **2008**, *32*, 496-504.

(158)   Wainwright, K. P.; Ramasubbu, A. *J. Chem. Soc., Chem. Commun.* **1982**, 277-278.

(159)   Bernier, N.; Allali, M.; Tripier, R.; Conan, F.; Patinec, V.; Develay, S.; Le Baccon, M.; Handel, H. *New J. Chem.* **2006**, *30*, 435-441.

(160)   Kimura, E. *Pure Appl. Chem.* **1986**, *58*, 1461-1466.

(161)   Kimura, E.; Koike, T.; Uenishi, K.; Hediger, M.; Kuramoto, M.; Joko, S.; Arai, Y.; Kodama, M.; Iitaka, Y. *Inorg. Chem.* **1987**, *26*, 2975-2983.

(162)   Kimura, E.; Koike, T.; Takahasi, M. *J. Chem. Soc., Chem. Commun.* **1985**, 385-386.

(163)   Iitaka, Y.; Koike, T.; Kimura, E. *Inorg. Chem.* **1986**, *25*, 402-404.

(164)   Houser, R. P.; Halfen, J. A.; Young, V. G.; Blackburn, N. J.; Tolman, W. B. *J. Am. Chem. Soc.* **1995**, *117*, 10745-10746.

(165)   Moore, D. A.; Fanwick, P. E.; Welch, M. J. *Inorg. Chem.* **1990**, *29*, 672-676.

(166)   Barefield, E. K. *Inorg. Chem.* **1972**, *11*, 2273-2274.

(167)   Barefield, E. K.; Wagner, F.; Herlinger, A. W.; Dahl, A. R. *Inorg. Synth.* **1976**, *16*, 220-225.

(168)   Hervé, G.; Bernard, H.; Le Bris, N.; Yaouane, J.-J.; Handel, H.; Toupet, L. *Tetrahedron Lett.* **1998**, *39*, 6861-6864.

(169)   McOmie, J. F. W.; West, D. E. *Organic Synthetic Collection* **1973**, *5*, 412-414.

(170)   Vankar, Y. D.; Rao, C. T. *J. Chem. Res., Synop.* **1985**, 232-233.

(171)   Niu, W.; Wong, E. H.; Weisman, G. R.; Peng, Y.; Anderson, C. J.; Zakharov, L. N.; Golen, J. A.; Rheingold, A. L. *Eur. J. Inorg. Chem.* **2004**, 3310-3315.

(172)   Niu, W.; Wong, E. H.; Weisman, G. R.; Sommer, R. D.; Rheingold, A. L. *Inorg. Chem. Comm.* **2002**, *5*, 1-4.

(173)   Harpstrite, S. E.; Beatty, A. A.; Collins, S. D.; Oksman, A.; Goldberg, D. E.; Sharma, V. *Inorg. Chem.* **2003**, *42*, 2294-2300.

(174)   Dong, Y.; Lawrence, G. A.; Lindoy, L. F.; Turner, P. *Dalton Trans.* **2003**, 1567-1576.

(175)   Fabbrizzi, L.; Montagna, A.; Poggi, A.; Kaden, T. A.; Siegfried, L. C. *J. Chem. Soc., Dalton Trans.* **1987**, 2631-2634.

(176)   Binkley, R. W.; Hehemann, D. G. *J. Org. Chem.* **1990**, *55*, 378-380.

(177)   Riley, J. G.; Grindley, T. B. *J. Carbohydr. Chem.* **2001**, *20*, 159-169.

(178)   Petchmanee, T.; Ploypradith, P.; Ruchirawat, S. *J. Org. Chem.* **2006**, *71*, 2892-2895.

(179)   Rodebaugh, R.; Debenham, J. S.; Fraser-Reid, B. *Tetrahedron Lett.* **1996**, *37*, 5477-5478.

(180) Park, M. H.; Takeda, R.; Nakanishi, K. *Tetrahedron Lett.* **1987**, *28*, 3823-3824.

(181) Lesk, A.; Nudelman, A. *Synth. Commun.* **1999**, *29*, 1405-1408.

(182) Hodgetts, K. J.; Wallace, T. W. *Synth. Commun.* **1994**, *24*, 1151-1155.

(183) Cappa, A.; Marcantoni, E.; Torregiani, E. *J. Org. Chem.* **1999**, *64*, 5696-5699.

(184) Kimura, E.; Uenishi, K.; Koike, T.; Iitaka, Y. *Chem. Lett.* **1986**, 1137-1140.

(185) Dong, Y.; Lindoy, L. F.; Turner, P.; Wei, G. *Dalton Trans.* **2004**, 1264-1270.

(186) Kimura, E.; Sasada, M.; Shionoya, M.; Koike, T.; Kurosaki, H.; Shiro, M. *J. Biol. Inorg. Chem.* **1997**, *2*, 74-82.

(187) Bloch, F.; Hansen, W. W.; Packard, M. *Phys. Rev.* **1948**, *70*, 474.

(188) Kimura, K.; Yamashita, T.; Yokoyama, M. *J. Chem. Soc., Perkin Trans. 2* **1992**, 613-619.

(189) Kimura, K.; Yamashita, T.; Yokoyama, M. *J. Chem. Soc., Chem. Commun.* **1991**, 147-148.

(190) Kimura, K.; Kado, S.; Sakamoto, H.; Sakai, A.; Yokoyama, M.; Tanaka, M. *J. Chem. Soc., Perkin Trans. 2* **1999**, 2539-2544.

(191) Kimura, K.; Sakamoto, H.; Uda, R. M. *Macromolecules* **2004**, *37*, 1871-1876.

(192) Toğrul, M.; Sünkür, M.; Kaynak, F. B.; Hoşgören, H.; Özbey, S. *J. Chem. Res.* **2003**, *2003*, 1014-1024.

(193) Bockstahl, F.; Graf, E.; Hosseini, M. W.; Suhr, D.; De Cian, A.; Fischer, J. *Tetrahedron Lett.* **1997**, *38*, 7439-7542.

(194) Linnane, P.; Shinkai, S. *Tetrahedron Lett.* **1995**, *36*, 3865-3866.

(195) Tanaka, M.; Kamada, K.; Ando, H.; Kitagaki, T.; Shibutani, Y.; Kimura, K. *J. Org. Chem.* **2000**, *65*, 4342-4347.

(196) Tanaka, M.; Kamada, K.; Kitagaki, T.; Shibutani, Y.; Yajima, S.; Sakamoto, H.; Kimura, K. *Chem. Commun.* **1999**, 1453-1454.

(197) Beeby, A.; Bushby, L. M.; Maffeo, D.; Williams, J. A. G. *J. Chem. Soc., Dalton Trans.* **2002**, 48-54.

(198) Tshuva, E. Y.; Gendeziuk, N.; Kol, M. *Tetrahedron Lett.* **2001**, *42*, 6405-6407.

(199) Hormnirum, P.; Marshall, E. L.; Gibson, V. C.; White, A. J. P.; Williams, D. J. *J. Am. Chem. Soc.* **2004**, *126*, 2688-2689.

(200) Cox, A. R. F.; Gibson, V. C.; Marshall, E. L.; White, A. J. P.; Yeldon, D. *Dalton Trans.* **2006**, 5014-5023.

(201) Massue, J.; Plush, S. E.; Bonnet, C. S.; Moore, D. A.; Gunnlaugsson, T. *Tetrahedron Lett.* **2007**, *48*, 8052-8055.

(202)   Land, E. J.; Porter, G. *Trans. Faraday Society* **1961**, *57*, 1885-1893.

(203)   Burai, L.; Tóth, É.; Moreau, G.; Sour, A.; Scopelliti, R.; Merbach, A. E. *Chem. Eur. J.* **2003**, *9*, 1394-1404.

(204)   Lebdušková, P.; Hermann, P.; Helm, L.; Tóth, É.; Kotek, J.; Binnemans, K.; Rudovský, J.; Lukeš, I.; Merbach, A. E. *Dalton Trans.* **2006**.

(205)   Mani, F.; Morassi, R.; Stoppioni, P.; Vacca, A. *J. Chem. Soc., Dalton Trans.* **2001**, 2116-2120.

(206)   Pittet, P. A.; Früh, D.; Tissières, V.; Bünzli, J.-C. G. *J. Chem. Soc., Dalton Trans.* **1997**, 885-900.

(207)   Aime, S.; Botta, M.; Fasano, M.; Marques, M. P. M.; Geraldes, C. F. G. C.; Pubanz, D.; Merbach, A. E. *Inorg. Chem.* **1997**, *36*, 2059-2068.

(208)   McRobbie, G. Thesis, The University of Hull, **2009**.

(209)   Zhao, G.; Bolton, S. A.; Kwon, C.; Hartl, K. S.; Seiler, S. M.; Slusarchyk, W. A.; Sutton, J. C.; Bisacchi, G. S. *Bioorg. Med. Chem. Lett.* **2004**, *14*, 309-312.

(210)   Xie, J.; Seto, C. T. *Bioorg. Med. Chem.* **2005**, *13*, 2981-2991.

(211)   Katayama, S.; Ae, N.; Kodo, T.; Masumoto, S.; Hourai, S.; Tamamura, C.; Tanaka, H.; Nagata, R. *J. Med. Chem.* **2003**, *46*, 691-701.

(212)   MacDonald, I. J.; Dougherty, T. J. *J. Porphyr. Phthalocyanines* **2001**, *5*, 105-129.

(213)   Pandey, R. K.; Zheng, G. In *The Porphyrin Handbook*; Kadish, K. M., Smith, K. M., Guilard, R., Eds.; Academic Press: London, **2000**; *Vol. 6*, p 157-230.

(214)   Zenkevich, E.; Sagun, E.; Knyukshto, V.; Shulga, A.; Mironov, A.; Efremova, O.; Bonnett, R.; Songea, S. P.; Kassem, M. *J. Photochem. Photobiol. B. Biol.* **1996**, *33*, 171-180.

(215)   Coutsolelos, A.; Guilard, R.; Bayeul, D.; Lecomte, C. *Polyhedron* **1986**, *5*, 1157-1164.

(216)   Eaton, S. S.; Fishwild, D. M.; Eaton, G. R. *Inorg. Chem.* **1978**, *17*, 1542-1545.

(217)   Buchler, J. W.; Puppe, L.; Rohbock, K.; Schneehage, H. H. *Chem. Ber.* **1973**, *106*, 2710-2732.

(218)   Feng, Y.; Ong, S. L.; Hu, J.; Ng, W. J. *Inorg. Chem. Comm.* **2003**, *6*, 466-468.

(219)   Coutsolelos, A.; Guilard, R.; Boukhris, A.; Lecomte, C. *J. Chem. Soc., Dalton Trans.* **1986**, 1779-1783.

(220)   Balch, A. L.; Latos-Grażyński, L.; Noll, B. C.; Phillips, S. L. *Inorg. Chem.* **1993**, *32*, 1124-1129.

(221)   DiPasquale, A. G.; Mayer, J. M. *J. Am. Chem. Soc.* **2008**, *130*, 1812-1813.

(222) Kadish, K. M.; Cornillion, J.-L.; Coutsolelos, A.; Guilard, R. *Inorg. Chem.* **1987**, *26*, 4167-4173.

(223) Kadish, K. M.; Boisselier-Cocolios, B.; Coutsolelos, A.; Mitaine, P.; Guilard, R. *Inorg. Chem.* **1985**, *24*, 4521-4528.

(224) Kadish, K. M.; Maiya, G. B.; Xu, Q. Y. *Inorg. Chem.* **1989**, *28*, 2518-2523.

(225) Balch, A. L.; Hart, R. L.; Parkin, S. *Inorg. Chim. Acta* **1993**, *205*, 137-143.

(226) Wojaczyński, J.; Latos-Grażyński, L. *Inorg. Chem.* **1995**, *34*, 1054-1062.

(227) Longo, F. R.; Finarelli, M. G.; Kim, J. B. *J. Heterocycl. Chem.* **1969**, *6*, 927-931.

(228) Gouterman, M.; Hall, R. J.; Khalil, G.-E.; Martin, P. C.; Shankland, E. G.; Cerny, R. L. *J. Am. Chem. Soc.* **1989**, *111*, 3702-3707.

(229) Kadish, K. M.; Araullo-McAdams, C.; Han, B. C.; Franzen, M. M. *J. Am. Chem. Soc.* **1990**, *112*, 8364-8368.

(230) Carvalho de Medeiros, M. A.; Cosnier, S.; Deronzier, A.; Moutet, J.-C. *Inorg. Chem.* **1996**, *35*, 2659-2664.

(231) Samaroo, D.; Soll, C. E.; Todaro, L. J.; Drain, C. M. *Org. Lett.* **2006**, *8*, 4985-4988.

(232) Weiss, R.; Pühlhofer, F.; Jux, N.; Merz, K. *Angew. Chem. Int. Ed.* **2002**, *41*, 3815-3817.

(233) van Nunen, J. L. M.; Folmer, B. F. B.; Nolte, R. J. M. *J. Am. Chem. Soc.* **1997**, *119*, 283-291.

(234) Tsuchida, E.; Komatsu, T.; Hasegawa, E.; Nishide, H. *J. Chem. Soc., Dalton Trans.* **1990**, 2713-2718.

(235) Sutton, J. M.; Clarke, O. J.; Fernandez, N.; Boyle, R. W. *Bioconjugate Chem.* **2002**, *13*, 249-263.

(236) Fuhrhop, J.-H.; Kadish, K. M.; Davis, D. G. *J. Am. Chem. Soc.* **1973**, *95*, 5140-5147.

(237) Bhattacharjee, M.; Mahanti, M. K. *Bull. Soc. Chim. Fr.* **1983**, *1*, 225-228.

(238) Bhattacharjee, M.; Mahanti, M. K. *Pol. J. Chem.* **1984**, *58*, 1099-1105.

(239) Mosinger, J.; Jirsák, O.; Kubát, P.; Lang, K.; Mosinger, B. *J. Mater. Chem.* **2006**, *17*, 164-166.

(240) Spellane, P. J.; Gouterman, M.; Antipas, A.; Kim, S.; Liu, Y. C. *Inorg. Chem.* **1980**, *19*, 386-391.

(241) Shaw, S. J.; Edwards, C.; Boyle, R. W. *Tetrahedron Lett.* **1999**, *40*, 7585-7586.

(242)   Liu, J. Y.; Jiang, Z. J.; Fong, W.-P.; Ng, D. K. P. *Org. Biomol. Chem.* **2008**, *6*, 4560-4566.

(243)   Charkoudian, L. K.; Pham, D.; Franz, K. J. *J. Am. Chem. Soc.* **2006**, *128*, 12424-12425.

(244)   Farrugia, L. J. *J. Appl. Crystallogr.* **1999**, *32*, 837-838.

(245)   Farrugia, L. J. *J. Appl. Crystallogr.* **1997**, *30*, 565.